BNL 51443

ISABELLE

PROCEEDINGS OF THE 1981 SUMMER WORKSHOP

VOLUME 1

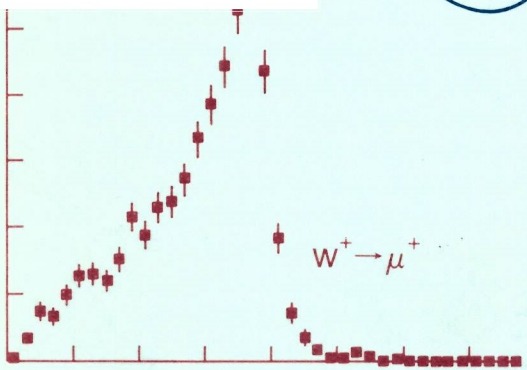

BROOKHAVEN NATIONAL LABORATORY
Upton, Long Island, New York, 11973

ISABELLE • 1981 WORKSHOP • VOL. 1 — LECTURES • BNL 51443



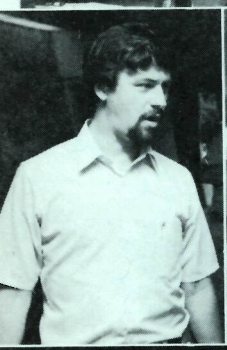

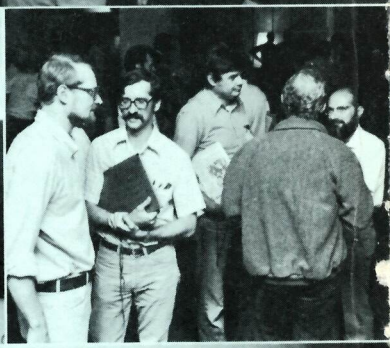
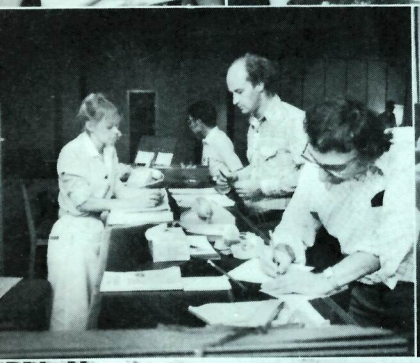


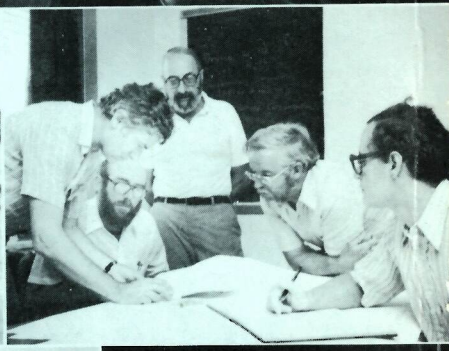


BNL 51443
UC-28
UC-34d
(Particle-Accelerators
and High-Voltage Machines;
Physics — Particles and Fields TIC-4500)

ISABELLE

PROCEEDINGS OF THE 1981 SUMMER WORKSHOP

JULY 20 — 31, 1981

VOLUME 1
LECTURES

BROOKHAVEN NATIONAL LABORATORY
ASSOCIATED UNIVERSITIES, INC.
UNDER CONTRACT NO. DE-AC02-76CH00016 WITH THE
UNITED STATES DEPARTMENT OF ENERGY

FOREWORD

The ISABELLE Summer Workshop, held at BNL from July 20 through July 31, was attended by 259 physicists representing 72 institutions. The discussions covered experimental areas, large detectors and detector technology, with a primary emphasis on physics opportunities, both with a phased and a full luminosity ISABELLE.

There was a consensus that physics with Phase I ($E_{cm} \approx 700$ GeV and $L \sim 2 \times 10^{31}/cm^2/sec$, with bunched beams) was feasible, important and exciting. It has been known for years that the orthodox gauge theories will be critically tested by studying the $W^{\pm}$, Z^0 and high $p_\perp$ phenomena. The Z^0 has a reasonable chance of being found at the $\bar{p}p$ colliders if luminosities reach $10^{30}/cm^2/sec$, but its properties will be difficult to decipher. Seeing the $W^{\pm}$'s or new heavy quarks is less probable and measuring their properties is even less likely. At ISABELLE these phenomena can all be studied with high precision. But the more exciting conclusion which emerged from the workshop was related to the question of what generates the $\sim$100 GeV masses of the W's and Z's. The answer could involve Higgs, technicolor, or other particles with masses ranging from 10.8 GeV to 1 TeV, with an intermediate mass scale of 200-300 GeV being a possible region of strong interest. Some of these models predict spectacular experimental signatures. It is clear that only ISABELLE with $L \sim 10^{32} - 10^{33}$, has an opportunity of addressing and resolving such questions.

The great interest in ISABELLE physics was also evidenced by the variety of large detectors (6 to date) that have evolved - characterized by magnetic field configurations ranging from solenoid through dipole and toroid to no field at all. The ability to extract the physics was re-examined, leptons and γ's being straightforward, with greater attention being paid to analyzing jet and multijet events and defining their properties, masses, $p_\perp$, etc. Many advances were also reported in detector R&D, for example, imaging Cerenkov counters, precision drift chambers, scintillating optical fibers. Although there were many problems to be solved, such as data handling and vertex detectors, there was

more confidence and less apprehension about our ability to solve them. Experimental areas look fine except for the rerouting of some trenches and exchanging areas #10 and #12 to more easily accomodate the ep option.

The question of options was discussed at length and in quite some depth. It seems natural to augment ISABELLE with an ep capability, especially with a separate ring. Electron energies of 10-20 GeV with luminosities of 10^{31} - 10^{32} look achievable and have stimulated great interest. The addition of a booster, Phase II, would also naturally allow for the study of heavy ion interactions for which enthusiasm seems to be growing, especially in the light of ISR results.

In summary, the Workshop was a very upbeat, enthusiastic, and successful meeting. With the opportunities for carrying out high energy experiments being limited at present and more so in the future, the community is beginning to reaffirm even more strongly the great physics potential of ISABELLE. The consensus is to get on with the project, get it done and perform the physics. A turn-on in '86 or '87 is what is desired.

N.P. Samios
S.C.C. Ting
Co-Chairmen

INTRODUCTION

The Workshop and these proceedings were organized into five parts:

		Organizers
1.	Lectures	Ling-Lie Chau
2.	Physics	M.A.B. Beg Ling-Lie Chau V. Fitch A. Mann
3.	Experimental Areas	R. Lanou S. Aronson
4.	Large Detectors	C. Baltay H. Gordon
5.	Detector Research and Development	W. Carithers T. Ludlam

During the two weeks of the Workshop authors gave us their drafts and figures. These were put into final form by BNL typists and draftsmen. Under the extremely tight time constraints we could not guarantee that everything has come out perfectly - we did the best job we could.

The Workshop and Proceedings were truly a herculean job and could not have been accomplished without the gracious help of many people. Kit McNally and Joyce Ricciardelli coordinated the Workshop from its inception. During the Workshop, they were joined by Penny Baggett and Pat Tuttle at the conference desk. The various amenities were organized by Pat Glynn, Bill Love, Mike Schmidt, Tom Rizzo, Larry Trueman and Peter Yamin.

For the Proceedings, Ken Foley served as managing editor, organizing the entire production in less than a month. The sections were ordered and edited by Ling-Lie Chau, Bob Lanou, Sam Aronson, Tom Ludlam and Frank Paige. We had an army of hard-working typists: Donna Early, Judy Ferrero, Barbara Gaer, Rae Greenberg, Isabell Harrity, Pat Knisely, Pat Lebitski, Sharon Smith, Kathy Tuohy, Pat Valli, and Diana Votruba. Drafting the myriad of figures was skillfully accomplished by Randy Bowles, Rip Bowman, Kathy Brown, Bill Dieffenbach, Sal Morano, and Sue Norton. The enormous job of copy preparation was done by Fern Coyle, Liz Russell and Joyce Ricciardelli. None of this would have been possible without the complete support of the Technical Photography and Graphic Arts Division.

Neil Baggett deserves special mention for his incomparable efforts in making this Workshop successful.

Howard A. Gordon
Editor-in-Chief

21 August 1981

Table of Contents

VOLUME 1

VOLUME 2

SECTION II - Physics

Page No.

VOLUME 4

SECTION V - Detector Research and Development

Participants
ISABELLE Summer Workshop July 20-31, 1981

Participant's name	Institution
K. Abe	University of Pennsylvania
A. Ali	DESY
K. Amako	University of Pennsylvania
E. W. Anderson	Iowa State University
T. W. Appelquist	Yale University
S. Aronson	BNL
F. W. Ascolese	BNL
V. Ashford	BNL
M. Atac	Fermilab
M. Atiya	Columbia University
J. Babcock	Carnegie-Mellon University
T. Bacon	Imperial College
N. Baggett	BNL
P. Baggett	BNL
N. Baker	BNL
C. Baltay	Columbia University
A. J. Baltz	BNL
Z. J. Banas	BNL
Z. Bar-Yam	Southeastern Massachusetts University
A. Bassetto	University of Trento, Italy
L. Baumel	Yale University/BNL
U. Becker	Massachusetts Institute of Technology
M. A. B. Beg	Rockefeller University
E. W. Beier	University of Pennsylvania
S. Beingessner	Carleton University
O. Benary	University of Tel-Aviv
J. Bensinger	Brandeis University
D. Berley	National Science Foundation
M. Bernias	BNL
K. Black	Yale University
S. Blatt	Yale University/BNL
B. Blumenfeld	Johns Hopkins University
S. Borenstein	York College of the C.U.N.Y.
G. Bozoki	BNL
P. Braccini	INFN-Pisa/CERN
J. Branson	Massachusetts Institute of Technology
M. Bregman	Nevis Laboratory
G. Bunce	BNL
M. Capell	Massachusetts Institute of Technology
W. Carithers	Lawrence Berkeley Laboratory
L.-L. Chau	BNL
M. Chen	Massachusetts Institute of Technology

S.-P. Chen	Institute of Atomic Energy, Beijing/BNL
C.P. Cheng	Institute of High Energy Physics, Beijing
Y. Cho	Argonne National Laboratory
T. S. Chou	BNL
J.H. Christenson	New York University
S. U. Chung	BNL
P. Clarke	SUNY, Stony Brook/BNL
W. E. Cleland	University of Pittsburgh
D. Coon	University of Pittsburgh
J. W. Cooper	University of Pennsylvania
P. Coteus	Columbia University
S. Csorna	Vanderbilt University
E. D. Courant	BNL
G. T. Danby	BNL
J. F. Donoghue	University of Massachusetts
J. Dowd	Southeastern Massachusetts University
D. S. Du	Institute of High Energy Physics, Beijing
P. Duinker	NIKHEF/DESY
R. Edelstein	Carnegie-Mellon University
F. Eiseler	CUNY
J. Elias	Fermilab
R. Engelmann	BNL
A. Erwin	University of Wisconsin
G. Y. Fang	Massachusetts Institute of Technology
R. Fernow	BNL
R. Field	University of Florida
J. Fischer	BNL
K. J. Foley	BNL
S. Frankel	University of Pennsylvania
W. Frati	University of Pennsylvania
W. R. Frisken	York University
G. Gammel	BNL
G. Giacomelli	University of Bologna
B. G. Gibbard	BNL
M. Goldhaber	BNL
P. Gollon	BNL
H. Gordon	BNL
P. D. Grannis	SUNY, Stony Brook
R. Gustafson	University of Michigan
S. Hagopian	Florida State University
V. Hagopian	Florida State University
H. Hahn	BNL
C. Hargrove	National Research Council of Canada
J. C. Herrerra	BNL

J. Hettema	BNL
H. Hilke	CERN
S. Holmes	Columbia University
H.-C. Hseuh	BNL
K. Huang	Massachusetts Institue of Technology
J. W. Humphrey	BNL
V. W. Hughes	Yale University
Y. Inagaki	BNL
N. Isgur	University of Toronto
J. Jackson	BNL
K. Jaeger	BNL
D. Jensen	University of Massachusetts
H. Jensen	Fermilab
R. Johnson	BNL
S. Kabe	KEK-Japan
T. Kalogerpoulos	Syracuse University
S. Kahn	BNL
G. Kane	University of Michigan
A. Kanofsky	Lehigh University
G. Kantardjian	CERN
H. Kasha	Yale University
S. Katcoff	BNL
E. Keil	CERN
W.-Y. Keung	BNL
J. Kirz	SUNY, Stony Brook
B. Knapp	Nevis Laboratory
H. Kraner	BNL
P. Kunz	SLAC
B. P. Kwan	BNL
T. F. Kycia	BNL
R. E. Lanou	Brown University
K. W. Lai	BNL, University of Arizona
L. Lasker	BNL
W. Lee	Columbia University
Y.Y. Lee	BNL
L. B. Leipuner	BNL
K. Li	BNL
P. Limon	Fermilab
S. Lindenbaum	BNL/CCNY
L. Littenberg	BNL
R. S. Longacre	BNL
W. A. Love	BNL
D. I. Lowenstein	BNL
D. Luckey	Massachusetts Institute of Technology
T. Ludlam	BNL

D. Makowiechi	BNL
K. Manivannan	SUNY, Stony Brook
A. K. Mann	University of Pennsylvania
V. Manzella	BNL
W. Marciano	Northwestern University
J. Martin	University of Toronto
J. Marraffino	BNL/Vanderbilt University
J. Marx	Lawrence Berkeley Lab
M. Marx	SUNY, Stony Brook
G. Massaro	NIKHEF/Amsterdam
T. Matsuda	Osaka University/ MIT
D. Maurizio	BNL
M. May	BNL
R. McCarthy	SUNY, Stony Brook
K. McDonald	Princeton University
A. Melissinos	University of Rochester
A. Metz	BNL/Harvard University
T. Meussen	BNL
D. Miller	Northwestern University
T. Miyachi	INS - Tokyo
M. Month	Department of Energy
W. M. Morse	BNL
A. H. Mueller	Columbia University
M. J. Murtagh	BNL
S. Murtagh	BNL
K. Nakagawa	University of Naples
A. Nappi	University of Pisa
P. Nemethy	Lawrence Berkeley Laboratory
J. Niederer	BNL
S. Nussinov	Massachusetts Institute of Technology
T. O'Halloran	University of Illinois
J. Okamitsu	Columbia-Nevis
B. Ovryn	BNL/University of Rochester
H. Paar	Columbia University/NIKHEF
F. E. Paige	BNL
J. A. Paradiso	Massachusetts Institute of Technology
Z. Parsa	Northwestern University
E. A. Paschos	BNL/Universitat Dortmund
A. Pascolini	University of Padua
R.M. Patel	McGill University
R. Peierls	BNL
A. Pevsner	Johns Hopkins University
O. Piccioni	University of California
H. Piekarz	BNL
J. Piekarz	BNL
R. Plano	Rutgers University
E. Platner	BNL

B. Pope	Princeton University
A. Prodell	BNL
S. Protopopescu	BNL
M. Pusterla	BNL
G. Rabinowitz	BNL
S. Raby	SLAC
V. Radeka	BNL
D. Rahm	BNL
R. R. Rau	BNL
G. Reiter	BNL
T. G. Rizzo	BNL
J. Roberts	Rice University
N. Rofail	BNL
C. Roos	Vanderbilt University
J. Rosen	Northwestern University
E. Rosenberg	Iowa State University
L. Rosenson	Massachusetts Institute of Technology
J. A. Rubio	JEN-Madrid
R. Rückl	University of Munich
J. Russell	Southeastern Massachusetts University
M. Sakitt	BNL
J. Sanford	BNL
J. Sandweiss	Yale University
D. Schildknecht	University Bielefeld
M. Schmidt	Yale University
L. S. Schroeder	Lawrence Berkeley Laboratory
W. Selove	University of Pennsylvania
W. P. Sims	BNL
A. Sinha	SUNY, Stony Brook
W. Sippach	Columbia University
E. J. Siskind	BNL
J. Skelly	BNL
P. Skybic	University of Oklahoma
S.D. Smith	BNL
G. Snow	University of Maryland
J. Spiro	BNL
R. M. Sternheimer	BNL
A. Stevens	BNL
H. Sticker	Rockefeller University
R. Strand	BNL
K. Strauch	Harvard University
I. Stumer	BNL
L. Sulak	University of Michigan
S. Sumorok	University of Birmingham/CERN
Y. Suzuki	Brown University
M. Tanaka	BNL
X. W. Tang	Institute of High Energy Physics, Beijing

M. J. Tannenbaum	BNL
S. Terada	BNL
G. Theodosiou	University of Pennsylvania
D. Theriot	Fermilab
J. Thompson	University of Pittsburg
S.C.C. Ting	Massachusetts Institute of Technology
F. G. Tinta	BNL
A. Tollestrup	Fermilab
M. Tran	University of California, Los Angeles
T. L. Trueman	BNL
M. Valdata-Nappi	INFN-Pisa
G. Voss	DESY
A. Walenta	BNL
W. G. Walker	BNL
W. Wallenmeyer	Department of Energy
P. Wanderer	BNL
J. Warnock	Massachusetts Institute of Technology
W. Weisberger	SUNY, Stony Brook
D. Wheeler	BNL
D. H. White	BNL
S. White	Rockefeller University
B. Wiik	DESY
A. Wijangco	BNL
B. F. Wilczek	University of California, Santa Barbara
H. H. Williams	University of Pennsylvania
W. Willis	CERN
R. R. Wilson	Columbia University
Y. S. Wu	Institute of Theoretical Physics, Beijing/ Institute for Advanced Study
P. Xue	Beijing/MIT
T. Yamanouchi	Fermilab
P. Yamin	BNL
C. N. Yang	SUNY, Stony Brook
T. Ypsilantis	Ecole Polytechnique
J. Zingman	Yale University; BNL

ISABELLE - OVERVIEW

N.P. Samios

ISABELLE, a proton-proton high energy intersecting storage accelerator, has as its main aim the study of proton-proton interactions at high center of mass energies E_{CM} = 360 GeV x 360 GeV = 720 GeV and high luminosities L = $10^{32}/cm^2/sec \rightarrow 10^{33}/cm^2/sec$. In contrast to several other colliders, this machine will be dedicated to a colliding beam physics program with six intersecting regions. The national and international situation concerning a variety of operating and proposed accelerators is shown in Table I. There is clearly a plethora of e^+e^- machines, five with energies between 7 and 40 GeV, the latest being PEP and PETRA with approval for the TRISTAN in Japan (60 GeV in 1986) and a strong likelihood for LEP at CERN (100 GeV in 1988). The hadron colliders are fewer in number with the CERN $\bar{p}p$ version having just recently attained beam with luminosities of $\sim 10^{26}/cm^2/sec$. The only newcomers to the fixed target machines are the Tevatron and UNK in the Soviet Union. The only ep under consideration is HERA at Hamburg, a 800 GeV p x 30 GeV e machine. It should be noted that these machines are complementary, each with their strengths and weaknesses. The e^+e^- machines are ideally suited to exploring s channel resonances in great depth. These are also attractive to theorists in that many of the processes are calculable. On the other hand one is restricted to moderate energies, the cost of such circular colliders being proportional to E^2_{cm}. Linear colliders have a promise of better scaling, cost $\sim E_{cm}$, but have yet to demonstrate feasibility. Limited luminosity, L = 5 x $10^{30}/cm^2/sec$ - $10^{31}/cm^2/sec$ also seems to be an attribute of such machines, an order of magnitude lower value than had been previously thought attainable. $\bar{p}p$ colliders are, in principle, the path to high energies since they involve a single ring of magnets. Still unknown are the attainable luminosities. Values of 10^{29} - $10^{30}/cm^2/$ sec are present target numbers, with much

information and knowledge to be gained in the next year with the CERN machine. This is to be contrasted with pp colliders which can attain high energies and high luminosities. The CERN ISR exceeded its design current, attaining 40 to 50 amps compared to a design value of 20 amps, thereby assuring luminosities of $10^{32}/cm^2/sec$ and higher for such machines at high energies. Of course, both the ISR with eight intersecting regions and ISABELLE with six are dedicated machines, while the $\bar{p}p$ colliders with only one or two regions also have competing fixed target programs. The rate at which events are accumulated is determined by the cross section and luminosity, $R = \sigma * L$. The cross section characterizing the strong interaction is of the order of millibarns, σ (strong) $\simeq 10^{-27} cm^2$ so that machines with luminosities of 10^{26}-$10^{28}/cm^2/sec$ can investigate such reactions. Electromagnetic cross sections are a factor of 1,000 smaller, σ (e-m) $\simeq 10^{-30} cm^2$, so that both e^+e^-, ep and hh machines with $L = 10^{30}/cm^2/sec$ have access to such interesting interactions. Going one step further, weak interactions have cross section σ (weak) $\simeq 10^{-33} cm^2$ or smaller, so that one clearly needs high luminosities, which only ISABELLE can supply, if one wants to systematically study such interactions. These machines with their pertinent parameters are displayed in Fig. 1. One notes the present operating machines clustering about the 30-60 GeV energy and 10^{30} -10^{31} luminosity regions, contrasting with those under construction at energies $\sim$100 GeV with as high luminosity as can be attained. ISABELLE, on these criteria, clearly has the best physics potential.

Before discussing the physics opportunities at ISABELLE, it is appropriate to digress a bit and look at possible lessons to be learned from our historical experience. The first observation I would make is that new physics is usually unearthed whenever one changes a pertinent physical parameter in a significant manner. This may involve temperature, distance, density, energy or intensity. The second lesson is that the major experimental discoveries made at most accelerators were not anticipated at

their inception. These are well known: for the AGS, CP violation, 2 ν's, Ω^-, J, Λ_c^+ and a host of other resonances; for Fermilab, T, T' and large $p_\perp$ behavior; and for SLAC, deep inelastic scattering, ψ, charmonium states, and charm mesons D,D*. Furthermore, the number of events needed for a discovery has varied from 1 to between 30 and 100. However, to exploit their properties, it was necessary to accumulate hundreds of events for the ϕ, thousands for the J/ψ and millions for the K^o. The last, parenthetical remark has to do with detectors. First, they need safety factors -- the 2 ν experiment which was a large extrapolation in detector size, 10 tons, found only 29 events. The split field magnet at the CERN ISR was specifically designed to look at low $p_\perp$ physics but the exciting physics occurred at large $p_\perp$. The message for ISABELLE is therefore clear; extend E, L and make the machine and the detectors reliable and flexible.

There are two major machine approaches proposed for ISABELLE. These are:

Approved - Large Aperture

E_{CM} = 360 GeV x 360 GeV = 720 GeV, B = 45 kgauss

L = 2 x $10^{32}/cm^2/sec \rightarrow 10^{33}/cm^2/sec$

Magnets - cos θ braid
2 layer cable - Palmer
Picture frame - Danby
3 layer cable - LBL-Taylor

Schedule and Cost: '87 $454M TEC
'88 $475M

Phased - E_{CM} = 350 GeV x 350 GeV = 700 GeV

Phase I - L = 2 x $10^{31} \rightarrow 10^{32}/cm^2/sec$

Small Aperture - Fermilab magnets 42 kgauss

Schedule and Cost: '86 $375M

Phase II - L = 10 x above

Booster 100 GeV

3 yrs. construction - $50-$100M

There are several very exciting possible machine options, especially ep and heavy ions. The Columbia group and their collaborators have investigated the former with parameters ranging from 10 GeV to 20 GeV e's on 350 GeV protons, with luminosities of 2×10^{31} and $9 \times 10^{31}/cm^2/sec$ respectively. The ability to longitudinally polarize the electrons is an important ingredient in each of these phases. The electron ring can be placed in the ISABELLE tunnel for an estimated $25M, in a separate tunnel for $40M and an additional $25M would increase the electron energy from 10 GeV to 20 GeV. The time scale for construction is three years from start of funding. With the addition of a booster for Phase II, the possibility of designing this machine to also accelerate heavy ions is clearly possible and desirable. The energy of such a booster would be above transition. The physics interest in such heavy ion collisions, α α, NeNe etc. has recently been stimulated by the results of Willis and his group at the CERN ISR. Finally, one should note that there is the distinct possibility that the e ring and the booster can be one and the same, at some added cost to each.

Physics

I would re-emphasize the search for the unknown as the primary goal for ISABELLE, as it has been for nearly all accelerators. The mass region from 40 GeV to 100 GeV should be explored with ease. The region of 100 GeV - 250 GeV will also be accessible, but will take a little longer. Both regions are extremely interesting, as will be discussed shortly. The former involves firm extrapolation of present knowledge and the latter region is more an area of speculation and probably the more interesting. There have been references to ISABELLE as a window on physics - I consider it to be more akin to a barn door, in contrast to other approaches which are peepholes.

Now, what are the basic physics considerations? First is the question of fundamental constituents, the number of quark flavors, We have u, d, c, s, b and no t up to a mass of 18 GeV. From our

observation of vector meson production (ϕ, J/ψ, Υ), we have noted a universal scaling phenomenon for the production and decay of such vector mesons into lepton pairs. This so-called Gaisser scaling works, from AGS, Fermilab to ISR energies, as shown in Fig. 2. Extrapolating to ISABELLE energies one predicts that in a 1,000 hour experiment a bump with an excess of 40 events can be accumulated for a vector particle mass of 60 GeV with a Phase I luminosity of 2×10^{31} and a mass of 80 GeV for a luminosity of 2×10^{32}. For comparison, the CERN collider is restricted to masses less than 40 GeV and the Fermilab collider to less than 50 GeV. If the mass of hidden ($t\bar{t}$) is greater than 100 GeV, then leptonic decays are severely depressed and one has to look for naked ($t\bar{d}$) and ($\bar{t}d$) production and decay. The cross section estimates for their production are in the picobarn range but again they are produced rather profusely. For a t mass of 50 GeV the phased ISABELLE with 2×10^{31} luminosity will produce 10^5 events in a 1,000 hour experiment and an order of magnitude more at the standard larger aperture ISABELLE. The challenge is to find these events. Recent work at the CERN ISR, where the Λ_c and possibly the Λ_b have been found, gives some optimism that it will be possible to do similar investigations for higher mass flavors.

As a function of time, the status of the intermediate vector bosons, $W^{\pm}$, Z^o has gone from reasonable expectation to firm orthodoxy. The great success of the Weinberg-Salam model in the lower energy regions gives confidence in the mass prediction for these particles, namely $m_{W^{\pm}} = 82$ GeV and $m_{Z^o} = 93$ GeV. Since the relevant scaling parameter $\frac{m}{E_{CM}} = \frac{100}{700} = .15$, the cross section variation in the region 700-800 GeV is of small consequence. Again one utilizes the scaling behavior of di-lepton production in pp interaction and the connection between electromagnetic and weak interactions to predict $W^{\pm}$ cross sections. Such predictions for the neutral member, the Z^o, does not scale but depends upon a knowledge of the parameter $\sin^2\theta_w$. In general for ISABELLE,

$$\sigma(W^{\pm}) = 3\,\sigma(Z^{o}) = 1.5\,\sigma(W^{-}) = 3 \times 10^{-33}\,cm^{2}$$

For reference: $\sigma(\bar{p}p)$ CERN = σ (pp) ISABELLE

$\sigma(\bar{p}p)$ Fermilab = (3-10) σ (pp) ISABELLE

In order to calculate rates, the canonical branching ratios of 3% for $Z^{o} \rightarrow \mu^{+}\mu^{-}$ and 8% for $W^{+} \rightarrow \mu^{+}\nu$ were used. In addition, further reduction by a factor of 4 for solid angle and detection efficiency were adopted, yielding a loss of 10^{-2} for Z^{o} and 2×10^{-3} for W^{+} detection. These factors could easily be an order of magnitude worse. When one puts all this together one obtains quite respectable rates. For instance in a 1,000 hour experiment with the above conditions, one would accumulate 700 $Z^{o} \rightarrow \mu^{+}\mu^{-}$ events and 4200 $W^{+} \rightarrow \mu^{+}\nu$. It is interesting to note that at this lower luminosity it would require 50 hours of data-taking to accumulate 40 $Z^{o} \rightarrow \mu^{+}\mu^{-}$, sufficient for its discovery, and 100 hours for 400 $W^{+} \rightarrow \mu^{+}\nu$, again the number needed for its discovery. Using this same criterion, one is sensitive to masses of 160 GeV at luminosities of 2×10^{31} and 225 GeV at 2×10^{32}. Thus, ISABELLE is in a position to measure the mass, branching ratios, $p_{\perp}$ distribution and other dynamical properties of these particles. It is instructive to look at the information content for various numbers of events. For instance, although 90 events are more than sufficient to discover the Z^{o}, that is about all. In Fig. 3 the $p_{\perp}^{2}$ distribution for lepton pairs from 90 Z^{o} events is shown. No discernible structure. This is to be contrasted in Fig. 4 with 400 events. In the same vein, the discovery of the W^{+} really depends on a shape measurement and a minimum of 400 events is required, with 1-2,000 events more desirable, as shown in Fig. 5.

I believe, however, that finding the source of the symmetry breaking, the particles that give the gauge bosons mass, will become the primary focus of ISABELLE as well as possibly providing the most exciting results. These may be Higgs particles with mass > 10 GeV, technicolor at 100-240 GeV or others. Again these cross sections are expected to be small, 10^{-35} - $10^{-36}\,cm^{2}$, and

ISABELLE's luminosity is needed to explore such issues. If one considers technicolor particles of mass 240 GeV, then one would produce ~3,000 events in 1,000 hours @ 2 x $10^{32}/cm^2/sec$. Again, a challenge to experimentalists.

There is a host of other topics that can be addressed; however, I am certain the speakers at the workshop will discuss these in great depth, so I'll just make a few remarks in passing. There is the question of lepton pair production and Drell-Yan scaling. It works rather well to within a factor of two, and one now wants to go to higher energies. ISABELLE will allow exploration to masses of 30-60 GeV at low and high $p_\perp$. As such, one can investigate the validity of QCD production and how scaling is broken. Of course jet studies come into their own at these high energies. What are the quark and gluon distributions? Experimentally, $p_\perp$'s of 100-200 GeV are attainable. Recently the importance of simple direct γ production has become apparent. These have been experimentally observed at the ISR and Fermilab and again they should be detected at ISABELLE even more easily with $p_\perp$'s of up to 60 GeV/c, interesting for deriving gluon distribution functions as well as other possibilities. Finally one should mention that we are indeed colliding protons with protons and thus studying the proton. Therefore, the total cross section, angular distribution of elastic scattering, multiplicities, particle distributions and character are all of interest but have been discussed at length at previous workshops. What we need now is data.

The experimental challenge is therefore straightforward. One wants to detect leptons, photons, and hadrons; in the latter case the guess is that jets will replace what in the old days were pions. There are trade-offs to be made involving resolutions (energy, momentum and position) counting rate and solid angle. We want it all but money will be finite so that taste and insight into the physics will come to the fore. And finally, remembering the lessons of the past, some flexibility is desired to allow for

following up the expected surprises.

Accelerator:

As is well known the concept is to use the AGS as an injector into ISABELLE. At present, the AGS is a 30 GeV accelerator producing 10^{13} protons per pulse. It can operate in two modes, Fast External Beam (FEB) with a cycle time of 1.5 sec for one turn extraction, and Slow External Beam (SEB) with a 2.5 sec cycle time and 1 sec flat top. The present plan is to utilize 3-5 x 10^{12} protons per pulse at 28 GeV and inject many such pulses into first one ring and then in the opposite direction in a second ring until one obtains amperes of beam. The beams can then be accelerated from 28 GeV up to 360 GeV in a fraction of an hour and then allowed to collide.

Most aspects of the project are going well. The lattice design, conventional construction, R.F., computer controls, cryogenics are in good shape. The main difficulty has been the magnets. They are superconducting: 700 dipoles and 300 quadrupoles needed for the two rings.

With regard to the large aperture magnets, four approaches are presently being pursued. These are 1) cos θ braid, 2) cos θ, 2 layer cable, 3) picture frame, monolithic conductor, and 4) intersecting ellipses, 3 layer cable. All are cold iron, warm bore magnets. The progress to date has been as follows:

1) Main ISABELLE effort. Magnets now can be made that achieve 45 kgauss in less than 10 quenches, and 50 kgauss in 20-30 quenches. However, the ramp rate behavior is marginal. Proper training and ramp rate behavior have been achieved in the quadrupoles with new medium resistance braid. This is to be tested soon in full scale dipoles. The field quality of both dipoles and quadrupoles is close to specification on the basis of data from 4 dipoles and 5 quadrupoles. One of the main strengths of these magnets is their ability to absorb their own energy during a quench.

2) The test of a full aperture five foot long dipole magnet is to take place at the end of July. This magnet has been en-

gineered to have proper performance characteristics for training, ramp rate and field quality.

3 & 4) Five foot long, full aperture models have achieved 60 kilogauss peak fields. The LBL version attained such values in four quenches at 4.2^{o}_{K} and higher fields at lower temperatures. Several more are under construction with plans for 15 full scale models.

There is also the possibility of a small aperture approach, namely through the use of Fermilab magnets with 42 kgauss magnetic field and full length, larger sagitta. A Task Force under the leadership of Kjell Johnsen consisting of ~30 physicists from BNL, LBL, Fermilab, Yale and Columbia have been examining this question since mid-May. Thus far, the lattice and matching sections, field quality of magnets, refrigeration, vacuum, injection and ejection have been looked at, with R.F., booster, cost and schedule to be stressed in the near future. No major difficulties with this approach have been found to date.

The advantage of the large aperture magnet is that of higher luminosity, with the disadvantage of not at this moment being a magnet clearly meeting all the necessary criteria. In the case of the small aperture, the magnet exists and if there are no unseen obstacles the time scale for an accelerator is shorter, '86. The disadvantage is the lower initial luminosity with the added cost of a booster needed to reach full luminosity.

The decision, to be made on September 1, is between the large and small aperture approaches. If the choice is the small aperture, we will proceed immediately, but one large aperture design will still be developed as a backup. If the decision is for the large aperture, one design will be selected by April of '82 and magnet production started by Oct. '83.

The charge to the workshop is therefore the following: consider the physics potential of the small aperture, phased ISABELLE; re-examine the physics of the full luminosity ISABELLE; consider the ep and heavy ion options; re-examine the experimental

areas, especially #10 and #12; and look at Detector R&D as well as the status of large detector systems.

ISABELLE is clearly an exciting project and it is indeed an appropriate time for a physics re-examination.

TABLE I. NATIONAL AND INTERNATIONAL SITUATION

COLLIDERS

E^+E^-	SPEAR	7 GeV	OPERATIONAL
	DORIS	10 GeV	
	CESR	10 GeV - 16 GeV	
	PEP	30 GeV	
	PETRA	40 GeV	
	(TRISTAN	60 GeV)	'86
	(LEP	100 GeV)	'88
$\bar{P}P$	(CERN	540 GeV)	'82
	(FNAL	2000 GeV)	'85
PP	ISR	62 GeV	
	ISA	800 GeV	'86 - '88

FIXED TARGET

P	AGS	30 GeV	
E	SLAC	40 GeV	
P	SERPUKHOV	80 GeV	
P	SPS, FNAL	400 GeV	
P	TEVATRON	1000 GeV	'83

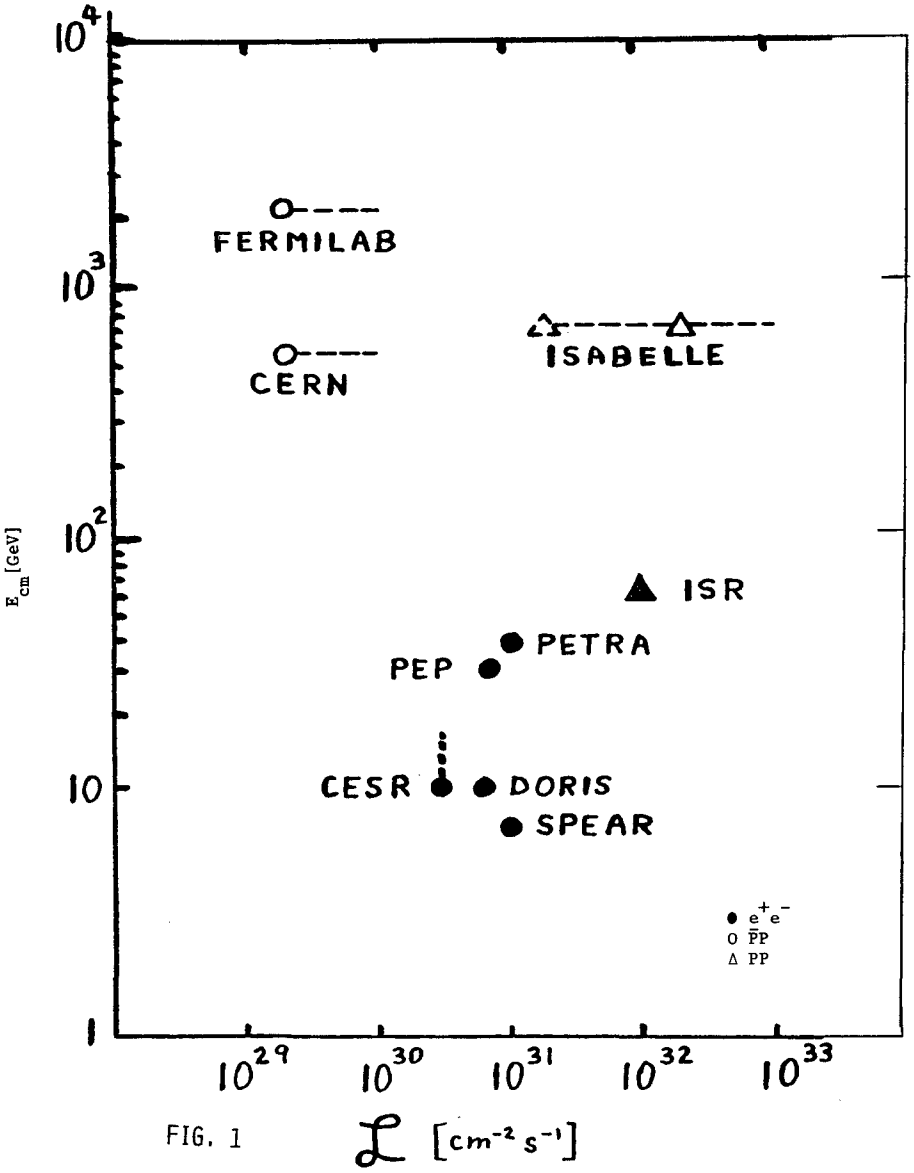
10^4
10^3
10^2
10
1
E_{cm} [GeV]
FERMILAB
CERN
ISABELLE
ISR
PETRA
PEP
CESR
DORIS
SPEAR
● e^+e^-
O $\bar{P}P$
Δ PP
10^{29}
10^{30}
10^{31}
10^{32}
10^{33}
$\mathcal{L}$ [$cm^{-2}s^{-1}$]

FIG. 1

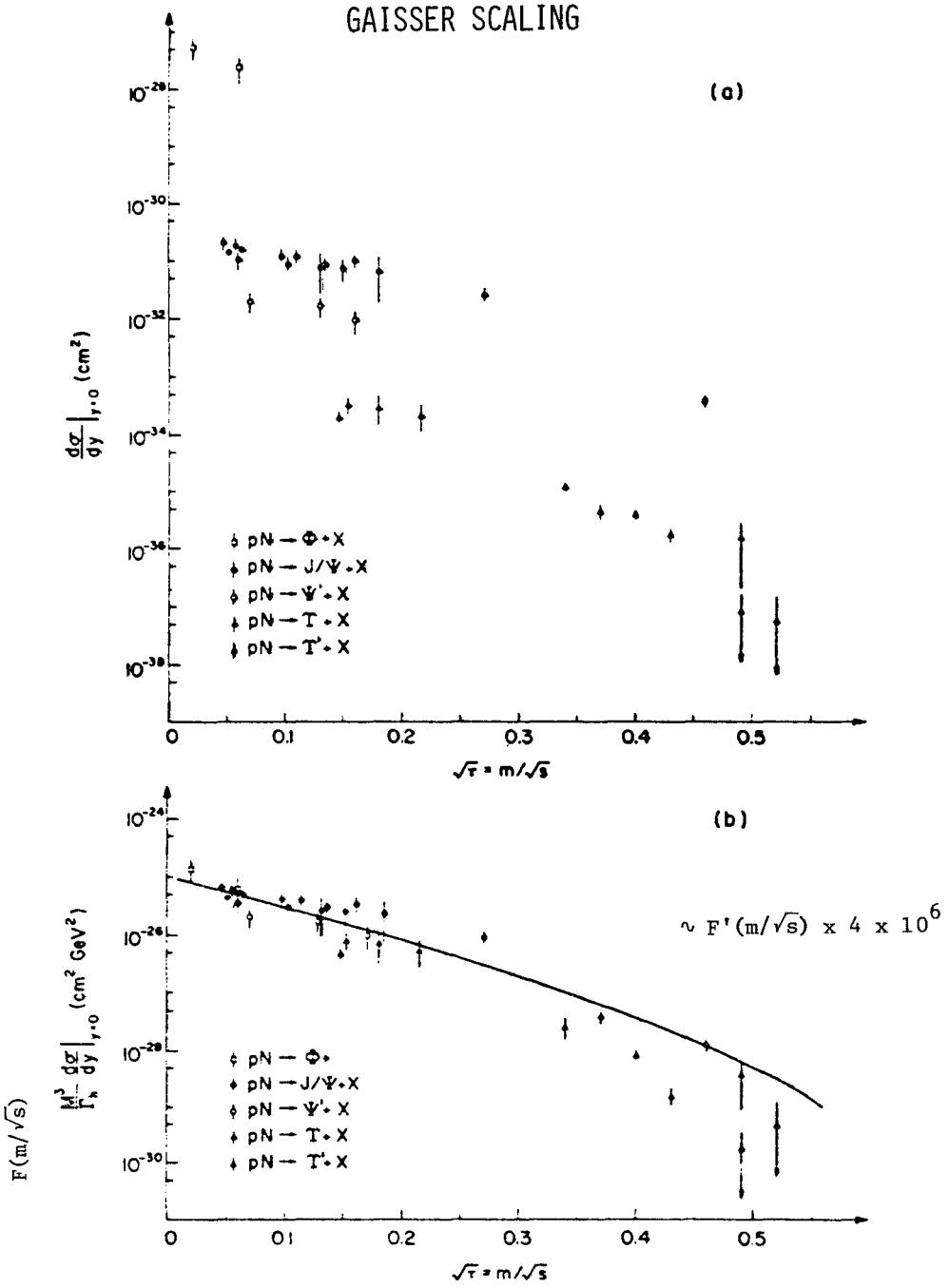
GAISSER SCALING
(a)
$\frac{d\sigma}{dy}\Big|_{y=0}$ (cm²)
pN → Φ + X
pN → J/Ψ + X
pN → Ψ' + X
pN → T + X
pN → T' + X
$\sqrt{\tau} = m/\sqrt{s}$
(b)
$\frac{M^3}{F_h}\frac{d\sigma}{dy}\Big|_{y=0}$ (cm² GeV²)
F(m/√s)
∼ F'(m/√s) x 4 x 10⁶
pN → Φ + X
pN → J/Ψ + X
pN → Ψ' + X
pN → T + X
pN → T' + X
$\sqrt{\tau} = m/\sqrt{s}$

FIG. 2

SPS

$Z^o \rightarrow \mu^+\mu^-$

90 Events

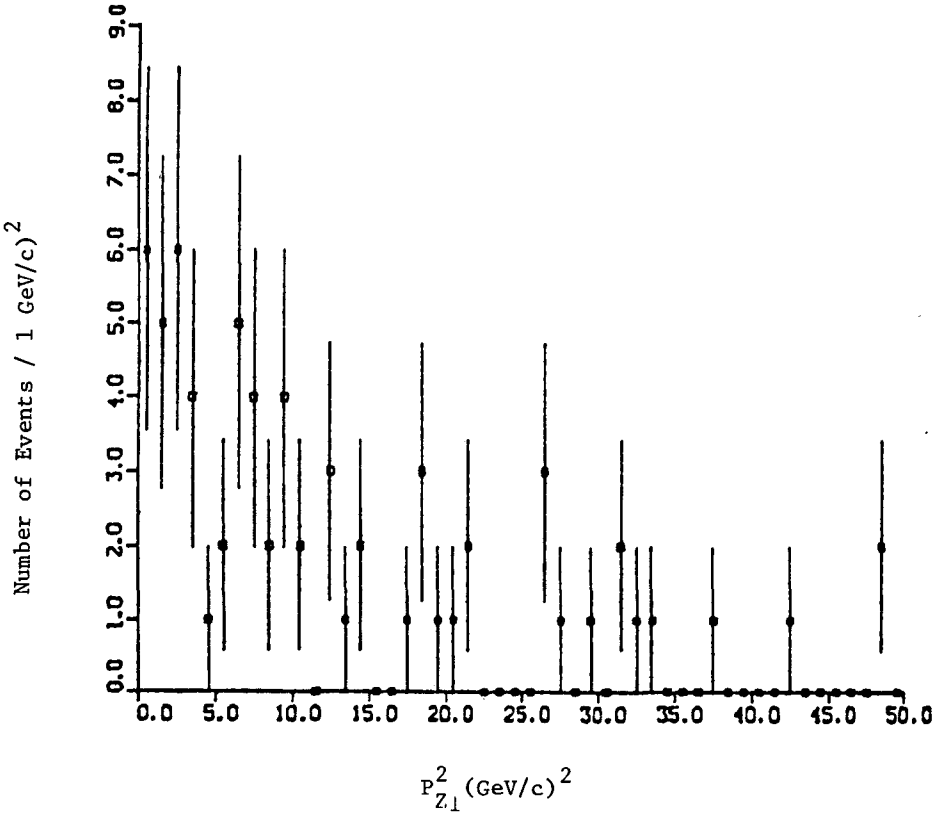

FIG. 3

ISABELLE

$z^o \rightarrow \mu^+\mu^-$

400 Events

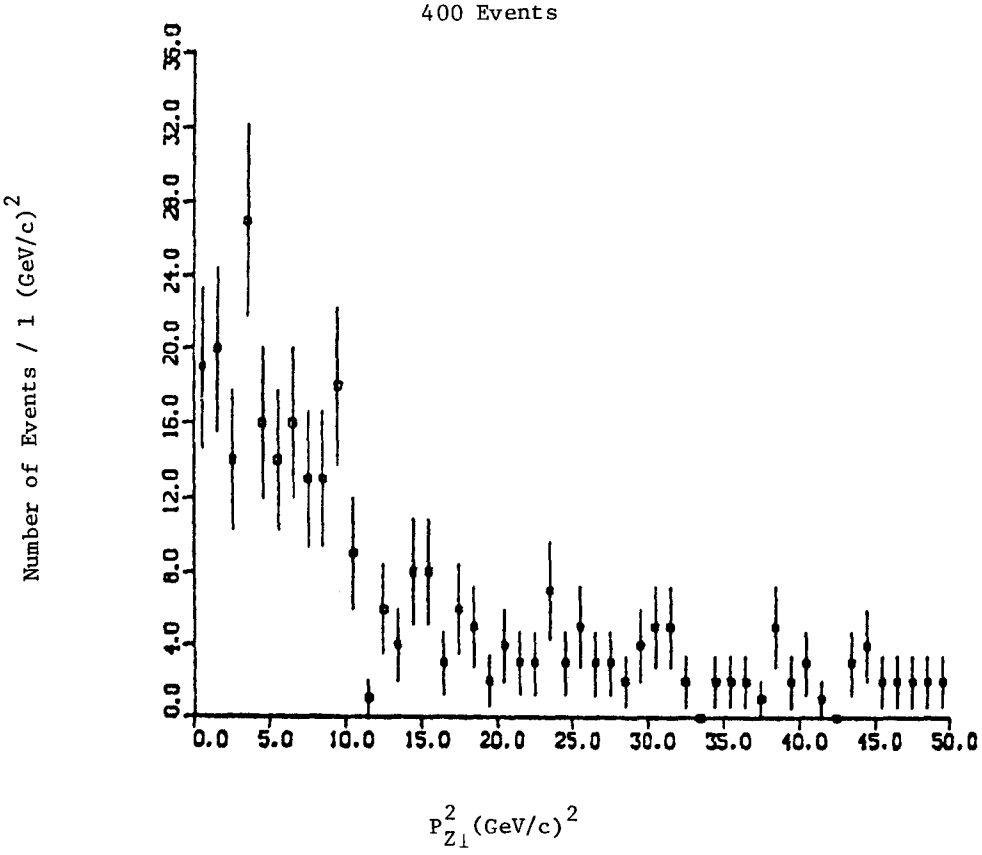

FIG. 4

ISABELLE

$W^+ \rightarrow \mu^+$

2,000 Events

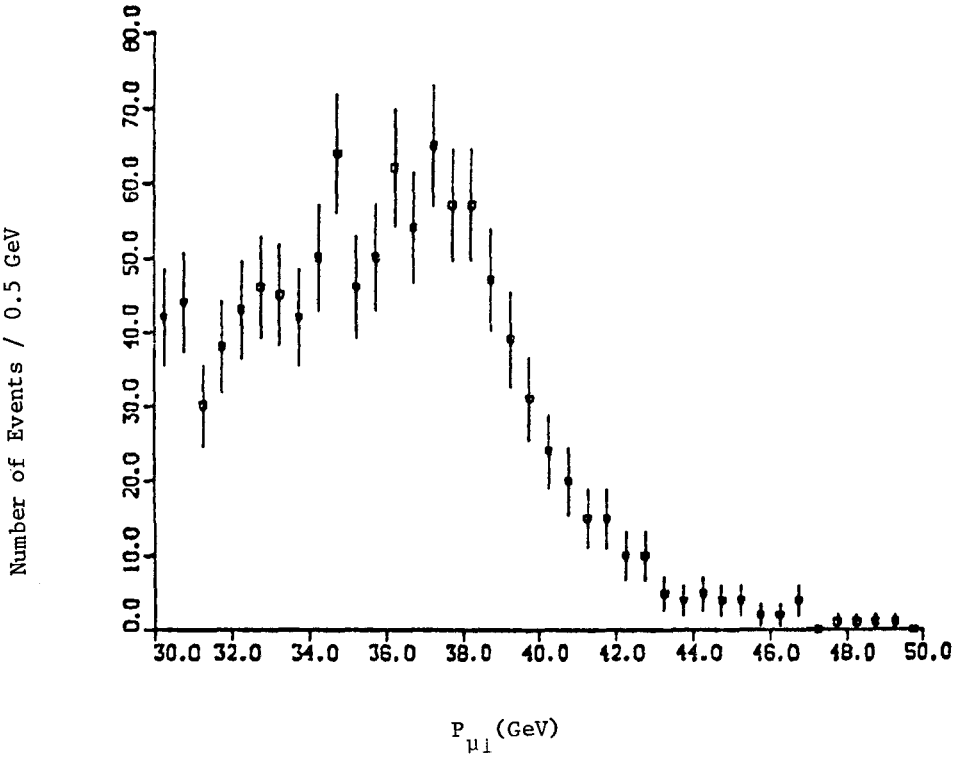

FIG. 5

SECTION I

LECTURES

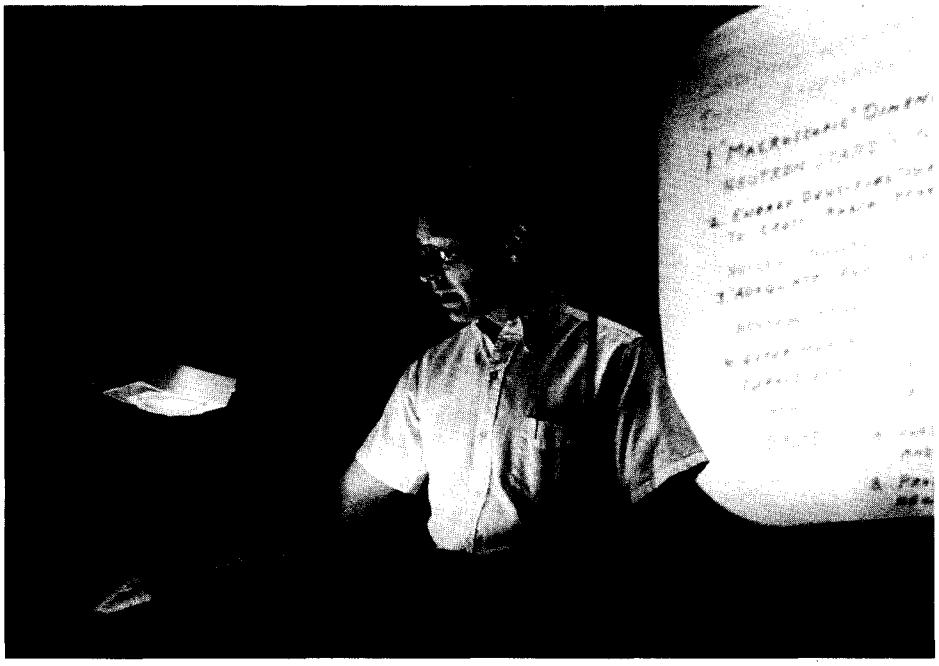

PERFORMANCE CHARACTERISTICS OF ISABELLE WITH FERMILAB MAGNETS

E.D. Courant
Brookhaven National Laboratory and SUNY, Stony Brook

ISABELLE is projected to produce p-p colliding beams of 8 amperes with a luminosity of about 2.5×10^{32} cm^{-2} sec^{-1} at an energy of 400 GeV per beam (with the luminosity extendable to 10^{33} by changes in the lattice).

This is to be accomplished by injecting successive pulses from the AGS at the edge of the ISABELLE magnet aperture, moving the beam to a stacking orbit on the other side, and repeating the procedure many times until the full 8 ampere beam is built up, requiring about 300 AGS pulses. The resulting beam is then to be accelerated to 400 GeV and debunched, and the beams in the two ISA rings collide in six places, intersecting at an angle of 11 milliradians.

This requires magnets having a usable aperture of around 8 cm and a peak field of 50 kilogauss.

You have all heard that the "cosθ - braid" magnets we have been developing for this purpose have not performed as they should, and that there are some doubts as to whether we can soon make magnets that do meet these requirements.

Some years ago there was a baseball manager named Leo Durocher. He is famous for Durocher's First Law: "Nice guys finish last". But he also formulated Durocher's Second Law, which is not as well known: "Many of the lies they are telling about us aren't even true!"

Nevertheless, suppose it is true that the cosθ braid magnets won't do. What then? It so happens that Fermilab, in the Energy Doubler (Tevatron) program, has developed a different superconducting magnet to the point where their magnets are apparently adequate for their purpose; these magnets are now in production at the Fermilab magnet factory.

Could we use these magnets for ISABELLE? (Assuming their factory kept going and produced magnets for ISABELLE after the Tevatron magnets are all built). If so, how would the ISABELLE performance change from our standard

scenario?

A task force under Kjell Johnsen, with members from Brookhaven, Berkeley, Fermilab, Yale and Columbia, has been exploring these questions in the last two months. I shall report on some of the work of the task force, mainly on the matters of changes of operation and performance.

First and foremost, the FNAL magnets have a much smaller aperture than the BNL magnets - a net good-field region of 4-5 cm instead of 8 cm. This means that the energy stacking scheme I just described will not work. We would be limited to injecting beams directly from AGS to ISA without multiple stacking and reprocessing of the bunches (which would require too much space); therefore the circulating beam in FISA would be limited to the same current as in the AGS, which is 0.6 amperes at 10^{13} protons per AGS pulse. Since the luminosity goes with the square of the current, this would seem to reduce L by two orders of magnitude to 1.4×10^{30}.

Furthermore the FNAL magnets are not designed for 50 kilogauss; we estimate that we could count on operating at 42 kilogauss. This would seem to reduce the energy to $42/50 \times 400 = 336$ GeV.

Fortunately one can do better than this in both luminosity and energy. The scenario for ISABELLE with Fermilab magnets (FISA) that we have worked out is as follows:

1. Inject AGS bunches directly into FISA with the rf at the same frequency (4.46 MHz) as in the AGS. This gives 57 bunches, 224 nanoseconds apart, with a circulating mean current of 0.6 amps.
2. Accelerate to top energy at this frequency and keep the beams bunched for collisions. The peak instantaneous current in the center of the bunch would be a respectable 11 amperes, and therefore the time average luminosity would be enhanced roughly by a factor (11/0.6) from the coasting beam value. This is not all the way to the ISABELLE goal, but down only one order of magnitude instead of two.

The FNAL magnets are longer than the BNL magnets. Therefore there will be fewer individual magnets and fewer spaces between them; thus we can fill a larger fraction of the circumference with magnets than in the standard case. Moreover the FNAL magnets have a cold bore vacuum chamber, which automatically does cryopumping; therefore we do not need space for external pumps in every

gap between magnets. So the inter-magnet gaps can be shorter as well as fewer. This leads to higher energy for a given field.

On the other hand, with the smaller aperture the field imperfections due to errors in conductor placement are relatively larger, and there is no room for compensating windings in the magnets (as there is in ISA-1). Separate compensating magnets ("spool pieces") have to be inserted in every half cell - these do take up space and reduce the energy/field ratio. Overall, though, the magnet packing factor in FISA is better than in ISA-1, and the energy at 42 kilogauss turns out to be 360 GeV rather than 336.

Several possible lattices for the FNAL magnets have been worked out by J. Claus, A. Garren and myself; Claus' lattice has been completed in the most detail.

Since the FNAL magnets are 40 cm wide as compared to 75 cm for the BNL cryostats, the two rings of FISA can be moved closer together (65 cm apart instead of 96 cm). This naturally leads to a smaller crossing angle: 7 milliradians instead of 11, and with it a higher luminosity for a given beam current. Furthermore the quadrupoles are also narrower; therefore the quadrupole doublets Q1-Q2 which produce a low β value at the crossing point can be moved closer to the crossing point (25 m instead of 30) and still permit the beam of one ring to avoid interference with the quadrupoles of the other. This leads to a smaller value of the amplitude function β at the crossing point - 3.1 m instead of 7.5 - and with is a reduced beam height, greater beam density, and higher luminosity.

Other features of the new lattice - probably of less interest to experimenters - are: the number of cells in the sextant arcs is 11 instead of 9, and the overall "tunes" are 19.6 horizontal, 22.6 vertical rather the 22.6 for both; this leads to some gain in the aperture needed for the beam.

The bottom line is, with the above lattice and reasonable assumptions about AGS beam quality:

$$L \text{ at } 360 \text{ GeV} = 2.75 \times 10^{31} \text{ cm}^{-2} \text{ sec}^{-1}.$$

The time structure of the luminosity is also of interest. Events occur during bunch collisions spread 224 nanoseconds apart; the instantaneous luminosity peaks at 5.2×10^{32} with a width in time having a σ of 3

nanoseconds. Thus with a total cross section of 50 millibarns, there will on the average be 0.31 events per crossing, and if a given event occurs, the probability of another event within the same bunch is again 31%. This imposes constraints on the time resolution of detectors.

Some other problems with the bunched-beam interaction scheme: the beam-beam interaction, usually measured by the "tune shift" of one beam caused by the other, leads to the equivalent of diffusive noise seen by the beam, which causes a slow blowup. For unbunched beams a tune shift up to around 0.005 units is generally expected to be tolerable (as confirmed by some ISR experiments). In the bunched case, the synchrotron energy and phase oscillations have the effect that a given particle sees a tune shift that is modulated in strength and phase. This results in additional randomization. We estimate (but not with great certainty) that, in the case here, this effect reduces the maximum allowable tune shift by something like a factor of 2 to 0.0025 - this should be all right but we cannot be absolutely sure. The value for the parameters just given is 0.0020.

Another potential cause of troubled is the longitudinal microwave instability, excited by the field of the image currents in the wall acting on the beam, and resulting in a stirring up of the beam and reduction of its density. The effect is inhibited by Landau damping due to the energy spread in the beam. In ISA-1 the effect is most severe at injection. In FISA it is less severe at injection, but at high energy the relative energy spread is very small, and the coupling impedance exciting the instability must be less than

$$\frac{Z}{n} < 10 \text{ ohms}$$

for Landau damping to kill the instability. This is comparable to the requirement we have been imposing on the ring for ISA-1.

A third effect: image currents induced in the chamber wall cause heating. If the wall is at cryogenic temperatures, this adds to the heat load in the refrigeration system. If the chamber walls are of stainless steel this heat load is estimated at 300 watts per FISA ring, which is of the order of 10-20% of the total cryogenic heat load - not negligible, but also not fatal. With a high conductivity plating on the vacuum chamber surface the effect could be

reduced considerably.

What can be done to improve the performance of this "Stage I" scenario?

Phase II: We may interpolate an intermediate energy accelerator ("booster") between AGS and FISA. This booster, being worked on by L.C. Teng and others, would be a storage ring similar to the original ISA-1, but with half the ISA circumference and conventional (warm) magnets; energy around 100 GeV. With some additional features, mainly long straight sections, such a booster or at least its tunnel might also be used for an electron storage ring for e-p collisions.

We stack in this booster from AGS as originally planned for ISA-1, until a current of 8 amperes is reached. Then accelerate to 100 GeV, transfer into half the FISA circumference, and repeat, filling all of FISA.

From 100 to 360 GeV we accelerate in FISA as in the original ISA-1, debunch, and run colliding beams in the DC mode as originally envisaged. The performance will be the same as ISA-1, except that the smaller crossing angle and lower β will give somewhat more luminosity. Further increases in luminosity can be achieved by the same tricks as planned for the "high luminosity" option of ISA-1: insert extra bending magnets near the crossing point to reduce the crossing angle, and retune the quadrupoles for a smaller central β. A luminosity of 10^{33} should then be attainable in this Phase IIA. (But a booster could also be added to the standard ISA-1 and enhance its luminosity even above 10^{33} if desired).

A more modest but still appreciable improvement can be obtained (Phase IA) without a booster, by reviving an idea originally suggested by Rena Chasman in 1972 (and discarded then because it could not easily go all the way to 8 amperes).

Change the AGS so that it accelerates a single intense bunch rather than 12 small ones. Intensity, say, 1/3 that of the normal AGS, e.g., 3.3×10^{12} protons or 0.2 amperes. With rf manipulation in the AGS, shorten this bunch so that it fits well within a single 4.46 MHz bucket. Transfer the bunch into one bucket of the FISA 4.46 MHz rf system, and repeat 57 times (or maybe 55 or 56 so as to leave a gap). Accelerate in FISA and collide either bunched or unbunched.

For this scheme we need: (a) extensive modification of the AGS rf system

(not yet worked out in detail); (b) a very fast kicker for injecting single bunches into FISA without disturbing the other bunches. The bunch length would be around half the spacing of 224 nanoseconds, so that the kicker has to turn on and off cleanly in 100 nanoseconds or better.

This scheme would put 2.4 amperes into FISA and lead to a luminosity

$$L = 1.4 \times 10^{32} \text{ (bunched mode)}$$

Instantaneous peak $L = 8.5 \times 10^{32}$ at center of bunch.

Alternatively, unbunched colliding with 2.4 amperes would give a luminosity of 3.2×10^{31} - more desirable than the luminosity of Phase I because the uniform duty cycle is easier to handle with most detectors.

To sum up: if ISABELLE were to be built with FNAL magnets instead of the BNL magnets (or some other large-aperture variant), the luminosity in Phase I would be down from the standard value by a factor of around 10 to 2.3×10^{31}, which is still a very respectable figure with which one could surely do a great deal of interesting physics. Adding a booster (Phase II) would restore the performance to the level originally planned. Intermediate performance could be obtained by alternate injection schemes requiring AGS modifications (Phase IA).

PROSPECTS AT HIGHER ENERGY

Frank Wilczek, Inst. for Theor. Physics, Santa Barbara, California 93106

I.

The orthodox model of particle physics is based on $SU_3 x SU_2 x U_1$ gauge theory. It is consistent with all known data. At higher energies we will be able to test the orthodoxy pretty stringently:

QCD: Quantitative tests should become feasible using order $\bar{g}^2$ effects. (So far, we have mostly order $1+g^{-2}$ effects such as scaling deviations in deep leptoproduction, which are much more difficult.) Most important of these are total widths and inclusive γ decays of heavy vector mesons, and high $p_\perp$ events (QCD Compton effect). At high $p_\perp$ the most promising look to be $\gamma \to \mu^+\mu^-$ and Z production, since fewer distribution functions are relevant. The $\sim 1/p_\perp^4$ asymptotics of hadronic production is a dramatic qualitative effect, as are multi-jet events.

$SU_2 x U_1$: Of course a big goal is to observe the Z and W directly. It is very interesting to get the Weinberg angle accurately, and to count neutrino species (by Z total width or "missing" high $p_\perp$ events). The Higgs sector is most interesting as we shall elaborate. The first goal here is to see if the Coleman-E. Weinberg proposal is right, $M_H = 10.8$ GeV. The standard Higgs particle may be produced in $t\bar{t} \to H\gamma$ (monochromatic γ), $Z \to ZH$ or $Z \to ZH \to \mu^+\mu^- H$, $Z \to t\bar{t}H \to$ many leptons, or directly by gluon fusion.

II.

The problems of the orthodox model are first of all lack of predictive power regarding quark and lepton masses, Cabibbo angle, types and number of elementary fermions, etc. These questions almost surely require extensions of the orthodoxy, the direction of which is at present unclear.

Second there is an internal problem, the strong CP problem. In QCD there is a possible interaction

$$L_I = \frac{\theta}{32\pi^2} \mathrm{Tr} G_{\mu\nu} \tilde{G}_{\mu\nu}$$

which represents a $\Delta S = 0$, P,T odd C even interactions. It will be induced

by radiative corrections in general and give a disastrously large contribution to the neutron electron dipole moment. Attempts to solve this problem involve "doubling" the Higgs sector which will give charged physical Higgs particles and perhaps an axion (whose existence is presently controversial).

III.

An extension of $SU_3 x SU_2 X U_1$ to SU_5 is almost part of the orthodoxy too. This extension helps a bit in relieving fermion proliferation (reducing the number of multiplets from 5 to 2 per family) but mostly leaves the basic problem of lack of predictive power intact. The success is a prediction of $\sin^2\theta_w$, which is very impressive. Most dramatic is the prediction of proton decay at an experimentally accessible rate.

Relevant to high energies is the suggestion that the Coleman-E. Weinberg value for M_H be taken seriously.

IV.

Problems of SU(5) and related theories:

i) Gauge hierarchy problem. How does a light doublet shed its colored partners? Where does the huge mass disparity come from? This is a very ugly feature.

ii) Overproduction of magnetic monopoles in the Big Bang.

Introduction of supersymmetric models can ease the first problem, some of these models (based on SU(7)) also ease the second. Supersymmetry, or absence of U(1) symmetry, must persist down to $\sim$ TeV. This would have most dramatic implications - "manifest" supersymmetry at high energies, fairly light magnetic monopoles.

The supersymmetric models drastically reduce the p-decay rate. They give good values for $\sin^2\theta_w$.

THE PRODUCTION OF PARTONS AND HADRONS IN e^+e^- ANNIHILATIONS AND IN HADRON-HADRON COLLISONS -- QUARK AND GLUON JET MODELS*+

R. D. Field

Particle Theory Group
University of Florida
Gainesville, Florida 32611

ABSTRACT

Monte-Carlo models for the production of parton showers in e^+e^- annihilations and in pp collisions are described. A new quark and gluon jet model is presented. It does not rely on the Feynman and Field parameterization but instead is based on perturbative QCD and simple phase-space ideas. The properties of 50 GeV jets are examined and the rates for producing these jets at Isabelle are calculated.

*Work supported in part by the U.S. Department of Energy under Contract No. DSR80136je7.
+Invited paper presented at the 1981 Isabelle Summer Workshop.

I. INTRODUCTION

The Feynman and Field quark jet parameterization (FF-model)[1] has served a useful purpose. It has provided a "standard" quark jet with limited transverse momentum with which various experiments could be compared. The model contains important physical ideas like a rapidity plateau and the effects of resonances but the model was never intended to be a fundamental theory. It is amazing how well the low energy ($E_{jet} < 6$ GeV) data agree with the FF parameterization.

One of the most exciting experimental observations of the past several years is the discovery that e^+e^- quark jets in the region $W=Q>12$ GeV do not agree with the FF-model.[2] In addition, there is mounting evidence that the discrepancy between the data and the FF-Model is in the direction expected from the theory of quantum chromodynamics (QCD).[3-5] Models based on a combination of perturbative QCD and the FF-model can be adjusted to describe quite well the data over the existing range $8<Q<36$ GeV.[6-8] These models involve first the generation of a parton final state. This state consists of either a quark and antiquark or a quark, antiquark, and gloun. Each parton in the final state is then allowed to "fragment" independently into hadrons according to the FF prescription.

The addition of the qqg final state coupled with the FF prescription is clearly the first thing one should try when analyzing the e^+e^- data. The agreement of this approach with the data certainly indicates that QCD is "on the right track". These comparisons indicate that nothing seen in the data is inconsistent with QCD. But have we provided QCD is the correct theory of strong interactions? Can we make precise predictions of what jets will look like at Q = 100 GeV? In my opinion more work must be done before we can answer these questions. Clearly at high energies where there are many quarks and gluons, it is not proper to allow each parton to fragment according to the FF-model. In fact, given what we now understand about perturbative QCD, it might be fruitful to abandon completely the FF-model in favor of models more closely connected with QCD.

If QCD is the correct theory of strong interactions then there should be a sizable rate for producing high energy jets ($E_{jet} \gtrsim 50$ GeV) in pp collisions with CM energies greater than 500 GeV. It is a challenge to see if we can predict what jets will look like at Isabelle energies ($\sqrt{s} \gtrsim 700$ GeV). Here there are many quarks and gluons and it does not make sense to fragment each parton according to the FF-model.

In this paper I would like to do two things. First, I would like to review and explain the Monte-Carlo model for producing final state partons in e^+e^- collisons developed by G.C. Fox and S. Wolfram.[9-13] In my opinion this is the best method for producing quark and gluon final states that are distributed according to perturbative QCD. The Monte-Carlo model produces not only the $q\bar{q}$ and $q\bar{q}g$ final state but also states containing many gluons (i.e., qqgg, qqggg, qqggqq, ...

etc.). It is therefore probably a better extrapolation to high energies. After discussing this Monte-Carlo I would like to examine several models for the way in which these final state partons turn into the observed hadrons. Stephen Wolfram and I have developed a somewhat ambitious model for the hadron final states. It is based on perturbative QCD (carried perhaps further than one can justify) and a simple phase space model of hadronization. This QCD phase-space model ("QCD-PS" model) conserves energy, momentum, and charge on an event by event bases. It can be compared to other schemes based on the FF parameterization in an attempt to ascertain how sensitive a particular observable is to the nonperturbative hadronization phase. Even if one is able to produce parton final states precisely according to perturbative QCD, it may be that at existing energies everything is dominated by the non-perturbative phase. I will not have the time to cover everything in this talk and some work is still in progress. A larger paper with all of our findings will be forthcoming. I will present some of our preliminary results here. The "QCD-PS" approach can also be used to produce final states in pp or $\bar{p}p$ collisions as well as for e^+e^- annihilations.

In Section II I will begin with a discussion of the "leading pole" approximation which is the basis of the Monte-Carlo which is explained in Section III. In Section IV I will examine the nonperturbative hadronization phase and present some phenomenology. In Section V I will examine applications to pp collisions and calculate jet rates at Isabelle energies. Section VI is reserved for summary and conclusions.

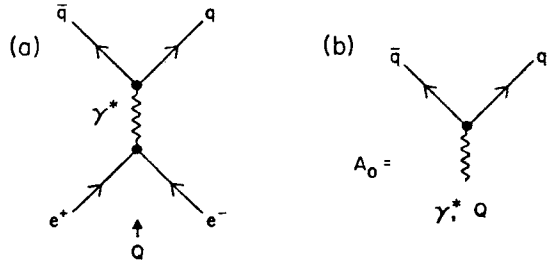

Fig. 2.1. (a) The lowest order "Born" amplitude for the production of a quark and antiquark pair through the annihilation of an electron-positron pair. (b) The lowest order "Born" amplitude, A_0, for the "decay" of a virtual photon of invariant mass Q into a quark-antiquark pair.

II. The "Leading Pole" Approximation

The "Born" cross section for an e^+e^- pair to annihilate and produce simply a $q\bar{q}$ pair is arrived at by squaring the amplitude as shown in Fig. 2.1a and is given by

$$\sigma_{tot}(e^+e^- \to \bar{q}q) = (\frac{4\pi}{3})e_q^2\,\alpha^2/Q^2, \qquad (2.1)$$

where Q is the e^+e^- CM energy and $\alpha = e^2/4\pi$ and e_q are the electric charge and quark charge, respectively. The correction to this due to the emission of a single real gluon in the process $\gamma^* \to \bar{q}qg$ contains three terms:

$$|A_R|^2 = c(s/t), \tag{2.2a}$$

$$|B_R|^2 = c(t/s), \tag{2.2b}$$

$$2A_R B_R^* = 2c(Q^4 - sQ^2 - tQ^2)/(st), \tag{2.2c}$$

where the coefficient c is given by

$$c = 32e_q^2 e^2 g^2 \tag{2.2d}$$

and where the amplitudes A_R and B_R are shown in Fig. 2.2. The invariants s, t, and u are given by

$$s = (p_1 + p_3)^2, \tag{2.3a}$$

$$t = (p_2 + p_3)^2, \tag{2.3b}$$

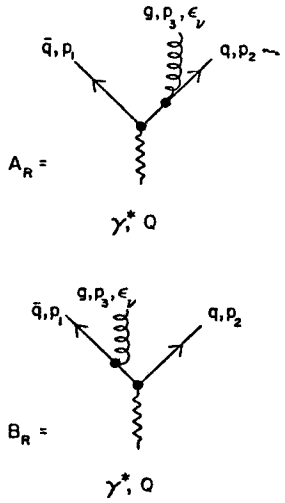

Fig. 2.2. Order α_s diagrams for the production of a real gluon, g, with momentum and polarization given by p_3 and ε_ν, respectively, in the process $\gamma^* \to \bar{q}qg$.

$$u = (p_1 + p_2)^2, \tag{2.3c}$$

where (for massless quarks and gluons)

$$s + t + u = Q^2. \tag{2.3d}$$

In (2.3) p_1 and p_2 are the 4-momentum of the outgoing antiquark and quark, respectively. p_3 is the 4-momentum of the gluon and Q^2 is the momentum squared of the virtual photon. Each of the three pieces in (2.2) is gauge dependent and the results above are for the Feynman gauge

$$\sum_{\text{pol}} \varepsilon_\nu \varepsilon^*_{\nu'} = - g_{\nu\nu'}, \tag{2.4}$$

where ε_ν is the polarization vector of the outgoing gluon. The complete amplitude is given by

$$|M_R|^2 = |A_R + B_R|^2 = c\left\{\frac{t}{s} + \frac{s}{t} - \frac{2Q^2 t}{st} - \frac{2Q^2 s}{st} + \frac{2Q^4}{st}\right\}, \tag{2.5}$$

and is, of course, independent of the choice of gauge.

It is convenient to introduce the dimensionless variables

$$x_i = 2E_i/Q \quad (i = 1,2,3). \tag{2.6}$$

For which energy conservation implies

$$x_1 + x_2 + x_3 = 2. \tag{2.7}$$

In terms of these x_i

$$s = Q^2(1 - x_2), \tag{2.8a}$$

$$t = Q^2(1 - x_1), \tag{2.8b}$$

$$u = Q^2(1 - x_3), \tag{2.8c}$$

and (2.2) becomes

$$|A_R|^2 = c(1 - x_2)/(1 - x_1) \tag{2.9a}$$

$$|B_R|^2 = c(1 - x_1)/(1 - x_2) \tag{2.9b}$$

$$2A_R B_R^* = 2c(x_1 + x_2 - 1)/[(1 - x_1)(1 - x_2)]. \tag{2.9c}$$

The complete amplitude squared is thus

$$|M_R|^2 = c\,\frac{x_1^2 + x_2^2}{(1-x_1)(1-x_2)}, \tag{2.10}$$

which results in a differential cross section for $e^+e^- \to \bar{q}qg$ given by

$$\frac{1}{\sigma_0}\frac{d\sigma}{dx_1 dx_2} = \left(\frac{2\alpha_s}{3\pi}\right)\frac{x_1^2 + x_2^2}{(1-x_1)(1-x_2)}, \tag{2.11}$$

where σ_0 is given by (2.1) and where $\alpha_s = g^2/4\pi$ is the strong interaction coupling constant. In arriving at (2.11) I have used three-body phase space given by

$$d\sigma_{(3)} = \frac{\pi^2 Q^2}{4}|M_R|^2\, dx_1 dx_2. \tag{2.12}$$

Equation (2.11) gives the probability of finding the outgoing antiquark and quark carrying fractional energies x_1 and x_2, respectively, after emitting a single gluon.

In order to compute the total rate for the production of a single gluon we must integrate the differential cross section in (2.11) over x_1 and x_2. The region of integration for massless quarks and gluons is

$$0 \leq x_2 \leq 1$$

$$1 - x_2 \leq x_1 \leq 1. \tag{2.13}$$

The total rate for single gluon emission in the massless case is thus

$$\sigma_{tot}(\text{real}) = \int_0^1 dx_2 \int_{1-x_2}^1 dx_1 \left(\frac{d\sigma}{dx_1 dx_2}\right), \tag{2.14}$$

which is infinite since the integrand in (2.11) diverges at $x_1 = 1$ and $x_2 = 1$. The origin of the divergence is clear. Consider the invariant mass t in (2.3b). In the massless limit

$$t = 2p_2\cdot p_3 = 2E_2\omega(1 - \cos\theta_{23}), \tag{2.15}$$

where θ_{23} is the angle between $\vec{p}_2$ and $\vec{p}_3$ and E_2 and ω are the energies of the outgoing quark and gluon, respectively. The differential cross section diverges when $t \to 0$ which results when the energy of the gluon goes to zero ($\omega \to 0$; "soft divergence") or when the outgoing quark and gluon become parallel ($\cos\theta_{23} \to 1$; "parallel divergence").

Even though the total rate for the production of a single gluon is infinite, the complete order α_s correction to the rate is not. This is because there is an order α_s correction to $\gamma^* \to \bar{q}q$ due to virtual gluons (see Fig. 2.3) which is also infinite in the limit of massless quarks and gluons. However, if one "regularizes" both the real and the virtual corrections in an appropriate manner and adds the two together then the result is finite in the limit of massless quarks and gluons.

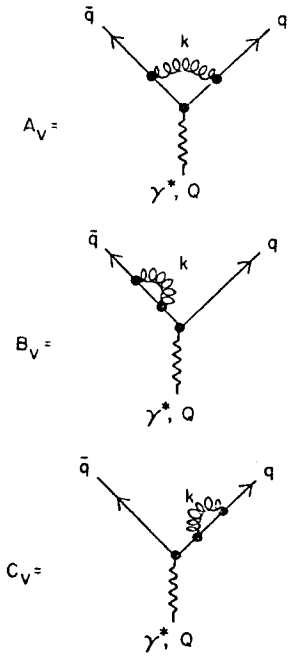

Fig. 2.3. Virtual gluon corrections to the process $\gamma^* \to \bar{q}q$.

For example, if we regularize by temporarily giving the gluon a fictious mass, m_g, then the regions of integration in (2.14) becomes

$$0 \leq x_2 \leq 1 - \beta,$$

$$1 - \beta - x_2 \leq x_1 \leq (1 - x_2 - \beta)/(1 - x_2), \tag{2.16a}$$

where

$$\beta = m_g^2/Q^2, \tag{2.16b}$$

and integrating over x_1 yields

$$\frac{d\sigma}{dx_2} = \left(\frac{2\alpha_s}{3\pi}\right)\sigma_0\left\{\left(\frac{1+x_2^2}{1-x_2}\right)\log\left[1/\beta\right] + \left(\frac{1+x_2^2}{1-x_2}\right)\log\left[x_2(1-x_2)\right]\right.$$
$$\left. - \frac{3}{2}\frac{1}{1-x_2} + \frac{1}{2}x_2 + \frac{1}{2} + \frac{\beta(2-x_2)}{(1-x_2)^2} + \frac{1}{2}\frac{\beta^2}{(1-x_2)^3}\right\}, \qquad (2.17)$$

where I have dropped terms that do not contribute in the limit $\beta \to 0$. Integrating (2.17) over x_2 is also easy and gives

$$\sigma_{tot}(\text{real}) = \left(\frac{2\alpha_s\sigma_0}{3\pi}\right)\left\{\log^2(\beta) + 3\log(\beta) - \frac{\pi^2}{3} + 5\right\}, \qquad (2.18)$$

where again terms that vanish in the limit $\beta \to 0$ have been dropped.

The order α_s contribution to the total rate $\gamma^* \to \bar{q}q$ from virtual gluon diagrams is given by

$$\sigma_{tot}(\text{virtual}) = \int\frac{d^4k}{(2\pi)^4}\left\{2A_0A_v^* + \frac{1}{2}\left[2A_0B_v^* + 2A_0C_v^*\right]\right\}, \qquad (2.19)$$

where A_0 is the "Born" amplitude in Fig. 2.1b and A_v, B_v, and C_v are the three amplitudes shown in Fig. 2.3. The integral is over the 4-momentum, k, of the virtual gluon. In the massive gluon regularization scheme (2.19) becomes

$$\sigma_{tot}(\text{virtual}) = \left(\frac{2\alpha_s\sigma_0}{3\pi}\right)\left\{-\log^2(\beta) - 3\log(\beta) + \frac{\pi^2}{3} - \frac{7}{2}\right\}, \qquad (2.20)$$

which when added to the real gluon contribution in (2.18) gives

$$\sigma_{tot} = \sigma_{tot}(\text{real}) + \sigma_{tot}(\text{virtual}) = \left(\frac{\alpha_s}{\pi}\right)\sigma_0, \qquad (2.21)$$

which is finite. Neither the log squared nor the log term in (2.18) contribute to σ_{tot}. They are both cancelled by the virtual graphs. Only the "constant" (non divergent) terms in (2.18) and (2.20) contribute to the total α_s correction to σ_{tot}.

To understand the "leading pole" approximation (LPA) we must change variables yet another time. This time let us introduce the Sudakov or light cone variables

$$\begin{aligned} E_i + (p_z)_i &= z_iQ, \\ E_i - (p_z)_i &= y_iQ, \end{aligned} \qquad (2.22)$$

where, as shown in Fig. 2.4, the z-axis is defined in the direction $\vec{p}_2 + \vec{p}_3$. The Sudakov variables for partons 2 and 3 satisfy

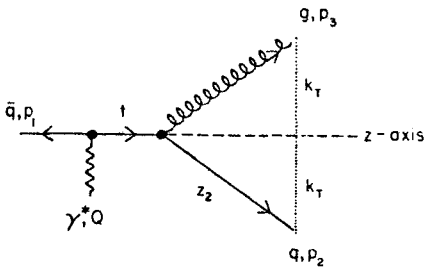

Fig. 2.4. Illustration of the "decay" of a quark, q, with invariant mass $\sqrt{t}$ into a gluon, g, and a quark carrying a fraction z_2 of its' $E+p_z$. The outgoing gluon has a transverse momentum, k_T, relative to a z-axis defined along the direction on the original quark.

$$\begin{aligned} &z_2 + z_3 = 1, \\ &y_2 + y_3 = \hat{t} = (1 - x_1), \\ &z_2 y_2 = z_3 y_3 = z_2(1-z_2)\hat{t} = k_T^2/Q^2, \\ &z_2 = x_2 - \hat{t}(1 - x_2)/(1- \hat{t}), \end{aligned} \tag{2.23a}$$

where

$$\hat{t} = t/Q^2, \tag{2.23b}$$

with t defined in (2.3b) and where k_T is the transverse momentum relative to the z-axis (i.e. relative to $\vec{p}_2 + \vec{p}_3$), which is simply the direction of parton 1 as shown in Fig. 2.4. The differential cross section in (2.11) when written in terms of z_2 and the invariant mass t of parton 2 and 3 becomes

$$\frac{1}{\sigma_0}\frac{d\sigma}{dz_2 d\hat{t}} = \left(\frac{2\alpha_s}{3\pi}\right)\left\{\frac{1+z_2^2}{\hat{t}(1-z_2)} - \frac{2(1-z_2(1-z_2))}{(1-z_2)} + \frac{\hat{t}(1+(1-z_2)^2)}{(1-z_2)}\right\}. \tag{2.24}$$

In regions where $k_T^2 = z_2(1-z_2)t$ is small. This differential cross section can be approximated by the first term. Approximating (2.24) by

$$\left(\frac{1}{\sigma_0}\frac{d\sigma}{dz_2 d\hat{t}}\right)_{LPA} = \left(\frac{2\alpha_s}{3\pi}\right)\frac{1+z_2^2}{(1-z_2)\hat{t}} \tag{2.25}$$

is known as the "leading pole" approximation. The virtual corrections can be included by writing

$$\left(\frac{1}{\sigma_0}\frac{d\sigma}{dz_2 dt}\right)_{LPA} = \frac{\alpha_s(t)}{2\pi t} P_{q\to qg}(z), \tag{2.26a}$$

where

$$P_{q\to qg}(z) = \frac{4}{3}\left(\frac{1+z^2}{1-z}\right)_+, \tag{2.26b}$$

and where the "+ function" is defined by

$$[f(z)]_+ = \lim_{\beta\to 0}\{f(z)\theta(1-z-\beta) - \delta(1-z-\beta)\int_0^{1-\beta} f(y)dy\}, \tag{2.27a}$$

which is well defined in a "distribution sense" and which has the property that

$$\int_0^1 [f(z)]_+ dz = 0. \tag{2.27b}$$

We will interprete (2.26) as the probability that a quark of invariant mass $\sqrt{t}$ propagates and "decays" into a quark and gluon carrying z and (1-z), respectively, of its $E+P_z$. We would like to construct e^+e^- final states with, for example, n gluons by multiplying the LPA probability in (2.26a) by itself n times. Unfortunately, if we examine the contributions to the LPA formula from the three terms in (2.2) we find (in the Feynman gauge)

$$|A_R|^2 = c(1-x_2)/(1-x_1) \xrightarrow{LPA} c(1-z_2)/\hat{t} \tag{2.28a}$$

$$|B_R|^2 = c(1-x_1)/(1-x_2) \xrightarrow{LPA} 0 \tag{2.28b}$$

$$2A_R B_R^* = 2c(x_1+x_2-1)/[(1-x_1)(1-x_2)] \xrightarrow{LPA} c\frac{2z_2}{(1-z_2)\hat{t}}. \tag{2.28c}$$

The sum of these terms gives, of course, the LPA result. However, since the interference term (2.28c) contributes to the result, we cannot simply multiply the probabilities of successive emissions. We must add the amplitudes first and then square. It does not appear as if we have "independent" emission.

This problem can be circumvented by an appropriate choice of gauge. In an axial gauge (2.4) is replaced by

$$\sum_{pol} \varepsilon_\nu \varepsilon_\nu^* = -g_{\nu\nu'} + \frac{n_\nu k_{\nu'} + n_{\nu'} k_\nu}{(n.k)} - \frac{n^2 k_\nu k_{\nu'}}{(n.k)^2}, \tag{2.29}$$

where k is the gluon momentum and n is an arbitrary 4-vector satisfying n.k = 0 (usually one also takes $n^2 = 0$). With the choice, for example, of

$$n = Q - p_2/x_2 \tag{2.30}$$

we have

$$|A_R|^2 = c\,\frac{1+x_2^2}{(1-x_1)(1-x_2)} \xrightarrow{\text{LPA}} c\,\frac{1+z_2^2}{(1-z_2)\hat{t}}, \tag{2.31a}$$

$$|B_R|^2 = c\,\frac{1-x_1}{1-x_2} \xrightarrow{\text{LPA}} 0, \tag{2.31b}$$

$$2A_R B_R^* = c\,\frac{-2}{(1-x_2)} \xrightarrow{\text{LPA}} 0. \tag{2.31c}$$

In this gauge the complete LPA result comes from the term $|A_R|^2$; interference terms do not contribute. Therefore, in this gauge (and in any axial gauge) the cross section for the emission of n gluons has the simple latter structure shown in Fig. 2.5. The

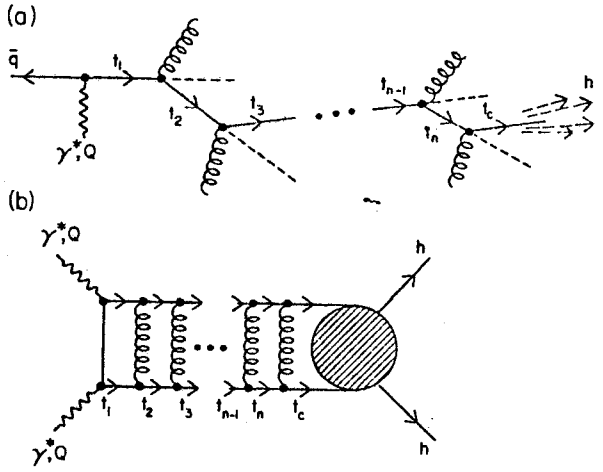

Fig. 2.5. (a) Illustration of the case where an initial quark produced by the "decay" of a virtual photon of invariant mass Q emits n gluons and has its' invariant mass is degraded from t_1 to t_c ($Q^2 > t_1 > t_2 > \ldots t_{n-1} > t_n > t_c$) whereby it subsequently fragments into a hadron, h. (b) Square of the amplitude for the process in (a) in the "leading pole" approximation. In an axial gauge interference terms do not contribute to leading order and the cross section takes on a simple ladder form.

total probability in the leading pole approximation is simply a product of the probabilities for each individual emission and the differential cross-section for the emission of n gluons from an outgoing quark becomes

$$\frac{d\sigma/\sigma_0}{dz_1 \ldots dz_n dt_1 \ldots dt_n} = \left[\frac{\alpha_s(t_1)}{2\pi t_1} P_{q\to qg}(z_1)\right]\left[\frac{\alpha_s(t_2)}{2\pi t_2} P_{q\to qg}(z_2)\right] \ldots \left[\frac{\alpha_s(t_n)}{2\pi t_n} P_{q\to qg}(z_n)\right], \tag{2.32}$$

where $P_{q\to qg}(z)$ is given in (2.26b), and where the invariant masses are ordered (see Fig. 2.5)

$$Q^2 > t_1 > t_2 > \ldots > t_{n-1} > t_n. \tag{2.33}$$

It is an easy matter to generalize the LPA cross section in (2.32) to include gluon jets as well. The LPA probability for a parton of type j (quark, antiquark or gluon) with invariant mass $\sqrt{t}$ to propagate from its' production and "decay" into partons of type j_1 and j_2 carrying fractions z and (1-z), respectively, of its' $E+p_z$ is given by

$$\frac{\alpha_s(t)}{2\pi t} P_{j\to j_1 j_2}(z), \tag{2.34}$$

where $P_{q\to qg}(z)$ is given in (2.26b) and

$$P_{g\to q\bar{q}}(z) = \frac{1}{2}\left(z^2 + (1-z)^2\right), \tag{2.35a}$$

$$P_{g\to gg}(z) = \frac{6(1-z+z^2)^2}{z(1-z)}. \tag{2.35b}$$

The total cross section (or probability) of any final state configuration of quarks, antiquarks, and gluons is given by the product of the probabilities for each individual emission. Namely

$$\frac{d\sigma/\sigma_0}{dz_1 \ldots dz_n dt_1 \ldots dt_n} = \left[\frac{\alpha_s(t_1)}{2\pi t_1} P_1(z_1)\right]\left[\frac{\alpha_s(t_2)}{2\pi t_2} P_2(z_2)\right] \ldots \left[\frac{\alpha_s(t_n)}{2\pi t_n} P_n(z_n)\right], \tag{2.36}$$

where $P_j(z)$ are the appropriate $P_{j\to j_1 j_2}(z)$ functions.

III. The Monte-Carlo Method -- Parton Final States[11-14]

We would like to generate Monte-Carlo events in which quarks and gluons are distributed according to the leading pole formula given in (2.36). I will illustrate the method of doing this by first considering the case in which quarks radiate gluons but where the gluons are not allowed to radiate or produce quark antiquark pairs (i.e. equation (2.32)).

It is necessary to introduce some cut-off procedure into the Monte-Carlo. Otherwise the Monte-Carlo will produce final states containing an infinite number of partons. A massless quark given enough time will radiate an infinite number of massless gluons. In the real world, on the other hand, quarks do not have an infinite amount of time to radiate because at some stage non-perturbative effects take over and hadrons are formed. It will turn out that one need only specify one cut-off parameter in the Monte-Carlo, which is taken as an invariant mass cut-off, $t_c = \mu_c^2$. Quarks with invariant mass less than μ_c will be allowed to propagate freely to the final state with no further radiation.

Given a quark with a maximum possible invariant mass of t_p, we must decide whether it will emit a resolvable gluon or not. Let $\pi_q(t_p,t_c)$ be the probability that a quark of maximum invariant mass $\sqrt{t_p}$ emits only unresolvably soft gluons (i.e. $z > 1-z_c$) until its invariant mass is degraded to t_c. This situation is illustrated in Fig. 3.1a. (Actually z_c is not a separate cut-off parameter, but is related to t_c.) To compute $\pi_q(t_p,t_c)$ we must integrate equation (2.32) over the appropriate regions. Namely,

$$\pi_q(t_p,t_c) = \sum_{n=0}^{\infty} \{\int_{t_c}^{t_p} \frac{\alpha_s(t_1)}{2\pi t_1} dt_1 \int_{t_2}^{t_1} \frac{\alpha_s(t_2)}{2\pi t_2} dt_2 \cdots \int_{t_c}^{t_{n-1}} \frac{\alpha_s(t_n)}{2\pi t_n} dt_n$$

$$\int_{\substack{z_1<1-z_c \\ z_1<z_c}} P_{q\to qg}(z_1)dz_1 \int_{\substack{z_2<1-z_c \\ z_2<z_c}} P_{q\to qg}(z_2)dz_2 \cdots \int_{\substack{z_n<1-z_c \\ z_n<z_c}} P_{q\to qg}(z_n)dz_n\}. \tag{3.1}$$

The integrations over t are nested because each t_i in the chain cannot be larger than the previous t_{i-1}. (See equation (2.33).) These nested integrals are easily done by first changing variables. We define

$$\kappa = \frac{2}{\beta_0} \log \{\alpha_s(t_c)/\alpha_s(t)\}, \tag{3.2}$$

then

$$\frac{d\kappa}{dt} = \frac{\alpha_s(t)}{2\pi t} \tag{3.3a}$$

with

$$\alpha_s(t) = 4\pi/(\beta_0 \log(t/\Lambda^2)) \tag{3.3b}$$

and

$$\beta_0 = 11 - \frac{2}{3} n_f. \tag{3.3c}$$

We are left with

$$\int_0^{\kappa_p} d\kappa_1 \int_0^{\kappa_1} d\kappa_2 \cdots \int_0^{\kappa_{n-1}} d\kappa_n = \frac{\kappa_p^n}{n!}, \tag{3.4}$$

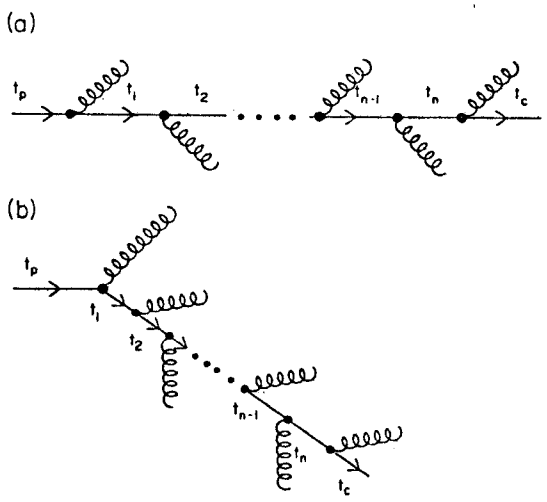

Fig. 3.1. (a) Illustration of the case where an initial quark of maximum invariant mass $\sqrt{t_p}$ emits n unresolvably soft gluons ($z>1-z_c$) until its' invariant mass is degraded to $\sqrt{t_c}=\mu_c$. This configuration of a quark and it's accompanying soft gluons is defined as an outgoing final state "quark". (b) Illustration of the case where one hard gluon is emitted followed by the emission of n unresolvably soft gluons.

where

$$\kappa_p = \frac{2}{\beta_0} \log \{\alpha_s(t_c)/\alpha_s(t_p)\} \tag{3.5}$$

Furthermore because of (2.27b) we have

$$\int_0^1 P_{q\to qg}(z)\, dz = 0, \tag{3.6}$$

which means that the integration over the soft gluon region can be arrived at by

$$\int_{\substack{z>1-z_c \\ z<z_c}} P_{q\to qq}(z)\, dz = -\int_{z_c}^{1-z_c} P_{q\to qq}(z) \equiv -\gamma_{NS}(z_c) \tag{3.7a}$$

with

$$\gamma_{NS}(0) = 0. \tag{3.7b}$$

We are left with

$$\pi_q(t_p,t_c) = \sum_{n=0}^{\infty} \frac{\kappa_p^n}{n!}(-\gamma_{NS}(z_2))^n = \exp[-\kappa_p\gamma_{NS}(z_c)], \tag{3.8}$$

or

$$\pi_q(t_p,t_c) = [\alpha_s(t_p)/\alpha_s(t_c)]^{d_{NS}} \tag{3.9a}$$

with

$$d_{NS} = 2\gamma_{NS}(z_c)/\beta_0. \tag{3.9b}$$

Given that a quark does decide to produce resolvable radiation then we must know how to produce its invariant mass. Its invariant mass distribution is given by (2.32) modified by possible subsequent emissions. What we must calculate is the invariant mass distribution for the situation in Fig. 3.1b in which one gluon is "hard" and all the rest are soft, $\Xi_q(t) = d\sigma/dt$. Actually we already know this because we know that if we integrate over $\Xi_q(t)$ we must get $1-\pi_q(t_p,t_c)$, namely,

$$\int_{t_c}^{t_p} \Xi_q(t)dt = 1 - \pi_q(t_p,t_c), \tag{3.10}$$

or

$$\Xi_q(t) = -\frac{d\pi_q(t,t_c)}{dt}, \tag{3.11}$$

and

$$\Xi_q(t) = \frac{\alpha_s(t)}{2\pi t}\gamma_{NS}(z_c)\pi_q(t,t_c). \tag{3.12}$$

The Monte-Carlo scheme then proceeds as follows:

(i) Starting with quark 1 in Fig. 3.2a decide whether it will radiate any "resolvable" radiation. This is done by generating a random number r from 0 to 1. If $r < \pi_q(t_p=Q^2,t_c)$ then this "quark" with its accompanying soft radiation is allowed to propagate freely and appears in the final state. If $r > \pi_q(t_p=Q^2,t_c)$ then it is allowed to radiate and we proceed to the next step.

(ii) If a quark does decide to radiate then its invariant mass is generated according to (3.12). This is done by generating another random number r from 0 to 1 and solving the following equation for t:

$$r = \frac{\int_{t_c}^{t}\Xi_q(t)dt}{\int_{t_c}^{t_p}\Xi_q(t)dt} = \frac{1-\pi_q(t,t_c)}{1-\pi_q(t_p,t_c)}. \tag{3.13}$$

The solution is

$$t/\Lambda^2 = (t_c/\Lambda^2)^b, \tag{3.14a}$$

with

$$b = [(1-r) + r\pi_q(t_p,t_c)]^{1/d_{NS}}, \tag{3.14b}$$

and with d_{NS} given in (3.9b).

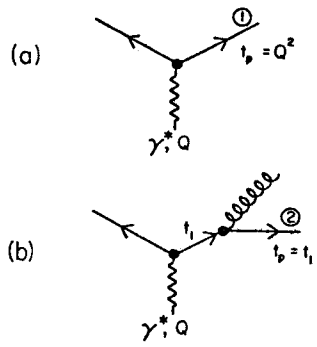

Fig. 3.2 (a) Illustration of the "decay" of a virtual photon of invariant mass Q into a quark with maximum invariant mass $\sqrt{t_p}=Q$ and antiquark. (b) The quark (1) in (a) subsequently "decays" into a gluon and a quark (2) of maximum invariant mass $\sqrt{t_p}=t_1$, where t_1 is the actual invariant mass of the gluon and quark (2).

(iii) The value of z for the decay is chosen according to the P(z) distribution in (2.26b). Here z is identified as the fraction of $E+|\vec{p}|$ rather than the fraction of $E+p_z$ as in (2.22). This change effects only subleading logs and allows for easier handling of the large and small z regions.[15] The $E+|\vec{p}|$ fractions satisfy $z_c>z>1-z_c$, and the momenta is distributed uniformly in azimuth.

(iv) Now quark 2 in Fig. 3.2b is examined. Its maximum invariant mass $\sqrt{t}$ is equal to the previous quarks choosen invariant mass $\sqrt{t_1^P}$. Again $\pi_q(t_p=t_1,t_c)$ is examined to decide whether or not further resolvable radiation is to be emitted. If not, then this "quark" along with its accompanying soft radiation is allowed to propagate to the final state. If radiation is to occur then the invariant mass of quark 2 is generated as in (ii).
(v) This process is continued until all quarks have decided to generate no further resolvable radiation with $t>t_c$.

It is easy to generalize the prescription to include the case where gluons "decay" as well. The probability that a parton of type j (quark or gluon) and maximum invariant mass $\sqrt{t}$ should evolve until it has $\sqrt{t}<\mu_c$ emitting only unresolvably soft ($z<z_c$ or $z>1-z_c$) partons is given by

$$\pi_j(t_p,t_c) = \sum_{n=0}^{\infty} \{\int_{t_c}^{t_p} \frac{\alpha_s(t_1)}{2\pi t_1}dt_1 \int_{t_c}^{t_1} \frac{\alpha_s(t_2)}{2\pi t_2}dt_2 \cdots$$
$$\int_{t_c}^{t_{n-1}} \frac{\alpha_s(t_n)}{2\pi t_n}\,dt_n \int_{\substack{z_1<1-z_c \\ z_1<z_c}} P_{j_1 \to All}(z_1)dz_1 \qquad (3.15)$$
$$\int_{\substack{z_2<1-z_c \\ z_2>z_c}} P_{j_2 \to All}(z_2)dz_2 \cdots \int_{\substack{z_n<1-z_c \\ z_n>z_c}} P_{j_n \to All}(z_n)dz_n\},$$

or

$$\pi_j(t_p,t_c) = [\alpha_s(t_p)/\alpha_s(t_c)]^{d_j}, \qquad (3.16a)$$

with

$$d_j = 2\gamma_j(z_c)/\beta_0 \qquad (3.16b)$$

and

$$\gamma_j(z_c) = \int_{z_c}^{1-z_c} P_{j \to All}(z)dz \qquad (3.16c)$$

$$\gamma_j(0) = 0. \qquad (3.16d)$$

Step (i) proceeds as before but using (3.15). Step (ii) is also the same except now the t-distribution is given by

$$\Xi_j(t) = -\frac{d\pi_j(t,t_c)}{dt}. \qquad (3.16)$$

Having determined that parton j is to radiate, and selected its invariant mass t step (iii) is modified slightly. It becomes

(iii') The decay products j_1 and j_2 ($j \to j_1+j_2$) and the value of z is determined according to (2.26b) and (2.35). The $E+|\vec{p}|$ fractions satisfy $z_c>z>1-z_c$, and the momenta are distributed uniformly in azimuth.

The partons j_1 and j_2 are allowed to evolve as was parton j, and the cascade continues until all partons have chosen to generate no further resolvable radiation with $t>t_c$.

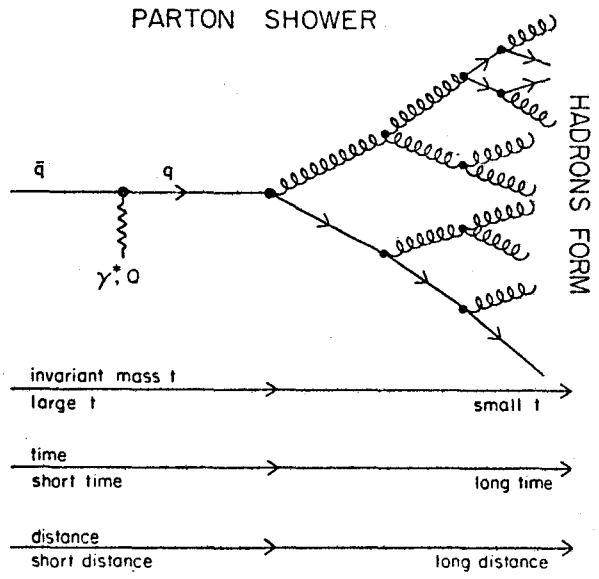

Fig. 3.3 Illustration of the development of a parton shower initiated by the "decay" of a virtual photon of invariant mass Q into a quark and antiquark. From left to right time and distance increases while the invariant masses of the partons (quarks and gluons) decreases. Finally, when the invariant masses become compariable to Λ hadrons are formed.

Parton showers generated in this manner can be viewed almost classically. "Virtual" partons will live for a time, $\Delta\tau$, determined by the degree to which they are off-shell

$$\Delta\tau \sim 1/\Delta E \sim (E+|\vec{p}|)/t \sim p/t \tag{3.17}$$

and then "decay", where p and t are the magnitude of the momentum and invariant mass, respectively, of the parton. The time for the emission of a gluon is roughly 1/p, so as long as

$$1/p \ll p/t \tag{3.18}$$

the independent emission (LPA) assumption is accurate. Equation (3.18) is satisfied except perhaps at early times where $t \sim Q^2$. The development of a parton shower is illustrated in Fig. 3.3. At early times (short distances) invariant masses are large (on the order of Q). Here interferences are important and gluons may be emitted at large angles where the LPA formula is not accurate. One can correct for this by using (at this stage) the complete order α_s formula in (2.24). At later times the invariant masses of the partons are smaller (because they are ordered as in (2.33)) and the angles of emission are small.[16] In this region one is justified in assuming independent emission, interferences are not important and the LPA approach correctly describes the development. At even longer times the invariant masses become small and compariable to Λ. Here $\alpha_s(t)$ is large, non-perturbative effects dominate, and the hadrons are formed. Presumably in this region interference effects are also important.

Figure 3.4 shows the space-time development of some typical parton showers initiated by the "decay" of a virtual photon with invariant mass Q = 200 GeV. The partons that choose not to produce any more resolvable radiation are assumed massless and appear as "final state" partons. These parton showers are in many respects analogous to electromagnetic showers, initiated by the entry of a high-energy electron into matter. In the electromagnetic shower case the initial particle is on shell, but is repeatly knocked off shell by interactions with nuclei in the matter. The electron generates a shower by successive Bremsstrahlung radiation of photons which in turn can produce e^+e^- pairs.

Figures 3.5 and 3.6 show the mean total multiplicity of partons and the mean fraction of the total energy carried by gluons, respectively, in parton showers with cut-off μ_c as a function of Q. The smaller μ_c is, the more partons one produces at a given Q and for a fixed Λ (of course, one must take $\mu_c > \Lambda$). It is interesting to note that nearly all the partons produced are gluons. As can be seen in Fig. 3.5, very rarely does one produce additional $q\bar{q}$ pairs in the LPA approximation. Since the hadron

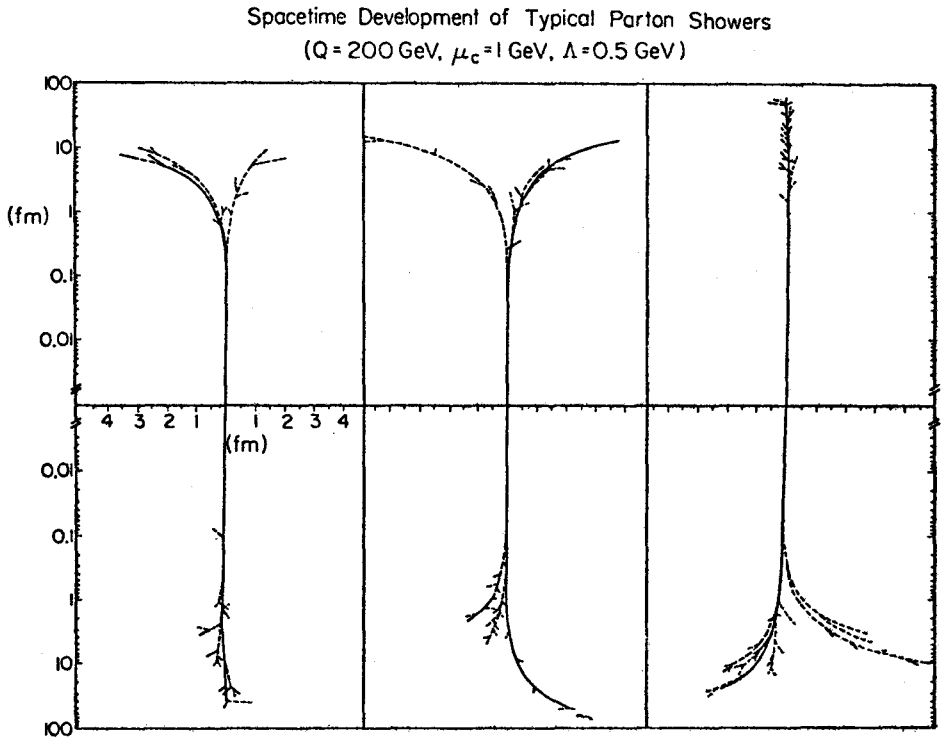

Fig. 3.4. Spacetime development of typical parton showers initiated by the "decay" of a virtual photon with invariant mass Q=200 GeV, traced until each parton has invariant mass below μ_c=1 GeV, and with Λ=0.5 GeV (taken from Ref. 13). Solid lines represent quarks while dashed lines are gluons.

final state contains many $q\bar{q}$ pairs, it is clear that we are not going to be able to construct a purely perturbative model for the formation of hadrons, which is not surprising. The perturbative structure of the parton showers can guide us, but the hadrons are going to have to be inserted by hand (i.e. by some non-perturbative model).

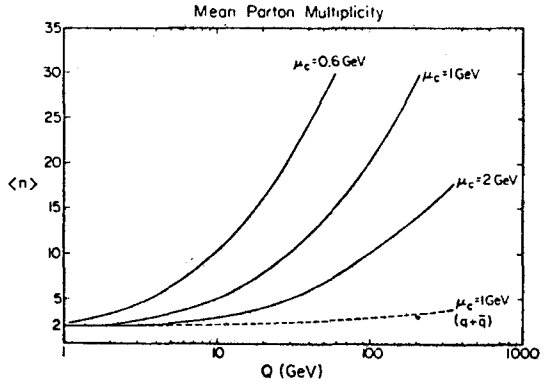

Fig. 3.5. Mean multiplicity of partons (quarks and gluons) produced in the "decay" of a virtual photon with invariant mass Q for various values of the cut-off μ_c with Λ=0.5 GeV (taken from Ref. 13). The dashed line gives the multiplicity of quarks and antiquarks.

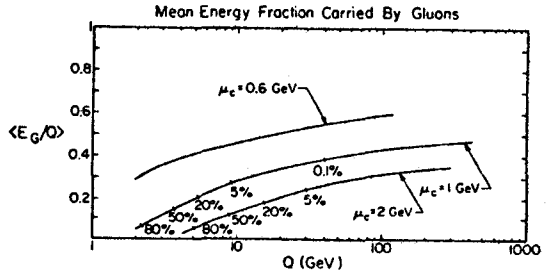

Fig. 3.6. Mean fraction of the total energy carried by gluons in the "decay" of a virtual photon with invariant mass Q and where the parton showers have been truncated when invariant masses fall below μ_c (taken from Ref. 13). The percentage of events in which no gluons were emitted above this cut-off is also marked.

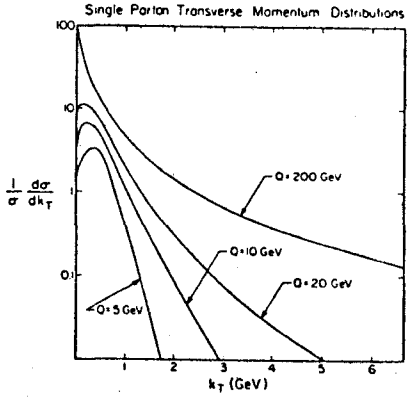

Fig. 3.7. Transverse momentum distributions for single partons produced in the "decay" of a virtual photon with invariant mass Q with respect to the primary $q\bar{q}$ direction and where μ_c=1 GeV and Λ=0.5 GeV (taken from Ref. 13).

Each off-shell parton "decay" produces a relative transverse momentum $k_T^2 \approx z(1-z)t$ of its products which when combined with the dt/t factor for each individual decay gives rise to the power law tail in the single parton k_T distribution shown in Figure 3.7. As the initial photon invariant mass, Q, increases, this tail in the k_T distribution becomes more prominent.

IV. Monte-Carlo Models — Hadron Final States

Given that the LPA Monte-Carlo approach produces parton showers in accordance with perturbative QCD, what can we say about what experiments measure; namely, hadron final states. Does the fact that we must convert perturbative parton showers into non-perturbative hadron showers mean that we loose our predictive power? Certainly not at extremely high energies since the non-perturbative pieces die off like various powers of 1/Q relative to the perturbative terms. But what is high energy? What about existing energies?

Before one can even attempt to answer these questions one must examine various models for the hadronization phase. Then one can compare the various approaches, examine the meriod of experimental observables, and come to some conclusions as to what is the "best" model for hadronization (i.e., the one most closely resembling nature) and what are the best observables to examine. Models for the hadronization can be divided into two classes. The

first class includes models in which the underlying parton shower, as illustrated in Fig. 3.3, is not allowed to develop very far. This corresponds to choosing a large value for the cut-off invariant mass μ_c. Models in this class generally rely on the FF-model to parameterize the manner in which the final state partons fragment into hadrons.

A. Models with μ_c large — the string picture

The first model in this class I will call the "QCD-FF-CM" model. In this model, which is illustrated in Figure 4.1 one chooses a large μ_c so that only a few gluons are produced in the parton shower. Each final state quark and gluon is then allowed to fragment independently in the e^+e^- cm frame according to the FF prescription. Versions of this approach, but were only the $q\bar{q}$ and $q\bar{q}g$ (and in some cases also the $q\bar{q}gg$) parton states are included, have been shown to agree quite well with the

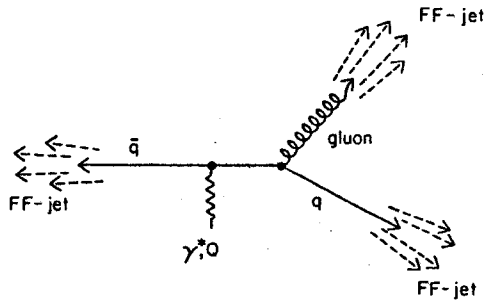

Fig. 4.1. Illustration of the "QCD-FF-CM" model in which each quark and gluon produced in the "decay" of a virtual photon of invariant mass Q is allowed to "fragment" independently in the e^+e^- CM frame according to the Feynman and Field prescription (FF-jet).

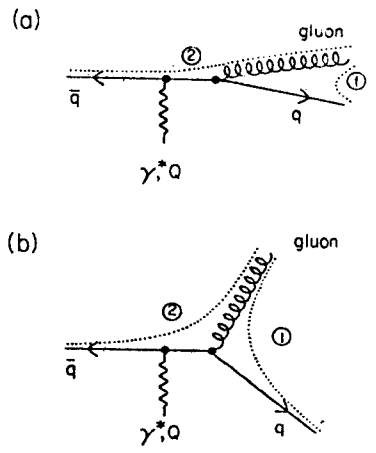

Fig. 4.2. (a) Illustrates the case where color "string" (1) has a small invariant mass while "string" (2) has an invariant mass nearly equal to the maximum value of Q. (b) Illustrates the case where both color "string" (1) and (2) have sizable invariant masses in the "decay" of a virtual photon with large invariant mass Q into a quark, antiquark, and gluon.

experimental data.[6,7] I have also verified that this approach can fit existing data, where I used Monte-Carlo generated parton showers with μ_c = 10 GeV and Λ = 0.5 GeV/c.

Although the "QCD-FF-CM" model fits quite well existing data. It is not appealing theoretically for several reasons. In a parton shower with several gluons or even with just $q\bar{q}$ and one gluon, if the gluon is not well separated from the q or the $\bar{q}$, then it is not sensible to allow the partons to fragment independently. When a quark and gluon are nearly parallel as in Fig. 4.2a then the pair should fragment as one jet, not as the sum of a gluon jet plus a quark jet. Only if the final partons are well separated as in Fig. 4.2b does allowing them to fragment independently make sense theoretically. Also, because of this double counting of overlaping parton jets it may be quite misleading to extrapolate the "QCD-FF-CM" model to high energies where there are many final state partons.

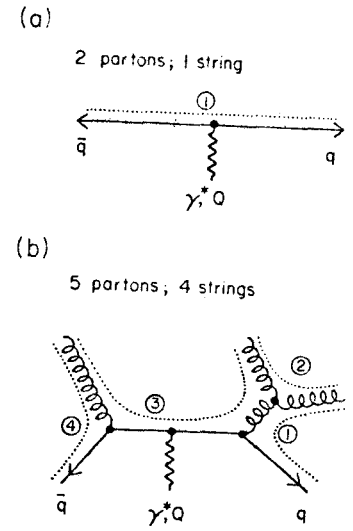

Fig. 4.3. (a) Illustrates the case where a virtual photon "decays" into two partons (a quark and antiquark) with one string (1) that labels the color separation. (b) Illustrates the case where a virtual photon "decays" into a quark, antiquark, and three gluons (a total of five partons). In this case there are four color strings (1)-(4).

Perhaps a more sensible approach is to keep tract of the color indices and to fragment the partons in the CM of the separating colors. For example, Fig. 4.3a shows a final state consisting of just a $q\bar{q}$ pair. We can imagine a color "string" connecting the quark of color a and the antiquark of color $\bar{a}$. In this case the CM of the "string" is the e^+e^- CM frame. This is not the case in Fig. 4.2b where there are 3 partons and 2 strings (since gluons have two color indices, two strings end on each gluon) and in Fig. 4.3b where there are 5 partons and 4 strings. It is an easy matter to generalize the parton shower Monte-Carlo to keep track of color indices so that one knows the final state string configuration. Each string is color neutral and we will consider it a color singlet.[17] The invariant mass of a string, m_s, is arrived at by dividing each gluon into a quark and antiquark carring a fraction ζ and $1-\zeta$ of its 4-momentum. The invariant mass, for example, of string number 1 in Fig. 4.4 is then

$$m_s^2 = (p_{q_a} + p_{\bar{q}_a})^2, \qquad (4.1a)$$

where

$$P_{\bar{q}_a} = \zeta P_{glue}. \tag{4.1b}$$

The distribution of ζ, $f_s(\zeta)$ (i.e., the "splitting function") is taken to be either

$$f_s(\zeta) = \delta(\zeta - 1/2) \tag{4.2a}$$

or

$$f_s(\zeta) = 1, \tag{4.2b}$$

(i.e. ζ is distributed uniformly from 0 to 1). One could, of course, choose any splitting function. However, the results are not very sensitive to this choice.

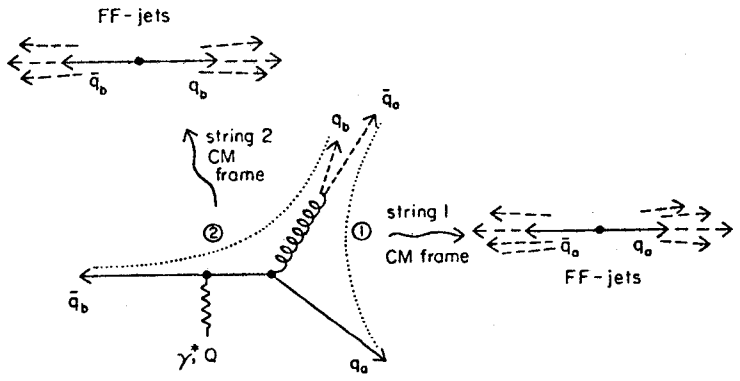

Fig. 4.4. Illustration of the "QCD-FF-string" model in which each color string (i.e., cluster) is parameterized by allowing it to "decay" in its' individual CM frame according to the FF-jet model. In order to determine the invariant mass of a string one must imagine the gluon as being made of a quark and an antiquark ($q_b \bar{q}_a$), each carrying a certain amount of the gluon's momentum with the total momentum of the pair being equal to that of the gluon.

If one combines the string approach with a large cut-off μ_c for the Monte-Carlo parton shower generator, one is left with rather large invariant masses to parameterize. As illustrated in Fig. 4.4, these subsystems are then parameterized by the FF model. I will refer to this approach as the "QCD-FF-string" model. This approach has the nice feature that when a quark and gluon in the shower become parallel as in Fig. 4.2a, the invariant mass of their connecting string goes to zero (string 1 in Fig. 4.2a). On the other hand, the other string (string 2 in Fig. 4.2a) has an invariant mass that approaches the total Q of the event. There is no double counting in this picture and three jet final states approach in a smooth manner the two jet configuration.

Differences between the "QCD-FF-CM" model and the "QCD-FF-string" model are due to the different choice in the frame for the fragmentation. For a given parton configuration these two models approach each other as the energy of the event is increased. In addition, the two models produce very similar results if the final state consists of widely separated partons and the energy is high. Fig. 4.5 shows the energy flow resulting from the two approaches at Q=W=10 GeV for the case where a quark, antiquark and gluon all have equal energies and are separated by 120°. At this energy there is a considerable difference between the two approaches even for the 120° configuration. At Q=W=30 GeV, on the other hand, the two approaches more closely agree as seen in Fig. 4.6. As can be seen in Fig. 4.7 and 4.8, for a $\bar{q}$-gluon separation of 60° there are extremely large differences in the two approaches particularly at the lower energies. At W=10 GeV and a separation of 60° the string approach produces events that resemble two jet events, while the CM approach produces events with an ordinary jet on the right balance by a high multiplicity of low momentum hadrons on the left. I find Fig. 4.7 to be quite interesting. It might be possible to decide whether nature more closely resembles the CM or the string picture by looking for certain correlations in the data. For example, the CM picture would seem to produce events with a large spread in the absolute value of the difference between left and right side multiplicities. I will investigate this further in the future.

Because the string approach produces events that more closely resemble two jet events than does the CM approach, it is necessary to use a larger value of Λ in the former if one is to fit the existing data.

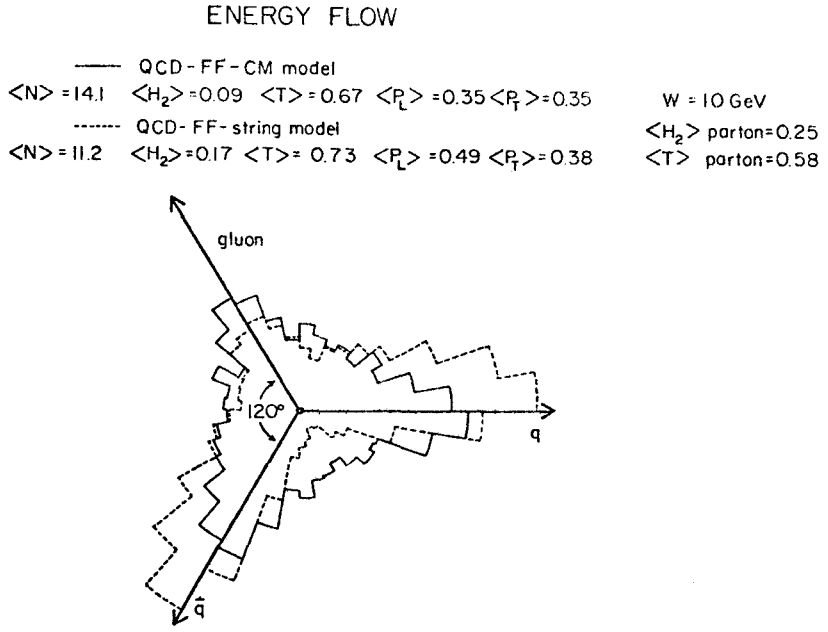

Fig. 4.5. Energy flow (histogram of the angle in the plane weighted by the energy) for hadrons produced by the "QCD-FF-CM" model (solid lines) and the "QCD-FF-string" model (dashed lines) for the case where a virtual photon of invariant mass Q=W=10 GeV "decays" into a quark, antiquark and gluon each of energy 3.33 GeV and with an angle of 120° between each. In the "QCD-FF-string" model the gluon "splitting function" in (4.2b) has been used (i.e. uniform distribution). Also listed is the average multiplicity of hadrons $\langle N \rangle$ and the mean parallel, $\langle p_L \rangle$, and mean transverse, $\langle p_T \rangle$, momentum of hadrons with respect to the sphericity axis. In addition, the mean H_2 and mean thrust, T, at both the parton and hadron level are given.

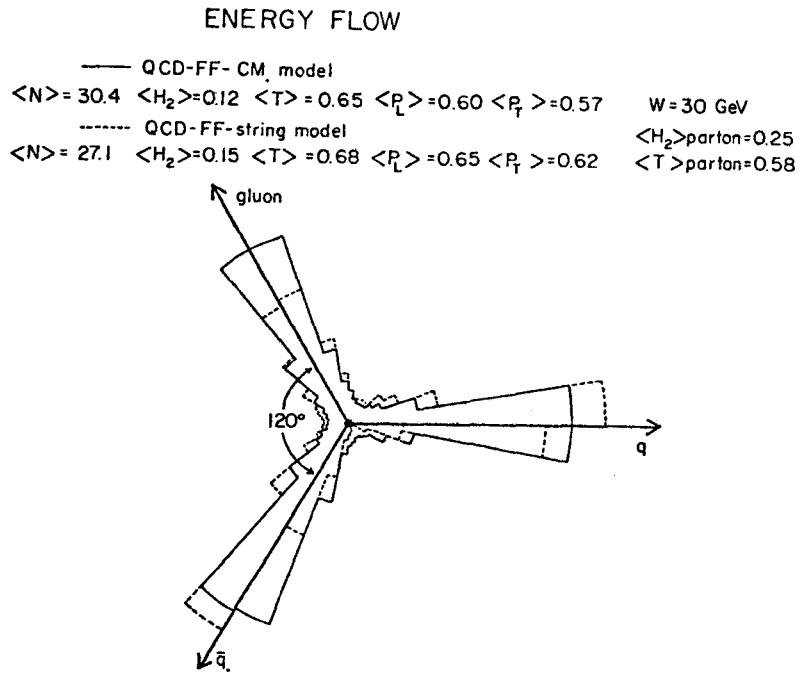

Fig. 4.6. The same as Fig. 4.5 but where each parton has an energy of 10 GeV resulting in a total CM energy of W=30 GeV.

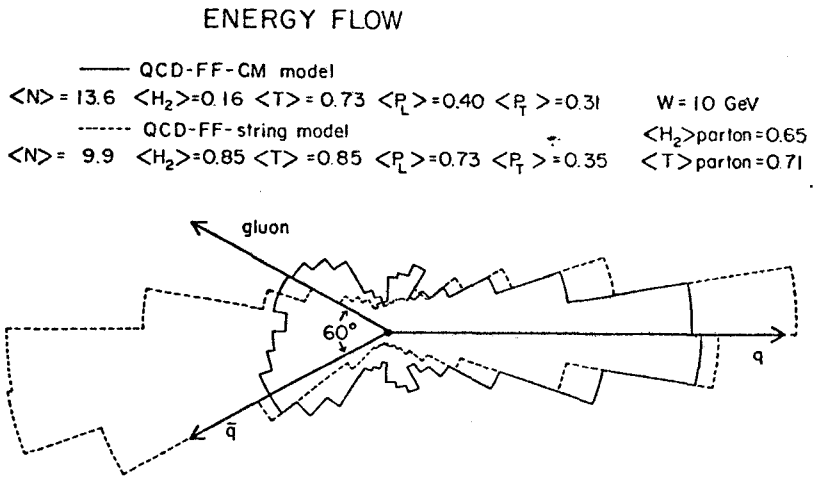

Fig. 4.7. The same as Fig. 4.5 but where the quark has an energy of 4.64 GeV while the antiquark and gluon have energies of 2.68 GeV and an angle of separation of 60° resulting in a total CM energy of W=10 GeV.

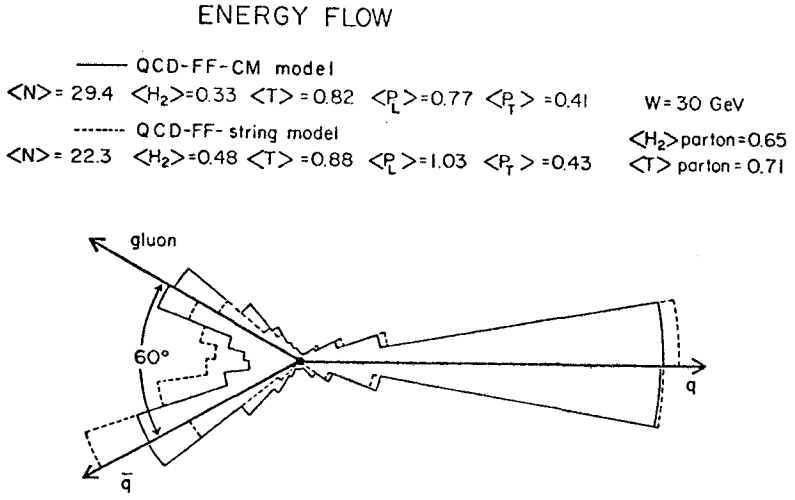

Fig. 4.8. The same as Fig. 4.5 but where the quark has an energy of 13.92 GeV while the antiquark and gluon have energies of 8.04 GeV and an angle of separation of 60° resulting in a total CM energy of W=30 GeV.

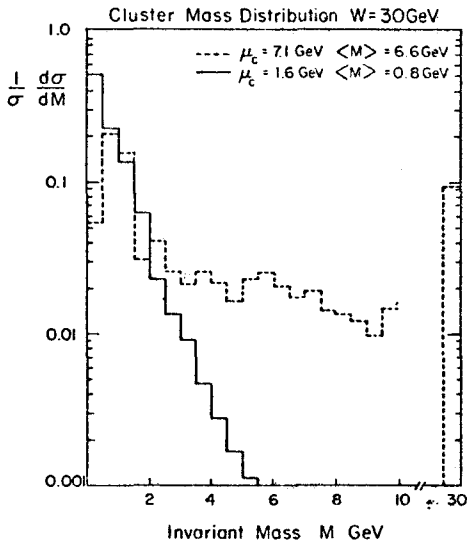

Fig. 4.9. Histogram of the individual cluster invariant masses, M, resulting from parton showers at W=Q=30 GeV with Λ=1.4 GeV and with the gluon "splitting function" given by (4.2b) (i.e. uniform distribution). The solid curves result from choosing a small cut-off μ_c=1.6 GeV and have a mean <M>=0.8 GeV, while the dashed curves result from choosing a large cut-off μ_c=7.1 GeV and have a mean <M>=6.6 GeV.

B. Ambitious approach (μ_c small) — "QCD-PS" model

It is quite interesting to see if we can take perturbative QCD a bit further by reducing the cut-off μ_c. This will produce showers with many partons even at existing energies. As can be seen in Fig. 4.9 the string invariant masses become quite small on the average once we allow μ_c to be small. This means that the insertion of hadrons in this approach reduces to the parameterization of low invariant mass color singlet subsystems (or clusters). If, for example, a $u\bar{d}$ color singlet cluster has a

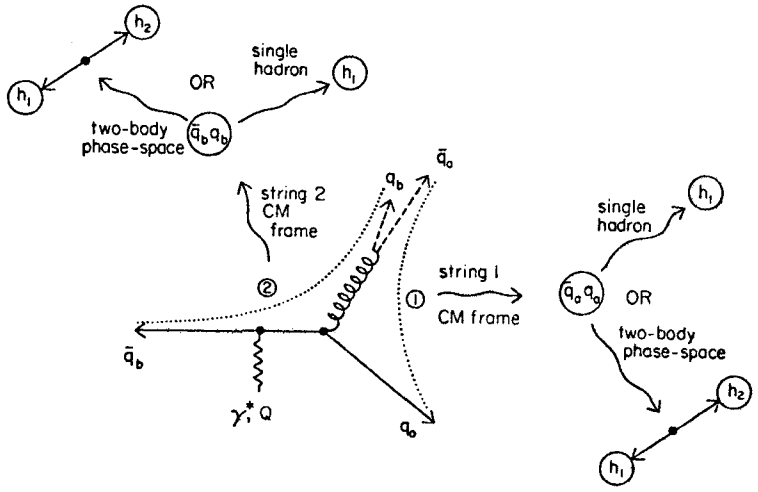

Fig. 4.10. Illustration of the "QCD-PS" model in which each color string (i.e. cluster) is allowed to become a single hadron (if the invariant mass is small enough) or is allowed to "decay" in its' CM frame into two hadrons (according to two-body phase-space).

invariant mass of say 500 MeV then it could appear in the final state as two pions, or three pions, or a ρ and a pion, or a K+ and a K-. There are many possibilities. In what I will call the "QCD-PS" model I have parameterized all color singlet subsystems by allowing them to "decay" uniformly in there center-of-mass according to two-body phase space as illustrated in Fig. 4.10. Two-body states containing vector and tensor mesions are included but are weighted by their phase space probability. In fact, I went crazy one night and coded in almost every two-particle combination in the particle tables, each weighted by its' phase space factor. One can even allow for baryons by allowing a cluster with, for example, $u\bar{d}$ quantum numbers to decay into a proton and an anti-neutron (again weighted by its phase space). In particular, all clusters with invariant mass above 300 MeV are allowed to "decay" into two hadrons

$$\text{Cluster} \longrightarrow M_1 + M_2 \qquad (4.3a)$$

where M_1 and M_2 are mesons belonging to the following SU(3) multiplets

(1) Pseudoscalar 0- Nonet (i.e. π, K, etc.) (4.3b)
(2) Vector 1- Nonet (i.e. ρ, ω, etc.) (4.3c)
(3) Tensor 2+ Nonet (i.e. A_2, f, etc.) (4.3d)
(4) Axial Vector 1+ Nonet (i.e. A_1, etc.) (4.3e)
(5) Axial Vector 1+ Nonet (i.e. B, etc.) (4.3f)
(6) Scalar 0+ Nonet (i.e. ϵ, etc.) (4.3g)

In addition, if a cluster has sufficient invariant mass it is allowed to decay into a baryon-antibaryon pair

$$\text{Cluster} \longrightarrow B_1 + \bar{B}_2, \tag{4.4a}$$

where B_1 and B_2 are baryons belonging to the following multiplets

(7) 1/2+ Octet (i.e. P, n_{++}etc.) (4.4b)
(8) 3/2+ Decaplet (i.e. Δ^{++}, etc.) (4.4c)

Each decay mode is weighted by its two-body phase space weight and with an additional spin weight of 2J+1. After a cluster decays into two hadrons, each of the two hadrons is then allowed to decay according to the decay modes in the particle tables. For example, if two ω mesons were produced the final multiplicity of the cluster would be six (each omega would decay into three pions). The dasher curve in Fig. 4.11 shows the average charged multiplicity of a single cluster of mass W. The multiplicity increases over the low mass region as the thresholds for the higher spin resonances are passed. It levels off at about 3.5 charged particles and becomes independent of the mass.

Some of the cluster invariant masses in Fig. 4.9 are quite small. It seems reasonable that if, for example, a $u\bar{d}$ color singlet cluster obtained an invariant mass of 140 MeV, that it should appear in the final state as a single pion. Unfortunately, the cluster invariant mass is a continuous distribution. Sometimes a $u\bar{d}$ cluster will have a mass of 50 MeV, sometimes 200 MeV, etc. Clearly nature is smarter than my Monte-Carlo. It produces color singlet clusters at just the precise mass of the pion. To account for this I allow extremely low mass clusters to become single hadrons. For example, any $u\bar{d}$ color singlet cluster with invariant mass below say 300 MeV is called a pion. In this approach pions (and kaons) have a variable mass. But on the average the pion mass is roughly 140 MeV. The "QCD-PS" model is illustrated in Fig. 4.10 and Fig. 4.11 which shows the resulting average charged multiplicity for complete e^+e^- events. As the e^+e^- CM energy, W=Q, increases, the number of partons (mostly gluons) in the shower increases. Thus, the number of strings (color singlet clusters) increases which means that the total multiplicity increases. As can be seen by examining Table 4.1, the total multiplicity is given roughly by the average number of clusters times the average hadron multiplicity per cluster.

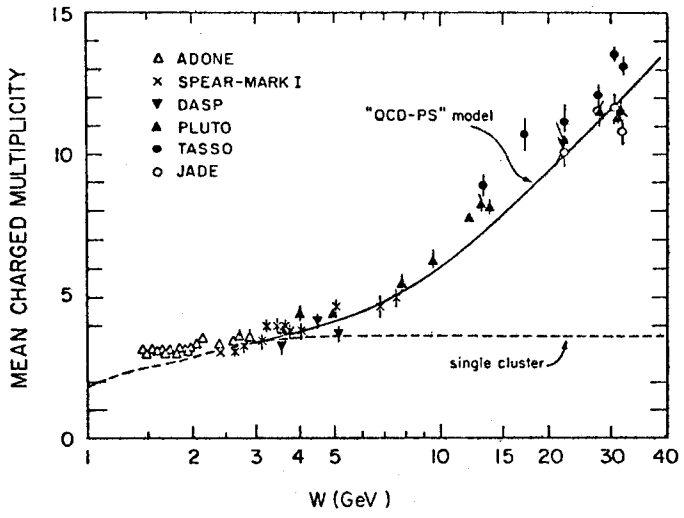

Fig. 4.11. Comparison of the data on the charged particle multiplicity in e^+e^- annihilations (Ref. 20) and results from the "QCD-PS" model. The dashed curve is the charged particle multiplicity resulting from the "decay" of a single cluster of invariant mass W in the "QCD-PS" approach.

C. Heavy quarks

Unfortunately, in e^+e^- annihilations one cannot compare a QCD model of the hadron final states without including a model for heavy quark production and fragmentation. It is even more unfortunate that heavy quarks tend to produce hadron final states that have a larger mean transverse momentum which is precisely the effect of adding the production of gluons to the light quark $q\bar{q}$ states. In addition, the decay of a heavy quark system can look like a three or four jet event. Thus, it becomes a tricky business to decide how much of the deviation of the large energy e^+e^- data from the naive FF-model is due to QCD gluons and how much is due to the production of the heavy quarks c and b. I will describe briefly the model I have used for the production and decay of heavy quarks. I have not yet checked how precisely the approach reproduces the data at, say, the upsilon mass.

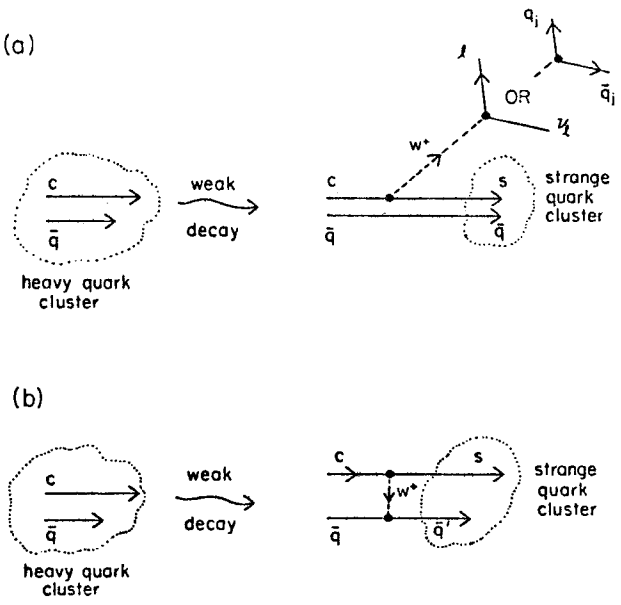

Fig. 4.12. Illustration of the model used for the "decay" of a heavy quark cluster (in this case a charm quark). (a) Illustrates the case where the charm quark decays weakly into an s-quark and a W+ boson which subsequently decays into either a lepton-antilepton pair or a quark-antiquark pair. The remaining strange quark cluster is allowed to decay according to the "QCD-PS" prescription. (b) Illustration of the case where the charm quark exchanges a W boson with the spectator quark resulting in a strange quark cluster which is then allowed to decay according to the "QCD-PS" prescription.

As explained by S. Wolfram[13] the parton Monte-Carlo model is easily generalized to include the production of heavy quarks. The cut-off parameter μ_c is replaced by

$$\mu_c^q = m_q + \mu_c \tag{4.5}$$

where q is a heavy quark with mass m_q. Clusters containing a heavy quark are more massive since their invariant mass will always be at least as large as the mass of the heavy quark, m_q.

The question is, "How do these heavy clusters decay into hadrons?". One way would be to use a model similar to (4.3) above but where M_1 or M_2 are mesons containing the heavy quark. One would then have to decay these mesons (i.e., the D's and D*'s) according to the known decay modes and guess at the unknown decay modes. I have not done this. Instead, I have used a model for the "decay" of these heavy quark clusters that is illustrated in Fig. 4.12.

In this approach one forms color singlet strings (or clusters) just as in the "QCD-PS" model. The light quark clusters are allowed to "decay" as described in Section IV-B above. The heavy quark clusters are allowed to undergo a weak decay in which, for example, the c-quark emits a W+ boson and becomes an s-quark. If the original heavy quark cluster was not electrically neutral then the situation is as in Fig. 4.12a and the W+ subsequently decays into either a lepton-antilepton pair (with probability 0.4) or a light $q\bar{q}$ pair (with probability 0.6). Any new $q\bar{q}$ pairs are treated just as an initial $q\bar{q}$ produced by the virtual photon. The resulting strange quark cluster in Fig. 4.12a "decays" according to the phase-space model in (4.3). The invariant mass distribution of the virtual W+ and the z-distribution of the remaining s-quark is generated according to perturbation theory.

If the heavy quark cluster is electrically neutral then there are two possibilities. The cluster may undergo either a weak decay according to Fig. 4.12a or the W+ could be reabsorbed by the spectator quark producing a strange quark cluster as in Fig. 4.12b. We have an adjustible parameter that specifies the relative probability of each. For the charm quark we have adjusted this parameter so the neutral $c\bar{q}$ clusters always proceed via Fig. 4.12b. Whereas, for the b-quark we have selected the parameter so that neutral $b\bar{q}$ clusters always decay according to Fig. 4.12a. In addition b-quarks are assumed to "cascade" to a strange quark by first emitting a W- becoming a charm quark and then emitting a W+. I must do more work before I can say how well this approach actually reproduces the data on heavy quarks.

D. Some e^+e^- observables

Let us now examine some comparisons with data. Keep in mind that I have not included any acceptance corrections nor have I included correction due to the emission of photons by the incoming e^+e^- pair (i.e. radiative corrections). Both these corrections are imortant if one wants to "finely tune" things so as to fit the data perfectly. Right now I am only interested in seeing if such an ambitious approach like the "QCD-PS" model has any chance at all in describing the data.

The first point that must be checked is whether a model in which one inputs only spherically symmetrical hadron states in the string CM frame (i.e., cluster rest frame), like the "QCD-PS" approach, can reproduce the dominant two-jet nature of the data. At first sight one may worry that the model might produce events that are too spherically symmetric. The great majority of the e^+e^- data resemble two jets. One finds that this is also true of the "QCD-PS" approach. For the great majority of events the gluons are not hard. They are along the direction of the initial quark or antiquark. Thus even though one is producing spherically symmetric subsystems in the cluster rest frame, when these subsystems are Lorentz boosted back to the e^+e^- CM frame the hadrons are also along the direction of the initial quark or antiquark and the event looks like two jets. I find this result quite pleasing. In a way it means that the two-jet nature of e^+e^- annihilations is predicted by perturbative QCD. The "QCD-PS" model produces two jet events that are not too different from the FF parameterization.

Occasionally at early times a gluon will be produced at large angles. Subsequent gluons will be at small angles with respect to the quark, antiquark, and the hard gluons resulting in a "three-jet" event. Similarly, but with even less likelihood, one may get two large angle gluons and a "four-jet" event, etc. In the version of the parton shower Monte Carlo that I use here, the exact "three-parton" matrix element is used. All states with more than one gluon are arrived at by use of the "leading pole approximation" explained in Section III. In addition I have used the gluon "splitting function" in (4.2b) (i.e. uniform distribution).

I used the following procedure in determining the cut-off parameter μ_c and the scale parameter Λ. First, I decided on a particular scheme for parameterizing the cluster "decay". Then, I adjusted μ_c and Λ to fit the observed charged particle multiplicity and transverse momentum distributions. I find it necessary to choose quite a large value for Λ. The results presented here for the "QCD-PS" model have Λ=1.4 GeV. This large value of Λ results from the use of the string picture which, as explained in Section III-A, produce events that more closely resemble "two-jets" than models that fragment in the e^+e^- CM frame. The "QCD-PS" model will produce events that are too "two-jetty" unless one increases Λ to a large value. (This is also true of the "QCD-FF-string" model.)

At this stage I don't think the fact that the string picture requires a large Λ means that it is wrong. I believe that both μ_c and Λ should be considered as free parameters. We have already included a particular set of subleading logs because of the manner in which the parton showers are generated.

Changing Λ also affects the subleading loss and it is not clear to me that under these circumstances we know what the best value of Λ to use is.

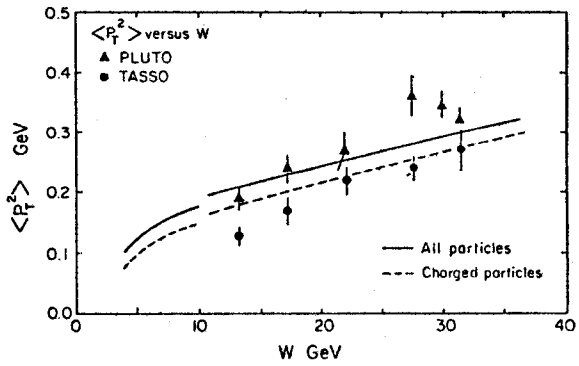

Fig. 4.13. Comparison of the data on the mean squared transverse momentum of charged hadrons in e^+e^- annihilations at a CM energy W (Ref. 21) and the results of the "QCD-PS" model.

(1.) Transverse momentum distributions

There are many observables in an e^+e^- event that one can examine. One of the simplest and most significent is the transverse momentum distribution relative to, say, the thrust axis. Fig. 4.13 shows the mean square transverse momentum versus the e^+e^- center of mass energy, W=Q, from both the data and the "QCD-PS" Model. In Fig. 4.14 I compare the data on the transverse momentum distributions at W=Q=12 and 30 GeV with the "QCD-PS" approach. The agreement, although not perfect, is quite reasonable. I have found no way to explain the large transverse momentum tail that appears at 30 GeV other than by the presence of gluons. Of course, this has already been noticed by many other theorists[6,7] and experimenters.[3-5] However, it also appears that the "QCD-PS" model can fit this phenomena as well as the other approaches.

In Fig. 4.15 I have compared the predictions of the "QCD-PS" Model with the transverse momentum distributions "in" and "out" of the plane at 12 and 30 GeV.[5] Again the agreement is reasonable.

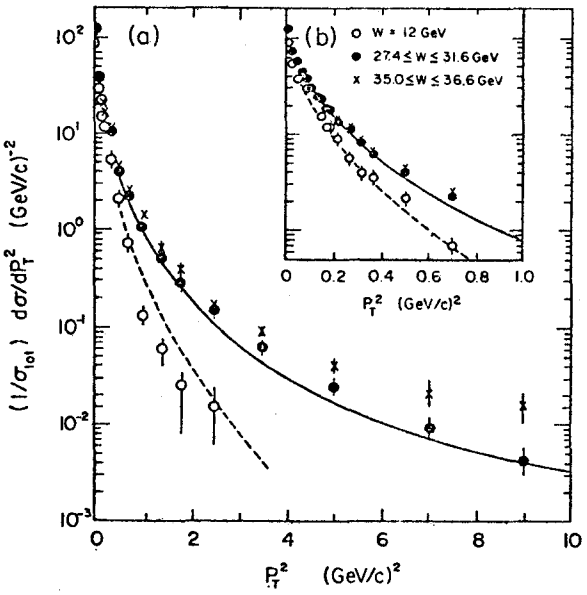

Fig. 4.14. Comparison of the data on the transverse momentum distribution of charged hadrons in e^+e^- annihilations (Ref. 21) and the results of the "QCD-PS" model at W=12 and 30 GeV (solid curves).

(2.) H_ℓ distributions

G. C. Fox and S. Wolfram[9,10] have defined shape parameters, H_ℓ, which are quite useful. For e^+e^- annihilations,

$$H_\ell = \sum_{i,j} \frac{|\vec{P}_i||\vec{P}_j|}{Q^2} P_\ell(\hat{P}_i.\hat{P}_j), \qquad (4.6)$$

where the $P_\ell(\cos\theta)$ are legendre polynomials and where the sum runs over all final hadrons, including the case i=j. For "two-jet"

events $H_{2\ell}$ is approximately one, while for isotropic events H_ℓ is approximately zero.

Fig. 4.16 and 4.17 shows a comparison of the data with the "QCD-PS" Model at W=12 and 30 GeV for the distribution of H_2 and H_4, respectively. Again the agreement is respectible.

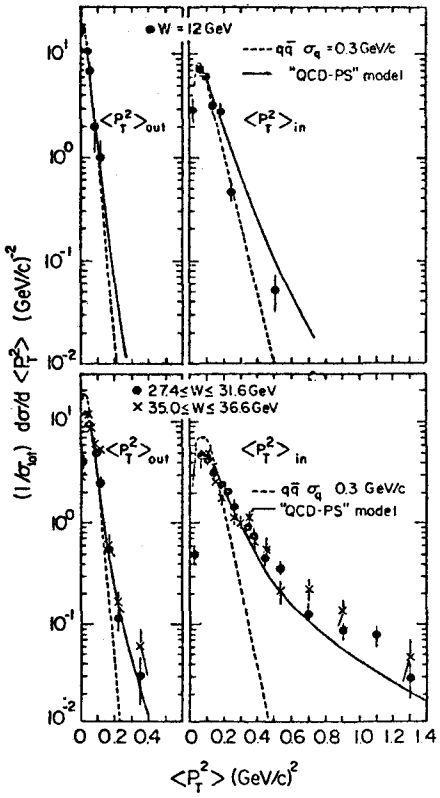

Fig. 4.15. Comparison of the data on the transverse momentum distributions "in" and "out" of the plane in e^+e^- annihilations (Ref. 5) and the results of the "QCD-PS" model at W=12 and 30 GeV (solid curves).

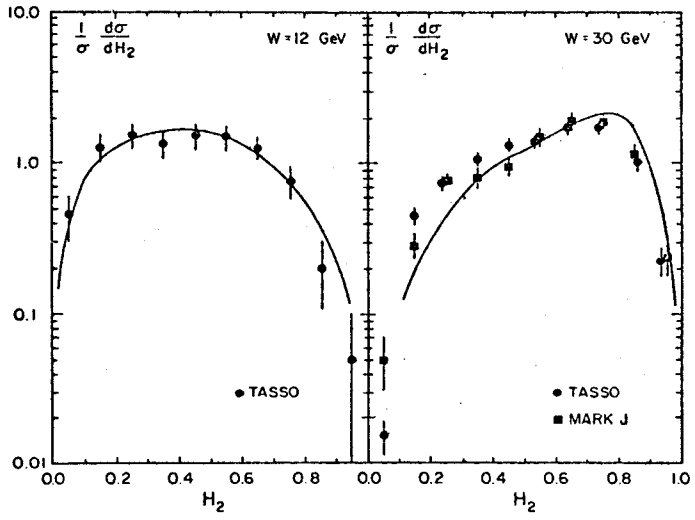

Fig. 4.16. Comparison of the data on the Fox-Wolfram H_2 distribution of hadrons in e^+e^- annihilations (Ref. 3 and Ref. 5) and the results of the "QCD-PS" model at W=12 and 30 GeV (solid curves).

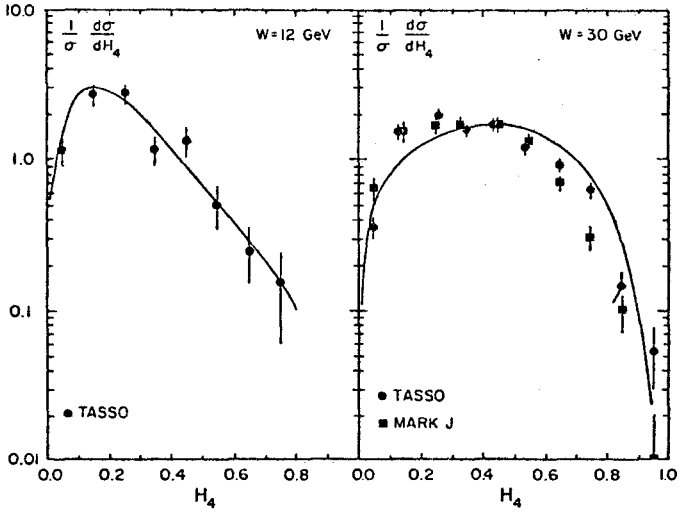

Fig. 4.17. Comparison of the data on the Fox-Wolfram H_4 distribution of hadrons in e^+e^- annihilations (Ref. 3 and Ref. 5) and the results of the "QCD-PS" model at W=12 and 30 GeV (solid curves).

Table 4.1.

Results of the "QCD-PS" model for e^+e^- annihilations at W=Q=4, 6, 11, and 30 GeV, where the cut-off μ_c=1.6 GeV and Λ=1.4 GeV. Mean parton (quark + antiquark + gluon) multiplicities, <N-parton>, and mean cluster multiplicities, <N-cluster>, are given. Also given is the fraction of the total energy carried by gluons, <E-glue>/Q; the average mass per cluster, <M>/cluster; and the percentage of clusters that were parameterized by a single hadron, % cluster=1 had. Hadron observables include the averge multiplicity, <N-had>; the charged multiplicity, <N-charged>; and the baryon multiplicity (proton + neutron), <N-baryon>, (there are of course an equal number of antibaryons). In addition, the average transverse, $\langle p_T$-had$\rangle$, average square transverse, $\langle p_T^2$-had$\rangle$, and average longitudinal, $\langle p_L$-had$\rangle$, momentum of the hadrons with respect to the sphericity axis are shown. Finally, the average sphericity, <S-had>, average thrust, <T-had>, and average H_2, $\langle H_2$-had$\rangle$, of hadrons are presented.

Q	4.0 GeV	6.0 GeV	11.0 GeV	30.0 GeV
<N-parton>	2.4	3.1	4.7	10.3
<E-glue>/Q	0.10	0.18	0.28	0.38
<N-cluster>	2.3	2.8	4.5	9.6
<M>/cluster	1.3 GeV	1.2 GeV	1.1 GeV	0.76 GeV
<N-had>/cluster	2.9	2.8	2.6	2.2
%cluster=1 had	9%	9%	18%	37%
<N-had>	6.5	8.0	11.8	20.7
<N-charged>	3.7	4.6	6.7	11.8
<N-baryon>	0.07	0.05	0.09	0.11
$\langle p_T$-had$\rangle$	0.27 GeV	0.31 GeV	0.36 GeV	0.40 GeV
$\langle p_T^2$-had$\rangle$	0.10 GeV^2	0.13 GeV^2	0.20 GeV^2	0.28 GeV^2
$\langle p_L$-had$\rangle$	0.46 GeV	0.59 GeV	0.76 GeV	1.3 GeV
<S-had>	0.33	0.29	0.24	0.11
<T-had>	0.80	0.83	0.85	0.91
$\langle H_2$-had$\rangle$	0.33	0.38	0.44	0.63

(3.) z-distributions — scale breaking

The "QCD-PS" model has an advantage over some of the earlier models used to fit the e^+e^- data since it automatically incorporates scale breaking within each of the jets it produces. Fig. 4.18 shows a comparison of the predictions of the "QCD-PS" model and the data on s $d\sigma/dz$, where z=2p (hadron)/Q. The data appear to scale, whereas the model exhibits a considerable amount of energy dependence. Now I know why previous models did not need to consider the Q^2 evolution of the jets. The data show almost no Q^2 dependence! I find this very interesting. If one is going to attribute the large transverse momentum tail in Fig. 4.14 to QCD gluons, then one must also observe scale breaking. In QCD you cannot have one without the other.[18]

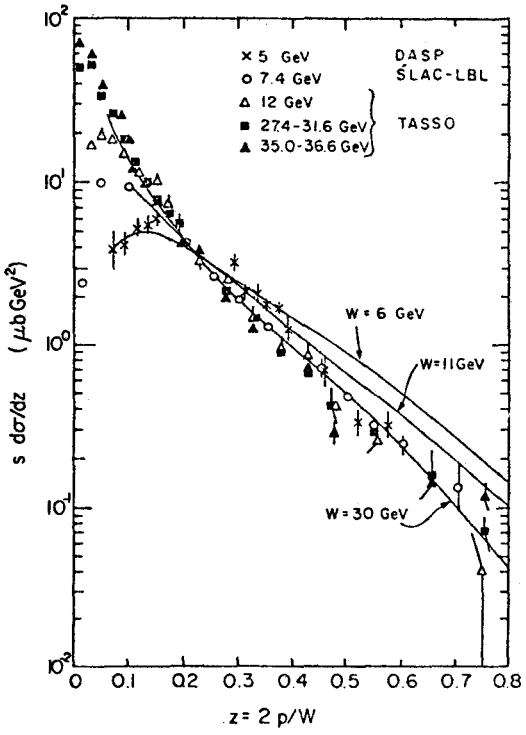

Fig. 4.18. Comparison of the data on the z-distribution of charged hadrons in e^+e^- annihilations (Ref. 20) and the results of the "QCD-PS" model, where z=2p(hadron)/W.

Perhaps the "QCD-PS" model overestimates the amount of scale breaking, since in order to fit the event shapes one needs a large value of Λ which in turn produces a large energy dependence of $s\,d\sigma/dz$. On the other hand, if QCD is indeed responsible for the observed event shapes then one must see some scale breaking. I suggest that the experimenters look for "scale breaking" in a somewhat different manner, one that should produce higher statistics. Let us define

$$N(Q,z_0)=\text{Multiplicity of particles with } z\geq z_0, \tag{4.7a}$$

where

$$z=2p(\text{hadron})/Q, \tag{4.7b}$$

and where p is the magnitude of the hadron momentum. For $z_0>0.5$, $N(Q,z_0)$ should decrease with increasing Q. For example, if we define the ratio of $N(Q,z_0)$ at two different values of Q by

$$R(Q,Q_0,z_0)=N(Q,z_0)/N(Q_0,z_0), \tag{4.8}$$

then Table 4.2 shows that the "QCD-PS" model predicts that $R(Q=30\ \text{GeV},Q_0=11\ \text{GeV},z_0=0.5)=0.72$ for charged hadrons. This is a big effect which could easily be tested experimentally.

Using the methods I presented in a recent summer school lecture,[19] we can deduce an analytic approximation for the ratio in (4.8). Leading order QCD predicts that if the quark "fragmentation" function, $D(Q,z)$ is given by

$$D(Q_0,z)=A(1-z)^r \tag{4.9}$$

at some reference energy, say Q_0, then it becomes

$$D(Q,z)\underset{z\to 1}{\sim}A\,\frac{\Gamma(r+1)}{\Gamma(r+1+\xi(Q))}\,(1-z)^{r+\xi(Q)} \tag{4.10a}$$

at the higher energy, Q, where

$$\xi(Q)=\frac{16}{3\beta_0}\log\{\alpha_s(Q_0^2)/\alpha_s(Q^2)\}, \tag{4.10b}$$

where $\alpha_s(Q^2)$ and β_0 are given by (3.3b) and (3.3c), respectively. (Note that $\xi(Q^2)=8\kappa/3$, where κ is given in (3.2).) The approximation in (4.10) is valid at large z and becomes exact as $z\to 1$. Integrating (4.9) and (4.10) gives

$$R(Q,Q_0,z_0)\underset{z_0\to 1}{\sim}\frac{\Gamma(r+2)}{\Gamma(r+2+\xi(Q))}\,(1-z_0)^{\xi(Q)}, \tag{4.11}$$

which is valid for large z_0.

Table 4.2 gives the results for $R(Q,Q_0,z_0)$ for the anlytic approximation in (4.11). Even for Λ as small as 100 MeV, there is a 20% drop in the charged particle multiplicity above z_0=0.6 between W=11 and 30 GeV. These effects should be experimentally measurable and are very important in establishing the correctness of perturbative QCD.

Table 4.2.

The ratio of the multiplicity of charged hadrons in e^+e^- annihilations with z=2p(hadron)/Q greater than z_0 at CM energy W=Q to that at energy Q_0=6 GeV, $R(Q,Q_0,z_0)$. Results are given for both the "QCD-PS" model with μ_c=1.6 GeV and the analytic approximation in (4.11).

Q(GeV)	QCD-PS model Λ=1.4 GeV z_0=0.5	QCD-PS model Λ=1.4 GeV z_0=0.6	analytic approx. Λ=1.4 GeV z_0=0.6	analytic approx. Λ=0.5 GeV z_0=0.6	analytic approx. Λ=0.1 GeV z_0=0.6
6	1.0	1.0	1.0	1.0	1.0
11	0.61	0.63	0.66	0.77	0.85
30	0.44	0.33	0.40	0.54	0.67
30/11	0.72	0.52	0.61	0.70	0.79

E. Dependence on the cut-off μ_c

If one really had a perfect model for both large and small mass clusters, then predictions presumably would not depend on the cut-off μ_c. Choosing μ_c large would stop the perturbative evolution in Fig. 3.3 at early times and one would have to parameterize the remaining shower and hadron formation by a complicated jet model (like the FF-model). On the other hand, if one choose μ_c small then one might only need a simple (perhaps phase-space model) to describe the remainder of the hadron shower. In fact, if one had a correct parameterization of hadron formation for times greater than $1/\mu_c$, then one could choose any μ_c and the results would be the same (i.e. the predictions would be independent of μ_c).

To test these ideas I have examined a mixed model. Clusters with invariant mass greater than 3.0 GeV are parameterized by two FF jets as in the "QCD-FF-string" model illustrated in Fig. 4.4. Clusters with a smaller invariant mass are parameterized by the "QCD-PS" approach illustrated in Fig. 4.10. I call this approach

the "QCD-FF-PS" model. To save computer money I have included only the pseudoscalar, vector, and tensor nonets in (4.3). A comparison of Table 4.1 and Table 4.3 shows that this makes little difference at W=30 GeV. In addition Table 4.3 shows that, although there is some dependence on μ_c, the dependence is not great. For example, at W=30 GeV the "QCD-FF-PS" model gives a charged multiplicity of 10.4 with μ_c=7.1 GeV, while the pure phase space approach with μ_c=1.6 GeV gives 11.2. For the former 48% of the clusters, on the average, were parameterized by the FF model, while the latter contained no FF jets. The cluster mass distribution for both extremes are shown in Fig. 4.9. There are many low mass clusters even with a large value of μ_c due to the heavy quark decay model used (see Section IV-C).

I am encouraged by these findings, but I am worried about the large value of Λ necessary in the string approach. I should also point out that, since the average cluster invariant mass decreases with increasing energy, the "QCD-FF-PS" model becomes equal to the "QCD-PS" model at high energy.

Table 4.3.

Results of the "QCD-FF-PS" model and the "QCD-PS" model for e^+e^- annihilations at W=Q=30 GeV with Λ=1.4 GeV and where only pseudoscalar P, vector V, and tensor T, mesons in (4.3) have been included. The observables are the same as Table 4.1 except that <N-FF> is the average number of clusters that are parameterized according to the FF prescription (i.e. clusters with invariant mass greater than 3.0 GeV).

	QCD-FF-PS model PVT-only	QCD-FF-PS model PVT-only	QCD-FF-PS model PVT-only	QCD-PS model PVT-only
μ_c	7.07 GeV	3.16 GeV	2.0 GeV	1.6 GeV
$\langle N^c$parton$\rangle$	2.5	4.4	7.2	10.3
<E-glue>/Q	0.09	0.24	0.32	0.38
<N-cluster>	2.5	4.1	6.7	9.6
<N-FF>	1.2	1.1	0.45	0.0
<M>/cluster	6.6 GeV	2.6 GeV	1.2 GeV	0.76 GeV
<N-had>/cluster	7.3	4.0	2.5	2.1
<N-had>	18.5	16.5	16.9	19.7
<N-charged>	10.4	9.3	9.5	11.2
$\langle p_{T_2}$-had$\rangle$	0.39 GeV^2	0.48 GeV^2	0.45 GeV^2	0.42 GeV^2
$\langle p_T$-had$\rangle$	0.27 GeV^2	0.40 GeV^2	0.36 GeV^2	0.31 GeV^2
$\langle p_L$-had$\rangle$	1.36 GeV	1.47 GeV	1.53 GeV	1.37 GeV
<S-had>	0.10	0.13	0.10	0.11
<T-had>	0.91	0.90	0.91	0.91
$\langle H_2$-had$\rangle$	0.62	0.60	0.64	0.63

F. Extrapolation to High Energy Jets

The next step is to extrapolate each of the above jet models to high energy and to compare the results. I have not had the time to do this yet, however, I do have some results from the "QCD-PS" model at Q = 100 GeV (i.e., 50 GeV jets). The cross section for producing jets with 50 GeV P_T in proton-proton collisions is quite large at Isabelle energies as will be examined in Section V.

Table 4.4 shows the average properties of a W = Q = 100 GeV e^+e^- event resulting from the "QCD-PS" approach. On the average an event contains about 40 particles 22 of which are charged. The average properties in Table 4.4 do not really give one a feeling of what 50 Gev jets look like. Fig. 4.19 and 4.20 show selected events at W = 100 GeV. In my opinion careful examination of these events reveals more about the nature of high energy jets than does the averages in Table 4.4. The event in Fig. 4.19 originated from a $c\bar{c}$ quark pair and contais $c\bar{c}+d\bar{d}+s\bar{s}+14$ gluons. The event is somewhat less "two-jetty" than the average. It has a thrust of 0.91 where the average at W = 100 GeV is 0.94. The event in Fig. 4.20 contains a $d\bar{d}$ quark pair plus 28 gluons and is somewhat mole "two-jetty" than the average (thrust = 0.955).

One quantity that helps give a feeling of what high energy jets look like is the maximum P_T in the event. This is shown in Table 4.5 together with the fraction of events with P_T-max less than 1,2,3 and 4 GeV. At W = 30 GeV 90% of the events have P_T-max less than 2.0 GeV, whereas at W = 100 GeV 62% of events are contained within P_T-max < 2.0 GeV. Even at W = 100 GeV 75% of all events are contained within P_T-max < 3.0 GeV. This means that 75% of the time the event has 100 GeV of energy completely contained within a cylindrical tube of radius 3.0 GeV.

Although the jets at W = 100 GeV are quite spectacular they are much softer and much more spread out than are the jets of the FF model. Table 4.6 shows that at W = 100 GeV there are only 2.1 particles, on the average, with momentum greater than 10 GeV. The average longitudinal momentum of a particle in 100 GeV e^+e^- annihilations is only 2.3 GeV, whereas $\langle P_T \rangle$ = 0.49 GeV (see Table 4.4). In spite of this softness, these jets should stand out clearly in pp collisions at Isabelle energies.

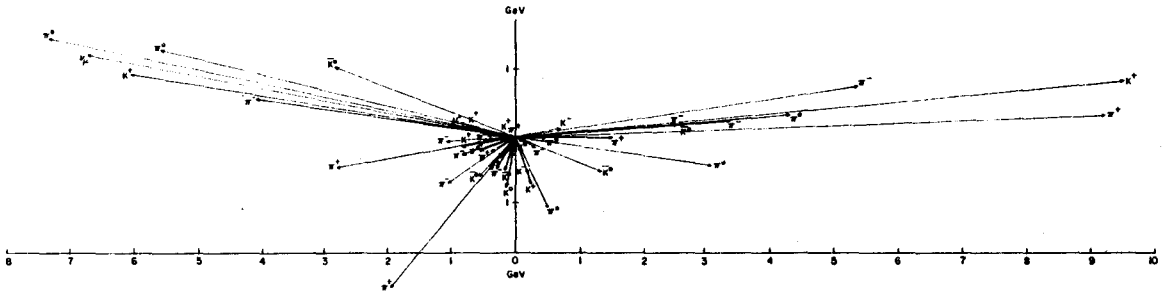

Fig. 4.19. An e^+e^- event at W=100 GeV from the "QCD-PS" model. The event contains a $\bar{c}c$, $\bar{d}d$, and $\bar{s}s$ quark pair together with 14 gluons resulting in 47 particles with 32 charged (π^0=7, π^+=10, π^-=12, K^+=6, K^0=2, K^-=3, $\bar{K}^0$=5, ν_μ=1, μ^-=1). In addition, the event has T=0.91, S=0.08, H_2=0.64, $\langle p_t^2 \rangle$=0.56 GeV^2, $\langle P_t^2\text{-out} \rangle$=0.13 GeV^2, and $\langle P_t^2\text{-in} \rangle$=0.43 GeV^2, which can be compared to an average event in Table 4.4.

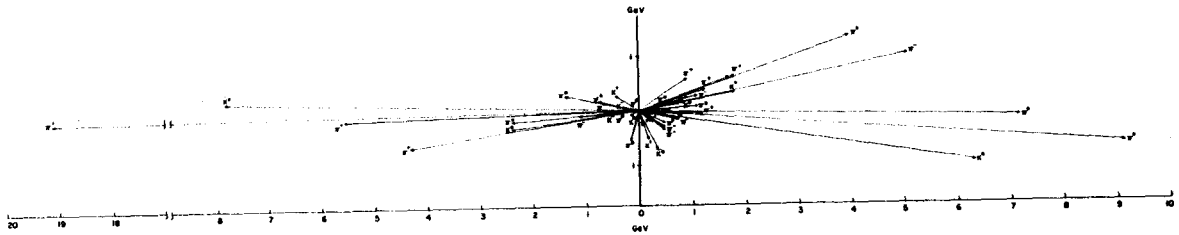

Fig. 4.20. An e^+e^- event at W = 100 GeV from the "QCD-PS" model. The event contains a $d\bar{d}$ quark pair together with 28 gluons resulting in 46 particles with 26 charged (π^o=13, π^+=9, π^-=10, K^+=4, K^o=3, K^-=3, K^o=4). In addition, the event has T = 0.96, S = 0.02, H_2 = 0.80, $\langle p_T^2 \rangle$ = 0.23 GeV^2, $\langle p_T^2\text{-out} \rangle$ = 0.06 GeV^2, and $\langle p_T^2\text{-in} \rangle$ 0.16 GeV^2, which can be compared to an average event in Table 4.4.

Table 4.4

Results of the "QCD-PS" model for e^+e^- annihilation at W=100 GeV, where the cut-off μ_c=1.6 GeV and Λ=1.4 GeV. The observables are the same as in Table 4.1.

<N-parton>	23.8
<N-cluster>	22.6
<M>/cluster	0.51 GeV
<N-had>/cluster	1.7
<N-had>	40
<N-charged>	22
$<P_t$-had>	0.49 GeV
$<P_t^2$-had>	0.66 GeV^2
$<P_L$-had>	2.3 GeV
<S-had>	0.06
<T-had>	0.94
$<H_2$-had>	0.75

Table 4.5

Results of the "QCD-PS" model for the maximum P_T of particles produced in an e^+e^- annihilation, where P_T is measured relative to the sphericity axis. Also given are the percentage of events with P_T-max less than 1,2,3, and 4 GeV.

	W=11 GeV	W=30 GeV	W=100 GeV
$\langle P_T\text{-max}\rangle$	0.83 GeV	1.2 GeV	2.2GeV
% events with P_T-max <1.0 GeV	75.5%	47.8%	25%
<2.0 GeV	99.6%	90.0%	62%
<3.0 GeV	100%	97.8%	75%
<4.0 GeV	-	99.6%	85%

Table 4.6

Results of the "QCD-PS" model for the multiplicity of particles with $z \geq z_0$, where z=2 p(had)/W.

z_0	W=11 GeV	W=30 GeV	W=100 GeV
0.0	11.8	20.7	39.8
0.1	6.7	6.3	5.2
0.2	3.4	2.7	2.1 (p=10 GeV)
0.3	1.8	1.3	0.90
0.4	0.93	0.64	0.44 (p=20 GeV)
0.5	0.48	0.30	0.26
0.6	0.25	0.12	0.05
0.7	0.12	0.04	0.03
0.8	0.05	0.01	0.01
0.9	0.007	0.001	-

V. The Rate for Producing Jets in pp Collisions at High Energy

A. Leading Order QCD Predictions

The jets in Fig. 4.19 and 4.20 are quite spectacular and should be easy to study in pp or $\bar{p}p$ collisions at high energy. I would like now to examine the question of the rate for these jets in pp collisions at Isabelle energies.

The leading order QCD prediction for the production of a jet of type c is given schematically by

$$E\, d\sigma/d^3p\,(s,P_T,\theta_{cm}) = \sum_{a,b} \int dx_a\, G_{A\to a}(x_a,Q^2)\, G_{B\to b}(x_b,Q^2)$$

$$(1/\pi)\, \hat{d\sigma}/\hat{dt}\,(\hat{s},\hat{t},Q;a+b\to c+d), \qquad (5.1)$$

where $G(x,Q^2_{\hat{}})$ are the "renormalization group improved" parton distributions and $d\sigma/dt$ is the differential cross section for parton-parton scattering $a+b\to c+d$, which is proportional to $\alpha_s^2(Q^2)$. The parton distributions are known fairly well. On the other hand, $\alpha_s(Q^2)$ is not known very precisely (i.e., we do not have a good determination of x).

It is interesting that the predictions for the jet cross section in Fig. 5.1 are not very sensitive to the precise value of Λ. This is due to two competing effects in equation (5.1). Although at fixed Q^2 the jet rate is proportional to $\alpha_s^2(Q^2)$, the extrapolation from low Q^2 is not that sensitive to $\alpha_s(Q^2)$. If $\alpha_s(Q^2)$ is large then there is more scale breaking in $G(x,Q^2)$ and thus less partons with high x within the proton at high Q^2. On the other hand, the parton cross section, $\hat{d\sigma}/\hat{dt}$, is large because $\alpha_s(Q^2)$ is large. If $\alpha_s(Q^2)$ is small then the parton cross section, $d\sigma/dt$, is small but there is less scale breaking in $G(x,Q^2)$ and thus more high x partons. Because of this the jet cross section of $W=\sqrt{s}=500$ GeV is relatively stable to changes in Λ. This means that one will not be able to use jet rate measurements to determine Λ, but it also means that the large rates predicted in Fig. 5.1, Fig. 5.2, and Fig. 5.3 should be observed. If they are not seen then QCD will be in a bit of trouble!

From Fig. 5.2 it is seen that at W=775 GeV the rate for producing jets with P_T greater than 50 GeV is about 100 mb. In phase I Isabelle should see about 7,200 events per hour with $P_T \geq 50$ GeV. This is quite a healthy rate and one should be able to perform detailed jet studies.

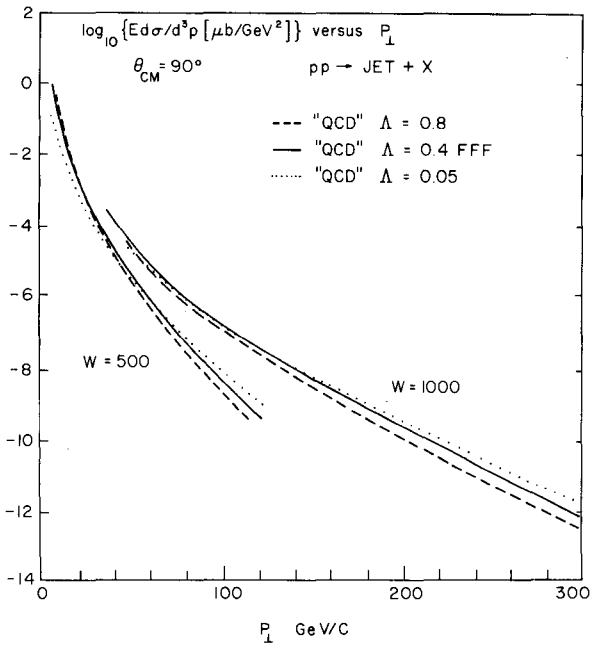

Fig. 5.1. Leading order QCD predictions of $Ed\sigma/d^3p$ for $pp \rightarrow Jet+X$ at $\theta_{cm}=90^\circ$ and $W=\sqrt{s}=500$ and 1000 GeV. Results are presented for $\Lambda=0.05$, 0.4, and 0.8 GeV.

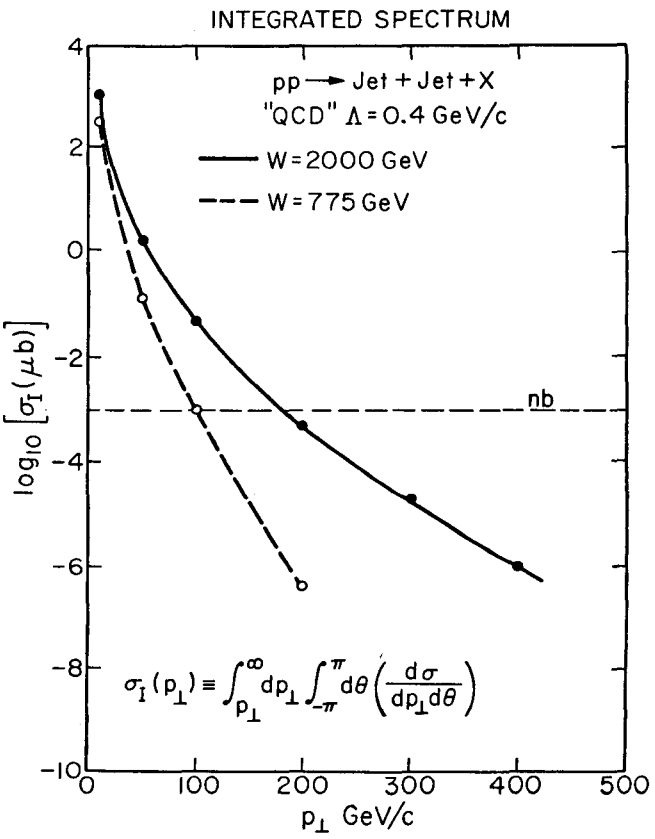

Fig. 5.2. Leading order QCD predictions for the integrated spectrum in pp→Jet+X at $W=\sqrt{s}=775$ and 2000 GeV.

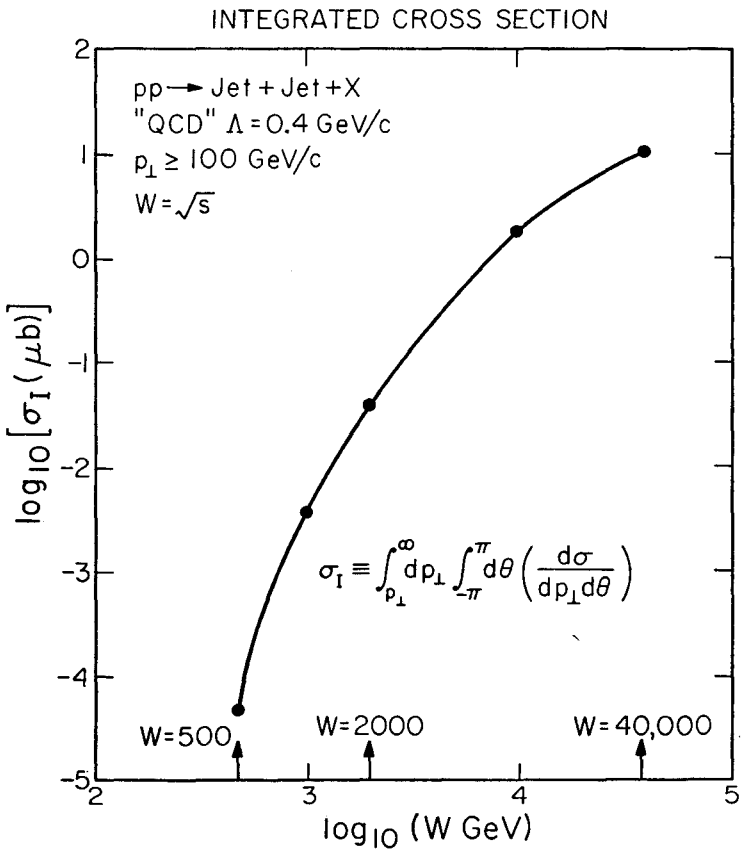

Fig. 5.3. Leading order QCD predictions for the total rate for producing jets with P_t greater than 100 GeV versus $W=\sqrt{s}$.

B. Monte-Carlo Model for Complete pp and $\bar{p}p$ Events

Geoffrey Fox has recently modified the parton shower Monte-Carlo model described in Section III to include the case where the partons are in the initial state (i.e., the Q^2 spacelike case). We should now be able to generate realistic pp and $\bar{p}p$ large P_T events like that shown in Fig. 5.4. In the initial state a parton of approximately zero mass radiates gluons and steadily gains invariant mass (i.e., becomes off-shell). It then undergoes a hard collision described by the appropriate two-to-two matrix element. The final state is described by the parton shower model just like e^+e^- annihilations.

The shower in the initial state is not only responsible for the scale breaking of the parton distributions within the initial hadrons but also causes the center-of-mass of the hard parton-parton collision to obtain some transverse momentum. This approach should allow us to study more precisely how transverse momentum is balanced in an event as well as to examine multijets produced at large P_T. I plan to pursue and develop this Monte-Carlo approach for pp and $\bar{p}p$ collisions within the next year. I am particularly interested in questions concerning trigger bias.

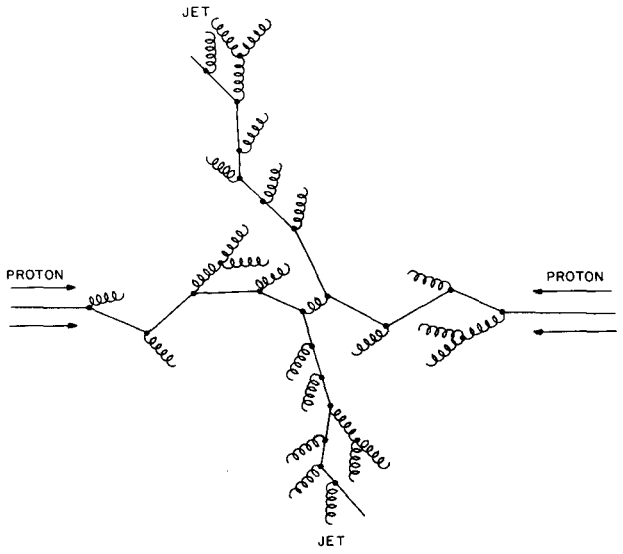

Fig. 5.4. Illustration of a large P_t event in proton-proton collisions. There is a parton shower in the initial state followed by a hard scattering. The final state is described by a parton shower analogous to e^+e^- annihilations (see Fig. 3.3).

VI. Summary and Conclusions

There have been many excellent papers, both experimental and theoretical, on applications of QCD to e^+e^- annihilations. I have purposefully not studied the literature in detail. I thought that it might be fruitful to perform an independent analysis of the data. For the most part my findings are the same as others. The data at energies greater than about W=10 GeV definitely begin to deviate from the naive FF-jet model. In addition, the discrepancy between the data and the FF model is in the direction expected from perturbative QCD. However, I do not feel that theoretical predictions in the existing energy range are as precise as some of the published papers would lead us to believe. Furthermore, I do not think we can be sure what events at, say W=100 GeV, will look like. The extrapolation of existing fits could be misleading.

A precise prediction from perturbative can be made only if the results are not sensitive to the assumed model for the manner in which the outgoing quarks, antiquarks, and gluons become the observed hadrons. My findings indicate that, over the existing energy range, predictions are sensitive to the particular hadronization model assumed. More work must be done before one can say whether the "QCD-PS" model is any "better" than the other models which are based on the FF prescription. In any case it is important to try different hadronization schemes. Only in this way can one tell if the measuring of a particular observable tests perturbative QCD or whether it gives us information about the manner in which quarks and gluons turn into the observed hadrons. Both are interesting.

I am certain, that with what we now know, we should be able to come up with a model for e^+e^- annihilations that is more closely connected to perturbative QCD than the FF prescription. The "QCD-PS" model is an attempt to do this. It is based on perturbative QCD in the leading pole approximation together with a simple phase-space scheme for the "decay" of color singlet clusters of partons. The model conserves energy, momentum, and charge on an event by event bases. In addition, it includes (in an approximate manner) the production of two, three, four, ..., etc. jets. The results presented here are encouraging. However, more work needs to be done. I am a bit leary about taking perturbation theory all the way down to $t_c/\Lambda^2=1.53$, which corresponds to $\alpha_s(t_c)\gtrsim 3.8$! For this reason the "QCD-PS" approach must be considered a model and not a theory.

The "QCD-PS" model can be used to extrapolate to high energies and examine the nature of jets. Jets with energies greater than about 50 GeV are quite spectacular even though they are much softer and much more spread out than FF-jets. The production rate for jets with P_T's greater than 50 GeV in pp collisions is quite large at Isabelle energies which should allow for detailed studies.

Finally, let me say that I believe QCD or something very similar to QCD is the correct theory of strong interactions. Scientifically, however, I do not feel that we have proven it to be correct. All data appear consistent with QCD, but calculations are not precise enough to prove its validity. I believe that the next generation experiments are crucial and I look forward to the data. Maybe there will even be some surprises.

Acknowledgements

This work was done in collaboration with Geoffrey Fox and Stephen Wolfram. I would like to thank Steve Ellis, and R. P. Feynman for useful discussions. In addition, I would like to thank both the MARK-J group and the TASSO group for giving me their preliminary results for the Fox-Wolfram H_ℓ distributions. After completing this work I found a paper by R. Odorico[22] in which he examines a parton shower Monte-Carlo model similar to the one by Fox and Wolfram. Finally let me congratulate the organizers on a most fruitful and enjoyable Isabelle Summer Workshop.

Footnotes and References

1. R.D. Field and R.P. Feynman, Phys. Rev. D15, 2590 (1977); Nucl. Phys. B138, 1 (1978).

2. Ch. Berger et al., (PLUTO-Collab.), Phys. Lett. 82B, 449 (1979). D.P. Barber et al., (MARK-J-Collab.), Phys. Lett. 85B, 463 (1979); Phys. Rev. Lett. 43, 830 (1979). R. Brandelik et al., (TASSO-Collab.), Phys. Lett. 86B, 243 (1979). Ch. Berger et al., (PLUTO-Collab.), Phys. Lett. 88B, 171 (1979).

3. D.P. Barber et al., (MARK-J-Collab.), Phys. Lett. 89B, 139 (1979). H. Newman (MARK-J-Collab.), invited talk given at the XXth International Conference on High Energy Physics, University of Wisconsin, Madison, 1980. P. Duinker, "Review of Electron-Positron Physics at Petra", DESY 81-012 (1981).

4. V. Hepp (PLUTO-Collab.), "Pluto Results on Jets and QCD", Talk given at the XXth International Conference on High Energy Physics, University of Wisconsin, Madison, 1980. Ch. Berger et al., (PLUTO-Collab.), Phys. Lett. 97B, 459 (1980).

5. S.L. Wu (TASSO-Collab.), invited talk at the XXth International Conference on High Energy Physics, University of Wisconsin, Madison, 1980. R. Brandelik et al. (TASSO-Collab.), Phys. Lett. 94B, 437 (1980).

6. P. Hoyer et al., DESY 79/21 (unpublished). P. Hoyer et al., Nucl. Phys. B161, 349 (1979).

7. A. Ali et al., Phys. Lett. 82B, 285 (1979); DESY 79/54. A. Ali, E. Pietarinen, G. Kramer, and J. Willrodt, DESY 79/86 (1979). A. Ali, Z. Physik C1, 25 (1979). A. Ali et al., Z. Physik C1, 203 (1979).

8. B. Anderson and G. Gustafson, Lund Preprint, LU TP79-2 (1979). B. Anderson and G. Gustafson, Z. Physik C3, 223 (1980).

9. Georffrey, C. Fox and Stephen Wolfram, Phys. Rev. Lett. 41, 1581 (1978); Nucl. Phys. B149, 413 (1979); Phys. Lett. B82, 134 (1979).

10. Geoffrey C. Fox and Stephen Wolfram, "A Gallimaufry of E^+e^- Annihilation Event Shapes", CALT-68-723 (1979) unpublished.

11. Geoffrey C. Fox and Stephen Wolfram, "A Model for Parton Showers in QCD", CALT-68-755 (1980), Nucl. Phys. B (to be published).

12. Stephen Wolfram, "Jet Development in Leading Log QCD", CALT-68-740 (1979) unpublished.

13. Stephen Wolfram, "Parton and Hadron Production in e^+e^- Annihilation", CALT-68-778, invited talk presented at the XV Rencontre de Moriond, March 1980.

14. The parton shower model presented here is quite similar to the "jet calculus" approach of Konishi, Ukawa, and Veneziano. K. Konishi, A. Ukawa and G. Veneziano, Nucl. Phys. B157, 45 (1979); Phys. Lett. 80B, 259 (1979).

15. Consider the "decay" of parton 1 into two partons, 2 and 3. For the z of the final partons to be maximal, they must have zero invariant mass. In this case, parton 2 has $z_2=(E_2+|\vec{p}_2|)/(E_1+|\vec{p}_1|)=2E_2/(E_1+|\vec{p}_1|)$. By energy conservation, $E_2=E_1-E_3<E_1$, and hence $z_2<2E_1/(E_1+|\vec{p}_1|)=1-(E_1-|\vec{p}_1|/E_1+|p_1|) =1-t_1/z_1^2Q^2) <1$, where z_1 is the $E+|\vec{p}|$ fraction for parton 1 with respect to the original γ momentum (see Fig. 3.2b). Since $t_1>\mu_c^2$, the soft diver gences in P(z) in (2.34) for gluon emissions are always avoided.

16. The strict ordering of the invariant masses in, Say Fig. 2.5a, (i.e. $Q^2>t_1>t_2...>t_n>t_c$) implies that the angles of gluon emissions are approximately ordered $\theta_1>\theta_2>...>\theta_n$. Large angle emissions occur early in the chain.

17. Strictly speaking color neural systems like $q_a\bar{q}_a$ need not be a color singlet. There are, for example, color neutron members of an octet. I have assumed here all the color neutral strings are color singlets.

18. Analytic calculations of he scale breaking of the quark fragmentation functions were presented in my Boulder lectures (Ref. 19) and in my Tokyo talk; R.D. Field, "Dynamics of High Energy Reactions", invited talk presented at the XIXth International Conference on High Energy Physics, Tokyo, 1978. See also, J.A. Hassan, "A Parameterization of the Scaling Violations to the Quark and Gluon Fragmentation Functions", University of Manchester Preprint M/C TH 80/32.

19. R.D. Field, "Perturbative Quantum Chromodynamics and Applications to Large Momentum Tranfer Processes", lectures given at the Boulder Summer School, University of Colorado, 1979; published by Plenum Press, Nato Advanced Study Institutes Series B, ed. K.T. Mahanthappa and J. Randa, 1980.

20. D. Pandoulas, Invited talk at the High Energy Conference (Wisconsin), 1980. R. Brandelik et al., (TASSO-Collab.), Phys. Lett. 94B, 444 (1980).

21. Ch. Berger et al., (PLUTO-Collab.), Phys. Lett. 81B, 410 (1978); 86B, 413 (1979); 86B, 418 (1979). R. Brandelik et al., (TASSO-Collab.), Phys. Lett. 83B, 261 (1979); 86B, 243 (1979); 89B, 418 (1980).

22. R. Odorico, Nucl. Phys. B172, 157 (1980).

STATUS OF PERTURBATIVE QCD

A.H. Mueller

Brookhaven National Laboratory
and
Columbia University*

I. INTRODUCTION

Over the past few years we have witnessed an enormous increase in our ability to calculate high energy processes from perturbative QCD.[1] In general one is able to calculate the energy dependence of certain measurable quantities in a process where a large momentum transfer occurs. In some cases, when the process is sufficiently inclusive, a complete calculation, including normalization, is possible. In this talk I would like to review some well known results very briefly and then discuss in some detail two processes which may soon be among those over which we have calculational control.

II. CLASSIC TESTS (OLD HAT)

A. $e^+e^- \to$ hadrons

A measurement of the total cross section for e^+e^- to go into hadrons is the simplest example of a quantity which is calculable in perturbative QCD at high energies. If we define $R = \sigma_{e^+e^- \to \text{hadrons}}/\sigma_{e^+e^- \to \mu^+\mu^-}$, then QCD tells us that

$$R = 3 \sum_F e_F^2 \left(1 + \alpha/\pi + C(\alpha/\pi)^2 + \ldots\right) \qquad (1)$$

The constant C is scheme dependent, but small in any reasonable renormalization scheme. The values one obtains for C are always of order 1. Experimentally $R \lesssim 3.97 \pm 0.06$[2] with a systematic error that may be as large as 0.4.

---

*Permanent Address

Theoretically $R \gtrsim 3.67\ (1+\alpha/\pi)$ which is in good agreement with the experimental value. This agreement of R between theory and experiment is an excellent test of asymptotic freedom, but as yet it does not furnish a good test of the radiative corrections in QCD.

B. Deeply Inelastic Scattering

QCD gives a good fit to the Q^2 dependence of νW_2 in electron, muon and neutrino scattering. I think the best test of QCD in these processes is the agreement between the ratios of anomalous dimensions and the data as extracted from a Perkins' plot.

III. PRETTY FIRM QCD PREDICTIONS

A. Jets in e^+e^- Annihilation

There are many theoretically clean results in e^+e^- annihilation. For example $d\sigma/dT$, $d\sigma/dEd\delta$, energy correlations, etc. So far the analysis of the data has needed a lot of noncalculable input such as Feynmann-Field fragmentation functions. The analysis of three jet events is also plagued by a present uncertainty in the size of the higher order QCD corrections.[3]

B. Jets and Single Particle Production in Hadron-Hadron Collisions

Consider the process hadron (p_1) + hadron (p_2) → hadron (p) + X, as illusrated in Fig. 1. It may also be that p represents a jet rather than a single hadron. In principle both jet and single particle cross sections are predictable in QCD. In the case of single hadron production at large transverse momentum this can be seen from Fig. 2.[4] There are four parts to the cross section. (i) The probability of finding a quark, k_1, in the hadron p_1 is determined from deeply inelastic scattering data. (ii) The probability of finding a quark, k_2, in the hadron p_2 is similarly determined. (iii) The "hard part" $k_1 + k_2 \to k + k_4$ is calculated in QCD. (iv) The probability of finding a hadron, p, in the quark k can be taken from e^+e^- annihilation data. There are two difficulties, however. (1) Higher order QCD corrections, though not completely done, appear to be large.[5] (Perhaps this will be like μ-pair production where the large corrections are essential for agreement with the data). (2) Higher twist effects may also be large. In the case of higher twist effects ISABELLE will be a real blessing as such corrections should be much diminished compared to present energies. The particle p may also be a

photon. In this case the photon distribution in a quark and in a gluon should be calculable in leading order. Overall the situation for large p_1 production should be very interesting at ISABELLE. It is even possible that such a process could furnish a striking test of QCD.

C. Hadron Form Factors

In Fig. 3 I have illustrated in very simple terms why one is able to partially determine the Q^2 dependence of elastic form factors.[6] Suppose that $\vec{p}$ is along the positive z-axis while $\vec{p}'$ is along the negative z-axis and that $|\vec{p}| = |\vec{p}'|$. The photon can only turn around a system which is spatially compact. The part of the process on the left hand side of Fig. 3 represents the wave function of the pion becoming a quark-anti-quark pair of size $|\Delta\vec{x}| \sim 1/Q$. The middle portion of the graph represents the hard part of the process where the almost point-like quark-anti-quark pair is turned around. The right hand part of the figure represents the quark-anti-quark pair expanding to fit into the normal pion wave function. The hard part of the amplitude is calculated in lowest order perturbation theory while the contraction of the wave function into an almost point-like system is calculable via the renormalization group as this is a short distance process. The unknown part of the process involves the matching of the renormalization group calculation onto the normal pion wave function. One finds

$$F_\pi(Q^2) \sim 16\pi^2 f_\pi^2 \alpha(Q^2)/Q^2 \left(1 + \sum_{2,4,\ldots} C_n (\ell n\, Q^2/\mu^2)^{-A_n} + \ldots\right). \qquad (2)$$

The A_N are known while the C_n depend on details of the pion wave function.

In the case of the nucleon form factor a similar result holds providing a certain Sudakov suppression occurs. This suppression is likely and should be provable using the techniques of Collins and Soper.[7]

As a theoretical accomplishment I think the work on elastic form factors is most impressive and it is a striking result that QCD perturbation theory can be used to determine such asymptotic behaviors. However, I do not feel that one will get very good tests of QCD from form factor measurements because of the smallness of the amplitude and also because the constants C_N in Eq. 2 are not determined within perturbative QCD.

III. PROCESSES WHERE SUDAKOV EFFECTS ARE PROMINENT

A. Massive μ-pair Production

In the parton model the μ-pair cross section, integrated over transverse momentum, is

$$\int \frac{d\sigma}{d^4q} d^2q_t = \frac{8\pi\alpha^2}{3N_c(Q^2)^2} \sum_F e_F^2 \{x_1 P^F(x_1) x_2 P^{\bar{F}}(x_2) + 1 \to 2\} \tag{3}$$

The dominant corrections in QCD simply add a Q^2 dependence to $P(x)$ so that $P(x) \to P(x,Q^2)$ exactly as in deeply inelastic scattering. The $\alpha(Q^2)$ correction[8] to the above equation gives the "K" factor which brings the theoretical predictions close to the experimental data. Unfortunately, it appears too difficult to do the order $\alpha^2(Q^2)$ effects completely so that the agreement between theory and experiment is possibly fortuitous. At very large values of Q^2 there are two distinct regions where $q_t^2/Q^2 \ll 1$. (i) $q_t^2 \lesssim (Q^2)^{c/1+c}$ where $c = 4c_F/11-2/3\ n_f = 16/25$ for 4 flavors. In this region

$$\frac{d\sigma}{d^4q} \simeq \frac{8\pi\alpha^2}{3N_c(Q^2)^2} \left(\frac{Q^2}{\Lambda^{*2}}\right)^{-c\ell n\ (1+c)/c} \sqrt{\frac{2c\ell nQ^2}{\pi(1+c)^2}} \sum_F e_F^2 \left\{\xi \frac{\partial}{\partial\xi} x_1 P^F(x_1,\xi) \right.$$

$$\left. \zeta \frac{\partial}{\partial z} x_2 P^{\bar{F}}(x_2,\zeta) + 1 \leftrightarrow 2\right\}\Big|_{\zeta=\xi=(Q^2)^{c/1+c}} \tag{4}$$

(ii) $q_t^2 \gtrsim (Q^2)^{c/1+c}$. In this region

$$\frac{d\sigma}{d^4q} \simeq \frac{8\pi\alpha^2}{3N_c(Q^2)^2} \sum_F e_F^2 \frac{q_t^2}{b} \frac{\partial}{\partial q_t^2} \left(x_1 P^F(x_1,q_t^2)\ x_2 P^{\bar{F}}(x_2,q_t^2)\right.$$

$$\left. + 1 \leftrightarrow 2\right) \times e^{-c\left(\ell nQ^2(\ell n\ell nQ^2 - \ell n\ell n\ q_t^2) - \ell n\ Q^2/q_t^2\right)} . \tag{5}$$

The forms given by Equations 4 and 5 depend on detailed Sudakov effects in QCD.[1,7,9] As of yet they are not rigorous consequences of QCD, but the work of Collins and Soper has gone a long distance toward establishing their validity. In principle the formalism of Collins and Soper allows one to calculate

Λ^* and even to calculate corrections to (4) and (5). So far these calculations have not been done.

In Fig. 4 is shown the qualitative q_t^2 behavior of the cross section. The striking feature is that as Q^2 becomes larger the $q_t = 0$ cross section decreases while the q_t distribution becomes flatter. In terms of parton distribution functions determined in deeply inelastic scattering the curves shown in Fig. 4 are completely calculable. However, because of the K-factor that is necessary in the integrated cross section it is important to do the $\alpha(Q^2)$ corrections to (4) and (5).

B. Wide Angle Elastic Scattering

As an example let us discuss π-π scattering. At fixed angle the Brodsky-Farrar counting rules give $d\sigma/dt = 1/s^6\ f(\theta)$ + logarithmic corrections, while the graphs found by Landshoff give $d\sigma/dt = 1/s^5\ f(\theta)$ + logarithmic corrections. It is now likely that the answer is part way between these two predictions[1] and that

$$\frac{d\sigma}{dt} \propto \frac{1}{s^5}\, s^{-4c\ell n\,(1+c)/c} \{(\text{calculable logarithmic s dependence}) \times (\text{calculable } \theta \text{ dependence}) + \text{corrections}\}. \tag{6}$$

As of yet there is no systematic treatment of the corrections to the dominant term, but such a treatment should be possible following Collins and Soper.[7]

IV. SOFT PARTICLE PRODUCTION AND MULTIPLICITY OF HADRONS IN A JET

Let $2Ep\ d\sigma/d^3p$ be the cross section for producing a hadron of any given type in an e^+e^- annihilation. Then

$$\bar{n}\sigma = \int 2E_p \frac{d\sigma}{d^3p} \frac{d^3p}{2E_p} \tag{7}$$

where $\bar{n}$ is the multiplicity of that hadron and σ is the total cross section for $e^+e^- \to$ hadrons. Now $d^3p/2E \propto \pi Q^2/2\ \omega d\omega$ where $\omega = 2pq/Q^2$ so that

$$\bar{n}\sigma = \int_{2P/Q}^{1} 2E \frac{d\sigma}{d^3p}\, \omega d\omega \tag{8}$$

where P is the mass of the particle p. Now for Ren > n_o, with n_o to be specified later,

$$(Q^2)^2 \int_0^1 2E\, d\sigma/d^3p\, \omega^n\, d\omega \underset{Q^2\to\infty}{\to} A_n\, E_n(Q^2) \tag{9}$$

with

$$E_n(Q^2) = e^{\int_{\mu^2}^{Q^2} d\lambda^2/\lambda^2\, \gamma_n(g^2(\lambda^2))} \tag{10}$$

Thus it is tempting to evaluate the Q^2 dependence of $\bar{n}$ from $E_1(Q^2)$. Unfortunately

$$\gamma_n(g^2) = a_1 \frac{g^2}{n-1} + a_2 \frac{(g^2)^2}{(n-1)^2} + \ldots$$

so that one cannot use lowest order perturbation theory in determining γ_1. The leading logarithms of the renormalization group correspond to the $a_1\, g^2/n-1$ term in γ_1 so that the average multiplicity is a problem to which the renormalization group does not directly apply.

Nevertheless a number of authors[10] have suggested that a more complete treatment of the dressed ladder graphs might give a way of evaluating $\bar{n}$. A proper treatment of dressed ladder graphs, in axial gauge, gives

$$\gamma_n = 1/2\, \left(-(n-1) + \sqrt{(n-1)^2 + 4\alpha c_A/\pi}\right)$$

which gives

$$\bar{n} \propto e^{2.4\sqrt{\ell n Q^2}}$$

for color SU(3) with 4 flavors. Furthermore one finds that a branching picture is valid as shown in Fig. 5 for gluons decaying into gluons. In this picture $p \ll k_2 \ll k_1$ for leading terms while

$$\frac{1-\cos\,\sigma(k_1,k_2)}{2} > p/k_2\,\frac{1-\cos\,\sigma(p,k_2)}{2} \quad \text{etc.}$$

as far as angular regions are concerned.

I have looked in perturbation theory in detail through three loops and find[11] that the above picture is essentially correct. I find that the anomalous dimension is consistent with

$$\gamma_\eta = 1/4\,\left(-(n-1) + \sqrt{(n-1)^2 + 8\,C_A\alpha/\pi}\right)$$

or

$$\bar{n} \propto e^{2.4\sqrt{\ell nQ^2}/\sqrt{2}}$$

a small change from the ladder graph calculation. Although non ladder graphs are important in this calculation their total effect is to modify the angular regions of the branching process so that $\ldots > \theta(k_i,k_{i+1}) > \theta(k_{i+1},k_{i+2}) > \ldots$ is the allowed region.

If the perturbative determination of $\bar{n}$ and $d\sigma/d\omega$ for small ω is upheld as one understands the problem more fully, and we are some distance from doing this, it would mean that the old picture of Bjorken, Casher, Kogut and Susskind is not correct in QCD and that strings do not form and break in a jet evolution into hadrons. This idea of a preconfinement, a color neutralization within perturbation theory, seems to be realized in the calculation of Field[12] presented at this workshop.

REFERENCES

1. See for example the review by A.H. Mueller, Physics Reports (to be published).
2. D. Cords, Proceedings of the XX International Conference on High Energy Physics, Madison (1981).
3. R.K. Ellis in Proceedings of the Conference on Perturbative QCD, Tallahassee (to be published).
4. R.P. Feynman, R.D. Field and G.C. Fox, Nucl. Phys. B128 (1977)1; B136 (1978)1.
5. R.K. Ellis, M.A. Furman, H.E. Haber and I. Hinchliffe, Nucl. Phys. B173 (1980) 39 and M.A. Furman (to be published).
6. G. Farrar and D. Jackson, Phys. Rev. Letters 43 (1979) 246; V.L. Chernyak and A.R. Zhitniski, Pisma Zh. Exp. Theo. Fiz. 25 (1977) 544; A. Efremov and A. Rodyushkin, Phys. Letters 94B (1980) 245; S. Brodsky and G.P. Lepage, Phys. Letters 87B (1979) 359, Phys. Rev. Letters 43 (1979) 545. A. Duncan and A.H. Mueller, Phys. Rev. D21 (1980) 1636, Phys. Letters 90B (1980) 159.
7. J.C. Collins and D. Soper (to be published).
8. J. Kubar-André and F.E. Paige, Phys. Rev. D19 (1979) 221; G. Altarelli, R.R. Ellis and G. Martinelli, Nucl. Phys. B157 (1979) 461; K. Harada, T. Kaneko and N. Sakai, Nucl. Phys. B155 (1979) 169; A.P. Contogouris and K. Kripfganz, Phys. Letters B84 (1979) 473, Phys. Rev. D19 (1979) 2207; J. Abad and Humbert, Phys. Letters B80 (1979) 286.
9. G. Parisi and R. Petronzio, Nucl. Phys. B154 (1979) 425.
10. A. Bassetto, M. Ciafaloni and G. Marchesini, Nucl. Phys. B163 (1980) 477; D. Amati, A. Bassetto, M. Ciafaloni, G. Marchesini and G. Veneziano, Nucl. Phys. B173 (1980 429; W. Furmanski, R. Petronzio and S. Pokorski, Nucl. Phys. B155 (1979) 253; K. Konishi, Rutherford Report RL79-035 (1979).
11. A.H. Mueller, Phys. Letters (to be published).
12. R. Field (these proceedings).

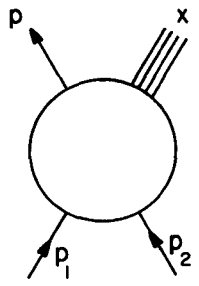

Fig. 1

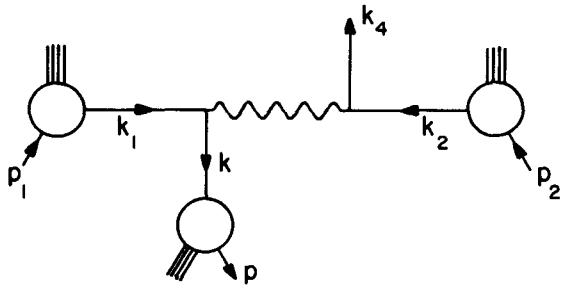

Fig. 2

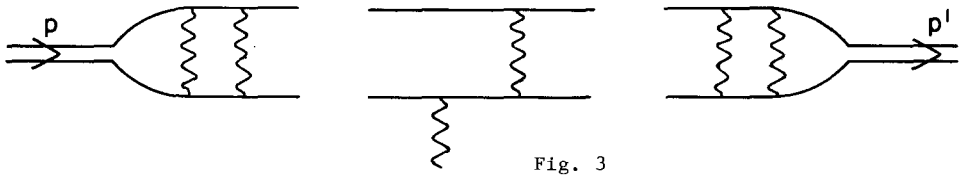

Fig. 3

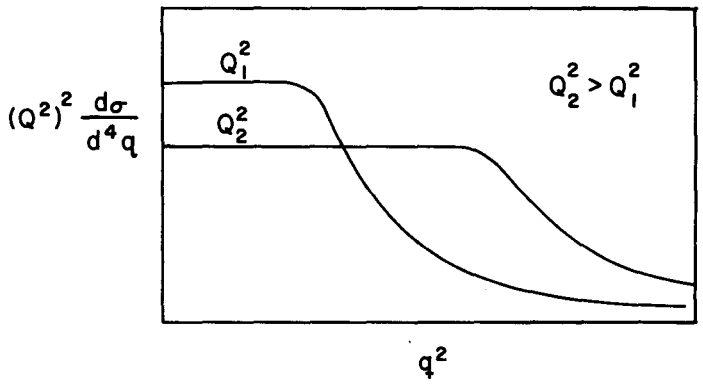

Fig. 4

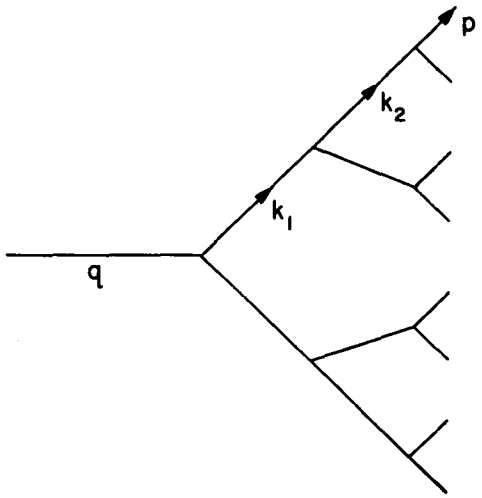

Fig. 5

AN EXPERIMENTAL PROGRAM TO STUDY THE PHYSICAL VACUUM: HIGH-ENERGY NUCLEUS-NUCLEUS COLLISIONS

W. Willis, CERN

I. THE PHYSICAL VACUUM IN CONFINING QCD

Quarks and gluons exist; they are nearly massless, but it is very hard or even impossible to knock them out of the proton. It is now widely believed that this strange state of affairs is due to the properties of the physical vacuum state as it now exists in our part of the Universe. On this view, the ground state of the vacuum is not that familiar in quantum electrodynamics (QED). That state is basically empty space, perturbed by fluctuations which occasionally give rise to a virtual electron-positron pair. In the quantum chromodynamic (QCD) theory of quarks and gluons, the stronger and more complicated forces give rise to a state which cannot be described as a perturbation on empty space. Instead, the physical vacuum has properties which resemble those of a physical medium. For example, the colour field is completely excluded, or at least strongly repelled, from a macroscopic volume of physical vacuum. This effect confines the quarks and gluons, which carry colour, inside the hadrons. On the scale of hadrons, quantum fluctuations make the phenomena more complex, but a simple picture postulates that the stong colour fields inside the hadron create a local volume of space more like the perturbative vacuum state, reverting to the physical vacuum state outside. This concept has been quantitatively expressed by the bag model, with some success.

This physical vacuum is also supposed to explain the origin of broken symmetries. An analogy is a perfectly symmetrical sphere of iron. Above the Curie temperature the state has spherical symmetry. At low temperature, the ground state will be magnetized, with the magnetic field pointing in an arbitrary direction determined by quantum fluctuations. The symmetry of the state has been broken, without any arbitrary direction entering in the laws of nature. By a quite similar mechanism, the parameters of the physical vacuum could determine the seemingly arbitrary breaking of symmetries in particle physics, though the fundamental laws remain symmetrical.

It seems that the physical vacuum has acquired properties reminiscent of Maxwell's ether. At least, so we are asked to believe. Maxwell introduced his ether for plausible reasons, but crucial experimental tests were found, and the theory was found wanting. In this Comment I discuss experiments for testing the idea that the physical vacuum is not idential to the perturbative one.

Our vacuum state has no consequences for the testing of special relativity, and probably none for (macroscopic) general relativity. Fortunately, another classical experiment on the vacuum is predicted to show striking results. The effect is due to the predicted instability of the physical vacuum state in the presence of high-energy density or matter density. Under these conditions, the lower-energy state is that based on the perturbative vacuum: empty space with real and virtual quarks and gluons traversing it, without colour confinement. This change to a qualitative different state is in fact expected to occur, under suitable conditions, as a sharp phase transition. The origin in this transition is that the physical vacuum state is supposed to arise from ordered virtual constituents which are disrupted by thermal agitations, or the colour fields of dense matter. The analogy of the iron sphere is again valid: the spontaneous symmetry breaking of the physical vacuum is a low-temperature phenomenon. The "Curie temperature" of the vacuum is of the order of the QCD scale parameters Λ.

II. AN IDEALIZED EXPERIMENT TO OBSERVE THE MELTING OF THE PHYSICAL VACUUM

Planck showed how far-reaching conclusions can be arrived at by analysing a volume of vacuum surrounded by walls in thermal equilibrium with the radiation in the interior. Let us follow him, adding equipment which will measure gluons as well as photons. In Fig. 1a we see a large box with thick walls at temperature T. The radiation emitted through a small aperature is measured. Alternatively, if we want to be sure of what happens in the middle of the box, a high-energy proton beam is sent through the aperture, and Compton scattering of photons and gluons is measured.

At low temperature, $T < \Lambda$, we will detect photons filling the box with the Planck distribution, but no gluons. Why not, since massless thermal gluons should be emitted by the walls? (If a mass is attributed to the gluons

it is surely << Λ.) The answer is supposed to be that the physical vacuum filling the box forces a thermal gluon back into the wall.

As the temperature of the wall is raised, there are more -- and more energetic -- thermal gluons emitted. They penetrate slightly further into the vacuum. Finally, the temperature approaches where the ordered structure of the virtual particles in the physical vacuum is so much disrupted by these assaults that the perturbative vacuum state is energetically preferred. Very near this temperature, large-scale fluctuation appears in the vacuum, with a mixture of colour-confining and unconfining regions. The phenomenon of critical opalescence will render the box opaque to the high-energy protons at that point (Fig. 1b).

Above the transition temperature, we will find freely propagating gluons and quarks filling the box (Fig. 1c). The situation at the small aperature is more complex, since it is a boundary with the physical vacuum in the world outside. Only constituent combinations which are colourless can make it to the outside world.

Suppose the walls are heated further. We note that the thermal energies of the constituents are > Λ, so that they are entering the regime of asymptotic freedom and their interactions are decreasing as they are heated. It seems there is no limit to the temperature. The "limiting temperature" observed in hadronic interactions must be a confinement effect, and indeed the Hagedorn temperature of 160 MeV is close to that estimated for the critical temperature.

The elements of this analysis which must be trasferred to a real experiment are the following:

i) The size of the box. The scale is given by Λ, $\sim$ 1/2 fermi. The size must be larger than that. Evidently, the proton is not large enough.

ii) The temperature. One should be able to sweep through the region 100-400 MeV, or thereabouts.

iii) A sufficient degree of thermal equilibrium must be established.

iv) The probes must be able to examine the <u>interior</u> of the "box" -- affording measurements of sufficient subtlety to distinguish the conditions above and below the transition, and the critical phenomena.

III. REAL EXPERIMENTS

First, I will mention some possible approaches along conventional experimental lines. Consider, first, proton-proton collisions. We know that the distributions of the particles in the "beam jets" as well as in high transverse momentum jets closely resemble those in the jets from high-energy e^+e^- annihilations[2]. The latter we may take to reflect the characteristics of the fragmentation of single quarks. It follows that ordinary pp collisions show no signs of the presence of many constituents, spread over a volume and in some sort of equilibrium -- the conditions we wish to produce. It is possible that some rare events in pp collisions are somewhat more suitable for our purpose, but it does not seem likely that they will go far enough towards satisfying the first three conditions above.

We can think of using protons incident on a nuclear target. Here again we can profit by a considerable body of knowledge from recent experiments[3]. For example, if we consider the system in which the proton is at rest, and consider the proton fragmentation products after it has been struck by the incident nucleus, we know that they are not very different from those after the proton has been struck by another proton. Consider, instead, the nucleus to be at rest. The proton passes through, making several collisions. The fast forward products do not fragment until they have left the nucleus (see the previous remark). The slower particles are emitted at larger angles, and do fragment inside the nucleus. Their fate is a hard one, however. These fragmenting particles have energies of a few GeV or less, and they enter a volume of cold nuclear matter where they are outnumbered by "stationary" nucleons at the odds of typically ten to one. They create feeble cascades, where the creation of a few pions is partially counterbalanced by pion absorption. No wonder that the observed increase in pion multiplicity, in comparison with pp collisions, is only between two and three in the heaviest nuclei. There is no possibility of heating a large volume to an interesting temperature. Instead, the energy provided is dissipated in a large mass of cold nuclear matter.

We come rather naturally to consider nucleus-nucleus collisions at high energy. First we note that accelerators, linear or cirular, act upon the charge. A fully stripped heavy ion has charge Z times that of a proton, and A times the mass, with $A \simeq 2Z$. The total energy of a nucleus produced by the

accelerator is thus about Z/2 times that of a proton from the same accelerator. Even for a medium-size nucleus, say argon, this is a huge factor. Given that we needed to heat a large volume, the fact that the energy is distributed over a number of particles is not a disadvantage. Quite the contrary, since this energy can be deposited in the target with reasonable efficiency, which is of course not the case when trying to heat a nuclear volume with one very high energy proton.

To give an idea of what should happen in such a collision, I shall estimate the number of pions produced, always assuming that there is no new physics at the level of the individual nucleon-nucleon collision. I should like to suppose that the energy is high enough so that there is a well-defined central region in rapidity, through the pion multiplicity may start to saturate at somewhat lower energies. In pp collisions, this occurs for lab energies of about 100 GeV. In nuclear collisions, the leading quarks are further degraded by multiple collisions, and the energy required is greater by $\simeq e^{\nu}$, where ν is the average number of collisions of the primary, ν = 2-4, depending on the A of the nucleus, or 0.5-10 TeV lab energies per nucleon, or (for comparison with cosmic ray events) a total energy of $\gtrsim 10^{14-15}$ ev. I shall also consider only central, i.e. head-on, collisions, since we can surely select them experimentally.

Suppose the target nucleus is struck by <u>one</u> proton of such an energy. We know what happens: the number of pions (including π^0) is, from the CERN Intersection Storage Rings (ISR), about 20 on the average. The effect of the nuclear target is to multiply this to about 50. Consider now that the nucleus is struck at the same time but at different points. Surely the number of pions produced is twice that produced by one proton. As the number of nucleon projectiles increases, the possibility of coherence between nearby nucleons arises. It is hard to see a motivation for such a coherence, and I believe it is not suggested by the cosmic-ray data[4]. A multiplicity linear in A cannot be far wrong, and thus for A of 200, the multiplicity could reach 10,000 pions.

Naively, we could suppose that these pions are created in the volume of the two nuclei before the system has had time to disassemble. Note, however, that if each pion is supposed to occupy the volume attributed to it in the bag

model, there is not room for that many pions. We may suppose that the matter is rather in the form of quarks and gluons, forming pions as the density fall to the appropriate value. Here, however, we make contact with the considerations on the role of the physical vacuum.

We know that the nucleus is made of nucleons, not a big bag of quarks. In fact, most of the volume inside a nucleus is occupied by the vacuum -- not by the nucleon bags. In the collisions just described, it seems very likely that the conditions are created where that physical vacuum is unstable, and at each point there is a transition to a perturbative vacuum filled with quarks and gluons. We then indeed have a big bag. The surface presumably emits pions as long as the temperature is high enough. In suggestive language, "the surface boils pions at the Hagedorn temperature". Arguments have been given that this state lasts "long enough". We will not attempt to follow this wild scenario to its end.

From another point of view, a novel aspect of the de-confining phase transition is that confinement is of necessity a long-range effect, and the transition necessarily produces long-range order. In the past, it has not been clear why there should be collective effects among many hadrons at particle physics energies. Now the confining properties of the physical vacuum guarantee such effects, within the orthodox theory. Having found circumstances where they are likely to occur, we must see if they can be observed.

IV. THE PROBLEM OF OBSERVABLES

The literature on this subject does not abound with good discussions of the quantities to be observed. One of the weaknesses, as well as strength, of the thermodynamical method is that one can proceed happily in a discussion using the thermodynamic variables without the necessity of explaining how they are to be measured. The problem becomes acute when there are strong temporal and spatial variations. A correct procedure would be to perform a Monte Carlo simulation at the constituent and vacuum level, but that is out of reach for the moment. We cannot yet renounce thermodynamical consideration.

We can begin the discussion by noting that most of the common observable are not very useful. Most hadrons will have at least scattered near the surface of the interaction volume, largely erasing the information about their

previous history. It is not sensible to go to such trouble to provide a good surface-to-volume ratio, and then selectively to observe the surface. Weakly interacting probes are called for. Most of our considerations must then deal with photons, or virtual photons oberved as leptons pairs[5].

The photons in question are of course direct photons, not those from meson decays. This suggests a rare particle, of order 1/137 compared to pions, but that can be misleading. For example, the point-like nature of the photon causes it to be much more common at high transverse momenta, where γ/Π° > 10% beyond 5 GeV/c. More complex phenomena are probably present at low P_T, where observations, so far all depending on lepton pairs, show a relatively copious production of virtual photons. The virtual photons have the advantage that the mass distribution carries some information, so that the temperature of an equilibrium source could in principle be read by either the mass distribution or the transverse momentum distribution. Experimentally, that have the advantage of avoiding contamination from pion decay, though the conversion to lepton pairs costs a factor of 10^3 in rate. As A increases, the ratio of volume (producing photons) increases more quickly than surface (producing pions). This further enhances the γ/Π° ratio, probably to values (> 10%) which can be measured directly[6].

The photons and leptons could be used in an attempt to observe the phase transition. The c.m.s. energy of the nuclei is varied, and the temperature indicated by the transverse momentum and mass distribution is determined. The rate of photon emission is then determined as a function of temperature. As the transition temperature is passed, the character of the particles producing the radiation changes, and one would expect a change in the number of the photons produced, or in the slope of the photon production versus temperature.

A variation of the baryon, or quark, density at fixed temperature will also allow a sweep across the transition. It is known from ISR data that the ratio of baryons to mesons varies strongly with rapidity. Though the variation will be somewhat smoothed out in nuclear collisions, this will give another convenient parameter to vary in the region of the phase transition.

Since we have only rough estimates of the transition temperature[7], rather crude notions of "temperature" in pp collisions, and as yet no direct data relevant to the temperature inside nuclear collisions[8], we cannot say anything

about the enrgies necessary to produce temperatures above the critical temperature. It seems clear that the energies investigated at Berkeley and Dubna, a few GeV per nucleon, are not sufficient. Conservative estimates in the region of limiting fragmentation, roughly corresponding to the energy range defined earlier for central region formation, seem to show energy densities of the required magnitude. In principal terms, keeping to accelerators at present existing or under construction, it seems that we must speak in terms of FNAL, SPS, ISR, or ISABELLE. Of course, experiments at the 10-15 GeV/nucleon would at least allow a better estimate to be made.

Another technique of observing the new phases based on calculations which show that heavy quarks will be much more common[9]. One then has to believe that they will survive the hadronization process, which seems plausible, but not certain.

Of course, it is easy to imagine many exotic and exciting forms of matter which can be created in these collisions, but I prefer to stick with an analysis of the fundamental phenomenon as we now understand it.

There are many interesting experimental questions associated with the large energy releases and large multiplicities present in these events, which I have discussed elsewhere[10].

FIGURE CAPTIONS

Fig. 1. Idealized experiment on "melting of the vacuum": a) Box at ambient temperature, showing thermal photons detected by Compton scattering of high-energy protons; b) at critical temperature, with large-scale fluctuations of the colour dielectric constant, and critical opalescence for protons; c) above transition, free gluons and quarks are detected in the middle of the box.

REFERENCES

1. A review is given in E. Shuryak, Phys. Report 61, 71 (1980).
2. M. Basile et al., Phys. Lett. 92B, 367 (1980).
3. W. Busza et al., Phys. Rev. Lett. 34, 836 (1975).
4. I. Otterlund et al., Proc. 15th. Int. Cosmic Ray Conf., Plovdiv, Bulgaria, 1977 (Bulgarian Acad. Sci., Sofia, 1978), Vol. 7, P. 40.
5. R. Anishetty, P. Koehler and L. McLerran, Phys. Rev. D22, 2793 (1980).
6. G. Domokos and J. Goldman, Phys. Rev. D23, 203 (1981). K. Kajantie and H. Miettinen, Helsinki HU-TFT-81-7 (1981).
7. E. Feinberg, Nuovo Cimento 34A, 391 (1976).
8. J. Engels, F. Karsch, I. Montvay and H. Satz, Bielefeld BI-TP 81/05 (1981). L. McLerran and B. Svetistsky, Phys. Lett. 98B, 195 (1981).
9. R. Hagedorn and J. Rafelski, Phys. Lett. 97B, 180 (1980). J. Rafelski, Frankfurt UFTP 55 (1981).
10. W. Willis, Preprint CERN-EP/81-21 (1981), to appear in the Proc. of the workshop on Future Relativistic Heavy Ion Experiments, GSI Darmstadt, 1980.

VACUUM MELTING

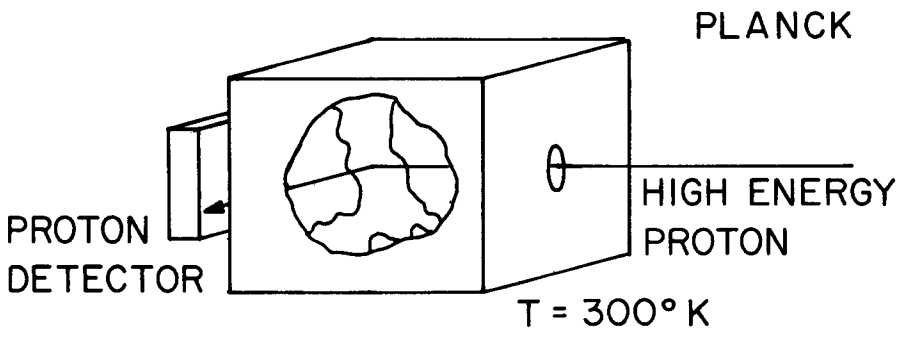

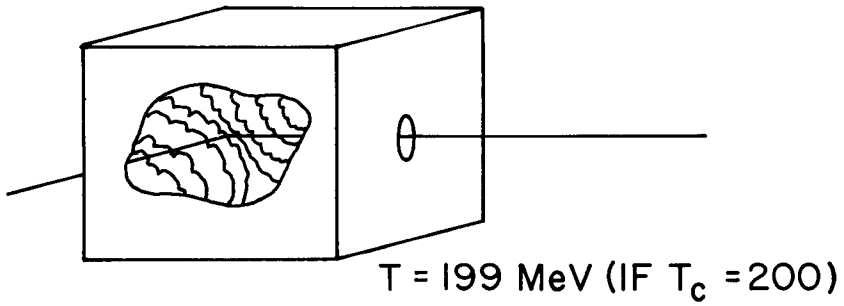

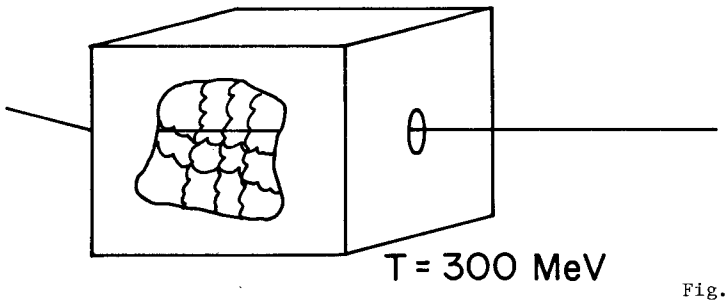

Fig. 1

PHOTONS

LEPTONS FROM pp INTERACTIONS

Frank E. Paige, BNL

Leptonic signatures for W mesons and heavy quark production at ISABELLE are discussed.

I. INTRODUCTION

It has long been recognized that leptons should be the best signature for W mesons produced in pp and $\bar{p}p$ interactions.[1,2] Leptons also provide good signatures for new heavy quark resonances[3] and for the associated production of heavy quarks.[4] Some recent work on these processes is reported here.

In Sections II and III the expected properties of W mesons and their production cross sections are reviewed. Many additional distributions have been given previously.[1,2,5] In Section IV a brief description is given of ISAJET,[6] a Monte Carlo event generator which simulates QCD jets, Drell-Yan processes, and minimum bias events. A few distributions for the $W^{\pm}$ and Z^{o} which are sensitive to their tranverse momenta are shown. In Section V preliminary results are given on the background to Drell-Yan processes from heavy quark semileptonic decays. The associated hadrons are found to provide an adequate means for separating the two types of events. In Section VI estimates are given for the production of new heavy quark resonances and their decay into $\ell^{+}\ell^{-}$. Such resonances should be observable at ISABELLE for masses below the Z^{o}. In Section VII the use of trilepton events as a signature for the associated production of heavy quarks is described. Finally, some implications for experiments are discussed in Section VIII.

II. PROPERTIES OF W MESONS

The standard SU(2)xU(1) gauge theory of electroweak interactions[7] is in good agreement with all existing data on charged and neutral weak currents. A fit of the lowest order cross sections to the data gives[8]

$$\sin^2 \theta_W = 0.23$$

Then the masses and widths of the $W^{\pm}$ and Z^{o} are determined. The lowest order mass formulas with n_q quarks and n_ℓ leptons give

$$M_W = \left(\frac{\pi\alpha}{\sqrt{2}\,G_F}\right)^{1/2} \frac{1}{\sin\theta_W} = 77.8 \text{ GeV}$$

$$\Gamma_W = \frac{G_F M_W^3}{6\pi\sqrt{2}} \left(3n_q + n_\ell\right) = 2.47 \text{ GeV}$$

$$M_Z = \frac{M_W}{\cos\theta_W} = 88.6 \text{ Gev}$$

$$\Gamma_Z = \frac{G_F M_Z^3}{6\pi\sqrt{2}} \sin^2(2\theta_W) \left[3 \sum_{q=1}^{n_q} (a_q^2 + b_q^2) + \sum_{\ell=1}^{n_\ell} (a_\ell^2 + b_\ell^2)\right]$$

$$= 2.49 \text{ GeV}$$

where a_i and b_i are the vector and axial couplings,

$$a_i = \frac{1}{\sin 2\theta_W} (T_{3i} - 2Q_i \sin^2\theta_W)$$

$$b_i = \frac{1}{\sin 2\theta_W} T_{3i}$$

These lowest order masses are the ones generally used here.

Both the mass formulas and the connections between $\sin^2\theta_W$ and experiment are subject to radiative corrections, which have recently been calculated by Marciano and Sirlin.[9] They find that for $\sin^2\theta_W$ defined by the $\overline{MS}$ prescription,

$$\sin^2\theta_W = 0.215 \pm 0.012$$

The corresponding masses including all the radiative corrections are

$$M_W = 83.0 \pm 2.4 \text{ GeV}$$
$$M_Z = 93.8 \pm 2.0 \text{ GeV}$$

Thus the radiative corrections shift the masses by more than 5%. The quoted errors are dominated by the experimental errors on $\sin^2 \theta_W$. Since experiments basically determine $\sin^2 \theta_W$ while $M_W \sim 1/\sin \theta_W$, it seems unlikely that they will be reduced by a large factor. Thus to test the standard model one should aim to determine M_W and M_Z with errors $\lesssim 1$ GeV.

Marciano and Sirlin[10] have also calculated the masses of the $W^{\pm}$ and Z^0 in the context of grand unified theories as functions of the QCD scale $\Lambda_{\overline{MS}}$

For the SU(5) model of Georgi and Glashow[11] they find

$\Lambda_{\overline{MS}}$ (GeV)	M_W(GeV)	M_Z(GeV)
0.1	82.8	93.6
0.2	83.6	94.2
0.3	84.0	94.6
0.4	84.6	94.9

Again an error of about 1 GeV seems appropriate.

Any e^+e^- machine with sufficient energy can presumably measure the Z^0 mass to a small fractions of 1 GeV, so the goal at ISABELLE should be to measure the difference of the $W^{\pm}$ and Z^0 masses. This is best done by measuring the $p_\perp$ distribution for $W^{\pm} \to \ell^{\pm}\nu$ and using the Z^0 data to unfold the transverse momentum. Such an analysis requires good statistics, which ISABELLE can provide.

III. W PRODUCTION

Cross Sections: Politzer[12] was the first to suggest that the cross section for a massive photon - or by a trivial extension for a W meson - could be computed perturbatively in QCD. It has now been shown[13] that the cross section integrated over the transverse momentum $q_\perp$ of the W is calculable to all orders in perturbation theory in terms of universal, nonscaling structure functions measurable in deep inelastic scattering. The leading term is given by the elementary cross section $\hat{\sigma}$ calculated in perturbation theory for the

Drell-Yan graph, Fig. 3.1. Thus must be folded with the structure functions, giving

$$\frac{d\sigma}{dM^2 dx_F} = \frac{1}{s\sqrt{x_F^2+4\tau}} \sum_q \sigma_{qq}(M^2)\, q(x_1,M^2)\, \bar{q}(x_2,M^2)$$

$$x_1 x_2 = \tau = M^2/s,\ x_1 - x_2 = x_F$$

Thus the only change from the original Drell-Yan model is the inclusion of scaling violations in the quark distributions.

Experimentally the Drell-Yan model works rather well for the existing $pp \to \ell^+\ell^- X$ and $\pi p \to \ell^+\ell^- X$ data except for the overall normaliation:[15]

$$\left[\frac{d\sigma}{dM^2 dx_F}\right]_{exp} = k \left[\frac{d\sigma}{dM^2 dx_F}\right]_{Drell\text{-}Yan}$$

$$k \simeq 2$$

However, the $O(\alpha_s)$ correction increases the cross section by a similar factor.[16] This means that there is no contradiction between theory and experiment, but also that QCD perturbation theory is not reliable for this process. Nevertheless the Drell-Yan model should be fully adequate for estimating expected rates.

To calculate cross section for W production one needs the structure function at $Q^2 = M_W^2$ as well as the elementary cross sections. Most of the calculations given here are based on the Owens-Reya parameterization,[17] which includes QCD scaling violations with $\Lambda_{\overline{MS}} = 0.5$ GeV. The more recent CDHS parameterization gives a considerably better fit to the data[19] but includes no scaling violations. Also, most recent analyses favor $\Lambda_{\overline{MS}} = 0.1$-$0.2$ GeV.[20] Fortunately at ISABELLE the typical value of x,

$$x \sim \frac{M}{\sqrt{s}} \sim 0.1$$

is such that these differences are not too important, but a better parameterization is clearly needed.

For $\sqrt{s}$ = 700 GeV and L = 2×10^{31} cm^{-2} s^{-1}, the parameters of ISABELLE - Stage I, the following cross sections and rates are obtained:

	σ(mb)	B(W→ℓ)	Rate/1000h
W^+	2.1×10^{-6}	1/12	1.3×10^4
W^-	1.1×10^{-6}	1/12	6.6×10^3
Z^o	7.0×10^{-7}	.03	1.5×10^3

For the $\ell^+\ell^-$ continuum with $\Delta M/M$=10% and the same energy and luminosity,

M(GeV)	$d\sigma/dMdy$ (mb/GeV)	Rate/1000h
20	4×10^{-9}	1700
30	7×10^{-10}	450
40	2×10^{-10}	170
50	7×10^{-11}	76
60	3×10^{-11}	39

The measurable range is somewhat limited, but for most purposes one can compare the continuum with the Z^o peak.

Transverse Momentum: The parton model neglects the transverse momentum $q_\perp$ of the W, and most previous calculations have used this approximation.[1,2,5] Recently considerable progress has been made in calculating the complete $q_\perp$ distribution in QCD. There are two distinct regions $q_\perp \curvearrowright M$ and $q_\perp \ll M$.

For $q_\perp \curvearrowright M$ there is only one large mass scale, and straightforward QCD perturbation theory should apply; the leading graphs are shown in Fig. 3.2. The cross section is $O(\alpha_s)$, and measurement of it would provide a direct test of gluon interactions. Higher order corrections are calculable in principle although very complicated.

For $q_\perp \ll M$ perturbation theory cannot be applied directly since it gives a series in α_s $\ell n^2(M^2/q_\perp^2)$ involving large logarithms. The first step in analyzing this region was carried out by Dokshitser, Dyakanov, and Troyan.[21] They summed the leading-log series to show that the probability for emitting

no gluons with transverse momentum $k_\perp > q_\perp$ was suppressed by the square of a Sudakov form factor

$$S = \exp\left\{-\frac{4}{3}\frac{\alpha_s}{\pi}\ln^2\left(\frac{M^2}{q_\perp^2}\right)\right\}$$

which vanishes faster than any power of M^2.

Parisi and Petronzio[22] used this result to argue that the cross section is calculable even for $q_\perp = 0$. The essential reason is that the cross section is negligible if all guons have small $k_\perp$, so gluons with substantial $k_\perp$ must be emitted even if the W has $q_\perp = 0$. Thus any primordial transverse momentum is washed out. Assuming that soft gluons behave like soft photons, Parisi and Petronzio carry out an explicit calculation. Asymptotically, they find

$$\frac{1}{\sigma}\frac{d\sigma}{dq_\perp^2}\Big|_{q_\perp = 0} \propto C_1\left(\frac{\Lambda^2}{M^2}\right)^{\eta_0}, \quad \eta_0 \simeq 0.60$$

$$\frac{\partial}{\partial q_\perp^2}\ln\left(\frac{d\sigma}{dq_\perp^2}\right)\Big|_{q_\perp = 0} \propto C_2\left(\frac{\Lambda^2}{M^2}\right)^{\eta_1-\eta_0}, \quad \eta_1 \simeq 0.91$$

Thus the contribution to the cross section from the small $q_\perp$ region vanishes like a fractional power of M^2. A more useful characterization of the shape is the width at half height of the distribution:

$$q_\perp \simeq 1 \text{ GeV at } M \simeq 10 \text{ GeV}$$
$$q_\perp \simeq 3 \text{ GeV at } M \simeq M_W$$

These widths are smaller than the mean values, which are dominated by the perturbative QCD tail.

The calculation of Parisi and Petronzio can be justified in the leading by approximation,[23] and the higher order correction are calculable.[24] The ability to calculate the distribution even at small $q_\perp$ is a remarkable feature of QCD, and one that will be very interesting to test at ISABELLE.

IV. ISAJET

ISAJET[6] is a Monte Carlo event generator for pp and $\bar{p}p$ interactions at ISABELLE energies. It forms the basis for many of the results presented here. The essential elements of the program are

(i) QCD cross sections for hadronic jets and Drell-Yan processes;

(ii) QCD scaling violations for jet fragmentation according to the Altarelli-Parisi equations;[25]

(iii) Fragmentation of the resulting quarks into hadrons using the Field-Feynman algorithm;[26]

(iv) Beam jet fragmentation;

(v) Resonance decay.

Most of their elements are familiar, but two require some further explanation.

Scaling Violations: Scaling violations are needed to get agreement between QCD and the single-particle cross sections measured at high $p_\perp$. Scaling violations in the longitudinal momentum along the jet axis have therefore been incorporated into ISAJET. The corresponding spread in transverse momentum about the jet axis -- and hence multi-jet events -- have been neglected in the present version. They should not significantly change any of the results given here.

Let $D_{h/i}(x,\xi)$ be the probability of finding a hadron h in a parton i with momentum fraction x and

$$\xi = \frac{1}{4\pi b_o} \ln\left(\frac{\alpha_s(Q_o^2)}{\alpha_s(Q^2)}\right), \quad b_o = \frac{33-2f}{12\pi}$$

Then $D_{h/i}$ satisfies[27]

$$D_{h/i}(x,\xi) = \sum_j \int_x^1 dy/y \; G_{j/i}(y,\xi) \; D_{h/j}(x/y,0)$$

where $G_{j/i}$ in turn satisifes the Altarelli-Parisi evolution equation[25]

$$1/2 \; \partial/\partial\xi \; G_{j/i}(x,\xi) = \sum_k \int_x^1 dy/y \; P_{jk}(x/y) \; G_{k/i}(y,\xi)$$

These equations immediately suggest a simple Monte Carlo procedure. First break the ξ range into small steps $\Delta\xi$, and in each step fragment the partons with the appropriate probabilities $P_{jk}\,\Delta\xi$. (The infrared devergence is removed by requiring that each parton have a momentum > 4 GeV). Then fragment the resulting partons into hadrons using the Q^2-independent Field-Feynman algorithm. This procedure is presumably reliable at not too small values of x for which the leading-log approximation is valid. It is not a priori reliable for small x or for the multiplicity, but in fact it gives reasonable agreement with other methods.

W Cross Section: The Parisi-Petronzio formula is not very suitable for generating events, so a simplified approximation is used. The cross section is basically taken from the $O(\alpha_s)$ graphs shown in Fig. 3.2. At large $q_\perp$ this gives the right result, while at small $q_\perp$ it has a $1/q_\perp^2$ singularity. This is removed by the substitution

$$\frac{1}{q_\perp^2} \to \exp\left\{-\frac{1}{2}\,\ell n\left[q_\perp^4 + \mu^4(Q)\right]\right\}$$

with $\mu(Q)$ chosen to give a width in agreement with that found by Parisi and Petronzio. This procedure of course has no fundamental basis. Its only justification lies in the fact that it gives a rapidity distribution integrated over $q_\perp$ and a total cross section in reasonable agreement with the Drell-Yan model.

Results: All distributions which depend mainly on the M or x_F dependence of the W cross section are essentially the same as given previously.[1,2,5] The $Z^o \to \ell^+\ell^-$ cross section as a function of $q_\perp$ is shown in Fig. 4.1. The limit for 1 event/GeV/1000h at $L = 2\times10^{31}\ cm^{-2}s^{-1}$ is

$$q_\perp = 45\ \text{GeV}.$$

QCD perturbation theory should certainly apply there, and the cross section will be a good test of gluon interactions and the gluon structure function.

The lepton distribution from $W^+ \to \ell^+\nu$ is shown in Fig. 4.2. There is still a rather clear Jacobean peak; it is not smeared very much by the $q_\perp$ distribution. The critical region is $p_\perp \simeq 1/2\ M_W$, and an expanded view of it is shown in Fig. 4.3 with the statistics expected in the first year of operation at

ISABELLE (assuming $L = 1 \times 10^{31}$ $cm^{-2}s^{-1}$ for 1000h and 25% efficiency). By comparing such distributions it appears possible to measure the $W^{\pm}$ mass to about 2 GeV.

The lepton rapidity distributions for $W^+ \to \ell^+ \nu$ and $W^- \to \ell^- \bar{\nu}$ are compared in Fig. 4.4a,b. The rather striking difference is a consequence of the V-A coupling of the $W^{\pm}$.

It would be interesting to measure $Z^o \to \nu\bar{\nu}$, since this branching ratio would determine the number of types of neutrinos. One possibility is to measure the total width of Z^o. Since $M_Z \simeq 89$ GeV, $\Gamma_Z \simeq 2.5$ GeV, and the $\nu\bar{\nu}$ branching ratio is 6%/type, a mass resolution of about 0.1% is needed to detect one additional neutrino species. This is obviously very hard except in e^+e^- machines. Corrections for QCD effects and for heavy quark masses must also be made.

Another approach is to look for $Z^o \to \nu\bar{\nu}$ directly at high $q_\perp$; the signature is then "something plus nothing." For $q_\perp > 50$ GeV the $Z^o \to \nu\bar{\nu}$ cross section at ISABELLE is 6.4×10^{-10} mb, giving a reasonable number of events at $L = 2 \times 10^{32}$ $cm^{-2}s^{-1}$. The QCD jet cross section is 8.7×10^{-5}, so a probability less than 10^{-5} of missing the second jet is needed. Heavy quark jets can give a large missing $p_\perp$ to a neutrino; the associated lepton must be detected. Finally, $W^{\pm} \to \tau^{\pm}\nu$ with $\tau^{\pm} \to$ hadrons is a serious background. This experiment is obviously very hard, but it may be worth some thought.

V. LEPTONS FROM HEAVY QUARKS

It was first pointed out by Pakvasa et al.[4] that semileptonic decays of heavy quarks would produce a substantial background for Drell-Yan proceses. To study this background about 75000 $c+\bar{c}$, $b+\bar{b}$, and $t+\bar{t}$ jet events in various $p_\perp$ ranges have been generated using ISAJET. The work is still in progress, and all results are preliminary.

The single lepton cross section $d\sigma/dp_\perp$ and the dilepton cross section ds/dM summed over $e^{\pm}$ and $\mu^{\pm}$ are shown in Fig. 5.1, 5.2. The events were generated using $\Lambda_{\overline{MS}} = 0.4$ GeV as the QCD scale. This gives a rather large scaling violation in the jet fragmentation, leading to a substantial suppression of high $p_\perp$ and high M events. Comparison with the Drell-Yan cross section gives

M(GeV)	$\frac{\sigma(Q\bar{Q}\to\ell^+\ell^-)}{\sigma(\gamma,Z\to\ell^+\ell^-)}$
20	3.3
30	.98
40	.38
50	.15
60	.045

Thus the background is still significant, even though it is substantially smaller than that found by Pakvasa et al. Since scaling violations change the result so much, it is planned to repeat the calculation with a smaller value of $\Lambda_{\overline{MS}}$.

The leptons from heavy quarks will occur within hadron jets, and this provides a good way to separate them from Drell-Yan leptons. Define

$$H_\perp = \left| \sum_h \vec{P}_{h_\perp} \right|$$

where the sum runs over all particles h except neutrinos having $|y_h - y_\ell| < 1$ and $|\phi_h - \phi_\ell| < \pi/4$. The $H_\perp$ distribution for Drell-Yan events with M = 50 GeV is shown in Fig. 5.3. The distributions for leptons in two $p_\perp$ ranges are shown in Fig. 5.4a,b. Making a cut at $H_\perp$ = 2 GeV gives the following efficiencies:

$\varepsilon = 0.91$ for Drell-Yan, M = 50 GeV

$\varepsilon = 0.15$ for $Q\bar{Q}$, $10 < P_{\ell_\perp} < 20$ GeV

$\varepsilon \leq 0.09$ for $Q\bar{Q}$, $20 < P_{\ell_\perp} < 20$ GeV.

(For the last value a smooth extrapolation to $H_\perp = 0$ has been made; a considerably smaller value would be found from the actual histogram.) Evidently this cut gives a suppression factor of about 10 per lepton, and presumably of about 100 for dilepton events. This is sufficient to make the background negligible even if the higher cross section of Pakvasa et al. is used.

VI. HEAVY $\bar{Q}Q$ RESONANCE

The decay of a heavy $Q\bar{Q}$ resonance into $\ell^+\ell^-$ is perhaps the cleanest signature for a new quark in pp interactions. While there is no well-established

theory for the production of such resonances, there is a successful phenomenology based on scaling.[3] The three-gluon width Γ_{3g} is a measure of the resonance coupling to light hadrons, so the production cross section should be proportional to it. In fact, the scaling relation[4]

$$\frac{d\sigma}{dy} = \bar{R}_o \Gamma_{3g} \left.\frac{d\sigma}{dMdy}\right|_{\text{Drell-Yan}}$$

$$\bar{R}_o = 1.5 \times 10^7 \quad \text{(for theoretical Drell-Yan)}$$

works rather well for he J/ψ and T systems, and even for the ϕ, as can be seen from the compilation of Kourkoumelis, et al.[29] While the scaled T cross section is about a factor of 2 lower than the J/ψ one, roughly 50% of the J/ψ comes from $\chi \to J/\psi + \gamma$.

The branching ratio into $\ell^+\ell^-$ can be calculated[4] from the matrix elements for decays into γ, Z^o, and three gluons and for free quark decay together with a fit for the wave function $|\Psi(0)|^2$ at the origin. The free quark decay width is proportional the $G_F^2 M_Q^5$ and so becomes dominant at sufficiently high masses, causing the $\ell^+\ell^-$ branching ratio to decrease rapidly above the Z^o mass. Therefore $Q\bar{Q}$ resonances cannot be used to search for very heavy quarks unless the generalized Cabibbo angles are for some reason small.

The background for such resonance is given by $\gamma, Z^o \to \ell^+\ell^-$. There is also a potential background from $c+\bar{c}$ and $b+\bar{b}$ semileptonic decays, but this can be removed by the method outlined in the previous section.

Combining the predicted cross sections and branching ratio gives the following rates/1000h for various masses at $L=2\times10^{31}$ cm^{-2}s^{-1}. The backgrounds are calculated assuming $\Delta M/M=1\%$.

M(GeV)	$B\frac{d\sigma}{dy}$ (mb)	$\frac{d\sigma^{(\gamma,Z)}}{dMdy}$(mb/GeV)	Signal	Background
40	3.9×10^{-9}	1.9×10^{-10}	378	23
50	1.1×10^{-9}	6.6×10^{-11}	108	10
60	3.4×10^{-10}	3.0×10^{-11}	33	5.0
70	1.1×10^{-10}	2.0×10^{-11}	11	4.2
80	3.8×10^{-11}	3.8×10^{-11}	3.8	8.8

With good mass resolution such resonances should be observable up to close to the Z^o mass, as can be seen either from the table or from the Fig. 6.1. Above that mass the tail of the Z^o and the rapidly decreasing branching ratio make the signal very poor.

VII. MULTILEPTON SIGNATURE FOR HEAVY QUARKS

For quark masses above those which can be seen as $\ell^+\ell^-$ resonances, it is necessary to look for associated production. The cross section for this is quite large; the problem is to find an adequate signature. In the absence of a vertex detector capable of observing charmed particle tracks, the most promisng approach[30] seems to be the study of trilepton events, $pp \to \ell^+\ell^+\ell^-X$. These can be produced by the sequential semileptonic decays of either $t+\bar{t}$ or $b+\bar{b}$ jets. The two sources can be separated by looking at various distributons involving the leptons. For example, in $b+\bar{b}$ events at least one of the $\ell^+\ell^-$ pairs must have a mass smaller than m_b.

The trilepton cross section[30] is shown in Fig. 7.1. By requiring that both $\ell^+\ell^-$ pairs have masses greater than m_b it should be quite straightforward to establish the existance of $t+\bar{t}$ production. The t mass must be determined by fitting the resulting distribution; no estimate of the accuracy of this determination has been made.

Another possible idea for determining m_t is to measure the lepton multiplicity as a function of he visible $p_\perp$ of the jets. The t quark will give more leptons, and its cross section will be suppressed at low $p_\perp$ because of its mass. No calculations have been done yet.

A trilepton signature has also been studied[30] for Higgs producton. The process

$$pp \to Z^oH^oX, \quad H^o \to \ell^+\ell^-$$

gives a characteristic peak and shoulder for $M_{\ell^+\ell^-}$, as is shown in Fig. 7.1. Unfortunately the cross section is small and the backgrounds are large.

VIII. IMPLICATIONS FOR EXPERIMENTS

Lepton detection has long been emphasized as the best way of studying the $W^{\pm}$ and Z^{o} in pp and $\bar{p}p$ interactions. Many refinements have been made in the calculations, but the original conclusions[1,2] remain substantially valid.

The cross section for the Drell-Yan continuum and for $\ell^{+}\ell^{-}$ pairs from semileptonic decays of heavy quarks are comparable, and both processes are interesting. To study them it is essential to be able to detect leptons within jets and to measure the correlation between the leptons and the associated hadrons. Typically the leptons will have only a small fraction of the jet momentum.

The ability to detect both electrons and muons simultaneously is of only marginal usefulness for $W^{\pm}$ and Z^{o} physics, but it could be quite important for other processes. Measuring $e^{\pm}\mu^{\mp}$ pairs would provide a direct experimental check on the background to Drell-Yan from heavy quark decays. Including both would gain a factor of $2^{3} = 8$ in the rate for trilepton cascades from heavy quarks. It would also give a much better handle on missing neutrinos. This should substantially improve the resolution on heavy quark jets if they can be identified by event topology or in some other way. Thus the detection of both e and μ deserves serious study, although it is obviously very difficult. Since narrow $e\mu$ resonances are not expected, good resolution on both does not seem necessary.

A vertex detector capable of observing the tracks of charmed particles might provide an alternative to $e\mu$ detection. The source of $e\mu$ events is heavy quark production, and all heavy quarks are expected to give charmed particles through the decay chain $t \to b \to c$. Of course such a vertex detector would also be valuable for studying non-leptonic decays.

ACKNOWLEDGMENTS

Many of the results reported here were obtained in collaboration with Serban Protopopescu. I also wish to thank Min Chen, Yee Keung, Larry Trueman, and Ling-Lie Wang for useful discussions. This work was supported by the U.S. Department of Energy under contract DE-AC02-76CH00016.

REFERENCES

1. R.F. Peierls, T.L. Trueman, and L.L. Wang, Phy. Rev. D16, 1397 (1977).
2. C. Quigg, Rev. Mod. Phys. 49, 297 (1977).
3. T.K. Gaisser, F. Halzen, and E.A. Paschos, Phys. Rev. D15, 2572 (1977).
4. S. Pakvasa, M. Dechantsreiter, F. Halzen, and D.M. Scott, Phys. Rev. D20, 2862 (1979).
5. F.E. Paige, BNL-27066 (1979).
6. F.E. Paige and S.D. Protopopescu, BNL-29777 (1981).
7. S. Weinberg, Phys. Rev. Letters 19, 1264 (1967); A. Salam, in Elementary Particle Theory: Relatavistic Groups and Analyticity (Almquist and Wiksell, 1968), pg. 367; S.L. Glashow, J. Iliopoulos, and L. Mainani, Phys. Rev. D2, 1285 (1970).
8. C. Baltay, XIX International Conference on High Energy Physics (Tokyo, 1978), pg. 882.
9. W.J. Marciano and A. Sirlin, Phys. Rev. D22, 2695 (1980).
10. W.J. Marciano and A. Sirlin, Phys. Rev. Letters 46, 163 (1981).
11. H. Georgi nd S.L. Glashow, Phys. Rev. Letters 32, 438 (1974).
12. H.D. Politzer, Nucl. Phys. B129, 301 (1977).
13. R.K. Ellis, H. Georgi, M. Machacek, H.D. Politzer, and D. Ross, Phys. Letters 78B, 281 (1978), Nucl. Phys. B152, 285 (1978); S. Libby and G. Sternman, Phys. Letters, 78B, 618 (1978), Phys. Rev. D18, 3252 and 4737 (1978); D. Amati, R. Petronzio, and G. Veneziano, Nucl. Phys. B140, 54 (1978); A. Mueller, Phys. Rev. D18, 3705 (1978).
14. S.D. Drell and T.M. Yan, Phys. Rev. Letters 25, 316 (1970), Ann. Phys. (N.Y.) 66, 578 (1971).
15. J.E. Pilcher, 1979 International Symposium on Lepton and Photon Interactions (Fermilab), pg. 185.
16. J. Kubar-Andre and F.E. Paige, Phys. Rev. D19, 221 (1979); G. Altarelli, R.K. Ellis, and G. Martinelli, Nucl. Phys. B157, 461 (1979).
17. J.F. Owens and E. Reya, Phys. Rev. D17, 3003 (1978).
18. J.G.H. DeGroot, et al., Z. Physik C1, 143 (1979).
19. D. Antreasyan, et al. Phys. Rev. Letters 47, 12 (1981).
20. A.H. Mueller, private communication.
21. Yu. L. Dokshitser, D.I. Dyakanov, and S.I. Troyan SLAC-TRANS-183 (1978); Phys. Reports 58C, 269 (1980).
22. G. Parisi and G. Petronzio, Nucl. Phys. B154, 427 (1979).
23. A.H. Mueller, these proceedings.
24. J.C. Collins and D.E. Soper, in preparation.
25. G. Altarelli and G. Parisi, Nucl. Phys. B126, 298 (1977).
26. R.D. Field and R.P. Feynman, Nucl. Phys. B136, 1 (1978).
27. J.F. Owens, Phys. Letters 76B, 85 (1978); T.A. DeGrand, Nucl. Phys. B151, 485 (1979).
28. F.E. Paige and S.D. Protopopescu, in preparation.
29. C. Kourkoumelis, et al. Phys. Letters 91B, 481 (1980). Note that this scaling relation is slightly different from the one used here.
30. W-Y. Keung, L.L. Chau Wang, and S.C.C. Ting, BNL-29598 (1981).

FIGURE CAPTIONS

Fig. 3.1: The Drell-Yan graph for W production

Fig. 3.2: The leading QCD graphs for W production at high $q_\perp$.

Fig. 4.1: The $Z^o \to \ell^+\ell^-$ cross section vs $q_\perp$ at $\sqrt{s}$ = 800 GeV.

Fig. 4.2: The $W^+ \to \ell^+\nu$ cross section vs $p_{\ell\perp}$ at $\sqrt{s}$ = 800 GeV.

Fig. 4.3: The $W^+ \to \ell^+\nu$ cross section vs $p_{\ell\perp}$ near the Jacobean peak. The statistics are those expected in the first year of ISABELLE operation.

Fig. 4.4: Lepton rapidity distributions. (a) $W^+ \to \ell^+\nu$. (b) $W^- \to \ell^-\bar{\nu}$.

Fig. 5.1: Single lepton cross section from heavy quarks vs. $p_\perp$.

Fig. 5.2: Dilepton cross section from heavy quarks vs. mass.

Fig. 5.3: Associated hadrons $p_\perp$ for Drell-Yan events with M=50 GeV. See text.

Fig. 5.4: Associated hadron $p_\perp$ for heavy quark events. (a) $10 < p_{\ell\perp} < 20$ GeV. (b) $20 < p_{\ell\perp} < 50$ GeV. See text.

Fig. 6.1: Predicted $Q\bar{Q}$ resonance cross sections and rates assuming L = 2×10^{31} $cm^{-2}s^{-1}$ and $\Delta M/M = 1\%$.

Fig. 7.1: Cross sections for $pp \to \ell^+\ell^+\ell^-X$ vs. $\ell^+\ell^-$ mass. From Ref. 30.

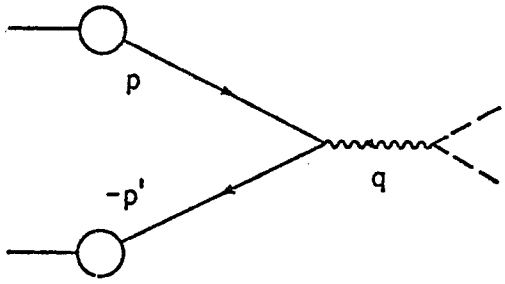

Fig. 3.1

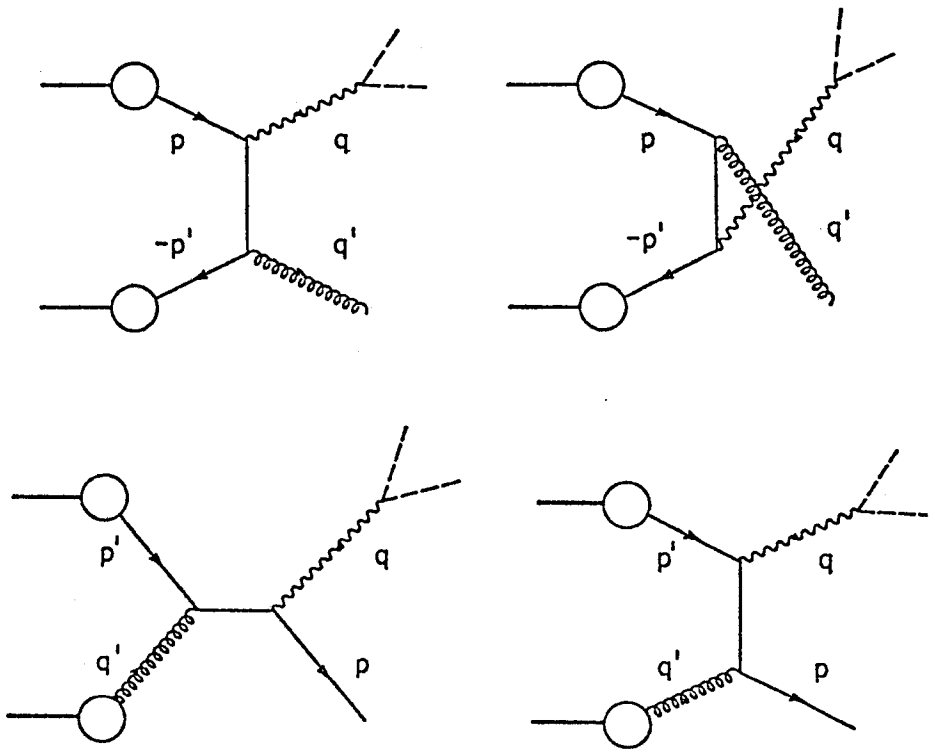

Fig. 3.2

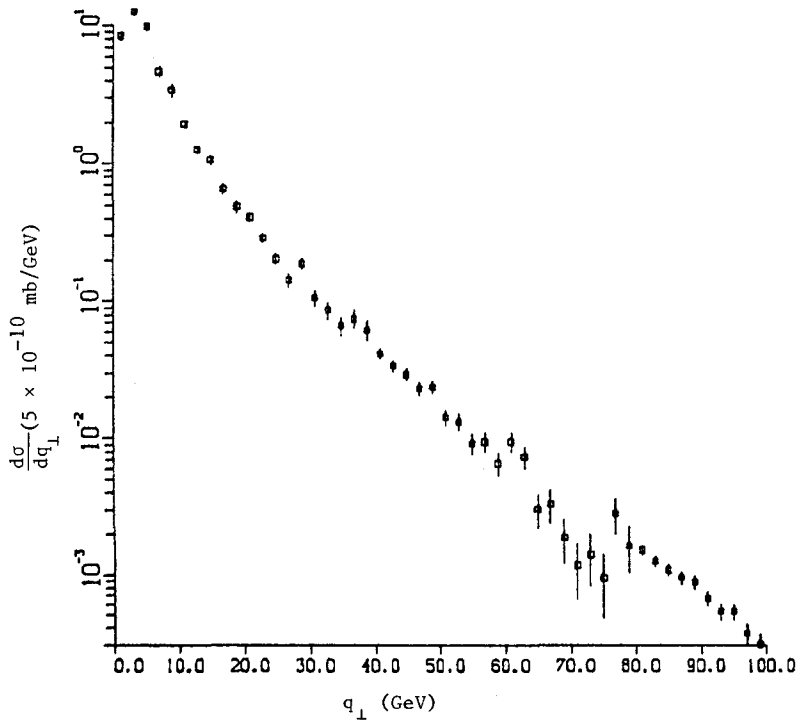
$\frac{d\sigma}{dq_\perp}(5 \times 10^{-10}$ mb/GeV)
10^{1}
10^{0}
10^{-1}
10^{-2}
10^{-3}
0.0
10.0
20.0
30.0
40.0
50.0
60.0
70.0
80.0
90.0
100.0
$q_\perp$ (GeV)

Fig. 4.1

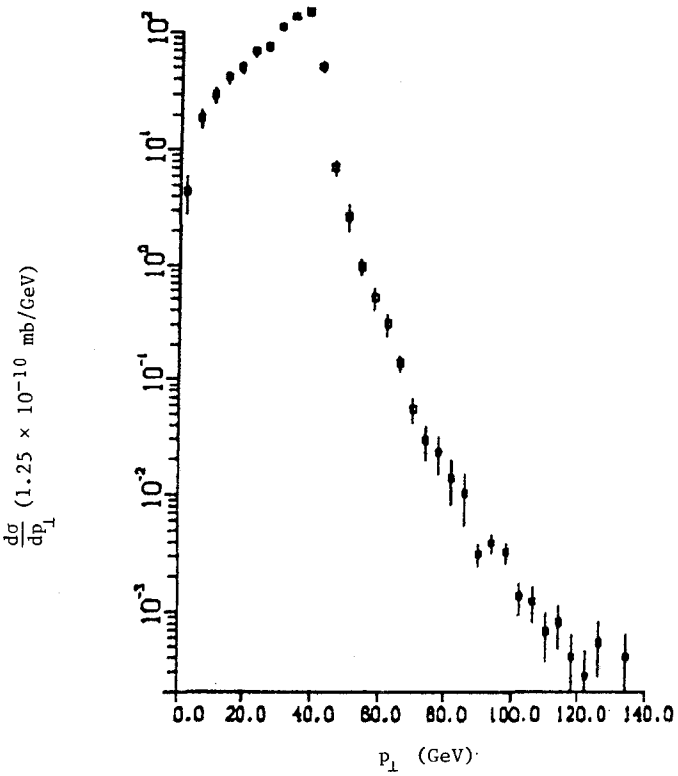
$\frac{d\sigma}{dp_\perp}$ (1.25 × 10^{-10} mb/GeV)
10^{2}
10^{1}
10^{0}
10^{-1}
10^{-2}
10^{-3}
0.0
20.0
40.0
60.0
80.0
100.0
120.0
140.0
$p_\perp$ (GeV)

Fig. 4.2

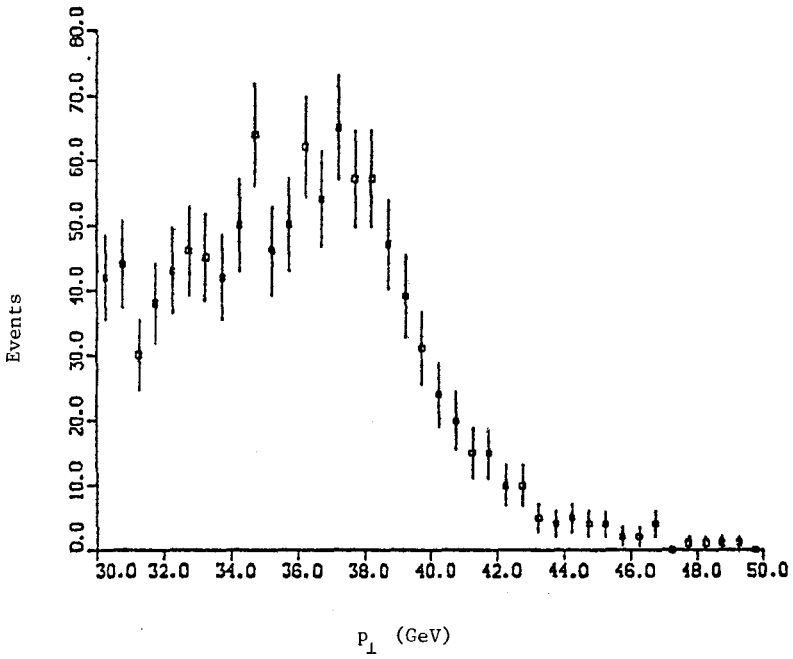
Events
0.0
10.0
20.0
30.0
40.0
50.0
60.0
70.0
80.0
30.0
32.0
34.0
36.0
38.0
40.0
42.0
44.0
46.0
48.0
50.0
$p_\perp$ (GeV)

Fig. 4.3

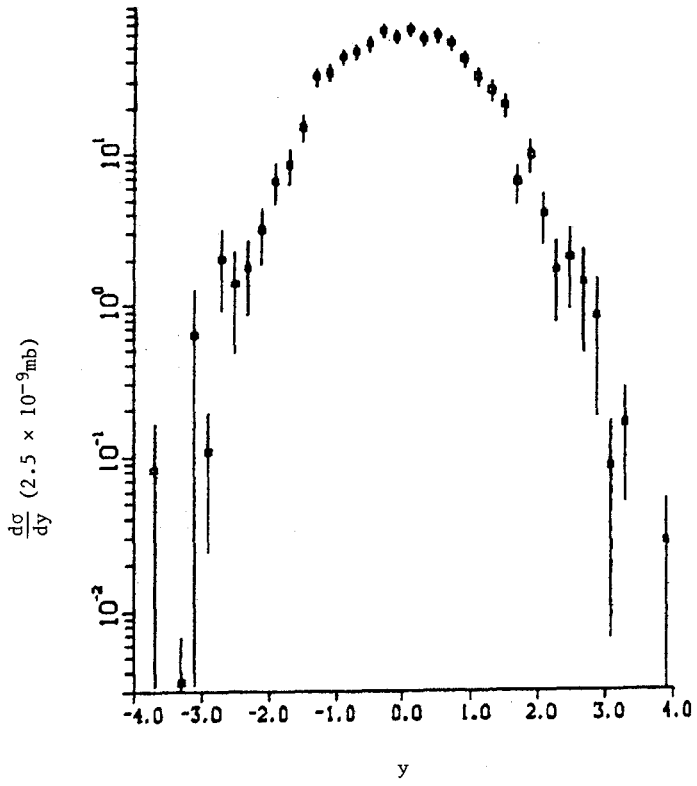
$\frac{d\sigma}{dy}$ (2.5 × 10^{-9}mb)
10^{1}
10^{0}
10^{-1}
10^{-2}
-4.0
-3.0
-2.0
-1.0
0.0
1.0
2.0
3.0
4.0
y

Fig. 4.4a

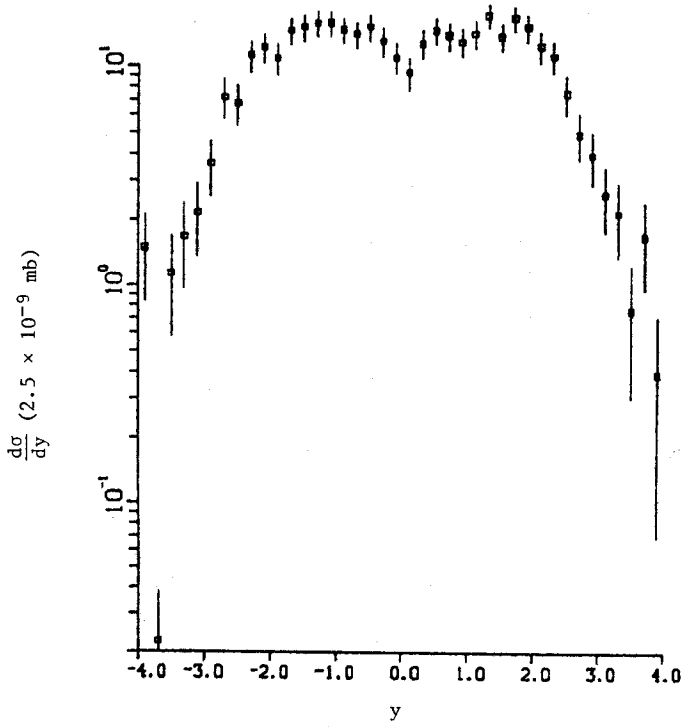

Fig. 4.4b

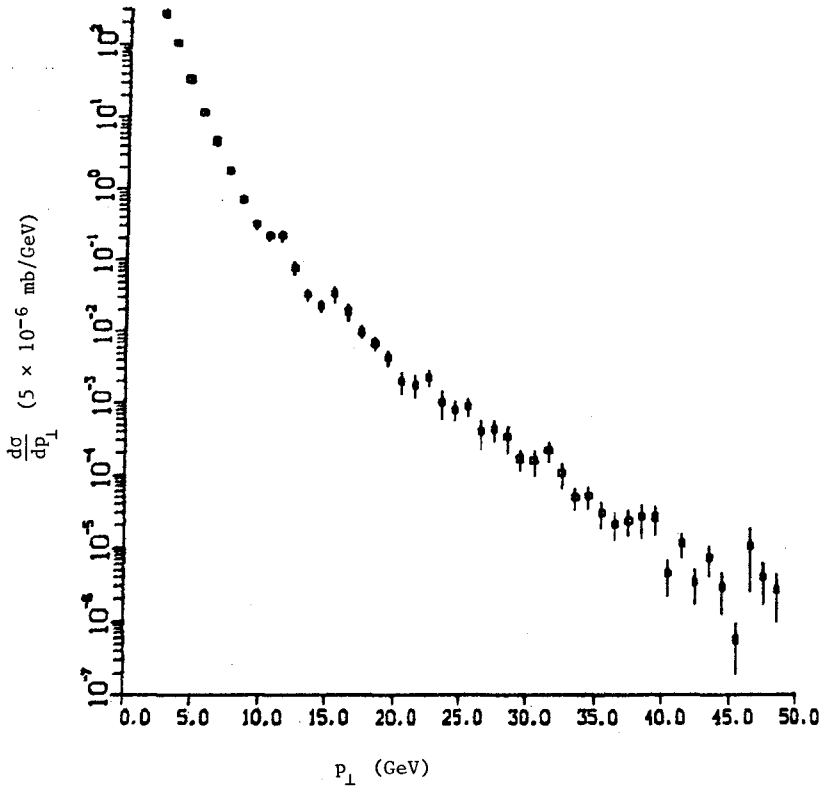
$\frac{d\sigma}{dp_\perp}$ (5 × 10^{-6} mb/GeV)
10^{3}
10^{2}
10^{1}
10^{0}
10^{-1}
10^{-2}
10^{-3}
10^{-4}
10^{-5}
10^{-6}
10^{-7}
0.0
5.0
10.0
15.0
20.0
25.0
30.0
35.0
40.0
45.0
50.0
$p_\perp$ (GeV)

Fig. 5.1

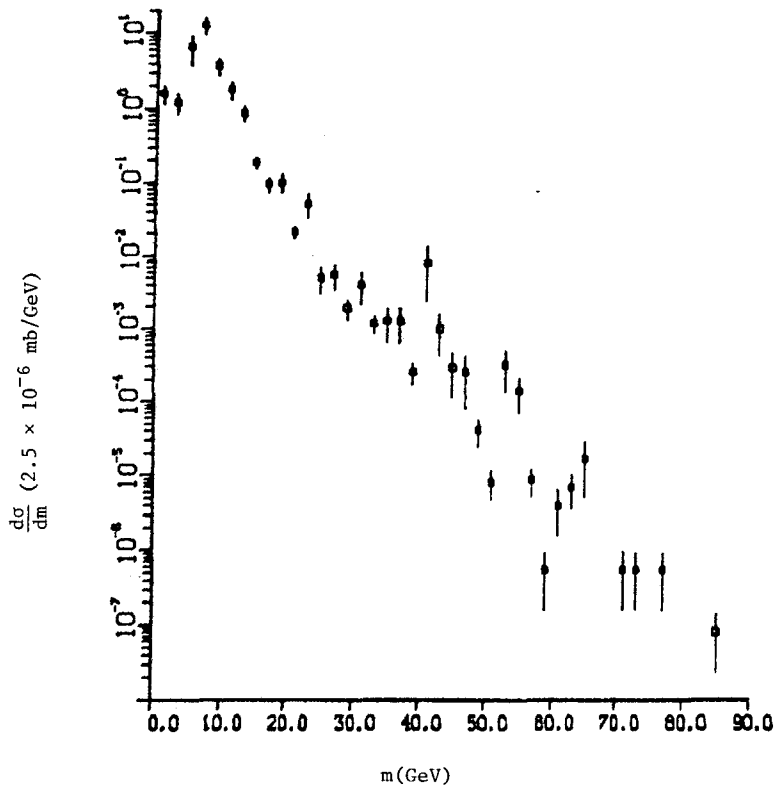
$\frac{d\sigma}{dm}$ (2.5 × 10^{-6} mb/GeV)
10^{-7}
10^{-6}
10^{-5}
10^{-4}
10^{-3}
10^{-2}
10^{-1}
10^{0}
10^{1}
0.0
10.0
20.0
30.0
40.0
50.0
60.0
70.0
80.0
90.0
m(GeV)

Fig. 5.2

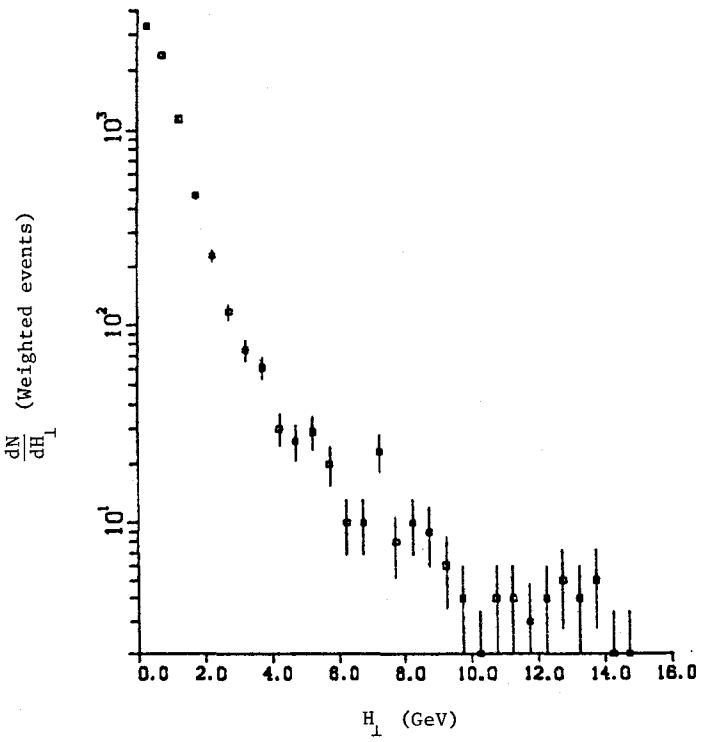
$\frac{dN}{dH_\perp}$ (Weighted events)
10^3
10^2
10^1
0.0
2.0
4.0
6.0
8.0
10.0
12.0
14.0
16.0
$H_\perp$ (GeV)

Fig. 5.3

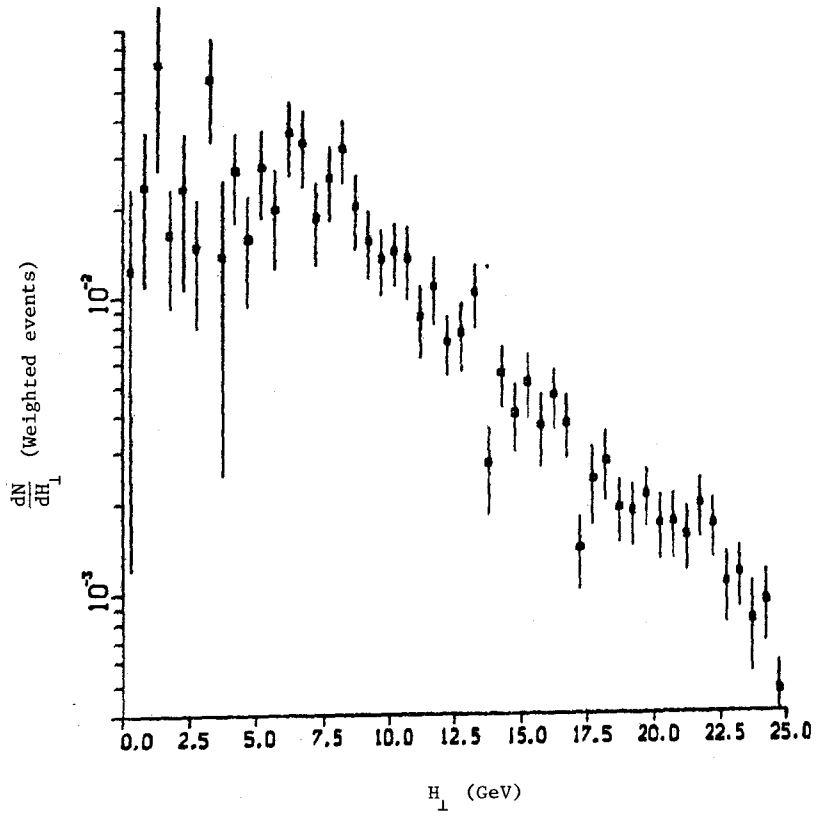
$\frac{dN}{dH_\perp}$ (Weighted events)
10^{-2}
10^{-3}
0.0
2.5
5.0
7.5
10.0
12.5
15.0
17.5
20.0
22.5
25.0
$H_\perp$ (GeV)

Fig. 5.4a

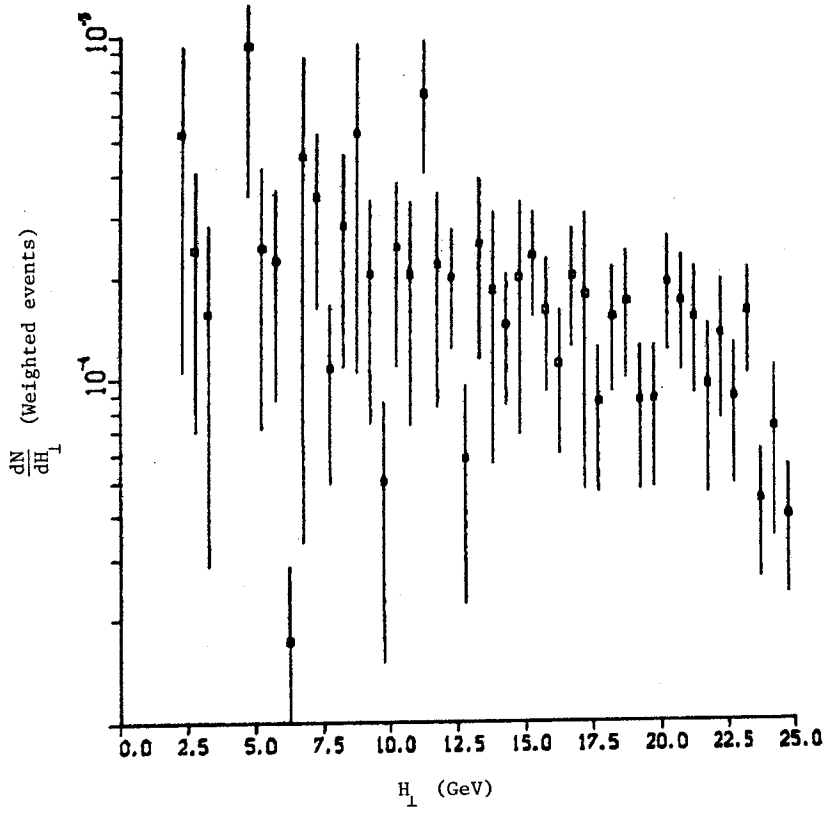
$\frac{dN}{dH_\perp}$ (Weighted events)
10^{-3}
10^{-4}
0.0
2.5
5.0
7.5
10.0
12.5
15.0
17.5
20.0
22.5
25.0
$H_\perp$ (GeV)

Fig. 5.4b

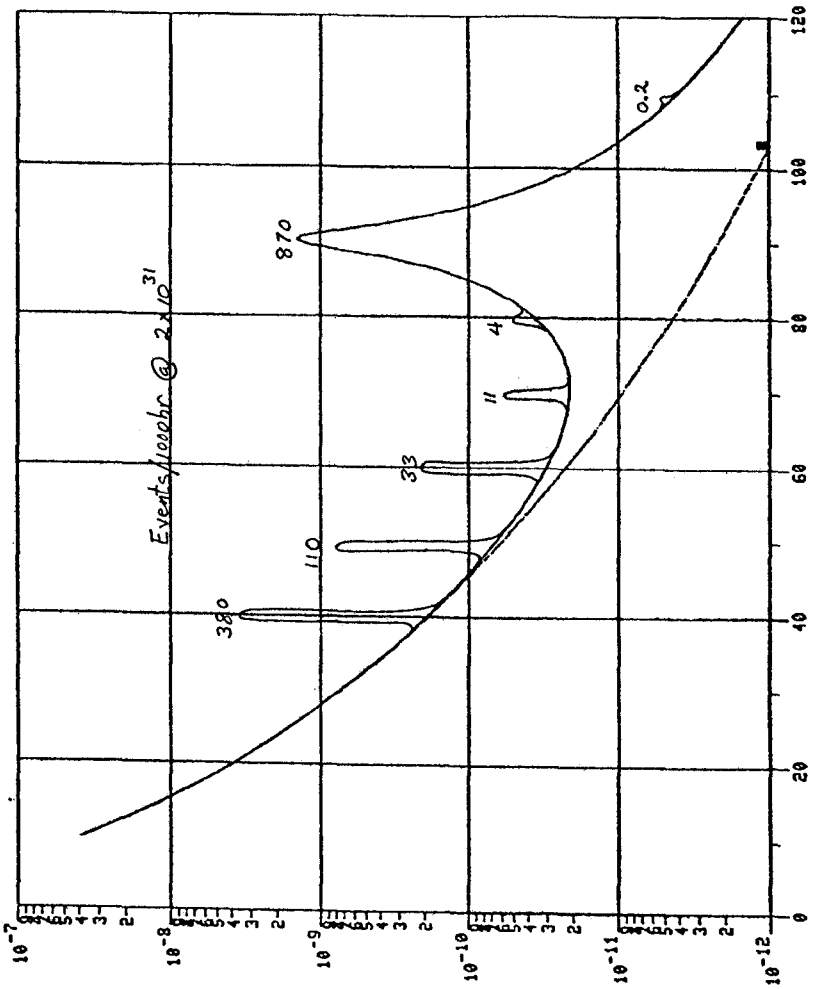
Events/100nbr @ 2x10^31
870
380
110
33
11
4
0.2
M(GeV)
B dσ/dMdy |y=0 (mb/GeV)

Fig. 6.1

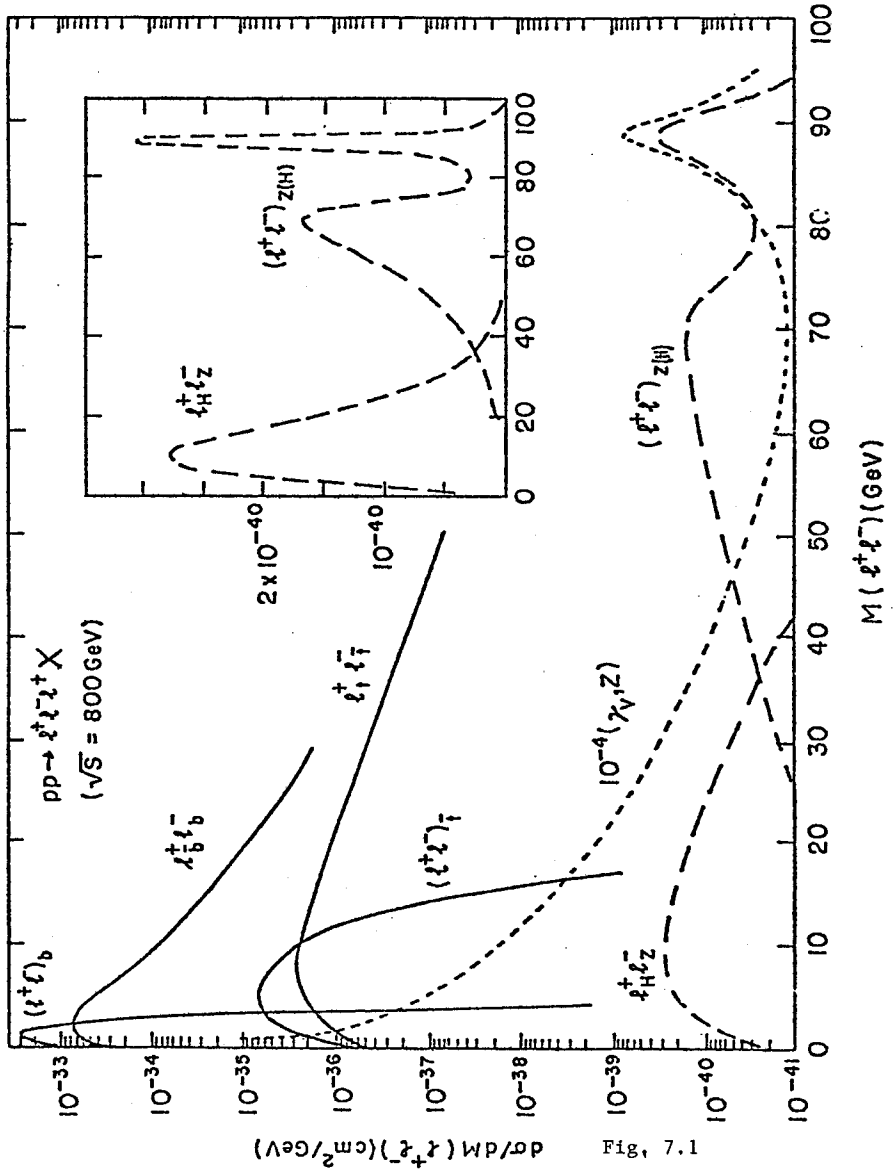
$pp \to \ell^+\ell^-\ell^+ X$
$(\sqrt{s} = 800\,GeV)$
$\ell_b^+\ell_b^-$
$\ell_t^+\ell_t^-$
$(\ell^+\ell^-)_t$
$10^{-4}(\gamma,Z)$
$\ell_H^+\ell_Z^-$
$(\ell^+\ell^-)_{Z(H)}$
$(\ell^+\ell^-)_b$
2×10^{-40}
10^{-40}
$d\sigma/dM(\ell^+\ell^-)(cm^2/GeV)$
$M(\ell^+\ell^-)(GeV)$

Fig. 7.1

PHYSICS FROM PETRA

P. Duinker, NIKHEF, Amsterdam, The Netherlands

Editors' Note: Dr. Duinker gave a thorough report of the physics from Petra, see his lecture, "Review of Electron-Positron Physics at Petra", The International School of Subnuclear Physics, Erice, Italy, 1980.

PHYSICS AT ISR ENERGIES

Lepton Pairs and High p_T

1981 ISABELLE Summer Study

Ulrich Becker

Massachusetts Institute of Technology

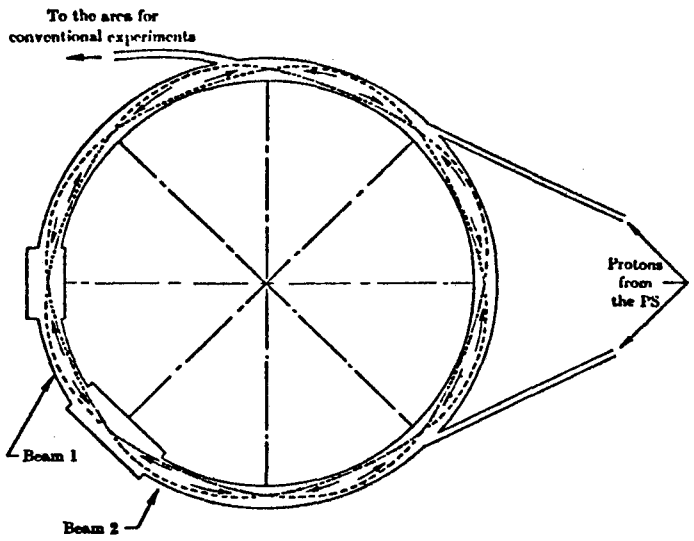
To the area for
conventional experiments
Protons
from
the PS
Beam 1
Beam 2

Figure 1

The ISR may be considered the ancestor of ISA, being a proton-proton collider. So we may start with a short history. The machine shown in Fig. 1 was designed to store protons of 12-31.5 GeV per beam. The ISR was completed in 1971 and at Amsterdam, Kjell Johnsen reported stable beams of 2A with lifetimes of weeks[1].

The luminosity of $\sim 10^{28}\ cm^{-2}/s^{-1}$ enabled measurement of total cross sections and multiplicities[2], and both were found to be rising logarithmically (see Figs. 2a and 2b). With quickly increasing luminosity, measurements of the shrinking elastic slope and more pronounced (deeper) diffractive minima became possible (Fig. 3). The design luminosity of $4 \cdot 10^{-30}$ was reached with 12 A beams in 1972. I myself witnessed the ISR exceeding its design luminosity by a considerable factor and remember data-taking in 1979 with 45 on 40 Amperes and $L = 3 \cdot 10^{31}\ cm^{-2}/s^{-1}$, making experiments fast and enjoyable, since the background stayed modest.

Clearly, this talk cannot give an account of all work done at the ISR, which is done anyway in excellent reviews[3]. Instead are presented some measurements of lepton pair production and high p_T phenomena which led to the understanding of constituents in the proton and show the influence of QCD.

---

(1) K. Johnsen, Proceedings of the 1971 Amsterdam Conf., 373.

(2) G. Giacomelli, ibid.

(3) M. Jacob, Physics Report 62 (1980).

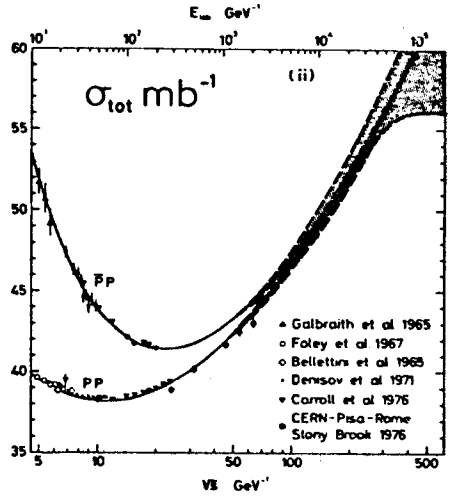

Figure 2a

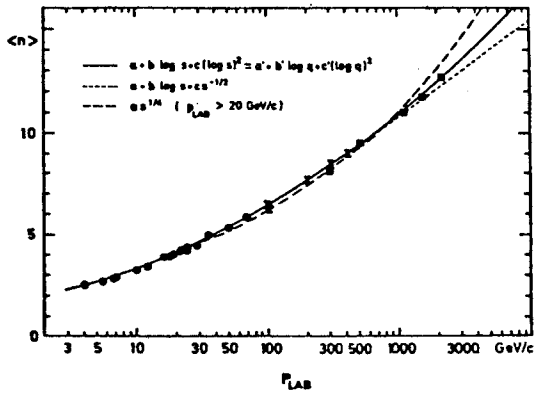

Figure 2b

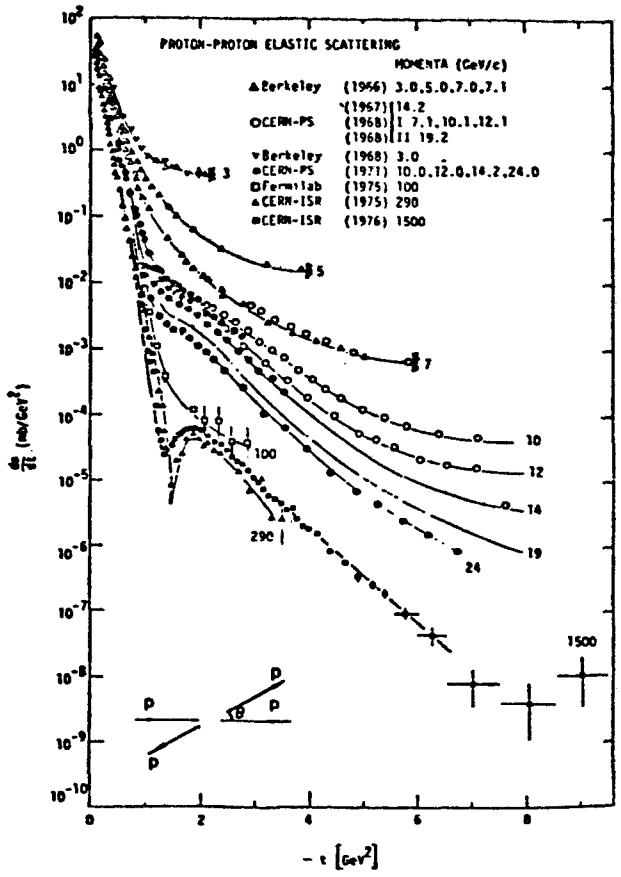
PROTON-PROTON ELASTIC SCATTERING
MOMENTA (GeV/c)
ΔBerkeley (1966) 3.0,5.0,7.0,7.1
(1967) 14.2
OCERN-PS (1968) I 7.1,10.1,12.1
(1968) II 19.2
▽Berkeley (1968) 3.0
◉CERN-PS (1971) 10.0,12.0,14.2,24.0
□Fermilab (1975) 100
▲CERN-ISR (1975) 290
■CERN-ISR (1976) 1500
3
5
7
10
12
14
19
24
100
290
1500
p
p
p
p
θ
$\frac{d\sigma}{dt}$ (mb/GeV^2)
$-t$ [GeV^2]

Figure 3

Large p_T phenomena

It started 1973 with the observation[1] of anomalously large yields of π mesons produced with large transverse momenta relative to the C.M. motion. Fig. 4a shows the early CCR (ref. 1a) π^o data compared to an exponential extrapolation of low p_T data. This hard scattering component could be explained as a production mechanism originating from smaller sources inside the proton. Lowest order QCD calculations[2] predict a p_T^{-4} behavior at large p_T. Fig. 4b shows accurate recent measurements[3] compared to the $p_T^{-8} \cdot F(X_T)$ parameterization which was found to hold for $p_T < 7$ GeV. We are at higher p_T values an excess approaching p_T^{-4}. In fact, the behavior is compatible with more detailed QCD calculations[2].

---

(1) M. Banner et al., Phys. Lett. 44B (1973), 537.
F.W. Büsser et al., Phys. Lett. 46B (1973), 471.
B. Alper et al., Phys. Lett. 44B (1973), 521.

(2) H.D. Politzer, Asymptotic freedom: an approach to strong interactions, Phys. Reports 14 (1974), 129. W. Marciano and H. Pagels, Quantum Chromodynamics, Phys. Reports 36 (1978), 137.
For a detailed discussion of the QCD analysis of large p_T production, see:
Jets in high energy collisions, Physica Scripta 19, Vol. 2 (1979).

(3) A.L.S. Angelis et al., Phys. Lett. 79B (1978), 505; A.G. Clark et al., Phys. Lett. 74B (1978), 267; C. Kourkoumelis et al., Phys. Lett. 84B (1979), 271.

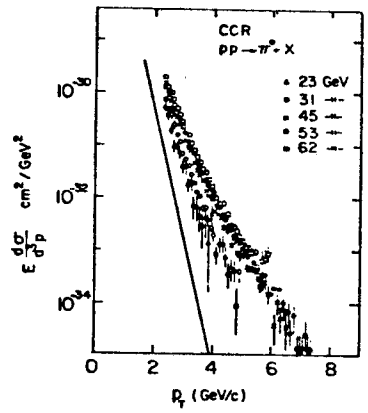

Figure 4a

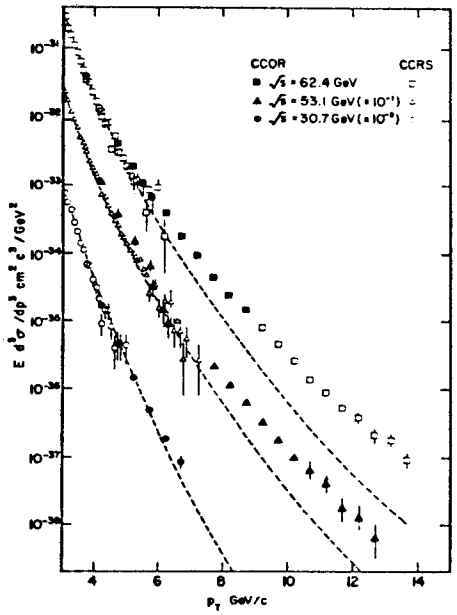

Figure 4b

Most surprisingly, the ratio of prompt electrons followed[1] the trend of the π^0's with a ratio of 10^{-4} as depicted in Fig. 5 for the example of the CCR data. With the advent of the J and charmed mesons, this ratio could be explained naturally[2].

The consequent step was to measure e-pairs, which the groups[1,3] did in different mass regions.

e^+e^- pair measurement[3]

The electron pairs are detected using four modules, each consisting of proportional chambers, plastic scintillator hodoscopes, lithium foil transition radiators followed by xenon linear proportional chambers which provided electron-hadron discrimination, and a lead/liquid-argon electromagnetic shower detector segmented laterally and longitudinally to provide measurement of the electron energy, and to achieve further rejection of hadrons. Each module covers 50° to 130° in polar angle and 40° in azimuth (see Fig. 6).

---

(1) Angelis et al., ibid; Clark et al., ibid; Kourkoumelis et al., ibid.

(2) L.M. Lederman, Phys, Rep. 26 (1976), 4.

(3) C. Kourkoumelis et al., CERN EP 80-08 and Phys. Lett.

Figure 5

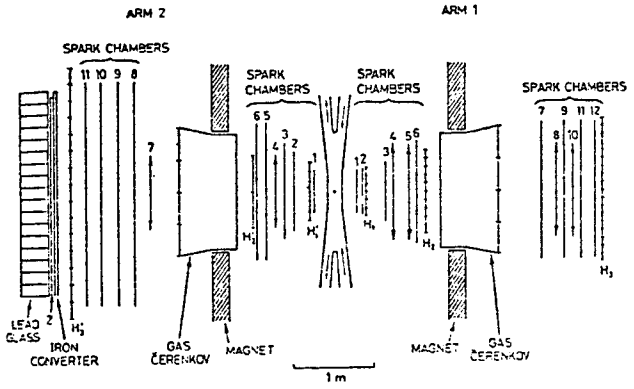

Fig. 12. Plan view of apparatus.

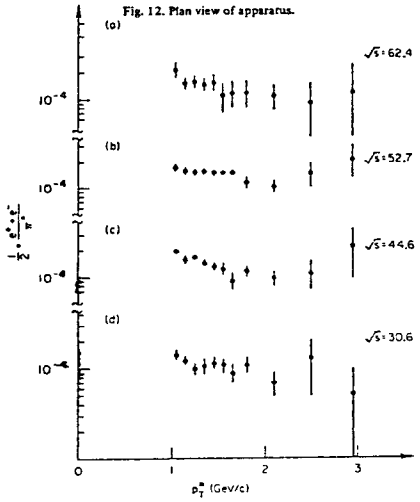

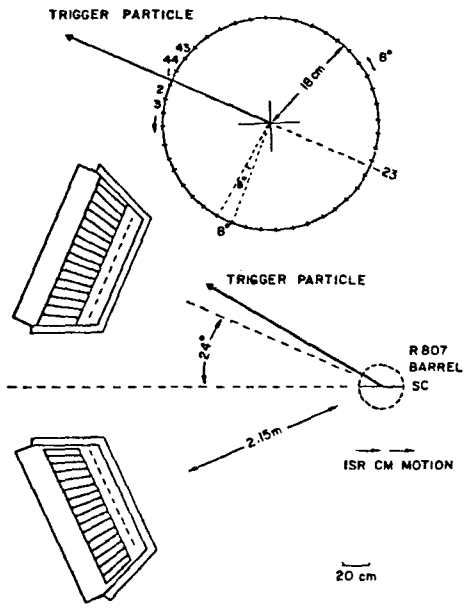
TRIGGER PARTICLE
43
44
3"
18 cm
6°
23
8°
TRIGGER PARTICLE
24°
R807
BARREL
SC
2.15m
ISR CM MOTION
20 cm

Figure 6

The four modules were run in two configurations. One, optimized for back-to-back electrons and hence high-mass pairs, was run for luminosities of 0.459 and 8.52×10^{37} cm^{-2} at $\sqrt{s}$ = 53, and 63 GeV.

The main sources of background are external and internal photon conversions, showers simulated by hadrons interacting in the calorimeter, and hadron tracks overlapping with electromagnetic showers. These are eliminated mainly by the requirements of minimum ionization, transverse and longitudinal shower distributions, and transition radiation generation respectively.

For example, in the mass interval $5 < m_{ee} < 6$ GeV for an overall efficiency of dielectron identification, $\epsilon = 0.11$, the residual background was estimated to be 30%. At higher masses, $8 < m_{ee} < 10$ GeV for the same ϵ, the level of the background is only 6%.

Figure 7 shows the dielectron cross section as a function of mass for the combined data at $\sqrt{s}$ = 53 and 63 GeV. A 50% uncertainty on the subtraction of the background was included in the error. These data were used to study Drell-Yan scaling after excluding the J and T resonances. Widening the $\tau = m^2/s$ region by including data from FNAL and ISR[1], the larger range of τ-values can be represented by :

$$m^3 \frac{d^2\sigma}{dmdy}\Big|_{y=0} = (2.60 \pm 0.13) \times 10^{-32} \exp\left((-2.0 \pm 0.7)\frac{m}{\sqrt{s}}\right)\left(1 - \frac{m}{\sqrt{s}}\right)^{9.7 \pm 0.4} \text{ cm}^2 \text{ GeV}^2,$$

(χ^2 of 72 for 57 degrees of freedom).

---

(1) D.K. Kaplan et al., Phys. Rev. Lett. 40 (1978), 435.

A.J. Clark et al., Nucl. Phys. B142 (1978), 29.

The confirmation of resonances in the mass region 1.5 to 2.4 GeV may question the use of these data as continuum.

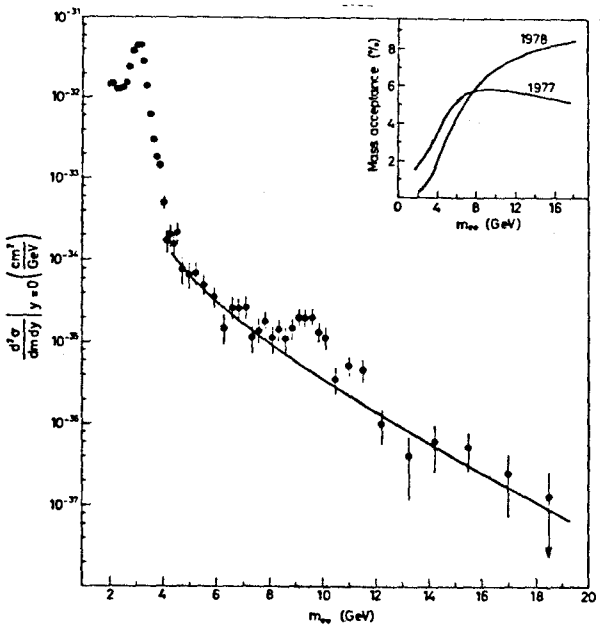

Figure 7

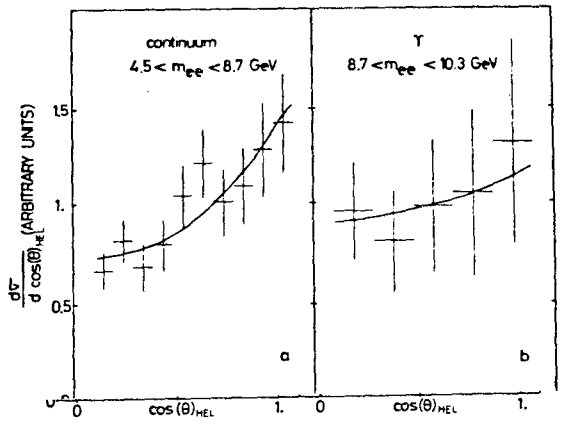

Figure 8

Fig. 8a shows the angular distribution of the e-pairs from the non-resonant mass region $4.5 < m_{ee} < 8.7$ GeV. The $1 + (1.2 \pm .3) \cos^2 \theta_H$ distribution lends strong support to the annihilation mechanism of Drell-Yan. In the T region, the distribution is flatter with a polarization of 0.79 ± 40 only. This diminishes to 0.31 ± 0.35 when 50% continuum is removed.

Fig. 9 shows the distribution as a function of p_T for different mass intervals for the restricted sample, where no other tracks or showers enter the same module with the electron. A comparison shows that the low multiplicity sample underestimates $\langle p_T \rangle$ by $6 \pm 4\%$. The data in Fig. 9 were not corrected for this effect. A fit was made to the form $d\sigma/dp_T^2 = A \exp(-bp_T)$. The resulting $\langle p_T \rangle$ is given in Table I. The results agree well with the excellent electron pair experiment using the superconducting solenoid[1].

$\mu^+\mu^-$ pair measurement[2]

The experiment measured the reaction

$$pp \rightarrow \mu^+\mu^- X \qquad (1)$$

It was carried out at the CERN ISR, as displayed in Fig. 10, at a center-of-mass energy of $\sqrt{s} = 62$ GeV and an integrated luminosity of $1.11 \times 10^{38} cm^{-2}$. This experiment has obtained 12300 muon pairs with an invariant mass above 2.8 GeV.

---

(1) A.L.S. Angelis et al., Phys. Lett. 87B (1979), 398.

(2) D. Antreasyan et al., Phys. Rev. Lett. 45, 863 (1980)

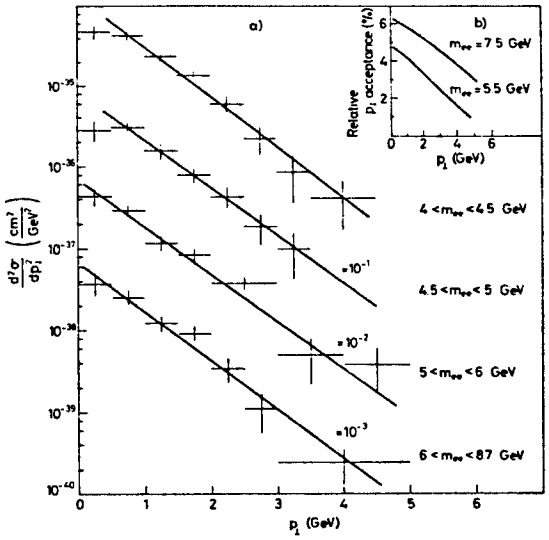

Figure 9

The $\langle p_T \rangle = 2/b$ were also consistent with a straight weighted average on the p_T.

$\langle p_T \rangle = 1.42 \pm 0.20$ GeV for $4.0 < m < 4.5$ GeV;
$\langle p_T \rangle = 1.46 \pm 0.10$ GeV for $4.5 < m < 5.0$ GeV;
$\langle p_T \rangle = 1.42 \pm 0.09$ GeV for $5.0 < m < 6.0$ GeV;
$\langle p_T \rangle = 1.43 \pm 0.09$ GeV for $6.0 < m < 8.7$ GeV;
$\langle p_T \rangle = 1.78 \pm 0.13$ GeV for $8.7 < m < 10.3$ GeV.

Table I

The high cross section of muon pair production, the small scaling variable values $\tau = m^2/s$, and the absence of nuclear shadowing corrections from pure pp collisions provide a sensitive search for new particles[1] and a test of scaling models[2].

The detector is shown in Figure 11. It is a large-acceptance spectrometer composed of seven magnetized iron toroids, excited to 18 kgauss and totaling 450 tons, which provide both the hadron absorber and the magnetic field for momentum amalysis of muons. The computer reconstruction of an event with mass 24.5 GeV/c^2 and p_T = 1.2 GeV/c is superimposed over the drawing. Chamber spacepoints are denoted by circles, and the shaded areas labeled "δ" represent the D-hodoscope interception points determined to within 25 cm.

To reduce background from hadron decays, the absorber starts ~ 40 cm from the interaction point. Muons are identified by penetration of 1.3 m magnetized iron requiring a minimum of 1.8 GeV/c.

Large size drift chambers determine the muon momenta. These chambers[3], of sizes up to 6.0 x 2.7 m^2, measure both coordinates twice with a resolution of σ = 430 μm. 4800 wires spaced at 10 cm cover 800 m^2 of sensitive area.

---

(1) J.J. Aubert et al., Phys. Rev. Lett. 33 (1974), 1404; S.W. Herb et al., Phys. Rev. Lett. 39 (1977), 252.

(2) S.D. Drell and T.M. Yan, Phys. Rev. Lett. 25, (1970), 316, 920.

(3) U. Becker et al., Nucl. Instrum. Meth. 128 (1975), 593.

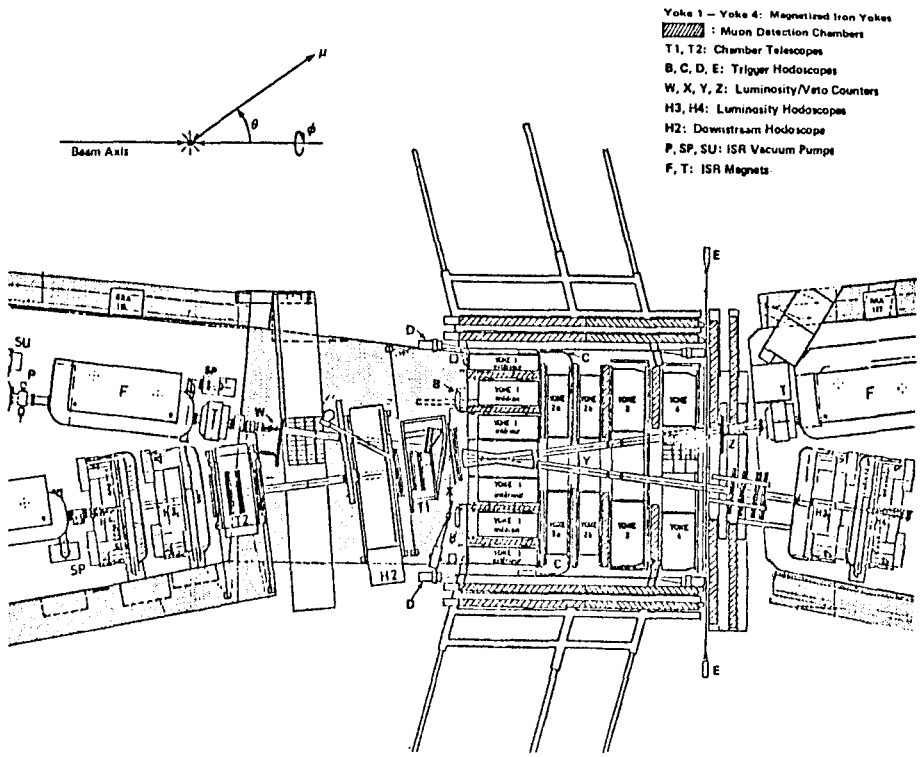
Yoke 1 – Yoke 4: Magnetized Iron Yokes
: Muon Detection Chambers
T1, T2: Chamber Telescopes
B, C, D, E: Trigger Hodoscopes
W, X, Y, Z: Luminosity/Veto Counters
H3, H4: Luminosity Hodoscopes
H2: Downstream Hodoscope
P, SP, SU: ISR Vacuum Pumps
F, T: ISR Magnets
μ
θ
φ
Beam Axis
SU
P
F
W
B
D
C
E
T1
T2
H2
SP
T
Z
Y
X

Figure 10

Around the interaction region an array of 136 small drift chambers measures charged tracks within $9^{o} < \theta < 171^{o}$ and $0 < \phi < 360^{o}$ with a precision of 0.3 mm along the beam and 2.6 mm transverse to it. This allows one to count associatied multiplicities, but without magnetic analysis. Chambers mounted further downstream extend the detection range down from $\theta = 1^{o}$. The observed muon tracks together with the hadron tracks determine the vertex.

For muon pairs the magnetic spectrometer has a large acceptance of $15^{o} < \theta < 120^{o}$ and $P_{\mu} < 1.8$ GeV. The large θ range implies a wide acceptance in $x \simeq 2P_{L}/\sqrt{s}$. Having little ϕ restriction the acceptance in p_{T}, the transverse momentum of the muon pair, is rather uniform for $m \leq 8$ GeV.

Mass spectrum

We have observed events with masses up to 25 GeV. The computer-reconstructed top view of one event with m = 24.5 GeV has been superimposed onto the cut view of the detector in Figure 11.

Figure 12a shows the observed mass spectrum of dimuon events. Drell-Yan contribution (0) and background (+) are indicated. The background from decay and punch-through of hadrons was calculated from the amount of like-sign muon pairs. It is negligible for m > 8 GeV.

The mass resolution is limited by multiple scattering in the iron. We expect $\Delta m/m = 11\%$ almost independent of mass. This is in good agreement with the direct measurement of J in Figure 12a, yielding 10.8%. There are 2580 events with m > 5 GeV, 1150 events with m > 8 GeV, and 3 events with m > 20 GeV. All events with m > 8 GeV have been visually scanned.

Two independent detection systems of small angle hodoscopes have recorded the luminosity. Over a period of 18 months they agreed to better than 6%.

FIGURE II THE SPECTROMETER - CUTAWAY VIEW

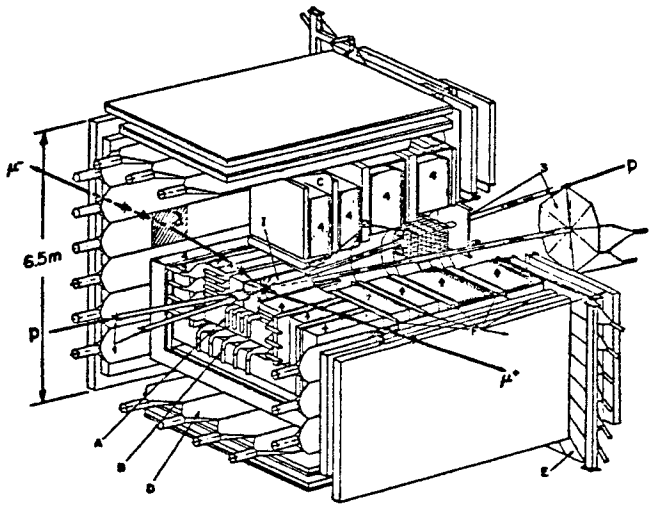

LEGEND:

1) Beam pipes
2) Lead absorbers
3) Luminosity and beam-veto monitors
4) Magnitized iron toroids
A) Inner hodoscope (there are 2 sets of A counters; the set described in the text is not shown)
B,D) Trigger hodoscopes coaxial with beamline
C,E) Trigger hodoscopes perpendicular to beamline
F) Drift chambers for muon detection
I) Interaction region and vertex detector

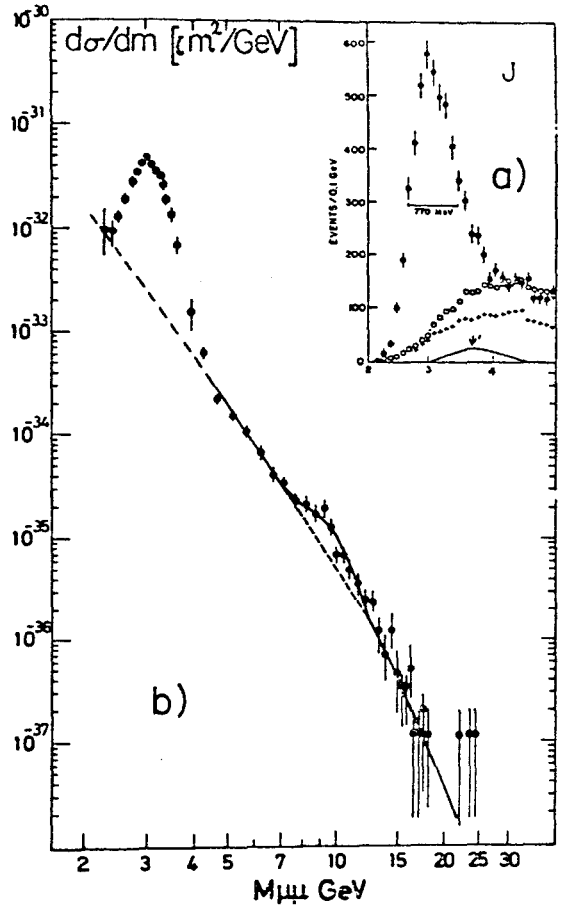

Figure 12

The mass acceptance for m > 5 GeV was calculated by Monte Carlo using a production mechanism of $d\sigma/dx_F\ dp_T\ d\cos\theta \sim (1 - |x_F|)^{3.0}\ \exp(-1.1\ p_T) \cdot (1 + \cos^2\theta_{cs})$ consistent with our continuum data. Multiple scattering, energy loss, trigger and fiducial constraints are taken into account. The resulting mass acceptance rises from 5% at m = 5 GeV to a plateau of 16% for m $\geq$ 8 GeV. It is insensitive to x_F and p_T distributions, but increases ~ 20% for isotropic emission in θ_{cs}, the Collins-Soper[2] angle.

An ansatz for the T resonances and a continuum was fitted to our cross section. The observed resonance shape is dominated by the resolution of the apparatus, $\Delta m/m = 11\%$.

$$\frac{d\sigma}{dm} = A\left\{\exp -\left(\frac{m - 9.46}{\sqrt{2} \cdot \Delta m}\right)^2 + 0.30 \exp -\left(\frac{m - 10.05}{\sqrt{2} \cdot \Delta m}\right)^2 + 0.15 \exp -\left(\frac{m - 10.4}{\sqrt{2} \cdot \Delta m}\right)^2\right\} + B\left\{\frac{(1 - m/\sqrt{s})^a}{m^4/\sqrt{s}}\right\} \quad (2)$$

We take a = 10 from Kinoshita et al.[3] and the relative T branching ratios from Ueno et al[4]. We obtain a good fit, with $\chi^2/DF = 27.4/26$ shown as the solid line in Fig. 12b.

The fitted A-value from equation (2) measures directly the integrated cross section for the T family. Our measured angular distribution in this mass region is consistent to be isotropic[1]. This implies a 20% reduction in the T cross section, as

---

(1) D. Antreasyan et al., Dynamics of high mass muon pairs produced at the ISR, Phys. Rev. Lett. (August, 1981)

(2) J.C. Collins and D.E. Soper, Phys. Rev. D16 (1977), 2219. θ_{cs} is the angle of μ^+ with respect to the average beam axis as seen from the dimuon system.

(3) K. Kinoshita et al., Phys. Rev. D17 (1977), 1834.

(4) K. Ueno et al., Phys. Rev. Lett. 42 (1979), 486.

mentioned. Thus we obtain

$$\sigma(T + T' + T'' \to \mu^+\mu^-) = (14.5 \pm 3.5)\ \text{pb}.$$

The mass region $2.8 < m < 5$ GeV is dominated by $J \to \mu^+\mu^-$ decay (see Fig. 12a). The continuum contribution was calculated from the fit (2) and subtracted. An acceptance at $m = 3.1$ GeV is calculated, weighted with $(1 - |x|)^{3.0} \exp(-1.5\, p_T)$ and isotropic decay. Since the acceptance peaks at $x = 0.2$ we quote:

$$B_{\mu\mu} \left.\frac{d\sigma}{dx}\right|_{\langle x\rangle = .2} (J) = (3.6 \pm 1.1) \times 10^{-32} \text{cm}^2.$$

Results - Scaling

In the Drell-Yan picture the dynamics depends only on the

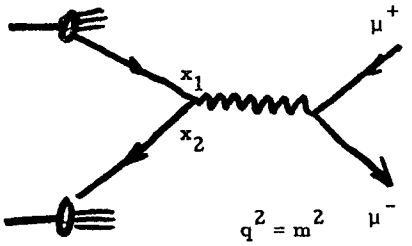

$$q^2 = x_1 x_2 \cdot s$$

$$\to \frac{m^2}{s} = x_1 x_2 = \tau.$$

fractional momenta x_1 and x_2 of the annihilating quarks, hence only on the scaling variable $\tau = m^2/s$, to lowest orders. The fitted value $B = (5.2 \pm 0.2) \cdot 10^{-33} \text{cm}^2\text{GeV}^2$ measures the continuum. If the exponent (a) in the ansatz is treated as a free parameter we find $a = 8 \pm 1$ with $\chi^2/\text{DF} = 22.1/25$.

There have been many excellent experiments on hadron-nuclear production of $\mu^+\mu^-$ pairs at Fermilab, where the measured cross section in the mass region $m > 5$ GeV is a factor of 10-100 lower than our cross section. Some of these experiments overlap with ours in τ and thus provide a unique opportunity to check the scaling phenomena of the time-like photon region.

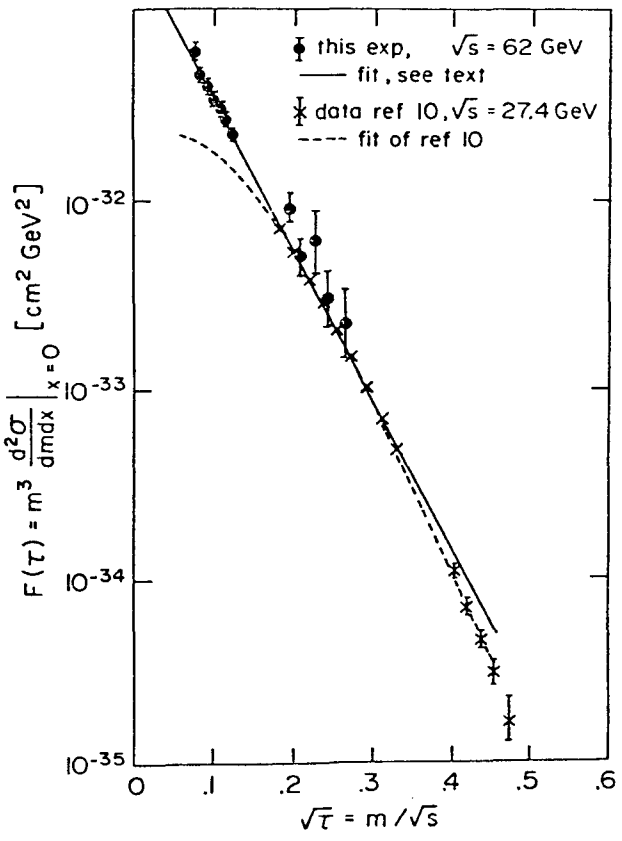
this exp, √s = 62 GeV
fit, see text
data ref 10, √s = 27.4 GeV
fit of ref 10
$F(\tau) = m^3 \frac{d^2\sigma}{dmdx}\Big|_{x=0}$ [cm² GeV²]
10⁻³²
10⁻³³
10⁻³⁴
10⁻³⁵
0
.1
.2
.3
.4
.5
.6
$\sqrt{\tau} = m/\sqrt{s}$

Figure 13

In the scaling model, $F(\tau) = m^3\, d^2\sigma/dmdx \,|_{x=0}$ depends only on the dimnsionless variable τ. We have converted our data in the mass range not affected by resonances (4.5-8 and 12.5-17 GeV). The result is shown in Figure 13 and the solid line represents our continuum fit recast into the scaling form:

$$F(\tau) = m^3 \left.\frac{d^2\sigma}{dmdx}\right|_{x=0} = (1.04 \pm 0.15)^* \, 10^{-32} \, (1-\sqrt{\tau})^{10}/\sqrt{\tau}\ \mathrm{GeV}^2\mathrm{cm}^2.$$

Our experiment overlaps with the high-statistics Fermilab experiment[2] at $\sqrt{\tau} \simeq 0.2$. The comparison is limited by the systematic uncertainty involved in an experiment using nuclear targets and by our statistical accuracy at masses above the T. Within these limitations, scaling holds despite the fact that cross sections in the same mass region differ by orders of magnitude. However, as can be seen in Fig. 13, the phenomenological ansatz used to describe the high statistics, low energy Fermilab data[2] is not valid in the very small τ region measured in this experiment.

We turn now to the more detailed production features of dimuon pairs.

---

(1) L.M. Lederman, Tokyo Conf., 580.

(2) J.K. Yoh et al., Phys. Rev. Lett. 41 (1978), 684.

Production Dynamics

The interest comes, of course, from the possibility of probing the internal proton structure with time-like photons. In particular, the model of Drell and Yan[1] views the μ pairs as originating from quark-antiquark annihilation; hence the production dynamics is related to quark distributions in the proton. Quantum Chromodynamics modifies this mechanism by invoking quark-gluon interaction terms[2]. The production of muon pairs with P_T larger than the confinement momenta of quarks is thus possible from hard gluon emission.

The data were accumulated with an integrated luminosity $L = 1.12 \times 10^{38}$ cm^{-2} at $\sqrt{s} = 62$ GeV as before and $L = 0.42 \times 10^{38}$ cm^{-2} at $\sqrt{s} = 44$ GeV in addition; both above the energy range of previous dimuon measurements[3] using nuclear targets. Beam-associated backgrounds and hadron track contaminations were suppressed by: (a) eliminating muon tracks parallel to the plane containing the ISR beams, (b) requiring the fitted χ^2 of each muon track to be consistent with multiple scattering, which eliminates hadron showers, and (c) requiring each muon to traverse at least 22 kgauss-meter of magnetized iron.

---

(1) S. D. Drell and T. M. Yan, Phys. Rev. Lett. 25, 316, 920 (E) (1970).

(2) These were studied in the inverse reaction of lepton pair annihilation, see: D. P. Barber et al., Phys. Report C3, 7, 1 (1980). For details on p_T, see: G. Altarelli et al., Phys. Lett. 76B, 351 (1978) and Phys. Lett. 76B, 356 (1978). Yu. L. Dokshitser et al., Phys. Reports 58, 269 (1980) and references therein.

(3) J. Branson et al., Phys. Rev. Lett. 38, 1344 (1977); J. K. Yoh et al., Phys. Rev. Lett. 41, 684 (1978); K. J. Anderson et al., Phys. Rev. Lett. 42, 944 (1979).

These cuts are sharper than before, but guarantee a clean sample with low background which can be obtained only from μ-pair measurement. The relatively high statistics of this experiment permits applications of ~~high~~ stringent cuts. Specifically, we have subdivided the $\sqrt{s}$ = 62 GeV data into mass intervals of 2-4, 5-8, 8-11 and 11-25 GeV with 4389, 1457, 536, 143 events respectively, and with relative background rates of 13, 19, 4 and 1% as computed from the rate of like-sign pairs. For the 44 GeV data, the mass intervals were 2-4, 5-8 and 8-17 GeV, with 897, 259, and 77 events and with 14, 10, and 1% background respectively. For both data sets the mass intervals 2-4 and 8-11 GeV are dominated by J and T resonances.

The experimentally measured resolutions were $\Delta m/m$ = 11%, in $x = p/p_{max}$ < 0.05 and 20% in p_T, above 1 GeV which agree with calculations by the Monte Carlo method. To obtain acceptances, the Monte Carlo program generated events with variables m', x', p_T', $\cos\theta_{cs}'$. Each event is weighted by the production mechanism:

$$\frac{d^4N}{dm'dp_T'^2dx'd\cos\theta'} = A\,\frac{(1-m'/\sqrt{s})^{10}}{m'^4/\sqrt{s}}\,(1-|x'|)^a\,e^{-bp_T}\,(1+c\cos^2\theta') \qquad (3)$$

and traced through the detector, taking into account multiple scattering and energy loss. The same program which treats the data reconstructs the "apparent" variables m, x, p_T, and cos θ. Fitting the event distributions in these variables to the measured events ensures accurate treatment of the resolution, and determines the parameters A, a, b, and c, which were used to calculate acceptances. The acceptance covers the x range from -0.1 to 0.8. The acceptance in p_T is roughly flat up to $p_T \simeq 8$ GeV for m > 8 GeV, and slowly drops as a function of p_T for lower pair masses. The acceptance in cos θ is peaked at 0^o.

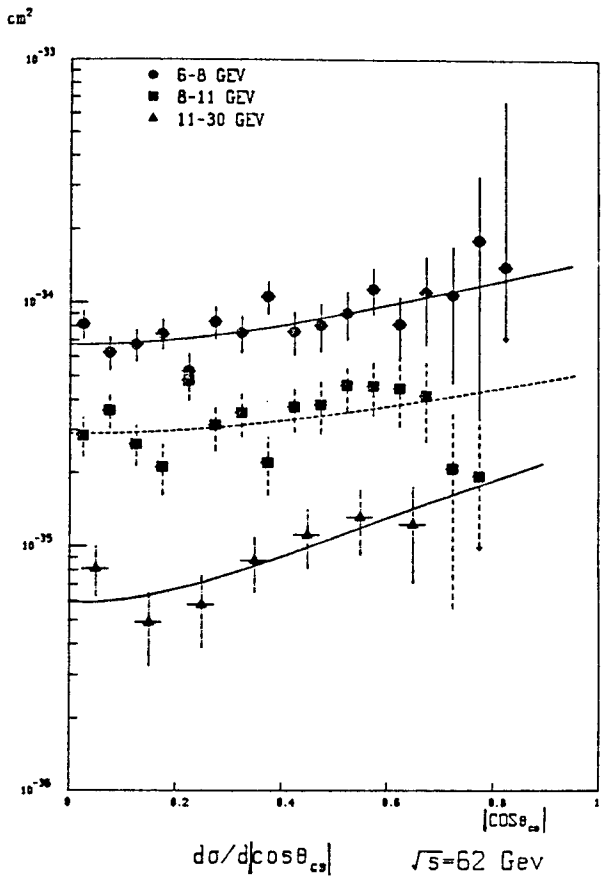

Figure 14

For the resonance-free region $5 < m < 8$ GeV at $\sqrt{s} = 62$ GeV, the angular distribution of the muons relative to the Collins-Soper axis was fitted with $(1 + c \cos^2\theta)$. We find $c = 1.0 \pm 0.5$, consistent with expectations from the Drell-Yan mechanism and with the e-pair measurements presented before. Similar results are obtained for other mass intervals above 5 GeV (see Fig.14) and the 44 GeV data, with indications of smaller polarization in the T region.

The asymmetric structure of the detector allows a detailed x-dependence measurement. Figure 15 gives the measured distributions in x for the 62 GeV data, which are empirically fitted by $(1-|x|)^a$, with $a = 2.7 \pm 0.3$, 3.3 ± 0.3, and 2.1 ± 0.3 for the 5-8, 8-11, and 11-25 GeV mass intervals respectively. In particular, we notice a higher a-value in the 8-11 GeV region (50% contribution from T resonances), and a slightly flatter behavior at $11 < m < 25$ GeV. The distributions agree quite well in shape with a Drell-Yan calculation of:

$$\left.\frac{d\sigma}{dm dx}\right|_{x=0} = \frac{8\pi\alpha^2\sqrt{s}}{m^4} \frac{\bar{u}(x)}{g} \left\{ 4\, u_v(x) + d_v(x) + \frac{21}{4}\, \bar{u}(x) \right\}$$

with specific structure functions[1]:

$$u_v(x) = 2.13\, x^{0.5}(1-x)^{2.8}$$
$$d_v(x) = 1.26\, x^{0.5}(1-x)^{3.8}$$
$$u_s = \bar{u} = d_s = \bar{d} = 2s = 2\bar{s} = 0.27(1-x)^{8.1}$$

The dashed line is the result of this calculation scaled up by an empirical factor 16.

---

(1) J. G. H. de Groot et al., Z. Phys. C1 (1979), 143.

J. Badier et al., Physics Letters 89B (1979), 145.

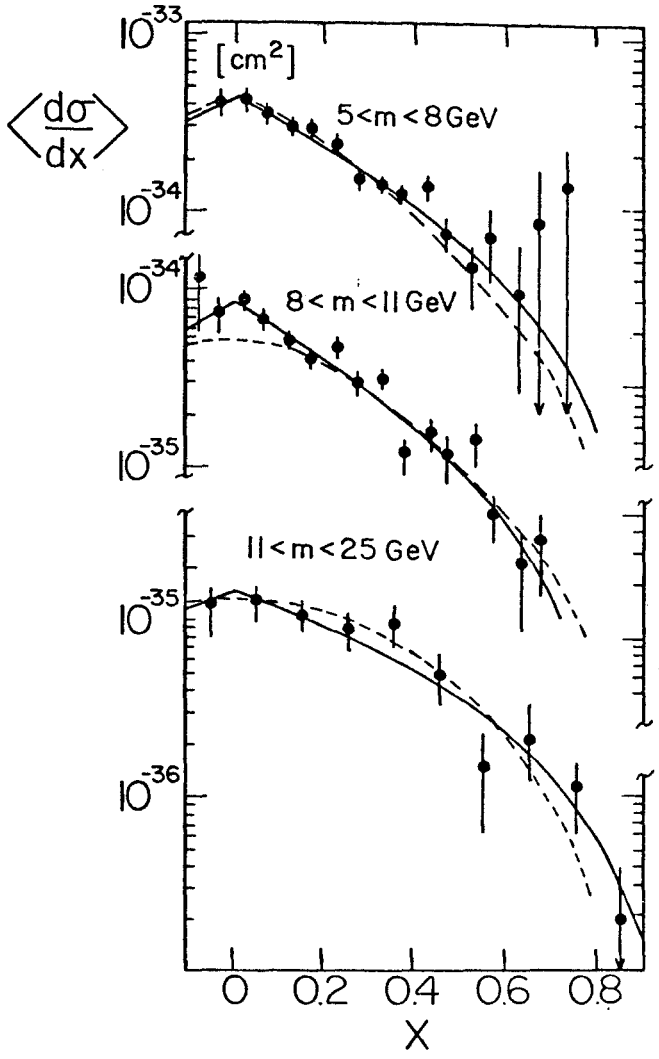
10^{-33}
[cm^2]
$\left\langle \frac{d\sigma}{dx} \right\rangle$
5<m<8GeV
10^{-34}
10^{-34}
8<m<11GeV
10^{-35}
11<m<25 GeV
10^{-35}
10^{-36}
0
0.2
0.4
0.6
0.8
X

Fig. 15

The cross section $d\sigma/dp_T^2$ is presented in Fig. 16 for the 62 GeV data and in Fig. 17 for 44 GeV data for different mass intervals. The quark confinement momenta with $\langle p_T \rangle \simeq 300$ MeV are expected to affect the region $p_T < 0.5$ GeV. Omitting the first bin, we obtain good fits to a simple exponential $Ae^{-b \cdot P_T}$ as stated in Table I. We observe large average transverse momenta $\langle p_T \rangle \simeq 2/b = 1.8\text{-}2.0$ GeV. In addition, the $\langle p_T \rangle$ values were independently calculated by summing individual events and weighting with the detector acceptance. We see good agreement in the values of $\langle p_T \rangle$ from the two different methods. The error in the J region is twice the statistical error due to the very limited range of acceptance. In the overlap mass region $2 < m < 11$ GeV our values are in agreement with electron pair measurements mentioned before.

Figure 18 summarizes our values of dimuon $\langle p_T \rangle$ obtained from the event counting methods together with the data of ref. 3 over a range of dimuon masses with $\sqrt{s}$ extending from 19 to 62 GeV. The large value of $\langle p_T \rangle$ and the increase of $\langle p_T \rangle$ with $\sqrt{s}$ cannot be understood in the Drell-Yan model but are in agreement with QCD predictions based on gluon-quark interaction[1].

We conclude that most dimuon production characteristics can be described by the quark-antiquark annihilation picture when it is expanded to include hard gluon processes of QCD to account for the measured large $\langle p_T \rangle$ values.

---

(1) H. Fritzsch and P. Minkowski, Phys. Letters 73B (1978), 80.

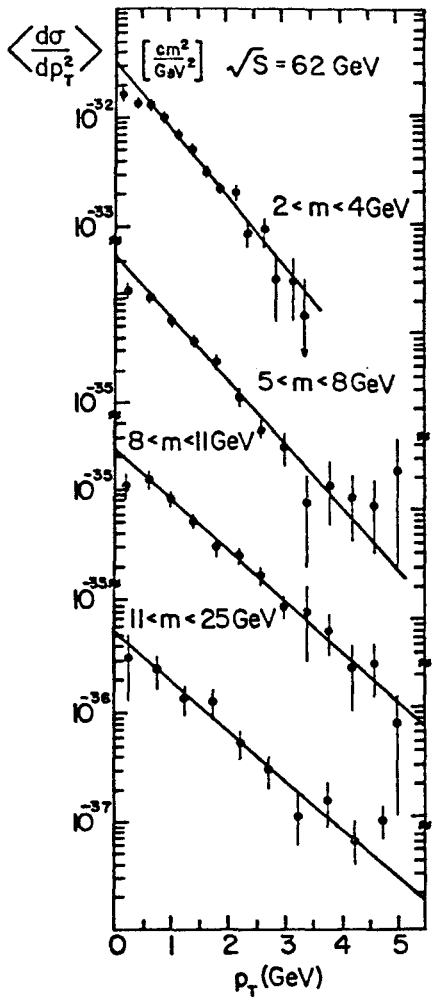
$\left\langle \frac{d\sigma}{dp_T^2} \right\rangle$
$\left[\frac{cm^2}{GeV^2}\right]$
$\sqrt{S} = 62$ GeV
10^{-32}
10^{-33}
10^{-35}
10^{-35}
10^{-35}
10^{-36}
10^{-37}
2<m<4GeV
5<m<8GeV
8<m<11GeV
11<m<25GeV
0 1 2 3 4 5
p_T(GeV)

Figure 16

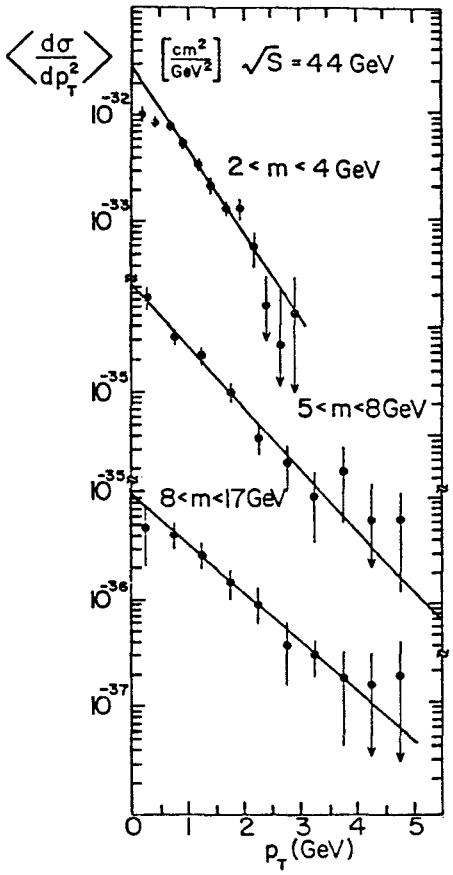
$\left\langle \frac{d\sigma}{dp_T^2} \right\rangle$
$\left[\frac{cm^2}{GeV^2}\right]$
$\sqrt{S}$ = 44 GeV
2 < m < 4 GeV
5<m<8GeV
8<m<17GeV
10^{-32}
10^{-33}
10^{-35}
10^{-35}
10^{-36}
10^{-37}
0
1
2
3
4
5
p_T (GeV)

Figure 17

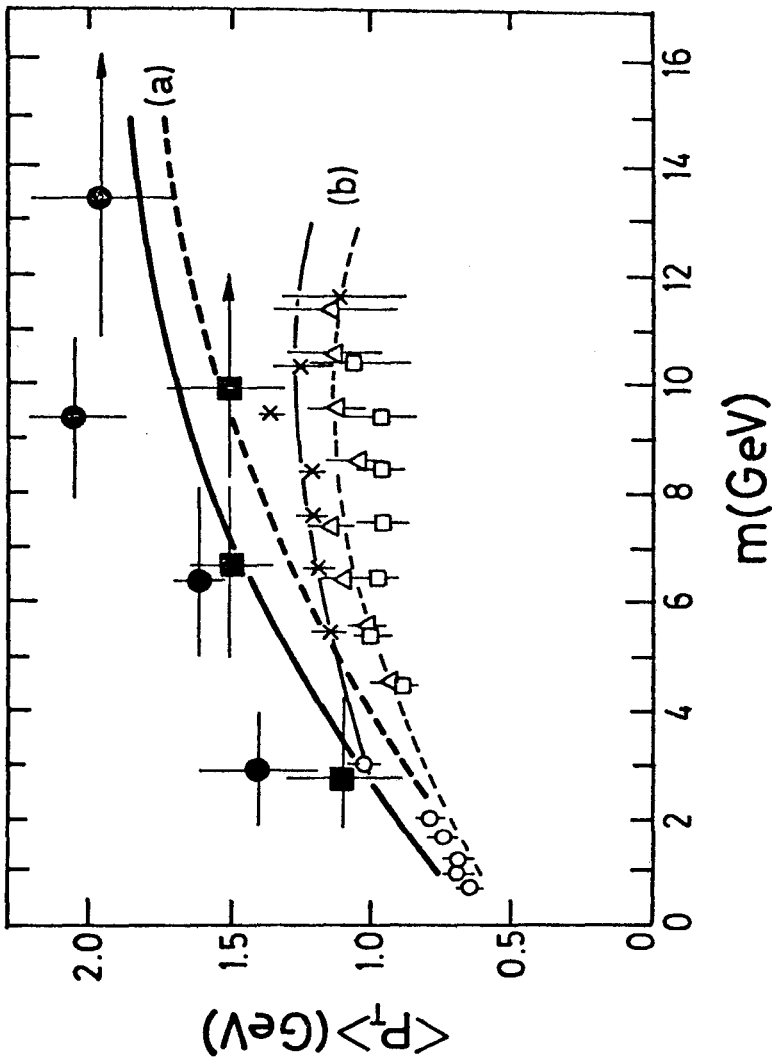

Fig. 18

TABLE I

Fits to $A \cdot e^{-b \cdot p_T}$, and average transverse momenta.

The errors include estimates of systematic uncertainties.

$\sqrt{s}$	Mass Range (GeV)	FIT χ^2/DF	$\frac{2}{b} \approx \langle p_T \rangle$ (GeV)	$\langle p_T \rangle$ from events (GeV)
62 GeV	2 → 4	7.9/10	1.4 ± 0.2	1.40 ± 0.20
	5 → 8	8.2/10	1.5 ± 0.1	1.60 ± 0.10
	8 → 11	2.9/10	1.9 ± 0.2	2.05 ± 0.15
	11 → 25	6.5/7	1.9 ± 0.4	1.95 ± 0.25
44 GeV	2 → 4	5.1/8	1.1 ± 0.2	1.10 ± 0.20
	5 → 8	4.3/7	1.5 ± 0.2	1.50 ± 0.15
	8 → 17	0.9/7	1.9 ± 0.4	1.50 ± 0.15

Observing QCD effects which act "scale breaking," we may give this aspect closer scrutiny. Instead of comparing to data on nuclear targets done at a different accelerator, we use our 44 and 62 GeV data to compare both continuum and resonances. Using the same apparatus and the same analysis ensures best treatment for the relative comparison of the mass spectra, which are presented in Fig. 19. With $\tau = m^2/s$, the data were compared to an ansatz

$$\frac{d\sigma}{dm} = A \frac{(1 - \sqrt{\tau})^{10}}{m^3 \cdot \sqrt{\tau}} + B \cdot T(m),$$

where $T(m)$ is the superposition of the three T resonances appearing as Gaussians of $\sigma(m) = 11\%$ resolution in our apparatus. For $m > 4.5$ GeV, a fit yields:

TABLE II

	A (nb • GeV^2)	B (pb • GeV)	σ_J (nb)	χ^2/DF
$\sqrt{s}$ = 62 GeV	5.76 ± .17	3.7 ± .6	41 ± 12	16.3/26
$\sqrt{s}$ = 44 GeV	5.47 ± .24	0.7 ± .4	15 ± 8	16.7/18

The ansatz gives good fit. The J was measured over a region of $0.1 < x < 0.3$; therefore we added $\sigma_J = B_{\mu\mu} \cdot dm/dx$ $(x = 0.2)$ to the table. The continuum contribution is shown as lines in Fig. 19. It is characterized by the value of A, which is the same for both energies within 5% or one standard deviation, hence confirming scaling between the two measurements in Fig. 19. The systematic differences between both measurements due to luminosity and event selection are estimated to be $\leq 5\%$. This relative agreement of 44 and 62 GeV data well matches the expectations of scalebreaking from QCD. In our range of small τ, the overall change of the integrated rate is estimated[1] to be ~ 4% only. Scaling was

(1) We thank R. Horgan, CERN, for this calculation.

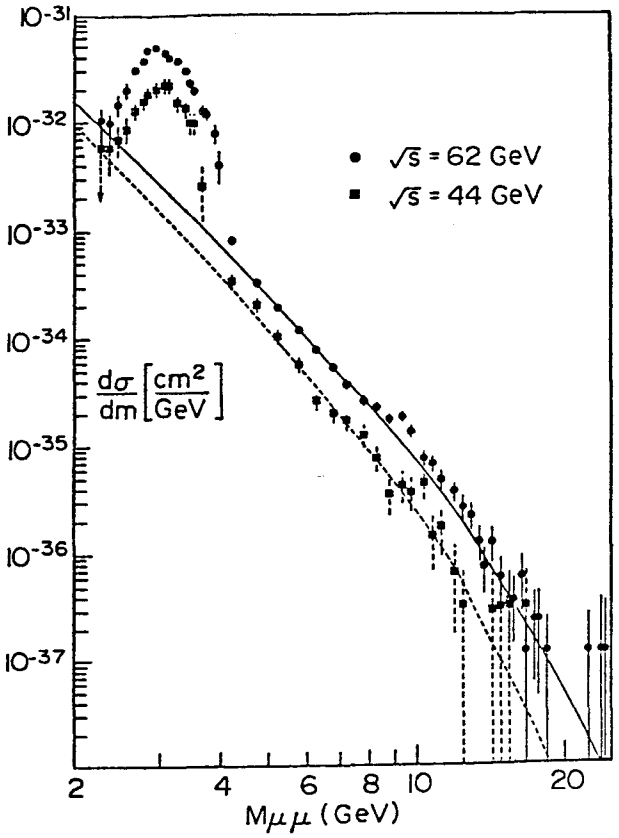
10-31
10-32
10-33
10-34
10-35
10-36
10-37
dσ/dm [cm²/GeV]
√s = 62 GeV
√s = 44 GeV
2
4
6
8
10
20
Mμμ (GeV)

Figure 19

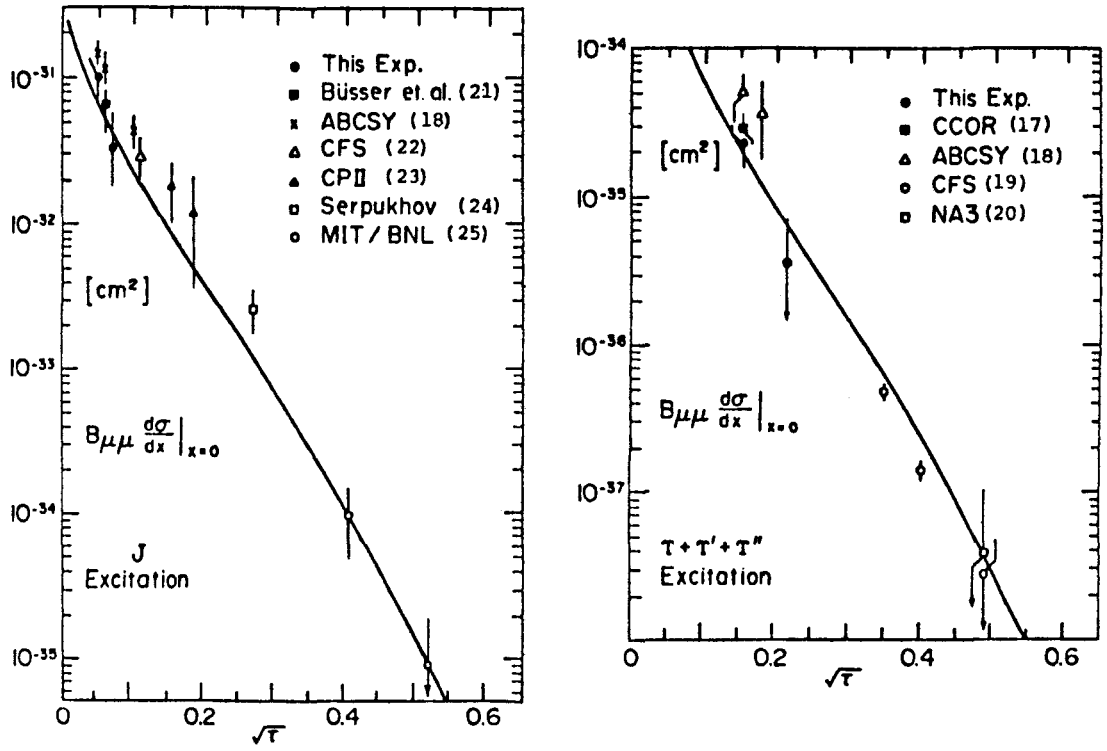
This Exp.
Büsser et al. (21)
ABCSY (18)
CFS (22)
CPII (23)
Serpukhov (24)
MIT / BNL (25)
[cm²]
Bμμ dσ/dx |x=0
J
Excitation
10⁻³¹
10⁻³²
10⁻³³
10⁻³⁴
10⁻³⁵
0
0.2
0.4
0.6
√τ
This Exp.
CCOR (17)
ABCSY (18)
CFS (19)
NA3 (20)
[cm²]
Bμμ dσ/dx |x=0
Υ + Υ' + Υ''
Excitation
10⁻³⁴
10⁻³⁵
10⁻³⁶
10⁻³⁷
0
0.2
0.4
0.6
√τ

Fig. 20

also found in relative measurements[1] at lower energies of $\sqrt{s}$ = 18 - 27.4 GeV at FNAL. Scaling is expected for the continuum, but with the values of Table II we note as an experimental fact that it holds for J and T resonances, too. This was also noticed by the ABCSY group. It is plotted, together with the original J cross sections measured at BNL, in Fig. 20. Amusingly, the shape of our continuum fit (with free normalization) describes the data well[2].

We turn now from the relative to the absolute size of the continuum cross section. There we have no uncertainty from nuclear target corrections; however, event selection and luminosity introduce a 10% overall uncertainty into the absolute cross sections. Therefore, comparing in Fig. 21 our cross sections to Drell-Yan estimates (dotted line) with specific structure functions as mentioned before, we observe a big discrepancy. We determine:

$$K = \frac{\text{measured cross section}}{\text{Drell-Yan prediction}} = 1.6 \pm 0.2.$$

This is different from the values K ≈ 2.2-2.4 from ref. 3); however, our experiment is carried out at two times higher C.M. energies and to higher Q^2 (= $m_{\mu\mu}^2$) values.

Alternatively we determine the sea quark structure function by fitting the 44 and 62 GeV data in the ranges 5 < m < 8 and m > 12.5 GeV with:

$$\left.\frac{d^2\sigma}{dm\ dX}\right|_{X=0} \simeq \frac{8\pi\alpha^2\sqrt{s}}{9m^4}\left(\frac{4}{9}\bar{u}(x)\right)\left(4u_v(x) + d_v(x) + \frac{21}{4}\bar{u}(x)\right)$$

---

(1) K. Ueno, et al., Phys. Rev. Lett. 42, 944 (1979).

(2) J. A. Paradiso, Thesis MIT, Feb. (1981), unpublished.

(3) J. Badier et al., Phys. Lett. 89B (1979), 145.

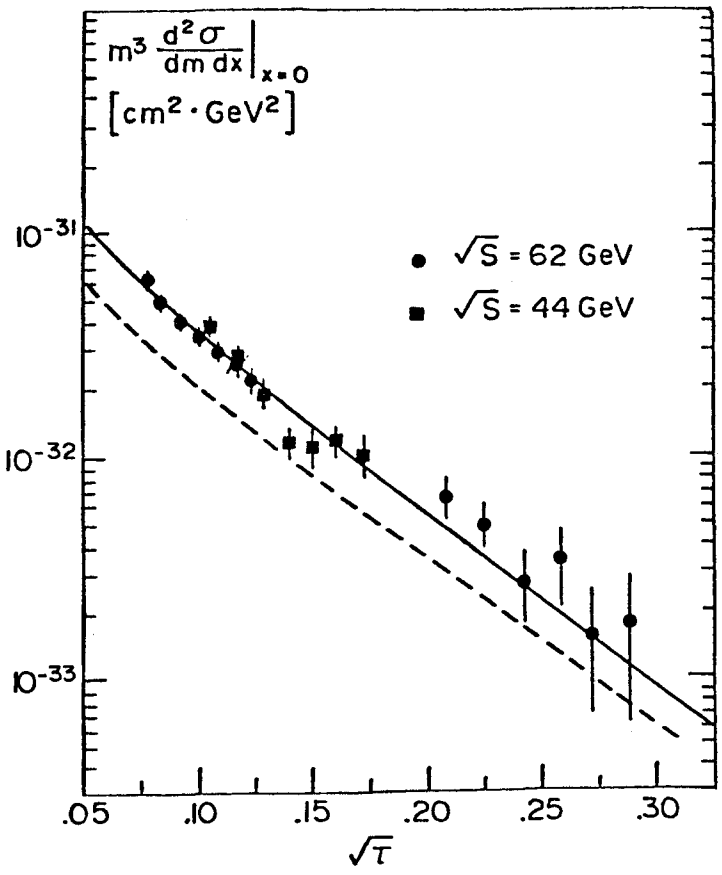
$m^3 \frac{d^2\sigma}{dm\,dx}\Big|_{x=0}$
$[cm^2 \cdot GeV^2]$
10^{-31}
10^{-32}
10^{-33}
$\sqrt{S}$ = 62 GeV
$\sqrt{S}$ = 44 GeV
.05
.10
.15
.20
.25
.30
$\sqrt{\tau}$

Fig. 21

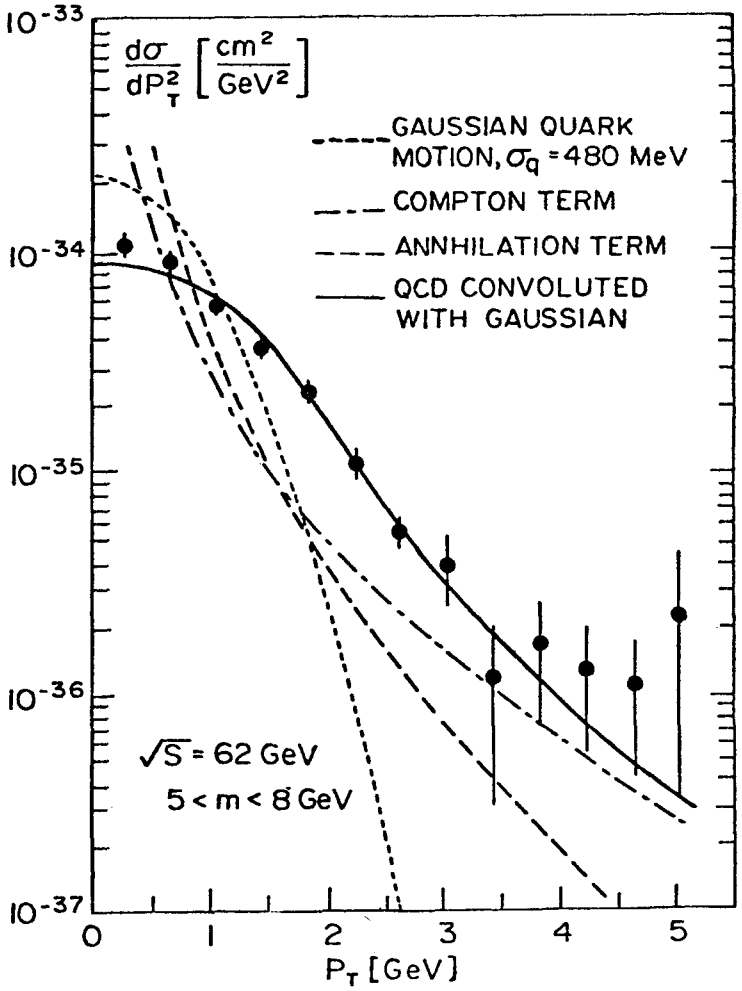
10^{-33}
10^{-34}
10^{-35}
10^{-36}
10^{-37}
$\frac{d\sigma}{dP_T^2}\left[\frac{cm^2}{GeV^2}\right]$
GAUSSIAN QUARK MOTION, σ_q = 480 MeV
COMPTON TERM
ANNHILATION TERM
QCD CONVOLUTED WITH GAUSSIAN
$\sqrt{S}$ = 62 GeV
5 < m < 8 GeV
0
1
2
3
4
5
P_T [GeV]

Fig. 22

where $x_1 = x_2 = \sqrt{\tau}$. We use the valence proton structure functions from inelastic neutrino scattering[1] $u_v(x) = 2.13\sqrt{x}\,(1-x)^{2.8}$ and $d_v(x) = 1.26\sqrt{x}\,(1-x)^{3.8}$, and take an ansatz for the sea of $\bar{u}(x) = \bar{d}(x) = A_s(1-x)^b$ with $s(x) = \bar{s}(x) = \frac{1}{4}(\bar{u}(x) + \bar{d}(x))$ and neglect c, b quarks. From a good fit with $\chi^2/DF = 6/17$ we obtain

$$\bar{u}(x) = (0.42 \pm 0.005)\,(1-x)^{(8.3 \pm 1.0)},$$

which is to be compared to $\bar{u}(x) = 0.27\,(1-x)^{8.1}$ from inelastic scattering. Whereas the shape is in accordance with neutrino measurements , the coefficient A_s reflects the K-factor. From QCD treatment of the Drell-Yan annihilation, one expects[2] an excess in the total production.

More specifically, QCD contributions manifest themselves in broadening the transverse momentum dependence of the dimuons tremendously. Fig. 22 shows a sample of $d\sigma/dp_T^2$ measured at 62 GeV and gives[3] the composition in terms of low order QCD graphs as stated.

Fig. 23 displays the $\langle p_T \rangle$ as a function of $\sqrt{s}$ for constant $\tau = m^2/s$, incorporating the new 44 GeV measurement and confirming the expected[2,3,4] linear rise of $\langle p_T \rangle$ with $\sqrt{s}$.

---

(1) J.G.H. de Groot et al., Z. Phys. C1, 143 (1979) and ref. 2 from previous page..

(2) For example, G. Altarelli et al., Phys. Lett. 76B, 351 (1978) and 356 (1978).

(3) R. D. Field, "Application to QCD," Caltech Preprint CALT-68-696 (1978) and CALT-68-739 (1979).

(4) Yu L. Dokshitser et al., Phys. Rep. 58, 269 (1980).

We are grateful for helpful conversations with R.D. Field, M. Jacob, L. Petronzio, F. Paige, and L.L. Wang.

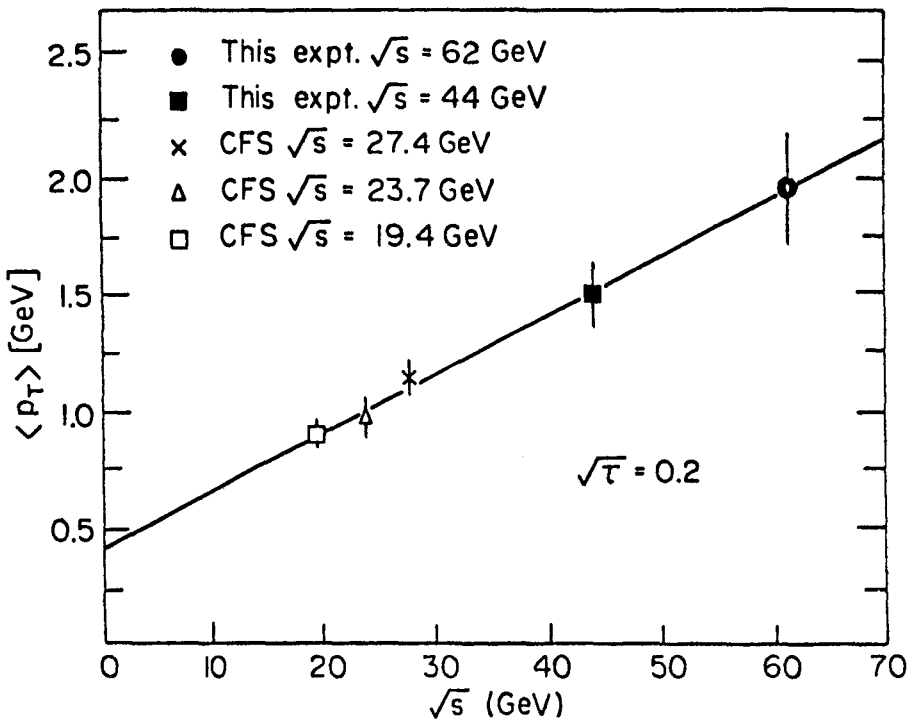
This expt. √s = 62 GeV
This expt. √s = 44 GeV
CFS √s = 27.4 GeV
CFS √s = 23.7 GeV
CFS √s = 19.4 GeV
√τ = 0.2
⟨pT⟩ [GeV]
√s (GeV)
2.5
2.0
1.5
1.0
0.5
0
10
20
30
40
50
60
70

Figure 23

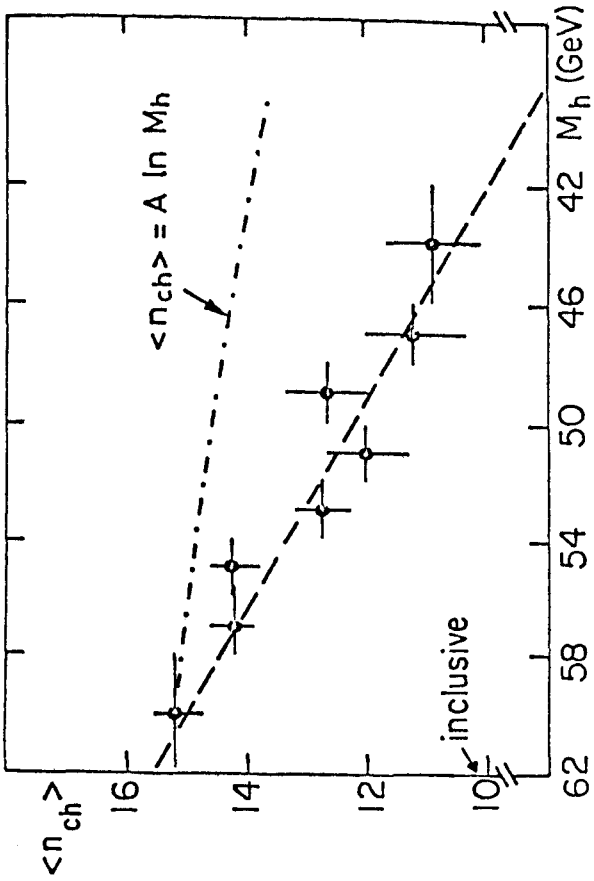
$\langle n_{ch} \rangle$
16
14
12
10
inclusive
$\langle n_{ch} \rangle = A \ln M_h$
62
58
54
50
46
42
M_h (GeV)

Figure 24a

A direct check of the QCD picture producing high p_T (Fig. 22) is possible. One expects the momentum balance of the μ-pair to be a quark or gluon jet which should--ignoring the intrinsic quark motion--roughly correspond to a jet observed in e^+e^- collisions with $E_{beam} \simeq p_T \cdot c$.

Fig. 23 shows the inner detector[1] built by the Pisa group. It enables us to count nearly all associated tracks of the reaction.

Fig. 24a shows the raw associated multiplicity in μ-pair events (after removing the two muons) as a function of the invariant mass of the final-state hadronic system. The data extrapolate to ~6 particles more than in unbiased inelastic events at $M_h = \sqrt{s} = 62$ GeV, and to ~0 multiplicity at $M_h = 0$ (the slope being 0.28 ± 0.04 particle/GeV). The dash-dotted curve represents a logarithmic dependence.

The comparison between multiplicities measured in e^+e^- annihilation and multiplicities associated with μ-pairs at $M_h = \sqrt{s}$ is given in Fig. 24b. The broken curve is a logarithmic fit to e^+e^- low energy data. ISR data with the energy of leading particles removed is also shown[2]. The full curve is a fit to the large energy ($10 < \sqrt{s} < 32$ GeV) e^+e^- data[3]. The dash-dotted curve is a fit to the pp inclusive multiplicity[4].

Fig. 25 displays $\langle n_{ch} \rangle$ versus p_T, in the hemisphere toward and away from the tranverse momentum of the μ-pair. The fitted curve to the away data (pp first 7 points) has a slope of 0.6 ± 0.2 particle per GeV/c, which is in accordance with jet

---

(1) D. Antreasyan et al., Associated hadronic production in μ-pair events at the ISR, subm. to Nucl. Phys. Also A. Bechini et al., N.I.M. 156 (1978), 181.

(2) M. Basile et al., Phys. Lett. 95B (1980), 311.

(3) Ch. Berger et al., Phys. Lett. 95B (1980), 313.

(4) W. Thome et al., Nucl. Phys. B129 (1977), 365.

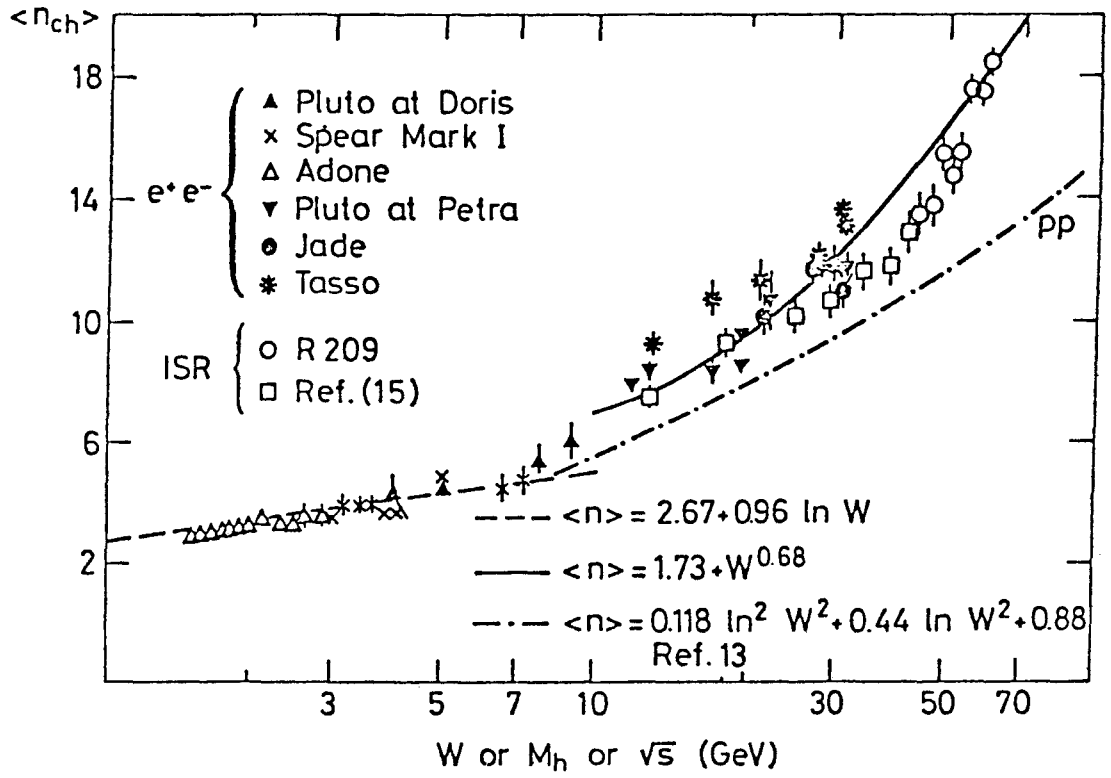
<n_ch>
18
14
10
6
2
e⁺e⁻
▲ Pluto at Doris
× Spear Mark I
△ Adone
▼ Pluto at Petra
● Jade
✱ Tasso
ISR
○ R 209
□ Ref. (15)
pp
<n> = 2.67+0.96 ln W
<n> = 1.73+W^0.68
<n> = 0.118 ln² W²+0.44 ln W²+0.88
Ref. 13
3
5
7
10
30
50
70
W or M_h or √s (GeV)

Fig. 24b

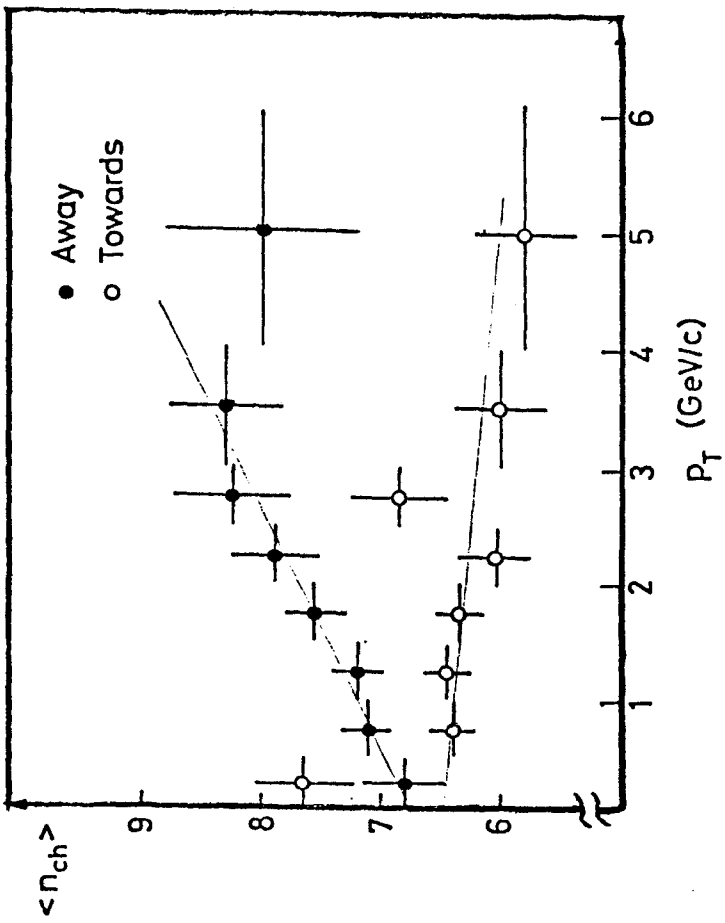

Fig. 25

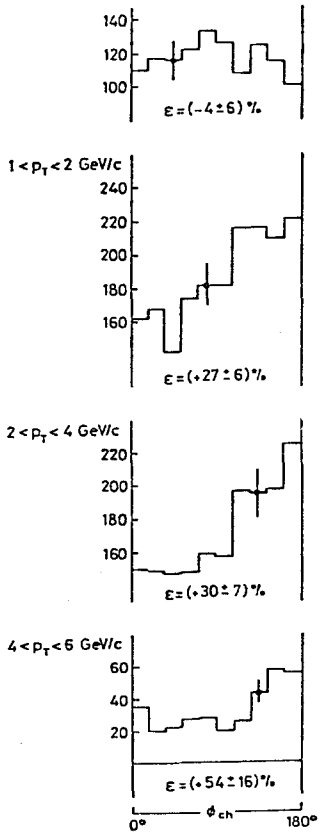
140
120
100
ε = (-4 ± 6) %
1 < p_T < 2 GeV/c
240
220
200
180
160
ε = (+27 ± 6) %
2 < p_T < 4 GeV/c
220
200
180
160
ε = (+30 ± 7) %
4 < p_T < 6 GeV/c
60
40
20
ε = (+54 ± 16) %
0°
φ_ch
180°

Figure 26

multiplicities of e^+e^- reactions. The width of these jet energies, however, will be very great, and it will be overshadowed by the other residuals of the inclusive reaction. Nevertheless, as Fig. 26 shows for masses of the hadronic system < 56 GeV (excluding J), a marked correlation occurs in azimuthal distribution of tracks at $|\theta| > 39^\circ$ relative to the muon pairs. ε is the excess in the backward hemisphere as compared to the forward hemisphere.

Direct γ production at large p_T was discovered by the ABCSY group[1] with W.J. Willis in 1978/79. The importance comes from the possibility of using the process

$$pp \to x + \gamma \text{ at large } p_T$$

to probe for the proton constituents[2]. As opposed to quarks and gluons, the photon is free of fragmentation obscuration. Viewing lepton pairs as virtual photons, the ideas are analogous except that the photon is real now and free of complications from resonances.

The apparatus consisted of two lead-liquid argon calorimeters[3], subdivided longitudinally and laterally with 5 mm resolution, allowing shower separation to 50 mm. Measurements were carried out between $\sqrt{s}$ = 31 and 63 GeV with fully resolving γ and π^0 over the p_T range measured 3.5 • 9 GeV. The data are shown in Fig. 27a; careful study of background from known decays of meson with one missing γ and merging π^0 have been calculated by Monte Carlo and are shown too.

---

(1) M. Diakonou et al., Phys. Lett. 87B (1979), 292; Phys. Lett. 91B (1980), 296; and Phys. Lett. 91B, 301.

(2) G.R. Farmer et al., Phys. Rev. Lett. 36 (1976), 1072, and R.D. Field, Proc. of 19th Conf. on H.E.P., Tokyo (1979), 743 and ref. therein.

(3) C. Kourkoumelis et al., CERN 77-06 (1977).

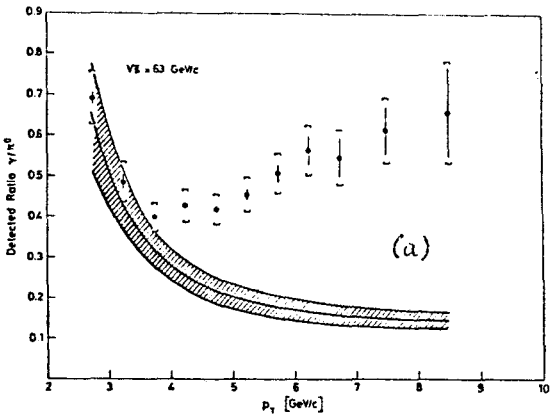
Vs = 63 GeV/c
Detected Ratio γ/π⁰
(a)
p_T [GeV/c]

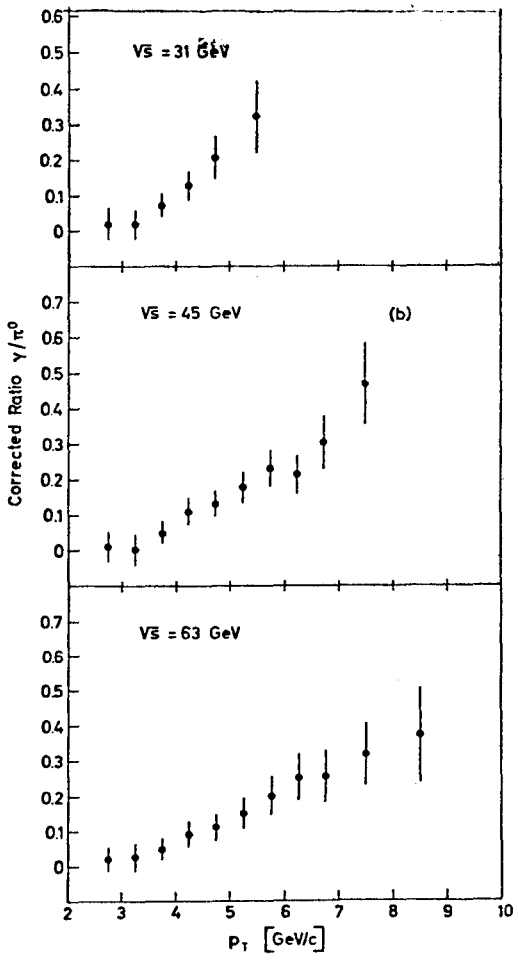
Vs = 31 GeV
Vs = 45 GeV
(b)
Vs = 63 GeV
Corrected Ratio γ/π⁰
p_T [GeV/c]

Figure 27

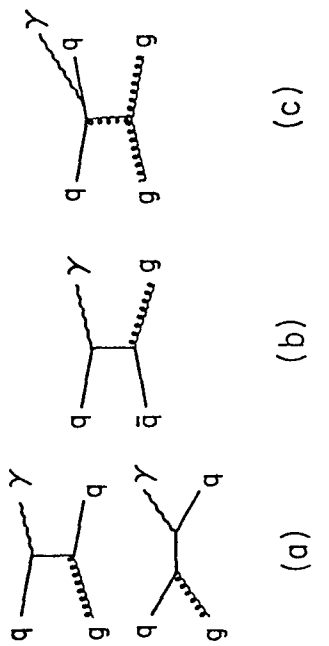

Figure 28

Fig. 27b shows the excess of direct γ's for various energies relative to π^0 after all background corrections are applied. No significant $\sqrt{s}$ dependence is seen, however there is a strong rise with p_T.

Recent calculations[1] have succeeded in duplicating the γ/π^0 measurements by considering the contributions of Fig. 28a, b, c.

Whereas the single photon is thought to proceed through scattering from quark or gluon, the high p_T π^0's are produced as leading fragments of proton constituents after hard scattering. Inserting a barrel of 44 scintillation counters around the intersection region allowed the study[2] of associated charge multiplicities for π^0 and γ. Defining the counter hit by the triggering particle as 1, Fig. 29b shows the distribution slightly peaking backward for 'minimum bias' events (beam-beam interaction with signal in barrel counters or calorimeter arms). Compared to those the π^0 (ϕ) and γ (χ) events with p_T = 6-7 GeV show a strong backward peak in Fig. 29a.

Differences between π^0 and γ become visible in Fig. 30. Fig. 30 gives the average multiplicity of counters hit in general, part a), for the hemisphere of the π^0 or γ. The multiplicity in the "away" hemisphere (Fig. 30b) is even more pronounced when corrected for multiple hits in the scintillators.

The local slope of ~ 0.5 particles/GeV for $3 < p_T < 6$ GeV agrees well with the multiplicity increase opposite to the dimuon pairs as discussed before. of 0.6 ± .2 Particles/GeV

---

(1) R. Horgan and P. Scharbach, Nucl. Phys. B181 (1981), 421; A. Contogouris, S. Papadopoulos, and J. Ralston, Megill Preprint, April, 1981; M. Dechantstreiter, F. Halzen, and D. Scott, DOE-EF-00881-198, DAMTP 81/6, March, 1981.

(2) M Diakonou et al., Phys. Lett. 91B (1980), 301.

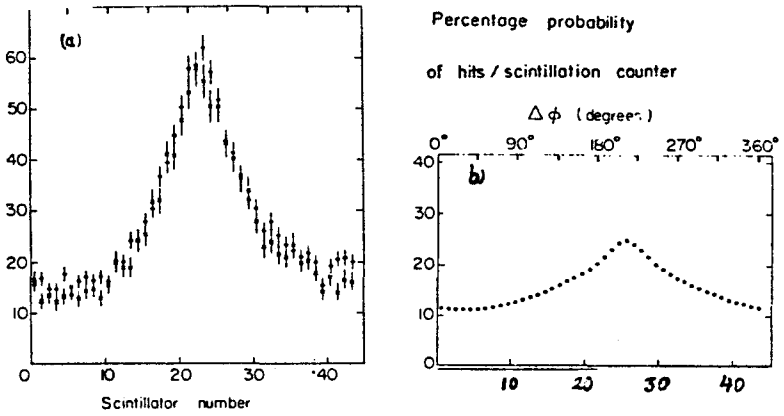

Figure 29

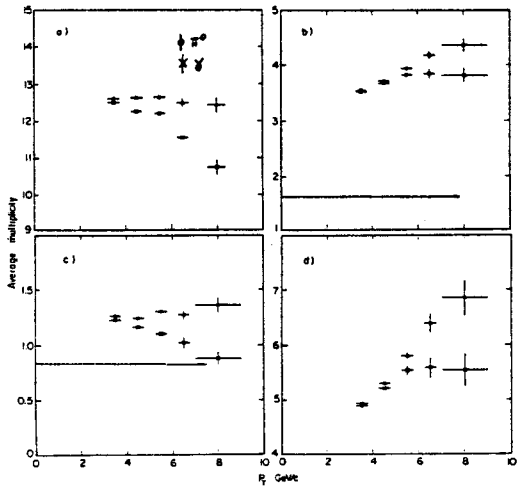

Figure 30

In a recent experiment done with the open axial field spectrometer[1] the charges of the associated particles can be distinguished, giving insight into the specific processes. Looking at the dominant γ contributions from Fig. 28a, one expects the γ to be unaccompanied by charged particles, because the p_T transfer keeps fragmenting constituents away. Furthermore, the most likely present quark is a u quark, which should manifest itself in the charge of the recoiling jet particles. For π^o's, on the other hand, a gluon jet should be dominantly[2] responsible, hence close by hadrons are expected.

Fig. 31 shows the $\Delta\phi$ distribution between neutral triggers with $p_T > 4.5$ GeV/c, and charged tracks with rapidity $|\eta| < 0.8$ and $p_T > 1.0$ GeV/c. Near $\Delta\phi = 0$ we see significantly fewer tracks for γ candidates than for π^o's. In the same figure we also display the signal near $\Delta\phi = 0$ for γ's after subtracting the background due to π^o's and η^o's expected in the γ candidate sample. If we assume that the associated multiplicity due to processes other than hard constituent scattering is given by that observed at $\Delta\phi \simeq 90^o$, then we see that there is a small but significant excess of tracks correlated with single photons at $\Delta\phi = 0^o$. The distribution for $\Delta\phi > 90^o$ exhibits the familiar away-side peaking with half width at half maximum of $\sim 25^o$. This distribution is essentially identical for γ and π^o candidates. Investigating the backward peak in terms of distribution in the variable $X_E = \vec{P}_c \cdot \vec{P}_\gamma / P_\gamma^2$ gives no significant difference for γ or π^o.

---

(1) E. Anassontzis et al., Contribution to the Intern. Conf. on HEP, Lisbon, July, 1981. I thank Drs. C.W. Fabjan and W.J. Willis for making the results available to me.

(2) M. Jacob in Techniques and Concepts of HEP, Plenum Pub., T. Ferbel, editor (1981).

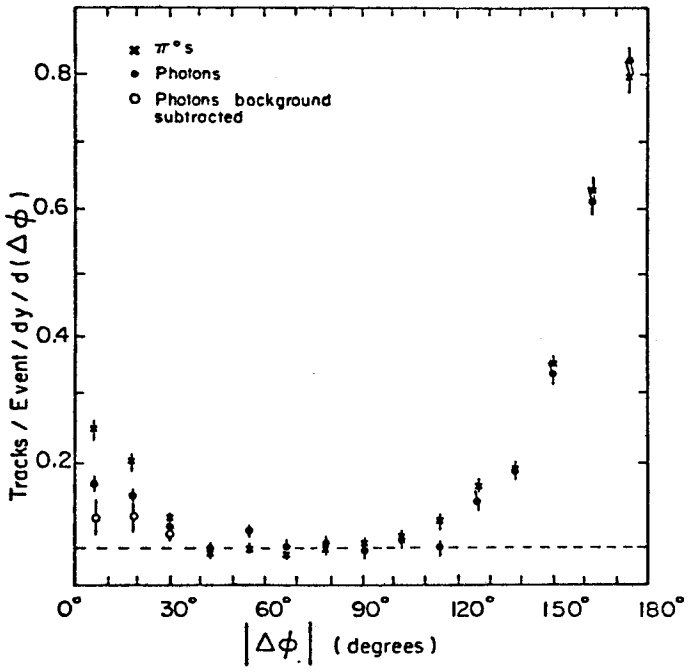
π°s
Photons
Photons background subtracted
0.8
0.6
0.4
0.2
Tracks / Event / dy / d(Δφ)
0°
30°
60°
90°
120°
150°
180°
|Δφ| (degrees)

Figure 31

Fig. 32a shows the ratio of the mean number of positive tracks to the mean number[1] of negative tracks (N^+/N^-) opposite γ's and π^o's as a function of X_E of the charged tracks. For π^o triggers the value is essentially constant at 1.1. For γ-triggered events the value rises slightly with X_E; for $X_E > 0.5$, N^+/N^- is 1.3 ± 0.2.

Part b) displays the same distribution as in Fig. 32a, but for events satisfying a cut requiring the total momentum of charged tracks in the direction of the neutral trigger to be less than 20% of the trigger momentum. For π^o triggers the distribution is essentially unchanged from Fig. 32a: $N^+/N^- = 1.2 \pm 0.2$ for $X_E > 0.5$.

Fig. 32c gives the charge balance of tracks of $\Delta\phi < 90^o$. The increase[2] with X_E can qualitatively be understood, because if the bremsstrahlung diagram (Fig. 28c) were a significant source of prompt γ's, we would expect a charge asymmetry in the associated tracks on the same side as the trigger γ; this is because the trigger γ is most likely to be associated with a u quark.

In conclusion, the charge correlations seen are in agreement with expectations from concrete constituent QCD pictures and continue the observations made from lepton pair production. They open a new field of study probably not foreseen at the start of the ISR. And why should it be different for ISA?

---

(1) See also: A. Angelis et al., Phys. Lett. 98B (1981), 115.

(2) A.G. Clark et al., Nucl. Phys. B160 (1979), 367.

THE LARGE EUROPEAN e^+e^- COLLIDER PROJECT LEP

E. Keil, CERN

I. INTRODUCTION AND SUMMARY

A large European e^+e^- Collider Project (LEP) has been under study at CERN since 1976. The history of these studies up to the 1979 US Particle Accelerator Conference has been described in a review paper.[1] Since that time the design study has been continued. A detailed description of LEP Version 8, the Pink Book,[2] was issued in August 1979. A review[3] of later developments was given at the 11th International Conference on High-Energy Accelerators in July 1980. This paper describes the most recent developments in the LEP Project which was submitted to the CERN Council in June 1980 for approval. It is hoped that Council will authorize the project in October 1981.

LEP Version 11 described here has a circumference of about 27 km. With an RF system consisting of 128 cavities and 16 1-MW klystrons the luminosity reaches a peak of about 10^{31} $cm^{-2}s^{-1}$ at 51.5 Gev. Enough space is foreseen in the lattice for a considerable extension of the RF system, permitting 90 GeV to be reached with room temperature RF cavities, and even more with superconducting ones. Progress of prototype work for the LEP magnet and RF systems is also briefly described.

II. MAIN PARAMETERS OF LEP VERSION 11

It was decided in summer 1980 that the construction of LEP would be undertaken in several phases. The main differences between the phases are the number of RF power sources, and the number and kind of RF cavities, either room temperature Cu or superconducting ones.

Earlier this year it was decided to reduce the LEP circumference by some 3950 m. The reason for this change is the geology of the LEP site which is shown in Fig. 1. LEP is almost tangential to the SPS at the center between the straight sections SS5 and SS6. Its level and inclination are chosen so that about 19 km of the circumference is in the molasse rock whose properties are well known from the construction of the SPS. The remaining 8 km, approximately, are in the limestone of the Jura mountains, about 4 km less than in the previous version of LEP.

Since the LEP position relative to the SPS is not changed, LEP will also penetrate some 1000 m less deep into Jura. It is hoped that in this manner geological layers which might cause serious difficulties in civil engineering can be avoided. The price to be paid for this safety is a small reduction of the peak energy for a given RF system.

In order to obtain a better knowledge of the geology a reconnaissance tunnel is under construction, as shown in Fig. 1. It starts with a vertical pit of some 75 m depth and continues with an almost horizontal tunnel of about 3 m diameter towards the experimental area P4 of LEP. By now, the pit is completed and the horizontal tunnel has been started. The tunnel will eventually be used for access to P4. In addition, several deep borings along the LEP perimeter are foreseen.

Phase 1 of LEP construction as presently defined includes:

i) the machine tunnel of about 27 km circumference described above,

ii) enough RF power and room-temperature RF cavities to operate LEP at 50 GeV in each beam with useful luminosity,

iii) and at least four fully equipped experimental areas out of a possible eight.

The most important parameters of LEP Version 11 are given in Table 1.

Fig. 2 shows a top view and a cross section of a typical underground experimental area at P2, P6 or P8. P4 will have a smaller experimental area and a nearly horizontal access tunnel.

III. FURTHER PHASES OF LEP CONSTRUCTION

The LEP circumference is much larger than the optimum value for a machine designed to operate in the neighborhood of 50 GeV in each beam. Therefore enough space is foreseen in the lattice to install more RF after the completion of Phase 1. How this is done is completely open now and not budgeted for. Basically there are two possibilities.

The installation of more room-temperature RF cavities is continued. How the maximum energy in LEP increases with the RF installed is shown in Table 2. Phase 1 corresponds to the column labelled 1/6 RF installed. Optimization between the capital and operating costs of the RF system requires that the installed power and the cavity length grow in proportion, bearing in mind that

the RF power is quantised due to the klystrons and that each klystron feeds a number of cavities which is a power of two. For the full RF installation the peak luminosity occurs at 85 GeV while it occurred at 88.8 GeV in the previous version of LEP[3].

The RF cavities are grouped in "RF stations" which are arranged systematically around the experimental area. A "full" RF stations contains 12 MW of RF power and 96 RF cavities with an active length of 203.6 m. A "partial" RF stations contains less power and fewer cavities, but because of the feeding arrangement the power must be a multiple of 4MW and the number of cavities a multiple of 32.

Progress in superconducting RF systems operating at 500 MHz has been very encouraging in several laboratories including CERN. If such cavities can be economically produced by industry in the late eighties or early nineties they could be installed in LEP immediately after Phase 1.

The performance with the superconducting RF system is shown in Table 3. The important parameter is the accelerating voltage gradient. The table gives the results for gradients from 2 to 5 MV/m which straddles the range of gradients which have already been achieved[4]. On the basis of these numbers we propose that all equipment going into the tunnel is suitable for operating at up to 125 GeV.

It should be obvious that the two possibilities of increasing the LEP energy - room temperature or superconducting RF cavities - present the two extreme solutions of a whole spectrum of possiblities.

IV. LATTICE LAYOUT

The LEP lattice consists of eight straight insertions and eight arcs. The insertions contain the low-β intersection regions and the straight section foreseen for the RF cavities as shown in Fig. 3. The dispersion vanishes in the whole insertion. It is matched to the value in the arcs by 16 dispersion suppressors between the insertions and the arcs. The dispersion matching is achieved by independently-powered quadrupoles rather than by leaving out bending magnets. The remaining straight sections are foreseen for wiggler magnets which are used to control the beam emittance and the bunch length. The first half cell of the dispersion suppressor from the crossing points has

magnets with only 10% of the normal field. Its purpose is to shield equipment around the crossing points from the penetrating synchrotron radiations generated in the arcs, which has a critical energy of 100 KeV at 51.5 GeV, and 440 keV at 85 GeV. The arcs have a standard FODO lattice consisting of 32 cells. The cell parameters are shown in Table 4. The phase advance in a cell is 90°. Hence, an even number of sextupoles (a family), having 180° phase shift between neighbors, can be connected to the same power supply. This results in at most four independent families in each half arc. Their strengths are adjusted so that the optimum chromaticity correction is achieved. Compared to existing machines the cells are longer and the phase advance is higher. This choice was made to keep the number of magnetic elements low, and the wasted space between them short which is more usefully occupied by bending magnets. The focusing in the arcs is chosen so that an adequately small beam size can be achieved up to energies approaching 125 GeV, possibly by using a change in damping partition numbers and a reduction of the coupling in addition. We propose to operate LEP at one tune in the whole energy range. This implies that at all energies below the maximum the beam emittance must be enlarged to fill the available aperture and to achieve the maximum luminosity.

V. INJECTION

For injection into LEP much use is made of the synchrotrons existing at CERN, and of existing transfer tunnels. A schematic layout is shown in Fig. 4, together with the transfer energies between machines and the numbers of circulating particles which decrease in sucessive machines due to transfer efficiencies. Electrons are accelerated in a 200 MeV electron linac. The gun current is 6 A and the current on target 2.5 A. The positrons are accelerated in a 600 MeV positron linac and accumulated in four branches circulating in the ACR ring. It acts as a buffer between the 100 Hz linacs and the PS and SPS synchrotrons which accelerate electrons or positrons every 12.5 s when LEP injection is interleaved with proton acceleration for fixed-target physics. The transfer energies, 3.5 GeV and 20 GeV, are a compromise. When they are increased, the number of RF cavities to be installed in the PS and the SPS goes up rather steeply, as does the synchrotron radiation power for which the PS and SPS vacuum chambers were not designed. At the same time the collective

phenomena in the subsequent machines which are hard to quantify and vary less steeply with energy become less severe.

VI. PERFORMANCE

The figures for LEP performance shown in Table 2 are based on four assumptions which must be re-examined as new experimental data from machines such as CESR, PEP and PETRA become available, and as more refined theories are developed. These four assumptions will be discussed in turn.

A. Beam-beam tune shift

The beam-beam tune shift limit is $\Delta Q = 0.03$, a factor of two lower than in previous versions of LEP. This value has been adopted because of the experimental evidence in CESR[5], PEP[6], and PETRA[7]. It must be noted that these observed values of ΔQ are about a factor of two lower than those observed in the previous generation of e^+e^- storage rings such as ADONE, SPEAR and VEPP-2M[8].

We assume that the beam-beam limit ΔQ does not continue to decrease when the size of the machine is increased by another factor of ten. This assumption is corroborated by a computer simulation[9]. Fig. 5 shows results of the computer simulation when the circulating current is varied. The simulation includes several effects due to errors in the machine and due to synchrotron oscillations which are known to deteriorate the luminosity. The beam emittances are also varied in proportion to the beam current without change in beam cross section $\Delta Q_o = 0.06$. We further assume that ΔQ does not depend on the number of bunches. This agrees with the observations in PEP[6].

B. Stored current

The LEP performance listed in Table 2 requires a stored current of about 3 mA in Phase 1 and up to about 5 mA in later phases. The two most worrying collective phenomena in LEP are turbulent bunch lengthening and coherent tune shifts of transverse head-tail modes at injection energy. Bunch lengthening in CESR, PEP and PETRA is small and does not lead to a current limitation. Experiments can therefore only be used to check quantitative predictions of bunch lengthening theories. A transverse instability is observed in PETRA when the coherent tune shift is of the order of the synchrotron tune Q_s, in qualitative agreement with a calculation of its parametric dependence.[10]

The turbulent bunch lengthening can be overcome by artificialy increasing the bunch length with dipole-octupole wigglers.[11] Our calculations indicate that both limitations should not prevent us from storing the currents mentioned above although the whole arsenal of diagnostic and feedback systems will be required to achieve this.

C. Vertical amplitude function

We assume that the vertical amplitude function β_y can be reduced to $\beta_y = 0.1$ m in the short insertion with a free space $\ell_x = \pm 5$ m, and to $\beta_y = 0.2$ m in the long insertion with $\ell_x = \pm 10$ m. Lower limits for β_y are determined by the chromaticity and by the bunch length. The severity of chromatic effects is proportional to $\ell_x/\beta_y \simeq 50$, which is not too far from the ratios actually achieved in CESR, PEP and PETRA. The bunch length σ imposes a lower limit on the ratio β_y/σ. Since the bunches in LEP are expected to be much longer than at zero-current the ratio β_y/σ is expected to be even smaller than in PETRA with mini-β insertions.[7] A computer simulation[9] has shown that reducing β_y below the values given above does not increase the achievable luminosity. This effect may be the ultimate limit to further reducing β_y by mini-β insertions. A tentative value of $\ell_x = \pm 3.6$ m has been adopted for further studies also involving experimental teams. It may eventually permit a reduction of β_y to 0.06 m. In Plan 1, the two different kinds of insertions will alternate around the machine. Hence the equipped experimental areas will all have the short insertion. The remaining areas may not be equipped with low-β insertions at the beginning. In order to operate LEP with 4 bunches it is necessary to equip them such that the ratio β_y/β_x is the same as in the experimental insertions.

D. Aperture

PEP is the only machine which operates with a horizontal beam emittance close to the design value and with a vertical emittance above it. In CESR and PETRA the actual values are below the design values. The choice of the LEP aperture follows the same principles but in addition allows for closed orbit distortions (±20 mm horizonatally, ±10 mm vertically) much larger than those which can be permitted in colliding-beam operation.[2] Hence the LEP aperture is not expected to present an additional performance limitation.

E. Conclusions on performance

The LEP performance quoted in Table 2 assumes a beam-beam tune shift $\Delta Q = 0.03$, the currents given and no other performance limitation. We hope to achieve this performance eventually. Soon after start-up the LEP performance is likely to be lower for one or another of the reasons discussed above or because equipment necessary for beam manipulations is not installed. Still, it ought to be possible to reach a luminosity above $10^{30} cm^{-2} s^{-1}$ fairly soon.

VII. PROTOTYPE WORK

A. Dipoles

The low bending field in LEP makes two drastic simplifications of the dipoles possible, namely (i) steel-concrete cores[12] and (ii) simple current bars instead of coils. Two full-size prototypes were built and tested[13] in collaboration with local firms. Each core is made of a stack of low-carbon steel laminations, 1.5 mm thick, separated by 4 mm gaps and embedded in a fine-grain sand and cement mortar. Mechanical measurements of the prototypes have shown a straightness in the vertical plane and a twist better than the tolerances by a factor of two. The straightness in the horizontal plane deteriorates in time due to differential shrinkage of the front and the back of the core. The mechanical rigidity corresponds to that known for mortar and is much higher than that of a typical laminated magnet. The magnetic measurements were also fully satisfactory. Two more contracts for a pair of dipoles each were placed with civil engineering firms in order to investigate the possibility of industrial production. Two of these dipoles have already arrived.

B. RF system

The main parameters of the LEP RF system are shown in Table 5. A novel feature of this system is that each of the five-cell accelerating cavities is coupled to a low-loss storage cavity. The system is excited at both its resonant frequencies so that the stored energy osillates between the two cavities at twice the bunch frequency. This reduces the overall losses by a factor 1.6. So far, the tests have been done at 500 MHz, using as a power source a klystron kindly provided by DESY. A coupled system of accelerating and storage cavities has been operated[14] up to the full power level required for LEP. The first prototype accelerating cavity for 350 MHz has arrived at

CERN and is being prepared for tests. The first prototype 1 MW CW klystron is due in a few months. A complete operating module should be ready late this year.

VIII. FUTURE PROSPECTS

The LEP position with respect to the SPS, the LEP circumference and the transfer tunnels linking the two machines have been chosen so that e-p collisions between the electrons circulating in LEP and protons circulating in a by-pass to the SPS are possible when the necessary equipment is installed.

VIV. ACKNOWLEDGEMENTS

This paper describes the work of the large number of people whose names may be found in ref. 2.

REFERENCES

1. W. Schnell, IEEE Trans. Nucl. Sci., NS-26, No. 3, 3130 (1979).
2. The LEP Study Group, CERN/ISR-LEP/79-33 (1979).
3. A. Hutton, Proc. XIth Internat. Conf. on High-Energy Accelerators, CERN 1980, 156 (1980).
4. Ph. Bernard et al., CERN/EF/RF 81-2 (1981).
5. B. McDaniel, IEEE Trans. Nucl. Sci. NS-28, No. 3, 1984 (1981).
6. J. Rees, IEEE Trans. Nucl. Sci. NS-28, No. 3, 1989 (1981).
7. J. Rossbach, IEEE Trans. Nucl. Sci. NS-28, No. 3, 2029 (1981).
8. S. Tazzari, IEEE Trans. Nucl. Sci. NS-28, No. 3, 2420 (1981).
9. S. Myers, IEEE Trans. Nucl. Sci. NS-28, No. 3, 2503 (1981).
10. R.D. Kohaupt, DESY 80/22 (1980).
11. A. Hofmann, J. Jowatt and S. Meyers, IEEE Trans. Nucl. Sci. NS-28, No. 3, 2392 (1981).
12. J.-P. Gourber and L. Resegotti, IEEE Trans. Nucl. Sci. NS-26, No. 3, 3185 (1979).
13. J.-P. Gourber and C. Wyss, IEEE Trans. Nucl. Sci. NS-28, No. 3, (1981).
14. P. Brown, H. Frischholz, G. Geschonke, H. Henke and I. Wilson, IEEE Trans. Nucl. Sci. NS-28, No. 3, (1981).

Table 1

General LEP Parameters

Machine circumference	26658.879	m
Average radius of arcs	3494	m
Bending radius	3104	m
Number of intersections	8	
Number of bunches per beam	4	
Horizontal betatron wave number	90.35	
Vertical betatron wave number	94.20	
Momentum compaction factor	1.928×10^{-4}	
Harmonic number	31320	
RF frequency	352.21	MHz

Table 2

Summary of Performance with Room Temperature RF

Fraction of RF installed	1/6	1/4	1/2	1	
Installed RF power	16	24	48	96	MW
Length of RF structure	271.5	407.2	814.4	1628.8	m
No. of RF stations	2 partial	2 full	4 full	8 full	
Max. energy (zero luminosity)	59.0	65.5	78.0	93.0	GeV
Max. current required	2.8	3.1	3.8	4.7	mA
Max. luminosity ($\Delta Q = 0.03$)	0.9	1.3	1.8	2.7	$\times 10^{31}$ cm^{-2} s^{-1}
Energy of max. luminosity	51.5	58.5	70.0	85.0	GeV

Table 3

Maximum Energies with Superconducting RF

Maximum accel. gradient MV/m	2 exp. areas with RF L_c = 407.2 m	4 exp. areas with RF L_c = 814.4 m	8 exp. areas with RF L_c = 1628.8 m
2.0	70.3	83.6	99.4
3.0	77.8	92.5	110.0
4.0	83.6	99.4	118.2
5.0	88.4	105.2	125.0

Table 4

Parameters of Lattice Period

Length of period			79.0 m
Magnetic length of Dipoles per period			70.1 m
Dipole field at 85 GeV			0.092 T
Bending radius			3.1036 km
Horizontal phase advance			90.0 degrees
Vertical phase advance			90.0 degrees
Magnetic length of quadrupoles (QF, QD)			1.60 m
QF strength			$-0.02269\ m^{-2}$
QD strength			$0.02268\ m^{-2}$
	β_x	β_y	D_x
Orbit parameters in QF	134.2	23.2	1.21 m
Orbit parameters in QD	23.2	134.2	0.59 m
Horizontal aperature			±59 mm
Vertical aperature			±33 mm

Table 5

Main RF System Parameters

	352/21		
Frequency			MHz
Number of klystrons	16	96	
Number of RF stations	2x2	8x2	
Nominal RF power output per klystron	1.0	1.0	MW
Waveguide losses	7.5	7.5	%
Length of active RF structure	271.5	1628.8	m
Number of five-cell cavities (each coupled to a storage cavity)	128	768	
Diameter of beam hole	100	100	mm
Effective shunt impedance	40	40	$M\Omega m^{-1}$
Filling time of coupled system	56.5	56.5	μs
Maximum circumferential voltage (zero beam current)	400	2400	MV

Fig. 1. Layout of LEP near the CERN site. The crossing points are labelled 1 to 8. The circle tangent to LEP is the SPS. The reconnaissance tunnel is the straight line starting at crossing point no. 4.

Fig. 2. Typical layout of an experimental area (P8) with access pits.

Fig. 3. Lattice layout and orbit functions near high-luminosity interaction point. Scales in meters.

Fig. 4. Schematic layout of the LEP injection system. Thick lines indicate existing installations. LSS1, LSS5, and LSS6 are long straight sections in the SPS. Details of $e^{\pm}$ injection into LEP are not shown.

Fig. 5. Variation of vertical blowup, luminosity and beam-beam tune shift width. The horizontal and vertical emittance is varied in proportion to the beam current. Realistic machine errors are included. The tunes are shown for optimum performance.

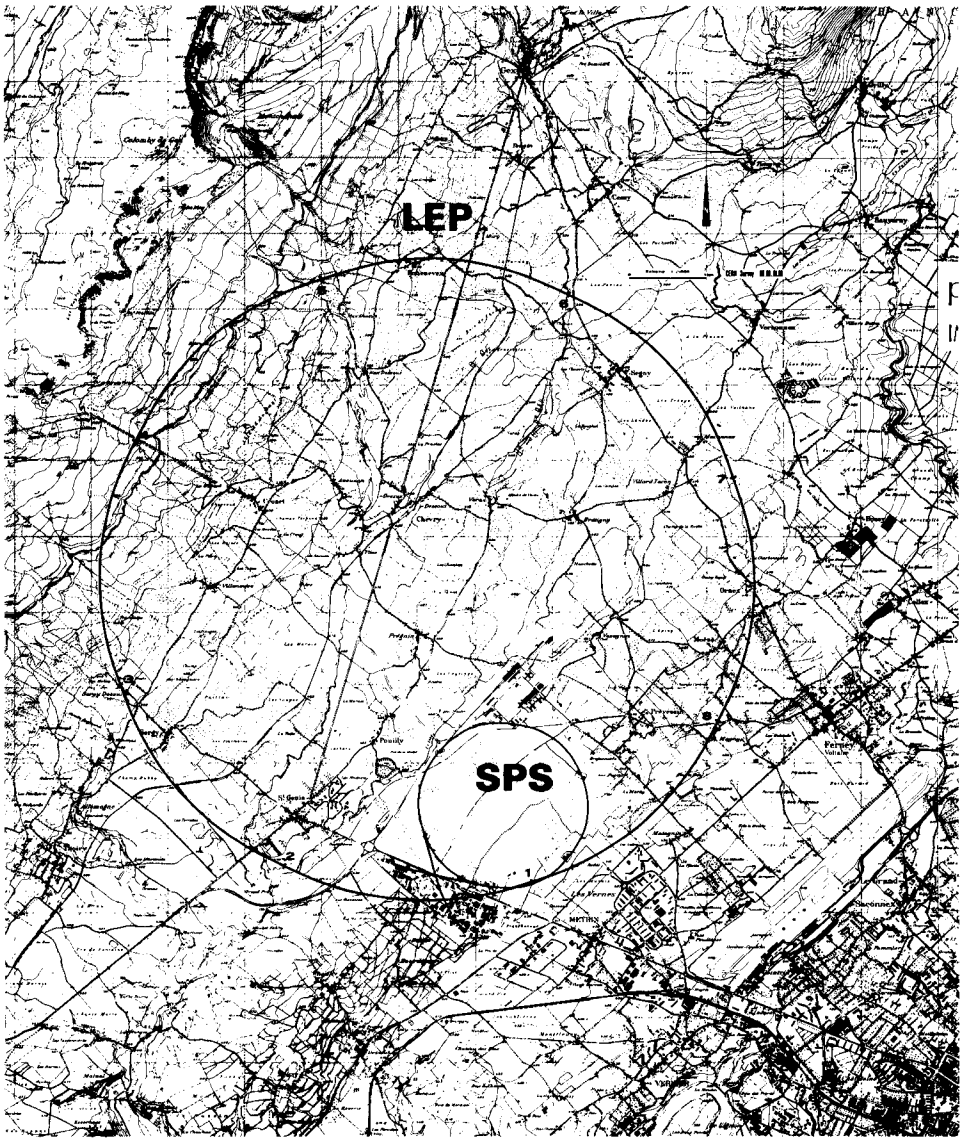

Fig. 1

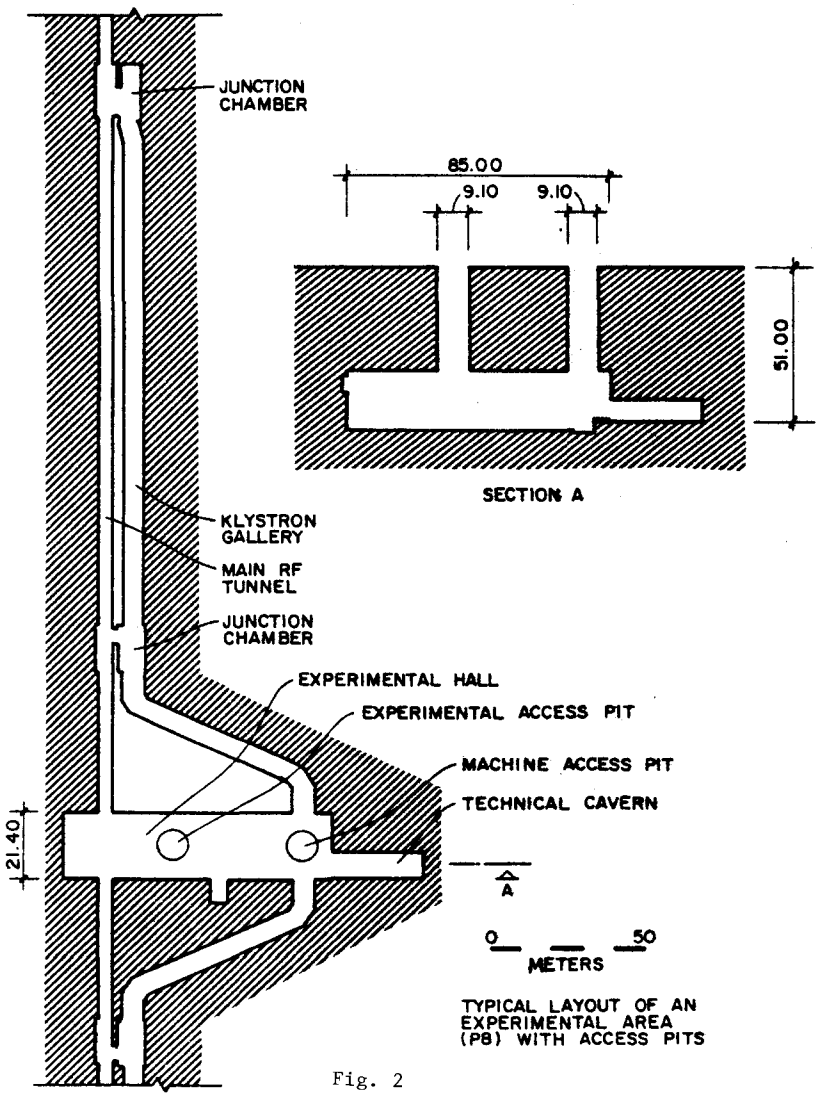
JUNCTION CHAMBER
85.00
9.10
9.10
51.00
SECTION A
KLYSTRON GALLERY
MAIN RF TUNNEL
JUNCTION CHAMBER
EXPERIMENTAL HALL
EXPERIMENTAL ACCESS PIT
MACHINE ACCESS PIT
TECHNICAL CAVERN
21.40
A
0
50
METERS
TYPICAL LAYOUT OF AN EXPERIMENTAL AREA (P8) WITH ACCESS PITS

Fig. 2

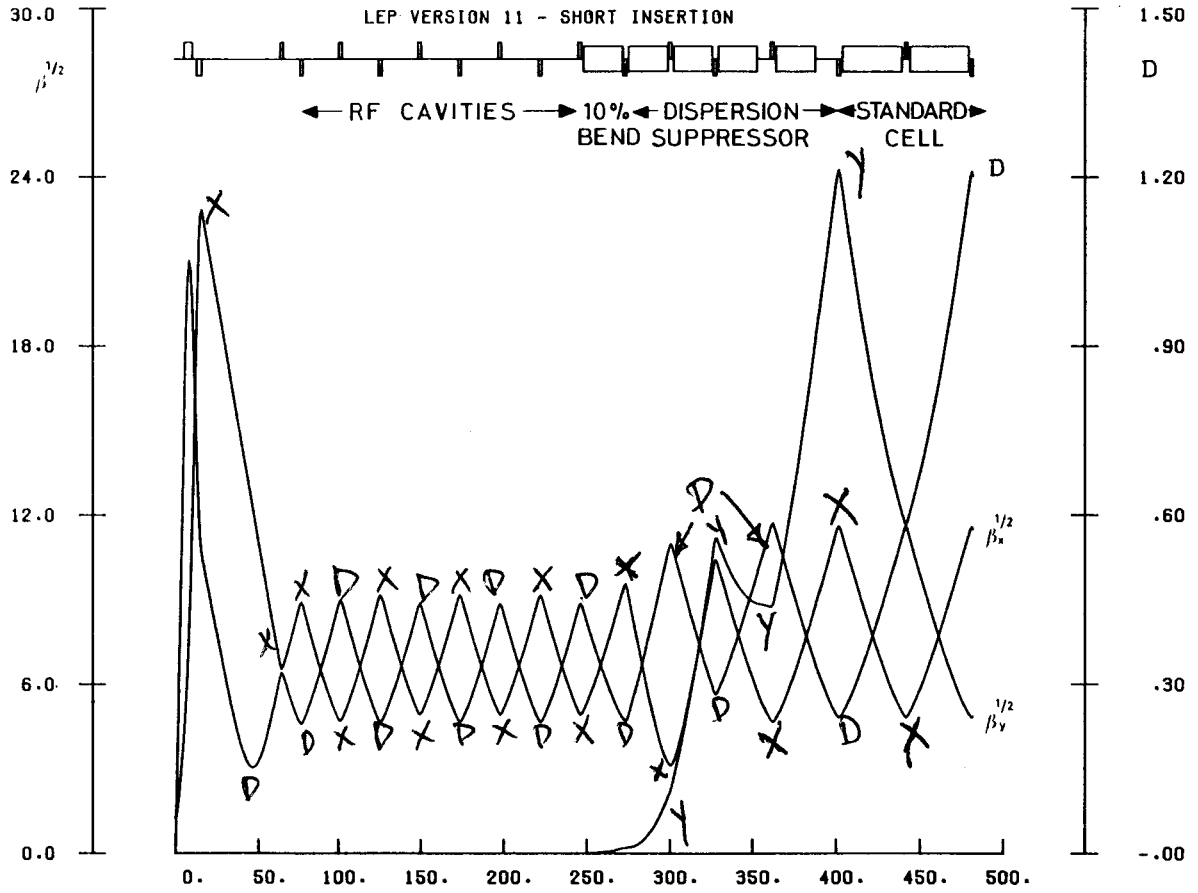
LEP VERSION 11 - SHORT INSERTION
RF CAVITIES
10%
DISPERSION
BEND SUPPRESSOR
STANDARD
CELL
D
30.0
24.0
18.0
12.0
6.0
0.0
1.50
1.20
.90
.60
.30
-.00
0.
50.
100.
150.
200.
250.
300.
350.
400.
450.
500.

Fig. 3

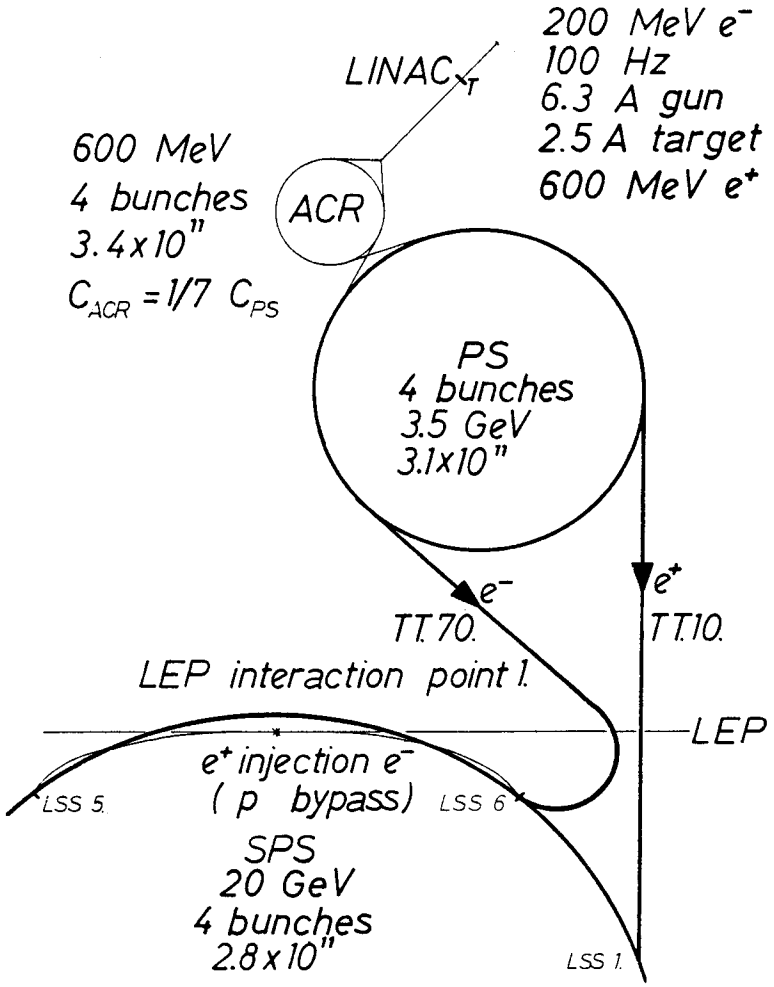
200 MeV e⁻
100 Hz
6.3 A gun
2.5 A target
600 MeV e⁺
LINAC
600 MeV
4 bunches
3.4x10¹¹
C_ACR = 1/7 C_PS
ACR
PS
4 bunches
3.5 GeV
3.1x10¹¹
e⁻
e⁺
TT 70.
TT 10.
LEP interaction point 1.
LEP
e⁺ injection e⁻
(p bypass)
LSS 5.
LSS 6
SPS
20 GeV
4 bunches
2.8x10¹¹
LSS 1.
24 e⁻ & 24 e⁺ cycles in LEP phase 1.

Fig. 4

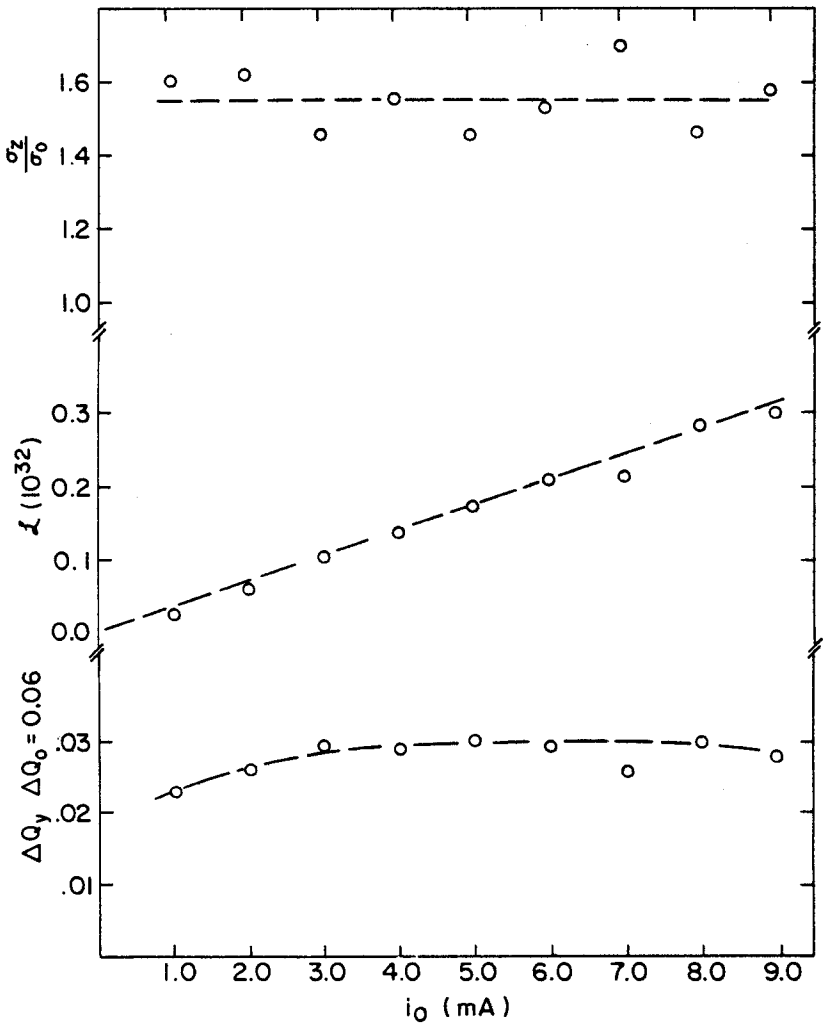
1.6
1.4
1.2
1.0
$\frac{\sigma_z}{\sigma_0}$
0.3
0.2
0.1
0.0
$\mathcal{L}$ (10^{32})
.03
.02
.01
ΔQ_y, $\Delta Q_0 = 0.06$
1.0
2.0
3.0
4.0
5.0
6.0
7.0
8.0
9.0
i_0 (mA)

Fig. 5

PHENOMENOLOGY OF THE HIGGS BOSON

A. Ali

Deutsches Elektronen Synchrotron, DESY

ABSTRACT

The phenomenology of the standard Weinberg-Salam Higgs boson is reviewed with particular emphasis on production mechanisms in high energy e^+e^- and hadron-hadron collisions. The production processes relevant for the ISABELLE and TEVATRON energies are discussed and their backgrounds estimated. It is argued that the toponium production and radiative decay provides the most hopeful reaction to detect a Higgs in both the e^+e^- and the hadron-hadron machines.

I. INTRODUCTION

The problem of understanding the mechanism of mass generation is perhaps the most fundamental problem in elementary particle physics. Closely associated with it is the nature of the weak interaction scale, namely, why is the Fermi coupling constant $G_F = 1.05 \times 10^{-5}\ m_p^{-2}$?

In the standard theory of electroweak interactions[1] the masses of the fermions and the gauge bosons, which mediate the weak interactions, are governed by an order parameter, $\langle\phi\rangle_o$, the vacuum expectation value of an elementary scalar, color and charge neutral particle, ϕ. The mechanism which brings about $\langle\phi\rangle_o \neq 0$ is now folklore and goes under the mystical name of spontaneous symmetry breaking. To be precise, one has a doublet of scalar Higgs fields $\phi = \begin{pmatrix}\phi^+ \\ \phi_o\end{pmatrix}$ having $SU(2)_L \times U(1)$ invariant couplings with the fermions and gauge bosons, and the Higgs potential has the form

$$V(\phi) = -\mu^2|\phi|^2 + \lambda|\phi|^4 \qquad (1.1)$$
$$\mu^2 > 0$$

In order that $V(\phi)$ has a minimum for finite $|\phi|^2$, one must have $\lambda > 0$. Minimizing the potential (1.1) one finds that the minimum is not at $\phi = 0$ but at a non-zero point determined by μ and λ.

$$|\phi|^2 = \mu^2/\lambda \equiv v^2/2 \qquad (1.2)$$

The situation that $v \neq 0$ is what is meant by having a spontaneously broken

symmetry. Now if one rescales the field $\phi \to \phi - v$, then the resulting theory can be arranged in such a way that the fields ϕ^+, $\phi^- = \bar{\phi}^+$ and $\chi = 1/\sqrt{2}\ i(\phi^o - \bar{\phi}^o)$ disappear from the lagrangian and these degrees of freedom become the longitudinal components of W^+, W^- and Z^o, respectively, which in turn become massive. This is what goes under the name of Higgs mechanism. The surviving scalar field, which we shall call H, has the form

$$H^o \equiv \frac{\phi^o + \bar{\phi}^o}{\sqrt{2}} - v \tag{1.3}$$

H is a physical field. Except mass, it has all the attributes of the vacuum. The reshuffled lagrangian has the form

$$\begin{aligned}\mathcal{L}(W,f) = V(H) + g_{fH}\,\bar{f}fH^o + \frac{1}{4}g^2\,W_\mu{}^+W^{\mu-}(H^o)^2 + g_{WH}(W_\mu{}^+W^{\mu-}H^o) \\ + g_{ZH}\,Z_\mu{}^2\,H^o + ...\end{aligned} \tag{1.4}$$

where the parameters g_{fH}, g_{WH} are completely determined in terms of the masses m_f, m_W, m_Z and the vacuum expectation value v. One has

$$\begin{aligned} g_{fH} &= m_f/v = (\sqrt{2}\,G_F)^{1/2}\,m_f \\ g_{WH} &= 2m_W{}^2/v = 2(\sqrt{2}\,G_F)^{1/2}\,m_W{}^2 \end{aligned} \tag{1.5}$$

The proportionality of the Higgs-fermion-fermion coupling and Higgs-Boson-Boson couplings to their masses is no accident. It follows from demanding that the Higgs couplings induce fermion and boson masses after spontaneous symmetry breaking.

The difficulty in having a clean signal in the search for H^o is precisely quantified through Eqs. (1.4), namely that the Higgs likes to couple to the fermions and bosons with an intrinsic strength proportional to their masses. Thus, the production rate in all lepton (e, μ, ν_e, ν_μ)-induced reactions is either zero or miniscule. In the same spirit the tree level couplings involving photons $g_{\gamma\gamma H}$ and the gluon g_{GGH} are zero, which is a consequence of gauge invariance. Thus $g_{\gamma\gamma H}$ (and g_{GGH}) are non-zero only in higher orders in α (and α_s), consequently the γ-induced and gluon-induced reactions are

also intrinsically very small. On the other hand the decays of the Higgs are dominantly into heavy fermions and bosons, leading to multiparticle final states thereby making the traditional $\mu^+\mu^-$ invariant mass searches prohibitively small.

The purpose of this talk is to review attempts in producing and detecting the Higgs boson using high energy machines already available and being planned. While the phenomenology of the Higgs boson will be reviewed in general, I will concentrate more on production mechanisms in the hadronic reactions which are more relevant for the purpose of the present meeting. The other reason is that the opportunities that high energy e^+e^- machines, like LEP, provide in Higgs searches have already been emphasized in the literature.[2] The role of hadron machines in Higgs searches has not received the attention it deserves. I will try to convince you that the intrinsic production cross sections for the Higgs in high energy proton-proton and proton-antiproton colliding machines are not small but the detection of the signal needs new thinking and strategies on the part of our experimental colleagues.

The plan of this talk is as follows. I will start by reviewing the bounds on and an estimate of the Higgs mass. I shall then discuss the various decay mechanisms. The production mechanisms of the Higgs boson is the main subject of this talk and I shall review them emphasizing in particular the radiative decay of the toponium,[3] $J_T \to H^o + \gamma$ and how to make use of this mechanism in hadronic processes. The radiative decay of toponium in my opinion provides the best chance of observing a Higgs both in the e^+e^- machines and at ISABELLE and TEVATRON, if the masses of the toponium and Higgs permit such a decay. Wherever relevant I shall compare the Higgs scenario with the hypercolor scenario of dynamical symmetry breaking,[4] which also admits (almost) point-like light (pseudo-)scalar particles, though this subject will be reviewed by Baqi Beg[5] and Gordy Kane[6] in separate talks in this meeting.

II. MASS OF THE WEINBERG-SALAM HIGGS BOSON UPPER BOUND ON m_{H^o}

The mass of the Higgs boson is in general not determined by the theory since it depends on the unknown quartic coupling constant λ in the Higgs potential (1.1). However an upper bound on m_{H^o} can be obtained in terms of an upper bound on λ. The coupling constant λ is bounded by $\lambda < 1$, otherwise the perturbation theory in λ breaks down. The precise bound is obtained if one considers the scattering of longitudinally polarized $W_L^+ W_L^- \to W_L^+ W_L^-$.[7] The amplitude via the γ and Z exchange is linearly divergent.

$$T^{\gamma,Z} \underset{s \to \infty}{\to} \frac{G_F}{\sqrt{2}} s(1 + \cos\theta); \; s = 4E_{W^\pm}^2 \tag{2.1}$$

This linear divergence (in s) is cancelled by the Higgs contribution giving

$$T^{\gamma,Z,H^o} \sim -\left(\frac{4G_F}{\sqrt{2}}\right) m_H^2 \tag{2.2}$$

Using the partial wave decomposition, one has

$$T = 16\pi \sum_J (2J + 1)\, t^J\, P_J(\cos\theta) \tag{2.3}$$

Unitarity bound for each partial wave is

$$|t^J| \leq 1 \tag{2.4}$$

For $J = 0$, this implies $T \leq 16\pi$ which translates to an upper bound on m_H^2.

$$m_H^2 \leq 4\pi \sqrt{2}/G_F . \tag{2.5}$$

The unitarity bound (2.5) could be refined by considering the 3-channel coupled system consisting of $W_L^+ W_L^-$, $1/\sqrt{2}\, Z_L Z_L$ and $1/\sqrt{2}\, H^o H^o$ which gives the bound

$$m_H^2 \leq \frac{8\pi\sqrt{2}}{3G_F} = 1 \text{ TeV}^2 \tag{2.6}$$

which is disappointingly large! If it turns out that nature has chosen a value for m_{H^o} close to its upper bound, then the Higgs boson is beyond the reach of all present and planned machines like LEP, ISABELLE and TEVATRON!

LOWER BOUND ON m_{H^o}

The lower bound on m_{H^o} comes by considering the radiative corrections to the Higgs potential (1.1). The 1-loop $[SU(2)_L \times U(1)]$ radiative correction gives the result

$$V(\phi) = -\mu^2|\phi|^2 + |\phi|^4 \ln(|\phi|^2/M^2) \times \left(\sum_{V=Z,W^{\pm}} 3m_V^4 + m_H^4 - 4 \sum_f m_f^2 \right) \tag{2.7}$$

where M is a mass parameter to absorb all $|\phi|^4$ terms in $V(\phi)$. The parameters μ and M are so chosen so that the vacuum is stable, i.e. $V(v^2/2) < V(0)$ where v is determined by demanding

$$\left. \frac{\partial V_{rad.}}{\partial \phi} \right|_{|\phi| = v/\sqrt{2}} = 0 \tag{2.8}$$

In the presence of radiative corrections, there is the amusing possibility that one could have $\mu^2 < 0$, and still arrange spontaneous symmetry breaking. However, in that case there will be several minima. It is conceivable that the theory (and the universe) is at the local minimum and will decay to the absolute minimum leading to catastrophic consequences. The rate of such a transition depends critically on m_{H^o}. It has been shown by Linde[8] that if $m_{H^o} > 260$ MeV, then the rate of this transition would be so slow that it is not of any immediate worry!

$$t(\phi_{min} = v/\sqrt{2} \to \phi_{min} = 0) > 10^{10} \text{yrs for } m_{H^o} > 260 \text{ MeV} \tag{2.9}$$

Of course, if m_{H^o} is close to the Linde bound, it will have important cosmological consequences.

Demanding $\phi_{min} \neq 0$ gives an upper bound on $(-\mu^2)$ which translates to a lower bound on m_{H^o}.[9]

$$m_H^2 = \left. \frac{\partial^2 V}{\partial \phi^2} \right|_{\phi = v/\sqrt{2} > (7.2 \text{ GeV})^2} > \frac{3}{16\pi^2 v^2} \sum_{V=W^{\pm},Z} m_V^4 \quad \text{for } \sin^2\theta_W = 0.20 \tag{2.10}$$

Thus, the present bounds on m_{H^o} are

$$1 \text{ TeV} > m_{H^o} \geq 7.2 \text{ GeV} \tag{2.11}$$

COLEMAN-WEINBERG ESTIMATE OF m_{H^o}

E. Weinberg and S. Coleman[10] have pointed out that one could set $\mu^2 = 0$, $\lambda > 0$ and achieve spontaneous symmetry breaking via radiative

corrections. It will then fix the mass of the Higgs boson to be

$$m_H^2 = \frac{3\alpha^2 v^2}{8}\left\{\frac{(2 + \sec^4\theta_W)}{\sin^{-4}\theta_W} - O(m_f/m_H)^4 + O(\alpha)\right\} \tag{2.12}$$

which gives (neglecting fermion mass and $O(\alpha)^3$ contributions) (v = 247 GeV)

$$m_H{}^o = 10.4\ \text{GeV}^{+0.5\ \text{GeV}}_{-0.4\ \text{GeV}} \text{ for } \sin^2\theta_W = 0.2^{+0.01}_{-0.01} \tag{2.13}$$

Thus, for the present value of the Weinberg-Salam-Glashow angle $\sin^2\theta_W$ = 0.215 it predicts $m_H{}^o \gtrsim 11$ GeV, which puts it above the mass of the heaviest observed bound $(Q\bar{Q})$ system Υ, Υ', Υ'' .... It should perhaps be remarked that the heavy fermion mass contribution decreases the estimate (2.13) for $m_H{}^o$ (though $\Delta m_H(f) < 10$ MeV for $m_f \leq 20$ GeV) and that the estimate of $m_H{}^o$ is based on one-loop calculations. The possibility (2.13) is very exciting from the point of view of the proposed e^+e^- and proton machines and I shall review the consequences of a Higgs with $m_H \lesssim 11$ GeV in this talk.

III. DECAYS OF THE WEINBERG-SALAM HIGGS BOSON

The decays of the Higgs boson are determined by the couplings in (1.4) and (1.5). There are <u>no</u> tree level couplings g_{H^oYY} or g_{H^oGG}. However, these couplings are induced at the 1-loop (QFD) level. Thus, the decays of H^o up to 1-loop level are:

$$\begin{aligned} H^o &\to Z^oZ^o \\ &\to W^+W^- \\ &\to \ell^+\ell^- \qquad \ell = e, \mu, \tau \\ &\to q\bar{q} \qquad q = u, d, s, c, b, t \\ &\to GG \\ &\to \gamma\gamma \end{aligned} \tag{3.1}$$

where the decays into weak gauge bosons are allowed only if $m_H{}^o > 2m_{W^\pm}, 2m_Z{}^o$, in which case the H^o decays would be totally dominated by these modes. The decay widths into Z^oZ^o and W^+W^- are given by

$$\Gamma(H^o \to W^+W^-) = \frac{G_F M_W^2}{8\pi\sqrt{2}}\, m_H \frac{(1 - x)^{1/2}}{x}(3x^2 - 4x + 4) \tag{3.2a}$$

$$\Gamma(H^o \to Z^oZ^o) = \frac{G_F M_W^2}{8\pi\sqrt{2}} \; m_H \frac{(1 - x')^{1/2}}{x'} \; (3x'^2 - 4x' + 4) \qquad (3.2b)$$

where

$$x = \frac{4M_W^2}{m_H^2}, \quad x' = \frac{4M_Z^2}{m_H^2} = \frac{x}{\cos^2\theta_W}$$

For $m_{H^o} \geq 200$ GeV, $\Gamma_{H^o} > 1$ GeV and the width increases very fast becoming bigger than m_{H^o} for $m_{H^o} \geq 1$ TeV. In that limit weak interactions become strong and the perturbation theory would break down, as I have already remarked. Leaving the question of producing a 200 GeV object apart, detecting such an object would be relatively easy through the modes

$$\begin{array}{l} pp(\bar{p}) \to H^o + x \\ \quad \hookrightarrow Z^oZ^o \\ \quad\quad \hookrightarrow \ell^+\ell^- \; (\ell = e, \mu, \tau) \\ \quad\quad \hookrightarrow \text{hadrons}, \; \ell^+\ell^- \end{array} \qquad (3.3)$$

and

$$\begin{array}{l} pp(\bar{p}) \to H^o + x \\ \quad \hookrightarrow W^+W^- \\ \quad\quad \hookrightarrow \ell^-\nu_\ell \\ \quad\quad \hookrightarrow \ell^+\nu_\ell, \; \text{hadrons} \end{array}$$

Note that such an object will not be confused with the technieta,[11] the massive colored pseudoscalar object present in technicolor/hypercolor theories which would decay predominantly into a $t\bar{t}$ pair, having very different event topologies. The color neutral pseudo-Goldstone boson, PGB, π'^o, even if it is massive ($m_{\pi'^o} > 2m_{W^\pm}$) will <u>not</u> decay at the tree level through the modes

$$\pi'^o \to Z^oZ^o, \; W^+W^- \qquad (3.4)$$

The couplings $g_{\pi'^oZ^oZ^o}$ and $g_{\pi'^oW^+W^-}$ are nonzero only at the one-loop level and hence very small.[12] The scenario of a heavy Higgs boson, $m_{H^o} > 2m_{Z^o}$, while somewhat discomforting from the point of view of production will have the redeeming feature that it's detection will be easy and it would not be confused with heavier pseudo-scalar objects of the hypercolor scenario.

Let us now concentrate on the scenario in which $m_{H^o} < 2m_{W^\pm}$, in that case the decays of H^o would be dominated by the heaviest fermion pair allowed by

phase space. The decay widths for $H^o \to \ell^+\ell^-$ and $H^o \to q\bar{q}$ are given by

$$\Gamma(H^o \to \ell^+\ell^-) = \frac{G_F m_\ell^2}{4\sqrt{2}\,\pi} m_H \left(1 - \frac{4m_\ell^2}{m_H^2}\right)^{3/2}$$
$$\Gamma(H^o \to q\bar{q}) = 3\,\frac{G_F m_q^2}{4\sqrt{2}\,\pi} m_H \left(1 - \frac{4m_q^2}{m_H^2}\right) \tag{3.5}$$

where the factor 3 for $H^o \to q\bar{q}$ is due to color.

Next we shall calculate the decays $H^o \to \gamma\gamma$,[13] and $H^o \to GG$.[3] These decays, which are allowed at the one-loop level, are quite amusing and if measured could be used as heavy quark counters. The effective $H^o \to 2\gamma$ coupling can be expressed as (see Fig. 1)

$$F(k_1, k_2, q) = \frac{2\alpha}{\pi v} I_{\mu\nu}(k_1, k_2)\, \varepsilon_\mu \varepsilon_\nu \tag{3.6}$$

where gauge invariance dictates that $I_{\mu\nu}$ be expressed as

$$I_{\mu\nu} = (k_{1\mu}k_{2\nu} - k_1 \cdot k_2\, q_{\mu\nu})I$$

and we decompose I according to the contributions from the fermion- and gauge boson-loop

$$I = I_W + \sum_f I_f \tag{3.7}$$

With this notation the decay width is given by

$$\Gamma(H^o \to 2\gamma) = \frac{G_F \alpha^2}{8\sqrt{2}\pi} m_H^3 \,|I|^2 \tag{3.8}$$

The two contributions to I can be calculated in a straight-forward way

$$I_W = \frac{-7}{4} + O(m_H^2/m_W^2) \tag{3.9}$$

$$I_f = N_c Q_f^2 L_f \tag{3.10}$$

where N_c is the color factor (=3), Q_f is the charge of the fermion in the loop and the factor L_f is given by

$$L_f = m_f^2 \int_0^1 dx \int_0^1 dy \,\frac{1 - 4xy}{m_f^2 - m_H^2 xy} \tag{3.11}$$

$$L_f \to \frac{1}{3}[1 + 0(m_H^2/m_f^2)], \; m_H^2/m_f^2 << 1$$

Thus, for large m_f, L_f becomes independent of m_f and counts the heavy fermion degrees. In particular, for a complete 3-generation family (e, μ, τ; u, d, s, c, b, t) we have

$$I(3) \equiv \sum_{3 \text{ gen.}} I_f = 0.7 \tag{3.12}$$

if (N-3) generations of heavy fermions exist then

$$I(N) = I(3) + \frac{8}{9}(N-3) \tag{3.13}$$

Putting (3.9) and (3.13) together, we get

$$\begin{aligned} I &\lesssim -1 \qquad \text{for } N = 3 \\ &\lesssim -0.1 \qquad \text{for } N = 4 \\ &\gtrsim 0.8 \qquad \text{for } N \geq 5 \end{aligned} \tag{3.14}$$

Thus, in principle, $BR(H^o \to 2\gamma)$ is a very sensitive way to 'feel' a fourth generation of fermions. In practice, however

$$\begin{aligned} BR(H^o \to 2\gamma) &\lesssim 4 \times 10^{-5} \; |I|^2 \text{ for } 2m_D < m_{H^o} < 2m_B \\ &\lesssim 4 \times 10^{-6} \; |I|^2 \text{ for } 2m_B < m_{H^o} < 2m_T \end{aligned} \tag{3.15}$$

which is hopelessly small.

Finally, we quote the result for the decay rate $\Gamma(H^o \to GG)$, for which only the heavy quarks contribute in the loop[3] (Fig. 2).

$$\Gamma(H^o \to 2G) = \frac{G_F N_F^2}{36\sqrt{2}\pi} \left(\frac{\alpha_s(m_H^2)}{\pi}\right)^2 m_H^3 \tag{3.16}$$

where N_F = number of heavy flavors. The decay rate $\Gamma(H^o \to 2G)$ is larger than the rate $\Gamma(H^o \to \mu^+\mu^-)$ for $m_{H^o} \geq 3$ GeV. However, it is still much smaller than the decay rate into the heaviest fermion pair. In addition $H^o \to 2G$ mode lacks a reliable trigger both in e^+e^- annihilation and hadron-hadron collisions and we shall not discuss it any more.

Traditionally, the searches for new particles (J/ψ, T) have been very successful in the hadron-hadron collisions through the mode $pp \to V + x$, $V \to \mu^+\mu^-$.

However, because of the peculiar $Hf\bar{f}$ couplings the branching ratio for $H^o \to \mu^+\mu^-$ is miniscule. To orient ourselves we note that

$$BR(H^o \to \mu^+\mu^-) \begin{cases} \gtrsim 2 \times 10^{-3} & \text{for } 2m_D < m_{H^o} < 2m_B \\ \gtrsim 2 \times 10^{-4} & \text{for } 2m_B < m_{H^o} < 2m_T \\ \leq 10^{-5} & \text{for } 2m_T < m_{H^o} < 2m_W \end{cases} \tag{3.17}$$

Thus, though the production of H^o in high energy hadron-hadron machines may be large, as we shall see in the next section, searching a peak in the $\mu^+\mu^-$ invariant mass would be a disappointing enterprise. Hadron machines require a useful trigger other than $\mu^+\mu^-$.

IV. PRODUCTION OF THE HIGGS BOSON

The Higgs production processes that I would like to discuss in this talk are:

i. Decays of vector bosons involving a Higgs

ii. Higgs production in pp and $p\bar{p}$ collisions

iii. Higgs production in lepton-hadron processes

and iv. Higgs production in e^+e^- annihilation.

Let me start with the production mechanism (i).

i. DECAYS OF VECTOR BOSONS INVOLVING A HIGGS

The vector particles in whose decays a Higgs boson may be produced are the Z^o boson and the bound heavy flavor vector meson, T and the yet to be discovered state toponium, J_T. The Higgs boson may also be produced in the decays of the charged vector bosons, $W^\pm$, however, I don't know how to produce $W^\pm$ copiously to detect branching ratios at the level of 10^{-4} which one expects in the decays $W^\pm \to H^o W^\pm$ [14]

$$\Big\lfloor \to \ell^\pm \nu_\ell,\ q\bar{q}$$

HIGGS IN THE DECAYS OF Z^o

There are two decay modes which have been advocated in the literature. The radiative decay[15]

$$Z \to H^o + \gamma \tag{4.1}$$

and the decay[16]

$$Z \to H^o + Z^o_{\lfloor \text{vir} \to \ell^+\ell^-} \tag{4.2}$$

In the standard model, the coupling $ZH^o\gamma$ is not allowed at the tree level.

At the one-loop level it can be calculated using the diagrams shown in Fig. 3. The matrix element for the process (4.1) can be written as

$$m = \varepsilon^{\mu}_{(\gamma)}\ m_{\mu\nu}\ \varepsilon^{\nu}_{(Z^o)} \tag{4.3}$$

Electromagnetic gauge invariance ($m_{\mu\nu} k^{\nu} = 0$) gives

$$m_{\mu\nu} = (k_{\nu} p_{\mu} - k\cdot p\ g_{\mu\nu})a \tag{4.4}$$

in terms of which the width can be expressed as

$$\Gamma(Z \to H^o + \gamma) = \frac{E_{\gamma}^{3} a^2}{12\pi} \tag{4.5}$$

leading to

$$\Gamma(Z \to H^o\gamma)/\Gamma(Z \to \mu^+\mu^-) \simeq \frac{\alpha^2}{\pi^2 \sin^2\theta_W} \left(\frac{E_\gamma}{M_Z}\right)^3 A^2 \simeq 2.6 \times 10^{-5}\left(\frac{E_\gamma}{M_Z}\right)^3 A^2 \tag{4.6}$$

The constant A from Fig. 3 is estimated to be

$$\begin{aligned} A_{(\text{Fermion loop})} &= \frac{4}{3\cos\theta_W}\left(1 - \frac{8}{3}\sin^2\theta_W\right) \\ &\simeq 0.7 \\ A_{(\text{W-boson loop})} &\simeq -\left|4.9 + 0.3(m_H^2/m_W^2)\right| \end{aligned} \tag{4.7}$$

leading to

$$\begin{aligned} \Gamma(Z \to H^o\gamma)/\Gamma(Z \to \mu^+\mu^-) &\simeq 7.8 \times 10^{-5}\left(1 - \frac{m_H^2}{m_Z^2}\right)^3 \\ &\simeq 10^{-6} \times \left(1 + .17\,\frac{m_H^2}{m_Z^2}\right) \end{aligned} \tag{4.8}$$

Even with this small rate one would have to look at

$$\begin{array}{l} Z^o \to H^o + \gamma \\ \qquad\ \ \big\lfloor \to \ell^+\ell^- \end{array} \tag{4.9}$$

Barbellini *et al.*[2] have calculated the background to the process (4.9) due to the decay mode

$$Z^o \to \ell^+\ell^-\gamma \tag{4.10}$$

and it looks formidable. Even after demanding that the photon be recoiling against $\ell^+\ell^-$, the signal from (4.9) would be buried in the background. In e^+e^- annihilation, where one could demand a monoenergetic photon, there may be some outside chance of observing (4.9) but in pp and $p\bar{p}$ collisions it is simply undoable.

Next, we discuss the process (4.2). In principle one could also look at the mode

$$Z^o \to H^o + Z^o_{\hookrightarrow q + \bar{q}}^{vir}$$

but its separation from the dominant Z^o decays ($Z^o \to q\bar{q}$) is not easy. The rate for (4.2) is given by[16]

$$\frac{1}{\Gamma(Z^o \to \mu^+\mu^-} \frac{d\Gamma}{dX_H}(Z^o \to H^o + \ell^+\ell^-) = \frac{\alpha}{4\pi \sin^2\theta_W \cos^2\theta_W} \tag{4.11}$$

$$x \frac{1}{(X_H - m_H^2/m_Z^2)^2} \left[1 - X_H + \frac{X_H^2}{12} + \frac{2}{3}\frac{m_H^2}{m_Z^2}\right]\left[X_H^2 - \frac{4m_H^2}{m_Z^2}\right]^{1/2}$$

where $X_H = 2E_H/m_Z$. The rates for $Z^o \to H^o\ell^+\ell^-$ and $Z^o \to H^o + \gamma$ are shown in Fig. 4. For $m_{H^o} \lesssim 10$ GeV it leads to a branching ratio

$$BR(Z^o \to H^o + \mu^+\mu^-) \lesssim O(10^{-5}) \tag{4.12}$$

which certainly is observable in a high luminosity Z^o-factory. A very good handle on the process (4.2) is obtained if one looks at the shape of the dimuon distribution which peaks at large values of $m_{\mu\mu}$.[16]

$$\frac{d\sigma}{dm^2_{\mu\mu}}(Z^o \to H^o\mu^+\mu^-)\Big|_\chi = 0 \tag{4.13}$$

where $\chi = 0.95\, m_H/m_Z$. The background to (4.2) comes from the dominant decay mode

$$Z^o \to Q\bar{Q} \to \mu^+\mu^- + X \tag{4.14}$$

However, this peaks at the low invariant mass of the dimuons, thus providing a clear signal. The invariant mass distribution, shown in Fig. 5, is a characteristic of the Higgs mode (4.2) and is very different if one considers instead the process involving a pseudo-Goldstone boson.

$$Z \to \pi'^{o} + Z^{o}_{vir} \quad (4.15)$$
$$\qquad\qquad\quad \hookrightarrow \mu^+\mu^-$$

Of course the rate expected for $Z \to \pi'^{o} + \mu^+\mu^-$ is prohibitively small.[12]

$$\frac{\Gamma(Z^o \to \pi'^o \mu^+\mu^-)}{\Gamma(Z^o \to H^o \mu^+\mu^-)} < 10^{-4} \quad (4.16)$$

The decay (4.2) in a Z^o factory is one of the most promising places to observe a Higgs if $m_{H^o} \lesssim 40$ GeV, beyond which both the branching ratio becomes very small and the signal to background separation no longer remains that good. In pp and $p\bar{p}$ machines (4.2) is buried under the background.

$$pp(p\bar{p}) \to Z^o + X \quad (4.17)$$
$$\qquad\quad \hookrightarrow \mu^+\mu^-$$

which is at least three orders of magnitude bigger than for the process[17]

$$pp(p\bar{p}) \to Z^o + X \quad (4.18)$$
$$\qquad\quad \hookrightarrow H^o + \mu^+\mu^-$$

The situation becomes better if one looks for the H^o signal in trilepton final state via

$$pp(p\bar{p}) \to Z^o + X \quad (4.19)$$
$$\qquad\quad \hookrightarrow H^o + \mu^+\mu^-$$
$$\qquad\qquad\quad \hookrightarrow \mu^\pm + X'$$

which has been calculated in Ref. 18 and shown in Fig. 6. The cross section for (4.19) is of order 10^{-39} cm^2 at ISABELLE and I guess the background from the Drell-Yan background to (4.19) may swamp the feeble signal. The use of (4.19) for Higgs search is going to be a formidable task.

HIGGS IN THE DECAYS OF QUARKONIA

Since the couplings of the Higgs boson to a fermion pair favors heavy fermions [see (1.5)], it immediately suggests that the search of Higgs will be profitable in processes in which heavy fermions are involved. Wilczek[3] suggested that if $m_{H^o} < m_T$ then it could be produced in the radiative decay

$$T(9.46) \to H^o + \gamma \quad (4.20)$$

The decay rate for (4.20) can be calculated using non-relativistic quark model and one obtains[3]

$$\frac{\Gamma(T \to H^o + \gamma)}{\Gamma(T \to \mu^+\mu^-)} = \frac{G_F m_T^2}{4\sqrt{2}\pi\alpha}\left(1 - \frac{m_H^2}{m_T^2}\right) \tag{4.21}$$

using the known branching ratio for $T \to \mu^+\mu^-$. (4.21) already gives an upper limit for the branching ratio $BR(T \to H^o + \gamma) < 2.5 \times 10^{-4}$. It has been pointed out in Ref. 19 that if m_{H^o} is close to m_T, then the estimate (4.21) should be corrected to take into account the dipole nature of the radiative decay. Correcting for this we multiply the right hand side of Eq. (4.21) by the dipole factor K, where a phenomenological estimate for K is[19]

$$K = \frac{\frac{m_T}{2}(1 - m_H^2/m_T^2)}{[\frac{m_T}{2}(1 - m_H^2/m_T^2) + \Delta]} \to 1 \qquad m_H^2/m_T^2 \ll 1 \tag{4.22}$$

and Δ is an onium potential dependent factor $\sim O(1\ \text{GeV})$. The K factor will further reduce the branching ratio depending upon the mass difference $(m_T - m_{H^o})$. The possibility (4.20) will soon be checked at CESR and DORIS. However, if the Coleman-Weinberg estimate of $m_{H^o} \gtrsim 11$ GeV is correct, then the decay (4.20) is not accessible. However the decay $J_T \to H^o + \gamma$ would have a large branching ratio in the decay of the (yet to be discovered) toponium state, J_T. The present experimental limit on the mass m_{J_T} from PETRA experiments is[20]

$$m(J_T) > 36.7 \tag{4.23}$$

implying

$$\frac{\Gamma(J_T \to H^o + \gamma)}{\Gamma(J_T \to \mu^+\mu^-)} > 0.13 \tag{4.24}$$

which is not a small number. On the other hand if the top quark mass is larger than $m_Z (\gtrsim 93\ \text{GeV})$, then J_T would decay dominantly via the weak interaction, thereby depleting the branching ratio for $J_T \to H^o + \gamma$. Since the

J_T production cross section both in e^+e^- annihilation and pp and $p\bar{p}$ collisions decreases with increasing m_{J_T}, we feel that an optimal situation for Higgs search is in the range $m_{J_T} \lesssim$ (40-60) GeV and of course with $m_{H^o} < m_{J_T}$.

The signatures for $J_T \to H^o + \gamma$ have been worked out in detail in Ref. 21, where it was shown that one could search for peaks in the inclusive photon energy distribution and analyze the hadronic junk recoiling against the photon. Since $BR(H^o \xrightarrow[b\bar{b}]{} 1\ell^\pm + X) \lesssim 0.64$, the hadronic jet will very often contain a charged lepton which would provide discrimination from decays of the type

$$J_T \to \gamma + GG \quad (4.25)$$
$$\qquad\qquad \hookrightarrow \text{glueball} \to \text{hadrons}$$

which otherwise could mock the decay

$$J_T \to \gamma + H^o \quad (4.26)$$
$$\qquad\qquad \hookrightarrow \text{hadrons}$$

In Table 1, we show the relative branching ratio $R_{H^o\gamma/\mu^+\mu^-} \equiv \Gamma(J_T \to H^o\gamma)/\Gamma(J_T \to \mu^+\mu^-)$ for some representative values of m_{J_T} and m_{H^o}.

The production of toponium in both the e^+e^- annihilation and pp ($p\bar{p}$) collisions has acquired a new interest, namely that it provides one of the most hopeful reactions to discover the standard Weinberg-Salam Higgs, if the phase space permits the decay (4.26). Perhaps it is worth remarking that in theories with dynamical symmetry breaking, the branching ratio for the process involving a color singlet neutral PGB, π'^o

$$J_T \to \pi'^o + \gamma \quad (4.27)$$

is comparable to the decay rate for $J_T \to H^o + \gamma$. We quote the relative rates[22]

$$\frac{\Gamma(J_T \to \pi'^o + \gamma)}{\Gamma(J_T \to \phi^o + \gamma)} \approx (\eta_{F'})^{-1} \quad (4.28)$$

where $\eta_{F'}$ is the number of hyperquark doublets. The dominant decays of O(10 GeV) π'^o are similar to those of H^o, namely

$$\pi'^o \to b\bar{b},\ c\bar{c},\ \tau^+\tau^-$$

though the details may differ.[23] We shall explore the search of the radiative decay $J_T \to H^o + \gamma$ in pp and $p\bar{p}$ collisions in the next section.

ii. HIGGS PRODUCTION IN pp AND $p\bar{p}$ COLLISIONS

DIRECT H^o PRODUCTION

The subprocesses that could lead to direct H^o production in pp and $p\bar{p}$ collisions are shown in Fig. 7. Thus, one could have a Drell-Yan type production

$$q + \bar{q} \to H^o \tag{4.29}$$

as well as the gluon fusion mechanism of Ref. 24

$$G + G \to H^o \tag{4.30}$$

leading to

$$p + p(\bar{p}) \to H^o + X \tag{4.31}$$

The production cross section for (4.31) through the subprocess (4.29) can be expressed in terms of rapidity distribution

$$\frac{d\sigma_H}{dy} \sim \frac{\pi}{6} \Sigma g_q^2 \, \tau m_H^{-2} [F_q(\tau^{1/2} e^y) F_{\bar{q}}(\tau^{1/2} e^{-y}) + q \leftrightarrow \bar{q}] \tag{4.32}$$

where

$$g_q = (\sqrt{2}\, G_F)^{1/2} m_q$$
$$y = \frac{1}{2} \ell n \left(\frac{E + p}{E - p}\right) \; ; \; \tau = m_H^2/s \tag{4.33}$$

$\sqrt{s}$ is the center-of-mass energy and $F_q(F_{\bar{q}})$ stands for the distribution function of finding a quark of flavor $q(\bar{q})$ inside the hadron. It should be remarked that m_q in the Yukawa coupling g_q is the current algebra mass because this is what the Higgs mechanism generates. Thus the coupling g_q is sizeable only for the heavy quarks but alas there are no heavy quarks in the proton! One could excite them from the proton (antiproton), but even at Q^2 available at ISABELLE and TEVATRON energies one would not excite enough $c\bar{c}$, $b\bar{b}$ and $t\bar{t}$ to make (4.32) appreciable. So, I shall neglect the subprocess (4.29).

Let us now consider the gluon fusion mechanism, Eq. (4.30). This leads to a rapidity distribution[24]

$$\frac{d\sigma_H}{dy} \sim \frac{\pi}{32} \left[\frac{\alpha_s(m_H^2)}{\pi}\right]^2 \frac{G_F}{\sqrt{2}} \frac{N_F^2}{9} \tau \, F_G(\tau^{1/2} e^y) \, F_G(\tau^{1/2} e^{-y}) \tag{4.34}$$

where $\alpha_s(m_H^2)$ is the QCD running coupling constant evaluated at $Q^2 = m_H^2$ and N_F is the number of heavy flavors ($m_Q > 0.2\ m_H$). The process (4.34) is small due to $\alpha_s(m_H^2)^2$. Using the experimental result

$$\int_0^1 \xi\ F_G(\xi)\ d\xi = 1/2 \tag{4.35}$$

and using $\xi F_G(\xi) = 3(1 - \xi)^5$, $N_F = 3$, one gets

$$\sigma(pp \to GG \to H^o + X) = \sigma(p\bar{p} \to GG \to H^o + X) \gtrsim 50\ \text{Pb} \tag{4.36}$$
for $\sqrt{s} = 800$ GeV; $m_H = 11$ GeV.

The cross section for the gluon fusion mechanism is shown in Fig. 8 as a function of $\sqrt{s}$. Note that the cross section for (4.31) at the ISABELLE and TEVATRON energies is not small.

To have some idea about the signal to background ratio, let us calculate the cross section $\sigma(pp \to H^o \to \mu^+\mu^-)$ for the optimistic case of $m_{H^o} \gtrsim 10$ GeV, with $BR(H^o \to \mu^+\mu^-) \gtrsim 2 \times 10^{-3}$. This gives for $\sqrt{s} \gtrsim 800$ GeV

$$\sigma(pp \to H^o \to \mu^+\mu^-) \gtrsim 10^{-37}\ \text{cm}^2 \tag{4.37}$$

The Drell-Yan background evaluated for $m(\mu^+\mu^-) \gtrsim 10$ GeV at $\sqrt{s} \gtrsim 800$ GeV is[25]

$$\sigma(pp \underset{DY}{\to} \mu^+\mu^- + X) \gtrsim 10^{-34}\ \text{cm}^2 \tag{4.38}$$

Thus, the $\mu^+\mu^-$ mode looks hopeless. It is clear that one has to look for some other trigger on H^o. I have no wisdom to offer except urging my experimental colleagues to start thinking about developing techniques to tag the $\tau^\pm$ produced in hadron-hadron collisions and develop jet mass reconstruction techniques,[26] which might ultimately help establish the Higgs signal. For pure fun let me quote the cross section (for $m_{H^o} \gtrsim 10$ GeV)

$$\sigma(pp \to H^o \to \tau^+\tau^-) \gtrsim O(10^{-34}\ \text{cm}^2) \tag{4.39}$$

which is comparable to the Drell-Yan process at $\sqrt{s}$ = 800 GeV for $m(\mu^+\mu^-) \gtrsim$ 10 GeV.

$$\sigma(pp \to \tau^+\tau^- + X) \gtrsim O(10^{-34}\ cm^2) \tag{4.40}$$

ASSOCIATED H^O PRODUCTION

The associated production of H^O in pp and $p\bar{p}$ collisions goes via the production of Z^O

$$pp(\bar{p}) \to Z^O + X \tag{4.41}$$

followed by the decays of Z^O

$$Z^O \to H^O + \gamma$$

and

$$Z^O \to H^O + Z^O \quad (Z^O \to \mu^+\mu^-)$$

discussed in the last section. I am afraid that the cross sections involved in any useful tag are of order 10^{-39} cm^2 or less at ISABELLE energies,[18] making the associated H^O production mechanisms unattractive for the Higgs search.

PRODUCTION OF H^O THROUGH H^O-P_b MIXING

This mechanism has been proposed by Ellis et al.[19] The point is that if the Coleman-Weinberg estimate of m_{H^O} is right, then we expect m_{H^O} to be in the mass range 10-11 GeV, though the one-loop result prefers $m_{H^O} \gtrsim$ 11 GeV. Thus if m_{H^O} is close in mass to the $P_b(\equiv {}^3P_o)$ state of the γ-family, then there could be appreciable H^O-P_b mixing leading to the process[19,27]

$$pp(\bar{p}) \to P_b + X \quad (P_b \to H^O) \tag{4.42}$$

Ruckl and Baier (see these proceedings) have recently calculated the inclusive production of the P_b state in pp and $p\bar{p}$ collisions and it is substantial. The production of H^O through (4.42) then depends on the mixing parameter C, which can be calculated in a non-relativistic quark model calculation[19]

$$C \gtrsim \left[\frac{27\sqrt{2}}{\pi} G_F\, m_{P_b}\, |R'(0)|^2\right]^{1/2} \tag{4.43}$$

where R'(0) is the derivative of the wave-function at the origin. The decay mode which is most favorable is

$$P_b \underset{\text{Mixing}}{\rightarrow} H^o \rightarrow (\tau^+\tau^-,\ c\bar{c}) \tag{4.44}$$

Putting everything together, one gets

$$\frac{\Gamma(P_b \rightarrow \tau^+\tau^-)}{\Gamma(P_b \rightarrow \text{all})} \simeq \frac{9\, G_F^{\,2}\, m_\tau^{\,2}\, m_{P_b}^{\,6}\left(1 - \frac{4m_\tau^{\,2}}{m_{P_b}^{\,2}}\right)^{3/2}}{128\,\pi^2\,\alpha_s^{\,2}(m_H^{\,2})(m_H^{\,2} - m_{P_b}^{\,2})^2} \simeq \frac{2.5 \times 10^{-7}}{(m_H - m_{P_b})^2} \tag{4.45}$$

where $\Delta H = m_H - m_{P_b}$ is expressed in GeV. For $\Delta M = 20$ MeV, (4.45) gives

$$\frac{\Gamma(P_b \rightarrow \tau^+\tau^-)}{\Gamma(P_b \rightarrow \text{all})} \simeq 6 \times 10^{-4} \tag{4.46}$$

which is rather small and presumably realistic if m_{H^o} is close to m_{P_b}. However, as an extreme example one could think of a scenario in which $\Delta M <$ 1 MeV such that $\Delta M \sim \Gamma(P_b \rightarrow \text{all})$. In that case there will be complete mixing in the P_b-H^o sector, making the perturbation theory estimate (4.43) of the mixing parameter inapplicable. In the event of complete mixing, one would have a situation very similar to the K^o-$\bar{K}^o$ system namely, there will be two states of P_b with

$$P_{b_{(\frac{1}{2})}} = \frac{1}{\sqrt{2}}\,(|H> \pm |P_b>) \tag{4.47}$$

having branching ratio $BR(P_b \rightarrow \tau^+\tau^-) \sim 10\%$ for both the states P_{b_1} and P_{b_2}! The prediction (4.47) has not yet been checked but it is clear that its validity would require an accidental degeneracy of m_{H^o} and m_{P_b} and in general such accidents are not very widespread in nature!

Perhaps, it is fair to say that if $\Delta M \simeq 100$ MeV, then the scenario (4.42) would lead to a marginal increase in the direct H^o production at the ISABELLE and TEVATRON energies.

PRODUCTION OF H^o THROUGH THE RADIATIVE DECAY $J_T \to H^o + \gamma$

In the last section I have discussed the exciting possibility of the process

$$J_T \to H^o + \gamma$$

which could be a large fraction of the rate for $J_T \to \mu^+\mu^-$, the traditional way of hunting for the vector mesons in hadron-hadron collisions. In this section I would like to advocate using the radiative decay of J_T to search for H^o in the pp and $p\bar{p}$ collisions at ISABELLE and TEVATRON. The process one should search for is

$$\begin{array}{l} pp(\bar{p}) \to J_T + X \\ \qquad\quad \lfloor\!\to H^o + \gamma \\ \qquad\qquad\quad \lfloor\!\to \ell^\pm + X' \end{array} \tag{4.48}$$

Depending on the mass difference $m_{J_T} - m_{H^o}$, the photon in (4.48) will be very energetic and will have a large p_T recoiling against a jet whose composition will depend on the mass of the H^o. If $m_{H^o} < 2m_B$, then the decay mode

$$H^o \to \tau^+\tau^-$$

could be as big as 25% of all the H^o decays, and one could look for

$$\begin{array}{l} pp(\bar{p}) \to J_T + X \\ \qquad\quad \lfloor\!\to H^o + \gamma\,(\text{large } p_T) \\ \qquad\qquad\quad \lfloor\!\to \tau^+\tau^- \end{array} \tag{4.49}$$

On the other hand if $m_{H^o} > 2m_B$, then the decays of H^o would be dominated by

$$H^o \to b\bar{b}$$

leading to the final state in (4.48). Since the branching ratio $H^o \to b\bar{b} \to \ell^\pm + X$ is about 2/3, there won't be any appreciable loss in the event rate. The requirement of large-p_T photon would reduce the background to (4.49) from the usual Drell-Yan background $pp(\bar{p}) \to \begin{array}{l} J_T + X \\ \quad\lfloor\!\to \tau^+\tau^- \end{array}$ and $pp(\bar{p}) \to \tau^+\tau^- + X$.

Requiring a prompt lepton in the hadronic shower recoiling against the large-p_T photon would reduce the background from the inclusive photon production background

$$pp \to \gamma + X \tag{4.50}$$

Next, we would like to calculate the rate for the process

$pp \to J_T + X$ (with $J_T \to H^o + \gamma$) and compare it with the rate for the background (4.50). There is a considerable amount of uncertainty involved in estimating the toponium production rate in pp and $p\bar{p}$ collisions. This is so because for large values of m_t, the wave-function becomes coulombic. In addition there are uncertainties about the diffractive component of $pp(\bar{p}) \to J_T + X$ as well as the contribution of the χ_T states to J_T production via the reaction $pp(\bar{p}) \to \chi_T + X$ (with $\chi_T \to J_T + \gamma$) to make a ball park estimate, we shall use Gaisser scaling,[28] which works for the J/ψ and T production in pp collisions within a factor 2. The quantity which scales is

$$\frac{d\sigma}{dy} = \tilde{R}^o \, \Gamma_{3g} \, \frac{d\sigma^{DY}}{dMdy} \tag{4.51}$$

where the coefficient $\tilde{R}^o$ has been calculated to be $\tilde{R}^o = 15 \times 10^{6}$.[28] Using this estimate for the production cross section, the rate for the quantity

$$(pp \to J_T + X)\ BR(J_T \to H^o + \gamma) \tag{4.52}$$

is tabulated in Table 2 for various representative values of m_{J_T} and m_{H^o} = 11 GeV at the ISABELLE energy $\sqrt{s}$ = 720 GeV. The numbers in the last column are the expected number of events assuming an integrated luminosity of 3.6×10^{39} (corresponding to 1000 hours of running time with $\mathcal{L} = 10^{33}$). We note that the event rates are quite encouraging. Rates for other allowed values of m_{H^o} can be obtained by combining Tables 1 and 2. For $m_{J_T} > m_Z$, the branching ratio $J_T \to \mu^+\mu^-$ becomes very small.

Let us now calculate the cross section for the background

$$pp(\bar{p}) \to \gamma + X$$

where the photon is produced, for example, in the subprocess $G + q \to \gamma + q$. The differential cross section $d\sigma/dp_T d\Omega$ has been evaluated in Ref. 25 to be

$$\left.\frac{d\sigma}{dp_T d\Omega}\right|_{\gamma_{p_T} = 30\ \text{GeV}} \simeq 1\ \text{Pb} \tag{4.53}$$

which is comparable to the production rate for the process

$$pp \to \begin{matrix} J_T + X \\ \hookrightarrow H^o + \gamma \end{matrix} \tag{4.54}$$

However, the background can be very much reduced by triggering in addition on a prompt lepton. One could even determine m_{H^o} by constructing the energy and momentum of the hadronic shower recoiling against the photon and measuring $d\sigma/dm_{\gamma\text{"}H^o\ \text{jet}\text{"}}$. This needs some effort and experience with hadronic jets at ISABELLE and TEVATRON energies.

The prospects of observing a Higgs signal in pp and $p\bar{p}$ collisions at high energies through the process (4.54) at the level of O(1 Pb) is exciting. One should point out that direct H^o production in pp and $p\bar{p}$ collisions through the gluon fusion mechanism is quite large at ISABELLE and TEVATRON energies. However, the Higgs so produced lacks a reliable trigger. Thus, the somewhat smaller production cross section for (4.54) is compensated by the relatively clean trigger that we have here advocated.

iii. HIGGS PRODUCTION IN LEPTON-NUCLEON PROCESSES

These processes include the reactions

$$\begin{aligned} \ell + N &\to \nu_\ell + H^o + X \\ &\to \ell + H^o + X \\ \nu_\ell + N &\to \nu_\ell + H^o + X \\ &\to \ell + H^o + X \end{aligned} \tag{4.55}$$

The lowest order processes involving the bremstrahlung off the lepton line are negligible. The next order diagrams involving double $W^{\pm}$ and Z^o exchanges are shown in Fig. 9. One could express the differential distribution corresponding to these diagrams as[29]

$$\frac{d^4\sigma}{dxdydx'dy'} = \frac{G_F^3 s^2 x'}{4\sqrt{2}\pi^3}\left[\left(1 + \frac{s}{m_W^2}xy\right)^2\left(1 + \frac{s}{m_W^2}x'y'\right)^2\right]^{-1}$$

$$\times \left[\{u(x',Q'^2) + c(x', Q'^2)\}f_1\right.$$

$$\left. + \{\bar{d}(x',Q'^2) + \bar{s}(x', Q'^2)\}f_2\right] \tag{4.56}$$

with $Q'^2 = -q^2 = sx'y'$,

$$x = \frac{-q^2}{2p\cdot q},\ x' = \frac{-q'^2}{2p\cdot q'},\ y = \frac{q\cdot p}{k\cdot p},\ y' = \frac{q'\cdot p}{k\cdot p}$$

f_1 and f_2 are kinematic factors for collisions of fermions with like and unlike helicities and are given by

$$f_1 = 1 - y + y' - \frac{x}{x'} - \frac{y'}{y} + \frac{xy}{x'} + \frac{2xy'}{x'y} - \frac{m_H^2}{s}\frac{(1-y)}{x'y}$$

$$f_2 = (1-y)\left[1 - \frac{x}{x'} - \frac{y'}{y} - \frac{xy'}{x'} + \frac{2xy'}{x'y} - \frac{m_H^2}{s}\frac{1}{x'y}\right] \tag{4.57}$$

The functions $u(x', Q'^2)$ etc., are the quark densities inside nucleon corresponding to the u quarks. In the low energy limit (i.e. $m_W \to \infty$), and neglecting any Q^2 dependence of the structure functions, one has

$$\sigma \sim \frac{G_F^3 s^2}{8\sqrt{2}\pi^3}\int_0^1 dx\,\frac{1}{6}\,x\,F_2(x) \tag{4.58}$$

using $\sigma(\nu_\mu \to \mu^-) = G_F^2 s/\pi$ gives

$$\frac{\sigma(\nu_\mu \to \mu^- + H^o + X)}{\sigma(\nu_\mu \to \mu^- + X)} \sim 3 \times 10^{-8}\left(\frac{E_\nu}{M_N}\right) \tag{4.59}$$

The cross section for other processes in (4.55) are even smaller. With $\sin^2\theta_W \simeq 0.22$, one has

$$\sigma(\nu \to \nu_H) = 2\sigma(\bar{\nu} \to \bar{\nu}_H) \simeq 0.04\,\sigma(\nu_\mu \to \mu^- + H) \tag{4.60}$$

and it looks hopeless.

At high energies, the results are shown in Fig. 10 for both the cases involving Q^2-independent and Q^2-dependent quark densities. Typically

$$\sigma(e + p \to \nu_e + H^o + X) < 10^{-37}\ \text{cm}^2 \quad \text{for } s = 10^7\ \text{GeV}^2 \tag{4.61}$$
$$< 10^{-39}\ \text{cm}^2 \quad \text{for } s = 10^4\ \text{GeV}^2$$

with QCD corrections reducing the rate by roughly a factor 2.

My conclusion is that ep and νp machines are not suitable to study the question of Higgs production at high energies.

iv. HIGGS PRODUCTION IN e^+e^- ANNIHILATION

e^+e^- machines are probably the last hope of the broken hearts who would like to see a Higgs in their life! The history of e^+e^- machines has been a success story which primarily could be traced back to their role as vector boson factories. Depending upon the energy resolution and the mass of the resonance as well as its width, the enhancement at these vector meson poles could be several thousand units of R, which compensates the intrinsically smaller cross section of the process $e^+e^- \to$ hadrons. Of course, the other advantage is that the initial state is very precisely known.

We have already discussed the potential role that vector bosons, J_T and Z^o could play in Higgs searches through the decays $J_T \to H^o + \gamma_{\text{monoenergetic}}$ and $Z \to H^o + \mu^+\mu^-$. If one could produce these vector bosons in abundance, then the vector boson factories have a much cleaner environment to study these decays. However if $m_{H^o} > m_{Z/2}$ and if $m_{H^o} > m_{J_T}$ then the vector boson factories cease their edge on other machines as far as Higgs search is concerned.

I shall now discuss some other processes in the context of e^+e^- machines.

1. $e^+e^- \overset{\gamma,Z}{\to} H^oH^o$

This is not allowed due to Bose symmetry.

2. Bremsstrahlung mechanisms

Here a Higgs can be bremsstrahlunged off the initial or final fermion line[2,27]

$$\frac{\sigma(e^+e^- \to \mu^+\mu^-H^o)}{\sigma(e^+e^- \to \mu^+\mu^-)} \sim G_F m_e^2 \ell ns \simeq 2.2 \times 10^{-11} \tag{4.62}$$

$$\frac{\sigma(e^+e^- \to \tau^+\tau^-H^o)}{\sigma(e^+e^- \to \mu^+\mu^-)} \sim 2.8 \times 10^{-4} \tag{4.63}$$

$$\frac{\sigma(e^+e^- \to t\bar{t}H^o)}{\sigma(\mu^+\mu^-)} \geq 0.1 \quad \text{for } m_t \geq 20 \text{ GeV} \tag{4.64}$$

However, it is very hard to identify H^o in the final state $t\bar{t}H^o$ since it lacks a good trigger.

3. $e^+e^- \to H^o$

$$\sigma(e^+e^- \to H^o) \simeq \frac{4\pi}{m_H^2} \frac{\Gamma(H^o \to e^+e^-)}{\Gamma(H^o \to \text{all})} \tag{4.65}$$

assuming

$$\Gamma(H^o \to Q\bar{Q}) \approx \Gamma_{\text{total}}(H^o)$$

$$\to BR(H^o \to e^+e^-) \simeq \frac{1}{3}\left(\frac{m_e}{m_Q}\right)^2$$

which gives

$$\begin{aligned} \Delta R(e^+e^- \to H^o) &\simeq \frac{3}{\alpha^2} BR(H^o \to e^+e^-) \\ &\simeq \frac{1}{\alpha^2} (m_e/m_Q)^2 \\ &\simeq 2 \times 10^{-3} \text{ for } 2m_D < m_{H^o} < 2m_B \\ &\simeq 2 \times 10^{-4} \text{ for } 2m_B < m_{H^o} < 2m_T \end{aligned} \tag{4.66}$$

4. $e^+e^- \to H^o + \gamma$ [30]

The one-loop diagrams are shown in Fig. 11 and one could express the result as

$$\frac{\sigma(H^o\gamma)}{\sigma(\mu^+\mu^-)} \simeq 4.8 \times 10^{-10}\, s(1 - m_H^2/s)^3 \left| I_W - \sum_F I_F \right|^2 \tag{4.67}$$

$$I_W \Big|_{\sqrt{s} = 30 \text{ GeV}} \simeq 1.7$$

$$I_F \Big|_{m_F \to \infty} \simeq 1/3 \text{ for } \begin{pmatrix} \nu_L \\ L^- \end{pmatrix} \text{ doublet}$$

$$\simeq 5/9 \text{ for } \begin{pmatrix} G \\ H \end{pmatrix} \text{ doublet}$$

This gives

$$\Delta R(H^o\gamma) \simeq O(10^{-6}) \qquad (4.68)$$

for $m_{H^o} \leq 20$ GeV

$20 \text{ GeV} \leq \sqrt{s} \leq 90$ GeV

an even difficult proposition than measuring $\Delta R(e^+e^- \to H^o)$!

5. $e^+e^- \to Z^oH^o$ [31]

This is the last process that I would like to discuss in my talk. Since the Z^oZ^oH coupling is large, one expects a huge cross section as the center-of-mass energy in e^+e^- ennihilation increases. The cross section can be expressed as

$$R_{ZH^o} = \frac{\sigma(Z^oH^o)}{\sigma(\mu^+\mu^-)} = \frac{3}{64}\left(\frac{m_Z}{38 \text{ GeV}}\right)^4 \frac{m_Z}{2\sqrt{2}\, m_H} \times [1 + (1 - 4\sin^2\theta_W)^2] \qquad (4.69)$$

which is not a small number. The ratio R_{ZH^o} peaks at $\sqrt{s} = m_Z + \sqrt{2}\, m_H$ and the rates at the peak assuming various values of m_{H^o} are shown in Table 3. The Z^o could be identified through

$$Z^o \to e^+e^-,\ \mu^+\mu^-$$

then

$$m_H^2 = (\sqrt{s} - E_Z)^2 - p_Z^2 \qquad (4.70)$$

The event rates corresponding to

$$e^+e^- \to Z^oH^o \qquad (4.71)$$
$$\hookrightarrow \ell^+\ell^-$$

are shown in the last column assuming optimistically a luminosity of 10^{31}. The table serves to show that LEP could at most see a Higgs of $m_{H^o} \leq m_{Z/2}$. The situation should be contrasted with the Higgs production through the gluon fusion mechanism in pp and $p\bar{p}$ collisions. My feeling is that at ISABELLE and TEVATRON, one would be able to explore a much larger range of m_{H^o} --- provided one could trigger on $\tau^+\tau^-$ and/or on the energetic jets in the decays of H^o.

V. CONCLUSION

The problem of understanding the mechanism that breaks chiral symmetry and gives fermions and gauge bosons their masses is not yet understood. Higgs mechanism is a possible solution. The standard Weinberg-Salam theory has a neutral Higgs, which is a physical particle. It's detection will strengthen our belief in the underlying framework. I reviewed attempts made to harness the Higgs.

Among the conceivable production mechanisms in proton-proton and proton-antiproton collisions, the most hopeful place is the process

$$pp(\bar{p}) \to \begin{matrix} J_T + X \\ \hookrightarrow H^o + \gamma \end{matrix} \quad \text{if } m_{H^o} < m_{J_T}$$

since it provides a rather powerful trigger. It will however need a high luminosity pp or $p\bar{p}$ collider, for example the phase II of ISABELLE. The gluon fusion mechanism $pp(\bar{p}) \to GG \to H^o + X$ has a potentially large cross section. It is imperative to develop a reliable trigger on H^o --- other than $\mu^+\mu^-$.

The production of vector boson J_T and Z^o in e^+e^- annihilation and the decays $J_T \to H^o + \gamma$, $Z \to H^o + \mu^+\mu^-$ and the reaction $e^+e^- \to Z^oH^o$ are the only other hopes of finding an H^o. However if m_{H^o} is large [$\geq$ 0(100 GeV)], then e^+e^- machines won't be able to see them simply because these machines run out of gas beyond $\sqrt{s}$ = 200 GeV. In that event pp and $p\bar{p}$ machines are the only hopes to see a Higgs, or any other particle or phenomenon, replacing the Higgs mechanism. Only pp and $p\bar{p}$ machines provide energies reaching $\sqrt{s} = \langle\phi^o\rangle \gtrsim 250$ GeV in a channel which could communicate with the vacuum. I am sure that when the pp and $p\bar{p}$ machines will probe the electroweak vacuum at $\sqrt{s} \gtrsim \langle\phi^o\rangle$, we are destined to observe new and fascinating phenomenon.

ACKNOWLEDGEMENT

I would like to thank M.A.B. Bég, J. Babcock, G.L. Kane, W.-Y. Keung, F.E. Paige and L.-L. Chau Wang for useful discussions. The hospitality of the Brookhaven National Laboratory is thankfully acknowledged.

REFERENCES

1. S. Weinberg, Phys. Rev. Lett. 19, 1264 (1967); A. Salam, in Proceedings of the Eighth Nobel Symposium on Elementary Particle Theory, Relativistic Groups and Analyticity, Stockholm, Ed. N. Svartholm (Almqvist and Wiksell, Stockholm, 1968).

2. See, for example, Proceedings of the LEP Summer Study, CERN Report 79-01 (1979) and G. Barbiellini et al., DESY Report 79/27 (1979).

3. F. Wilczek, Phys. Rev. Lett. 39, 1304 (1977).

4. S. Weinberg, Phys. Rev. D19, 1277 (1979); L. Susskind, Phys. Rev. D20, 2619 (1979).

5. M.A.B. Bég, Proceedings of the 1981 ISABELLE Summer Workshop.

6. G.L. Kane, Proceedings of the 1981 ISABELLE Summer Workshop.

7. B.W. Lee, C. Quigg and H. Thacker, Phys. Rev. Lett. 38, 883 (1977); M. Veltman, Acta Phys. Pol. (June 1977), Phys. Lett. 70B, 253 (1977).

8. A.D. Linde, JETP Lett. 19, 183 (1974).

9. A. Linde, JETP Lett. 23, 64 (1976); S. Weinberg, Phys. Rev. Lett. 36, 294 (1976); P. Frampton, Phys. Rev. Lett. 37, 1378 (1976).

10. S. Coleman and E. Weinberg, Phys. Rev. D7, 1888 (1973); see also, S. Weinberg, Phys. Rev. D7, 2887 (1973).

11. S. Dimopolous, S. Raby and G.L. Kane, Nucl. Phys. 182B, 77 (1981); see also, G.L. Kane, Ref. 6.

12. A. Ali and M.A.B. Bég, DESY Report 80/98; see also, J. Ellis, M.K. Gaillard, D.V. Nanopolous and P. Sikivie, Nucl. Phys. 182B, 529 (1981).

13. J. Ellis, M.K. Gaillard and D.V. Nanopolous, Nucl. Phys. B106, 292 (1976).

14. A. Ali, DESY Report 81/18 (1981).

15. R.N. Cahn, M.S. Chanowitz and N. Fleishon, LBL Report No. LBL-849 (1978).

16. J.D. Bjorken, SLAC Report No. PUB-1866 (1977).

17. L.-L. Chau Wang, Brookhaven Report, BNL 28781-R (1981).

18. W.-Y. Keung, L.-L. Chau Wang and S.C.C. Ting, Brookhaven Report BNL 29598 (1981).

19. J. Ellis, M.K. Gaillard, D.V. Nanopolous and C.T. Sachrajda, CERN Report TH. 2634 (1979).

20. P. Duinker, Talk at the EPS Meeting, Lisbon, Portugal (1981).

21. A. Ali and G. Nikenberg, Z.f. Physik C3, 147 (1979).

22. Ali and Bég in Ref. 12.

23. A. Ali, H.B. Newman and R.Y. Zhu, DESY Report 80/110 (1981); see also, J. Ellis et al. in Ref. 12.

24. H. Georgi, S.L. Glashow, M. Machacek and D.V. Nanopolous, Phys. Rev. Lett. 40, 692 (1978).

25. F.E. Paige, BNL Report BNL 27066 (1979) and private communication.

26. For such techniques in e^+e^- annihilation see J.P. Babcock and R.E. Cutkosky, Carnegie-Mellon University Report COO-3066-71 (1981) and J.P. Babcock, Proceedings of the 1981 ISABELLE Workshop.

27. H.E. Haber, G.L. Kane and T. Sterling, Nucl. Phys. B161, 493 (1979).

28. This estimate is based on the work done by F.E. Paige (unpublished result). For Gaisser scaling, see also S. Pakvasa et al., Phys. Rev. D20, 2862 (1979).

29. S. Midorikawa and M. Yoshimura, Univ. of Tokyo report INS-Rep.-348 (1979).

30. J.P. Leveille, Wisconsin Report COO-881-86 (1979).

31. B. Ioffe and V. Khoze, Sov. J. Part. Nucl. 9, 50 (1978); J. Ellis, M.K. Gaillard and D.V. Nanopolous in Ref. 13; B.W. Lee, C. Quigg and H.B. Thacker, Phys. Rev. D16, 1519 (1977).

TABLE 1

The ratio $\frac{\Gamma(J_T \to H^o + \gamma)}{\Gamma(J_T \to \mu^+\mu^-)}$ in the Weinberg-Salam model

m_{H^o} (GeV) \ $m(J_T)$ (GeV)	40	60	80
10	.14	.32	.58
20	.11	.29	.55
30	.065	.24	.50
40		.18	.44
50		.10	.35
60			.25
70			.13

Table 2

Production cross section for the process $pp \to J_T + X \to H^o + \gamma + X$ using Gaisser scaling. The numbers correspond to using $m_{H^o} \simeq 11$ GeV, $\sqrt{s} = 720$ GeV, $BR(H^o \to 1\ell^{\pm} + X) = 0.64$ and an integrated luminosity of 3.6×10^{39}.

$M(J_T)$ (GeV)	$\sigma(pp \to J_T + X \hookrightarrow H^o + \gamma)$	# Events $pp \to J_T \to H^o + \gamma \hookrightarrow \geq 1\ell^{\pm} + X$
40	1.0 Pb	2300
50	0.5 Pb	1150
60	0.22 Pb	500
70	0.1 Pb	230
80	0.04 Pb	$\sim$ 100

TABLE 3

Expected rates for the process $e^+e^- \to Z^oH^o$ at the peak value $\sqrt{s} = m_Z + \sqrt{2}\, m_H$. The entries in the last two columns are obtained for $\mathcal{L} = 10^{31}$ cm^{-2} sec^{-1} and a branching ratio $Z^o \to \ell^+\ell^- = 3\%$ (Barbiellini et al. in Ref. 2).

M_H(GeV)	$\sqrt{s}$ (GeV)	$\frac{\sigma(Z^o + H^o)}{\sigma_{pt}}$	$\frac{\# H^o + Z^o}{10^3 \text{ hrs.}}$	$\frac{\# H^o\ell^+\ell^-}{10^3 \text{ hrs.}}$
10	104	4.7	1458	44
30	132	1.56	280	$\sim$ 9
45	154	1.04	138	$\sim$ 4
60	175	0.78	82	$\sim$ 3

FIGURE CAPTIONS

Fig. 1 Feynman diagrams for the decay $H^o \to 2\gamma$.

Fig. 2 Feynman diagram for the decay $H^o \to 2G$.

Fig. 3 Feynman diagram forthe decay $Z^o \to H^o + \gamma$.

Fig. 4 Decay rates for $\Gamma(Z^o \to H^o + \gamma)/\Gamma(Z^o \to \mu^+\mu^-)$ and $\Gamma(Z^o \to H^o + \mu^+\mu^-)/\Gamma(Z^o \to \mu^+\mu^-$ for different values of m_H/m_Z from Ref. 15.

Fig. 5 Dimuon invariant mass distribution in the decay $Z^o \to H^o + \ell^+\ell^-$ from Ref. 16.

Fig. 6 Distribution of the dilepton invariant mass $m(\ell^+\ell^-)$ in $pp \to \ell^+\ell^-\ell^\pm X$ at $\sqrt{s}$ = 800 GeV from the sources

(i) decays of $b\bar{b}$ and $t\bar{t}$ produced in pp collisions.

(ii) Drell-Yan process $pp \to (\gamma, Z^o) \to \ell^+\ell^-$ along with a third lepton produced with a probability 10^{-4} and

(iii) $pp \to Z^o + H^o + X$ followed by $Z^o \to \ell^+\ell^-$ and $H^o \to \ell^\pm + X$.

Label $\ell_i\ell_j$ denotes leptons originated from particle i and j respectively and $(\ell^+\ell^-)_i$ denotes leptons from the same parent, from Ref. 18.

Fig. 7 (a) 'Drell-Yan' mechanism for $p + p(\bar{p}) \to H^o + X$.

(b) Gluon fusion mechanism for $p + p(\bar{p}) \to H^o + X$.

Fig. 8 Production cross section for $NN \to GG \to H^o + X$ (N = p or $\bar{p}$) for m_{H^o} = 11 GeV (from W.Y. Keung).

Fig. 9 Feynman diagrams for Higgs production in lepton-nucleon scattering processes $\ell + p \to \nu_\ell + H^o + X$ and $\ell + p \to \ell + H^o + X$.

Fig. 10 (a) Cross sections for $e + p \to \nu_e + H^o + X$ shown in Fig. 10 as a function of $(\text{CM energy})^2$. Solid and dashed curves correspond to parton model with and without a QCD correction. Cases A, B and C are results for m_{H^o} = 10, 100 and 200 GeV.

(b) Same as (a) but for smaller range of s. Curves A, B and C are results with m_{H^o} = 10, 20 and 30 GeV, from Ref. 29.

Fig. 11 Diagrams for the process $e^+e^- \to H^o + \gamma$.

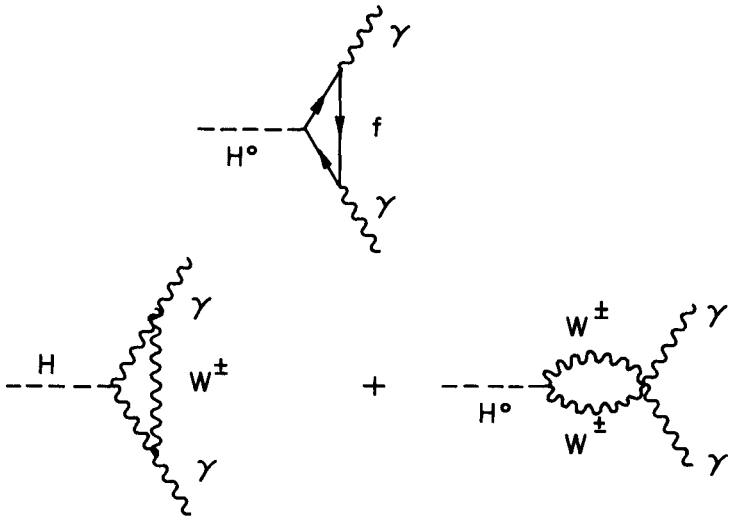

Fig. 1

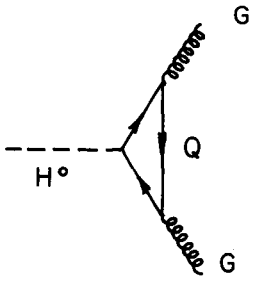

Fig. 2

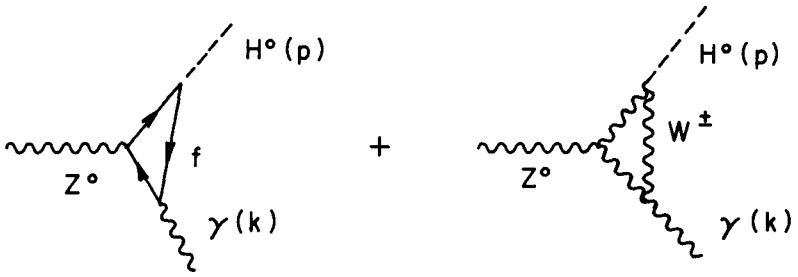

Fig. 3

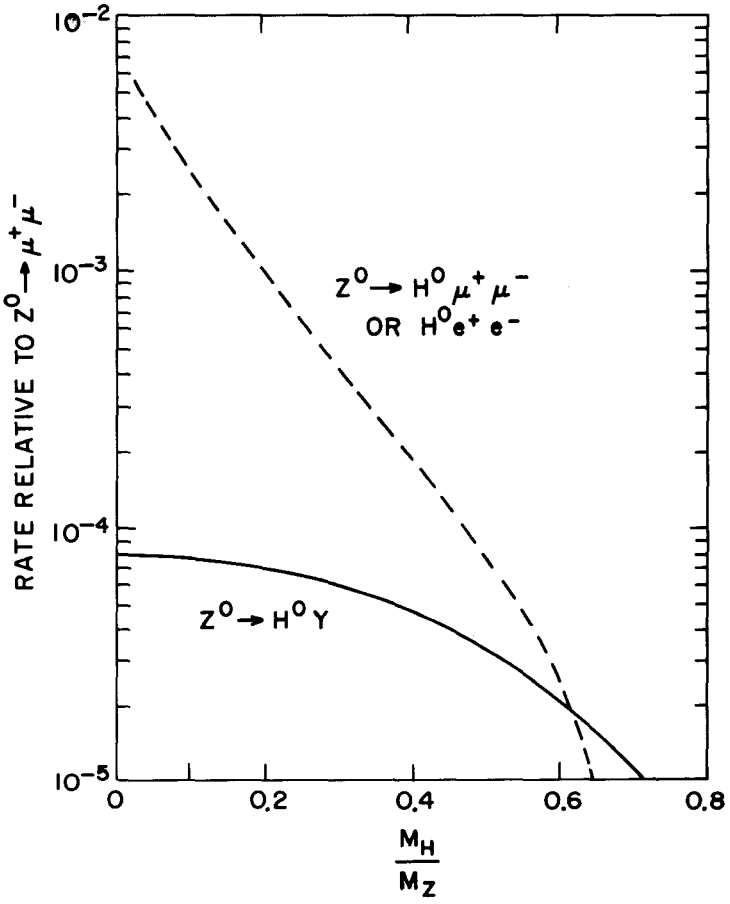
10^{-2}
10^{-3}
10^{-4}
10^{-5}
RATE RELATIVE TO $Z^0 \to \mu^+\mu^-$
$Z^0 \to H^0\mu^+\mu^-$
OR $H^0e^+e^-$
$Z^0 \to H^0Y$
0
0.2
0.4
0.6
0.8
$\frac{M_H}{M_Z}$

Fig. 4

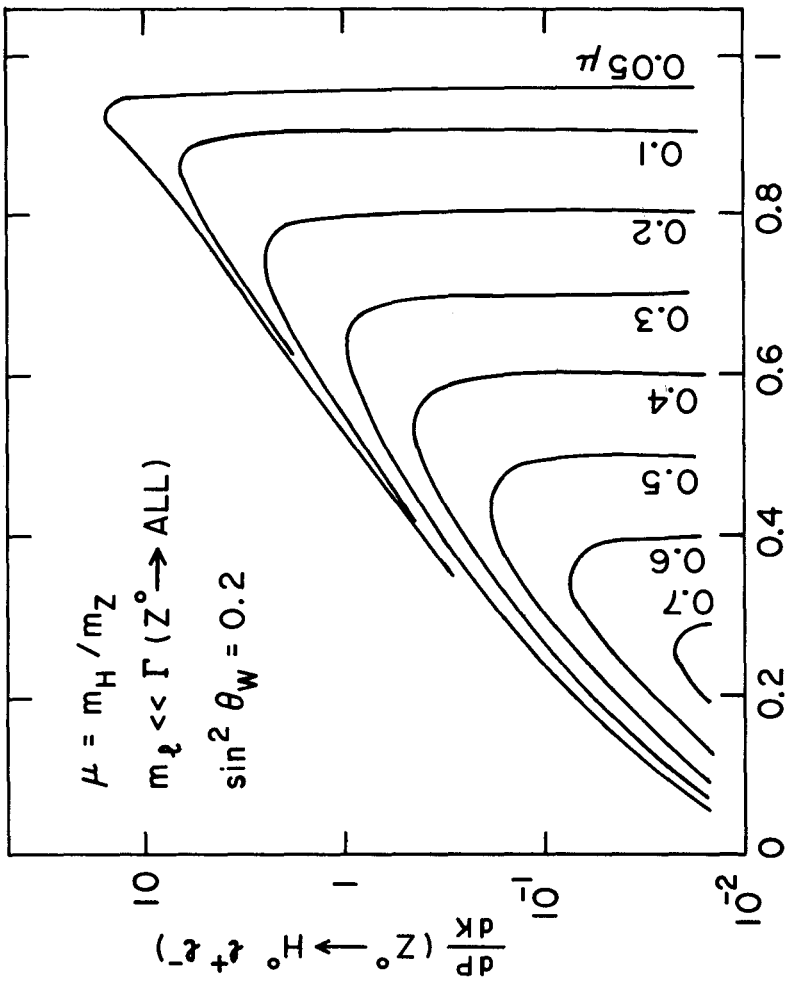
$\frac{dP}{dK}(Z^0 \to H^0 \ell^+\ell^-)$
10
1
10^{-1}
10^{-2}
0
0.2
0.4
0.6
0.8
1
$K = m_{\ell^+\ell^-}/m_Z$
$\mu = m_H/m_Z$
$m_\ell << \Gamma(Z^0 \to ALL)$
$\sin^2\theta_W = 0.2$
0.7
0.6
0.5
0.4
0.3
0.2
0.1
0.05

Fig. 5

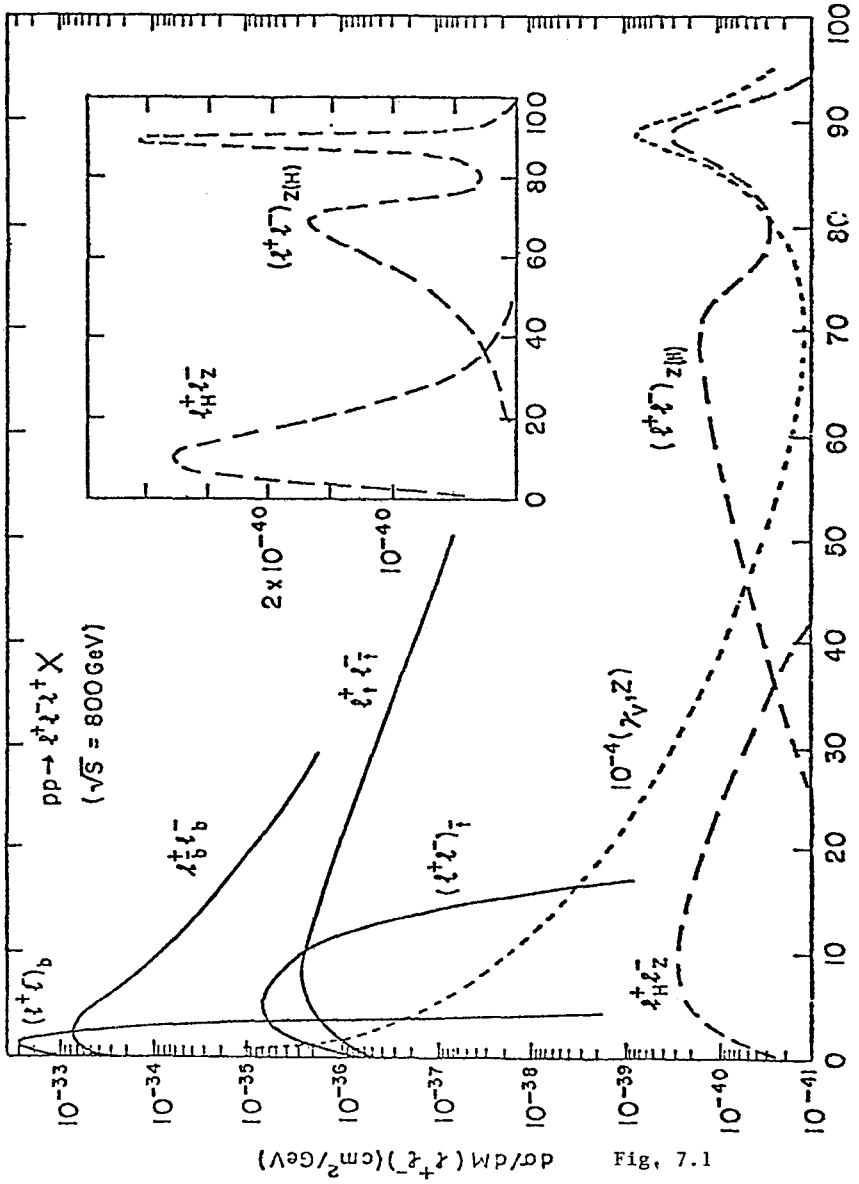
$pp \to \ell^+\ell^-\ell^+ X$
$(\sqrt{s} = 800\,GeV)$
$\ell_b^+\ell_b^-$
$\ell_1^+\ell_1^-$
$(\ell^+\ell^-)_b$
$(\ell^+\ell^-)_{\tilde{t}}$
$10^{-4}(\gamma,Z)$
$(\ell^+\ell^-)_{Z(H)}$
$\ell_H^+\ell_Z^-$
2×10^{-40}
10^{-40}
$d\sigma/dM(\ell^+\ell^-)(cm^2/GeV)$
$M(\ell^+\ell^-)(GeV)$

Fig. 7.1

Fig. 6

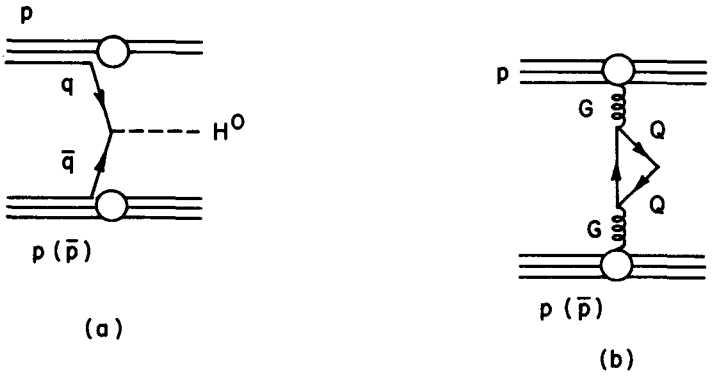

Fig. 7

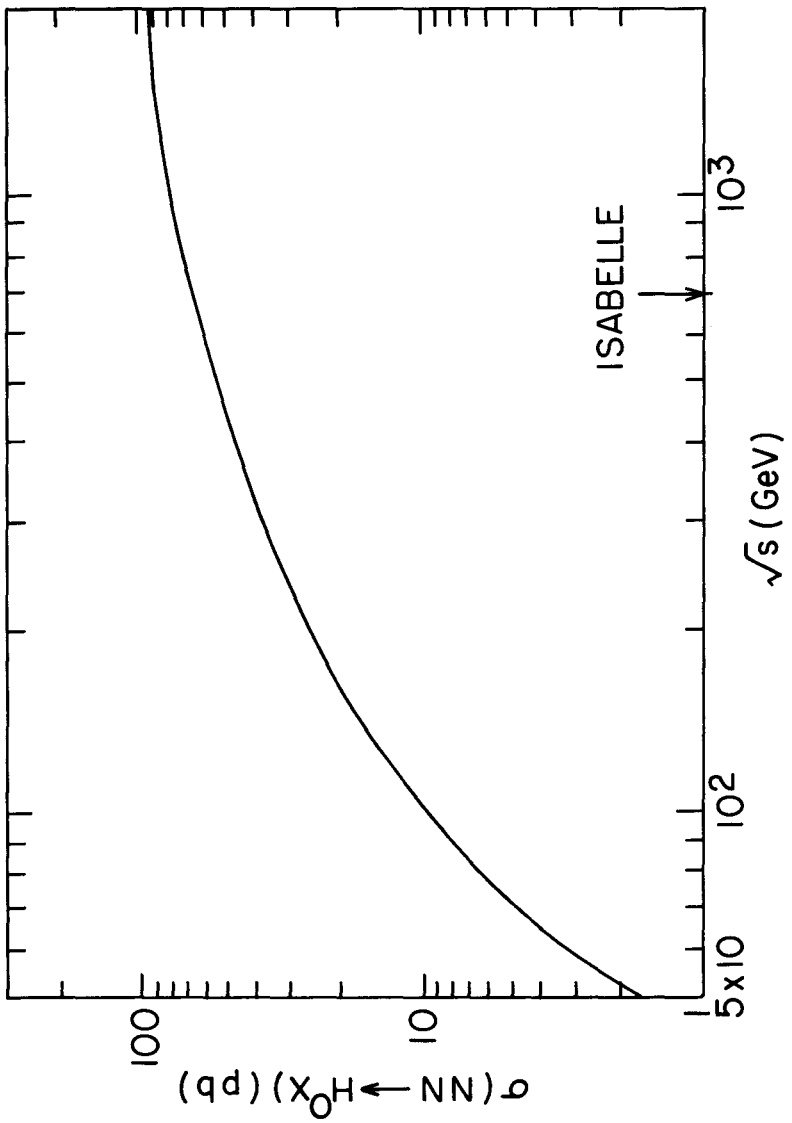

Fig. 8

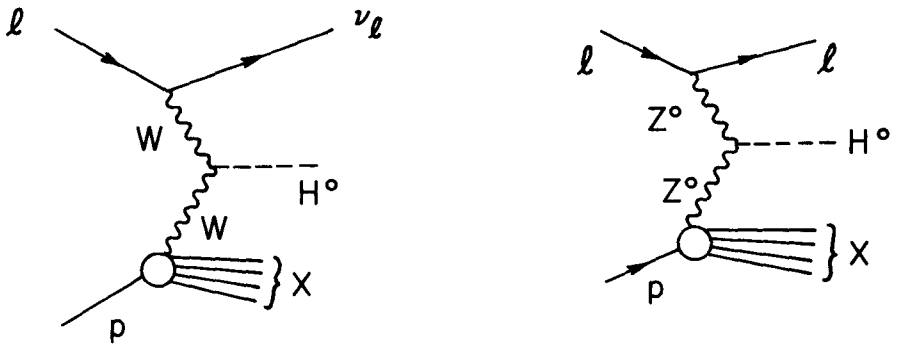

Fig. 9

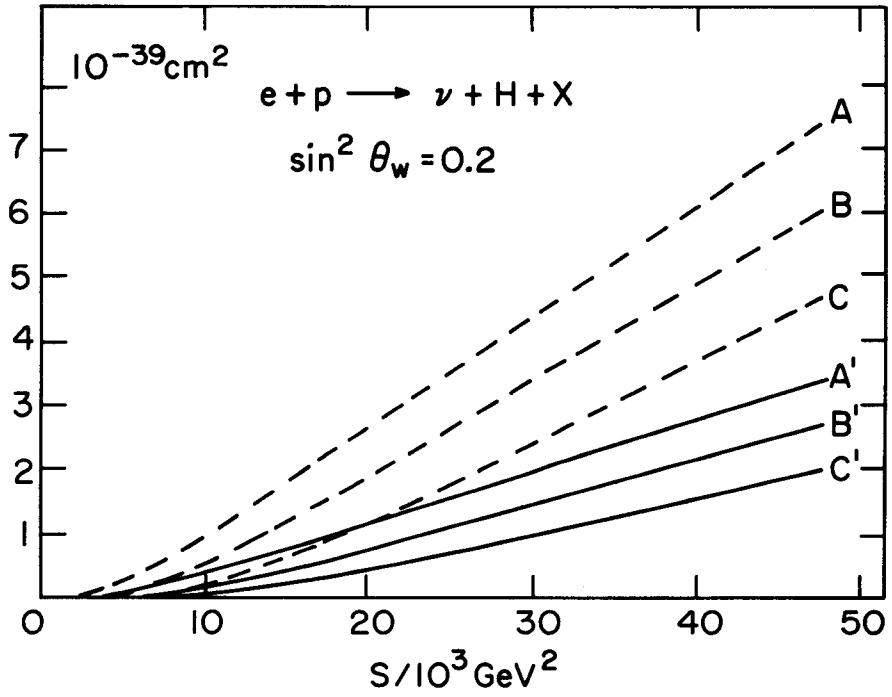
10^{-39}cm^2
e + p ⟶ ν + H + X
sin^2 θ_w = 0.2
A
B
C
A'
B'
C'
7
6
5
4
3
2
1
0
10
20
30
40
50
S/10^3 GeV^2

Fig. 10a

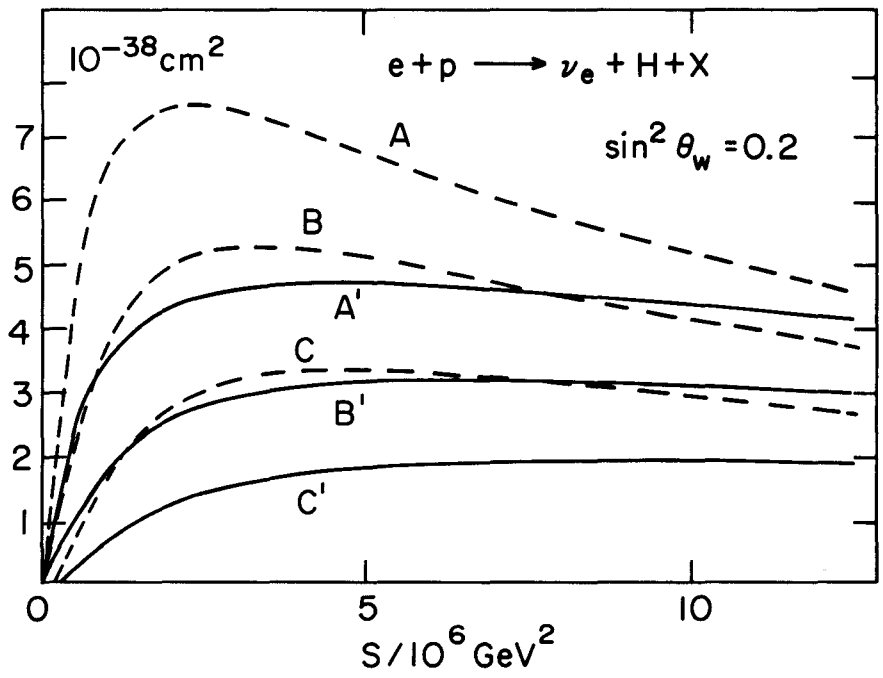
10^{-38}cm^2
e+p ⟶ ν_e + H+X
$\sin^2\theta_w$ =0.2
A
B
A'
C
B'
C'
7
6
5
4
3
2
1
0
5
10
S/10^6 GeV^2

Fig. 10b

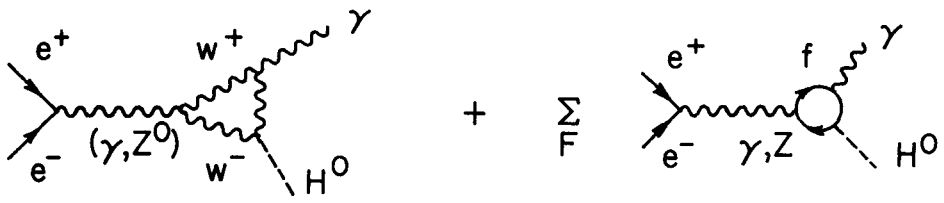

Fig. 11

"HIGGS" PHYSICS AT ISABELLE

G.L. Kane, Randall Laboratory of Physics, University of Michigan

In the standard electroweak theory it is possible to include the presence of gauge boson and fermion masses, but there is no deep understanding of the physical origin of mass. New scalar bosons are required, but their properties are not calculable (particularly if, as most people who have examined the problem expect, at least two Higgs doublets are required).

Two ways have been found that might make sense of scalars. Both approaches give large numbers of interesting interactions and particle states. Supersymmnetry is one promising possibility, discussed briefly elsewhere in the proceedings. Here we will concentrate on the "dynamical symmetry breaking" mechanism. Beg has reviewed the general theory in his talk and I will discuss the experimental implications. Most of the results are from Ref. 1. While there is not yet a good technicolor theory, I think that is due more to the lack of a clever solution than to any problem with the basic idea. The production of η_T has been studied in Ref. 2, 3 and 4; we will quote some results from Ref. 4 below.

In the dynamical theories new fermions are assumed, with an appropriate new non-Abelian group. Broken symmetries give rise to pseudo-Goldstone bosons (pGB), which get mass from color, electroweak, and additional interactions. In any theory where the new fermions carry color, the colored pGB get mass

$$m^2 \approx \alpha_s \Lambda_T^2$$

where $\Lambda_T \approx 700$ GeV is the mass scale of the theory, and there is a coefficient of order unity. The η-like colored octet η_T is the main state of interest; it gets a mass of order 240 GeV.

A large number of interesting states can arise (see Ref. 1). Here we emphasize η_T and the other main state relevant to ISABELLE, the charged colorless states $P^{\pm}$ which get a mass of about 8 GeV (Ref. 1). All others have cross sections or decays which make them difficult to find. The states $P^{\pm}$ are expected to couple to the heaviest fermions, and have decays $\tau\nu$, $c\bar{s}$, $c\bar{b}$, $c\bar{u}$. The last two may be suppressed by mixing angles--perhaps $c\bar{b}$ and $c\bar{s}$

are about equal. All estimates of decays of technicolor states are highly model dependent. In the model of Ref. 1, the $\tau\nu$ mode has a branching ratio of 90%. These states could be seen in e^+e^- interactions at PETRA, PEP. They have not been seen,[5,6] which may require them to have mass above 15 GeV, contrary to the simplest expectation, or a very particular pattern of decay branching ratios. No explicit analysis of the data is yet published, but soon the situation will get clearer. Since b-quarks at CESR do not decay via a two body charged Higgs mode, we can conclude $m_H > m_b$.

The importance of $P^{\pm}$ for ISABELLE is via t-quark production and decay. If there is a charged Higgs (whatever the physics origin) with mass $m_H < m_t - m_b$, then the decay $t \to Hb$ is semiweak and totally dominates the usual decay $t \to b\bar{f}f'$ (f,f' are any fermion doublet). So, the t-quark and the charged Higgs will be found simultaneously! Plans to search for t-quarks should take this decay mode into account. Since $m(P^{\pm}) \approx 8$ GeV, it is expected that if technicolor ideas are right the t will always decay $t \to bP^+$. Which mode is occurring should be observable from the jet structure and from the violations of universality (e.g., $H^+ \to \tau^+\nu$ but not $\mu\nu$ or $e\nu$, whereas $W^+ \to \tau\nu$, $\mu\nu$, $e\nu$ equally).

Most important for ISABELLE is the state η_T. Not only is its mass approximately known, but its production cross section is approximately calculable. If the whole technicolor approach makes sense, we can apply[1,2] current algebra ideas to the coupling of η_T to gauge bosons, and since it is colored it couples to gluons just as a π° couples to $\gamma\gamma$, with a calculable amplitude.

This gives a production cross section

$$\left(d\sigma/dy\right)_{y=0} = \pi^2\left(\frac{\Gamma(\eta_T \to gg)}{m^3(\eta_T)}\right) G(x_1)G(x_2)$$

where G(x) is the gluon distribution function in a proton (see Ref. 1 for Γ). Since η_T is point-like at low energies, $\Gamma \sim m^3$ and Γ/m^3 in the cross section is independent of m. The production cross section as a function of $m(\eta_T)$ then depends only on the gluon distribution function and scaling violations, and

can be reliably estimated; it is shown Fig. 1. The cross section for η_T production is 128 times that for an elementatry Higgs of the same mass, and 8 times that of an uncolored composite boson of the same mass. Fig. 1 shows σLT for 10^7 sec to see more or less what could be produced in a year, using the luminosities shown. The hatched regions show estimates for the corrections due to scaling violations, and the lower estimates are expected to be valid. The reader can correct for different L or T if desired.

Reference 4 shows a number of useful curves for η_T production and detection via its main mode $t\bar{t}$, with calculations of signal-to-noise, decay angular distributions and effective mass plots.

In general we expect the dominant decay to be

$$\eta_T \to t\bar{t}$$

where t is the heaviest fermion (η_T is a good source of new heavy fermions). For $m_t = 25$ GeV, $\Gamma(\eta_T \to tt) \approx 1$ GeV. Next most important are $\Gamma(\eta_T \to gg) \approx \Gamma(\eta_T \to b\bar{b}) \approx 60$ MeV. η_T will be easily found by using the $t\bar{t}$ mode. The η_T is produced essentially at rest, and gives $t,\bar{t}$ back-to-back isotropically, with very large P_T. The $t,\bar{t}$ decay gives a 4 jet event (or 3 jets + a lepton + missing energy, or six jets, etc.) which has little background. The jets are reconstructed to make $t,\bar{t}$ and then (assuming $t,\bar{t}$) the effective mass is plotted and a peak is detected at $m(\eta_T)$.

Once it is found, various tests can be done to determine the character of the new peak. The size of the cross section is important. The precence or not of $\mu^+\mu^-$, e^+e^-, $\nu\bar{\nu}$ modes and whether universality (e.g., the relation between $\Gamma(t\bar{t})$ and $\Gamma(b\bar{b})$) is violated will tell us. The presence of a gg mode (for spin zero) or 3g mode (spin 1) will distinguish from a vector quarkonium state. Rare decays ($\sim 1\%$) like $\eta_T \to gZ^\circ$ will be very clear signals. So altogether it will be fun to decide what we have once it is found.

Perhaps the main point is to emphasize that the particles and interactions discussed above are real possibilities for the physics that explains the origin of mass and for the next major discoveries in particle physics.

REFERENCES

1. S. Dimopoulos, S. Raby, and G.L. Kane, Nucl. Phys. B182 (1981) 77.
2. J.D. Bjorken, private communication.
3. F. Hayot and O. Napoly, Saclay preprint.
4. G. Girardi, P. Mery, and P. Sorba, LAPP preprint.
5. H. Meyer, private communication from Pluto data.
6. P. Duinker, these proceedings.

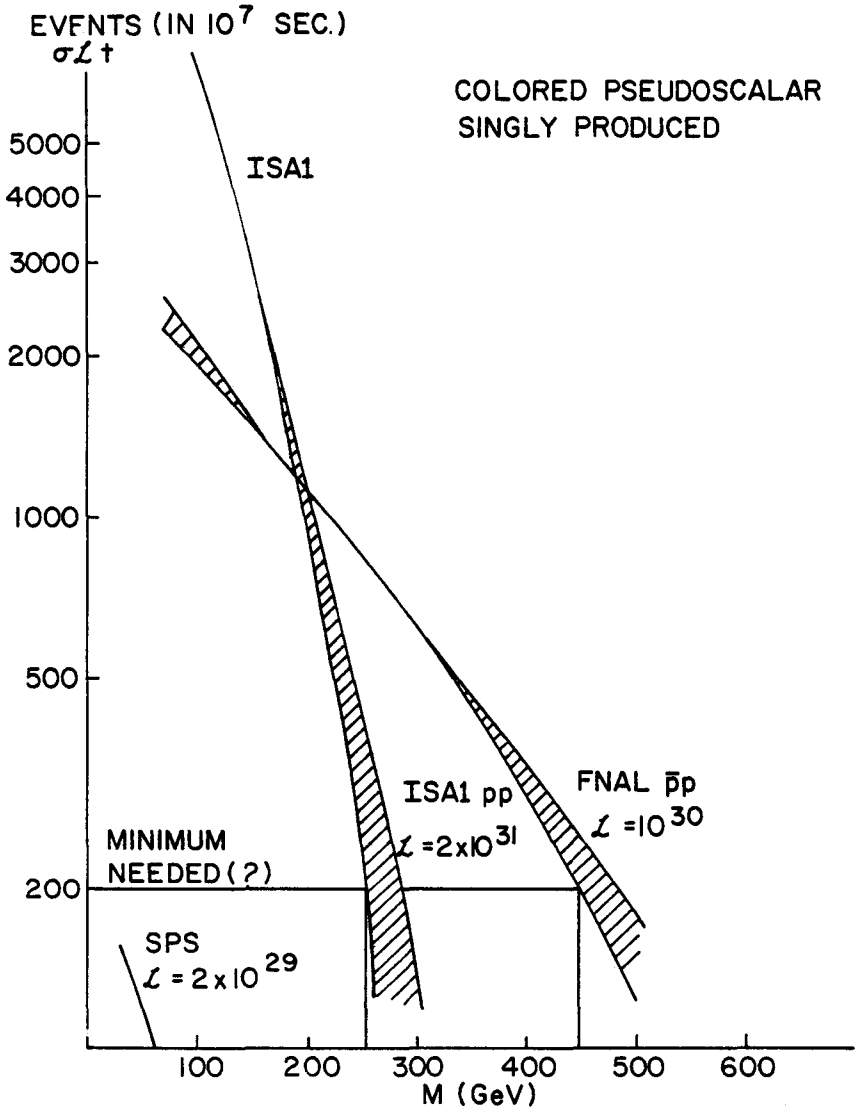
EVENTS (IN 10^7 SEC.)
$\sigma \mathcal{L} t$
COLORED PSEUDOSCALAR
SINGLY PRODUCED
5000
4000
3000
2000
1000
500
200
ISA1
ISA1 pp
$\mathcal{L} = 2 \times 10^{31}$
FNAL $\bar{p}p$
$\mathcal{L} = 10^{30}$
MINIMUM
NEEDED (?)
SPS
$\mathcal{L} = 2 \times 10^{29}$
100
200
300
400
500
600
M (GeV)

Fig. 1

EXPERIMENTAL IMPLICATIONS OF NEW THEORETICAL IDEAS

M.A.B. Bėg, The Rockefeller University

ABSTRACT

Physical implications of some new theoretical ideas, which can be subjected to experimental scrutiny at e^+e^- and pp colliders, are briefly discussed.

I. INTRODUCTION

Conventional wisdom, in elementary particle physics, decrees that matter consists of quarks and leptons and that interactions between these fermions arise via gauge principles based on the groups

$$SU(5) \supset SU(3)_C \times SU(2)_L \times U(1)$$

where $SU(3)_C$ is the strong color group, $SU(2)_L \times U(1)$ is the electroweak group and SU(5) is the currently fashionable grand-unification group. The pattern of symmetry-breaking, which permits these groups to describe physical reality, is constructed with the help of auxiliary spin-0 or Higgs fields by a method of careful planning; the spin-0 fields are judiciously chosen and coupled so as (a) to yield current masses for the quarks and leptons and (b) to trigger the Higgs mechanism in such a way as to leave the eight color gluons and the photon massless, endow the weak bosons $W^{\pm}$ and Z with masses of O(100 GeV) and give masses of $O(10^{15}$ GeV) to the twelve remaining gauge bosons. In the following[1], any theoretical construct which attempts to reproduce the known physics by alternate -- hopefully simpler — paths shall be deemed to be a "new theoretical idea."

II. MOTIVATION FOR THE CURRENT CROP OF NEW IDEAS

The orthodox picture, outlined above, is unsatisfactory on at least two counts.

First, the proliferation of quarks and leptons has reached a point where one begins to wonder if one is dealing with "elementary particles" at all. A

glance at Table I is enough to convince one that the quest for economy in the description of the structure of matter, which underlay the introduction of the quark model, has not been successful.

Second, the use of elementary Higgs fields, in the manner described above, destroys the essential simplicity of the gauge theoretic approach. The various mass scales which appear are put in by hand, via judicious choice of vacuum expectation values; the theory has little predictive power, it enables one to fit experimental curves but affords little insight into the nature of the dynamics.

The ideas summarized below were proposed as attempts to improve on the canonical theory; unfortunately, as of the time of this writing, no logically consistent alternative which can reproduce the known phenomenology has been found.

III. COMPOSITE MODELS OF QUARKS AND LEPTONS

The quark-model[2], with its ability to explain meson and baryon spectra, suggests a rather simple solution to the problem of quark-lepton proliferation: posit a few bits of spin 1/2 ur-matter (superquarks, say) with a color-like degree of freedom (call it C" or supercolor), generate interactions by gauging C", and let these superquarks be the internal constituents of quarks and leptons. While, in general, one should treat sub-leptons and sub-quarks as distinct entities, let us note that quark-lepton unification may be achieved in a painless (?) way by simply declaring that the superquarks in leptons are identical to the ones in quarks.

The dynamics of a composite model for the electron, for example, is very different from that of the quark-model of the nucleons; the difference stems primarily from the fact that the compton wavelength of the electron is five to possibly ten orders of magnitude larger than the electron radius[1]. The experimental upper bound on the radius, R_e, is 2×10^{-3} f; consideration of the gyromagnetic anomaly, in the absence of accidental or contrived cancellations yields $R_e < 2 \times 10^{-7}$ f; these numbers are to be compared with $m_e^{-1} \simeq 400$ f. A natural way to resolve this "two length problem" is to assume that there exists a symmetry limit in which m_e is exactly zero and that the relevant symmetry is only minutely broken. One is thereby led to posit that, unlike QCD

which chooses the Nambu-Goldstone (N-G) phase, QC"D chooses the Wigner-Weyl (W-W) realization[3] -- type (a), to be precise — for the accidental chiral group in flavor space. If the W-W phase is possible, there is a neat, indeed serendipitous implication[1]: there are no light flavor nonsinglet states in the spectrum with spin > 1/2.

An example of a composite fermion model which -- despite the many shortcomings that have been discussed elsewhere[1] — is appealing, because of its stark simplicity, is the Karari-Shupe model[4]. We abstract two features which may well survive the model in its present form: (a) the interpretation of the known electroweak doublets as excited modes of the first generation, cousisting of the quarks (u,d) and leptons (ν_e,e-) and (b) the expectation that there exist even higher quark-like and leptonic excitations. Existence of such excitations, as well as flavor-number nonconserving transitions between the known generations, will therefore be deemed to herald the composite nature of quarks and leptons.

A needed parameter is Λ_{SC}, the characteristic mass in QC"D. For purposes of orientation as to orders of magnitude we shall use two extreme values: 1TeV and 10^3 TeV.

IV. COMPOSITE HIGGS BOSONS, DYNAMICAL SYMMETRY BREAKING AND HYPERCOLOR

The virtues of implementing the Higgs mechanism in a dynamical way[5], in the framework of the hypercolor scenario[6], have been emphasized in many places; it would be pointless to go over the same terrain. Suffice it to say that hypercolor appears to have the potential for furnishing an elegant description of weak interactions and providing a natural resolution of the gauge-hierarchy problem. At this time, however, there is no satisfactory working model; the basic desideratum, of generating current quark masses without disturbing the Weinberg-Salam relationship between W and Z masses and in the framework of a natural GIM mechanism, remains unfulfilled. Nonetheless, we may abstract some implications of the general strategy which are likely to endure; these may profitably be tested at ISABELLE and LEP.

It is important to bear in mind that, within the framework of existing theoretical constructs, hyperquarks lend a new dimension to the problem of quark proliferation. One can not plausibly identify QC'D, the QCD-like theory

which underlies the hypercolor scenario, with QC"D; the quintessential feature of QC"D -- which permits it to play a role in weak interactions -- is its choice of the N-G mode for the global chiral group in flavor space, in contrast to QC"D which chooses the W-W mode.

V. MODEL INDEPENDENT EXPERIMENTAL IMPLICATIONS

We list some experimental signals whose significance can be gauged without reference to any specific model.

A. Signatures of Composite Fermions:

(a) Form factors for quarks and leptons, above and beyond the normal expectation from radiative corrections.

Measurement of the energy dependence of cross-sections for $e^+e^- \to \ell^+\ell^-$, $q\bar{q}$ etc. could in principle yield information about form factors. Unfortunately, however, effects signalling structure are not expected to be important until we have c.m. energies comparable to Λ_{SC}; at such energies the magnitude of the cross section is rather small: $\sigma \curvearrowdown 10^{-43}\text{cm}^2$ for $\Lambda_{SC} \curvearrowdown 10^3$ TeV to $\sigma \curvearrowdown 10^{-37}$ cm^2 for $\Lambda_{SC} \curvearrowdown 1$ TeV.

(b) Intergeneration Transitions.

None have so far been seen at low energies; the present limit on $\mu \to e\gamma$ (Branching Ratio $< 1.9 \times 10^{-10}$) is consistent with $\Lambda_{SC} \curvearrowdown 10^3$ TeV.

(c) Heavy quark and lepton excitations.

These offer interesting possibilities; they would make themselves manifest through super-heavy hadronic (B=1) and leptonic (L=1) resonances which can be studied with high-energy machines. The range of expected masses may be gleaned from Table II.

(d) Non-canonical values for $W^{\pm}$ and Z-masses. Many of the composite models proposed[1] are unable to accommodate the Weinberg - Salam values for W and Z masses:

$$m_W \cong 84 \text{ GeV}$$
$$m_Z \cong 95 \text{ GeV}$$

Failure of ISABELLE to detect intermediate bosons at these masses would indeed be a major discovery.

B. Signatures of Hypercolor:

(a) New spectroscopy of hyperhadrons (i.e. hadrons which are hypercolor singlet composites of hyperquarks). Mass scale $\curvearrowright 2\,\Lambda_{HC} \simeq 1$ TeV.

(b) Pseudo-Goldstone Bosons (PGBs) in mass range 10 GeV - 100 GeV.

(i) Charged PGBs in $e^+e^- \to \pi'^+\pi'^-$ (necessary but not sufficient to establish hypercolor).

(ii) Neutral PGBs produced in reactions which can be studied with high luminosity colliders. All of the reactions listed below warrant careful experimental study; observation of any of them will provide valuable information about the nature of the Higgs mechanism.

LEP Experiments[7]:

$$e^+e^- \to J_T \to \pi'^o + \gamma \qquad (1a)$$

$$e^+e^- \to J_T \to \phi^o + \gamma \qquad (1b)$$

$$e^+e^- \to Z \to \pi'^o + \mu^+\mu^- \qquad (2a)$$

$$e^+e^- \to Z \to \phi^o + \mu^+\mu^- \qquad (2b)$$

$$e^+e^- \to \text{"Z" or "}\gamma\text{"} \to \pi'^o + Z \qquad (3a)$$

$$e^+e^- \to \text{"Z"} \to \phi^o + Z \qquad (3b)$$

ISABELLE Experiments[8,9]:

$$pp \to J_T + X \qquad (4)$$

$$\downarrow \begin{cases} \pi'^o + \gamma & (4a) \\ \phi^o + \gamma & (4b) \end{cases}$$

$$pp \to \pi'^o + Z + X \qquad (5a)$$

$$pp \to \phi^o + Z + X \qquad (5b)$$

$$pp \to \pi'^{o} + X \tag{6a}$$

$$pp \to \phi^{o} + X \tag{6b}$$

Here π'^{o} is a flavor-neutral PGB, ϕ^{o} is the left-over Higgs of the canonical methodology and "Z" means a virtual Z. The dominant mechanism for the last two reactions is two-gluon fusion; the mechanism is operative for π'^{o} in models in which hyperquarks carry the attribute of color.

Note that the rate for ϕ^{o} and π'^{o} production is comparable in reactions (1a) - (1b), (4a) - (4b) and (6a) - (6b) for any reasonable choice of parameters. With an unreasonable choice, one can enhance the cross section for π'^{o} production to the point where 2(a) and (2b), for example, proceed at comparable rates; the dimuon invariant mass distribution, however, is very different in the two cases.

A general handle for distinguishing π'^{o} from ϕ^{o}, in reactions where they can be produced at comparable rates, is provided by the parity tests of ref. 10. $\{\phi^{o} \to D\bar{D}$ (Yes), $\pi'^{o} \to D\bar{D}$ (No) etc.$\}$ These parity tests actually follow from CP - invariance if π'^{o} is flavor neutral -- an expectation in all existing models for the lightest neutral PGBs.

Cross sections for the reactions listed above have been calculated by various authors, and I refer you to the literature.[1] The reaction which seems most promising for ISABELLE is (6a); for $m_{\pi'^{o}} \lesssim 50$ GeV, $\sqrt{s} = 700$ GeV, the cross section is

$$\left(\frac{d\sigma}{dy}\right)_{y=0} \simeq 10^{-35}\ \text{cm}^2 \left(\frac{N_C'}{4}\right)^2 \left(\frac{n_F'}{4}\right)^2 n \tag{7}$$

where N_C' is the number of hypercolors, n_F' is the number of hyperflavor doublets and we have summed over all n π'^{o}-like states. ($n \simeq n_F'$ for $n_F' \gg 1$). y is the π'^{o} rapidity. For $n_F' = 4$, $n = 1$, Eq. (7) agrees with the result quoted in ref. 9.

REFERENCES AND FOOTNOTES

1. For a fuller discussion of some of the topics considered here, and a comprehensive list of references, see: M.A.B. Bég, Rockefeller University Report No. 81/B/9. [To appear in the Proceedings of the EPS Int. Conf. on High Energy Physics, Lisbon, Portugal (1981)].
2. M.A.B. Bég, B.W. Lee and A. Pais, Phys. Rev. Lett. 13, 514 (1964).
3. B.W. Lee, "Chiral Dynamics" (Gordon and Breach Science Publishers, New York, 1972).
4. H. Harari, Phys. Lett. B86, 83 (1979); M.A. Shupe, ibid B86, 87 (1979).
5. M.A.B. Bég and A. Sirlin, Annu. Rev. of Nucl. Sci. 24, 379 (1974).
6. S. Weinberg, Phys. Rev. D13, 974 (1976); L. Susskind, ibid. D20, 2619 (1979).
7. A. Ali and M.A.B. Bég, Phys. Lett. B103, 376 (1981).; M.A.B. Bég, Proc, of VPI Workshop on Weak Inst. as Probes of Unif. ed. G.B. Collins, L.N. Chang and J.R. Ficenec (Am. Inst. of Phys., New York, 1981) p. 505.
8. L.L. Chau Wang, BNL Report No. 28781-R (1980).
9. S. Dimopoulos, S. Raby and G.L. Kane, Nucl. Phys. B182, 77 (1981).
10. M.A.B. Bég, H.D. Politzer and P. Ramond, Phys. Rev. Lett. 43, 1701 (1979).

Table 1

"Elementary" Particles	1981	1964 Before the Quark Model
Spin 1/2 Fermions:		
Leptons	6	4
Hadrons	15+3(?)	8
Spin 1 Bosons:		
Massless	9	1
Massive	3(?)+12(??)	9
Spin 0 Bosons	1(?)+108(??)	9
Spin 3/2 Fermions	0	10

Spectrum of "elementary" particles in 1981 contrasted to that in 1964. Entries followed by a single question mark correspond to hitherto unobserved particles which are required by the Weinberg-Salam theory; entries followed by a double question mark correspond to the additional particles which would occur in SU(5)-based grand unification. The supergravity enthusiast may wish to delete the null entry in the 1981 column and insert his favorite number, followed by an appropriate number of question marks.

Table II

Λ_{SC}	m(q*)		m(C*)
	$\bar{\alpha}_{QCD}(\Lambda_{SC})\Lambda_{SC}$	$\bar{\alpha}_{QCD}(\Lambda_{SC})^2\Lambda_{SC}$	$\bar{\alpha}_{QED}(\Lambda_{SC})\Lambda_{SC}$
1. TeV	110 GeV	12 GeV	8 GeV
10^3 TeV	60 TeV	4 TeV	9 TeV

Sample of expected masses for excited quarks and leptons in a class of composite models. (Cf. S. Weinberg, Texas preprint (1981)). To interpolate between the extreme values of Λ_{SC}, one way use:

$$\bar{\alpha}_{QCD}(\Lambda_{SC})^{-1} = 1.11 \ln (\Lambda_{SC}/300 \text{ MeV});$$

$$\bar{\alpha}_{QED}(\Lambda_{SC})^{-1} = 128 - 1.7 \ln (\Lambda_{SC}/84 \text{ GeV})$$

H E R A

B.H.Wiik
Deutsches Elektronen-Synchrotron DESY, 2000 Hamburg 52 - Notkestrasse 52 - Germany.

1. Introduction

The possibility of reaching very high energies by colliding electrons with protons was recognized[1] a long time ago, but despite many attractive features no e p - facility has ever been constructed.

DESY has proposed to construct HERA, a large electron-proton colliding beam facility on a site adjoining the present site. HERA is designed to collide 820 GeV protons with 30 GeV electrons in 4 interaction regions yielding 314 GeV in the center of mass system corresponding to a maximum momentum transfer squared of 98400 GeV^2.

A feasibility study[2] of this project carried out in collaboration with ECFA has been completed. The project has received strong support from the German high energy physics community and in 1980 the report, endorsed by ECFA, was forwarded to a committee appointed by the German Minister of Science and Technology to evaluate this and other large science projects. In its report issued earlier this year the committee recommended that HERA is built with the construction starting in 1984. Towards the middle of 1980 a group to review the feasibility report and to prepare a more technical study was formed. This group was rather broadly based with some 50 physicists and engineers from 21 European Institutions participating in the study besides DESY staff. This study[3] is now completed and forms the basis for the prototype work already in progress.

2. The physics motivation for HERA

Studies of lepton-hadron interactions have in the past provided much of the basis for our present knowledge of elementary particles and their interactions. It has been found that the incident electron interacts directly with one of the quarks in the nucleon as shown in Fig. 1. The interaction is mediated by a space-like current charged or neutral and the current is defined by the kinematical quantities Q^2, ν or the scaling variables x and y as given in Fig. 1.

The study of neutral and charged weak currents is one of the prime motivations[4] for constructing a large electron-proton colliding beam facility. Indeed the properties of charged currents at small distances can only be studied using colliding electron-proton machines. It is crucial that the new accelerator can explore the

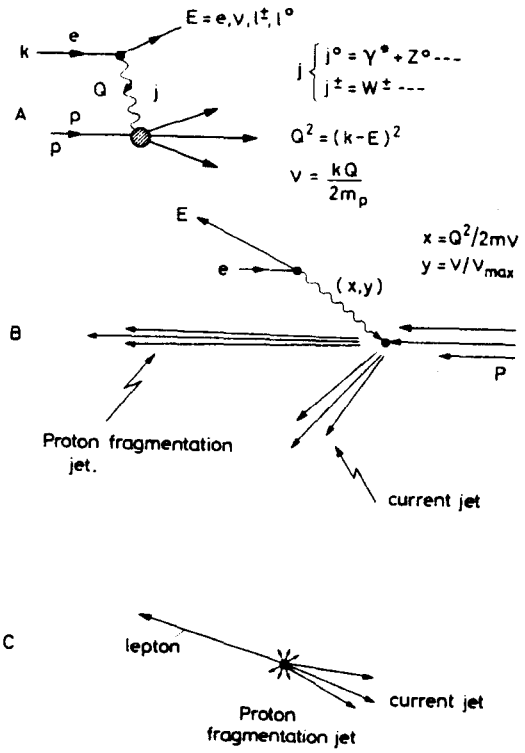

Fig. 1
Kinematics of deep inelastic electron-proton collisions.

region above 100 GeV in the center of mass system since this is the presumed mass scale of weak interactions where new phenomena might be expected to occur. Measurements with both electrons and positrons in well defined helicity states are needed to untangle electromagnetic and weak effects and to determine the properties of the weak current. Measurements with left handed positrons or right handed electrons are very sensitive probes for new weak currents.

The proliferation of leptons and quarks is a strong incentive to search for substructure or excited states of these particles. HERA is well suited for such measurements. The spectrum of electron-like leptons can be explored up to 250 GeV and the structure of quarks investigated down to distances of 10^{-17} cm - order of magnitude smaller than what is presently known.

A measure of an electron-proton collider is therefore the number of events produced with a momentum transfer above 10^4 GeV^2. The number of such events depends not only on the luminosity, but also an available centre of mass energy.

How far out in Q^2 these processes can be followed also depends on the visibility of the events - i.e. what is the lowest acceptable counting rate ? We will now address these questions in turn.

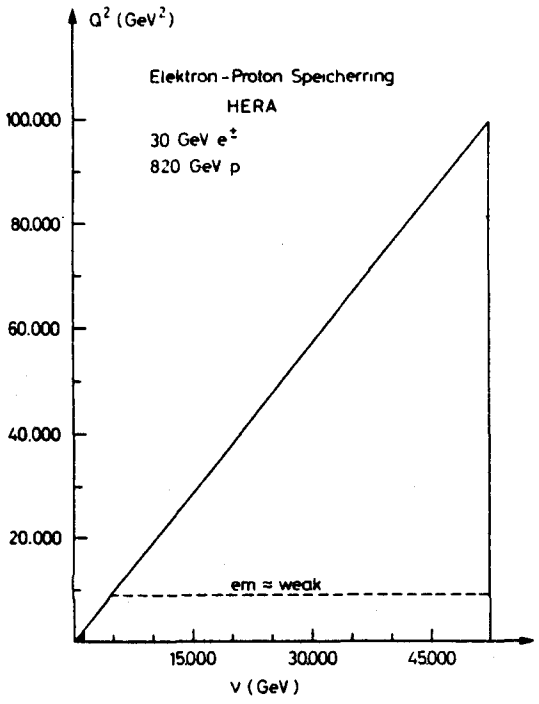

Fig. 2 - Kinematical region in Q^2 and ν which can be explored with HERA.

The kinematical region available with HERA is equivalent to that of a 52 TeV fixed target machine and is shown in Fig. 2. The scale is set by the black dot in the lefthand corner representing the region which can be explored using a 1 TeV muon or neutrino beam on a fixed target. Such beams will become available at FNAL in 1983. It is clear that HERA allows us to study a kinematical region well outside that available with present or planned fixed target machines.

The Q^2 value roughly corresponding to the characteristic mass of the weak interaction squared is shown as the dotted line. A large kinematical region is available beyond these Q^2 values. We will now briefly discuss how far this region can be explored.

The final state in deep inelastic electron-proton interactions is rather striking and easy to recognize among the much more numerous beam gas events. As indicated in Fig. 1 B and C the scattered lepton appears at a large angle with respect to the beam axis and the corresponding transverse momentum is balanced by the struck quark which fragments into a jet of hadrons appearing on the opposite side of the beam axis. The remains of the proton give rise to a forward jet of hadrons with no net transverse momentum with respect to the beam axis. Because of the imbalance between the incident electron and the proton momenta the particles will in general emerge in the forward direction along

the proton direction. The proton jet, the quark jet and the lepton define a plane (containing also the beam axis) with small momenta transverse to the plane and large momenta in the plane.

A polar diagram describing the kinematic of the final lepton (upper part of the figure) and of the current jet (lower part) at the top HERA energy of 30 GeV electrons on 820 GeV protons is shown in Fig. 3. For a given Q^2 and x the energies and the angles of the lepton and the jet in the laboratory system are obtained by joining the relevant points of the upper and the lower parts of the diagram with the origin. Note that the laboratory angles for the lepton and the current jet are quite large for a typical Q^2-value of 10 000 GeV^2.

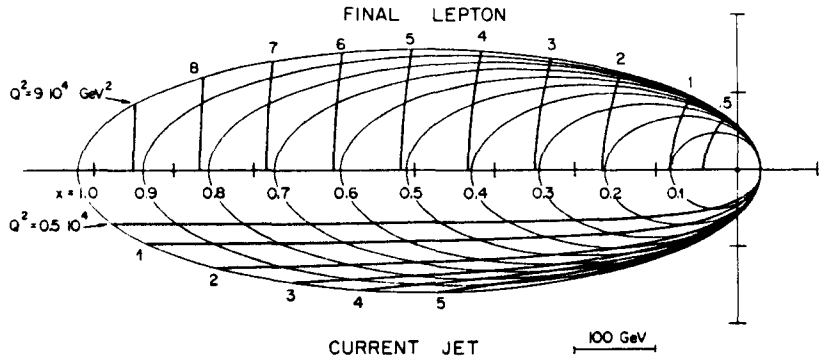

Fig. 3 - Kinematics for ep → e'qX. The scattered electron kinematics in terms of Q^2 and x is given on the upper half, the kinematics for the current jet on the lower half. The laboratory angles and the energies can be read off directly by connecting points with a given x and Q^2 with the origin.

It seems rather unlikely to confuse a deep inelastic electron-proton event with a background event such that counting rates on the order of one a day are acceptable. The available Q^2 range is therefore limited not by visibility but rather by luminosity. In Fig. 4 the average luminosity needed to produce 100 charged current events a year with $Q^2 > Q_0^2$ is plotted versus Q_0^2 for various values of the center of mass energies. The year is assumed to have 5000 hours and

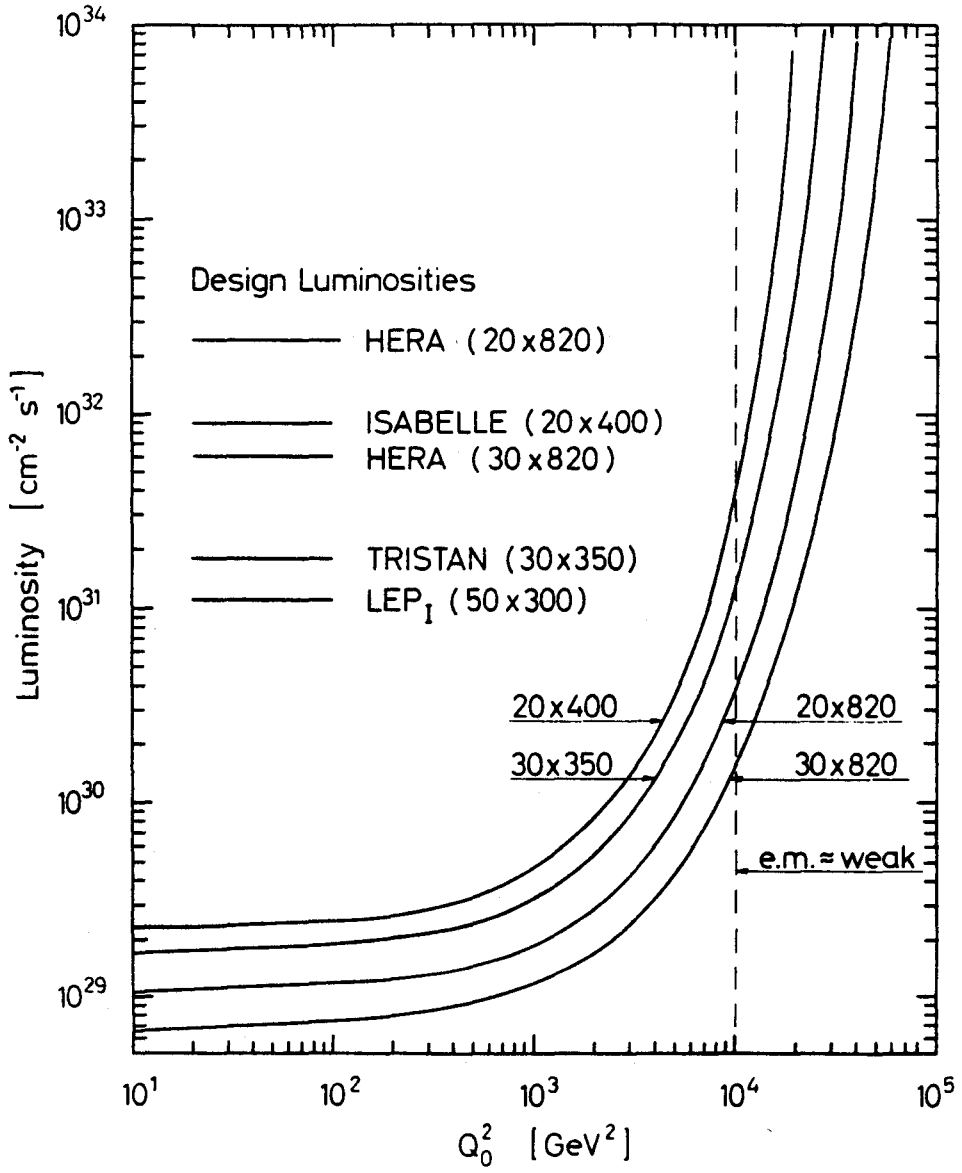

Fig. 4 - The average luminosity needed to produce 100 charged current events with $Q^2 > Q_0^2$ in 5000 hours of running versus Q_0^2 for various center of mass energies.

the rate is evaluated in the standard model[5] with one charged vector boson. Note that it is possible to explore Q^2 values up to 2000 - 3000 GeV^2 even with a luminosity as low as 2×10^{29} $cm^{-2}sec^{-1}$. To produce 100 charged current events with $Q^2 > 10\,000$ GeV^2 per year requires a luminosity of 1.5×10^{30} $cm^{-2}sec^{-1}$ - a factor of 40 below the HERA design luminosity. To obtain the same number of events with $Q^2 > 10\,000$ GeV^2 by colliding 20 GeV electrons with 400 GeV protons requires an average luminosity of 3×10^{31} $cm^{-2}sec^{-1}$ - or a factor of 20 higher than at HERA. Note that for a luminosity of $10^{32}cm^{-2}sec^{-1}$ we expect 100 charged current events a year with $Q^2 \gtrsim 40\,000$ GeV^2.

We will now discuss some of these processes in more detail.

2.1 Charged current events

Present data are all consistent with a lefthanded current which is mediated by a single charged vector boson with a mass around 80 GeV. However, present experiments can only probe the weak interaction at Q-values which are small compared to the characteristic mass scale of the weak interactions. The observed simplicity of the charged current might well only reflect the static limit studied so far and a rich structure with many vector bosons, some perhaps giving rise to righthanded currents, might appear at higher energies. Measurements at HERA will enable us to investigate the region well beyond 80 GeV and answer these questions.

From a purely experimental point HERA has some unique features compared to present fixed target experiments.

- Very high energy.
  The beam is equivalent to a monoenergetic neutrino beam with an energy up to 52 TeV
- Choice of helicity.
  It will presumably be possible to change the helicity of the incident lepton - i.e. the cross section for left and righthanded electrons (or positrons) can be measured directly.
- Visibility.
  The target is massless and can be surrounded by fine grained detectors including particle identification.
- Favourable kinematics.
  The lepton, the current jet and the target fragmentation jet are presumably

well separated in space and the event is easily recognized.

The number of charged current events expected in a bin dxdy = $(0.2)^2$ after one month of data taking with an unpolarized 30 GeV electron beam colliding with protons of either 820 GeV or 200 GeV is shown in Fig. 5, assuming a luminosity of 10^{32} $cm^{-2}sec^{-1}$. The rates were estimated in the standard model[5] with m_W = 78 GeV and formfactors parametrized according to Buras and Gaemers[6]. Given the distinctive signature of a charged current event it seems possible to measure the cross section for values of Q^2 up to 4 x 10^4 GeV^2.

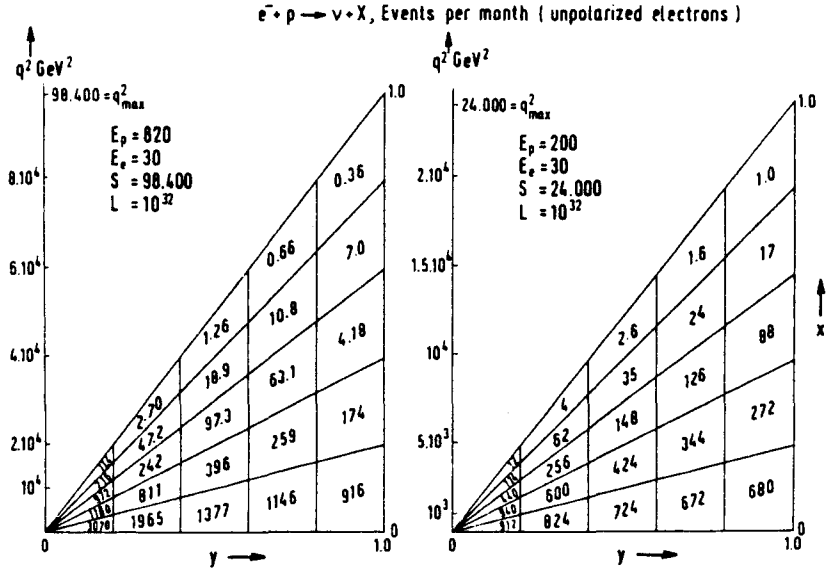

Fig. 5 - Number of charged current events produced per month of running time. In bins dxdy = $(0.2)^2$ assuming the standard model.

The expected counting rate for $e^- p \to \nu X$, evaluated with the assumptions listed above, is plotted in Fig. 6 versus Q^2 for various propagator masses. It is clear that HERA experiments can be used to determine the mass of the propagator as long as it is below say 400-500 GeV. The data can also be used to determine whether the charged current is damped by a single vector boson as presently believed or by several. As an example, a model containing two vector bosons has

been evaluated with the assumption that they have the same coupling constant at $Q^2 = 0$ and that one of the vector bosons has a mass of 78 GeV. The expected event rate for the two vector boson model, normalized to the standard model event rate, is plotted in Fig. 7 versus Q^2 for various mass values of the second vector boson. The effects are large.

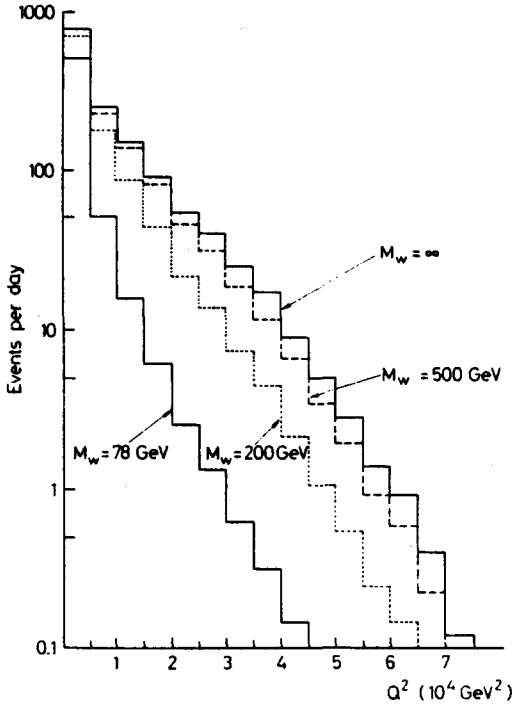

Fig. 6
Events per day for
$e^- + p \rightarrow \nu + X$
in Q^2 bins of 5000 GeV^2
with the standard assumptions.

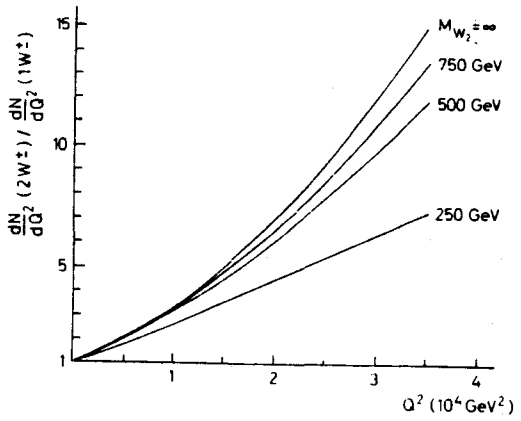

Fig. 7
Ratio dN/dQ^2 (two $W^\pm$) / dN/dQ^2 (one $W^\pm$) for different mass values of the second $W^\pm$.

The existance of righthanded currents can of course be deduced directly from a measurement of $\sigma(e_R^- p \to \nu X)$ or $\sigma(e_L^+ p \to \bar{\nu} x)$.

2.2 New Fermions

HERA is ideally suited to produce electronlike charged or neutral leptons and new heavy quarks which couple to the u or d quarks in the proton. We know that such couplings are rather weak in the standard model, however, new currents may exist. Indeed the basic fermions must have excited states if they are not pointlike. The rate for producing a heavy quark from a light quark is plotted in Fig. 8 with the mass of the lepton at the upper vertex (Fig. 1) as a parameter. The rates were evaluated with the assumptions listed above plus the assumption that the new current couples with the same strength as the old one. Leptons and quarks with masses up to 150 - 200 GeV can be found in this way. The decay of these particles lead to rather spectacular signatures $L^0 \to e^- Q q'$ - i.e. the events consist of two large angle jets in addition to the forward target jet. The jet resulting from the decay of the heavy lepton will contain electrons.

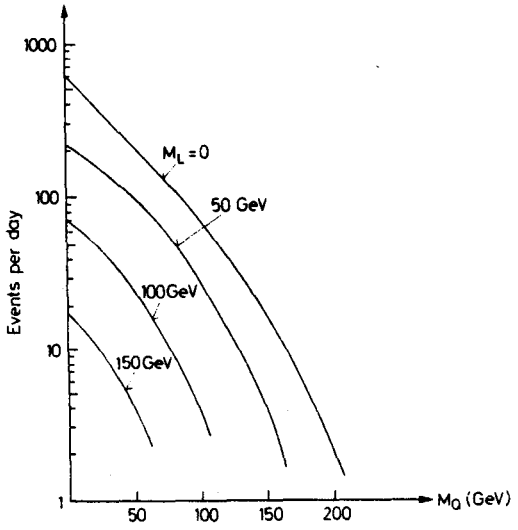

Fig. 8a
Number of events per day for $e^- + p \to L^0 + Q + X$ at $s = 9.6 \times 10^4$ GeV^2 assuming left-handed couplings, unpolarized electrons, $m_{W'} = 78$ GeV, Buras-Gaemers QCD parametrization with $\Lambda = 0.5$ GeV and a luminosity of 10^{32} cm^{-2}s^{-1}.

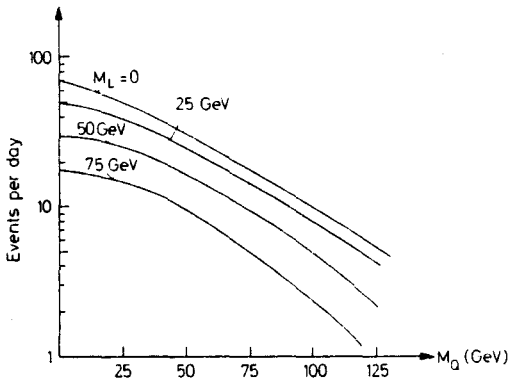

Fig. 8b
Same as Fig. 8a but with $m_{W'} = 150$ GeV.

2.3 Neutral Currents

One photon exchange and Z^0 exchange contribute (Fig. 1) coherently to $e + p \to e' + X$ and both contributions are of similar strength at HERA energies. Measurements of this process can therefore decide if indeed the electromagnetic and the weak interactions are manifestations of a single force and if this unification occurs as conjectured in the standard model[5] or if a more complicated mechanism involving many $Z^{0'}$s is realized in nature. The number of neutral current events produced in a bin $dxdy = (0.2)^2$ per day by 30 GeV electrons colliding with 820 GeV protons and a luminosity of 10^{32} cm^{-2} s^{-1} is plotted in Fig. 9. Again due to the characteristic topology of deep inelastic events HERA can extend the Q^2 range from the present few hundred GeV^2 out to some 30000 GeV^2.

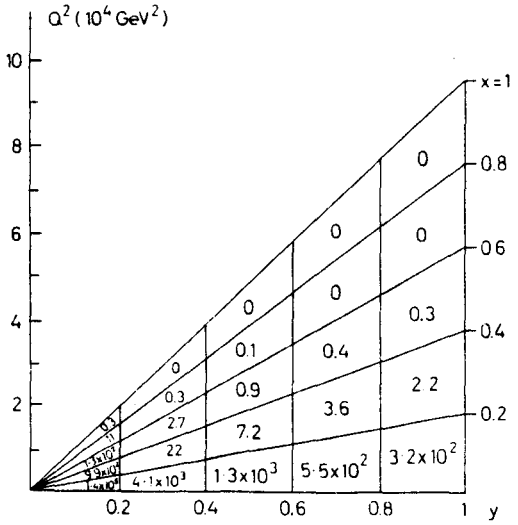

Fig. 9
Number of events per day for $e^- + p \to e^- + X$ at $s = 9.6 \times 10^4$ GeV^2 and the standard assumptions.

The presence of a weak current in the amplitude has clear signatures.

1) Parity violation

$$\sigma(e_L^- p \to e^-, X) \neq \sigma(e_R^- p \to e^-, X)$$

$$\sigma(e_L^+ p \to e^+, X) \neq \sigma(e_R^+ p \to e^+, X)$$

This effect can only be caused by a neutral weak current.

2) Appearant C-violation

$$\sigma(e_L^- p \to e^-, X) \neq \sigma(e_L^+ p \to e^+, X)$$

$$\sigma(e_R^- p \to e^-, X) \neq \sigma(e_R^+ p \to e^+, X)$$

Two-photon exchange will also give rise to a charge asymmetry. This effect, however, is expected to be of order $\alpha/\pi \ln Q^2/m^2$ with $m \sim 300$ MeV. At large values of Q^2 this effect is small compared to the charge asymmetry caused by Z^0 exchange and it has furthermore a different Q^2 dependence. The two photon effects can be determined at relatively low values of Q^2 where Z^0 exchange has a small effect only.

3) The presence of a $1-(1-y)^2$ term which is not allowed in the one photon exchange approximation. This effect cannot be caused by two photon exchange.

The size of these effects in the standard model is shown in Fig. 10 where the ratio for the left and righthanded electrons and positrons is plotted as solid line versus y for $x = 0.25$ and $s = 9.8 \times 10^4$ GeV^2. Note that the rates are sufficient to determine these asymmetries in a few months of running.

A measurement of these asymmetries can be used to pin down the properties of the neutral weak current. Suppose that $SU(2)_L \times SU_R(2) \times U(1)$ is realized in nature. The dotted lines in Fig. 10 show the cross sections expected in this model with the mass of the second Z^0 at 224 GeV. It is clear that the two models can be separated.

New flavour changing neutral currents might also appear. Such currents could lead to spectacular processes like $e^- d \to \tau^- b$.

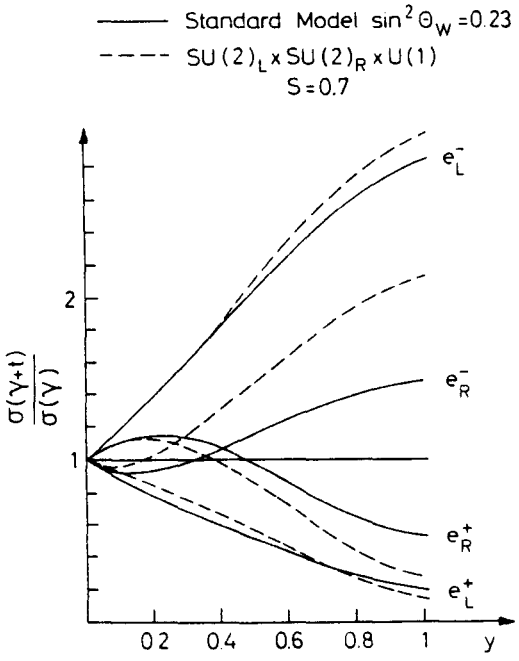

Fig. 10
The ratio $\sigma(\gamma + Z^0) / \sigma(\gamma)$ at $x = 0.25$ and $s = 9.6 \times 10^4$ GeV^2 for two different weak interaction models.

2.4 Test of Strong Interactions

QCD[7] makes clear, unambigous predictions for deep inelastic processes.

Such a prediction for non-singlet moments is plotted in Fig. 11 versus Q^2. Note that the value of the moments in QCD is nearly constant for Q^2 above 1000 GeV^2. This is a very strong prediction unique to QCD. For example a simple power behaviour expected in other types of field theories can mimic the observed behaviour over the present available Q^2 range - however, it will deviate from the QCD predictions at large values of Q^2. This constancy makes it also easy to observe thresholds like color liberation if they should occur. Measurements of the final state hadrons will enable us to carry out detailed test of QCD.

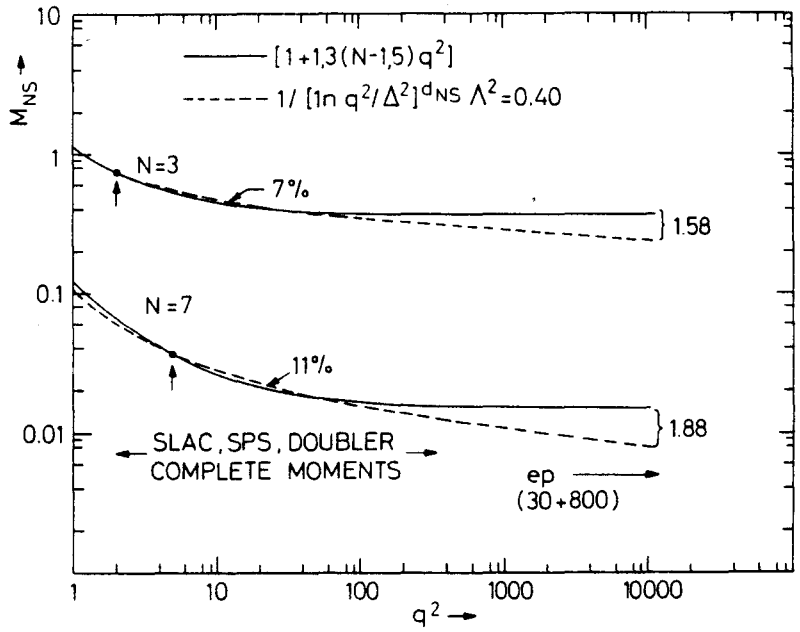

Fig. 11 - A simple $1/Q^2$ power behavior compared with the QCD logarithmic behavior for non-singlet moments.

2.5 Probing Quarks and Leptons

Faced with the large numbers of leptons and quarks many physicists find it natural that these entities are made up of new building blocks. With HERA we can probe the fermion structure down to distances of 10^{-17} cm corresponding to 10^{-4} of the size of the proton.

If the leptons have a size we would expect to observe a leptonic form factor and ultimately the production of excited leptons. The cross section would be modified by a form factor $F(Q^2) = 1 / (1 + q^2/M^2)$ giving rise to a scaling violation which is very different from that expected in QCD. A 10% measurement at 4×10^4 GeV^2 would be sensitive to a mass of the order of 1 TeV.

An excited lepton could decay into $e + \gamma$, $e + Z^o$ and $e + W$ leading to peaks in the invariant spectrum.

The cross section would also be modified in a similar manner, if the quark has a structure - i.e. again one might probe down to distances of $(1\ TeV)^{-1}$. Again there might be excited quark states.

Another possibility is that the proton contains new gluon-like particles which interact neither weakly nor electromagnetically. These particles would show as a step in the momentum fraction of the protons carried by the quarks. Example of such particles are the spin 1/2 gluinos expected in supersymmetric theories. In a new class of elementary particle interactions - technicolour forces - there will be constituents carrying both lepton and baryon numbers. Such particles might be produced directly in e p collisions if they have a mass below 200 GeV.

2.6 Low Q^2-physics

The electron beam of HERA is equivalent to a well collimated bremsstrahlungs-beam with an endpoint energy of 52 TeV. The photon-proton luminosity is typically on the order of a few percent of the electron-proton luminosity - i.e. around 10^{30} $cm^{-2}s^{-1}$ corresponding to some 10^7 hadronic events per day. Several interesting processes like deep inelastic Compton scattering, the QCD analogues of Compton scattering and Bethe-Heitler processes can be investigated at HERA.

3. The Machine

3.1 General Description

The layout of HERA is shown in Fig. 12. The machine has a fourfold symmetry; four 360 m long straight sections are joined by four arcs with a geometric radius of 779.2 m yielding a total circumference of 6336 m. HERA consists of two rings, one for electrons (positrons), the other for protons and the rings cross in the middle of the long straight sections. The rings will be burried some 10 - 20 m below the surface to avoid any disturbance of the urban surroundings. The tunnel traverses largely land belonging either to the Federal Government or to the City of Hamburg and it intersects the PETRA ring some 20 m below the surface. The physical plant can thus be located on the DESY site and only short injection paths are needed to connect PETRA and HERA. The site, according to records made available by the Geologisches Landesamt in Hamburg is well suited for tunneling. This has now been confirmed by a series of 60 drillings made along the circumference of the ring. The tunnel will be drilled using special boring machines equipped with driving shields. These machines, protected by the driving shield, can bore tunnels below the water table without the use of pressurized air. This method has been extensively used in Hamburg and is well adapted to the requirements posed by the HERA tunnel.

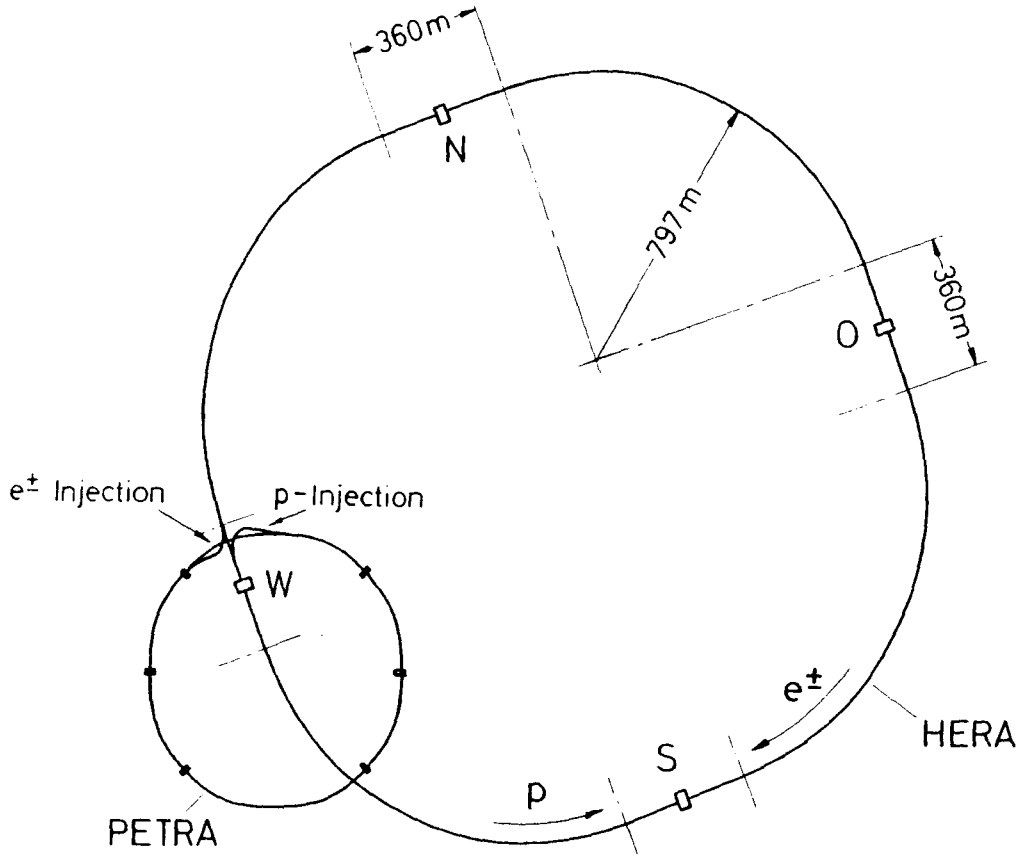

Fig. 12 - Layout of HERA

A total floorspace of 875 m^2 is available for experiments compared to the 650 m^2 available in a typical PETRA Hall. The beam traverses the hall some 5.5 m above the floor level. Machine components like klystrons, power supplies and compressors are located in a multistory structure built at the side of the hall and above the hall, providing a total area of some 3600 m^2. This structure including the hall will be completely covered after construction and only the access roads and a small one story building will be visible on the surface. Fig. 13 shows a vertical cut through an experimental building parallel to the beam line.

The planning board of the city of Altona has recently approved the detailed plans for the construction of the tunnel and the experimental areas on the site proposed.

3.2 Parameters and Performance

The general parameters of HERA are listed in Table 1. The energy of the electron beam can be varied between 35 GeV and 10 GeV where the upper limit is determined by the available RF power of 13.2 MW and the lower limit by the damping time. At the nominal energy of 30 GeV the transverse polarisation builds up in 19.5 min compared to an expected lifetime of several hours.

The maximum induction of the HERA magnets is chosen to be 4.53 Tesla compared to 4.3 Tesla for the FNAL Tevatron[8] or 5.0 Tesla, the design values for Isabelle[9]. This yields a maximum proton energy of 820 GeV. The lower limit on the proton energy for long term storage is determined by the effect of persistent currents in the superconducting coils. The relative importance of these currents decreases with energy as they cause constant higher multipole fields disturbing the dipole field. An estimate of these effects, based on the FNAL magnets, shows that it should be possible to inject protons at 40 GeV and store them down to energies of about 100 GeV.

In experiments[10] with a stored bunched beam in the SPS it has been found that the bunch length should be no more than about 30% of the bucket length. If this condition is violated, then RF noise will lead to a loss of beam. We have chosen 208 MHz as the RF frequency for the proton beam. At this frequency the bunch will be stable with an RF voltage of 25 MV, a voltage which can be provided with high Q cavities at a modest power consumption.

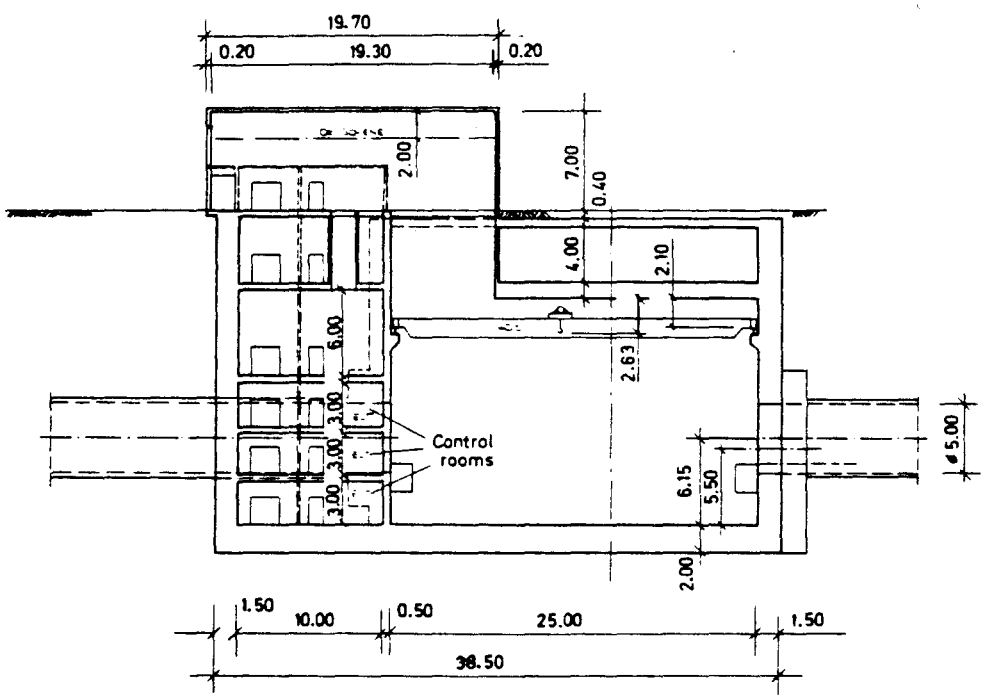

Fig. 13 - Vertical cut through an experimental building parallel to the beams.

Table 1 - Basic parameters

	p-ring	e-ring	units
Nominal energy	820	30	GeV
$s = Q^2_{max}$	98400		GeV^2
Luminosity	0.6×10^{32}		$cm^{-2}s^{-1}$
Polarization time		20	min
Number of interaction points	4		
Length of straight sections	360		m
Free space for experiments	15		m
Circumference	6336		
Bending radius	603.8	540.9	m
Magnetic field	4.53	0.1849	T
Total number of particles	6.3×10^{13}	0.76×10^{13}	
Circulating current	480	58	mA
Energy range	200 → 820	10 → 35	GeV
Emittance $(\varepsilon_x/\varepsilon_z)$	0.47/0.24	1.6/0.16	10^{-8}m
Beta function β^*_x/β^*_z	3/0.3	3/0.15	m
Dispersion function D^*_x/D^*_z	0/0	0/0	m
Beam-beam tune shift $\Delta Q_x/\Delta Q_z$	0.0006/0.0009	0.008/0.014	
Beam size at crossing σ^*_x	0.12(0.91)**	0.22	mm
Beam size at crossing σ^*_z	0.027	0.013	mm
Number of bunches	210		
Bunch length	9.5	0.93	cm
RF frequency	208.189	499.667	MHz
Maximum circumferential voltage	100***	290	MV
Total RF power	4-6	13.2	MW
Filling time	20	15	min
Injection energy	40.0	14.0	GeV
Energy loss / turn	1.4×10^{-10}	142.3	MeV
Critical energy	10^{-6}	111	keV
Heat loss at 4.3 K	13.2		kW
Lead cooling gas rate	42.5		g/s
Design refrigeration power at 4.3K	20		kW
Design lead gas rate	64		g/s

* At the interaction point
** Including the bunch length
*** 25 MV is foreseen initially corresponding to 1 - 1.5 MW.

For the electron RF system we have chosen 500 MHz, the frequency adopted for the other DESY machines. This choice allows us to exploit fully both the expertise and the hardware available at DESY and makes it attractive to construct the RF system in stages. The final stage employs 192 cavities and a total RF power of 13.2 MW, sufficient to reach 35 GeV electron energy with zero current.

The luminosity of an electron-proton colliding ring is given by

$$L = \frac{f_o \cdot n_b \cdot N_e \cdot N_p}{2\pi(\sigma_{xp,eff}^2 + \sigma_{xe}^2)^{1/2} (\sigma_{zp}^2 + \sigma_{ze}^2)^{1/2}}$$

In this formula f_o is the revolution frequency, n_b the number of bunches in each ring, N_e and N_p the number of electrons and protons per bunch respectively, $\sigma_{xp,eff} = (\sigma_{xp}^2 + (\sigma_{sp} \cdot \phi)^2)^{1/2}$ with σ_{sp} denoting the proton bunch length and ϕ the crossing angle assumed to be ± 10 mrad, σ_{xe} is the width of the electron beam and σ_{zp} and σ_{ze} the height of the proton and the electron beam respectively.

The beam sizes are all defined in the interaction point and are calculated from the emittance of the two beams. In the case of the electron beam, the horizontal emittance at a given energy and cell length is determined by the phase advance per cell. The vertical emittance depends on coupling between the horizontal and vertical plane which we computed to be 10%. The main contricution to this coupling comes from the vertical bends in the spin rotator. In the case of the proton beam the emittances are determined by the injector.

The luminosity is proportional to the number of bunches. We have chosen 210 bunches in each ring spaced 96 ns apart with a gap of about one microsecond required by the fast ejection system.

The luminosity was then evaluated with the following assumptions:

1) The maximum number of protons per bunch $N_p \lesssim 3 \times 10^{11}$. This is a factor of 3 above the bunch current which has been stored in the SPS. However, note that HERA will have a much smoother vacuum chamber and a much higher peak RF voltage.

2) The electron RF power is limited to 13.2 MW.

3) The limits for the electron and the proton tune shifts are

$$\Delta Q_e \leq 0.025$$

$$\Delta Q_p \leq 0.0025.$$

The resulting luminosity is plotted in Fig. 14 as a function of proton energy for various values of the electron energy. The parameters limiting the luminosity is listed in the brackets. Note that the luminosity at the highest electron energies is limited by the beam currents and at the lowest electron energies by the tune shifts.

A peak luminosity on the order of 3×10^{32} is reached for 20 GeV electrons colliding with 820 GeV protons. The luminosity is still about 6×10^{31} $cm^{-2}sec^{-1}$ for 30 GeV electrons and 820 GeV protons.

3.3 Injection

The injection system is capable of filling the electron ring of HERA with 210 bunches of 14 GeV electrons (positrons) with a maximum intensity of 1.3×10^{11} particles per bunch in 15 min (25 min). The proposed injection system is based on Linac II, the DESY synchrotron and PETRA for electrons and on Linac II, PIA, the DESY synchrotron and PETRA for positrons.

The proton injection scheme is also to a large extent based on existing accelerators. Protons from a new 50 MeV linear accelerator are injected into the DESY synchrotron, accelerated to 7.5 GeV and transferred to PETRA where they are accelerated to 40 GeV, the maximum possible energy, and injected into HERA.

The field at injection has a strong sextupole component resulting from persistent currents with a small contribution from winding errors. Using the measured[8] values of the sextupole field we find that the resulting chromaticity at 40 GeV is nearly an order of magnitude larger than the natural chromaticity. The average sextupolfield will be corrected by bucking coils mounted directly onto the beampipe. The remaining effects caused by the fluctuations have been investigated[3] using a fast tracking program. The program includes multipoles up to order 16 as thin lenses in the middle of the dipole magnet. The strengths of the multipoles are gaussian distributed with an rms width taken to be 1/3 of the

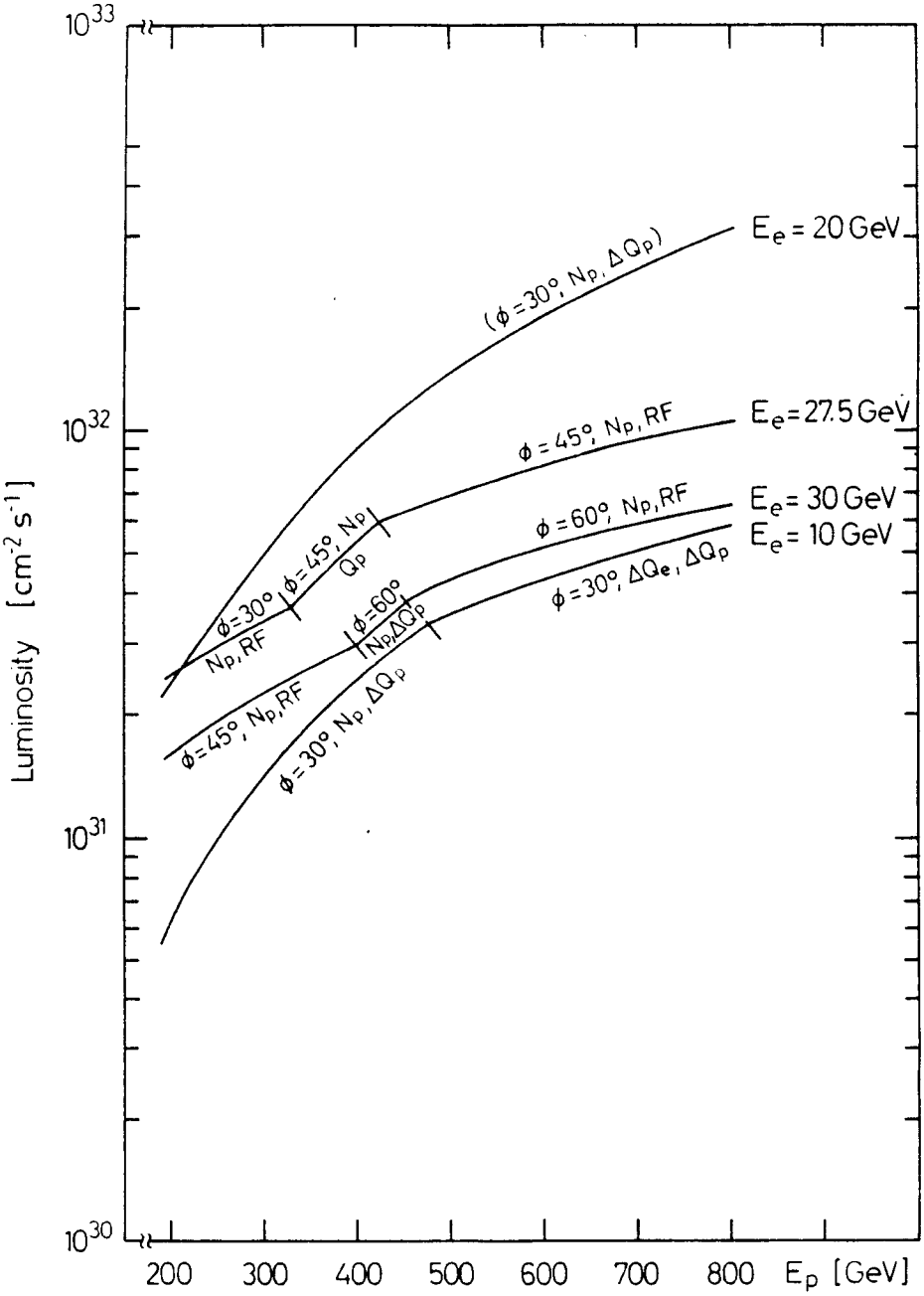

Fig. 14 - Luminosity as a function of the proton energy for various electron energies. The luminosity limiting parameters are indicated.

maximum tolerable value required for the FNAL magnets. The persistent currents are assumed to fluctuate by at most ± 10%. The rms value of the closed orbit distortions was 1 mm.

A simple arrangement of two sextupol families is used to correct the natural chromaticity ($\xi_x = \Delta Q_x/(\Delta p/p) = -62$, and $\xi_z = \Delta Q_z/(\Delta p/p) = -88$). In the arcs one family is located close to the focusing quadrupoles and the other close to the defocusing quadrupoles. The sextupoles in the straight section are located adjacent to the quadrupoles at positions where the horizontal and vertical betatron oscillations are decoupled and the dispersion is large.

The maximum value of the initial amplitude leading to a stable oscillation is determined by tracking an ensemble of 16 particles through the HERA magnet structure. To determine the stability limit we followed the ensemble for 100 turns in the case of a constant energy and for 300 turns when synchrotron oscillations are included. The tracking is done assuming that the half aperture of the elements in the regular lattice is 30 mm and infinite for elements in the straight section. An amplitude is stable if no particles are lost and unstable if at least one particle is lost.

The nonlinear acceptance of the machine at the injection energy of 40 GeV is shown in Fig. 15. The maximum value of the initial betatron amplitude A_i which yields a stable oscillation is plotted versus particle momentum. The amplitude is plotted at the position of a regular lattice focusing quadrupole. The lower value of the error bar corresponds to the maximum stable, the upper value of the error bar to the minimum unstable amplitude found by the program. The working point of the machine is $Q_x = 32.145$ (33.138) and $Q_z = 35.135$ (35.107) for the upper (lower) curve.

The upper curve shows the acceptance with only the chromaticity correcting sextupoles included. The lower curve shows the acceptance with both persistent current sextupoles and multipoles included. Including all nonlinear effects redueces the aperture by 20 - 30% compared to the aperture with only the chromaticity correcting sextupoles present.

Measurements[11] at the ISR found a beam lifetime on the order of 18.5 hours with the vertical collimators set at 2.2σ. We therefore assume that the available aperture should be at least $(\Delta p/p \cdot D) + 2.2\sigma_x$ at injection, where $\Delta p/p$ is the

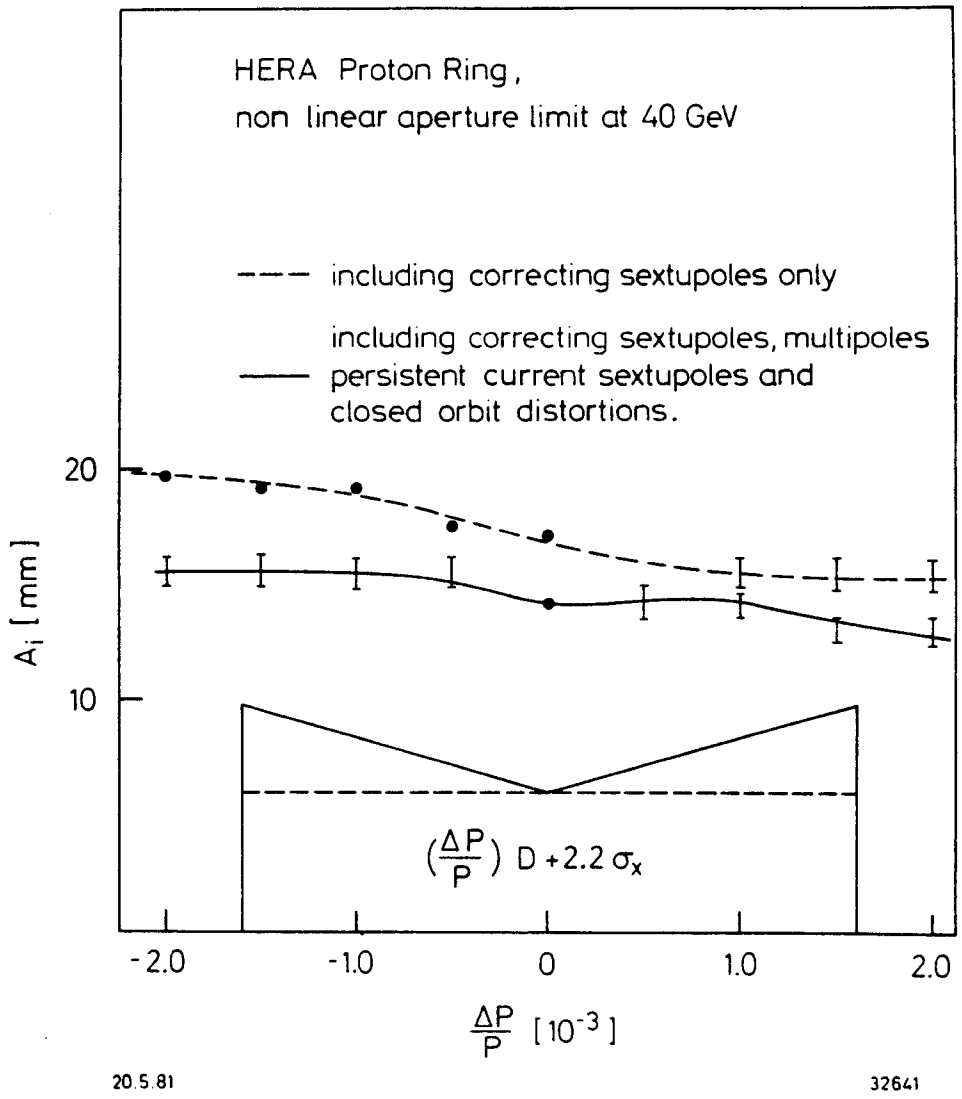

Fig. 15 - Maximum stable initial amplitude versus relative energy deviation at 40 GeV.

total momentum spread and $\sigma_x = \sqrt{\varepsilon_x \cdot \beta_{max}}$. At 40 GeV $D^{max} \cdot \Delta p/p = 3.0$ mm and $\sigma_x = 2.77$ mm.

This aperture, plotted in Fig. 15, is comfortably smaller than the non-linear aperture determined by the tracking program. The emittance growth due to beam-gas and intra beam scattering has been evaluated[2,3] and found to be negligible for injection times on the order of half an hour.

The non-linear aperture was also determined at 820 GeV. The high energy aperture plotted in Fig. 16 is slightly larger than the aperture found at 40 GeV since persistent current effects can be neglected at high energies. The beam size defined as above is now much smaller since the betatron part of the amplitude decreases as $1/\sqrt{E}$ and the momentum spread is reduced from 1.6 $^{o}/_{oo}$ to 0.95 $^{o}/_{oo}$. The non linear aperture is on the order of $20\sigma_x$ and clearly sufficient to store the beam for tens of hours.

3.4 The lattice

Both rings have a periodic FODO cell structure consisting of equidistant focusing and defocusing quadrupoles which alternate in sign. The magnet structure of the standard cells is depicted in Fig. 17. As much of the intervening space as possible is filled with bending magnets in order to reach the highest proton energy and in case of the electron machine, to minimize synchrotron radiation. A short straight section placed to one side of each quadrupole provides space for sextupole magnets, orbit detecting pickups, correction dipoles and vacuum equipment together with other beam detection equipment and correction windings.

The HERA lattice parameters are listed in Table 2.

3.5 The interaction region

The interaction region in an electron-proton colliding ring is rather complex. Firstly it must bring the two beams with rather different properties into collision. The arcs must be matched into the long straight sections such that the dispersion is suppressed. Furthermore the spin of the electron which is transverse in the arcs must be turned by $\pm\pi/2$ to become parallel or antiparallel to the beam direction in the interaction point and be restored to the transverse direction upon reentering the arcs. Minimizing the depolarization caused by the

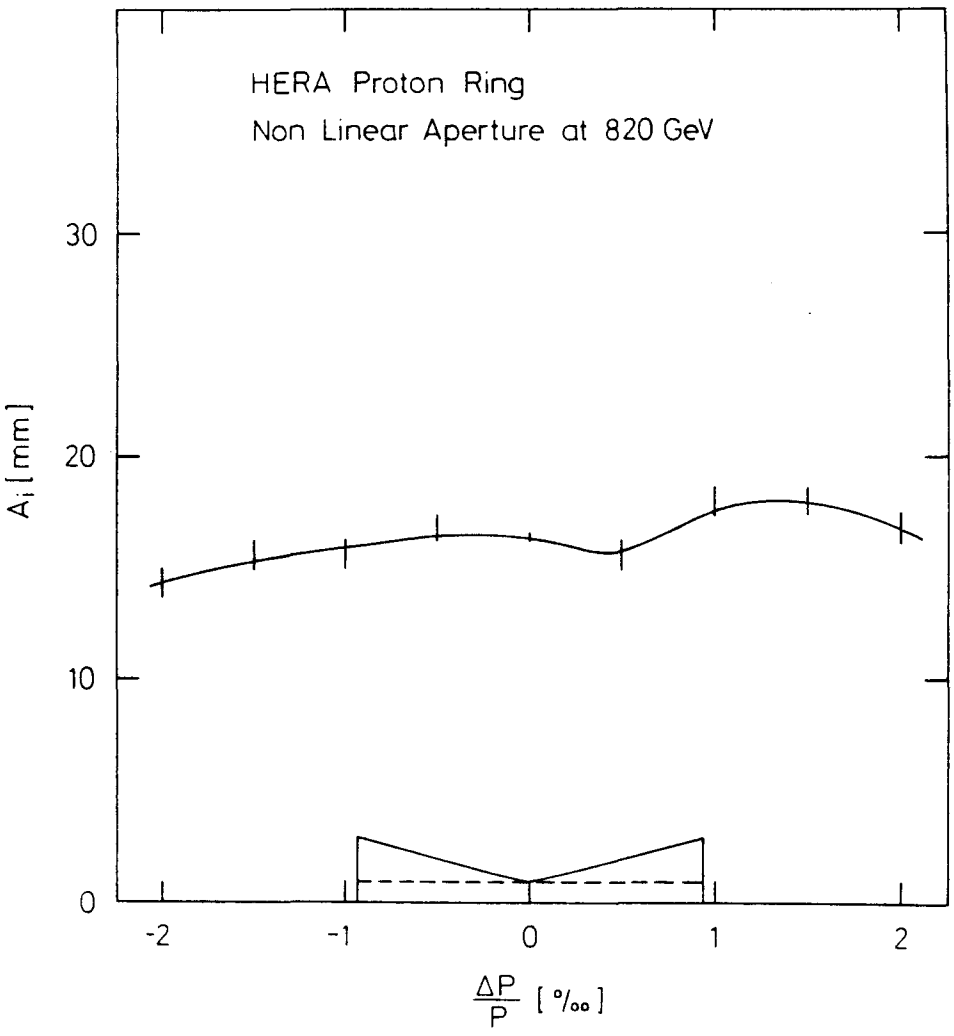

20 5.81

Fig. 16 - Maximum stable initial betatron amplitude versus relative energy deviation at 820 GeV.

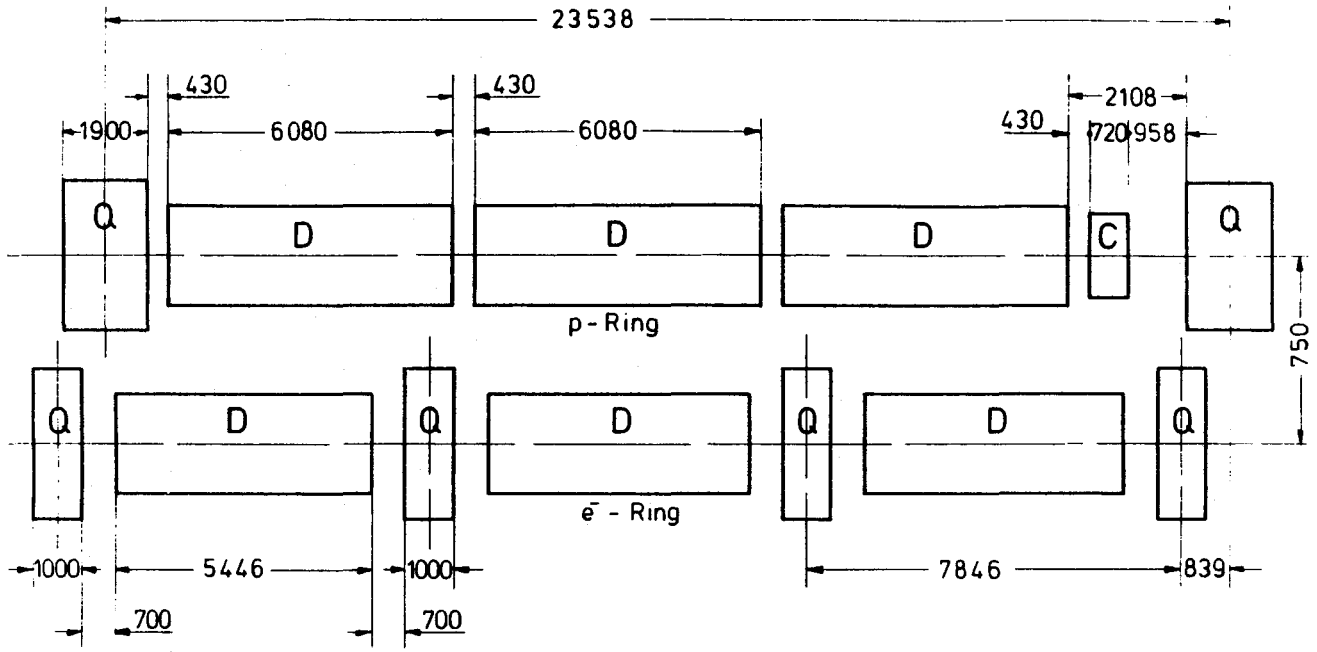

Bending angle $\alpha = \frac{2\pi}{624} = 1{,}007 \times 10^{-2}$

Fig. 17 - Lattice for the electron, and the proton ring.

Table 2 - HERA lattice parameters

	p-ring	e-ring
Energy (GeV)	820	30
Circumference (m)	6336	
Number of superperiods	4	
Lattice	FODO	
Straight section length	360 m	
Normal cells / octant	9	34.5 *
Dispersion suppressing cells / octant	4	2
Number of dipoles / cell	6	2
Magnetic length of dipole (m)	6.08	5.446
Aperture of bending magnet (mm)	60.0 ø	70 x 40
Bending radius (m)	603.8	540.9
Magnetic length of quadrupole (m)	1.90	1.00
Aperture of quadrupole (mm)	60.0 ø	50.0 ø
Betatron phase advance / cell	90^{o}	60^{o}
Momentum compaction	$1.315 \cdot 10^{-3}$	$0.495 \cdot 10^{-3}$
Transition energy (GeV)	25.9	
Working point Q_x / Q_z	32.14/35.14	48.3/48.2
Cell quadrupole focal length (m)	16.6	7.8
Cell quadrupole gradient (T/m)	91.2	12.7
Amplitude function β^{max} (m)	80.4	27.2
Amplitude function β_{min} (m)	13.8	9.1
Dispersion D^{max} (m)	1.9	0.39
Dispersion D_{min} (m)	0.92	0.24

* The horizontal bend of each spinrotator is equivalent to that of 2.5 normal cells.

spin rotator introduce further constraints. Sufficient space for the RF cavities and the magnets for the injector and the ejector must also be found.

A detailed layout of the intersection region is given in Fig. 18. The beams cross in the horizontal plane of the electron ring at an angle of $\pm$ 10 mrad in the middle of the long straight section. A horizontal crossing was chosen since the beam size in the horizontal plane is larger than the beam size in the vertical plane. The crossing angle is in principle a free variable. The large crossing angle chosen makes it possible to design the machines without common elements such that the energies can be varied independently. The luminosity remains the same as in the earlier design, since the increase in horizontal beam size can be compensated by bringing the proton quadrupoles closer to the interaction point thus reducing the vertical beam size. A free distance of $\pm$ 7.5 m around the interaction point is available for experiments. In this design the spin is turned into the longitudinal direction by an 80 m long rotator installed at the end of the arc and restored to the transverse direction by a similar rotator positioned at the entrance to the next arc.

The rotator is shown in more detail in Fig. 19. The spin of an electron is aligned antiparallel and that of a positron parallel to the direction of the magnetic field in the arcs - i.e. the spin is always pointing upwards. The spin is rotated by $\pi/4$ in the first vertical bend, precessed by $-\pi$ in the horizontal magnet and rotated by $-\pi/4$ in the second vertical bend. The spin, after this magnet sequence, is pointing along the direction of flight and the next two vertical bends simply restore the original beam direction without changing the spin direction.

Both helicities can be obtained by reversing the sign of the vertical bending magnet in the rotators and reposition the magnets vertically by 80 cm.

The horizontal magnet in the rotator is a part of the lattice and must bend the particles by a fixed angle of 50.35 mrad in addition to precess the spin by π. The rotator is therefore optimized for a fixed energy of (27.5 $\pm$ 0.5) GeV.

The large distance between the interaction point and the last bend in the rotator minimizes the amount of synchrotron radiation which reaches the detector. In each straight section nearly 200 m is available for the RF system and the injection and the ejection system.

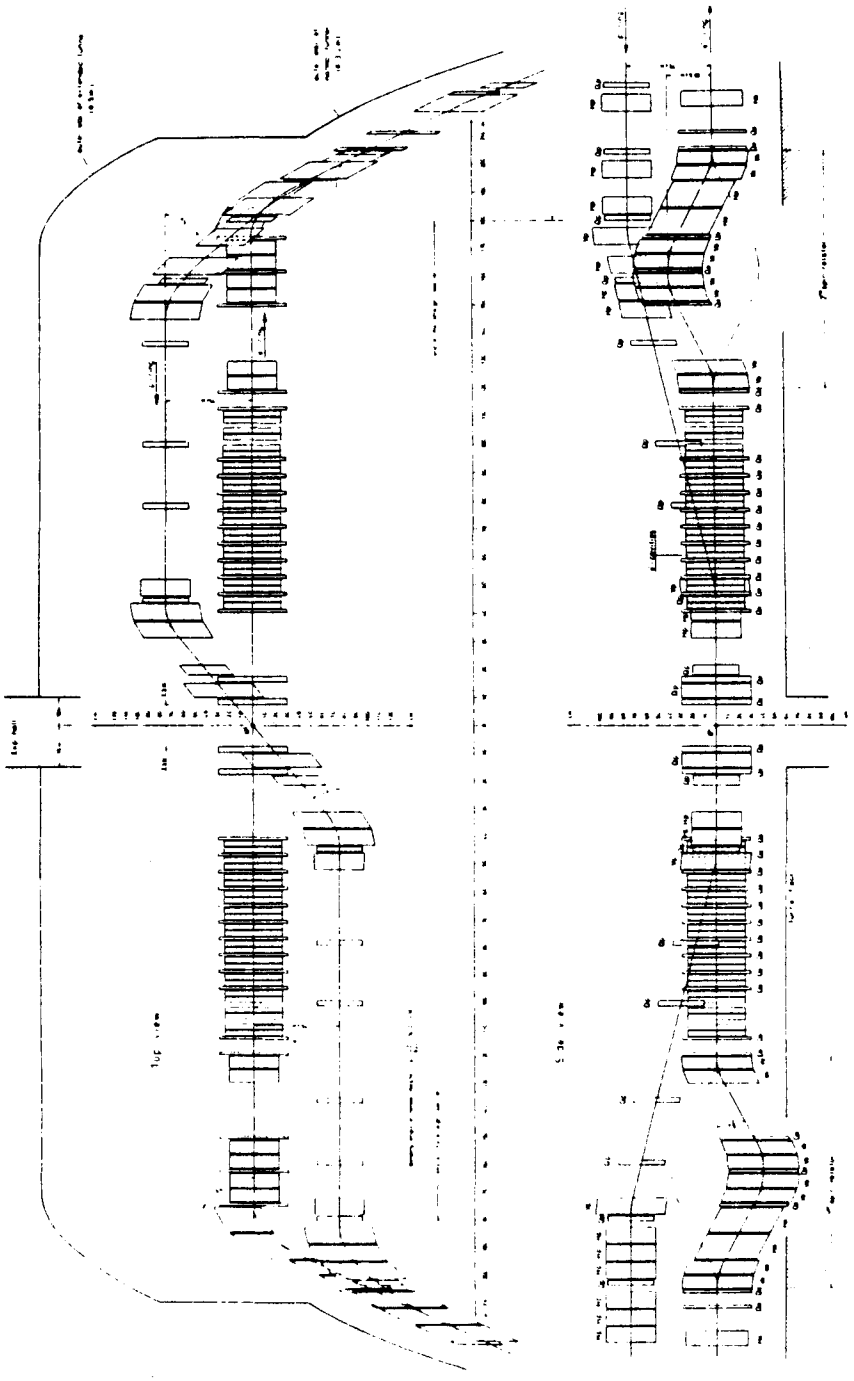

Fig. 18 - Layout of the interaction region.

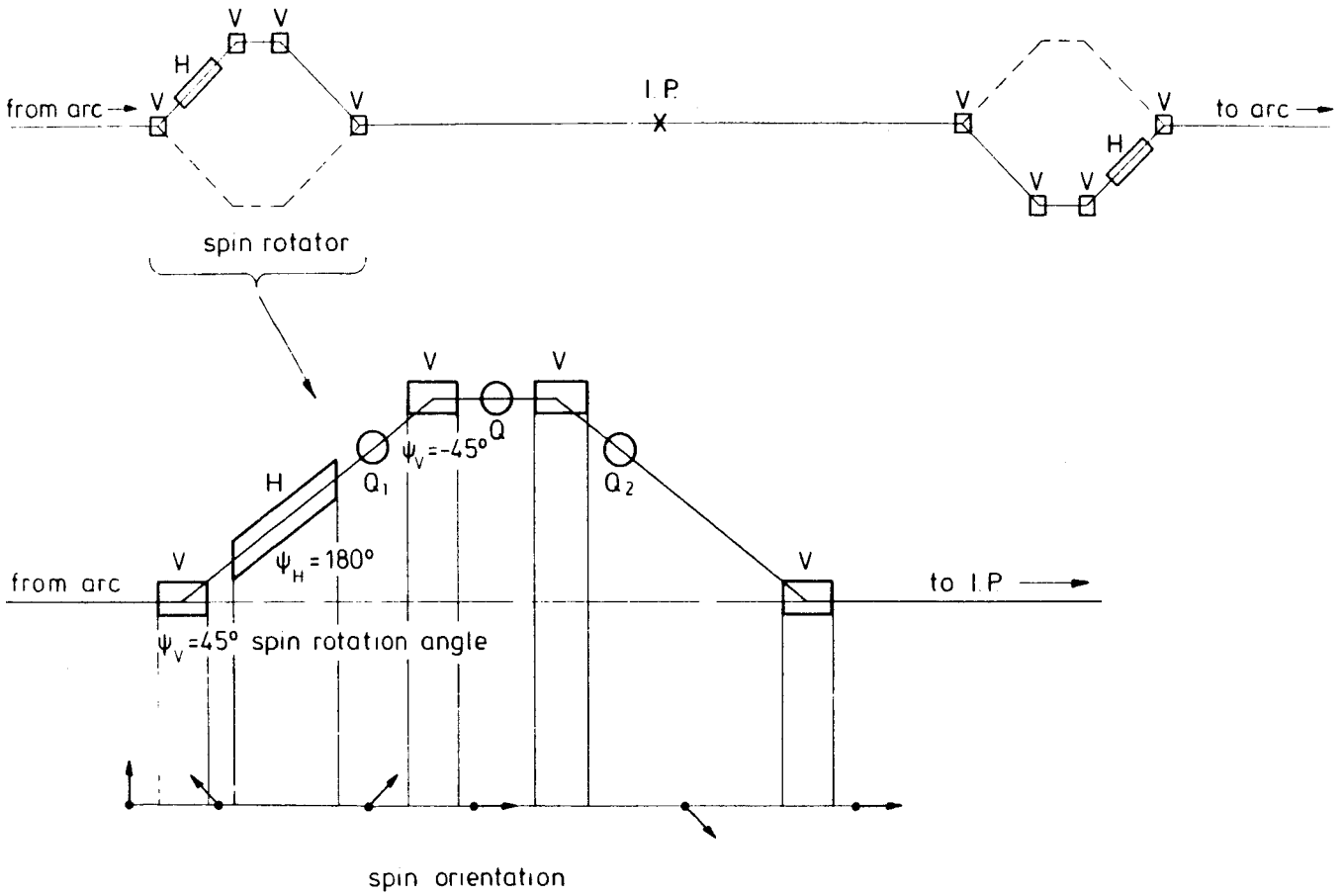

Fig. 19 - Spin rotator.

The properties of the rotator have been investigated using the SLIM program[12]. With the present design we find a longitudinal polarization of about 60% in each of the four interaction regions. Note that a transverse polarization of 70% has been obtained in PETRA with a single beam and that some polarization with colliding beams has been observed[13] for the first time at high energies.

3.6 Components of the electron ring

The electron ring of HERA is similar to the PETRA machine except that the circumference is larger by a factor of 2.75. Although the PETRA components in principle could be used directly, some changes, based on PETRA experience, are made to simplify the design and to reduce the cost.

The RF system is similar to the one used at PETRA except that the cavity will be designed with seven cells instead of five and a reduced hole size between adjacent cells. These design changes should increase the shunt impedance per meter by 50% to R = 18 MΩ/m and reduce power consumption.

The cross section of a dipole magnet with vacuum chamber and a pump is shown in Fig. 20. The dipole is excited by a single turn conductor traversing the entire ring. The stray field is cancelled by a second conductor mounted at the wall of the tunnel with the current flowing in the opposite direction. The slots in the lamination equalize the length of the field lines in the yokes and lead to a field uniformity of the order of 10^{-4} over the magnet aperture.

The vacuum chamber, 40 mm high and 80 mm wide, will be made of copper pipe 4 mm thick. We plan to use discrete pumps spaced 1 m apart. Only the part of the beam pipe facing the coil and the magnet gap will be covered by a 5 mm thick lead sheet. In this arrangements less than 10^9 rad is absorbed by the organic coil insulation during the estimated life time of the machine. At 30 GeV about 97.5% of the radiated synchrotron power is absorbed in the copper beam pipe and the lead with 2% ($\sim$ 40 Watt/m) absorbed by the magnets and a small fraction (0.5%) escaping through the magnet gap.

The magnets can easily handle this power without additional cooling and can hence be used without any changes as a synchrotron radiation shield.

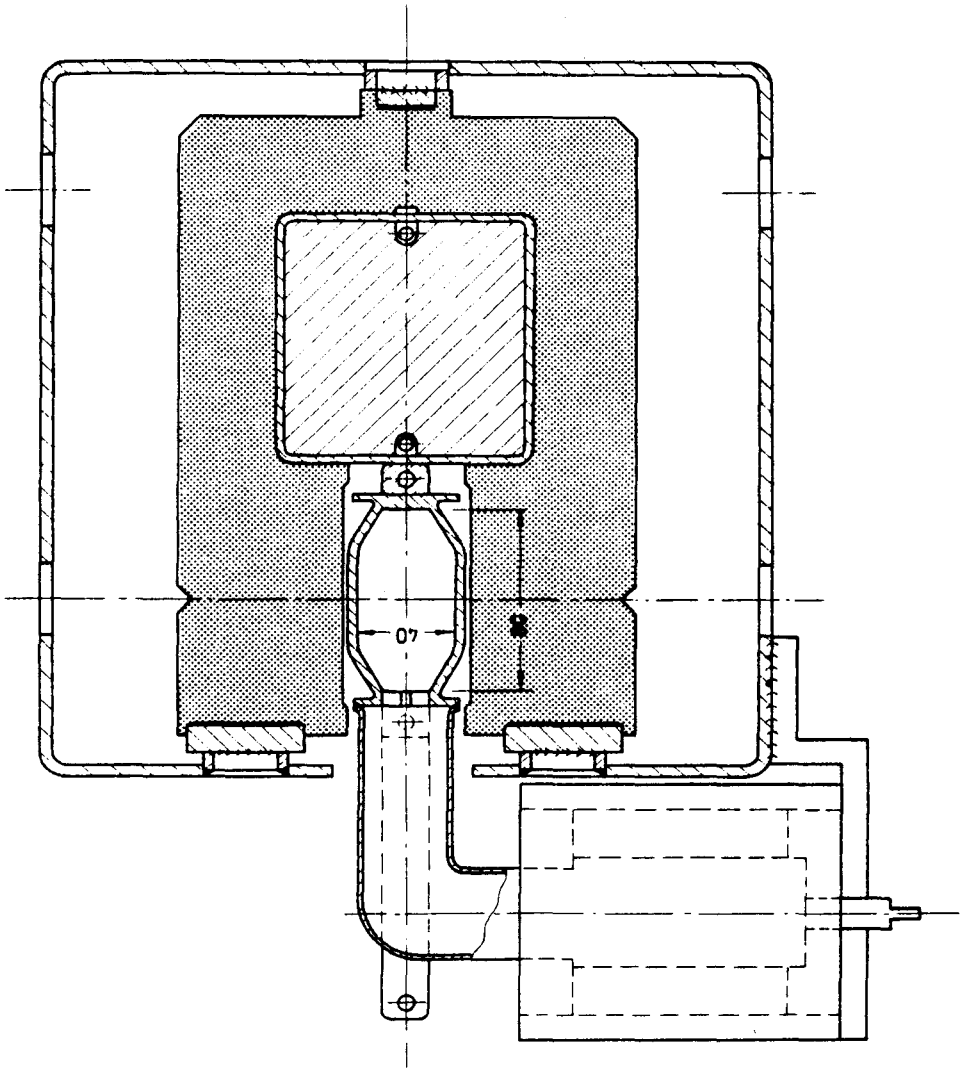

Fig. 20 - Cross section of the vacuum chamber with the lead shielding in the dipole magnet.

3.7 Components of the Proton Ring

The proton ring of HERA will be constructed using superconducting magnets. The conductor will be a niobium titanium superconductor imbedded in a copper matrix.

The dipole magnets are rather similar to the FNAL magnets and have a warm iron and a cold bore. The heat losses in the vacuum pipe will be minimized by Cu-plating the inner walls of the chamber and by making a very smooth chamber without clearing electrodes. This avoid any excessive heat load on the refrigeration system even for the short, intense proton bunches in HERA.

A vertical cut through a dipole magnet is shown in Fig. 21. The cryostat is mounted inside a 436 mm wide and 352 mm high iron yoke using four sets of six tie rods each. The heat loss through the tie rods is small and this system allows us to adjust the coil within the iron following magnetic measurement without warming up the magnet. In the present design the dipole field is approximated by a two shell conductor arrangement fixed by precision stamped stainless steel collars as in the FNAL design.

The magnets are cooled by one phase helium. At the end of each octant the one phase helium is expanded and the ensuing two phase helium is returned through the magnets in good thermal contact with the one phase helium thus ensuring a constant temperature of the coolant. The heat shield is maintained at 50 K by passing cold He gas through the outer cryostat.

The parameters of the dipole and quadrupole magnets are listed in Table 3.

Table 3 - Superconducting magnet parameters

Parameter	Dipole	Quadrupole
Number of magnets	656	304
Magnetic length (m)	6.08	1.90
Induction (T)	4.53	
Gradient (T/m)		91.2
Bore (mm)	60	60
Nominal current (A)	5582	5582
Load factor (at 4.6 K)	0.89	0.86
Stored energy (kJ)	560	76
Mass (kg)	5750	448

1 Cryostat vacuum
2 Coils
3 Iron yoke
4 50 K shield
5 2 phase He
6 1 phase He
7 Collars
8 Beam vacuum
9 Suspension rod
10 Steel girder
11 Sextupole correction

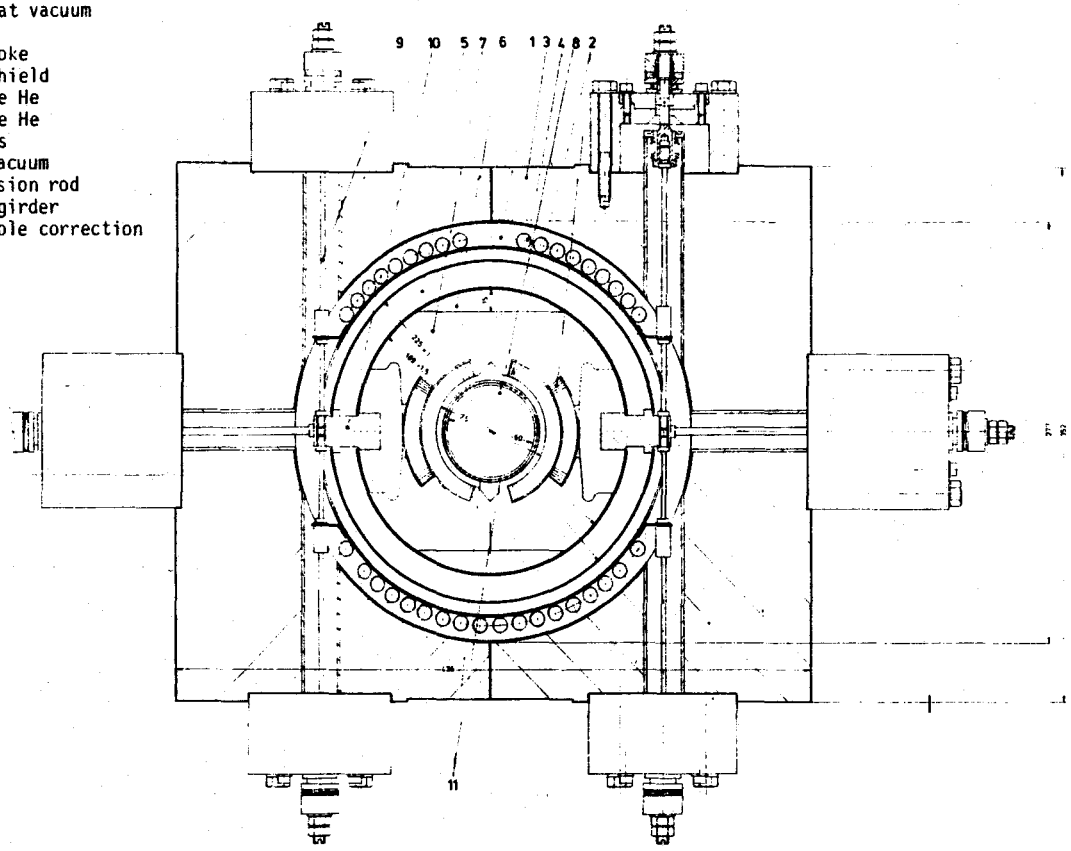

Fig. 21 - Cross section of a superconducting dipole magnet.

The layout of the refrigeration system is shown in Fig. 22.

A central compressor system is located near experimental hall West on the DESY site. The compressor capacity will be subdivided into six units, each with 1/4 of the normal flow rate. Extra capacity is thus available either to shorten the cooldown times or to ensure continuous operation in the case of maintenance or repairs. The high pressure helium is distributed around the ring to four refrigeration units, one located in each experimental hall.

Each refrigerator cools the two neighbouring octants and the magnets located in the long straight section. The refrigerator capacity is 50% higher than the normal load such that the machine can continue operation even if one unit fails. The total heat load under normal running conditions is 13.2 kW at 4.3 K and 42.5 g of liquid He per second. The heat loss at 50 K is 45 kW. This can be compared to the total refrigeration power of 20 kW at 4.3 K and 64 g liquid helium per second. The refrigeration power at 50 K is 68 kW.

For the proton RF we propose to use the 200 MHz system now being developed[14] at CERN for the SPS. This system is modular with each RF cavity having its own small amplifier on top and vacuum pump underneath. We propose to install 48 groups of 3 single cell modules. The total cell length will amount to 104 m and the maximum voltage is 100 MV with an RF power between 4 - 6 MW. As the final power amplifier we propose to use the longlife tetrode currently being developed by European Industry. Test with a prototype cell at CERN have given very encouraging results[14].

The HERA design will now be forwarded to the government with a request for funding. If we are lucky we could then observe e p collisions before the thirtieth anniversary of the first proposal to collide electrons with protons.

68%

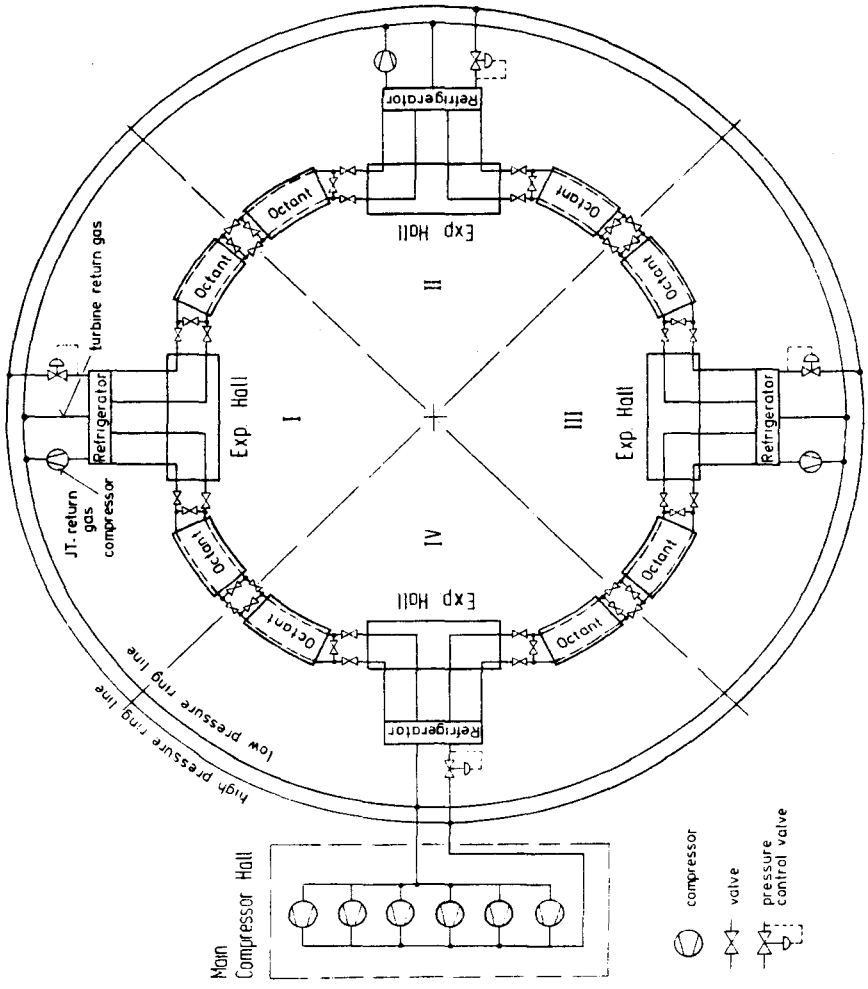

Fig. 22 - Layout of the magnet cooling circuit.

References:

1) H.G.Hereward, K.Johnsen, A.Schock and C.J.Zilverschoon,
Proc. 3rd International Conference on High Energy Accelerators, Brookhaven 1961
L.Goldzahl and E.G.Michaelis, CERN 66-12 (1966);
C.Pellegrini, J.Rees, B.Richter, M.Schwartz, D.Möhl and A.Sessler,
Proc. 8th International Conf. on High Energy Accelerators, CERN 1971
H.Gerke, H.Wiedemann, B.H.Wiik and G.Wolf,, DESY H-72/22 (1972)

2) Report of the Electron-Proton Working Group of EXFA, Study of the Proton-Electron Storage Ring Project HERA, ECFA 80/42 - 17 March 1980 - DESY HERA 80/01

3) HERA, A proposal for a Large Electron-Proton Colliding Beam Facility at DESY, DESY HERA 81/10

4) For an early complete discussion on the physics which can be carried out with a large electron-proton colliding ring see:
C.H.Llewellyn-Smith and B.H.Wiik, DESY 77/38 (1977)
CHEEP-An ep facility in the SPS:
J.Ellis, B.H.Wiik and K.Hübner (editor) CERN 78-02
and Ref. 2

5) S.L.Glashow, Nucl.Phys. 22, 579 (1961)
S.Weinberg, Phys.Rev.Lett. 19, 1267 (1967)
A.Salam, Proc. 8th Nobel Symposium, Stockholm,
Almquist and Wiksells, Stockholm 1968 p. 363

6) A.J.Buras and K.J.F.Gaemers, Nucl.Phys. B 132, 249 (1978)

7) H.Fritzsch, M.Gell-Mann and H.Leutwyler, Phys.Lett. 47B, 365 (1973)
F.Gross and F.Wilczek, Phys.Rev.Lett. 30, 1343 (1973)
H.D.Politzer, Phys.Rev.Lett. 30, 1346 (1973)
For reviews see:
H.D.Politzer, Phys.Reports 146, 129 (1974)
M.Marciano and H.Pagels, Phys. Reports 366, 1373 (1978)

8) Superconducting Accelerator Design Report,
Fermi National Accelerator Laboratory (1979)

9) ISABELLE, a 400 x 400 Proton-Proton Colliding Beam Facility,
Brookhaven National Laboratory, BNL 50718

10) D.Boussard et al., IEEE Transaction on Nuclear Science NS-26, No. 3 (1979)

11) K.Hübner, private communication

12) The SLIM program was written by A.Chao at SLAC, SPEAR 200/PEP 257, SLAC 1977

13) Private communication from the PETRA polarization group

14) C.Zettler, private communication

GRAND UNIFICATION AND BEFORE*

W. J. Marciano, Northwestern University
A. Sirlin, New York University

I. $SU(3)_C \times SU(2)_L \times U(1)$ Parameters

The "standard" $SU(3)_C \times SU(2)_L \times U(1)$ model of strong and electroweak interactions contains the following parameters:[1] 1) It has three independent couplings g_3, g_2 and g_1. The QCD coupling g_3 is often parameterized in terms of the mass scale $\Lambda_{\overline{MS}}$, while g_2 and g_1 are generally traded off for the electric charge e and the weak mixing angle θ_W via the relationships $e^2 = g_2^2 \sin^2\theta_W$ and $\tan^2\theta_W = 3g_1^2/5g_2^2$. 2) There are two intermediate vector boson masses m_W and m_Z which are related by $m_W = m_Z\cos\theta_W$ and an arbitrary Higgs scalar mass m_ϕ. 3) Of its nine fermion masses m_e, m_μ, m_τ, m_d, m_s, m_b, m_u, m_c and m_t, all except, m_t have phenomenologically measured values. From e^+e^- annihilation PETRA data, one has the lower bound $m_t \gtrsim 18$ GeV. (A theoretical analysis by A. Buras[2] finds $m_t \simeq 26 \pm 7$ GeV.). 4) There are three quark mixing angles θ_1, θ_2, θ_3 and a CP violating phase δ. In addition, there may be neutrino masses, lepton mixing angles, new generations of fermions, etc. As experimentalists measure these parameters with better precision, theorists seek natural relationships (such as $m_W = m_Z\cos\theta_W$) in an attempt to understand their origin. Such relationships are generally obtained by constraining the theory with additional symmetries. In that regard we now know how to correlate the three couplings g_3, g_2 and g_1 through grand unification.[3] Unfortunately, the origin of masses and their interrelationships are not as well understood. This problem of masses should be a signal that something fundamental is lacking in our present theories.

Before describing the predictions of the SU(5) Georgi-Glashow model[3] and speculating on what new physics may populate the great desert (between 10^2 GeV and 10^{14} GeV) suggested by such theories, we will briefly review the

---

*Talk presented by W.J. Marciano.

present experimental status of $\alpha = e^2/4\pi$, $\Lambda_{\overline{MS}}$ and $\sin^2\theta_W$. These low energy parameters already provide precise predictions for the masses and decay rates of the $W^{\pm}$ and Z^0, as we shall see.

1) $\underline{\alpha}$: Josephson effect measurements of the fine structure constant α give[4]

$$\alpha^{-1} = 137.035987 \tag{1}$$

This long distance coupling (defined at zero momentum transfer) is related to the short distance coupling[5] $\hat{\alpha}(m_W)$ defined by modified minimal subtraction $\overline{MS}$ in the dimensional regularization scheme with μ, the 't Hooft[6] unit of mass equal to m_W by

$$\hat{\alpha}^{-1}(m_W) = \alpha^{-1} - \frac{2}{3\pi}\sum_f Q_f^2 \ln(m_W/m_f) + \frac{1}{6\pi} + \ldots \tag{2a}$$

where the sum is over all charged fermions and ... refer to higher order terms. Including QCD effects, this relationship implies (for $\Lambda_{\overline{MS}}$ = 0.4 GeV and m_t = 20 GeV)[1]

$$\hat{\alpha}^{-1}(m_W) \simeq 127.49 \tag{2b}$$

This value will subsequently be used in our SU(5) analysis.

2) $\underline{\Lambda_{\overline{MS}}}$: The QCD coupling $\hat{\alpha}_3(\mu) = \hat{g}_3^2(\mu)/4\pi$ is also defined by modified minimal substraction. It is generally parametrized by a mass scale $\Lambda_{\overline{MS}}$ such that for $m_c < \mu < m_b$ (i.e. an effective 4 flavor theory)[1]

$$\hat{\alpha}_3(\mu) = \frac{12\pi}{25\ln(\mu^2/\Lambda^2_{\overline{MS}})}\left[1 - \frac{462}{625}\frac{\ln\ln(\mu^2/\Lambda^2_{\overline{MS}})}{\ln(\mu^2/\Lambda^2_{\overline{MS}})}\right] \tag{3}$$

Using this parametrization, fits to scaling violations in electroproduction find $\Lambda_{\overline{MS}} \simeq 0.4$ GeV, while perturbative analyses of e^+e^- → hadronic jets and upsilon decay tend to give smaller values near 0.2 GeV. To be conservative, we will subsequently employ the range 0.1 GeV < $\Lambda_{\overline{MS}}$ < 0.6 GeV in our SU(5) analysis.

Using the value of $\hat{\alpha}_3(\mu)$ at $\mu = \sqrt{10}$ GeV given by Eq. (3) and employing the QCD beta function to evolve this coupling up to $\mu = m_W$, we find (for six flavors with m_t = 20 GeV) the following values of $\hat{\alpha}_3(m_W)$ and $\hat{\alpha}(m_W)$*

$\Lambda_{\overline{MS}}$ (GeV)	m_W (GeV)	$\hat{\alpha}_3(\sqrt{10}$ GeV)	$\hat{\alpha}_3(m_W)$	$\hat{\alpha}^{-1}(m_W)$
0.1	82.8	0.1732	0.1015	127.56
0.2	83.6	0.2106	0.1127	127.53
0.3	84.0	0.2423	0.1207	127.51
0.4	84.4	0.2721	0.1271	127.49
0.5	84.6	0.3019	0.1328	127.47
0.6	84.8	0.3325	0.1379	127.46

Table I.

The values of m_W used in the above table are consistent with the SU(5) analysis in section II.

3) $\sin^2\theta_W$: Presently, the best experimental determination of $\sin^2\theta_W$ comes from deep-inelastic neutrino scattering via the measurement of $R_\nu \equiv \sigma(\nu_\mu + N \to \nu_\mu + X)/\sigma(\nu_\mu + N \to \mu^- + X)$.[7] Including the effect of radiative corrections on both the neutral and charged current cross-sections in R_ν, we found after a detailed analysis[8]

$$\sin^2\hat{\theta}_W(m_W) = 0.215 \pm 0.010 \pm 0.004 \quad (\text{From } R_\nu) \tag{4}$$

where ±0.004 is the estimated theoretical uncertainty. The renormalized quantity $\sin^2\theta_W(m_W)$ is defined by modified minimal subtraction, $\overline{MS}$, with $\mu = m_W$.[9] We note that the corrected value in Eq. (4) is about 5% smaller than lowest order estimates. The primary source of this reduction is our finding that the parameter ρ^2 which has the lowest order value 1 in the Weinberg-Salam model is reduced by radiative corrections (for $m_t \simeq 20$ GeV and $m_\phi \simeq m_Z$) to[8]

$$\rho^2 \simeq 0.983 \quad (\text{theory}) \tag{5}$$

*For further details regarding the calculations in this paper, see ref. 1.

Since ρ^2 and $\sin^2\theta_W$ are correlated, this shift alone in ρ^2 leads to a 3.6% reduction in $\sin^2\theta_W$. We might point out that a combined phenomenological analysis of deep-inelastic neutrino and antineutrino scattering data found[7]

$$\rho^2_{exp.} \simeq 0.998 \pm 0.050 \qquad (6)$$

which is consistent with Eq. (5).

In the case of the Yale-SLAC e-D asymmetry measurement,[10] we found after including the dominant radiative corrections[1,11]

$$\sin^2\hat{\theta}_W(m_W) = 0.216 \pm 0.020 \qquad (7)$$

Averaging the results in Eqs. (4) and (7), one finds[1]

$$\sin^2\hat{\theta}_W(m_W) = 0.215 \pm 0.012 \quad \text{(Average)} \qquad (8)$$

This is the experimental value that should be compared with predictions from grand unified theories.[9]

From the result in Eq. (8) and our previous calculations of the radiative corrections to $W^\pm$ and Z^0 mass formulas,[5,12] we find

$$m_W = \frac{38.5 \text{ GeV}}{\sin\hat{\theta}_W(m_W)} = 83.0 \pm 2.4 \text{ GeV} \qquad (9)$$

$$m_Z = 93.8 \pm 2.0 \text{ GeV}. \qquad (10)$$

These $SU(2)_L \times U(1)$ predictions are about 5% larger than analyses which neglect radiative corrections. Since the decay rates of the $W^\pm$ and Z^0 increases like the mass cubed,[13] this mass shift gives rise to about a 16% increase in the decay widths. So, using $m_Z = 93.8$ GeV, $\sin^2\theta_W(m_W) = 0.215$ and $m_t = 20$ GeV, one finds for the Z^0's total width (including QCD corrections)[13]

$$\Gamma(Z^0 \to \text{all}) = 3.02 + 0.18\ (N_\nu - 3)\ \text{GeV}. \qquad (11)$$

where N_ν is the number of distinct neutrino species. A precise measurement of the Z^0's total width (to within about 0.2 GeV) will tell us the total number of massless (or light) neutrino species. (Will N_ν turn out to be 3?)

What if deviations from the predictions in Eqs. (9) and (10) are found? Very large differences would signal dramatic new physics such as additional Z's and W's, mixing effects etc. Small differences could imply more subtle effects. For example, if it turns out that $m_t > m_W$ (rather than $\simeq$ 20 GeV as we assumed), the Z^0 mass prediction is modified to[14]

$$m_Z = 93.8 \pm 2.0 - 0.38 \frac{m_t^2}{m_W^2}\ \text{GeV} \qquad (12)$$

Obviously, the results in Eqs. (9) - (12) emphasize the need for very precise determinations of the $W^\pm$ and Z^0 masses and their decay properties.

II. Grand Unified Theories

In this section we review the predictions of a class of grand unified theories (GUTS) generically denoted by G, the best known and simplest of which is the Georgi-Glashow SU(5) model.[3] The basic assumption employed is that G contains only two symmetry breaking mass scales m_S (the super-heavy unification mass) and m_W, such that the pattern of symmetry breaking associated with each of these mass scales is

$$G \xrightarrow[m_S]{} SU(3)_c \times SU(2)_L \times U(1) \xrightarrow[m_W]{} SU(3)_c \times U(1)$$

(This situation is certainly realized in the G = SU(5) model.) Taking G to be a simple Lie group requires $g_{G_0} = g_{3_0} = g_{2_0} = g_{1_0}$, i.e. all bare gauge couplings must be equal. In addition, defining the electric charge operator

as in the SU(5) model implies $\sin^2\theta_W{}^0 = e_0{}^2/g_{2_0}{}^2 = 3/8$ and $e_0{}^2/g_{3_0}{}^2 = \alpha_0{}^2/\alpha_{3_0}{}^2 = 3/8$. The bare parameter $\sin^2\theta_W{}^0$ is elevated from an infinite adjustable counterterm parameter (its role in the Weinberg-Salam model) to a rational number. As a simplification, we assume that all physical Higgs scalars which belong to $SU(2)_L$ isodoublets have mass $\simeq m_W$ (we allow N_H such doublets) and all other physical scalars have mass m_S.

SU(5) Analysis: Given the above assumptions, the effective low energy $SU(3)_c \times SU(2)_L \times U(1)$ couplings $\hat{\alpha}_i(m_W) \equiv \hat{g}_i{}^2(m_W)/4\pi$, $i = 1,2,3$ can be easily computed in terms of the grand unified coupling $g_G(m_S)$. Such calculations were initially carried out in the pioneering work of Georgi, Quinn and Weinberg[15] and have since been refined and extended by others.[16] We exhibit here the final results of our calculations.[1]

In terms of m_S/m_W, N_H (number of light Higgs isodoublets), n_g (number of fermion generations), $\hat{\alpha}(m_W)$, $\hat{\alpha}_i(m_W)$ and $\hat{\alpha}_i(m_S)$, $i = 1,2,3$, one finds from direct calculation and a renormalization group summation of the leading and next to leading logs.[1*]

$$\frac{\hat{\alpha}(m_W)}{\hat{\alpha}_3(m_W)} = \frac{3}{8}\left[1 - \frac{66 + N_H}{6}\frac{\hat{\alpha}(m_W)}{\pi}\ln\left(\frac{m_S}{m_W}\right) + \frac{\hat{\alpha}(m_W)}{2\pi} + \frac{\hat{\alpha}(m_W)}{4\pi}\right.\{$$

$$\frac{272 - \frac{176}{3}n_g}{11 - \frac{4}{3}n_g}\ln\left(\frac{\hat{\alpha}_3(m_S)}{\hat{\alpha}_3(m_W)}\right) + \frac{-\frac{136}{3} + \frac{40}{3}n_g}{\frac{22}{3} - \frac{4}{3}n_g - \frac{1}{6}N_H}\ln\left(\frac{\hat{\alpha}_2(m_S)}{\hat{\alpha}_2(m_W)}\right)$$

$$\left.\left. + \frac{\frac{4}{3}n_g}{-\frac{4}{3}n_g - \frac{1}{10}N_H}\ln\left(\frac{\hat{\alpha}_1(m_S)}{\hat{\alpha}_1(m_W)}\right)\}\right]\right. \qquad (13)$$

*The estimates given here do not include all Higgs contributions to the next to leading logs. There is an additional small contribution which has recently been calculated by D.R.T. Jones and quoted by D. Unger and Y.-P. Yao.[17]

$$\sin^2\theta_W(m_W) = \frac{3}{8}\Big[1 - \frac{110 - N_H}{18}\,\frac{\hat{\alpha}(m_W)}{\pi}\,\ell n\Big(\frac{m_S}{m_W}\Big) + \frac{5\hat{\alpha}(m_W)}{18\pi}$$

$$+ \frac{\hat{\alpha}(m_W)}{4\pi}\Big\{\frac{-\frac{16}{9}n_g}{11-\frac{4}{3}n_g}\,\ell n\,\Big(\frac{\hat{\alpha}_3(m_S)}{\hat{\alpha}_3(m_W)}\Big) + \frac{\frac{680}{9} - \frac{236}{9}n_g}{\frac{22}{3} - \frac{4}{3}n_g - \frac{1}{6}N_H}\,\ell n\Big(\frac{\hat{\alpha}_2(m_S)}{\hat{\alpha}_2(m_W)}\Big)$$

$$+ \frac{\frac{16}{9}n_g}{-\frac{4}{3}n_g - \frac{1}{10}N_H}\,\ell n\Big(\frac{\hat{\alpha}_1(m_S)}{\hat{\alpha}_1(m_W)}\Big)\Big\} \qquad (14)$$

Although they may look complicated, these formulas are actually very convenient for obtaining precise SU(5) predictions and examining their dependence on N_H and n_g.

Taking $n_g = 3$, $\hat{\alpha}_1(m_S) = 0.0243$ and the values for $\hat{\alpha}(m_W)$, $\hat{\alpha}_3(m_W)$ in Table I (also using $\hat{\alpha}_2(m_W) \simeq 0.037$ and $\hat{\alpha}_1(m_W) \simeq 0.0165$), one finds from Eq. (13)[1]

$$\frac{m_S}{m_W} = 6.5 \times 10^{12} \times 10^{-0.19(N_H-1)} \times (\Lambda_{\overline{MS}}/0.4\ \text{GeV})^{1.04} \qquad (15)$$

When this value for m_S/m_W is inserted in Eq. (14), one obtains the SU(5) prediction[1]

$$\sin^2\hat{\theta}_W(m_W) = 0.2083 + 0.004(N_H-1) + 0.006\ \ell n\Big(\frac{0.4\ \text{GeV}}{\Lambda_{\overline{MS}}}\Big) \qquad (16)$$

For $N_H \geq 1$ and $0.1\ \text{GeV} \leq \Lambda_{MS} \leq 0.6\ \text{GeV}$, this SU(5) prediction is in excellent agreement with the experimental average $\sin^2\hat{\theta}_W(m_W) = 0.215 \pm 0.012$ found after including radiative corrections;[8] a tremendous success for the SU(5) model.

Using $m_W = 38.5\ \text{GeV}/\sin\hat{\theta}_W(m_W)$ and the SU(5) estimate for the proton lifetime[9] (with $n_g = 3$)

$$\tau_p \simeq 10^{-28\pm1} \ (m_S \text{ in GeV})^4 \text{ yr} \qquad (17)$$

one finds from Eqs. (15) and (16)

$$\tau_p \simeq 9 \times 10^{30\pm1} \times 10^{-0.76(N_H-1)} \times (\Lambda_{\overline{MS}}/0.4 \text{ GeV})^{4.16} \text{ yr} \qquad (18)$$

Note that each increase in N_H by one Higgs doublet decreases the proton lifetime by a factor of 0.17 (if no other changes are made). Given the present experimental bound

$$\tau_p^{exp} \gtrsim 10^{30} \text{ yr.}$$

one sees that there cannot be too many light Higgs doublets in the SU(5) model, i.e. from Eq. (18) $N_H \lesssim 3$. For the minimum case $N_H = 1$, the SU(5) model's predictions as a function of $\Lambda_{\overline{MS}}$ are illustrated in Table II.

$\Lambda_{\overline{MS}}$ (GeV)	$\sin^2\hat{\theta}_W(m_W)$	m_W (GeV)	m_Z (GeV)	m_S (GeV)	τ_p (yr)
0.1	0.216	82.8	93.6	1.4×10^{14}	$4 \times 10^{28\pm1}$
0.2	0.212	83.6	94.2	2.7×10^{14}	$5 \times 10^{29\pm1}$
0.3	0.210	84.0	94.6	4.1×10^{14}	$3 \times 10^{30\pm1}$
0.4	0.208	84.4	94.9	5.5×10^{14}	$9 \times 10^{30\pm1}$
0.5	0.207	84.6	95.1	7.0×10^{14}	$2 \times 10^{31\pm1}$
0.6	0.206	84.8	95.3	8.5×10^{14}	$5 \times 10^{31\pm1}$

Table II

If any quantity in Table II is precisely measured, all the others are determined. The next generation of accelerators should measure m_W and m_Z with high precision. The values obtained will then be used to determine $\sin^2\hat{\theta}_W(m_W)$, $\Lambda_{\overline{MS}}$ and even the proton lifetime (within the SU(5) framework).

III. A Fourth Generation?

Is there a fourth generation of fermions? Some large GUTS based on SO(N) groups require an even number of generations, thereby suggesting at least a fourth generation. Mass sum rules in some dynamical symmetry breaking schemes[18] call for fermion masses $\gtrsim m_W$, implying the existence of new heavy fermions. In addition, to be able to account for the observed baryon asymmetry of the universe in the framework of SU(5) may require the introduction of at least a fourth generation.[19] Furthermore, there are no real arguments against a fourth generation*; hence we consider it a viable possibility. Indeed, its introduction may eventually shed light on the origin of CP violation and help provide us with a basic understanding of quark masses and mixing angles.

In this section we describe the effect of a fourth generation on the SU(5) predictions for $\sin^2\hat{\theta}_W(m_W)$ and τ_p. Calling the fourth generation members ν_E, E, U and D, we assume $m_E \approx 33$ GeV and $m_D \simeq m_W$. (These values simplify our analysis and seem reasonable; our results are rather insensitive to this specific assumption.) In a leading log approximation, our results are independent of m_U; however, one expects m_U to be near m_W. For these mass values $\hat{\alpha}_3(m_W)$ is unchanged while $\alpha^{-1}(m_W)$ decreases by 0.20 and $\hat{\alpha}_1(m_S)$ increases from 0.0243 to 0.0287. Using these numbers in Eq. (13), with $n_g = 4$, we now find [1,20]

$$\frac{m_S}{m_W} = 7.9 \times 10^{12} \times 10^{-0.19(N_H-1)} \times \left(\frac{\Lambda_{\overline{MS}}}{0.4\ \text{GeV}}\right)^{1.04} \qquad (20)$$

Comparing this result with Eq. (15), we see that adding a fourth generation increases the unification mass by about 20%. Inserting the expression in Eq. (20) into Eq. (14) (with $n_g = 4$) yields

$$\sin^2\hat{\theta}_W(m_W) = 0.2079 + 0.004(N_H-1) + 0.006\ \ell n(0.4\ \text{GeV}/\Lambda_{\overline{MS}}) \qquad (21)$$

*Even helium production within the framework of big bang cosmology is consistent with 4 distinct neutrino species.

A slight decrease of 0.0004 compared with the 3 generation prediction in Eq. (16), i.e. only a 0.2% reduction.

To obtain the proton lifetime prediction appropriate for the case of four generations, we must modify the usual SU(5) results in the following ways. Since $\hat{\alpha}_1(m_S)$ is larger for four generations, this effect reduces τ_p (which is proportional to $\hat{\alpha}_1^{-2}(m_S)$) by a factor of 0.72. Also, the one loop enhancements to the decay rate formulas are increased, which further reduces τ_p by a factor of 0.84. In total, we find for four generations, the prediction in Eq. (17) is modified to[1]

$$\tau_p \simeq 0.6 \times 10^{-28\pm1} \times (m_S \text{ in GeV})^4 \quad \text{yr} \qquad (22)$$

Inserting the value of m_S obtained from Eq. (20) into Eq. (22) gives

$$\tau_p \simeq 1.2 \times 10^{31\pm1} \times 10^{-0.76(N_H-1)} \times (\Lambda_{\overline{MS}}/0.4 \text{ GeV})^{4.16} \text{ yr} \quad (23)$$

Comparing this result with the 3 generation prediction in Eq. (18), we find that τ_p has increased overall by about 30%, not a very significant change (given the other uncertainties in τ_p).

In summary, going from 3 to 4 generations causes fairly insignificant modifications in the SU(5) model's predictions. (A fifth generation causes similar changes which can be easily obtained from Eqs. (13) and (14).) The existence of a fourth generation would have important implications for high energy accelerators. It will lead to a larger Z^0 width, a new charged heavy lepton, and a host of new hadrons. Heavy quarkonia states should be carefully searched for at facilities such as ISABELLE.

IV. Exotic Quarks, Technicolor??

Might there be very heavy hadronic matter formed as bound states of exotic quarks such as color sextets[21] or very strongly interacting techniquarks which bind by the hypothetical technicolor interaction[22] (or

one of the other equivalent schemes)? The existence of such non-standard quarks would imply a plethora of new hadrons waiting to be discovered at high energies. One or more of the members of this new spectrum of particles might even be stable (at least as stable as the proton); an exciting possibility. Furthermore, chiral symmetry breaking in the exotic (or techni) quark sector could provide a dynamical generation of $W^{\pm}$ and Z^0 masses and leave over many fairly light pseudo-Goldstone bosons (PGBs). Indeed, most technicolor scenarios[23] envision neutral and charged PGB's in the 5-50 GeV region. Can such new fermions be accommodated in the SU(5) model without destroying its prediction for $\sin^2\hat{\theta}_W(m_W)$? What would they imply for τ_p? Unfortunately, a viable technicolor GUT has not been found and color sextets have to be incorporated into SU(5) via rather large complicated fermion representations;[24] hence precise statements regarding modifications of the SU(5) predictions are not possible. We can unite (extended) technicolor and SU(5) in a semisimple way through the gauge group $SU(N_c') \times SU(5)$ (N_c' = number of technicolors). This involves adding N_c' new fermion generations to the SU(5) model which form a $SU(N_c')$ fundamental representation.[23] The consequences of such a scenario have been partly explored.[23] One finds[23] that such a theory has many PGB's below the technicolor mass scale of $\simeq 0.5 - 1$ TeV (where the techni-rho, eta, A_1 etc. reside).

Without considering a specific example, we can make the following general observations regarding the effects of new heavy exotic quarks on $\sin^2\hat{\theta}_W(m_W)$ and τ_p in the SU(5) model.

1) New generations of fermions which are approximately mass degenerate influence the SU(5) predictions mainly at the two loop level; hence as demonstrated in section III, they do not cause large modifications. We found that a new generation slightly reduces $\sin^2\hat{\theta}_W(m_W)$ and increases τ_p.

2) Introducing light (colorless) charged Higgs scalars has the opposite effect, $\sin^2\hat{\theta}_W(m_W)$ increases while τ_p is reduced. The dynamical symmetry breaking scenarios we are discussing do not have elementary scalars; however; the PGB's will effectively play the same role in a detailed renormalization group analysis. Hence, the two effects just

mentioned should occur and they will tend to cancel. Therefore, one may be able to populate the 100 GeV - 1 TeV region with lots of new exotic quarks (and their vast hadronic spectrum) without significantly altering the SU(5) predictions for $\sin^2\hat{\theta}_W(m_W)$ or τ_p. Of course, the above argument is mainly qualitative; specific models should be thoroughly checked by extending our renormalization group analysis in section II to each particular case (a straightforward exercise).

V. Summary

Given the present experimental value $\sin^2\hat{\theta}_W(m_W) = 0.215 \pm 0.012$, we find that the standard $SU(2)_L \times U(1)$ model predicts $m_W = 83.0 \pm 2.4$ GeV and $m_Z = 93.8 \pm 2.0$ GeV (including radiative corrections). If the $W^\pm$ and Z^0 are found to have these masses, it will mark a spectacular triumph for the standard model. Precise measurements of the $W^\pm$ and Z^0 decays will be very important. The total width of the Z^0 will provide us with the total number of neutrino species and if the Higgs mass m_ϕ is light, the decays $Z^0 \to \phi^0 + \mu^+ + \mu^-$ and $Z^0 \to \phi^0 + \gamma$ may be detectable. Verification or negation of the standard model should be the highest priority of the next generation of accelerators.

The Georgi-Glashow SU(5) model provides an elegant framework for unifying weak, electromagnetic and strong interactions. Its major success is the prediction of a value for $\sin^2\hat{\theta}_W(m_W)$ which is now in excellent agreement with experiment. Proton decay experiments will provide a crucial test of the SU(5) model's prediction that τ_p lies in the range $10^{30} \sim 10^{32}$ yr. Symmetry so constrains the parameters of this model, that a single precise measurement of one quantity (such as m_Z) provides values for many others, e.g. (for one light Higgs doublet)

$$\Lambda_{\overline{MS}} = 0.4 \text{ GeV } \exp[(m_Z - 94.9)/1 \text{ GeV}] \qquad (24)$$

Our analysis of the SU(5) model's dependence on the number of fermion generations indicates that its predictions are fairly insensitive to the addition of a fourth generation. Given the present proliferation of quark

and lepton species, the existence of a fourth generation would not be surprising. Experimentalists should be on the lookout for a new charged heavy lepton with mass > 18 GeV, new onia, and other new heavy hadronic matter.

Our present lack of a fundamental understanding of the origin of masses has given rise to much speculation regarding exotic new quarks.[21] If quark sextets exist, we can look forward to a totally new kind of heavy hadronic spectroscopy which may contain stable heavy particles. The technicolor scenario also envisions considerable new physics at around $0.5 \sim 1$ TeV accompanied by light PGB's which should be observable at ISABELLE. We have argued that incorporating new fermions into the SU(5) model may not significantly affect its predictions for $\sin^2\hat{\theta}_W(m_W)$ and τ_p.* Hence, even the staunchest SU(5) advocates should not be surprised by the discovery of a plethora of new very heavy hadron states.

The standard model has been very successful in accommodating low energy phenomenology; however it leaves too many questions (particularly regarding masses) unanswered. It can not be the complete story. Current speculation regarding technicolor has failed to overcome these theoretical shortcomings. Perhaps radical new ideas are needed. Multiply charged scalars or stable fractionally charged particles might be examples of radical new physics waiting to be uncovered. Hopefully, totally unanticipated discoveries will be made at ISABELLE and they will inspire the creativity of theorists.

---

*In some supersymmetric theories, $\sin^2\theta_W(m_W) \simeq 0.21$, but τ_p increases by several orders of magnitude and is rendered unobservable. Cf. F. Wilczek's talk in these Proceedings.

REFERENCES

1. For a more detailed discussion of the standard model see W. J. Marciano and A. Sirlin, Proceedings of the Second Workshop on Grand Unification, Ann Arbor, Michigan, April (1981).
2. A. Buras, Phys. Rev. Lett. 46, 1354 (1981).
3. H. Georgi and S. Glashow, Phys. Rev. Lett. 32, 438 (1974).
4. Cf. T. Kinoshita, in New Frontiers in High-Energy Physics edited by A. Perlmutter and L. Scott (Plenum Press, New York 1978) p. 127.
5. W. Marciano, Phys. Rev. D20, 274 (1979).
6. G. 't Hooft, Nucl. Phys. B61, 455 (1973).
7. J. Kim, P. Langacker, M. Levine and H. Williams, Rev. Mod. Phys. 53, 211 (1980); I. Liede and M. Roos, Nucl. Phys. B167, 397 (1980).
8. A. Sirlin and W. Marciano, "Radiative Corrections to $\nu_\mu + N \to \mu^- + X$ and their Effect on the Determination of ρ^2 and $\sin^2\theta_W$", to be published in Nucl. Phys. B.
9. W. Marciano and A. Sirlin, Phys. Rev. Lett. 46, 163 (1981).
10. C. Prescott et al., Phys. Lett. 77B, 347 (1978); 84B, 524 (1979).
11. W. Marciano and A. Sirlin, Proceedings of the VPI workshop on Weak Interactions as Probes of Unification (1980).
12. A. Sirlin, Phys. Rev. D22, 971 (1980).
13. D. Albert, W. Marciano, D. Wyler and Z. Parsa, Nucl. Phys. B166, 460 (1980).
14. W. Marciano and A. Sirlin, in Proceedings of the Cornell Z^0 Theory Workshop, edited by M. Peskin and S.-H. Tye, 1981, p. 40.
15. H. Georgi, H. Quinn and S. Weinberg, Phys. Rev. Lett. 33, 451 (1974).
16. Ref. 1 contains an extensive list of references on GUTS.
17. D. Unger and Y.-P. Yao, Univ. of Michigan preprint UM HE 81-30.
18. A. Carter and H. Pagels, Phys. Rev. Lett. 25, 43 (1979).
19. G. Segre and M. Turner, Phys. Lett. 99B, 399 (1981).
20. Similar results were independently obtained by M. Fischler and C. Hill, Fermilab-Pub-81/43-THY May (1981).
21. Cf. W. Marciano, Phys. Rev. D21, 2425 (1980).
22. S. Weinberg, Phys. Rev. D13, 974 (1976); 19, 1277 (1979); L. Susskind, ibid. 20, 2619 (1979).
23. M.A.B.Beg, H.D. Politzer and P. Ramond, Phys. Rev. Lett. 43, 1701 (1979); E. Eichten and K. Lane, Phys. Lett. 90B, 125 (1980); M. Peskin, Nucl. Phys. B175, 197 (1980); S. Dimopoulos, S. Raby and G. Kane, Nucl. Phys. B182, 77 (1981).
24. H. Georgi and S. Glashow, Nucl. Phys. B159, 29 (1979).

FNAL $\bar{p}p$ PROJECT

A. V. Tollestrup

Fermi National Accelerator Laboratory*

I. OVERVIEW

The Tevatron I project at Fermilab was approved and funded in FY 1981. This project calls for construction of a $\bar{p}p$ source capable of producing a luminosity of 10^{30} at center of mass energies of the order of 2 TeV or 3 ergs. In addition, provision was made for two experimental areas; one at B0 and the second at D0. A large detector is being constructed as a Laboratory facility at B0, and a workshop was held for the D0 area where a number of groups presented a wide range of proposals.

The time schedule for this facility is as follows:

1. Finish Saver installation during the period of June to December 1982. At present, well over half of the collared coils have been constructed. Cryostat production is at the rate of 12 per week, and the Magnetic Test Facility is measuring finished dipoles at a rate of 10 to 12 per week. These production rates are consistent with finishing the Saver from the schedule mentioned above.
2. Commission the Saver starting from CY 1983.
3. Construction of the assembly hall and collision hall from the fall of 1981 to the summer of 1983. The collision hall involves a penetration into the tunnel, and its construction will be synchronized with the final phase of Saver installation.
4. Construction of the Source starting in 1982 and finishing in 1984.

*Operated by Universities Research Association under Contract with the United States Department of Energy.

5. Detector construction from the present through 1984.

6. Commissioning the Source starting in the summer of 1984.

The schedule for the construction of D0 is still under discussion. In addition, studies have recently shown that it should be possible to bypass the main ring around the collision hall. The cost and the impact of this option on the program is being studied.

In this report, I will discuss the status of the Source, the collision hall, and the detector. Finally, I would like to compare the potential for colliding beam physics at the Tevatron with that of ISABELLE.

II. SOURCE

A detailed design for the Source has been presented in "The Fermilab Antiproton Source Design Report of June 1981." Here a design that generates $\bar{p}$'s at the rate of 7.9×10^9 per hour is presented. The $\bar{p}$'s are then cooled by longitudinal stochastic cooling. Next, they are decelerated, and the cooling is repeated. After three such cycles, the $\bar{p}$'s are injected into an accumulator ring where they are cooled in all three dimensions by electron cooling. After an elapsed time of 12.7 hours, 10^{11} $\bar{p}$'s have been accumulated. They have a $\Delta p/p$ of .1 percent and an emittance of 1π mm-mrad in each plane. The antiprotons are then formed into three bunches and reaccelerated to 1 TeV for colliding beam physics.

Many technical hurdles for the Source design have been overcome, and the projected luminosity of 10^{30} is realistic.

This proposal was reviewed in detail in June 1981 by a committee appointed by the Director. The conclusion of this committee was that the design was technically correct and could form a basis for our program. However, they also pointed out that the potential at FNAL was much greater than was being

exploited in the design and consequently urged the Laboratory to be more bold. They suggested that FNAL has a potential factor of 10 greater $\bar{p}$ production rate when compared to CERN, and that this could be achieved by use of techniques that have already been demonstrated. Using the previous work as a basis, a scheme along the lines suggested has been developed, and the complete design will be available before 1982 for an enhanced Source.

CERN is paving the way in this new technology. Many of the techniques they have developed are adaptable for use at FNAL. However, it is also true that there are vast differences between the two machines and that the potential resides at Fermilab for higher $\bar{p}$ production rates and higher luminosities. In addition, our biggest physics advantage is our higher collision energy.

III. DETECTOR

The detector is being built as a facility at Fermilab and will be installed in a collision hall at B0. The group at present consists of six universities: University of Chicago, University of Illinois, Harvard University, Purdue University, Texas A&M University, and University of Wisconsin. In addition, there are three national laboratories: Fermi National Accelerator Laboratory, Argonne National Laboratory, and Lawrence Berkeley Laboratory. Finally, we have collaborators from Italy (Frascati and University of Pisa) and Japan (KEK and University of Tsukuba). In addition, valuable help has been received from the California Institute of Technology. An overall view of the detector is given in Figs. 1 and 2. This detector covers an angular region from 2° to 178° in the laboratory system. The central magnetic detector covers the region from 10° to 170° and will roll in and out of the collision hall as a unit. The detectors covering 2° to 10° and

170° to 178° consist of toroids with tracking and hadron/electron calorimetry and will be assembled in their respective areas by means of transfer carts that are designed to move large pieces of equipment between the assembly hall and the collision hall.

The central detector consists of tracking chambers around the beam pipe and a 1.5 Tesla axial field produced by superconducting solenoid. Next in radius are electron calorimetry, hadron calorimetry, and finally muon tracking chambers.

Extensive model tests have produced a design for the electron and hadron calorimeters for this detector, and construction of these components is now underway. Model tests of the solenoid have been successfully carried out in Japan, and final design is now underway. Design and construction of prototypes for the tracking chambers is also underway.

A brief description of the design principles used for this detector is now given. The rapidity interval covered by 2 TeV pp collisions is -7.6 to +7.6. High p_T jets (100 GeV) and massive particles have a more restricted region in rapidity. Our detector will cover the region from 2° to 178° or $-4 < y < 4$.

The calorimetry of the central detector is divided into towers such that the granularity is about .1 units in y and 15° in $\Delta\phi$. There is some interpolation in $\Delta\phi$ because each tower is read out by means of two independent phototubes. These tubes look at the two edges of the scintillator plates in constant ϕ planes, and hence the ϕ resolution will be better than the 15°. Early studies were carried out using as a model the decay of a heavy quark of mass 50 GeV. This quark was assumed to decay into three jets, and the granularity of the calorimeter was investigated in order to determine

how many cells were necessary to reconstruct the individual jets and obtain the mass of the parent quark. These studies indicated that 500 or more cells in the region of $\theta = 45^{o}$ to 135^{o} would be sufficient to resolve the jet structure and measure mass. Fewer cells could reconstruct the mass of the parent quark but would lose the substructure. This then fixed the granularity in the central region. Fig. 3 shows the mass spectrum expected from a calorimeter with 640 elements in the central region.

The end plugs as well as the forward calorimeters will utilize gas calorimetry with cathode pads for readout. This choice was dictated by the very difficult mechanical and magnetic problems encountered in this region as well as the requirement for increased spatial resolution. The gas calorimetry provides for greater flexibility of readout than scintillator technology does.

In the forward and backward region, the hadron shower size becomes large enough so that the resolution in both Δy and $\Delta\phi$ is reduced. Hence, at angles less than 10^{o}, the calorimeters are moved further from the interaction points so that a typical QCD jet can still be resolved. Fig. 4 shows the resolution of the calorimetry in ϕ and y with typical QCD jets superimposed.[2]

Extensive studies were made of requirements for a magnet and the direction of its field. The reason for a field are diverse but when taken together, become decisive. Some of these are:

1. Increased information about particle charge in new and unexpected phenomena.
2. Enhanced πe separation.
3. Muon momentum measurement.

4. Help in ascertaining and maintaining the calibration of the calorimeters.

5. Asymmetries expected in some decays requires knowledge of the μ or e sign.

6. Enhanced momentum measurement of low momentum particles.

A solenoid was chosen because of its ease of construction and integration into the machine. It does not sweep particles from the leading beam jets into the detector and in addition, there is a large amount of experience and expertise in the physics community with tracking for this geometry. It obviously fails to provide information below about 30°, and so this region will be covered by magnetized iron toroids which will measure the momentum of muons in this angular region.

This completes a rather cursory description of the detector. A more complete description will be available shortly from Fermilab in the form of the CDF Detector Design Report. The design of the calorimetry has been intensively pursued during the last year, and agreements are now being drafted for construction of the various components. The construction will take place largely over the three year period from 1982 to 1984 and will be closely coordinated with the construction of the $\bar{p}$ Source.

IV. COLLIDING AREAS

There will be two colliding areas available for $\bar{p}p$ experimentation; one at B0 and a second at D0. The detector just described will go in the area at B0 and will be a major Laboratory facility. The Director has issued a call for proposals for the D0 area, and the detailed developments of plans for this facility will be heavily dependent upon the proposals that are

received. The B0 assembly hall and collision hall are nearly complete and ready for Title I approval, and we wish to have the Title II ready by October.

Figs. 5 and 6 show a view of the collision hall and the assembly hall as well as the support area. The first two are nearly 40 ft. below ground level while the support area is at the surface.

The collision hall consists of a region of a length 100 ft. Its width varies as shown. The central region is slightly deeper and provides a nearly cubical space 50 ft. x 50 ft. and 40 ft. high for housing the central detector which can move in and out. The two smaller halls in the forward and backward region contain magnetized iron toroids and electron and hadron calorimetry. A bypass is provided around the outside of this region for servicing the main ring in the Tevatron. The floor is a concrete pad 4 ft. thick in order to support the weight of the detector elements. The assembly hall is located parallel to the collision hall and separated from it by a tunnel in which a retractable shielding door is placed, which when removed from the tunnel can be stored at either side in the assembly hall. The assembly area is covered by a 50 ton crane, and in addition, transfer carts will be provided to move heavy equipment from the assembly area into the forward and backward collision halls. The floor level not occupied by the transfer carts or the central detector is raised 4 ft. in order to facilitate work on the detector and its components and to facilitate support of the components in the forward and backward halls. The building at ground level will provide adequate room for assemblying the smaller components of the detector. Fig. 7 shows an outline of the B0 area and with the same scale, the CERN UA1 Pit and the BNL Major Facility 8.

In addition to the support, the assembly, and the collision areas, this building will contain a fixed electronics house for the detector. The cabling problems presented by this decision as well as the division of the electronics between the detector and the electronics house has not yet been resolved. A $\bar{p}$ source with a high production rate will obviously make it more practical to obtain access to components of the detector within the collision hall during running. Placing more of the electronics immediately at the detector simplifies the cabling but increases the need for highly reliable electronics.

A large detector such as has been described here is obviously a very versatile instrument for physics. However, there are many regions where it has obvious deficiencies. For this reason and for the reason that Fermilab desires an increased user participation in its $\bar{p}$ colliding beam program, a second collision area will be provided. The Director has called for proposals for experiments in this area. The area will not accommodate a major facility such as we have been describing but will be dedicated to more highly specialized experiments that supplement the major facility. The design of this area iwll be influenced by the proposals that are received and approved by the PAC.

V. BYPASS

An examination of all of the detector drawings shows the main ring beam pipe passing through the detector 25 in. above the Tevatron center line. This obviously poses difficulties for all of the detector elements that the main ring beam must pass through. A configuration of the main ring that would allow it to bypass the collision hall has been sought for a long time. It has recently become clear that such a configuration for the main ring

exists and that the main trick is to bend the main ring in the vertical direction to pass over the collision hall.[3] In order to keep the path length fixed in the main ring, the orbit must move to a slightly smaller radius. The details of various schemes are now being carefully examined and evaluared. Since such a bypass may be as long as 1,500 ft., it will involve considerable expense and additional engineering in the main ring runnel. It is unlikely that such a bypass could be installed before the Source is commissioned. However, the ultimate opportunity to remove the main ring from interference with the detector is an exciting prospect.

VI. PHYSICS

Inevitably, the physics capability of ISABELLE pp collisions at less than 800 GeV in the center of mass system will be contrasted with the $\bar{p}p$ colliders. In particular, this question will arise in trying to evaluate the proposed[4] Phase I ISABELLE (using FNAL magnets) with a luminosity of 2.7×10^{31}. The ultimate outcome of this discussion will have to consider problems of funding, politics, and physics. However, here I would like to restrict these remarks to physics and technology.

The $W^{\pm}$ and the Z^{o} will probably have been discovered at CERN by the time either ISABELLE or TeV I is operational. It is also true that the fundamental properties of the Z^{o} are better studied in an $e^{+}e^{-}$ machine such as LEP. In the past, physicists have been extremely successful in deducing the fundamental properties of a particle from a very small number of events. It is not productive to argue about the relative numbers of these particles that will be produced per hour at the various machines. A better comparison is given by a set of curves that compares colliders in terms of the luminosity

of quark-quark collisions.[5] Thus, the interaction rate for any given channel can be computed from these luminosity curves times the fundamental cross section. It forms an easy way to compare various machines. Clearly, qq interactions will be enhanced in pp collision, and $\bar{q}q$ interactions will be suppressed. The gg interactions are relatively insensitive to the type of particles. Curves from Ref. 5 are presented in Figs. 8 through 10, and they incorporate the scaling violations as calculated by QCD. (It is useful to make transparencies of these curves so that they may be compared for different machine energies and luminosities.)

It is seen that at the same luminosity, CERN $\bar{p}p$ and ISABELLE pp are essentially equivalent. However, a comparison of TeV I shows that for W = 100 GeV, a factor of 10 lower machine luminosities leaves TeV I equal to ISABELLE, and for W greater than 200 GeV, TeV I is superior even for a ratio of 100 in basic luminosity. These curves display the enormous leverage that energy has over luminosity in the search for high mass states.

The remaining figures show the results of calculations for high p_T jets, single π^o, single γ, and $W^{\pm}$ or Z production. For instance, at a p_T of 100 GeV/c, there is a factor of 100 difference in the jet cross section between $\sqrt{s}$ = 2000 and $\sqrt{s}$ = 500 for jets.

In summary, it is clear that any comparison between ISABELLE and the $\bar{p}p$ machines must take into account the following:

1. The intermediate vector boson will have been discovered. Comparing machines by comparing W production rates is not meaningful. CERN will have had too long a lead time.
2. $\bar{p}$ source technology is new and advancing rapidly. A luminosity equal 10^{31} is realistic to achieve.

3. The higher energy of TeV I gives it an advantage of approximately 100 or more for high p_T states.

From the above considerations, it appears that a machine with a Phase I luminosity of 2.7×10^{31} may be marginal in its appeal.

These considerations are offset by the fact that at ISABELLE there will be more than two interaction regions and that the machine is a dedicated facility. Furthermore, at the luminosities quoted for Phase I, the beam-beam tune shift is not large, and one is not making a big extrapolation into regions of unknown machine stability. Until the luminosity is raised, the problem of multiple interactions in a beam bunch does not seem serious.

The above is a summary of the colliding beam program at FNAL. CERN is aggressively pushing their own programs. ISABELLE will be born into a very competitive environment - one of new technologies that are advancing rapidly.

These considerations plus others such as funding, access of the university community to facilities, and the support and development of new accelerator technology will have to guide the future of ISABELLE.

REFERENCES

1. A Longer Note on Top Quarks, G. Fox and L. Romans, FNAL Pub. CDF-70. Also, private communication, Irwin Gaines.
2. CDF Design Report.
3. Private Communication, T. Collins. Also, D. Johnson and R. Huson.
4. Preliminary Report of the Task Force to Study the Possibility of Using Fermilab Magnets in ISABELLE, BNL, June 12, 1981.
5. Comparing Collider Capabilities, C. Quigg, FNAL Pub., July 8, 1981.

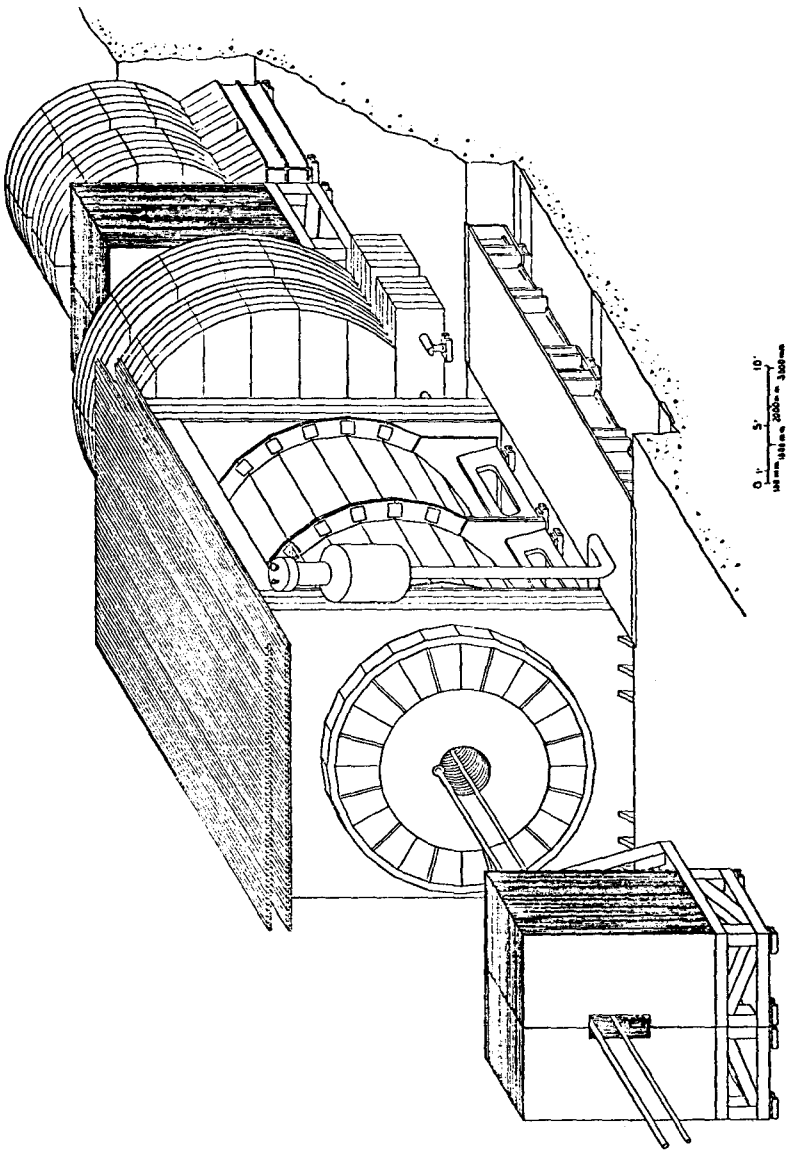

Fig. 1

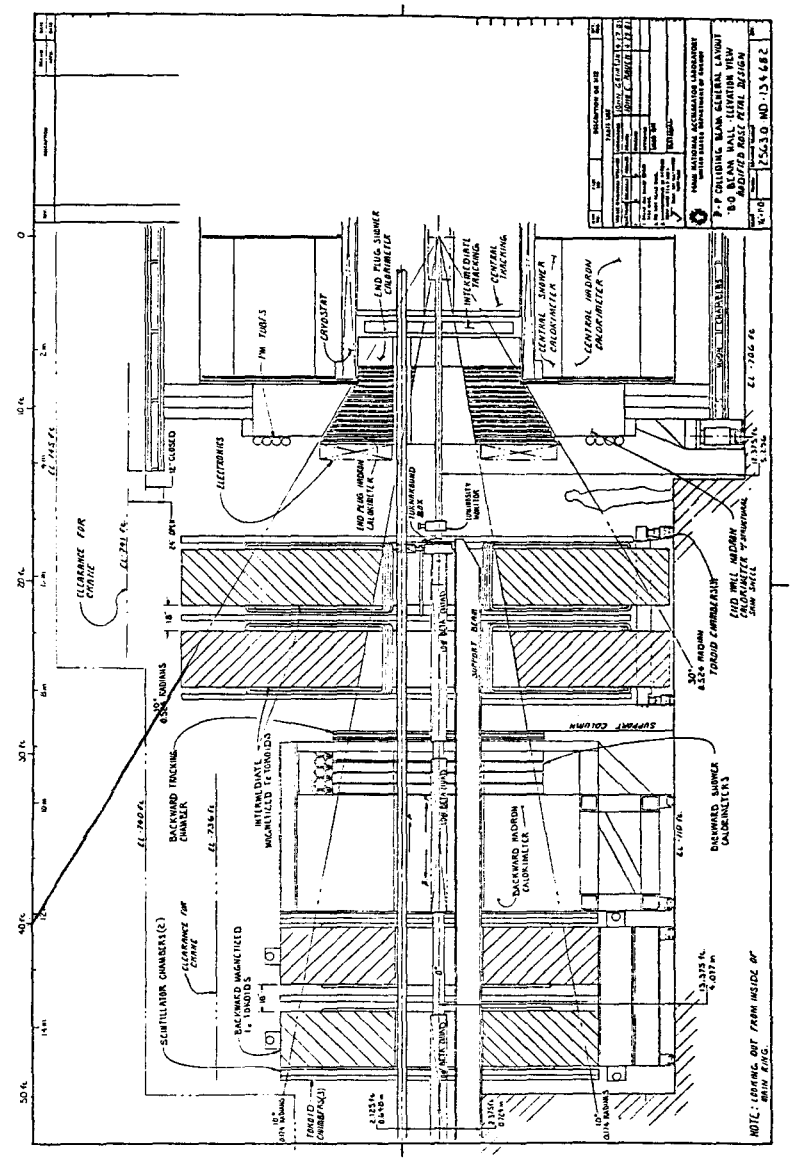
CLEARANCE FOR CRANE
BACKWARD TRACKING CHAMBER
SCINTILLATOR CHAMBERS(2)
BACKWARD MAGNETIZED IRON TOROIDS
TOROID CHAMBERS(2)
INTERMEDIATE MAGNETIZED IRON TOROIDS
SUPPORT BEAM
SUPPORT COLUMN
BACKWARD HADRON CALORIMETER
BACKWARD SHOWER CALORIMETERS
END WALL HADRON CALORIMETER
STEEL SHELL
TOROID CHAMBERS
CRYOSTAT
END PLUG SHOWER CALORIMETER
INTERMEDIATE TRACKING
CENTRAL TRACKING
CENTRAL SHOWER CALORIMETER
CENTRAL HADRON CALORIMETER
ELECTRONICS
END PLUG HADRON CALORIMETER
COLUMBIA MONITOR
P-P COLLIDING BEAM GENERAL LAYOUT
'80 BEAM WALL - ELEVATION VIEW
MODIFIED BASE METAL DESIGN
NOTE: LOOKING OUT FROM INSIDE OF MAIN RING

Fig. 2

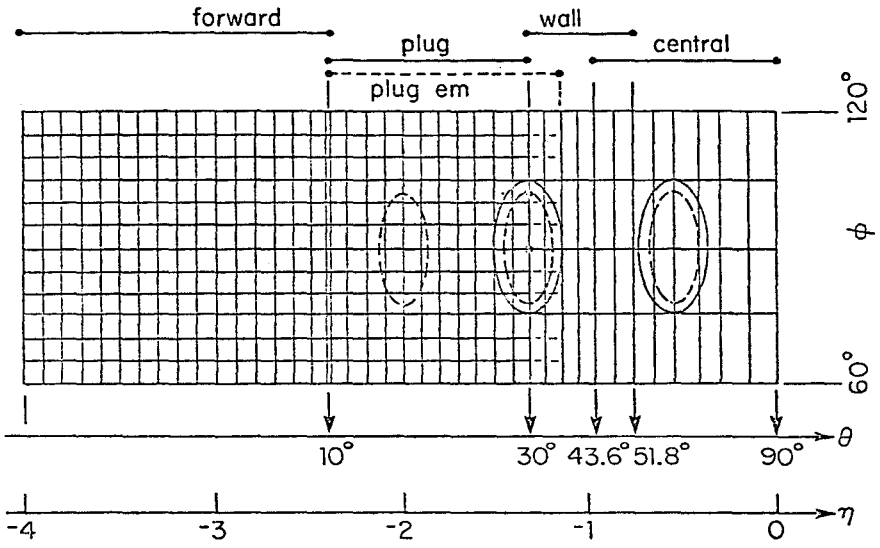
forward
plug
wall
central
plug em
120°
φ
60°
θ
10°
30°
43.6°
51.8°
90°
η
-4
-3
-2
-1
0

Fig. 3

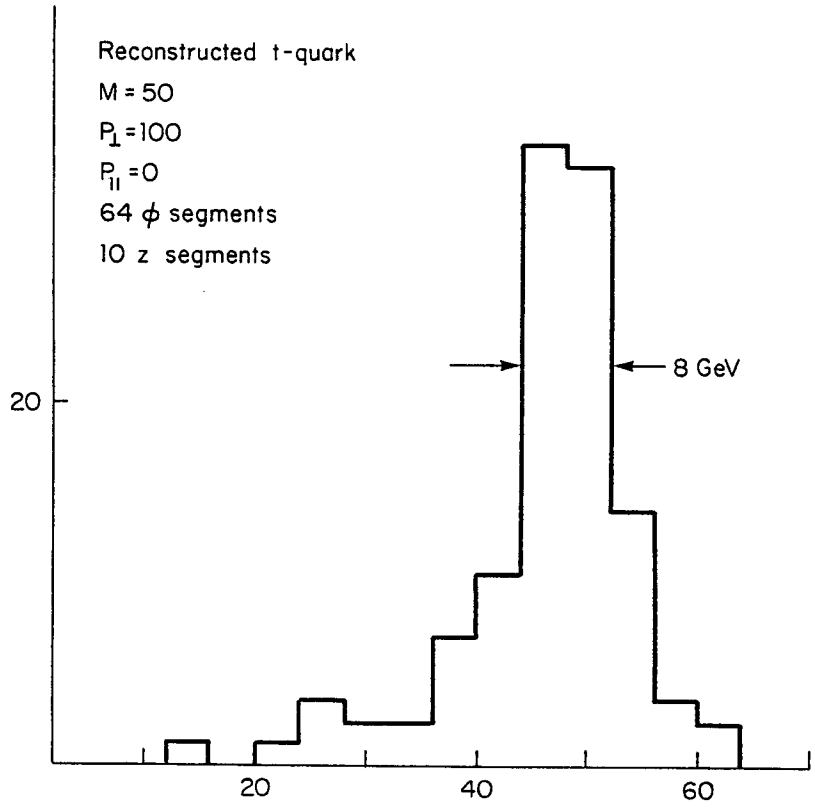
Reconstructed t-quark
M = 50
$P_\perp$ = 100
$P_{||}$ = 0
64 ϕ segments
10 z segments
8 GeV
20
20
40
60

Fig. 4

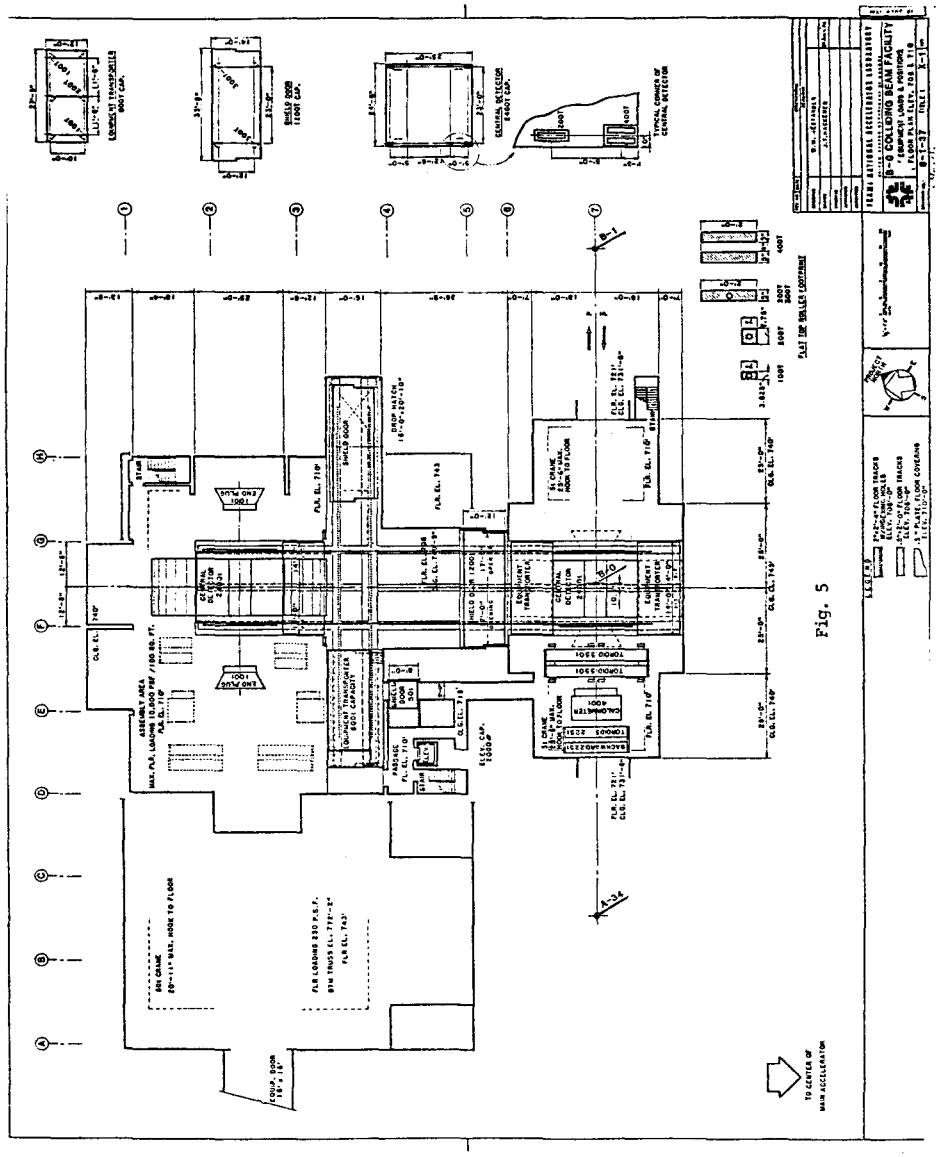

Fig. 5

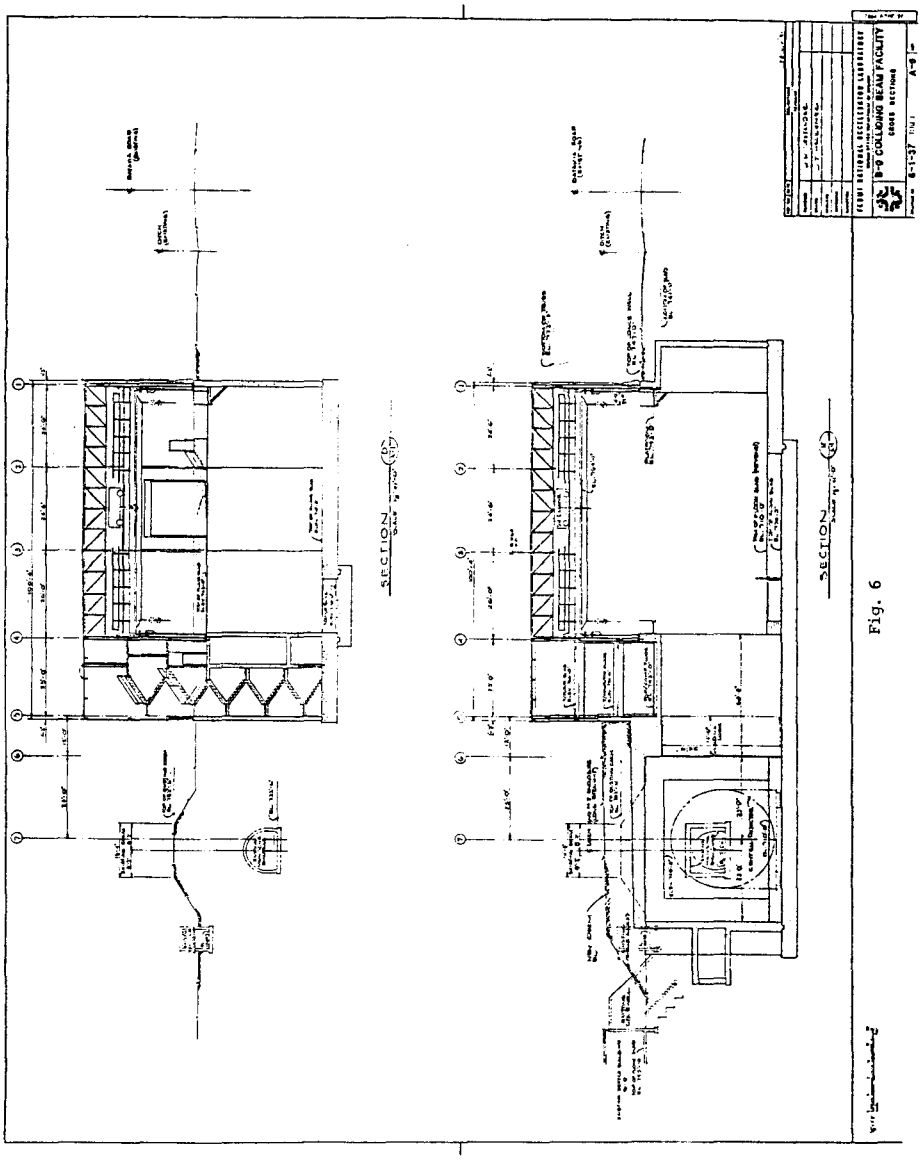

Fig. 6

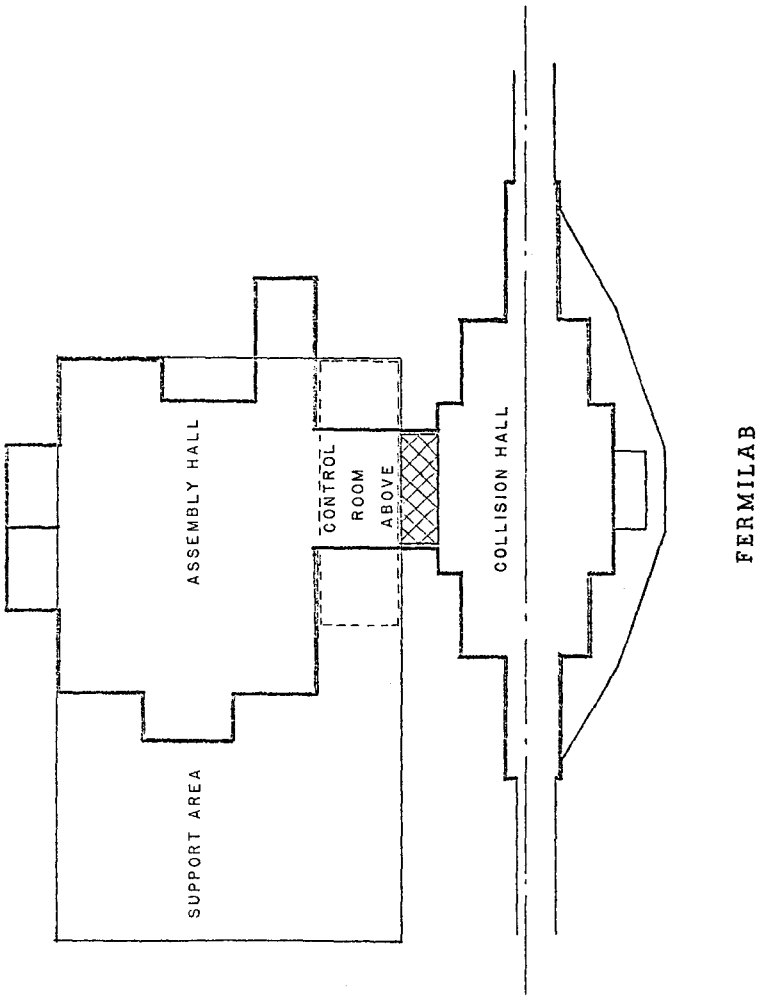
ASSEMBLY HALL
CONTROL ROOM ABOVE
COLLISION HALL
SUPPORT AREA
FERMILAB

Fig. 7a

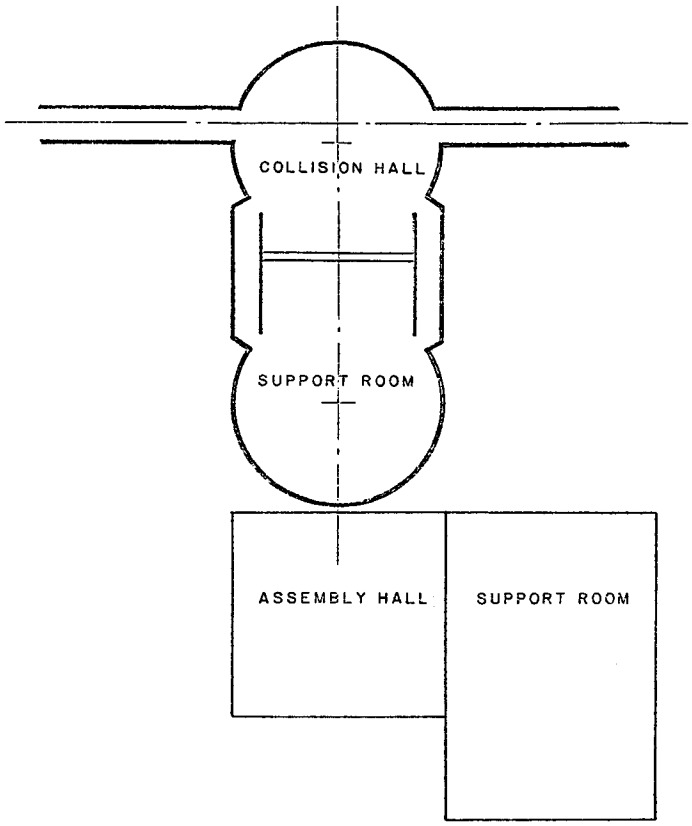

CERN

Fig. 7b

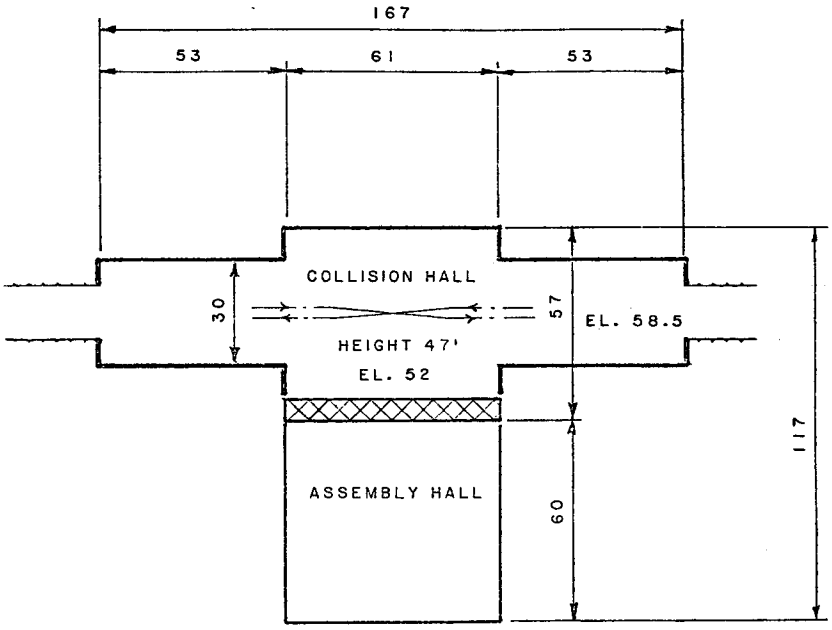

B N L

MAJOR FACILITY 8

Fig. 7c

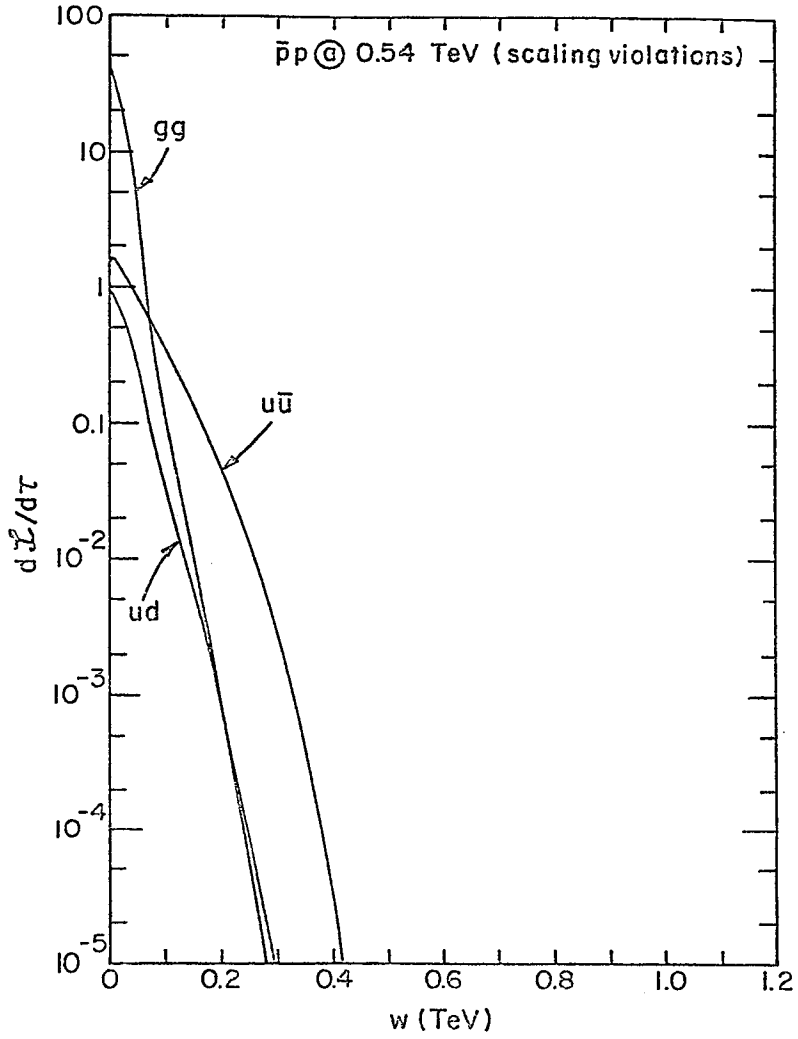
$\bar{p}p$ @ 0.54 TeV (scaling violations)
gg
$u\bar{u}$
ud
$d\mathcal{L}_p/\mathcal{L}_p$
w (TeV)
100
10
1
0.1
10^{-2}
10^{-3}
10^{-4}
10^{-5}
0
0.2
0.4
0.6
0.8
1.0
1.2

Fig. 8

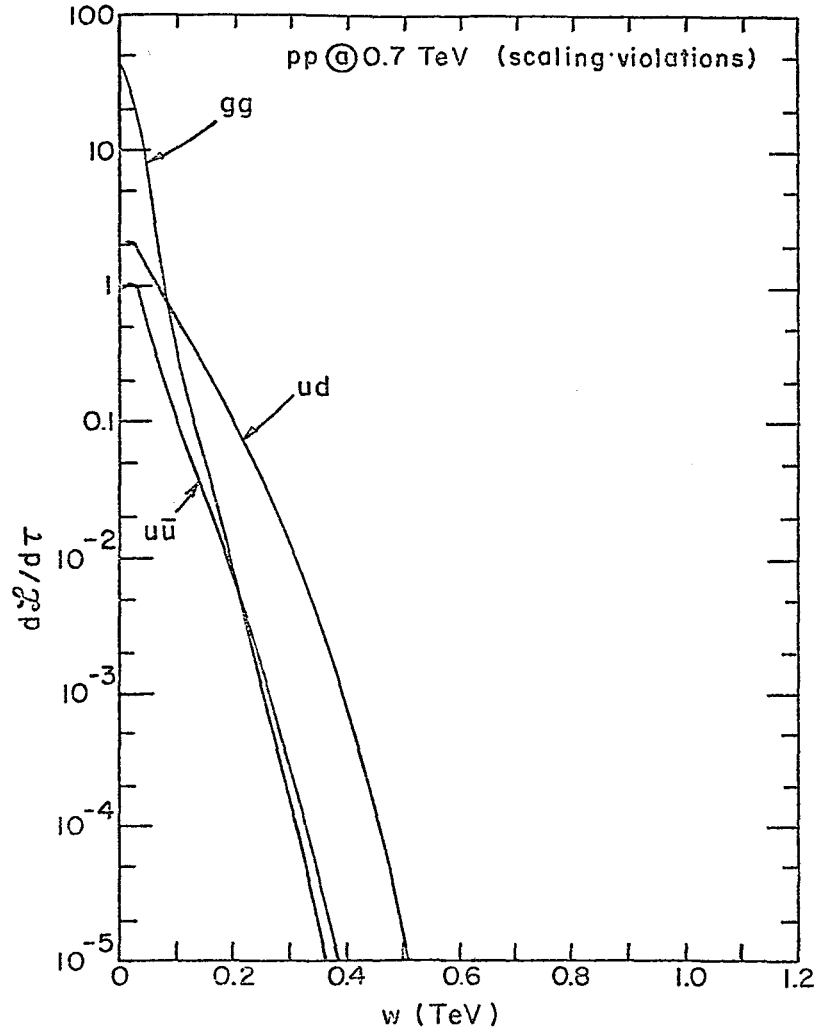
pp @ 0.7 TeV (scaling violations)
gg
ud
$u\bar{u}$
$\tau\, d\mathcal{L}_{pp}/d\tau$
100
10
1
0.1
10^{-2}
10^{-3}
10^{-4}
10^{-5}
0
0.2
0.4
0.6
0.8
1.0
1.2
W (TeV)

Fig. 9

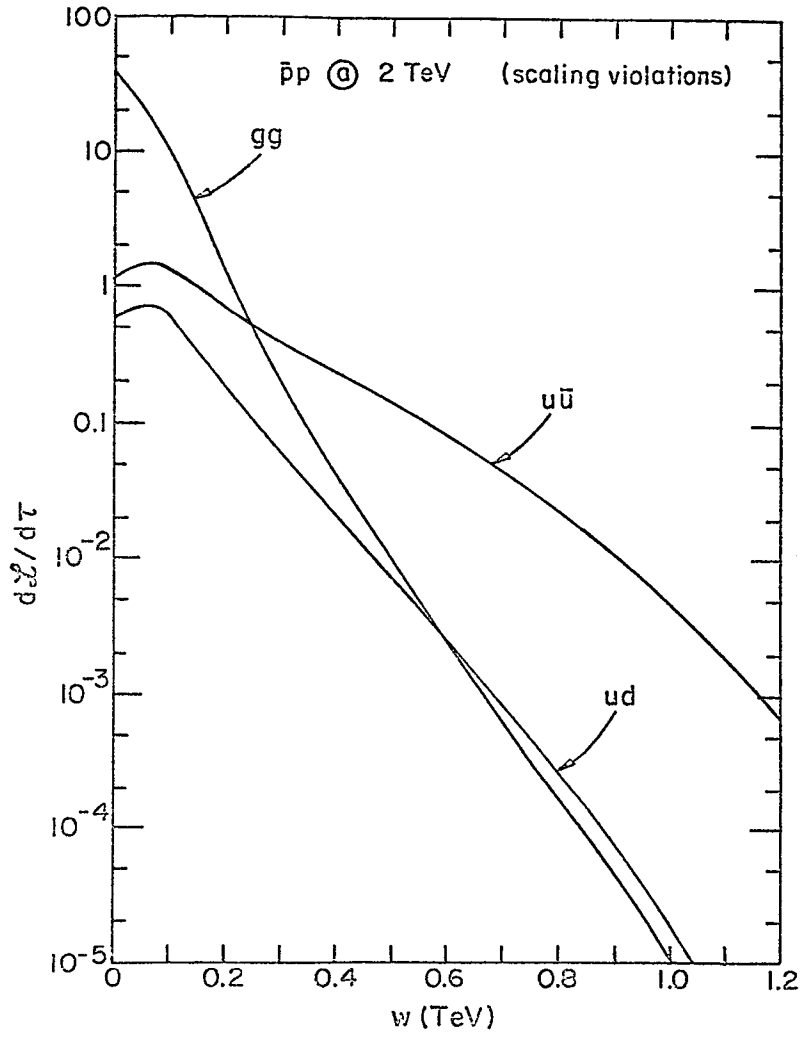
100
10
1
0.1
10^{-2}
10^{-3}
10^{-4}
10^{-5}
$d\mathcal{L}/d\tau$
$\bar{p}p$ @ 2 TeV (scaling violations)
gg
$u\bar{u}$
ud
0
0.2
0.4
0.6
0.8
1.0
1.2
W (TeV)

Fig. 10

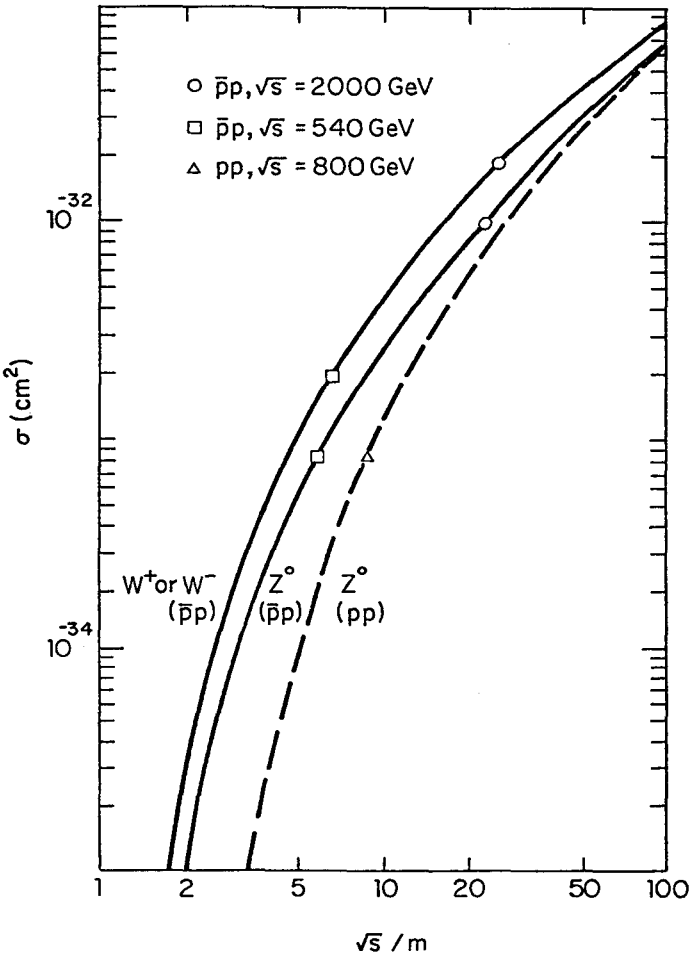
o p̄p, √s = 2000 GeV
□ p̄p, √s = 540 GeV
△ pp, √s = 800 GeV
10^-32
10^-34
σ (cm²)
W⁺ or W⁻ (p̄p)
Z° (p̄p)
Z° (pp)
1
2
5
10
20
50
100
√s / m

Fig. 11

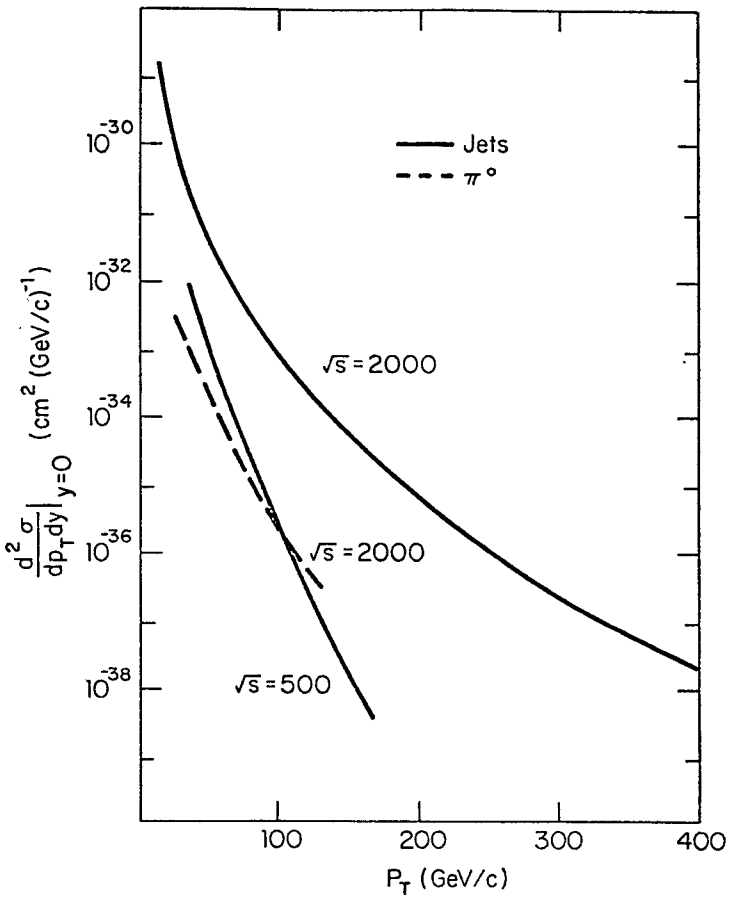
Jets
π°
√s = 2000
√s = 2000
√s = 500
10^{-30}
10^{-32}
10^{-34}
10^{-36}
10^{-38}
$\frac{d^2\sigma}{dp_T dy}\Big|_{y=0}$ (cm² (GeV/c)⁻¹)
100
200
300
400
P_T (GeV/c)

Fig. 12

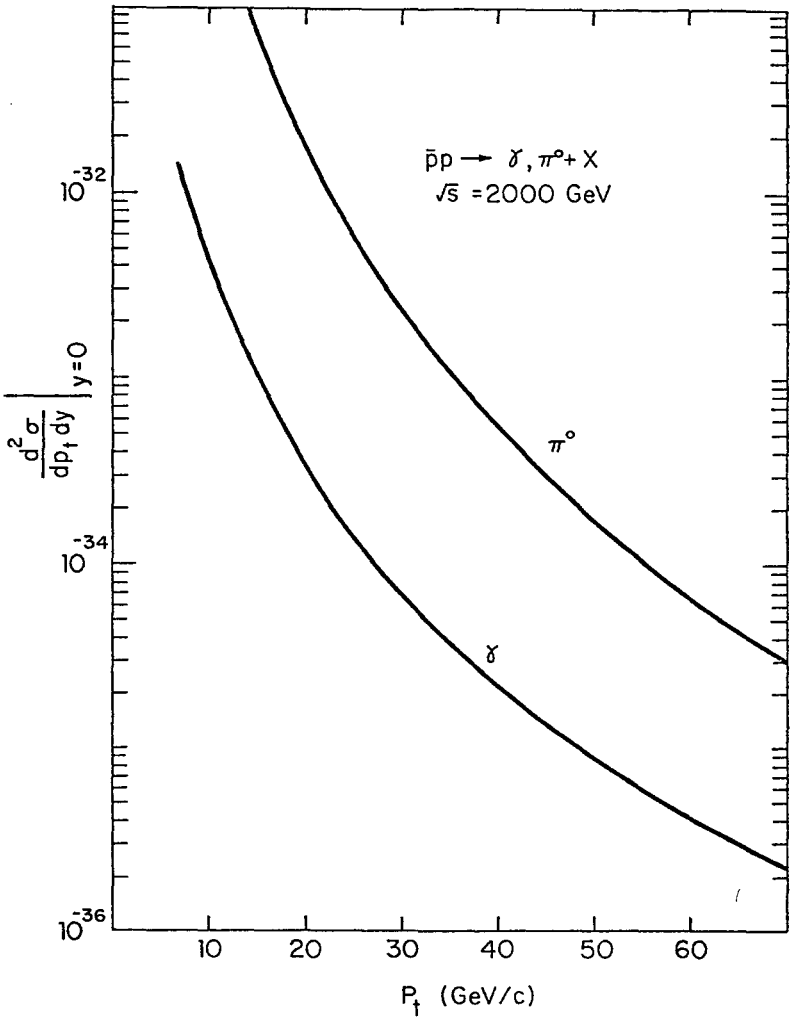
$\bar{p}p \rightarrow \gamma, \pi^0 + X$
$\sqrt{s}$ =2000 GeV
π^0
γ
$\frac{d^2\sigma}{dp_t dy}\Big|_{y=0}$
10^{-32}
10^{-34}
10^{-36}
10
20
30
40
50
60
P_t (GeV/c)

Fig. 13

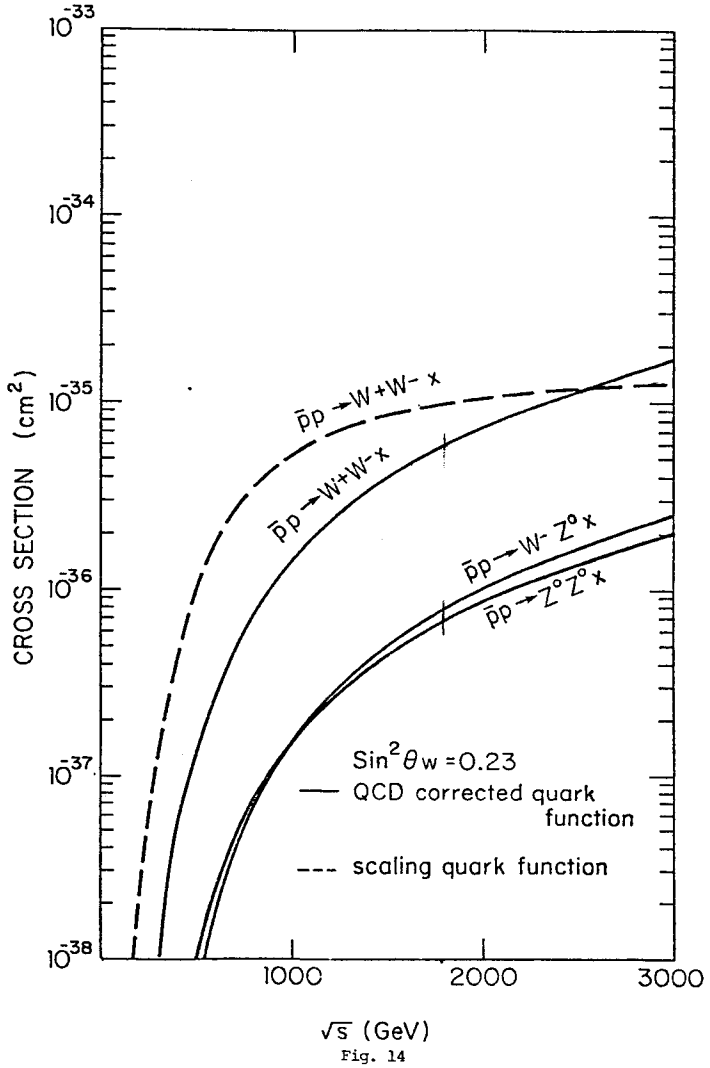
CROSS SECTION (cm²)
10⁻³³
10⁻³⁴
10⁻³⁵
10⁻³⁶
10⁻³⁷
10⁻³⁸
p̄p → W⁺W⁻ x
p̄p → W⁺W⁻x
p̄p → W⁻ Z⁰x
p̄p → Z⁰Z⁰x
Sin²θw = 0.23
QCD corrected quark function
scaling quark function
1000
2000
3000
√s (GeV)

Fig. 14

THE ep OPTION AT ISABELLE

R. R. Wilson, W. Lee, S. Holmes
Columbia University

Editors' Note: Professors R. R. Wilson, W. Lee, and S. Holmes gave very instructive and promising lectures on the ep options at ISABELLE. Please see the report of Group VIII on "High Energy ep Physics", p. 655-737.

AFTER DINNER SPEECH AT THE ISABELLE WORKSHOP

C.N. Yang
SUNY, Stony Brook

These are difficult times for our field.

I was recently visiting Japan where I spent a day at the KEK. Ozaki and Takahashi, old friends from Brookhaven and Stony Brook showed me around. They explained to me that they are planning to build Tristan, and that they have enough money but not enough experimental physicists. Later on while giving a seminar, I started by saying that their laboratory has a unique problem among the high energy laboratories in the world today, that of how to spend a lot of money while everyone else has shrinking budgets.

The workshop which will conclude tomorrow has been a useful and necessary one. Many new ideas about the Isabelle accelerator and about experimental and theoretical physics for Isabelle were discussed. Options were analyzed in detail and argued out. All of these are important for planning the detailed steps to be taken with respect to this important machine and the physics projects associated with it. At this time of budgetary difficulties such detailed discussions are not only useful but absolutely necessary.

Having said all this, however, I would like to emphasize that if history is to repeat itself, then the most important physics to come out of Isabelle is likely to be in areas that were not discussed at this workshop, in areas that could not possibly be discussed at this workshop. Experience has told us that every time high energy physicists move into a new domain of experimentation, almost invariably important and oftentimes profound new physics are opened up in directions that were not foretold at the time of planning for these new domains of experimentation.

Let me start with a negative example. In the year 1898 A.A. Michaelson wrote in the University of Chicago's catalog:

> "While it is never safe to affirm that the future of Physical Science has no marvels in store even more astonishing than those of the past, it seems probable that most of the grand underlying principles

> have been firmly established and that further advances are to be sought chiefly in the rigorous application of these principles to all the phenomena which come under our notice. An eminent physicist has remarked that the future truths of Physical Science are to be looked for in the 6th place of decimals."

It is perhaps not pointless to remind ourselves of the folly of Michaelson's statement, since there are a number of colleagues who seem to think today that the underlying principles of fundamental physics are all firmly in hand.

To take more recently examples, in the late 1940s when the Berkeley Cyclotron was being constructed, the feeling was that it would make possible experiments which would tell us the forces between nucleons. Once those forces were known, it was thought the whole of nuclear physics would be cleaned up. As we all know, that was not the contribution that the Berkeley Cyclotron eventually made to physics. In fact, a complete understanding of nuclear forces is still not in sight today. Next came the Cosmotron and the Bevatron. The main contributions of these two machines, which really started the discipline of high energy physics, were not envisaged at the time of their construction. For example, no one foresaw the large number of resonances discovered with the Bevatron at the time that it was being planned. If we next think about the AGS and the PS, we find that the most important contributions by these two machines: the two-neutrino experiment, the discovery of Ω^-, of CP violations, of neutral currents, of J/ψ, were all beyond the scope of deliberation at the time these machines were under construction. The same is also true of SPEAR.

Let me repeat, history has told us over and over again that whenever a new domain of experimentation is opened up for high energy physics, then with overwhelming probability, the most important discoveries to be made are not foreseen at the time of the planning of the new domain of experimentation.

In 1964, Luke Yuan of Brookhaven asked about thirty physicists to write short articles concerning the prospects of high energy physics. I was one of them. The articles were all written after serious deliberations. Rereading them today what is striking is that no one had foreseen what the physics of the 1970s was to be like.

Perhaps the most interesting passage in that collection of articles was in Julian Schwinger's "The Future of Fundamental Physics." Let me read this passage to you to conclude my short talk. Schwinger was discussing the importance of continuing research in high energy physics. He said:

> "And one should not overlook how fateful a decision to curtail the continued development of an essential element of the society can be. By the Fifteenth Century, the Chinese had developed a mastery of ocean voyaging far beyond anything existing in Europe. Then, in an abrupt change of intellectual climate, the insular party at court took control. The great ships were burnt and the crews disbanded. It was in those years that small Portuguese ships rounded the Cape of Good Hope."

Chen Ning Yang

A PERSONAL VIEW OF THE ISABELLE PROJECT

Samuel C. C. Ting

Massachusetts Institute of Technology

I. INTRODUCTION

One of the most important tasks an experimental physicist has is to select the right experiment to perform at the right accelerator at the right time. In the next ten years, the high energy physics community will be fortunate to have opportunities to work on (a) the 100 GeV e^+e^- colliding beam accelerator in Geneva, Switzerland, known as LEP, (b) a 2 TeV $p\bar{p}$ collider at FNAL, or (c) the high intensity 800 GeV proton-proton collider, ISABELLE.

The principal physics interests for LEP would be the study of Z^0 physics, which includes the counting of neutrinos, the searching for Higgs, and the measuring of the weak angle, $\sin^2\theta_w$. LEP will also be useful in the search for new quark-antiquark states such as toponium. Experiments on strong interactions off resonance are very difficult to perform. This is because the hadron production cross section is very small at $\sqrt{s} \sim 100$ GeV. It would be difficult to obtain more than a few hundred hadron events per year at LEP.

The $p\bar{p}$ collider at Fermilab will certainly explore some of the strong interaction physics at TeV regions and will be more competitive than the CERN $p\bar{p}$ collider at 540 GeV. However, because of the luminosity limitations it perhaps will not have the capacity to search for new particles much beyond 100 GeV mass.

The principal physics interest at ISABELLE would be the utilization of its high luminosity to search for new, unpredicted phenomena, thus making a fundamental advance in our understanding of particle physics.

II. HISTORICAL PERSPECTIVE

In the past, the physics of e^+e^- accelerators and proton accelerators have played complementary roles. Some of the major discoveries produced from these two types of machines are summarized in Table I. I want to review the results from the presently highest-energy machine of each type.

A. Recent Results from the ISR

Some of the most notable results from the ISR include the rising total cross section, the discovery of high p_T physics, the observation of lepton pairs, and the observation of single photon production.

The mass spectrum of the electron pair experiment by Willis, Palmer and collaborators is shown in Figure 1. This figure indicates that a) one can perform a high statistics e^+e^- experiment in a large solid angle detector on proton-proton colliders, and b) had one been given the opportunity to perform this experiment earlier, both the J and the T particles could have been easily discovered.

The results of the μ-pair experiment by Becker, Braccini et al., are shown in Figures 2, 3, 4. Figure 2 shows that the measured cross section exhibits clear scaling behavior between $\sqrt{s}$ = 44 and 62 GeV and is within a factor 1.6 of the standard Drell-Yan prediction. This factor 1.6 can be explained from QCD corrections. Figure 3 shows the measured $x = p_{||}/p_{max}$ distribution as a function of μ-pair mass. Figure 4 shows the measured average p_T as function of $\sqrt{s}$ compared with QCD model predictions. It shows good agreement between the data and the model.

The result of a very important direct photon experiment is shown in Figure 5. The photon yield cannot be explained by known particle decays, and it varies insignificantly with energy $\sqrt{s}$. A natural explanation of this is the quark bremsstrahlung.

The results from the ISR provide a reliable reference for projecting some of the potential physics yields at ISABELLE.

B. Recent Results from PETRA

When PETRA was first proposed, there were many theoretical predictions on the mass of the sixth quark. Most of the theoretical predictions centered on a toponium state below the mass of 30 GeV. There were also speculations on new leptons, on possible violations of QED, etc. The five PETRA groups, JADE, MARK-J, CELLO, PLUTO, and TASSO, have produced concurrent and complementary results. Some of the highlights of PETRA results are:

a) Search for Toponium

Figure 6 shows the summarized results on measurement of R compared with the predictions with five-quark contributions and six-quark contributions. The results clearly indicate that the top mass is larger than 18 GeV. Figure 7 shows the latest scanning results from the MARK-J group, carrying the search up to 36.7 GeV and looking for possible narrow resonance states. This figure illustrates one of the difficulties of electron-positron accelerators in that to search for narrow states, one must vary the machine energy continuously in small steps. This is very time-consuming. Figure 8 exhibits results from the MARK-J group in measuring the thrust distribution of inclusive muon events. The inclusive muon distribution gives a better signal to discover new flavor productions. As shown in Figure 8, both charge 2/3e and charge 1/3e quarks can be ruled out by the data.

b) Gluon Physics

Figure 9 compares the broad jet oblateness distribution $\frac{1}{N}\frac{dN}{dO_B}$ seen in the data with QCD, $q\bar{q}$, and a $q\bar{q}$ model with an $\exp(-P_t/a)$ fragmentation distribution. It shows that the observation of an excess of planar events in agreement with QCD predictions is not a proof of hard gluon emission. With the high statistics now available and the ability to measure the total energy of each event, we can perform detailed investigations of the energy flow pattern of the 3-jet events with various models, as shown in Figure 10. The unfolded energy flow diagram clearly indicates that of all the models tested, only the QCD model is in agreement with the data.

Recently there has been an important study of gluon spin. The results from TASSO group, shown in Figure 11, indicate that the data is in good agreement with the assumption that the gluon has spin-1.

c) Tests of Quantum Electrodynamics

One of the more concrete results from PETRA has been the test of QED from electron, muon, and tau pair production. The results indicate that all the known charged leptons are point-like with a radius $< 10^{-16}$ cm. Figure 12 shows the comparison of μ-pair production data from PETRA groups with the predictions of quantum electrodynamics, indicating clear agreement between theory and data at extremely small distances.

d) Search for New Leptons

Recently the MARK-J group has searched for the excited state of the muon $\mu^* \rightarrow \mu\gamma$ which decays into an ordinary muon and a photon from the reaction

$$e^+e^- \rightarrow \mu^{*-}\mu^+$$
$$\mu^{*-}\mu^{*+}$$

with a total integral luminosity of $12340\,nb^{-1}$ in the energy region $27.4 \leq \sqrt{s} \leq 36.7$ GeV. The predicted background from higher order QED is twelve events. The MARK-J group observed eleven events. No excited muons have been found.

Figure 13 shows the results of the search for sequential heavy leptons. Again, up to a mass of 16 GeV no new heavy leptons have been found. In the framework of supersymmetric theories, spin-0 partners of the muon and the electron are expected to decay into an ordinary electron (muon) and a photino. The results of the search for spin-0 electrons from the CELLO group is shown in Figure 14. Again, the data rules out spin-0 electrons up to a mass of 16.6 GeV.

e) Electroweak Effects

One of the major experimental achievements in the last decade has been the determination of the parameters of the electroweak theory. The theory of Glashow-Weinberg-Salam (GWS) is characterized by a parameter denoted $\sin^2\theta_w$. Neutrino-nucleon scattering experiments yield a value of $\sin^2\theta_w = 0.229 \pm 0.009 \pm 0.005$ (systematic error).

The MARK-J data, which is used to test electroweak theories, consists of measurements of the angular distribution of Bhabha scattering, of the

muon pair and tau pair production cross sections, of the $\mu^+\mu^-$ charge asymmetry and the hadron production rate as a function of $\sqrt{s}$. In the framework of GWS we find $\sin^2\theta_w = 0.27 \pm 0.08$.

MARK-J also fits g_V^2 and g_A^2 in the more general context of single Z^o models, and find $g_V^2 = -0.05 \pm 0.10$ and $g_A^2 = 0.21 \pm 0.18$ with $\chi^2 = 14.4$ for 23 degrees of freedom. These results, including correlations, can be converted into an allowed region in the $g_V - g_A$ plane, as shown in Figure 15. Also shown in the figure are neutrino electron scattering data $\nu_\mu e^- \to \nu_\mu e^-$, $\bar{\nu}_\mu e^- \to \bar{\nu}_\mu e^-$, $\bar{\nu}_e e^- \to \bar{\nu}_e e^-$, which limit the possible value of g_A and g_V to two regions in the $g_V - g_A$ plane around ($g_V = 0$, $g_A = -1/2$) and ($g_V = -1/2$, $g_A = 0$). Combining the MARK-J and the neutrino scattering data, the second solution is ruled out with more than 95% confidence. This confirms the conclusions drawn on the basis of deep inelastic neutrino nuclear scattering and polarized electron deuterium scattering data, but without recourse to models of hadron production by the weak neutral current.

To summarize, even though PETRA has a high luminosity of $1.5 \times 10^{31} cm^{-2}/sec$ at 36.7 GeV compared to the output of SPEAR and DORIS, the physics at PETRA has not been as stimulating.

III. COMMENTS ON ISABELLE

A. The Completion Date of ISABELLE

In the history of particle physics the completion time of accelerators is not necessarily the decisive factor in their ultimate usefulness, as evidenced by the following examples:

a) the 6 GeV electron accelerator, CEA, was finished years ahead of a similar accelerator at DESY;

b) the CERN 28 GeV proton synchrotron was finished one year ahead of the AGS at Brookhaven;

c) the 400 GeV Fermilab accelerator was finished many years ahead of the CERN SPS.

The physics output of all these accelerators has been very competitive and compatible with that of all the others.

To make a quantitative comparison of the physics potential of ISABELLE, Dr. Samios has provided an operational scenario, shown in Table II, of intensities of the CERN $p\bar{p}$ collider, the FNAL $p\bar{p}$ collider, the phased ISABELLE approach, and the large-aperture ISABELLE. From Table II one can calculate the Z^o and the $W^{\pm}$ yield as function of time for all three machines (Figures 16-17). In Figure 18 we show the relative sensitivity to search for heavier mass Z^o's of the large-aperture ISABELLE, with luminosity $10^{33} cm^{-2}/sec$, and the other two $p\bar{p}$ colliders. In Figure 19 we show the production cross section for high p_T physics with the large-aperture ISABELLE. If toponium exists there is a clean method to detect Higgs particles by triggering on hard ($\geq$ 20 GeV) photon together with a recoiling jet containing at least one muon. As seen from Figure 20, with a Higgs particle mass of 11 GeV there is a good chance of detecting the Higgs particle at ISABELLE.

Figures 17-20 show clearly the potential of ISABELLE for studying the properties of Z^o, $W^{\pm}$ and high p_T phenomena compared to competing machines in either the phase approach or the large-aperture approach. These figures also indicate **the uniqueness of ISABELLE, because of its high luminosity, to search for as yet unsuspected phenomena.**

B. Style of Brookhaven Research

Traditionally, Brookhaven has enjoyed excellent guidance from its directors of high energy physics. Drs. M. Goldhaber, R. Cool, R. R. Rau have been instrumental in setting up the style of the laboratory and encouraging much participation from university communities.

The current deputy director for high energy physics, Dr. N. Samios, is an extraordinary scientist. His many discoveries include work on the production decays and lifetimes of Λ^o's and θ^o's, the first experimental demonstration of nonuniversality of weak decays (the leptonic decay rate for strange particles being less than expected), the determination of π^o parity, Dalitz pair distribution of π^o, the discovery of ϕ (1020) and Ξ^* (1530), the discovery of η (960), the discovery of Ω^-, the discovery of F^* (1500), the discovery of Ξ (2030), the first observation of bare charm Σ_c^{++} and Λ_c^+, and the verification of the Weinberg-Salam gauge model. There are very few physicists who have achieved such an extraordinary record. His proven physics intuition as shown by his accomplishments will be a major factor in the future success of ISABELLE.

C. Experimental Considerations

To utilize the high intensity of ISABELLE, it is important to recognize that a careful, precise experiment requires large amounts of systematic technical development. In Tables III, IV, and V, I list the difficulties due to rate, the need for high resolution, and the need for good hadron lepton rejection. As shown in Table III, the phased approach of ISABELLE implies that there is a 10% chance for two events in the trigger counters plus a 20% chance in the 1 cm drift chamber and 100% probability for 2 events in 5 cm drift space. Triggering with a microprocessor would therefore be extremely difficult. Table IV shows that in order to obtain a mass resolution of 1% for electron pairs the problem of

calibration and stability for many counters must be studied, and to obtain 1% resolution for muon pairs, one needs a resolving power $B\ell^2 = 24\ kG\text{-}m^2$ and a B constant to < 1% together with a mechanical accuracy of locating the signal wires to < 30 μm. Table V shows that to detect $W^{\pm}$ at large p_T, one needs a π/μ rejection of approximately 10^4. Tables VI, VII, VIII, and IX are examples of important experimental requirements, possible solutions, and items of research and development on track detectors, on shower detectors, on particle identification, and on data processing.

Of particular interest is the effort being carried out by Professor B. Pope to study a toroidal magnet configuration to be used at ISABELLE. Toroidal magnets are excellent devices for colliding beam accelerators. In the last decade, many experimentalists--at DORIS and at the ISR--have proposed experiments utilizing toroids. In the summer study of 1977, there was also a proposal by W. Busza, M. Chen, G. Danby, L. Rosenson, and D. Lowenstein on the use of toroids. Large-sized toroids have many mechanical problems. There are normally a few thousand tons of force on the outside coils. These toroids are now being extensively pursued in the fusion projects and hopefully this will give us some insight into the enormous amount of engineering problems involved.

D. Time Schedule for Detector

In a colliding beam accelerator, because of the limitation of luminosity, a high sensitivity experiment requires a 4π detector. In the last decade many large detectors have been built. Some examples are:

1. At the ISR at CERN.
   - the superconducting solenoid detector at Intersection 1, which was used in the discovery of the high p_T phenomena,
   - the magnetized iron detector at Intersection 2, which was used to study the production mechanisms of dimuons,

- the multipurpose split-field magnet used to discover a new particle, Λ_b,
- the axial field magnet detector now being constructed by Willis.

2. At the $p\bar{p}$ collider at CERN:
   - a 4π solid angle detector with dipole magnet known as UA1 (shown in Figure 21),
   - a 4π detector with emphasis on detecting electrons and photons, known as UA2.
3. At Fermilab $p\bar{p}$ collider:
   - a 4π superconducting magnet detector (FNAL-CDF). This detector cost approximately $40 M to equip.
4. At PETRA. The history of PETRA can be summarized as follows:

	1975	PETRA was approved
February	1976	Frascati meeting on physics at PETRA
Autumn	1976	5 experiments were approved (CELLO, JADE, MARK-J, PLUTO, and TASSO)
Summer	1978	First storage of beams
November	1978	First collision for high energy physics
Winter	1980	Mini low-β insertions
	1981	All detectors will be fully equipped.
		Data taking in process.

The above statistically significant sample shows that it takes four to five years to finish a detector.

E. Participation in the ISABELLE Experiment

I am very pleased to learn that already there are many experimental groups actively designing experiments for ISABELLE. I list examples of three experiments:

1) The LAPDOG experiment is a high resolution spectrometer focusing upon electrons, photons, and π^o's. The participants are shown in Table X, the physics goals are shown in Table XI, and a plan view and an end view of the detector are shown in Figures 22 and 23. The group has already performed experimental tests of large arrays of lead-glass counters and is in the process of preparing a proposal to ISABELLE.

2) The dipole detector, a large group of physicists from Brookhaven, Columbia University, and the University of Pennsylvania, is performing systematic design studies of a large-aperture dipole spectrometer, the plan view and top view of which are shown in Figures 24 and 25. This is a general purpose detector designed to measure leptons, hadrons, particle correlations, energy flow, new particles, etc. My opinion is that this is an excellent detector which can be readily constructed and will be very versatile and useful for many years. The preliminary estimate of the cost of this detector is about $40 M.

3) The muon detector, a group of physicists from Brookhaven, Brandeis, Florida, MIT, NIKHEF (in The Netherlands), Osaka, Paris, Peking, Pisa, Vienna, and Wyoming, has been designing a 4π detector measuring

- $\mu^+\mu^-$
- $\mu^\pm$ + jet
- jet + jet
- $\mu^+\mu^-\mu^\pm$ + jet
- $\mu^+\mu^-\mu^+\mu^-$

with a mass resolution $\frac{\delta M_{\mu\mu}}{M_{\mu\mu}} \simeq 1\%$ at a mass of 100 GeV.

The plan view of the detector is shown in Figure 26. The intersection region is surrounded by a calorimeter, the design of which is shown in Figures 27, 28, 29.

In the last two years a 40 man-year effort involving the magnet and the large chambers has been put into systematic development for the instrumentation of this detector. The magnet development was carried out together with the National Magnet Laboratory at MIT and the large drift chamber development was carried out with the Draper Laboratory in Cambridge, Massachusetts.

The chamber has 5 m long signal wires parallel to the beam and to the magnetic field of the solenoid. They are supported in the middle so that the momentum determination of muons emitted in either hemisphere is unobstructed. The chamber is assembled with 96 segments of 160 wires each, 15,360 total. A segment of this chamber is shown in Figure 30. The chamber itself is considerably larger than existing chambers at PETRA or PEP. To understand these large chambers, four independent development projects were carried out at MIT, at Brookhaven, and at NIKHEF:

1. To understand the influence of magnetic fields, a one-wire model was built to measure the Lorentz deflection, and to choose a good gas so that the chamber can work at less than four atmospheres of pressure. The arrangement is shown in Figure 31.
2. To understand the problem of 5 m length wire, a 10-wire module was built and operated in a specially built 20 kgauss field solenoid. Extensive tests of this chamber indicate that with one support in the middle, one can indeed obtain the desired resolution from such long wires. The test arrangement is shown in Figure 32.
3. To control the systematic error to < 30 μm, a full segment of the chamber was constructed with 160 wires. The arrangement is shown in Figures 33 and 34. The chamber frame is supported at six points from

the chamber carrier, and they are remotely adjustable with the feedback system using optical fibers and CCD devices.

4. To insure that there is no cross-talk between wires so that the resolution increases as $1/\sqrt{N}$, a large chamber with 100 wires and with dimensions $150 \times 100 \times 40\ cm^3$ (Figure 35) was also tested at the Brookhaven beam.

So far all the test results agree with expectations and, indeed, one is quite confident that with this detector we can reach a mass resolution of 1%.

Tables XII and XIII are the production schedules of chamber and magnet, prepared by professional engineers.

After two years of effort, I can only emphasize that there are many problems still to be solved, and in order to meet the schedule of 1987 one has to continue at a vigorous pace both with the research and development phase and the construction phase of this detector.

IV. CONCLUSION

To summarize, the physics of ISABELLE is unique. It is the only accelerator with true potential for discoveries beyond our expectations. In order to exploit the physics, one needs to start preparing experiments now.

ACKNOWLEDGEMENTS

I wish to thank Dr. Nicholas Samios for his kind hospitality at this stimulating and exciting workshop. I wish also to acknowledge discussions with Drs. L. L. Chau, N. Samios, and A. H. Walenta of Brookhaven, Dr. A. Ali of DESY, and Drs. U. Becker, D. Luckey, and M. Chen of MIT.

TABLE I:
SOME OF THE MAJOR ACCOMPLISHMENTS
FROM PP AND $e^+ e^-$ ACCELERATORS.

PP	$\sqrt{s}$ (GeV)	e^+e^-
Ω^-, ϕ, K_o, J	10	Q.E.D., J/ψ
Λc, 2ν, ...		
Υ, Λb, HIGH $P_\perp$	10 – 60	Q.E.D., GLUON PHYSICS
		Υ FAMILY,
	100	Z^o
$W^{\pm}$, MORE Z^o.....	~700	

TABLE II:
A SCENARIO FOR THE NEXT GENERATION
OF COLLIDING BEAM ACCELERATORS.

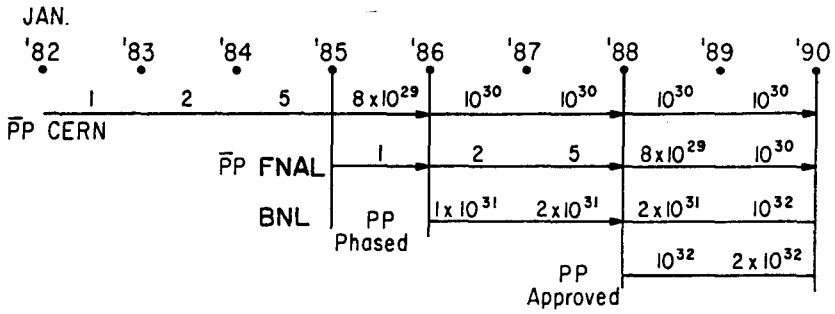

		Areas
CERN:	$\bar{P}P$ 540 GeV Jan. '82 •	(1 + 1)
	$\mathcal{L}$ = 10^{29} — 10^{30} 5 yrs 1,000 hrs/yr.	
FNAL:	$\bar{P}P$ 2,000 GeV Jan. '85 •	(1 + 1)
	$\mathcal{L}$ = 10^{29} — 10^{30} 5yrs 1,000 hrs/yr.	
BNL:	PP I) 700 GeV •	(3+3)
	$\mathcal{L}$ = 10^{31}, 2×10^{31}, 2×10^{31} II) 10^{32}	
	1,000 hrs, → 2,000 hrs.	
	PP 720 GeV •	(3+3)
	$\mathcal{L}$ = 10^{32} 2×10^{32}	
	1,000 hrs 2,000 hrs.	

TABLE III

EXP CONSIDERATIONS I : RATE

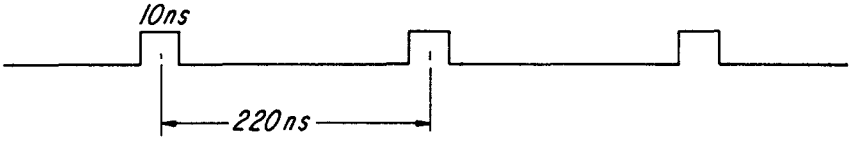

AVERAGE RATE : $\sigma \cdot L = 6 \times 10^{-28} \cdot 3 \cdot 10^{31} = 1.8 \times 10^{6}/s$

INST RATE : $1.8 \times 10^{6} \times 40 \times 22 = 1.6 \times 10^{9}/s$
$\langle n \rangle \langle DF \rangle$

$\Rightarrow$ 10% for 2 event in 10ns → TRIGGER COUNTER

20% " 220ns → 1cm DRIFT SPACE

100% " 1μs → 5cm DRIFT SPACE
→ μ-PROCESSOR

EXP CONSIDERATIONS II : RESOLUTION

$\Gamma \approx \alpha m$ $\qquad \frac{\Delta M}{M} \sim 1\%$

$P + P \longrightarrow e^+ e^- + X$

$\frac{\Delta M}{M}$: LIMITED BY CALIBRATION OF 4π SHOWER COUNTERS

$P + P \longrightarrow \mu^+ \mu^- + \ldots\ldots$

$$\frac{\Delta M}{M} = \frac{1}{\sqrt{2}} \frac{50\ \text{GeV}}{.03} \cdot \frac{\sigma}{B \cdot \ell^2} \sqrt{\frac{720}{N+5}} = 1\%$$

$\sigma = 140\mu$

$N = 160$

$B \cdot \ell^2 = 24\ \text{KG} - \text{M}^2$

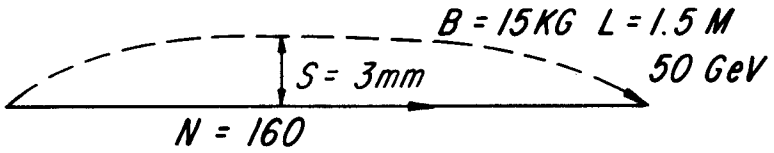

B CONSTANT TO < 1%

MECHANICAL ACCURACY OF WIRES < 30μ

TABLE V

EXP CONSIDERATIONS III HADRON REJECTION:

at $W^{\pm} \rightarrow \mu^{\pm}$ $\quad P_{\perp} \approx 20\,GeV$

$\pi/\mu \approx 10^{4}$

TABLE VI

DETECTOR DEVELOPMENT OF PARTICULAR SIGNIFICANCE TO ISABELLE

TRACK DETECTORS

REQUIREMENT	EXAMPLE OF SOLUTION	RESEARCH/DEVELOPMENT
$\Delta p/p^2 \leq 10^{-4}$ GEV^{-1}	LARGE PRECISION DRIFT CHAMBER	PRECISION MECHANICS ON LINE POSITION CONTROL LASER CALIBRATION LARGE MAGNET (SUPERCOND.)
$\sigma \leq 20\ \mu$	TIME EXPANSION DRIFT CHAMBER	STUDY OF PRIMARY IONIZATION, DRIFT, DIFFUSION, READ-OUT
	SEMICONDUCTORS WITH STRIP READOUT	MANUFACTURING, READ-OUT

TABLE VII

SHOWER DETECTORS

REQUIREMENT	EXAMPLE OF SOLUTION	RESEARCH/DEVELOPMENT
10^4 SEGMENTS	PROPORTIONAL WIRE SAMPLING	STABILITY, CALIBRATION, SHOWER DEVELOPMENT CONSTRUCTION
$\sigma_T \lesssim 1$ NS (TIME RESOL.) $\Delta T < 50$ NS (MEMORY)	PARALLEL PLATE SAMPLING	STABILITY, CALIBRATION, SHOWER DEVELOPMENT, CONSTRUCTION

Table VIII

Particle Identification

Requirement	Example of Solution	Research/Development
$10^3..10^4$ segments	gas ionization Cerenkov counters	optics, proportional photon counters
analysis in jet	dE/dx	calibration by pulsed x-ray or laser
compact detector	imaging Cerenkov-counter	UV-detector development

TABLE IX

DATA PROCESSING

REQUIREMENT	EXAMPLE OF SOLUTION	RESEARCH/DEVELOPMENT
FAST SIGNAL PROCESSING FOR TRIGGER	OPTICAL PROCESSOR	FINE GRAINED LIGHT EMITTING & RECEIVING DEVICES
$T_{DEL} \leq 200$ NS	FAST SEMICONDUCTOR PROCESSORS	SPECIFICATIONS
DATA REDUCTION	μ-PROCESSORS, EMULATORS	SPECIFICATIONS

TABLE X

LAPDOG

A HIGH RESOLUTION SPECTROMETER AT LARGE ANGLES, FOCUSSING UPON ELECTRONS, PHOTONS AND π^0.

BROOKHAVEN: L. AHRENDS, S. ARONSON, H. FOELSCHE, B. GIBBARD, P. WANDERER, H. WEISBERG, P. YAMIN

BROWN UNIV.: D. CUTTS, R. LANOU

COLUMBIA UNIV.: P. FRANZINI

STONY BROOK: R. ENGELMANN, P. GRANNIS, J. KIRZ, J. LEE-FRANZINI, M. MARX, R. McCARTHY

TABLE XI

PRIMARY PHYSICS GOALS

I) HIGH TRANSVERSE MOMENTUM PARTICLE PRODUCTION

(π°, DIRECT γ, $e^\pm$)

II) HIGH MASS STATES

e^+e^- (Z° WIDTH, ($t\bar{t}$) SEARCH, DRELL-YAN CONTINUUM)

σ_{Mee} AT $Z^\circ < 1$ GeV

III) MULTILEPTON EVENTS

(WITH MUON IDENTIFICATION THROUGH THE MAGNET)

AT LUMINOSITY = $10^{32}\,cm^{-2}\,sec^{-1}$:

~1 DETECTED $Z^\circ \rightarrow e^+e^-$/hr

~1 DETECTED ($t\bar{t}$) $\rightarrow e^+e^-$/day

~1 π°/hr at Pt = 50 GeV/c

~1 DIRECT γ/hr at Pt = 20 GeV/c if $\gamma/\pi^\circ = 0.1$

TABLE XII

LONG RANGE PROJECTION
PRELIMINARY DRAFT OF PRODUCTION SCHEDULE
CENTRAL CHAMBER

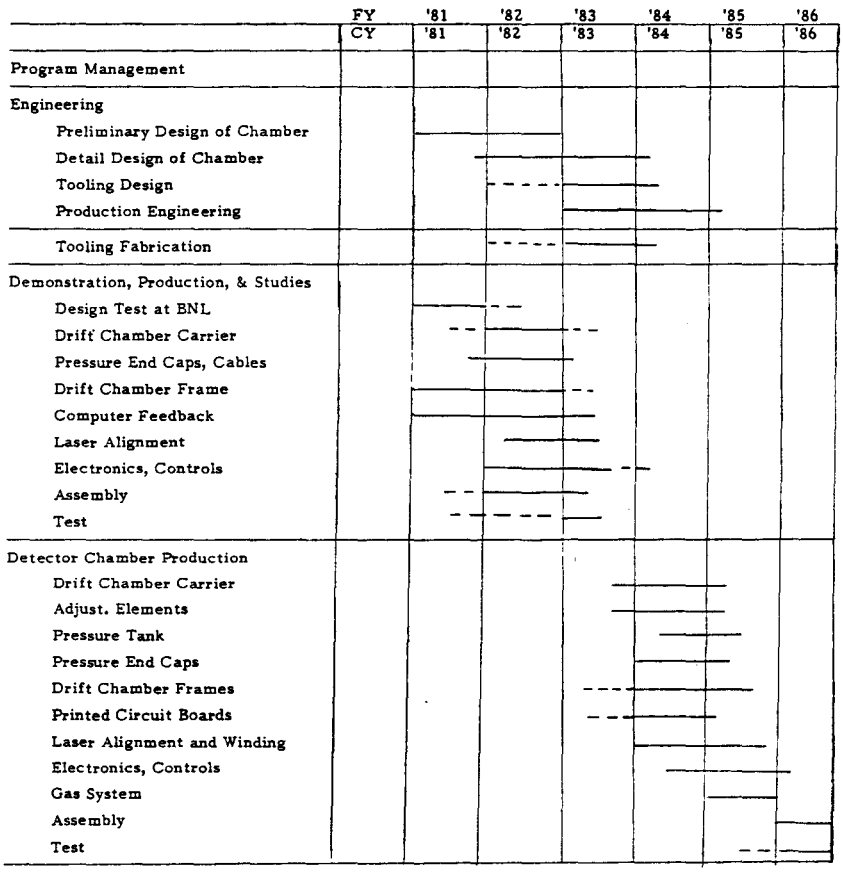

TABLE XIII

MAGNET

PRELIMINARY DRAFT OF PRODUCTION SCHEDULE

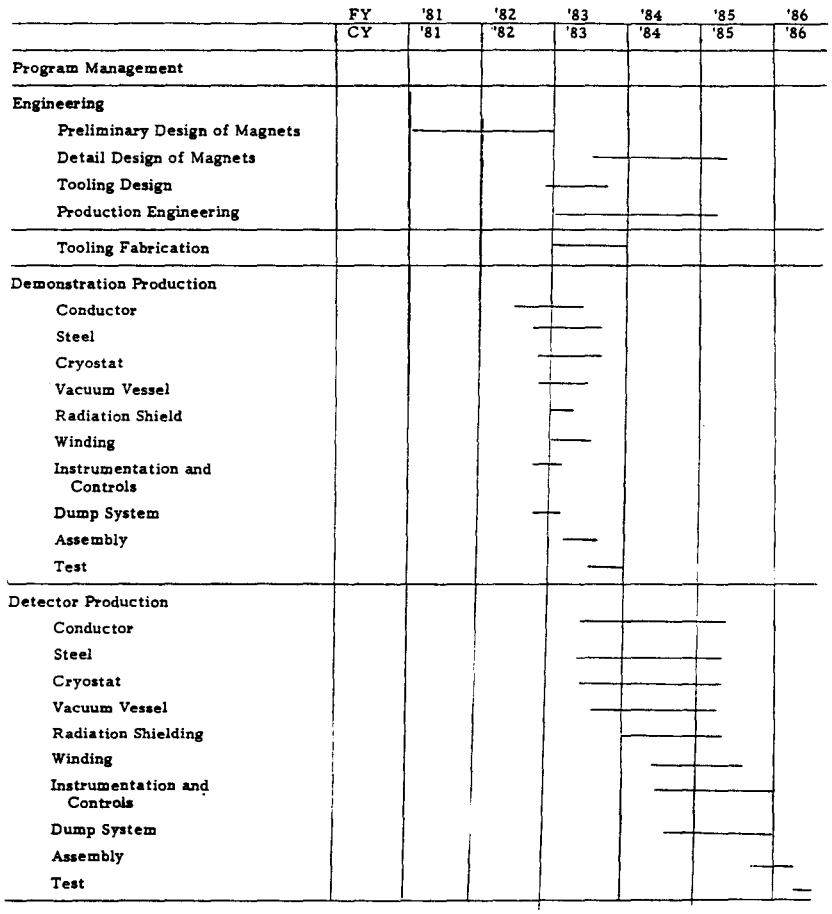

FIGURE CAPTIONS

Fig. 1 The cross section $(d^2\sigma/dmdy)_{y = 0}$ versus mass for the data at $\sqrt{s}$ = 53 and 63 GeV combined. The curve is a result of the fit to the continuum. The mass acceptance was calculated for isotropic decay distributions and production uniform in rapidity with p_T dependence $d\sigma/dp_T^2 \sim \exp(-bp_T)$, where b = 1.4 GeV^{-1}. (CERN EP 80-08).

Fig. 2 Scaling comparison of the 44 and 62 GeV continuum muon pair data. The dotted line is the Drell-Yan prediction with structure functions from neutrino data. The shape agrees well; however, the normalization is a factor 1.6 lower. The solid line is our fit to the sea distribution $(0.42 \pm 0.01)(1 - x)^{8.3 \pm 1.0}$. (U. Becker, private communication).

Fig. 3 Distribution of dimuons in Feynman x for three mass intervals. The solid line is the fit to the form $(1 - x)^{\alpha}$. The dashed line is a Drell-Yan calculation scaled up by a factor of 1.6. (Phys. Rev. Lett. 47, 12, 1981).

Fig. 4 Dimuon $\langle p_T \rangle$ as a function of $\sqrt{s}$ at $\sqrt{\tau}$ = 0.2. The linear rise of $\langle p_T \rangle$ is predicted from lowest order QCD. (U. Becker, private communication).

Fig. 5

Top Observed ratio of γ/π^0 at $\sqrt{s}$ = 63 GeV. Inner error bars are statistical errors. The outer error bars include possible systematic effects due to calorimeter non-linearity. The solid curve shows the Monte Carlo calculation for the ratio assuming no direct γ production. The shaded area indicates the one standard deviation systematic errors on the Monte Carlo simulation.

a, b, c Final results for the γ/π^0 ratio after background subtraction and correction for relative efficiency a) at $\sqrt{s}$ = 31 GeV; b) at $\sqrt{s}$ = 45 GeV; c) at $\sqrt{s}$ = 63 GeV. (Phys. Lett. 91B, 296 and 301, 1980).

Fig. 6 Measurement of average R value compared with udscb and udscbt quark model predictions. (P. Duinker Report, Lisbon Conference, 1981).

Fig. 7 R values measured during the energy scan between 33.0 and 36.7 GeV. Each point corresponds to 40 nb^{-1} on average. The line is the mean R value of 3.75 ± 0.05. (P. Duinker Report, Lisbon Conference, 1981).

Fig. 8 Measured thrust distribution for inclusive muon events compared with model predictions. (MARK-J group).

Fig. 9 The broad jet oblateness distribution $\frac{1}{N}\frac{dN}{dO_B}$. The data are compared with the predictions of the QCD and $q\bar{q}$ models. (MARK-J group, MIT preprint 115, 1981).

Fig. 10 (a) Comparing the data with QCD and $q\bar{q}$ models, using energy flow diagrams in the thrust major event plane for events with $O_B > 0.3$, with $T_n < 0.98$ and $\theta_{minor} < 60^o$.

(b) The unfolded energy flow diagram of Fig. 10a compared with the models of QCD, $q\bar{q}$, phase space, and a $q\bar{q}$ model with an $\exp(-p_T/650\ \text{MeV})$ fragmentation distribution. (MARK-J group, MIT preprint 115, 1981).

Fig. 11 Observed distribution of the data in the region $x_1 < 0.90$ as a function of the $\cos \bar{\theta}$ angle. The solid line is the prediction for a vector gluon, the dashed line the prediction for the scalar gluon. Both curves are normalized to the number of events in the histogram.

This angle $\cos \bar{\theta}$ is obtained by boosting the 3-parton system in such a way that partons 2 and 3 are in their rest frame. Neglecting the masses of quarks and gluons, $\cos \bar{\theta}$ can be written as

$$\cos \bar{\theta} = \frac{x_2 - x_3}{x_1} = \frac{\sin \theta_2 - \sin \theta_3}{\sin \theta_1}$$

(See R. Marshall Report, Lisbon Conference, 1981.)

Fig. 12 Observed cross section for the reaction $e^+e^- \to \mu^+\mu^-$ compared to the predictions of QED (solid curve). (P. Duinker Report, Lisbon Conference, 1981).

Fig. 13 Number of events expected for the production of a new (sequential) heavy lepton as a function of mass. The inset shows the number of events expected in the τ sample from tau and heavy lepton production. We observe a total of 52 τ events. The dashed line corresponds to the 95% confidence level upper limits. (MARK-J group, Phys. Rev. Lett. 45, 1904, 1980).

Fig. 14 Number of events expected for the production of a spin-0 partner s_e of the electron as a function of mass. The upper limit of events (95% confidence) and the mass range excluded are also indicated. (P. Duinker Report, Lisbon Conference, 1981).

Fig. 15 Results obtained from neutrino experiments and the MARK-J experiment expressed in terms of limits on g_V and g_A. The region in between the concentric ellipses corresponds to 68% confidence limits from the neutrino electron scattering experiments. The two black areas indicate the two allowed regions for g_V and g_A from the combined neutrino data. The shaded area represents the 95% confidence limit contour from the MARK-J experiment. (Phys. Rev. Lett. 46, 1663, 1981).

Fig. 16 Accumulated events for $Z^o \to \mu^+\mu^-$ in one 4π detector of running for large-aperture ISA (a), for phased ISA (b1, b2), for FNAL $p\bar{p}$ collider (c), and for CERN $p\bar{p}$ collider (d).

Fig. 17 $W \to \mu^+\nu$ yields at different colliders.

Fig. 18 Yield of $Z^o \to \mu^+\mu^-$ as a function of Z^o mass for the large-aperture ISA (a), for FNAL $p\bar{p}$ (c), and for CERN $p\bar{p}$ (d), assuming 1000 hours per year of running at ISA.

Fig. 19 Events per day per GeV steradian for high p_T QCD jets for the large-aperture ISA.

Fig. 20 Summary of a production mechanism and yield for detecting Higgs particles at ISA (mass of Higgs particles is assumed to be 11 GeV).

Fig. 21 Experiment UA1: A 4π solid angle detector for the SPS used as a proton-antiproton collider at a center-of-mass energy of 540 GeV.

Fig. 22 Plan view of LAPDOG detector.

Fig. 23 End view of LAPDOG detector.

Fig. 24 Plan view of the Brookhaven, Columbia, Pennsylvania dipole detector.

Fig. 25 Top view of dipole detector.

Fig. 26 Schematic of the large solenoid muon detector. C is hadron calorimeter. D is precision drift chamber. H is muon drift chamber. K is end cap drift chamber.

Fig. 27 Side view of muon detector where A, B, and C are electromagnetic calorimeters, D, E, F, and G are hadron calorimeters.

Fig. 28 Details of electromagnetic calorimeters shown in Fig. 27.

Fig. 29 Assembly schematic of the calorimeters shown in Fig. 27.

Fig. 30 A schematic view of one segment of the precision drift chamber showing pressure vessel, carrier ring, and so forth.

Fig. 31 Test arrangement with an x-ray source for a one-wire chamber to choose different gases and to measure the Lorentz angles for different gases at different pressures.

Fig. 32 Photograph of experimental arrangement on the AGS floor showing 5 m long 10-wire module drift chamber (mounted inside an aluminum tube). The 20 kG field is provided by a specially made solenoid which can traverse along the wire direction.

Fig. 33 Schematic drawing of the feedback system at 6 points on a wire plane.

Fig. 34 (a) One segement of the wire plane under test conditions. The 6 mechanical gauges are clearly visible.

(b) Detail of the feedback system at one of the 6 points.

Fig. 35 A 100-wire module built in Amsterdam and used at the AGS to test $1/\sqrt{N}$ law.

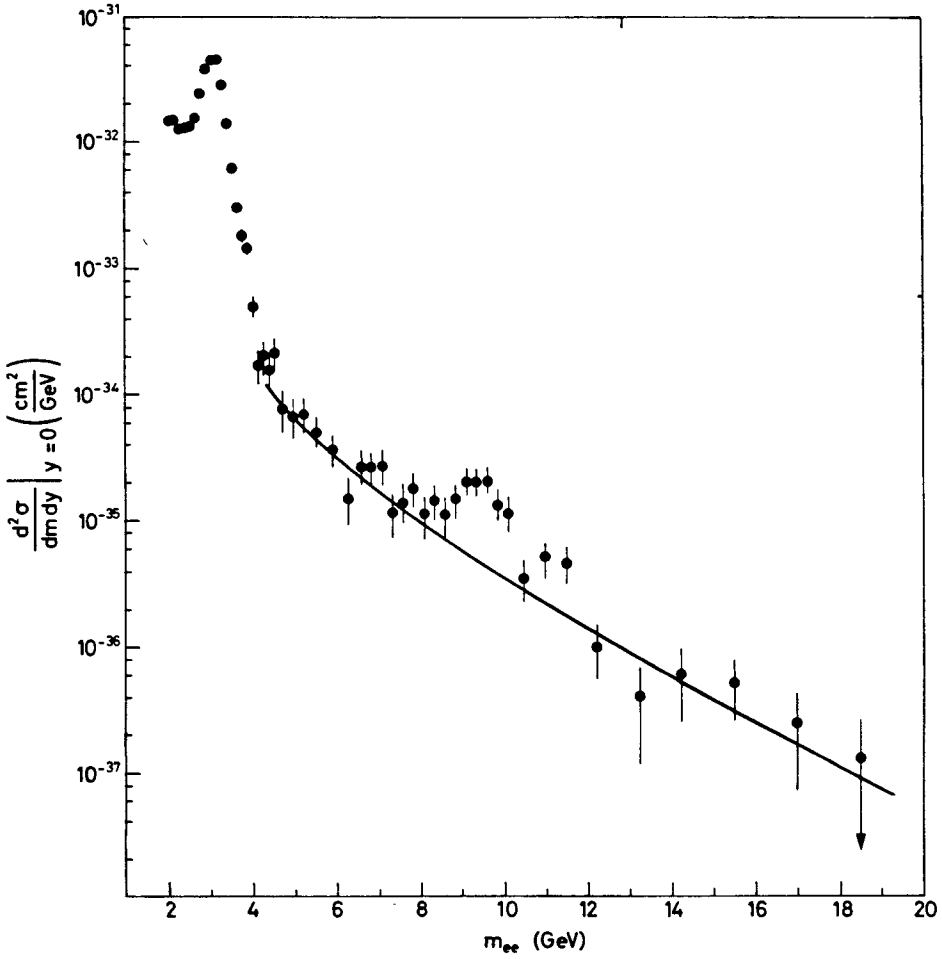
10^{-31}
10^{-32}
10^{-33}
10^{-34}
10^{-35}
10^{-36}
10^{-37}
$\frac{d^2\sigma}{dm\,dy}\Big|_{y=0}\left(\frac{cm^2}{GeV}\right)$
2
4
6
8
10
12
14
16
18
20
m_{ee} (GeV)

Fig. 1

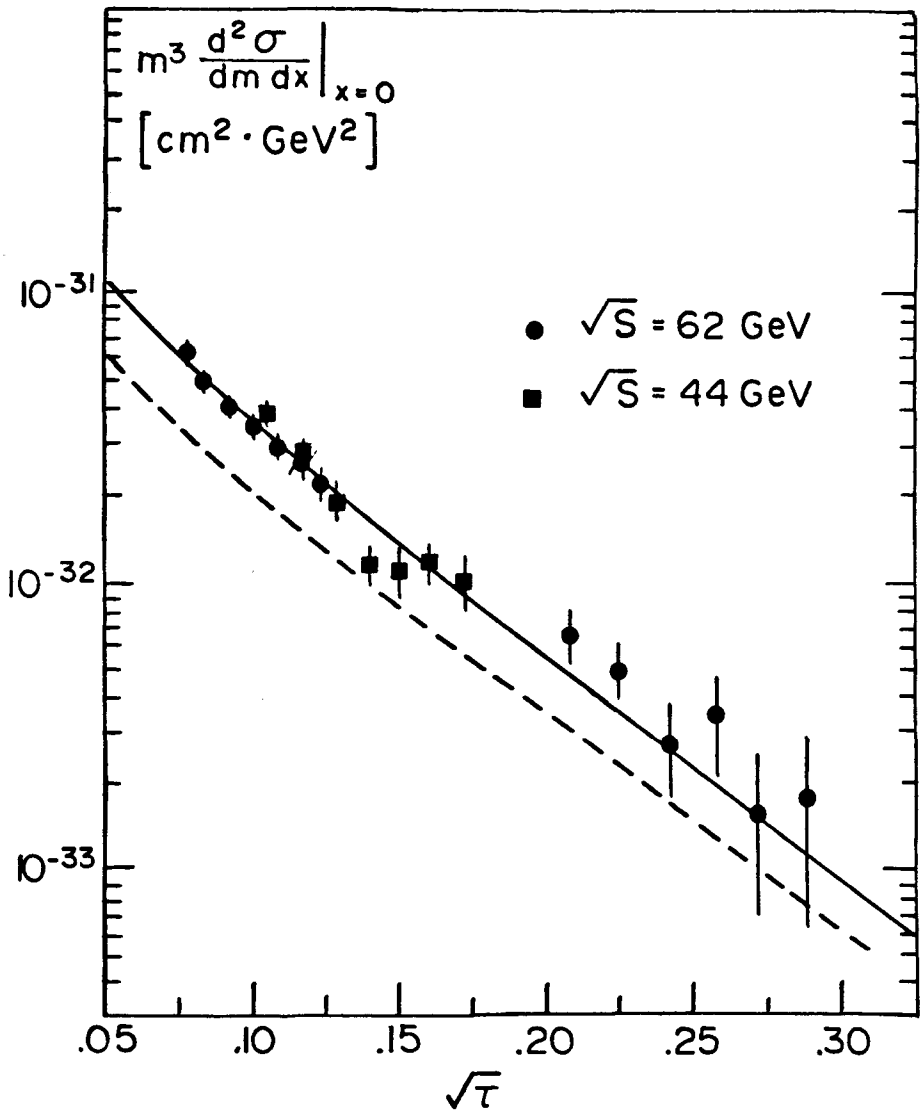
$m^3 \frac{d^2\sigma}{dm\,dx}\Big|_{x=0}$
$[cm^2 \cdot GeV^2]$
10^{-31}
10^{-32}
10^{-33}
$\sqrt{S}$ = 62 GeV
$\sqrt{S}$ = 44 GeV
.05
.10
.15
.20
.25
.30
$\sqrt{\tau}$

FIGURE 2

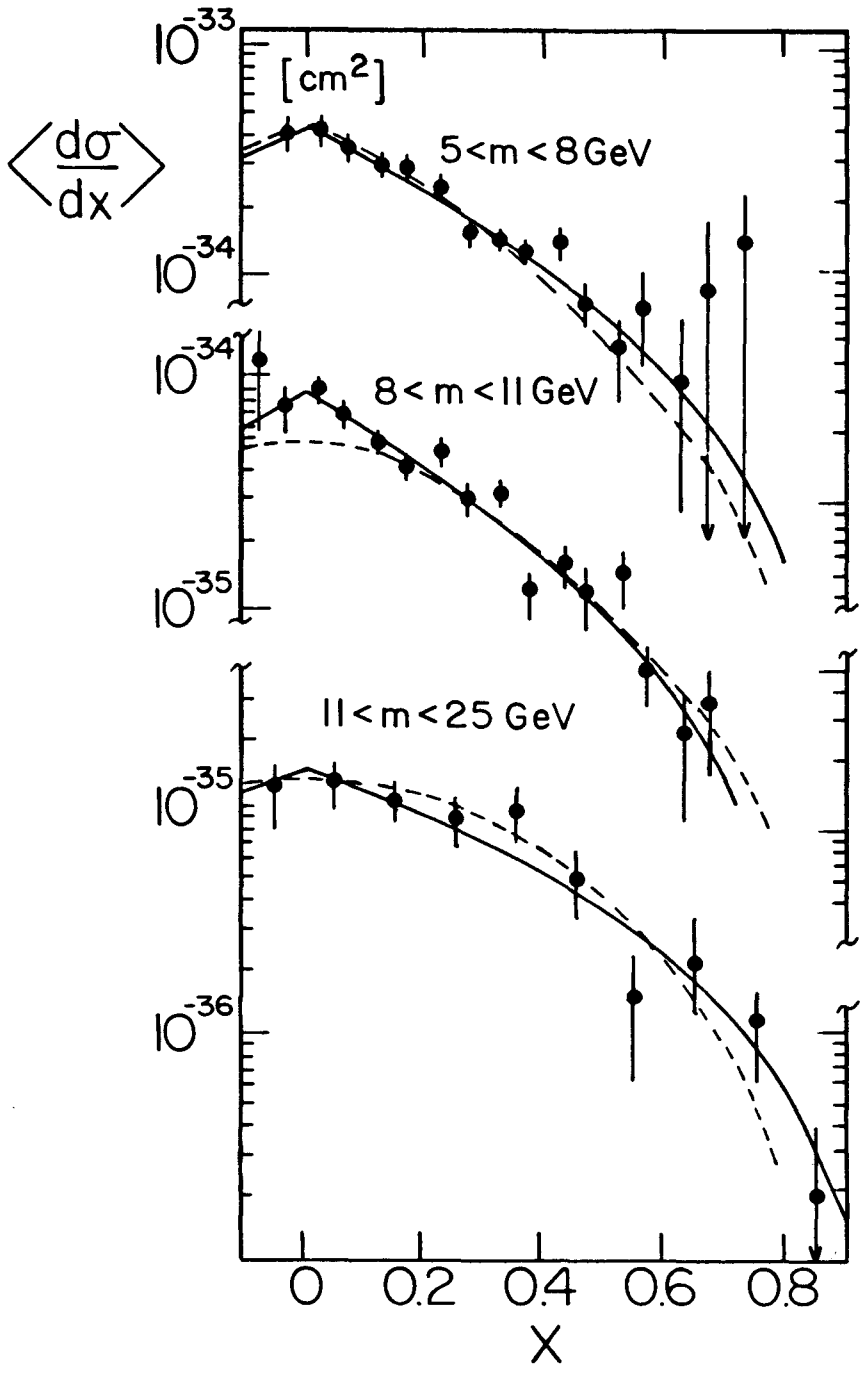
10^{-33}
[cm^2]
$\left\langle \frac{d\sigma}{dx} \right\rangle$
5<m<8 GeV
10^{-34}
10^{-34}
8<m<11 GeV
10^{-35}
11<m<25 GeV
10^{-35}
10^{-36}
0
0.2
0.4
0.6
0.8
X

FIGURE 3

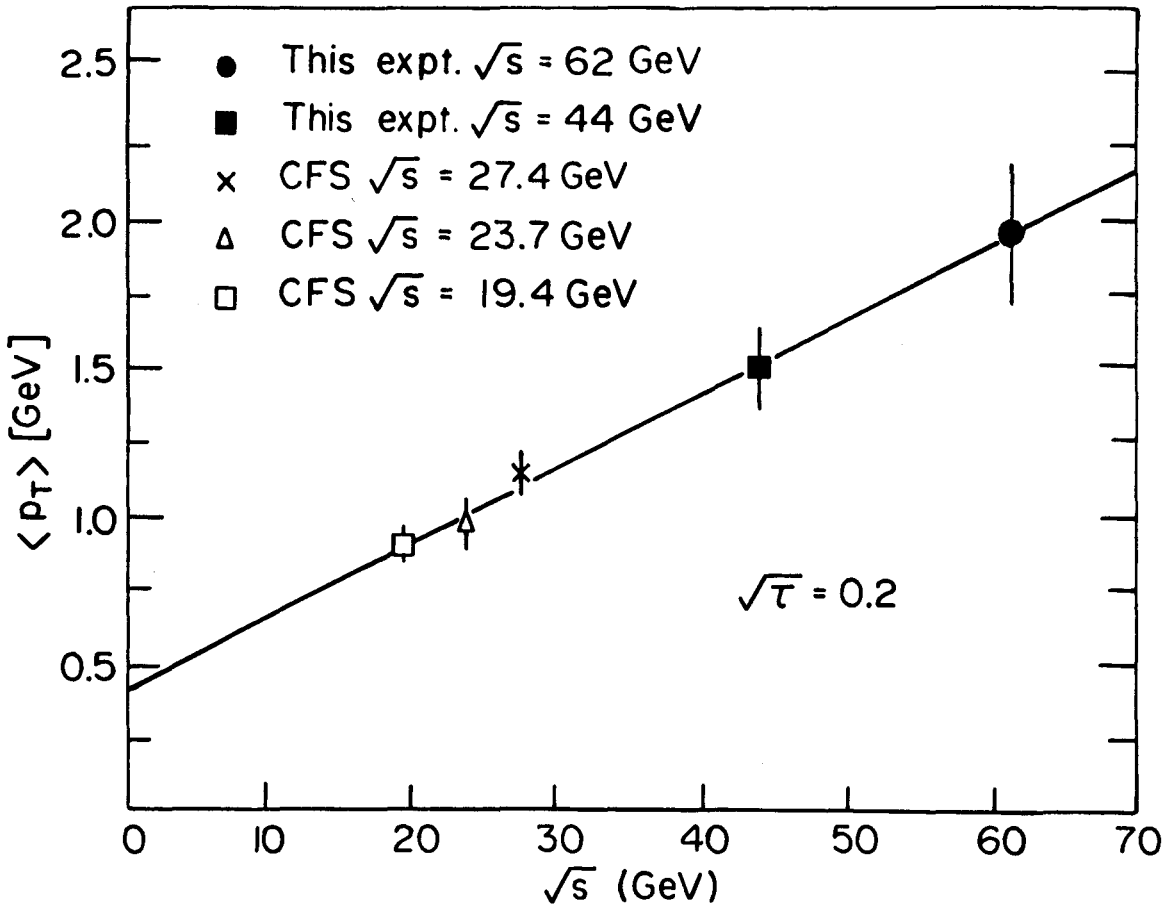
This expt. √s = 62 GeV
This expt. √s = 44 GeV
CFS √s = 27.4 GeV
CFS √s = 23.7 GeV
CFS √s = 19.4 GeV
√τ = 0.2
⟨pT⟩ [GeV]
√s (GeV)
2.5
2.0
1.5
1.0
0.5
0
10
20
30
40
50
60
70

FIGURE 4

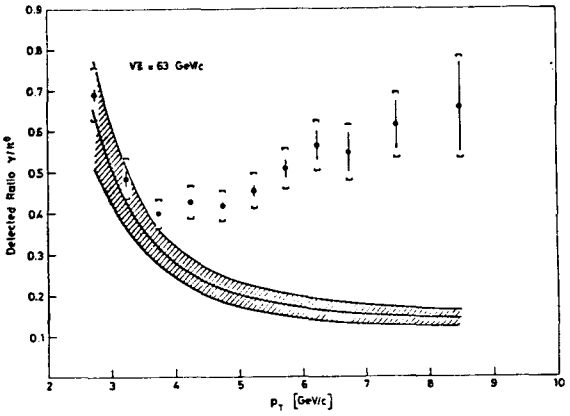
√s = 63 GeV/c
Detected Ratio γ/π⁰
p_T [GeV/c]

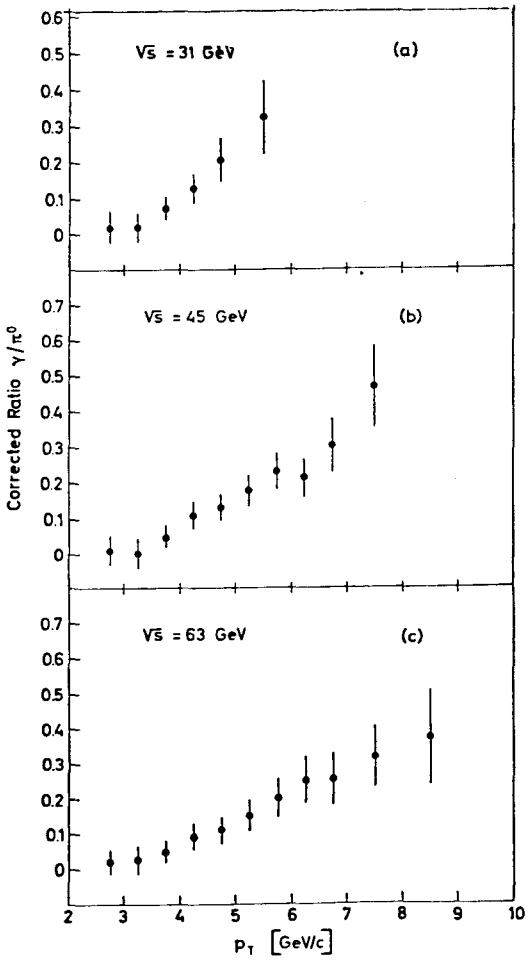
√s = 31 GeV
(a)
√s = 45 GeV
(b)
√s = 63 GeV
(c)
Corrected Ratio γ/π⁰
p_T [GeV/c]

FIGURE 5

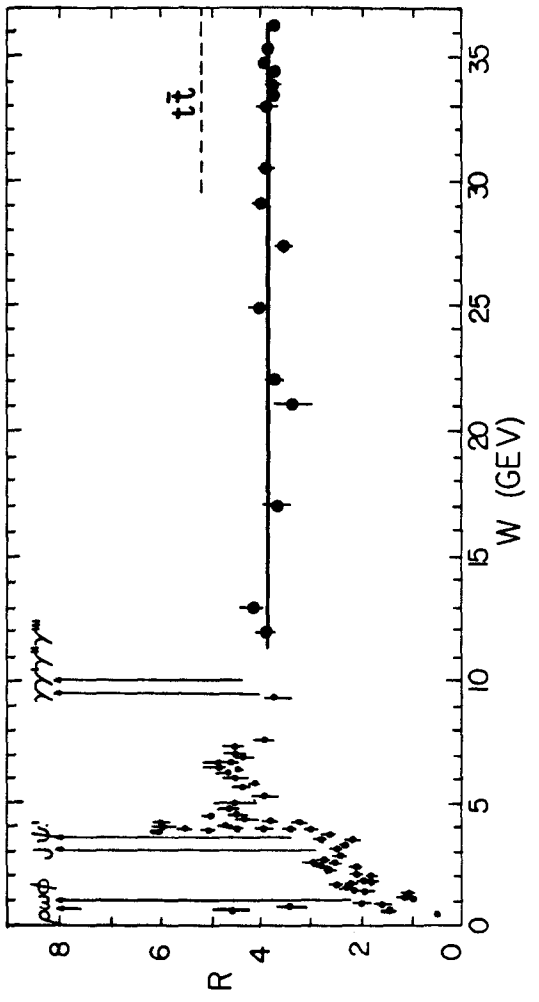

FIGURE 6

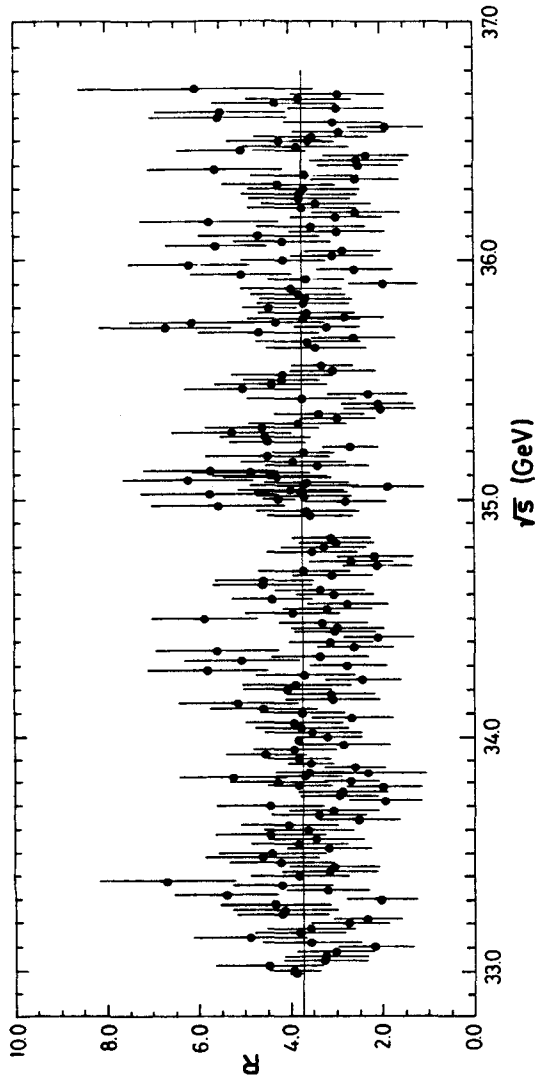

FIGURE 7

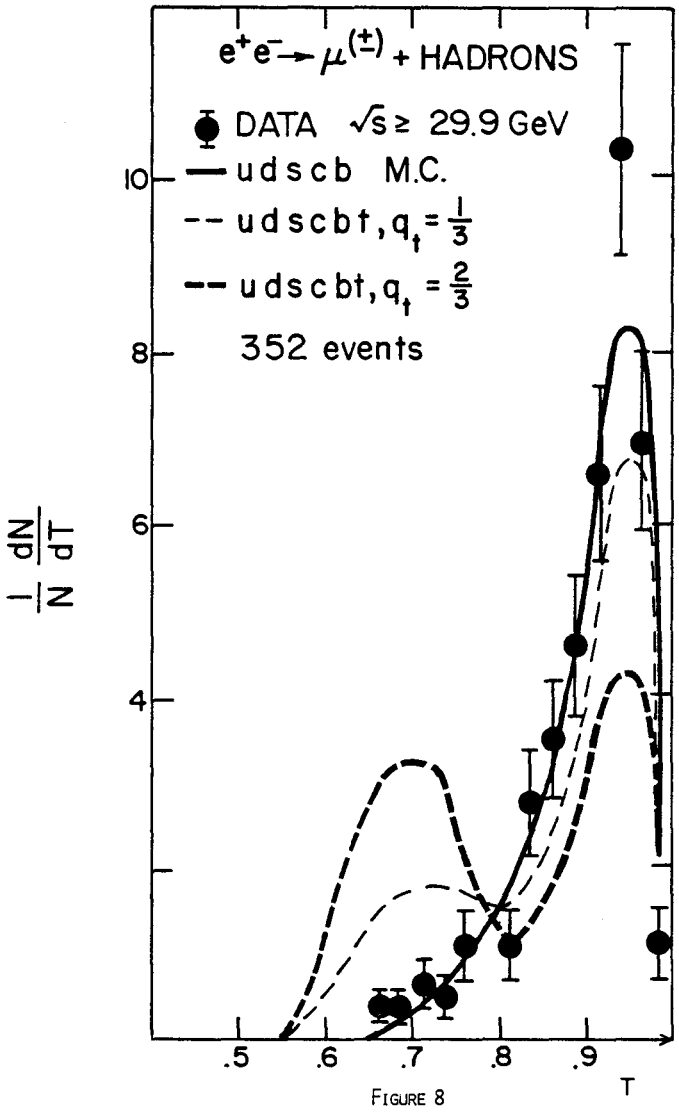
$e^+e^- \to \mu^{(\pm)}$ + HADRONS
DATA $\sqrt{s} \geq 29.9$ GeV
udscb M.C.
udscbt, $q_t = \frac{1}{3}$
udscbt, $q_t = \frac{2}{3}$
352 events
$\frac{1}{N}\frac{dN}{dT}$
10
8
6
4
.5
.6
.7
.8
.9
T

FIGURE 8

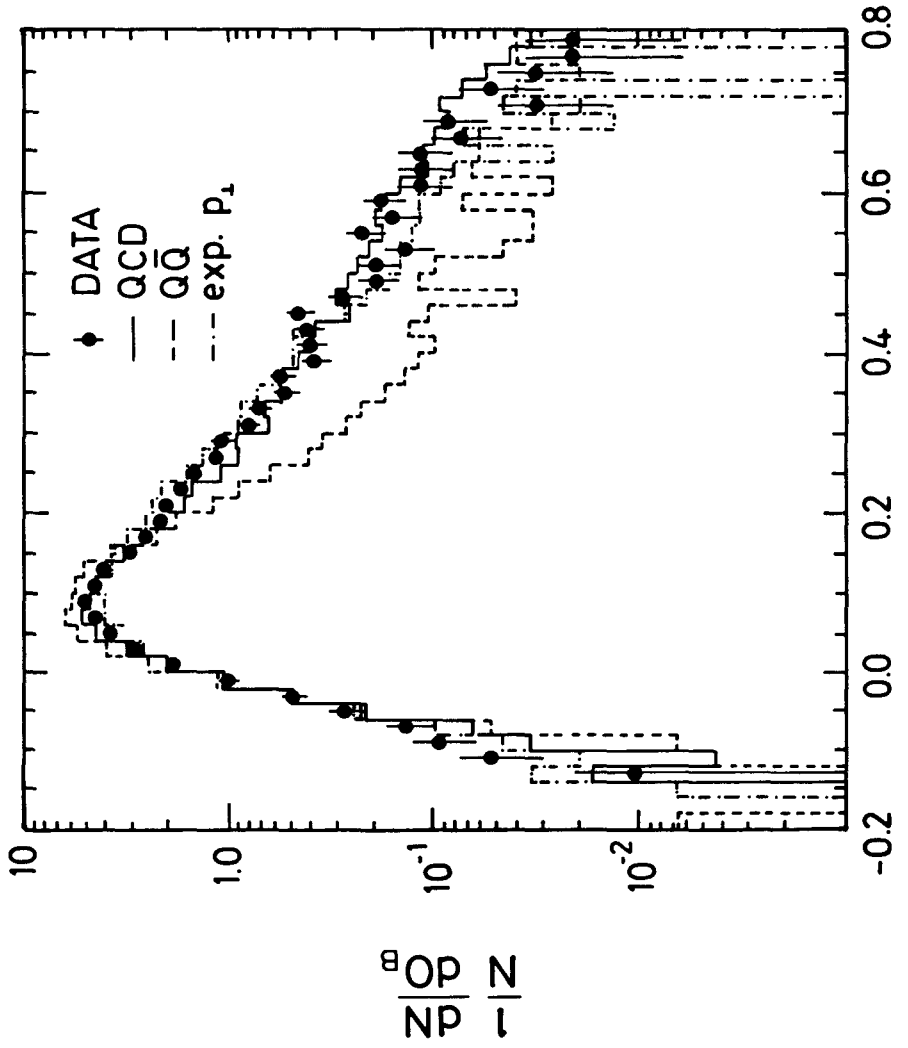

FIGURE 9

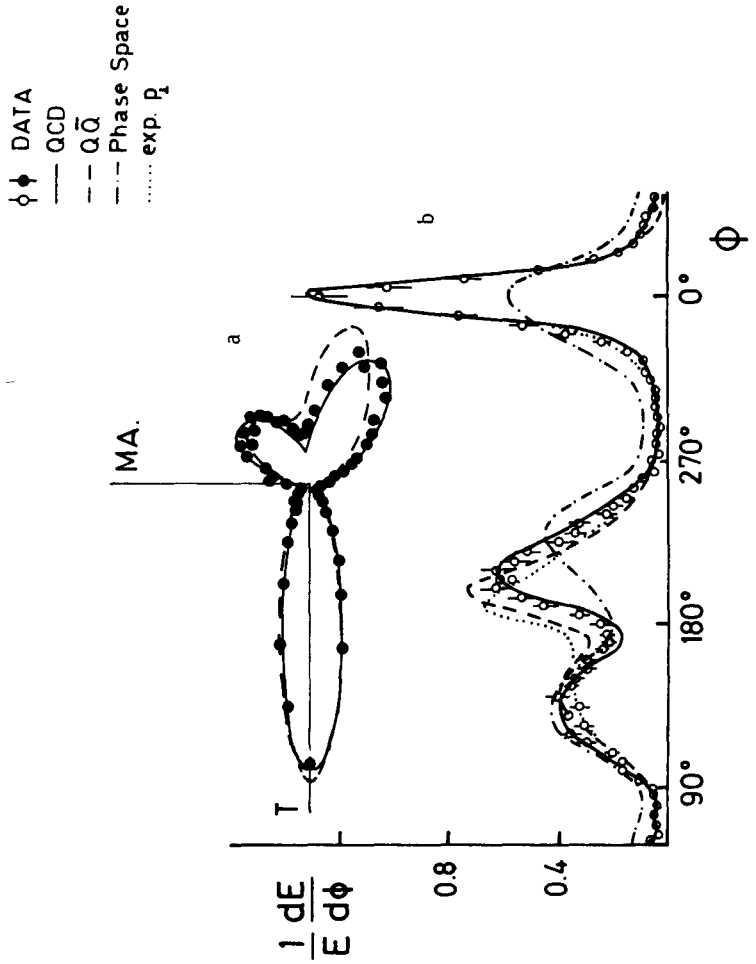
DATA
QCD
QQ̄
Phase Space
exp. p_t^2
MA.
T
a
b
$\frac{1}{E}\frac{dE}{d\phi}$
0.8
0.4
90°
180°
270°
0°
ϕ

FIGURE 10

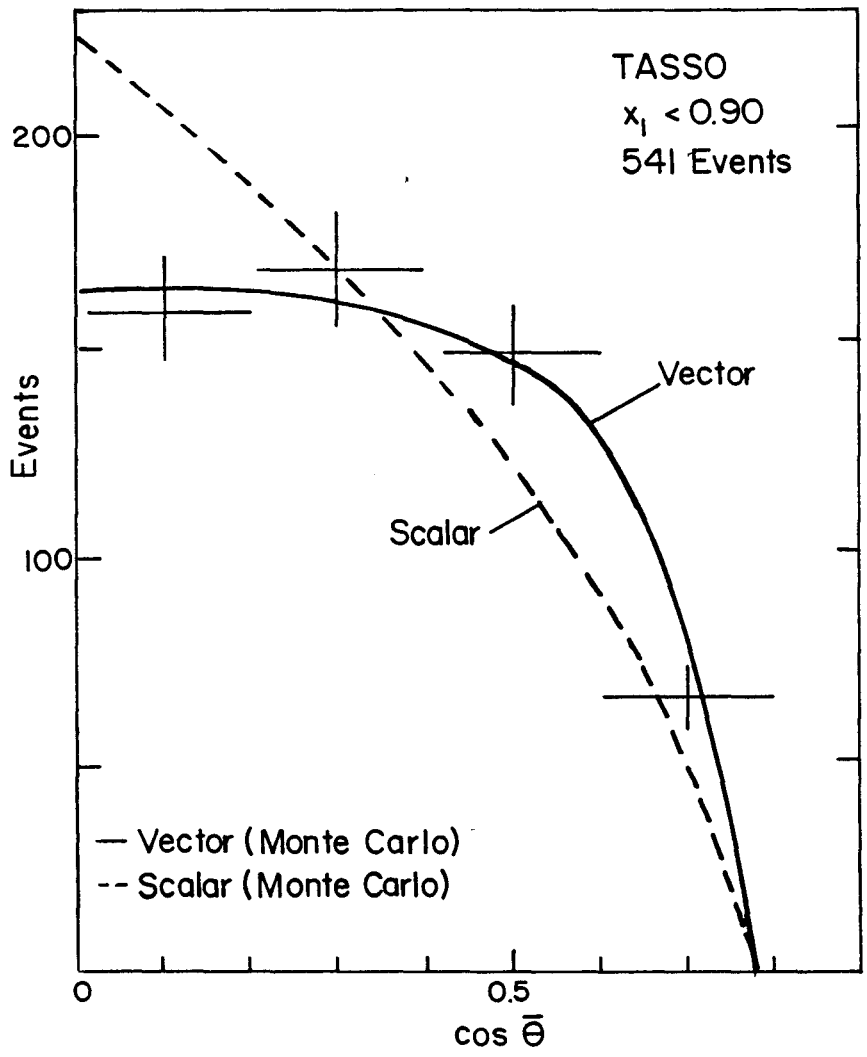
TASSO
$x_1 < 0.90$
541 Events
200
100
Events
Vector
Scalar
— Vector (Monte Carlo)
-- Scalar (Monte Carlo)
0
0.5
cos $\bar{\theta}$

FIGURE 11

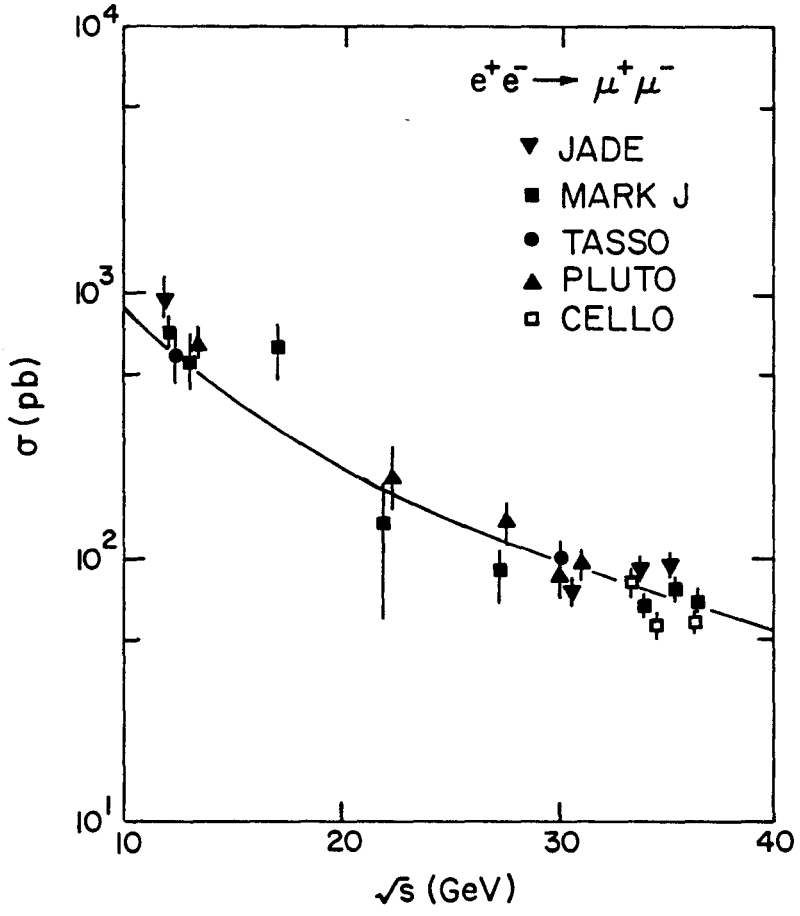
10^4
10^3
10^2
10^1
$e^+e^- \rightarrow \mu^+\mu^-$
JADE
MARK J
TASSO
PLUTO
CELLO
σ (pb)
10
20
30
40
√s (GeV)

FIGURE 12

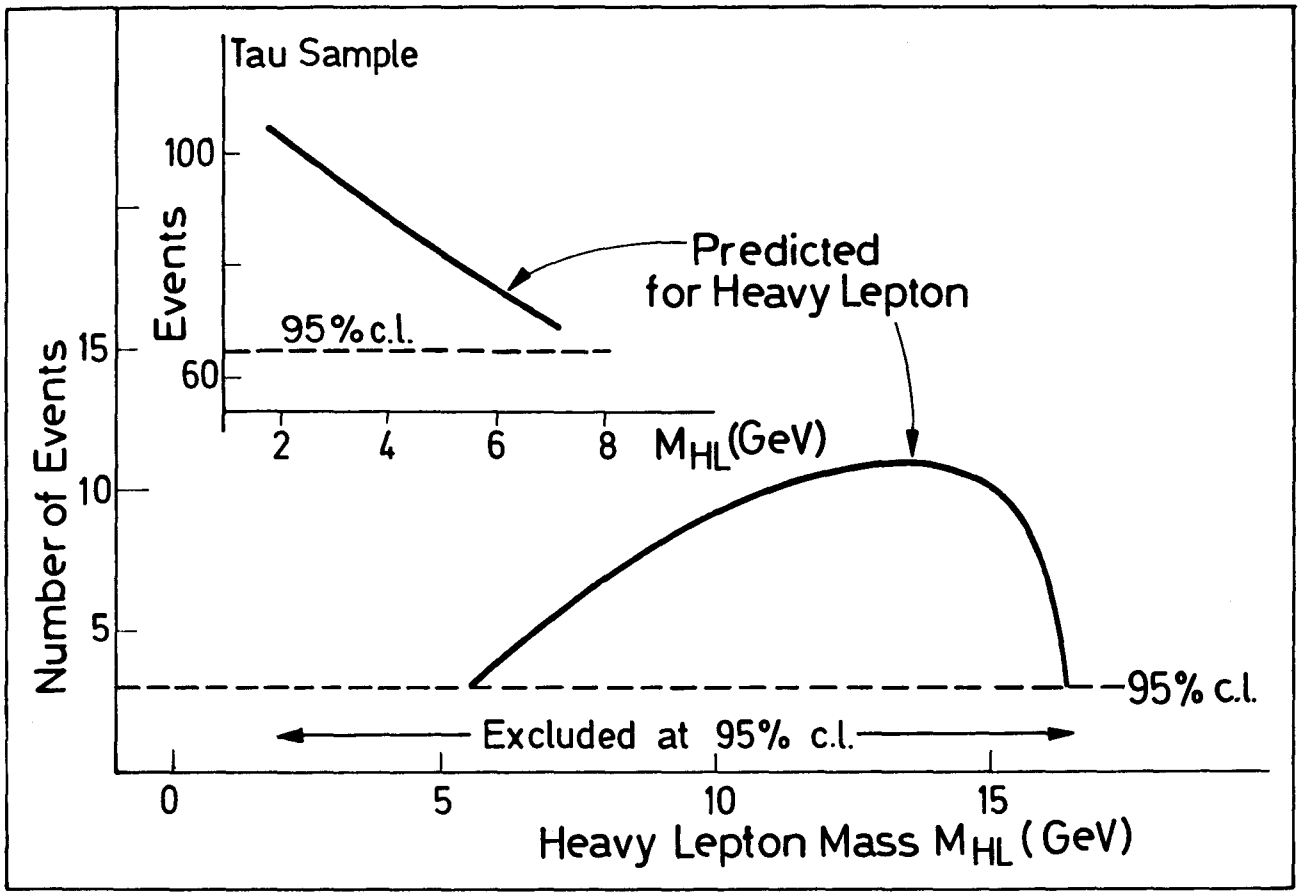
Tau Sample
100
Events
60
95% c.l.
2
4
6
8
M_{HL}(GeV)
Predicted
for Heavy Lepton
Number of Events
15
10
5
95% c.l.
Excluded at 95% c.l.
0
5
10
15
Heavy Lepton Mass M_{HL} (GeV)

FIGURE 13

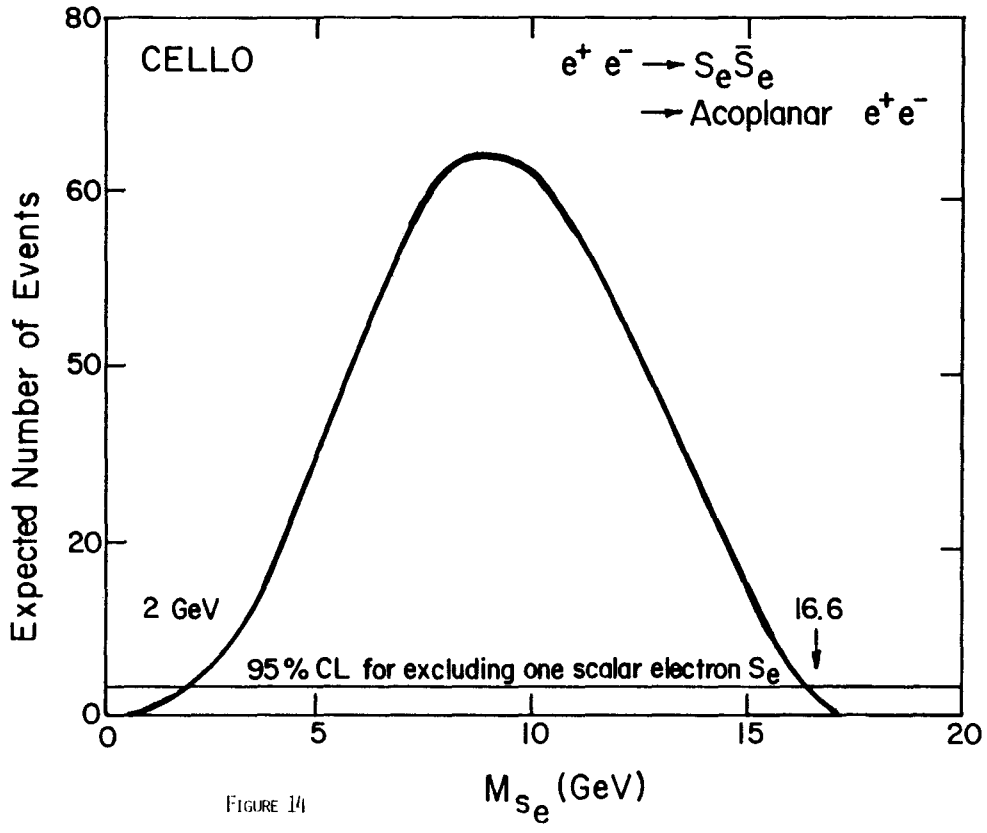
CELLO
$e^+ e^- \rightarrow S_e \bar{S}_e$
Acoplanar e^+e^-
Expected Number of Events
80
60
50
20
0
2 GeV
16.6
95% CL for excluding one scalar electron S_e
0
5
10
15
20
M_{S_e} (GeV)

FIGURE 14

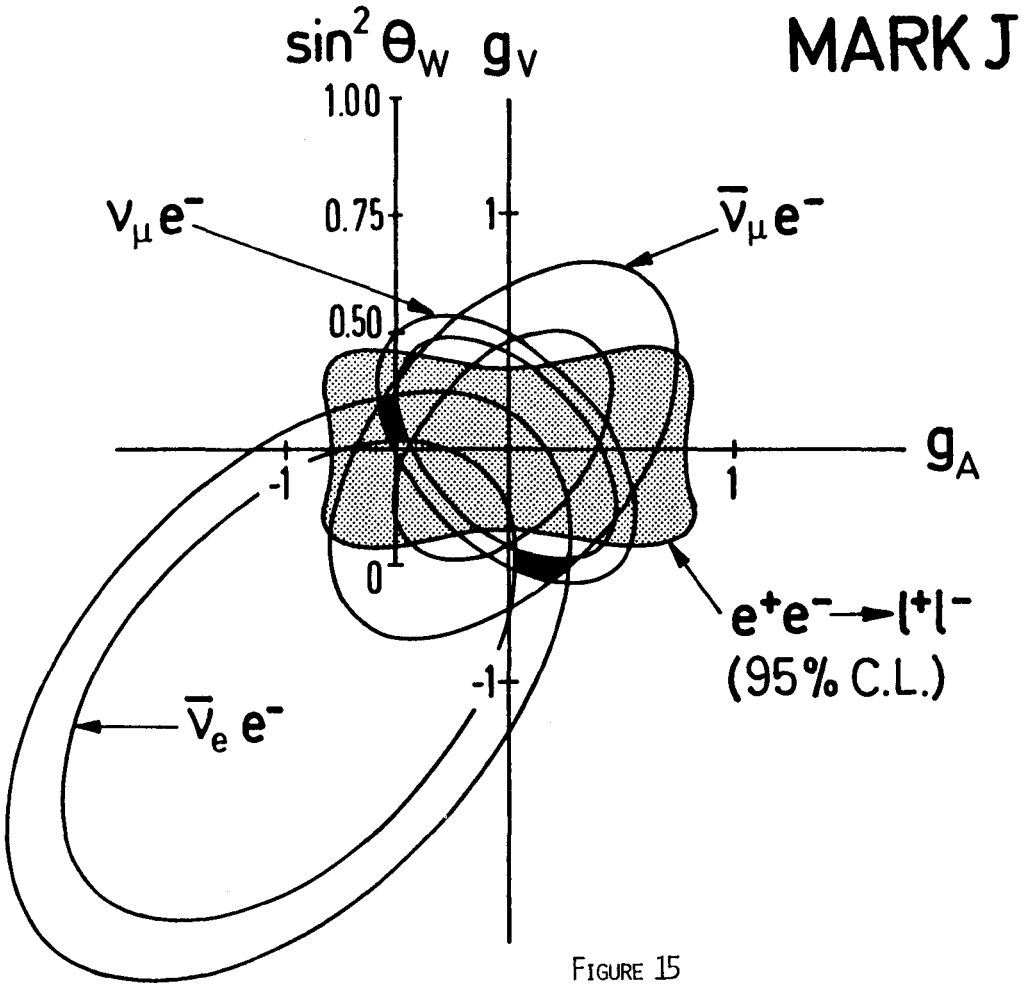

FIGURE 15

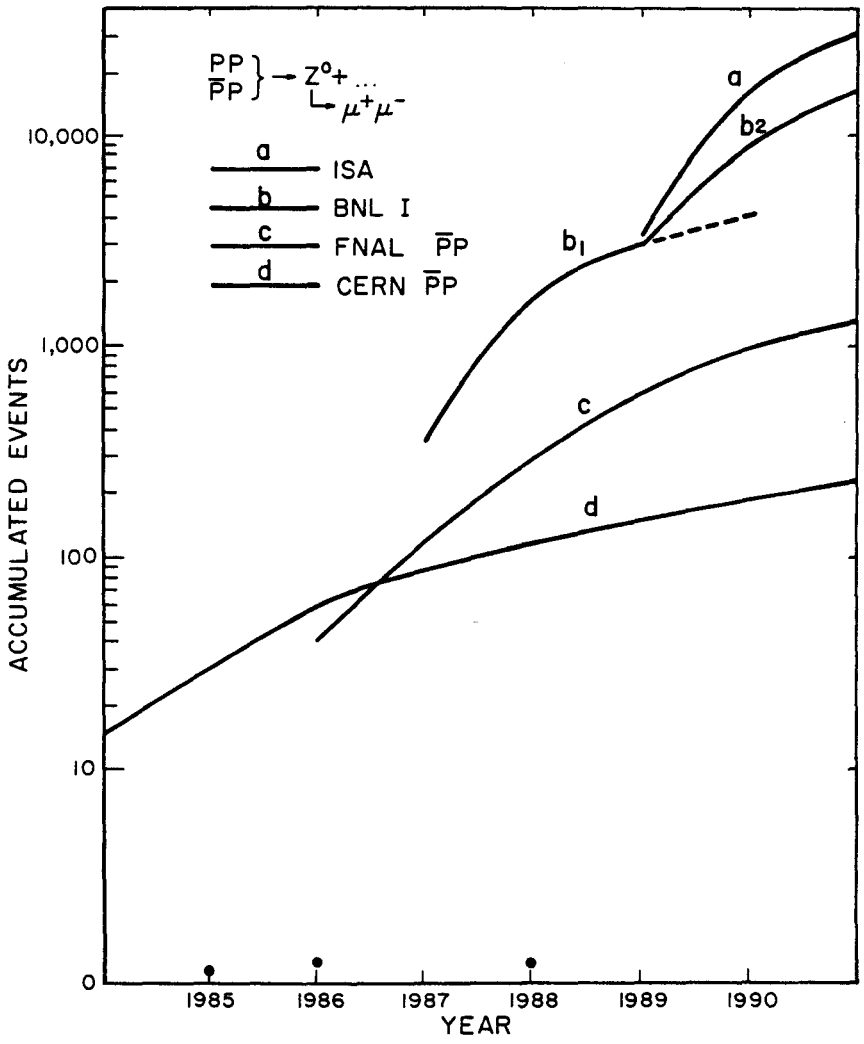
PP
P̄P → Z° + ...
↳ μ⁺μ⁻
a ISA
b BNL I
c FNAL P̄P
d CERN P̄P
a
b2
b1
c
d
10,000
1,000
100
10
0
ACCUMULATED EVENTS
1985
1986
1987
1988
1989
1990
YEAR

FIGURE 16

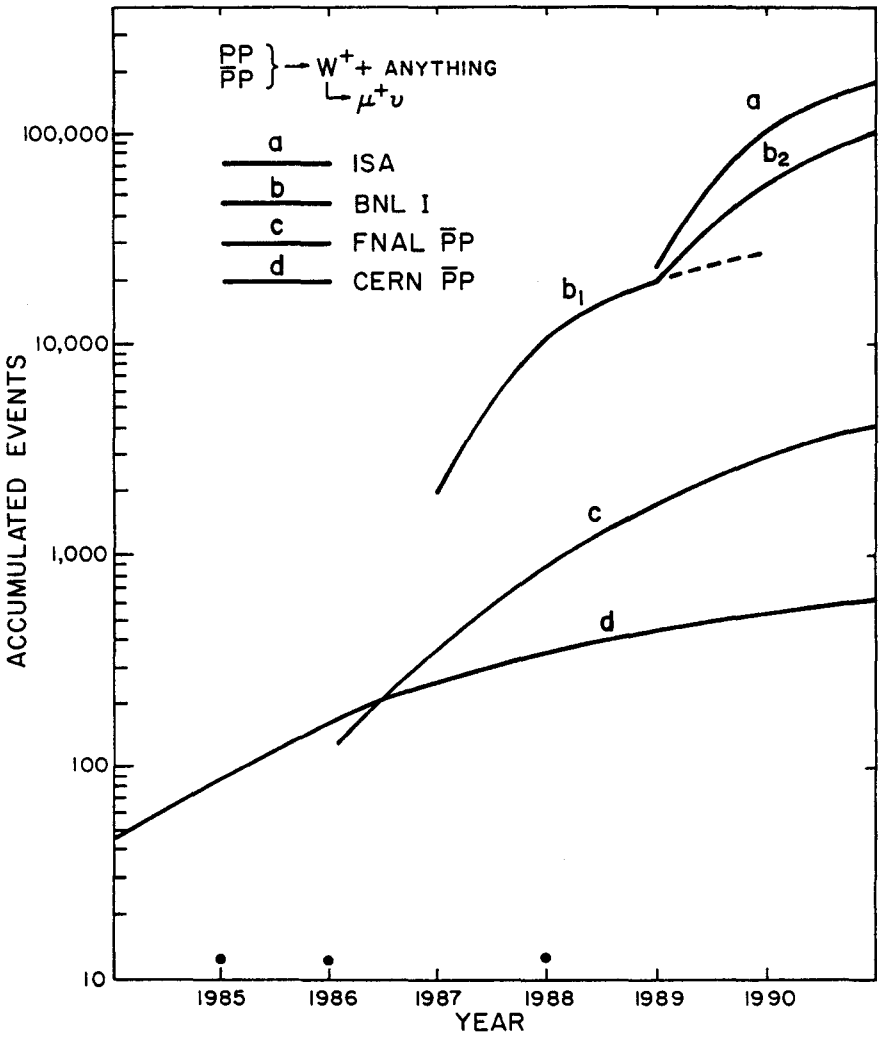
PP
P̄P
W+ + ANYTHING
μ+ν
a
ISA
b
BNL I
c
FNAL P̄P
d
CERN P̄P
a
b2
b1
c
d
100,000
10,000
1,000
100
10
ACCUMULATED EVENTS
1985
1986
1987
1988
1989
1990
YEAR

FIGURE 17

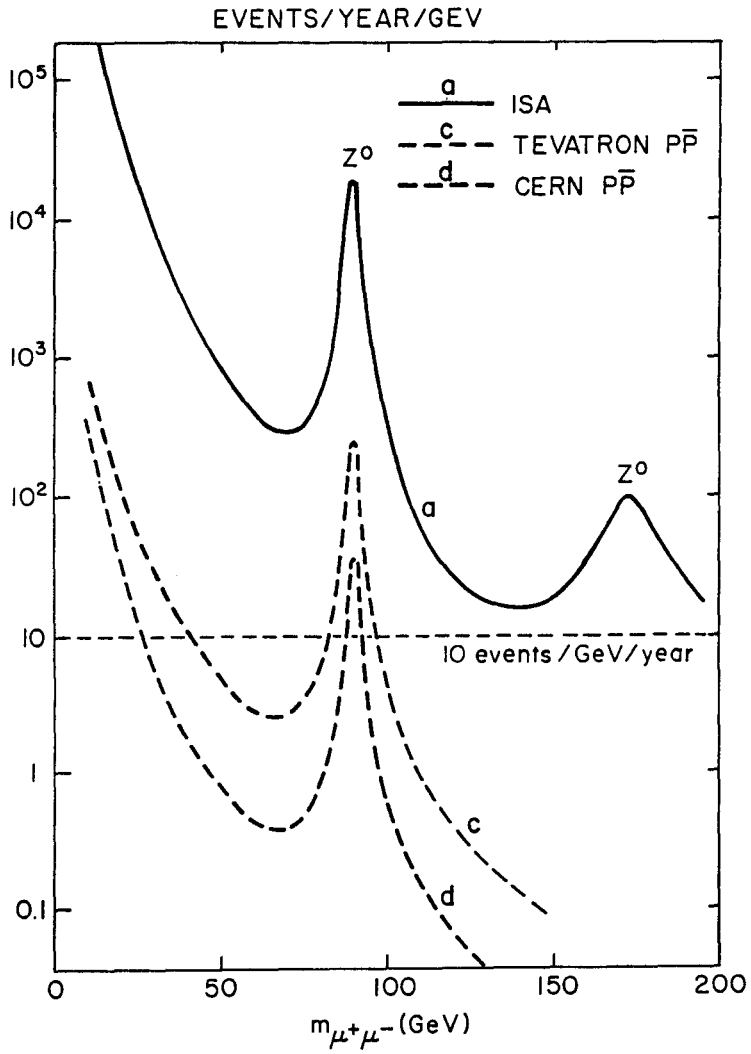

SEARCH FOR Z's

FIGURE 18

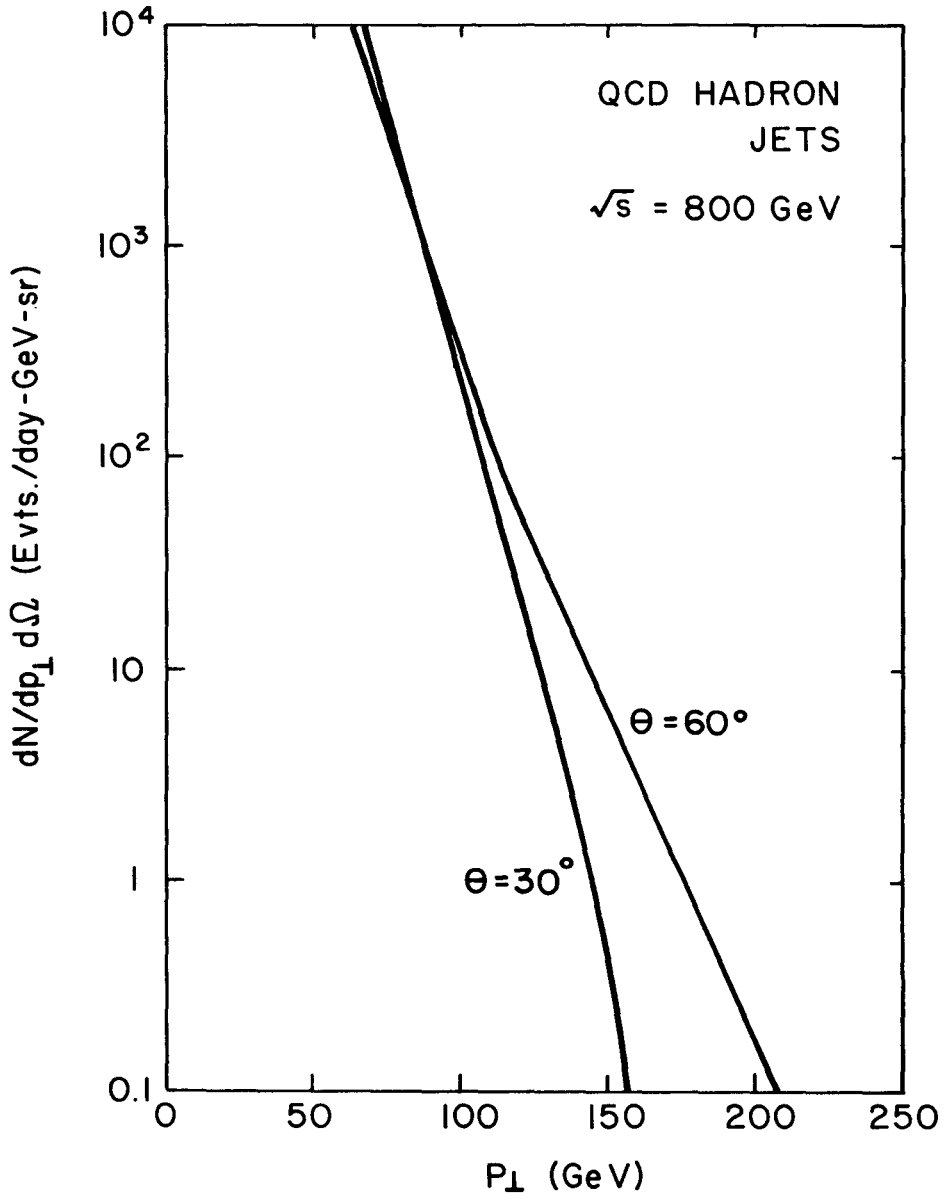
QCD HADRON
JETS
√s = 800 GeV
θ=60°
θ=30°
dN/dp⊥ dΩ (Evts./day-GeV-sr)
P⊥ (GeV)
10⁴
10³
10²
10
1
0.1
0
50
100
150
200
250

FIGURE 19

HIGGS

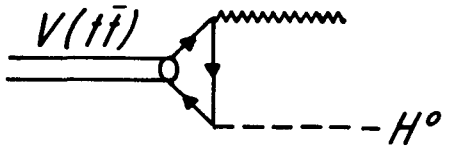

EXPERIMENTAL SIGNATURE:

$PP \rightarrow (t\bar{t}) + X$

$\hookrightarrow H^0 + (\gamma)$

$\hookrightarrow b\bar{b},\ c\bar{c},\ \tau\bar{\tau} \rightarrow (\mu's + X')$

TRIGGER: Hard (≥ 20 GeV) Photon + Recoiling Jet ($\geq 1\mu$)

WITH $\int \mathcal{L}\,dt = 10^{33}\,cm^{-2}\,sec^{-1} \times 10^{3}\,h$

M_V (GeV)	$\sigma(PP \rightarrow V \rightarrow H^0\gamma + X)$ (pb)	No. of Events
40	1.0	2300
60	0.2	500
80	0.04	~100

BACKGROUND: Invariant Mass $m[\gamma, H^0]$ provides good identification against QCD single photon (and π^0)

FIGURE 20

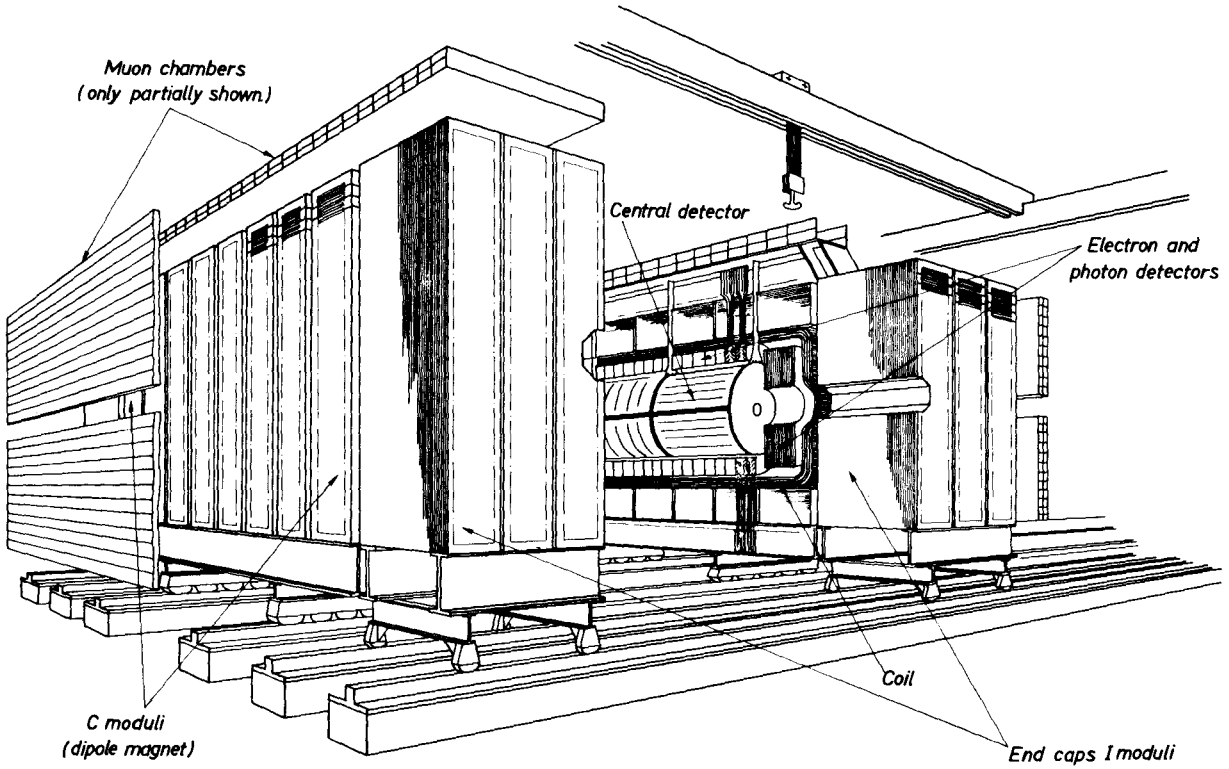
Muon chambers
(only partially shown)
Central detector
Electron and
photon detectors
Coil
C moduli
(dipole magnet)
End caps I moduli

FIGURE 21

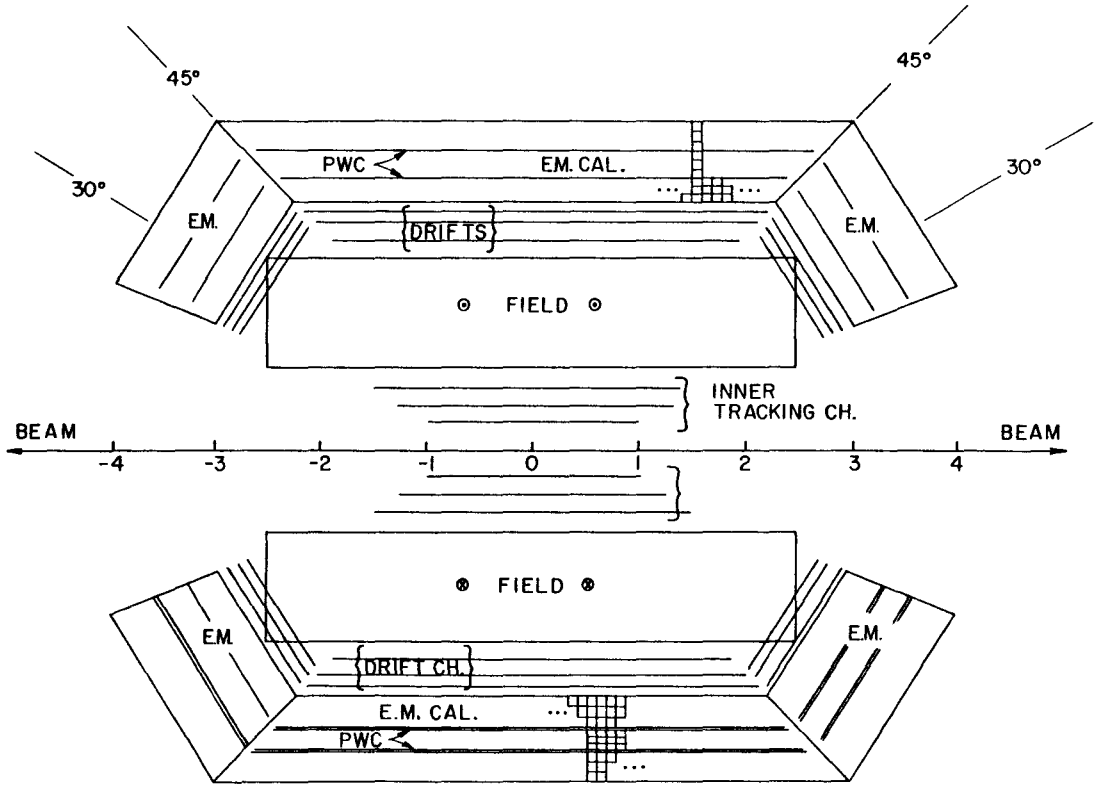

PLAN VIEW
FIGURE 22

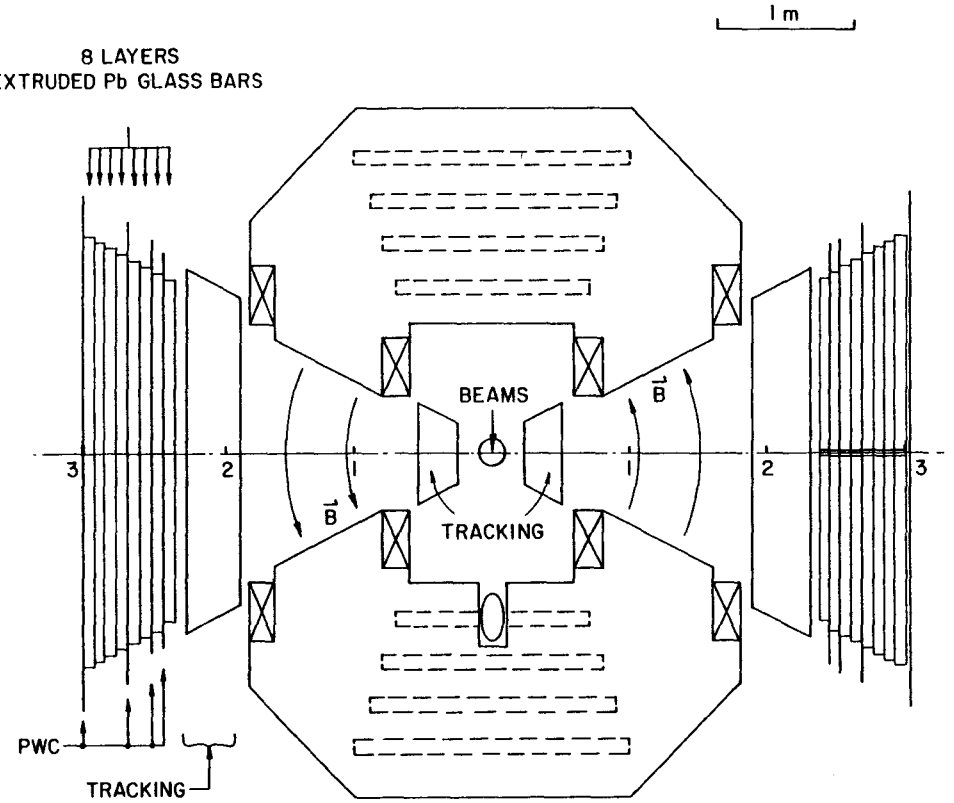

END VIEW
FIGURE 23

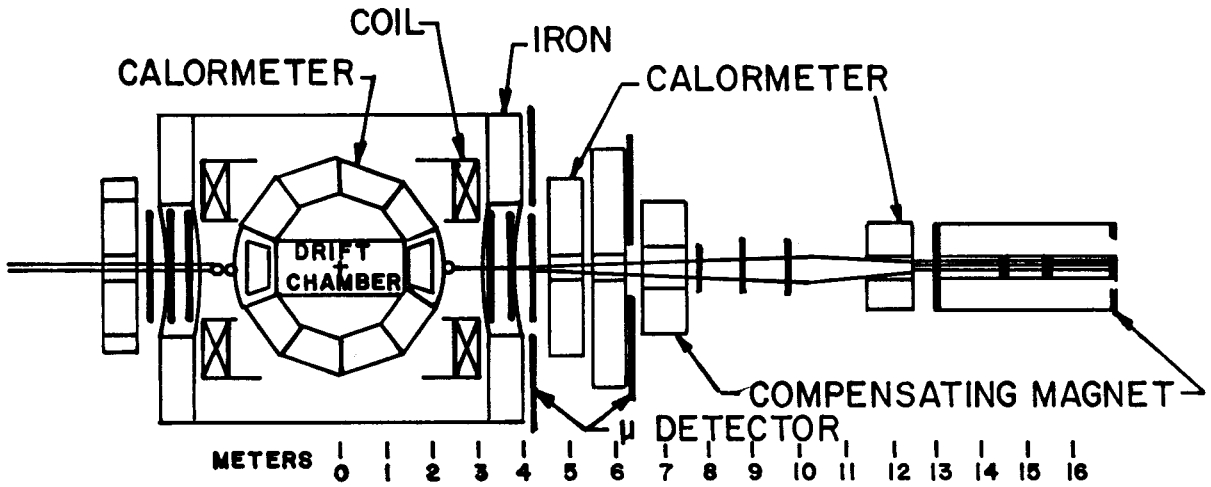

PLAN VIEW

FIGURE 24

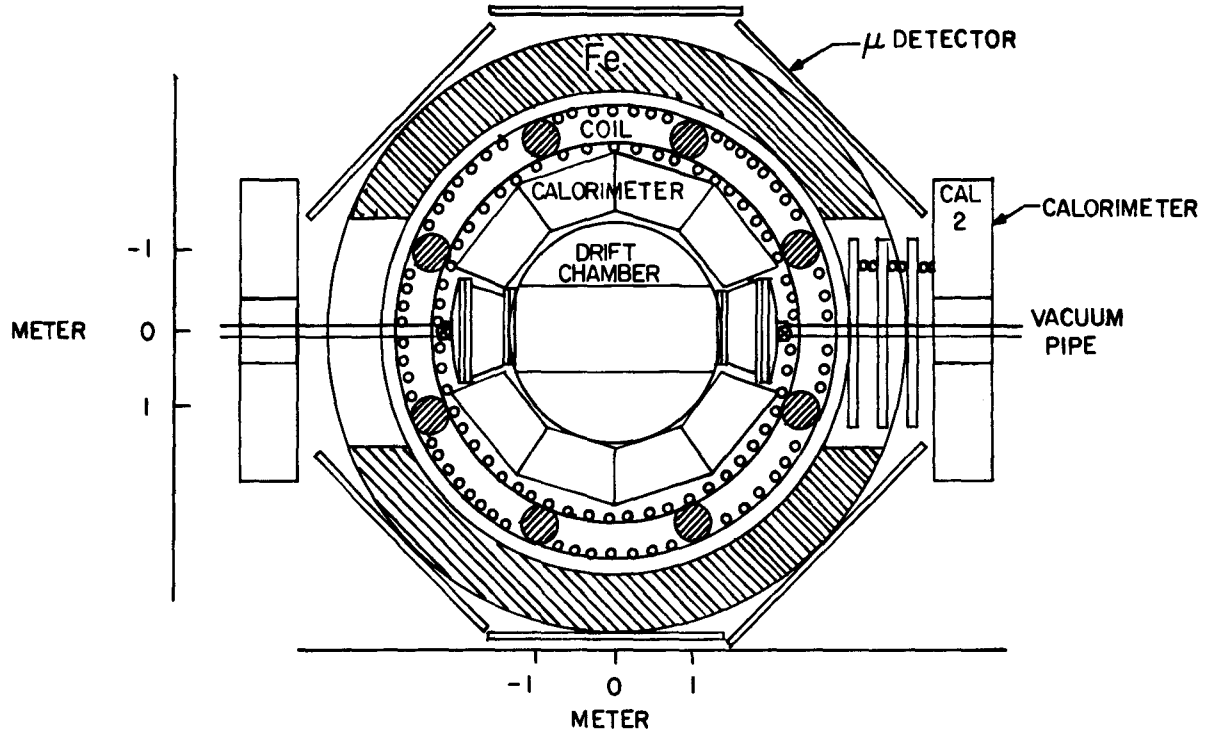
μ DETECTOR
Fe
COIL
CALORIMETER
DRIFT
CHAMBER
CAL
2
CALORIMETER
VACUUM
PIPE
METER
-1
0
1
-1
0
1
METER

FIGURE 25

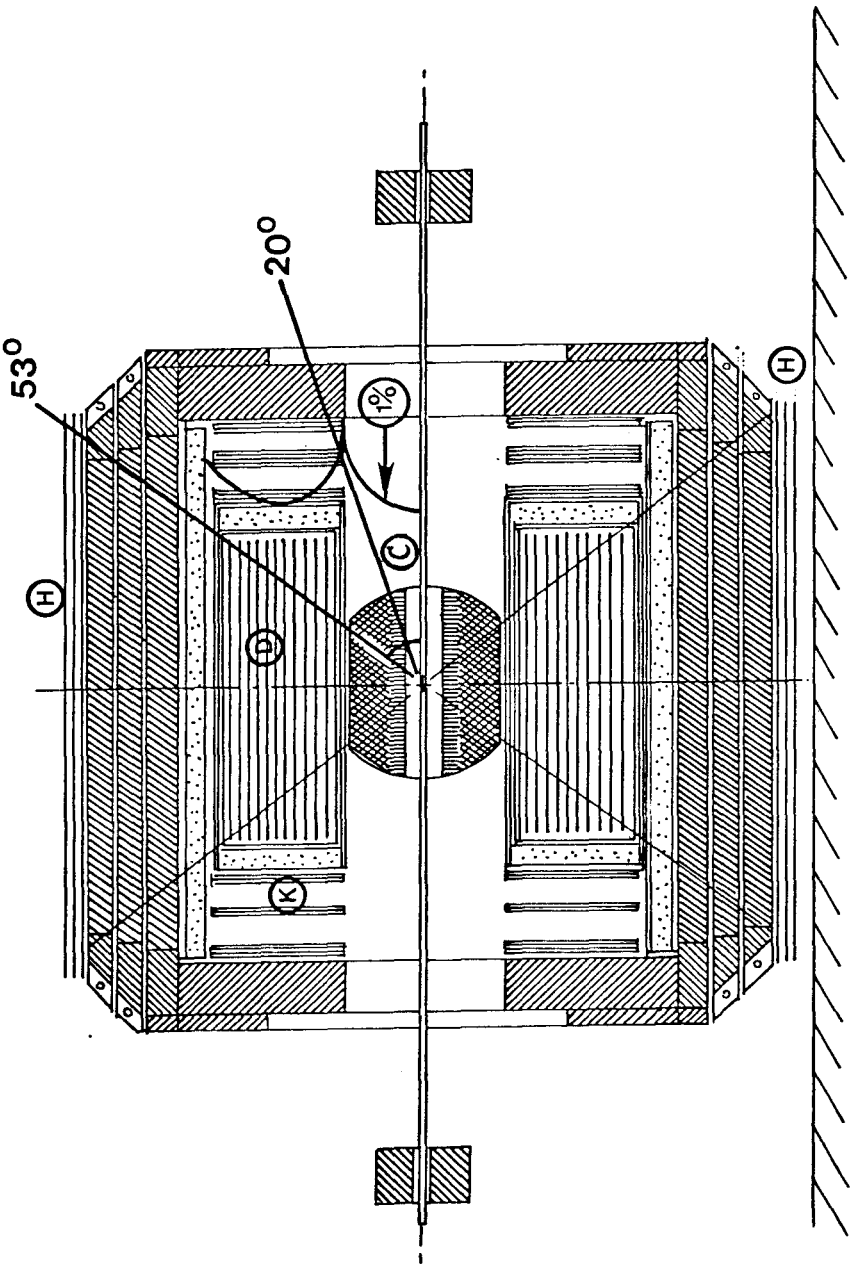

FIGURE 26

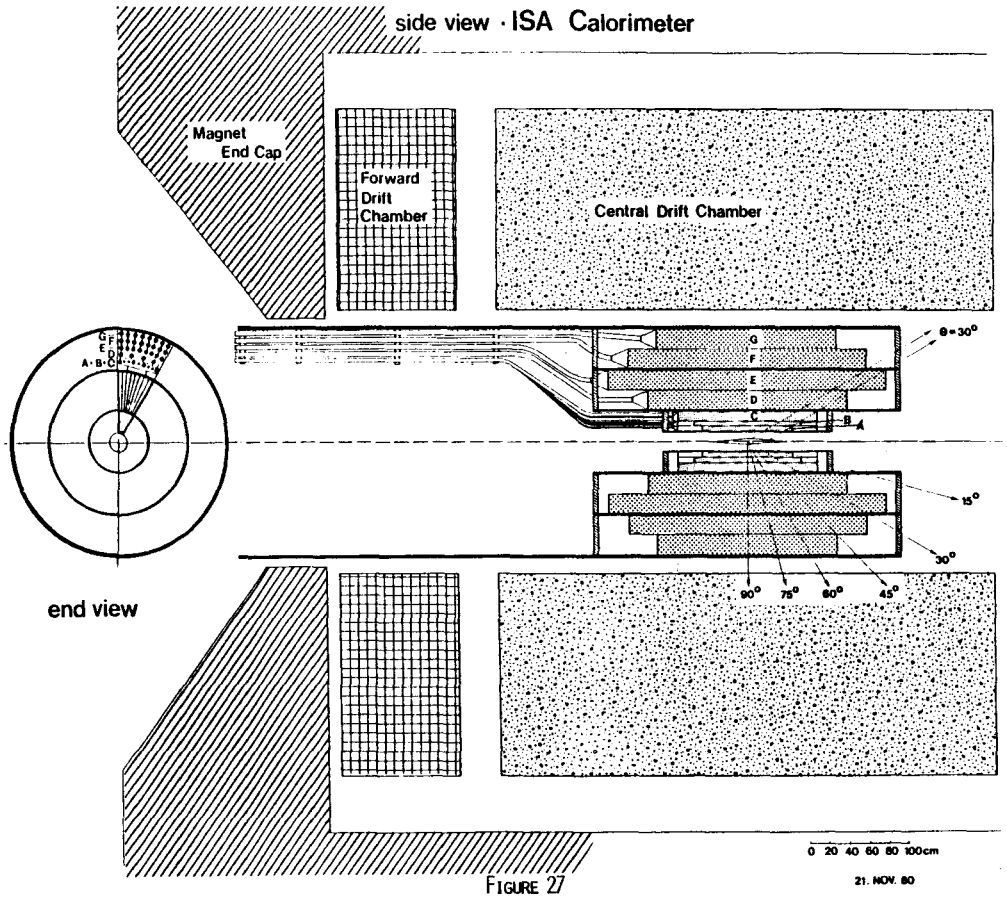
side view · ISA Calorimeter
Magnet
End Cap
Forward
Drift
Chamber
Central Drift Chamber
θ=30°
15°
30°
90°
75°
60°
45°
end view
0 20 40 60 80 100cm
21. NOV. 80

FIGURE 27

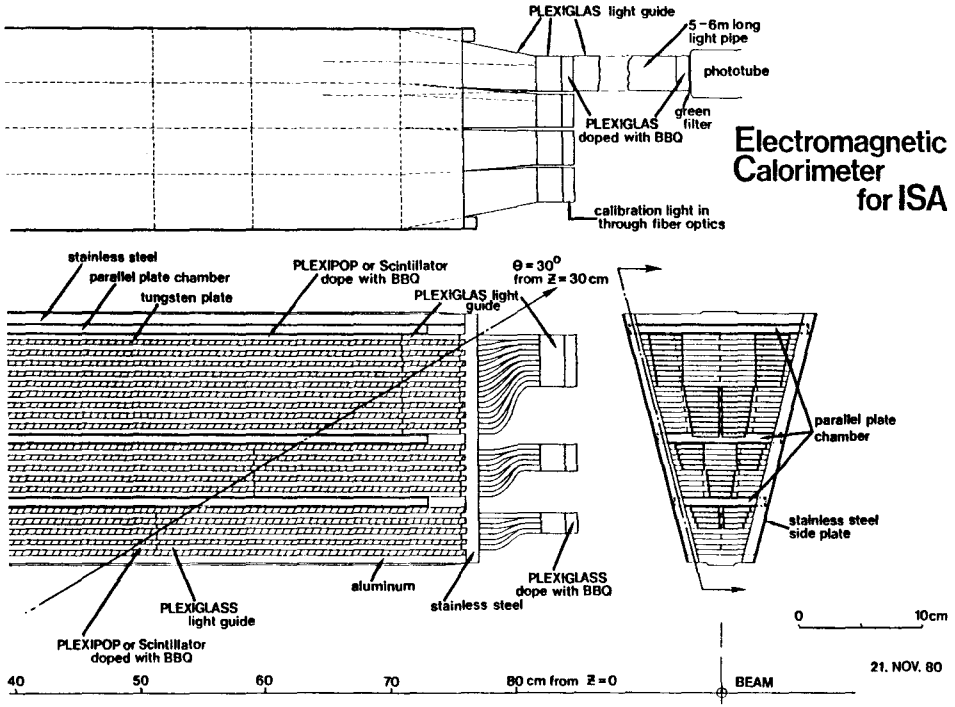
PLEXIGLAS light guide
5-6m long light pipe
phototube
green filter
PLEXIGLAS doped with BBQ
calibration light in through fiber optics
Electromagnetic Calorimeter for ISA
stainless steel
parallel plate chamber
tungsten plate
PLEXIPOP or Scintillator dope with BBQ
PLEXIGLAS light guide
θ = 30° from z = 30 cm
parallel plate chamber
stainless steel side plate
aluminum
stainless steel
PLEXIGLASS dope with BBQ
PLEXIGLASS light guide
PLEXIPOP or Scintillator doped with BBQ
0
10cm
40
50
60
70
80 cm from z = 0
BEAM
21. NOV. 80

FIGURE 28

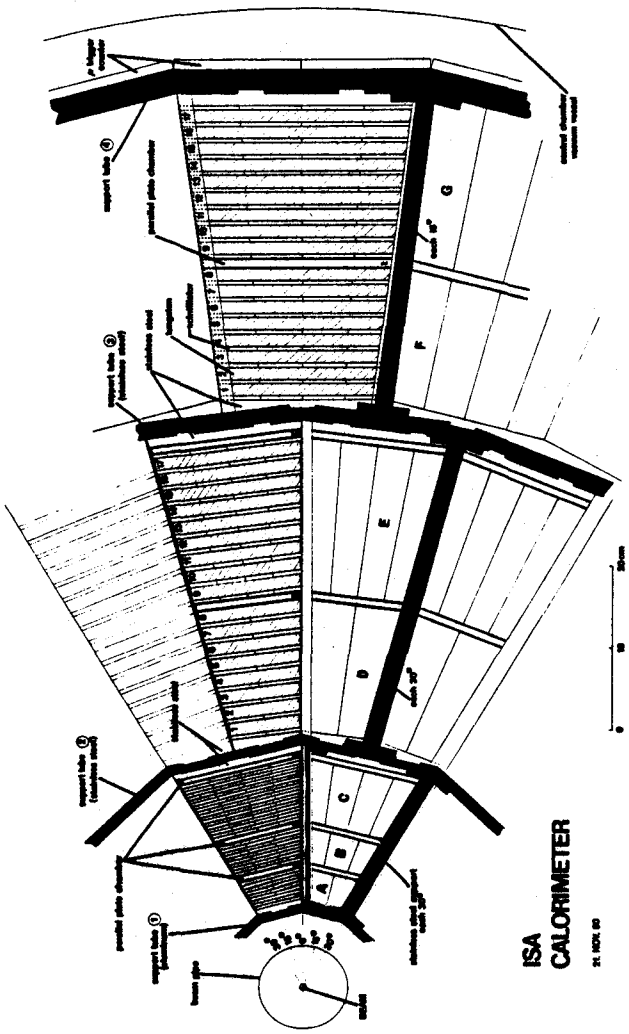

FIGURE 29

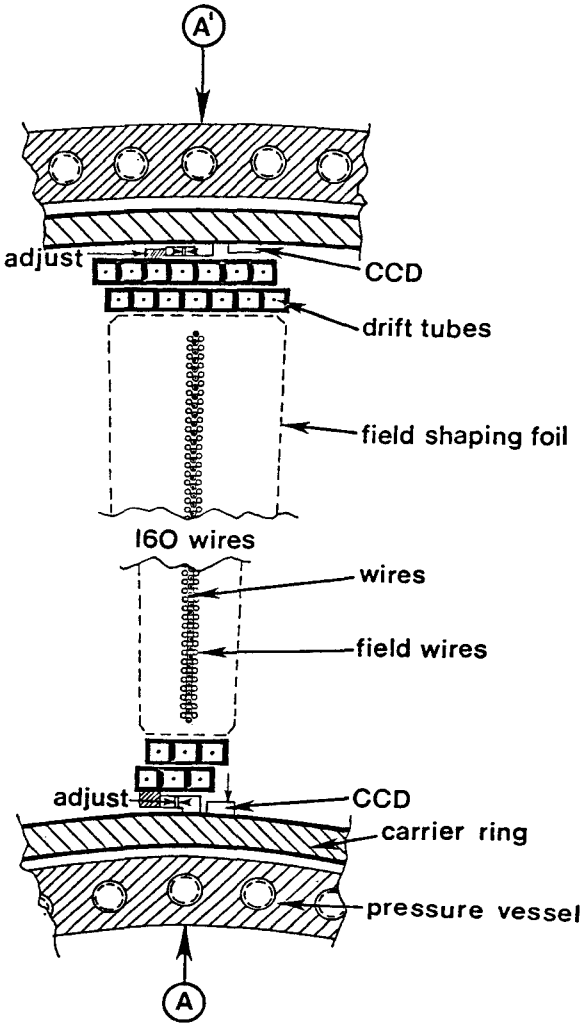
A'
adjust
CCD
drift tubes
field shaping foil
160 wires
wires
field wires
adjust
CCD
carrier ring
pressure vessel
A

FIGURE 30

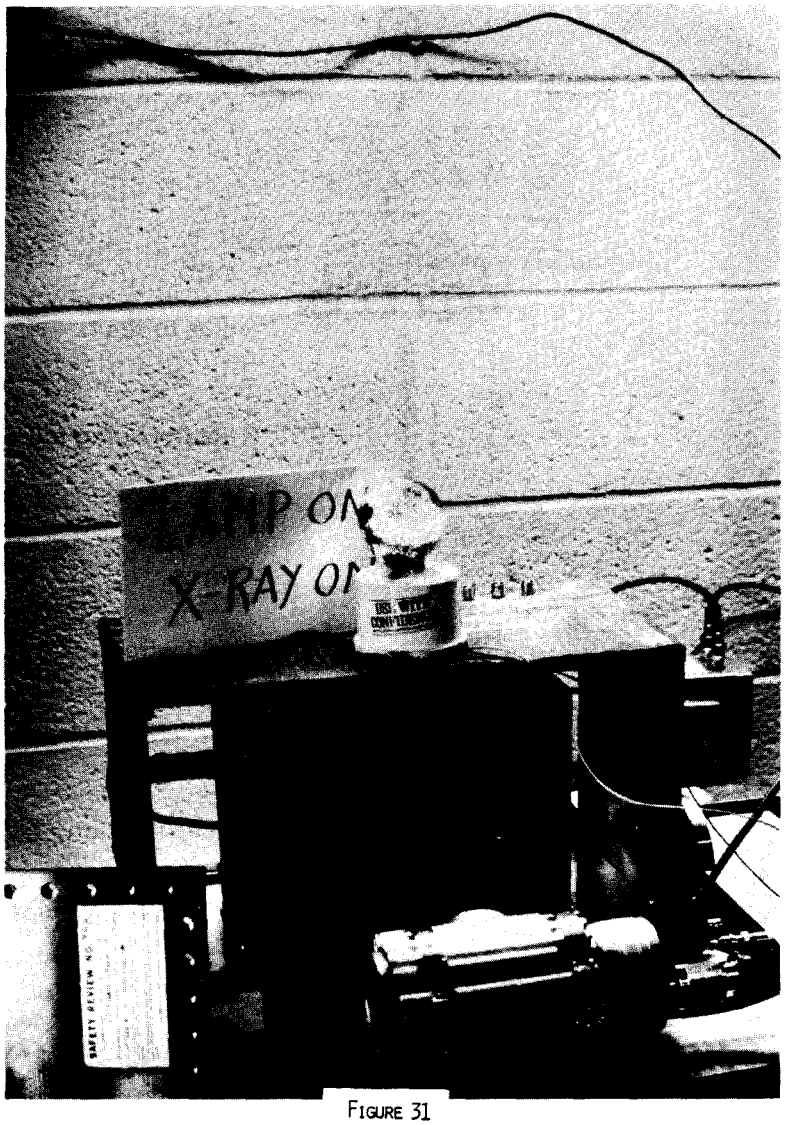

FIGURE 31

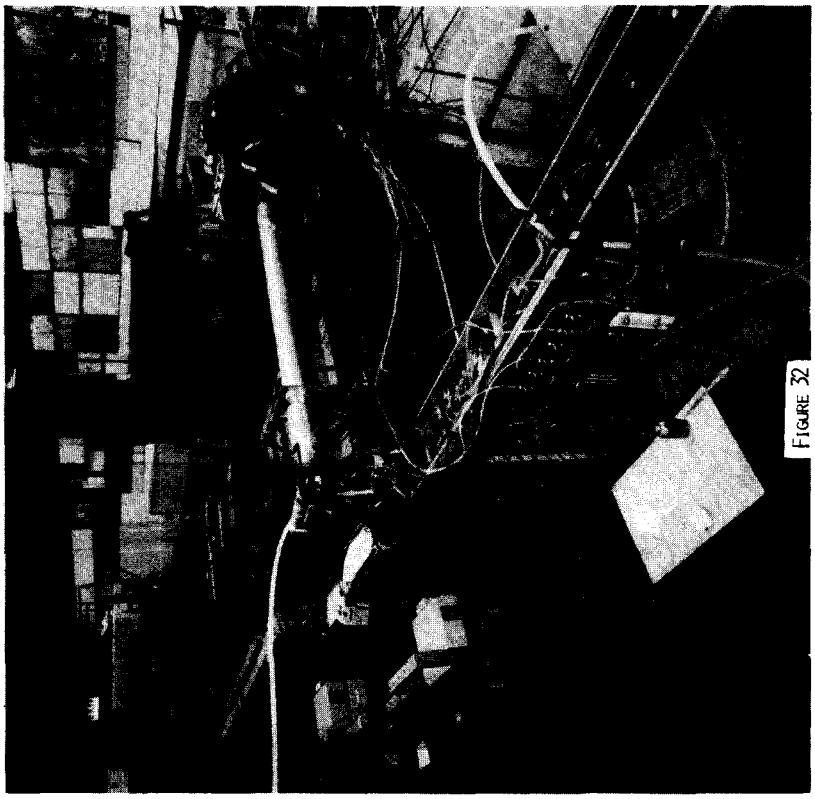

FIGURE 32

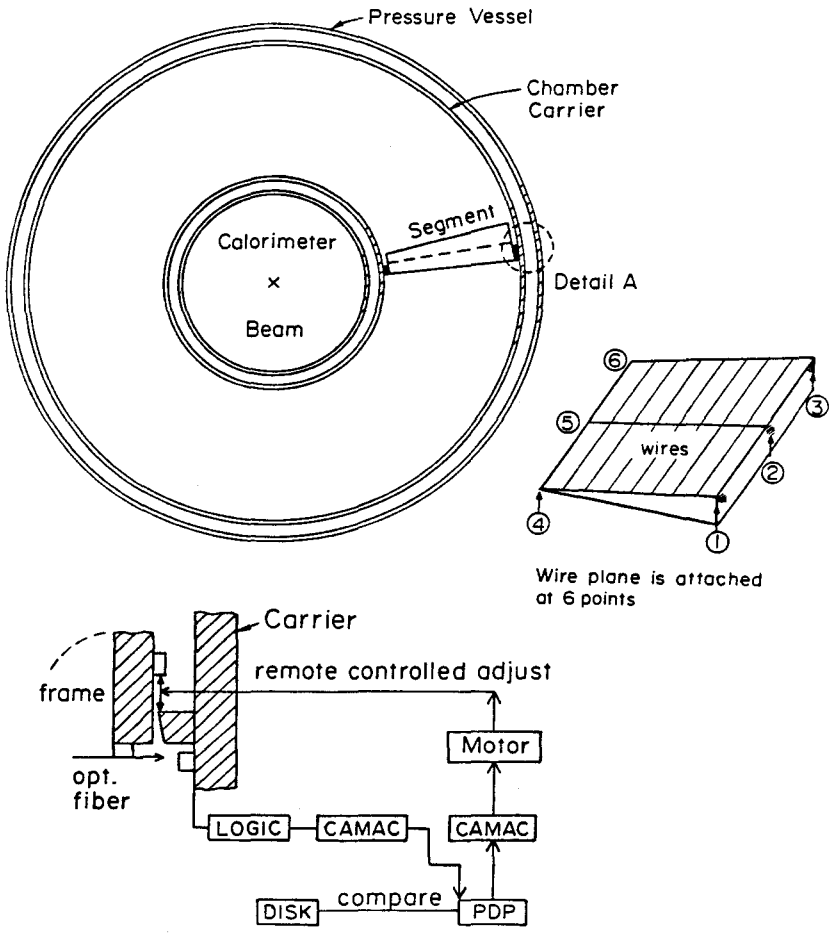
Pressure Vessel
Chamber
Carrier
Calorimeter
×
Beam
Segment
Detail A
⑥
⑤
③
wires
②
④
①
Wire plane is attached
at 6 points
Carrier
frame
remote controlled adjust
Motor
opt.
fiber
LOGIC
CAMAC
CAMAC
DISK
compare
PDP

FIGURE 33

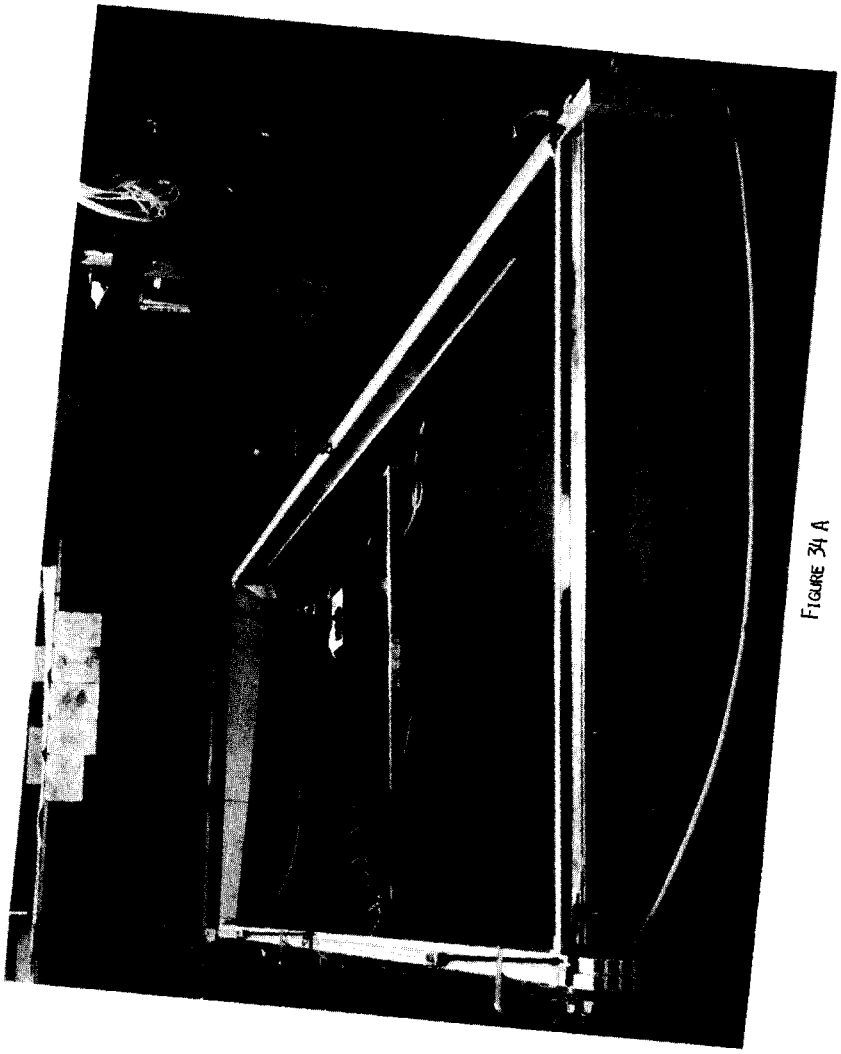

FIGURE 34 A

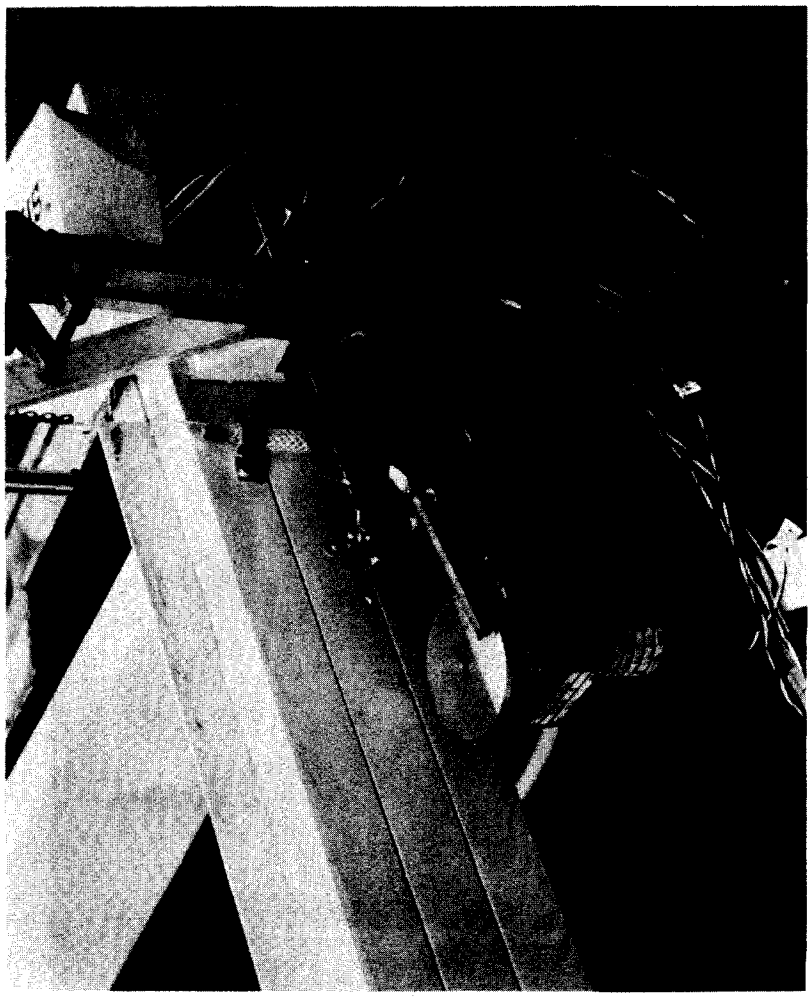

FIGURE 34 B

FIGURE 35

SUMMARY REMARKS

N. P. Samios

I would like to take this opportunity to make a few brief remarks mainly concerning the physics discussed at this workshop. The importance of luminosity and energy for colliders was certainly reaffirmed. The mass scales that we know of, to date, are 1-30 GeV for quark flavors, $m \simeq 100$ GeV for W's and Z's and higher mass onia with cross sections $\simeq 10^{-33} cm^2$, the grand unified level of 10^{15} GeV which is for theorists (not experimentalists at present) and a region from 10.8 GeV (Higgs) to 300 GeV which may turn out to contain a wealth of new particles, e.g., technicolor, with cross sections $\simeq 10^{-35} cm^2$ which would be accessible with ISABELLE luminosities. In fact, I consider this to be the area that has the highest probability of containing surprises and producing the most exciting physics at ISABELLE. At this point I would also like to give some advice, namely, to beware of fads. Such things occur in our field from time to time; however, we should be deeper in our commitment to projects than some speculative theory or wrong experiment. I remind you that the predicted proton lifetime changed by more than 8 orders of magnitude, 10^{32} yrs. $\rightarrow 10^{40}$ yrs. by just going from SU(5) to SU(7) or invoking supersymmetric theories. As far as luminosity is concerned, one really needs $I > 10^{31}/cm^2/sec$ just because σ (strong) $\simeq 10^{-27} cm^2$, σ (e-m) $\simeq 10^{-30}$ cm^2 and σ (weak) $< 10^{-33} cm^2$. The importance of luminosity is brightly illuminated if we recall the CEA bypass experience. The R measurement clearly indicated new and exciting physics; however, all the ψ's, χ's, D's were left to other machines, not because of energy but insufficient luminosity. In this regard, pp machines are straightforward, the ISR is the prototype, and ISABELLE should, with high confidence have a luminosity of 2×10^{32} or higher. $\bar{p}p$ colliders, on the other hand, are more akin to an experiment, high energies but design luminosities of 2×10^{29} to 10^{30}, a factor of 1,000 less than pp. Furthermore if the physics and

high energies turn out to be due more to gluons than to quarks, then luminosity is even more important.

If one takes a historical perspective one can consider the 1950's - 1960's as the era of hadron machines. Most of the

magnets, implying an '87 completion with a higher luminosity, i.e., 2×10^{32}. I welcome written comments from the participants of this workshop. Anticipating success on one of these tracks, we will start to consider a schedule for proposals at the end of the year.

It is time to think deeply and hard and realize that ISABELLE with pp, ep and heavy ions is the cornerstone of the U.S. High Energy Physics Program. It is our intent to implement this program.

AUTHOR INDEX

Volume 1 contains pages 1-402 + δ
Volume 2 contains pages 403-804
Volume 3 contains pages 805-1134
Volume 4 contains pages 1135-1488

U.S. GOVERNMENT PRINTING OFFICE: 714-037#14